REPORT DOCUMENTATION PAGE

Form Approved
OMB No. 0704-0188

1. AGENCY USE ONLY *(Leave blank)*	2. REPORT DATE	3. REPORT TYPE AND DATES COVERED
	10 June 1999	Annual Report, 1 June 98 - 31 May 99

4. TITLE AND SUBTITLE

Use of Suction Piles for Mooring of Mobile Offshore Bases

5. FUNDING NUMBERS

Grant
N00014-97-1-0887

6. AUTHOR(S)

Sangchul Bang

7. PERFORMING ORGANIZATION NAMES(S) AND ADDRESS(ES)

South Dakota School of Mines and Technology
501 E. St. Joseph St.
Rapid City, SD 57701

8. PERFORMING ORGANIZATION REPORT NUMBER

9. SPONSORING / MONITORING AGENCY NAMES(S) AND ADDRESS(ES)

Office of Naval Research
800 North Quincy St.
Arlington, VA 22217-5660

10. SPONSORING / MONITORING AGENCY REPORT NUMBER

11. SUPPLEMENTARY NOTES

a. DISTRIBUTION / AVAILABILITY STATEMENT

APPROVED FOR PUBLIC RELEASE

12. DISTRIBUTION CODE

13. ABSTRACT *(Maximum 200 words)*

The research includes a feasibility study to determine the practicability, efficiency, and applicability of the suction piles for their use as part of the mooring system in deep water. It examines the effects of various pertinent geometric and material parameters of suction piles through analytical and experimental studies. Analytical performance study is completed. Laboratory experiments on suction piles in sand are also completed with those in clay are still continuing. Verification of mooring line analysis through field tests are also completed.

14. SUBJECT TERMS

suction pile, experimental testing, analytical parametric study, performance study, mooring line analysis, field verification

15. NUMBER OF PAGES
9 pages with CD

16. PRICE CODE

17. SECURITY CLASSIFICATION OF REPORT	18. SECURITY CLASSIFICATION OF THIS PAGE	19. SECURITY CLASSIFICATION OF ABSTRACT	20. LIMITATION OF ABSTRACT
			UL

USE OF SUCTION PILES FOR MOORING OF MOBILE OFFSHORE BASES

(ONR Grant No. N00014-97-1-0887)

Task 2 Completion Report: Analytical Performance Study

(July 1, 1997 – Sep. 30, 1998)

Submitted to

Naval Facilities Engineering Service Center
Port Hueneme, CA

by

Sangchul Bang and Yeongki Cho

Department of Civil and Environmental Engineering
South Dakota School of Mines and Technology
Rapid City, SD 57701

Mar., 1999

Table of Contents

	Page
1. INTRODUCTION	6
2. PERFORMANCE STUDY OF SUCTION PILES WITH LINEAR ELASTIC SOIL PROPERTIES	7
2.1 Material and Loading Parameters	8
2.2 Description of Pile Cross-Sections	9
2.3 Results	10
2.3.1 Behaviors under horizontal loads	10
2.3.2 Behaviors under vertical loads	15
2.3.3 Results from various cross-sections	16
2.4 Summary	17
3. PERFORMANCE STUDY OF SUCTION PILES IN SAND WITH ELASTO-PLASTIC SOIL PROPERTIES	19
3.1 Material and Loading Parameters	20
3.2 Example Input Data	21
3.3 Description of Pile Cross-Sections	23
3.4 Results	23
3.4.1 Behaviors under horizontal loads	25
3.4.2 Behaviors under vertical loads	29
3.4.3 Behaviors under inclined loads	31
3.4.4 Additional results	33
3.5 Summary	33
3.5.1 General conclusions	33

3.5.2 Pile failure loads 34

3.5.2.1 Pile failure based on horizontal displacement 35

3.5.2.1 Pile failure based on vertical displacement 35

3.5.3 Soil minor principal stresses 36

3.5.4 Pile von Mises stresses 37

3.5.5 Analysis with unsymmetric global stiffness matrix 38

4. PERFORMANCE STUDY OF SUCTION PILES IN CLAY WITH ELASTO-PLASTIC SOIL PROPERTIES 39

4.1 Extended Hyperbolic Drucker-Prager Plasticity 40

4.2 Material and Loading Parameters 42

4.3 Example Input Data 44

4.4 Description of Pile Cross-Sections 46

4.5 Results 46

4.5.1 Behaviors under horizontal loads 47

4.5.2 Behaviors under vertical loads 51

4.5.3 Behaviors under inclined loads 54

4.5.4 Additional results 56

4.6 Summary 56

4.6.1 General conclusions 56

4.6.2 Pile failure loads 58

4.6.2.1 Pile failure based on horizontal displacement 58

4.6.2.2 Pile failure based on vertical displacement 59

5. ADDITIONAL PERFORMANCE STUDY OF SUCTION PILES 60

5.1 Description of Parameters 60

5.1.1 Width of flange 61

5.1.2 Loading point 61

5.1.3 Pile diameter change 62

5.1.4 Layered soil condition 62

5.2 Material and Loading Parameters 63

5.3 Results 63

5.3.1 Effect of flange 63

5.3.1.1 Behaviors of suction piles in Sand 64

5.3.1.2 Behaviors of suction piles in clay 67

5.3.1.3 Additional results 70

5.3.2 Effect of loading point 70

5.3.2.1 Behaviors of suction piles in Sand 71

5.3.2.1.1 Behaviors under horizontal loads 71

5.3.2.1.2 Behaviors under 45-degree inclined loads 74

5.3.2.2 Behaviors of suction piles in clay 76

5.3.2.2.1 Behaviors under horizontal loads 76

5.3.2.2.2 Behaviors under 45-degree inclined loads 79

5.3.2.3 Additional results 81

5.3.3 Effect of pile diameter change 81

5.3.3.1 Behaviors of telescopic piles in sand 82

5.3.3.2 Behaviors of telescopic piles in clay 84

5.3.3.3 Additional results 87

5.3.4 Effect of layered soil condition 88

5.3.4.1 Suction piles with group-I soil conditions 88

5.3.4.2 Suction piles with group-II soil conditions 91

5.3.4.3 Additional results 93

5.4 Summary 94

5.4.1 General conclusions 94

5.4.1.1 Flange width 94

5.4.1.2 Loading point 95

5.4.1.3 Diameter change 96

5.4.1.4 Layered soil condition 97

5.4.2 Pile failure loads 97

6. CONCLUSIONS 98

6.1 Linear Elastic Analysis 98

6.2 Elasto-Plastic Analysis with Sand 99

6.3 Elasto-Plastic Analysis with Clay 100

6.4 Effects of Additional Parameters 101

6.4.1 Flange width 102

6.4.2 Loading point 102

6.4.3 Diameter change 103

6.4.4 Layered soil condition 104

7. REFERENCES 105

8. FIGURES AND TABLES 106

1. INTRODUCTION

An analytical performance study on suction piles was conducted to identify the most effective geometry of suction piles under various external loading conditions and various suction pile and soil geometric and material properties. First, a qualitative analytical performance study was conducted to examine the behaviors of 11 different pile cross-sectional shapes under vertical and horizontal loads using linear elastic soil material properties. Three suction pile cross-sections which exhibited the best overall performances were selected at the end of this study.

The three selected pile cross-sections were then studied in detail using plastic soil material properties, i.e., linear extended Drucker-Prager plasticity for sand and hyperbolic extended Drucker-Prager plasticity for clay. Vertical, horizontal, and inclined loads were applied incrementally to failure and responses of the pile and soil were observed.

Additionally, the effects of the flange at the top of the pile, the point of the mooring line attachment, the telescopic pile cross-section, and the layered soil properties on the overall performance of the suction pile were examined.

ABAQUS version 5.7 (1), a finite element method of analysis software written by Hibbit, Karlsson & Sorensen, Inc., was utilized for the entire analytical performance study. In addition, FEAMAP software (5) was used for the easy performance of pre- and post-processing of input and output such as three dimensional mesh generations and graphical display of output, etc.

It is noted that the solutions of the analysis such as displacements and stresses are presented in the form of color intensity contours. The majority of these figures are included in a separate volume of the report – APPENDIX: Results of Analysis.

2. PERFORMANCE STUDY OF SUCTION PILES WITH LINEAR ELASTIC SOIL PROPERTIES

The purpose of this study is to identify a set of the most efficient cross-sectional shapes of the suction pile in terms of lateral and vertical resistance prior to the detailed analysis with plastic soil properties. It was assumed that the length and thickness of the pile and the contact area between the pile and the soil remained the same for all shapes in order to maintain the same amount of pile material. A circular pile 30 feet in diameter and 30 feet in length was selected as the control. Eleven additional cross-sections were selected according to the above conditions and their behaviors analyzed.

The objective of this study is to compare qualitatively the responses of various pile cross-sections under lateral and vertical loads using linear elastic soil properties. This is to limit the number of cross-sections to be considered in the detailed quantitative analysis with plastic soil properties.

The study included eleven different cross-sections. This resulted in thirty different modes due to different directions of the horizontal loads and aspect ratios, i.e., the ratio between the width and length of their branches or cells. The selected pile cross sections are the ones that have been widely used in conventional piling. They include circular, triangular, square, Y-shaped, cross-shaped, clover shaped with three or four

leaves, and clusters of three or four circles. The cross-sectional profiles selected for the study are shown in Figure-1.

For the detailed finite element analysis, the selected cross-sections were expanded into three-dimensional columns to simulate the suction piles of uniform cross-sections. Figure-2 shows the three dimensional finite element grid used for the analysis of a suction pile with a circular cross-section.

2.1 Material and Loading Parameters

It was assumed that the soil was homogeneous and isotropic and its behaviors could be described completely by two parameters, Young's modulus (E) and Poisson's ratio (ν), i.e., linear elastic material properties. The following soil parameters were selected to represent typical seafloor soil properties.

$E = 5{,}000$ psf

$\nu = 0.499$

AISI 4340 steel was chosen for the pile material. The detailed parameters are summarized below. G represents the shear modulus and σ_y indicates the stress limit or the yield stress.

$E = 29{,}000{,}000$ psi

$G = 11{,}000{,}000$ psi

$\nu = 0.32$

σ_y = 215,000 psi for tension

240,000 psi for compression

156,000 psi for shear

The loads were applied at the center of the pile cap along with the horizontal or vertical direction. The horizontal loads were applied to study the suction pile behavior associated with the lateral resistance, and the vertical loads for the pull-out behavior. The applied load remained as 300,000 lbs for either horizontal or vertical direction.

2.2 Description of Pile Cross-Sections

The detailed dimensions of each pile cross-section were determined based on the constant pile-soil contact area. In addition, the length of the pile was fixed as 30 feet. A circular pile of 30 feet in diameter and 30 feet in length was selected as the standard pile. The contact area of this circular pile with the soil is (900 x π) ft^2. A total of 23 cross-sectional shapes were studied as shown in Table-1. As can be seen from the table, the cross-sections with Y-shape, cross-shape, clover shape, and clustered circles were further divided into subshapes with various cell or branch dimensions. The detailed dimensions of the pile cells are defined in Figure-3 and listed in Table-1. It should be noted that the ratio inside the parenthesis in Table-1 indicates the ratio between the larger and shorter lengths of rectangular branches of Y-shaped or cross-shaped pile cross-sections.

As shown in Table-1, pile cross-sections with more cells or branches tend to have smaller value of w due to the imposed condition of constant contact area between the soil and pile. It is noted that, as the ratio of the longer and shorter lengths of rectangular branches of cross- and Y-shaped cross-sections changes, the face width of the pile does not change much. Consequently, piles with slender rectangular branches did not necessarily yield better results. It was observed that the face width of the pile more or less governed the pile resistance.

2.3 Results

2.3.1 Behaviors under horizontal loads

To investigate the behaviors of piles with various cross-sections under horizontal load, the maximum lateral displacements from the output of the finite element analysis were compared, since piles experiencing smaller lateral displacements under the same conditions were believed to be more efficient. In addition, the maximum horizontal normal compressive and minor principal stresses of the soil and the maximum horizontal normal tensile and major principal stresses within the pile top were also compared to study the performance of piles with various cross-sections.

In order to minimize the element size effect when generating the finite element mesh, this study attempted to keep the same sizes of the soil elements near the pile or the pile elements near the point of loading for all cross-sections considered. However, it was not entirely possible to maintain the element sizes exactly the same. As a result, the

comparisons described below may include certain inherent errors. This is more evident for the stress comparisons, since the stresses are calculated at the geometric centers of the elements. The resulting errors are not however considered significant. The results are summarized in Table-2.

1) Pile horizontal displacements

The maximum horizontal displacement due to the horizontal point load applied at the center of the pile cap always occurred at the top of the pile toward the loading direction, whereas the minimum displacement occurred at the bottom of the pile as shown in Figure-4. The difference in pile movements along the vertical direction indicates that the pile was experiencing a rotational movement. Because of the relatively high stiffness of the pile material, no difference in horizontal displacements on any given horizontal pile cross-section was observed (Figure-5).

As shown in Table-2, the circular cross-section yielded the smallest maximum horizontal displacement of 0.463 feet. The horizontal displacement of 0.478 feet for Y-shape cross section with aspect ratio of 1:1 was the next smallest. Hexagon and triangle cross-sections produced the same displacements of 0.539 feet. The remaining cross-sections underwent much higher horizontal displacements. The five best cross-sections in terms of the smallest horizontal displacement are listed in Table-3 in order of increasing magnitude.

The maximum horizontal displacement is more or less related to the face width (W) of the pile. As shown in Figure-6, the maximum horizontal displacement generally decreases with the increases in the face width of the pile.

2) Horizontal normal soil stresses

Since the compressive stress developed within the soil is directly related to the soil failure and thus to the lateral resistance of the pile, the horizontal normal soil compressive stresses resulting from the horizontal point load applied at the center of the pile cap were selected for comparison. As indicated previously, the comparison of stresses may include certain errors due to the fact that in the finite element method of analysis stresses are evaluated at the centers of elements.

The maximum horizontal normal soil compressive stress was always generated at the tip of the advancing side of the pile. On the other hand, the receding side of the pile experienced tensile stresses due to the nature of the elastic analysis.

As shown in Table-2, the smallest horizontal normal soil compressive stress was generated with the hexagonal cross-section. The five best cross sections in terms of the maximum horizontal normal soil compressive stress due to a horizontal load are listed in Table-4. It is noted that the maximum stress values were selected considering the direction of the horizontal load, i.e., the worse condition. For instance, the cross (1:2) cross-section experienced the maximum horizontal normal soil compressive stress of -1,038.5 psf when the load was applied between the branches (indicated as cross2 (1:2) in Table-2), whereas the stress of -1,201.4 psf resulted when the load was applied along the centerline of the branch (indicated as cross1 (1:2) in Table-2). -1,201.4 was therefore selected as the maximum horizontal normal soil compressive stress associated with the cross (1:2) cross-section.

Figure-7 shows the scatter plot between the maximum horizontal normal soil compressive stress and the maximum horizontal soil displacement. As can be seen, the stresses are linearly proportional to the displacements.

3) Minimum soil minor principal stresses

The minimum minor principal stress of the soil was selected for additional comparison, since this describes the absolute maximum soil compressive stress. The complete results are included in Table-2. They are similar to those of the maximum horizontal normal soil compressive stresses. The five best cross-sections with respect to the minimum soil minor principal stress are listed in Table-5.

The relationship between the maximum displacement and the minimum soil minor principal stress also shows a similar pattern with the maximum soil horizontal normal stress, i.e., the stress increases as the displacement increases (Figure-8).

4) Maximum horizontal normal pile tensile stresses

In general, the steel material fails due to the developed tensile stress under most circumstances. Therefore, the maximum horizontal normal pile tensile stress was considered for comparison. Please note that the cylindrical outer surface of the pile was modeled by either shell elements in the case of curved surfaces or plate elements in the case of plane surfaces. The stresses used for the comparison were along the outer surfaces of the plate/shell elements. However, the maximum horizontal normal pile tensile stresses on the outside surface of the pile were found to be greater than those on the inside

surface of the pile in almost all cases. Therefore, only the maximum horizontal normal pile tensile stresses developed on the outside surface of the pile were compared.

The maximum horizontal normal pile tensile stresses on the outside surface of the pile always developed near the point of the load application at the pile cap. The five best cross-sections in terms of the smallest maximum horizontal normal pile tensile stress are listed in Table-6.

The relationship between the maximum horizontal normal pile tensile stress on the outside surface of the pile and the maximum horizontal pile displacement is shown in Figure-9. Though some scatter in data points is evident, generally the maximum horizontal pile tensile stress is proportional to the maximum pile horizontal displacement.

5) Maximum pile major principal stresses

The maximum pile major principal stresses developed on the outside surface of the pile were also compared, since this describes the absolute maximum tensile stress within the pile. Table-2 indicates the magnitude of such stress for all cross-sections considered.

The five best cross-sections with respect to the smallest maximum pile major principal stress are shown in Table-7. The maximum pile major principal stress generally increased with the increase in the maximum pile horizontal displacement, as shown in Figure-10.

6) Relationship between soil stresses and pile stresses

The maximum horizontal normal soil compressive stresses generally increased with the increase in the maximum horizontal normal pile tensile stress as shown in Figures-11. Note that the data points near the coordinate origin are those with no branches or cells, while the data points further away from the origin are those with branches or cells.

The relationship between the maximum pile major principal stress and the minimum soil minor principal stress also shows a similar pattern with that between the maximum horizontal normal pile tensile stress and the maximum horizontal normal soil compressive stress as shown in Figure-12.

2.3.2 Behaviors under vertical loads

To investigate the behaviors of suction piles with various cross-sectional shapes under a vertical load applied at the center of the pile cap, sixteen different modes were examined. As was the case with the horizontal load, the displacements were the primary factors considered for the comparison. Other parameters considered for additional comparisons include the maximum pile major principal stress and the minimum soil minor principal stress.

The elements and nodal configurations used for the study of the pile behavior under the horizontal load were used without change for studying the effects of the vertical load except the direction of the load. The results of the analysis are summarized in Table-8.

1) Maximum pile vertical displacements

As expected, the maximum pile vertical displacement due to the applied vertical point load at the center of the pile cap was always observed at the point of loading. Figure-13 shows the distribution of the pile vertical displacements due to 300,000 lbs of tension applied at the center of the pile top. As shown in Table-8, smaller pile vertical displacements were evident for cross-sections with branches and cells such as clustered circular sections, Y-shaped sections, and cross-shaped sections. This is mainly because the face width of the pile is relatively small for these cross -sections.

2) Minimum soil minor principal stresses

The minimum soil minor principal stress, i.e., the absolute maximum soil compressive stress, was generated around the point of loading. The five best cross-sections in terms of the smallest minimum soil minor principal stress are listed in Table-9.

3) Maximum pile major principal stresses

The maximum pile major principal stress, i.e., the absolute maximum pile tensile stress, on the outside surface of the pile always occurred near the point of loading. The five best cross-sections in terms of the smallest maximum pile major principal stresses are listed in Table-10.

2.3.3 Results from various cross-sections

The appendix of this report (figure numbers starting with "A") includes some of the results from the analysis with circular, Y-shape, clover shape with three leaves, and clustered circle with four cells under a horizontal load of 300,000 lbs. The results include; (1) horizontal displacements, (2) horizontal displacements on a vertical plane along the horizontal load direction, (3) horizontal normal stresses of the pile on the pile surface, (4) horizontal normal stresses of the soil on the pile surface, (5) major principal stresses of the pile on the pile surface, and (6) minor principal stresses of the soil on the pile surface.

2.4 Summary

Based on the results of comparisons, the cross-sectional shape of the pile has a significant effect on the performance of the pile. There also exists a general trend in terms of the overall behavior of the pile with a given cross-sectional shape. In general, the horizontal pile displacement due to the horizontal point load at the center of the pile cap decreases with the increase in the face width of the pile. All stresses of the soil or pile increase with the increase in the horizontal displacement. The critical response of the pile under the vertical point load at the center of the pile cap is concentrated near the point of loading and, therefore, the soil vertical displacement does not dictate the overall maximum vertical displacement.

1) Behaviors of soil under horizontal loads

Circle, Y-shape (1:1), square, Y-shape (1:2), triangle, and hexagon cross-sections have been identified to be the most effective shapes of the pile in terms of the maximum horizontal pile displacement. Hexagon, Y-shape (1:1), cross (1:2), circle, and triangular sections have been shown as the most effective cross-sectional shapes in terms of the soil stresses.

2) Behaviors of pile under horizontal loads

Circle, Y-shape (1:1), square, triangle, and hexagon cross-sections have been shown as the most effective in terms of the pile stresses.

3) Behaviors of soil under vertical loads

Circle, C-circle3, Y-shape (1:1), triangle, and cross (1:1) cross-sections are the five best shapes in terms of the soil stresses.

4) Behaviors of pile under vertical loads

Circle , cross (1:1), Y-shape (1:1), cross (1:3), and cross (1:2) cross-sections are the five best shapes in terms of the pile stresses.

Based on the findings described above, it may be concluded that circle, Y-shape (1:1), hexagon, and triangle cross-sections are the most effective in terms of providing resistance against both horizontal and vertical loads.

3. PEFORMANCE STUDY OF SUCTION PILES IN SAND WITH ELASTO-PLASTIC SOIL PROPERTIES

The purpose of this study is to investigate the detailed behaviors of the suction piles embedded in sand and subjected to various loading conditions. The behavior of the sand was characterized with elasto-perfectly plastic material properties.

As described in Chapter 2, linear elastic analyses were performed, prior to the elasto-plastic analyses, to identify the effects of various pile cross-sections. Three different cross-sections selected from the linear elastic analyses were used in this study. The selected cross-sections include: 1) circular, 2) Y-shaped, and 3) triangular cross-sections. The dimensions of the pile and the pile material properties remained the same as the linear elastic analysis. The loads were applied along the horizontal direction, vertical direction, and direction inclined at 45 degrees to the horizontal. All loads were applied at the center of the pile cap.

The initial linear elastic behavior of the sandy soil was described by Young's modulus (E) and Poisson's ratio (υ), whereas the subsequent plastic behavior was modeled by the extended Drucker-Prager plasticity model. In the extended Drucker-Prager plasticity model, yielding of the material is described differently in tension and compression. In general, relatively smaller resistance against tension than compression is allowed, i.e., the kinematic hardening plastic behavior.

To eliminate the relative deformations of the pile itself near the point of loading, the stiffness of the pile was assumed to be very large, i.e., the pile was almost rigid. The finite element details used for the previous linear elastic analysis were directly utilized without change except the loads and boundaries. The outer boundary of the solution

domain was changed to rollers in order to avoid the stress concentrations as experienced in the linear elastic analysis that utilized fixed boundaries.

3.1 Material and Loading Parameters

The following sandy seafloor soil properties were used for the analysis. The plasticity parameters were quoted from Shugar (8).

Fundamental Soil Parameters

Buoyant Unit Weight (γ_b) = 47.6 pcf

Friction Angle (ϕ) = 26.0 deg (corresponding to slope angle of 46.2 deg, in linear extended Drucker-Prager model)

Lateral Earth Pressure Coefficient (K_o) = 1-sinϕ = 0.56

Linear Elastic Soil Parameters

Young's Modulus (E) = 864,000.0 psf

Poisson's Ratio (υ) = 0.3

Extended Drucker-Prager Plasticity Soil Parameters

Friction Angle = 46.2°

Angle of Dilation = 21.5°

Yield Stress in Compression = 2,016.0 psf

Initial Void Ratio = 0.563

The pile material properties remained the same as the linear elastic analysis. The loads were applied at the center of the pile cap along the horizontal, vertical, or 45-degree inclined direction. The inclined load was applied by a combination of the horizontal and vertical loads. For example, an inclined load of 100 lbs at 45 degrees was equivalent to 71.71 lbs of horizontal and vertical loads. The loads were increased until the solutions did not converge.

3.2 Example Input Data

The following input data file was prepared for ABAQUS version 5.7 to simulate the elasto-perfectly plastic sandy soil behaviors due to the load applied at the center of the pile cap. Data for nodes and elements generation, boundary conditions creation, output control, etc. are not included below. Any command preceded by ** is ignored by ABAQUS, i.e., it is "commented out." Initial field geostatic stress condition was also established by the command of "*STEP."

```
** GROUP nodes and elements----------------------------------------------------------
*NSET,NSET=ALL,GENERATE
1,2140,1                    (all nodes are named by ALL)
*ELSET,ELSET=SOIL,GENERATE
1,3228,1                    (all soil elements are named by SOIL)
** FEAMAP Material 1 : AISI 4340 Steel-----------------------------------------------
```

*MATERIAL, NAME=M1 (begin the definition of a material named M2)

*ELASTIC,TYPE=ISO (specify elastic properties)

4.176E+9,0.32 (Young's Modulus=4.176E+9 psf, Poisson's ratio=0.32)

** FEAMAP Material 2 : Soil Properties----------

*MATERIAL, NAME=M2 (begin the definition of a material named M2)

*ELASTIC (specify elastic properties)

864000.0,0.3 (modulus of elasticity = 864,000 psf, Poisson's ratio =0.3)

*DRUCKER PRAGER (specify extended Drucker Prager plasticity model with non-associate flow)

46.2,1.0,21.5 (friction angle = 46.2 deg., angle of dilation = 21.5 deg.)

*DRUCKER PRAGER HARDENING,TYPE=COMPRESSION (specify hardening or yield behavior in compression for Drucker Prager material)

2016.0,0.0 (elastic perfectly plastic behavior specified, residual stress = 2,016 psf for all strain)

*INITIAL CONDITIONS, TYPE=RATIO (specify initial void ratio)

ALL,0.563 (all node points are assigned an initial value of 0.563)

*INITIAL CONDITIONS, TYPE=STRESS,GEOSTATIC (specify initial geostatic stress condition)

SOIL, 0.,0.,-47.6,-1.,0.56,0.56 (all soil elements are assigned an initial effective stress by linear interpolation with two points, (depth, stress)=(0.ft,0.psf) and (-1ft, -47.6psf) and lateral stress coefficient at rest (k_o) = 0.56)

** GEOSTATIC STEP----------

*STEP (start to set up equilibrium for geostatic condition)

*GEOSTATIC

*BOUNDARY

```
14,1                    (node=14, x-direction is constrained)
                        (all boundaries are specified continuously)

*DLOAD

SOIL, BZ,-47.6          (body force =-47.6pcf in z-direction for all soil elements)

*END STEP

**LOAD STEP-----------------------------------------------------------------

*STEP,INC=1000          (start to analyze for a concentration load)

*STATIC

*CLOAD,OP=NEW

2100,1,100000.          (horizontal load=100,000lbs applied at node=2100)

*END STEP
```

3.3 Description of Pile Cross-Sections

The detailed dimensions of each pile cross-section were determined based on the constant pile-soil contact area. A circular pile of 30 feet in diameter and 30 feet in length was selected as the standard pile. The cross-sectional profiles selected for the study are shown in Figure-14. It is noted that two different directional loads were analyzed for triangular and Y-shaped cross-sections because the different loading directions resulted in different behaviors of the suction pile.

3.4 Results

In the extended Drucker-Prager plasticity model, the hardening behavior of the soil follows a kinematic hardening rule, i.e., a much smaller tensile resistance than the compressive resistance of the soil is used than would be expected in typical soils. Figure-15 shows the horizontal soil normal stress distributions at two nodes for the circular cross-section under various magnitudes of horizontal load. Node 667 was located at the advancing side of the pile (resulting in soil compression), whereas node 621 was located at the receding side of the pile (resulting in tension). When the soil elements started to yield in tension, the maximum horizontal soil tensile stress developed at node 621 increased at much slower rate than the increase in horizontal load. It converged to the ultimate stress of about 1,260.0 psf, which corresponded to the horizontal load of about 3,500,000 lbs as shown in Figure-15. However, the horizontal soil normal compressive stress developed at node 667 increased continuously with the increase in horizontal load due to the soil hardening process. Th solution did not converge with the horizontal loads over 7,000,000 lbs.

Since the pile cross-section experiencing smaller displacements under the same loading condition is believed to be more efficient, the maximum total and horizontal/ vertical pile displacements were primarily observed. These displacements are defined in section 3.4.1. In addition, the minimum minor principal stresses of the soil were compared, since this describes the largest compressional stress. Also, von Mises stresses within the pile were considered to study the responses of the pile due to the applied load. In von Mises theory, failure by yielding occurs when, at any point within the body, the distortion energy per unit volume in a state of combined stress becomes equal to that

associated with yielding in a simple tension. Yielding does not depend on the hydrostatic tensile or compressive stresses. The von Mises stress is expressed as

$$\text{von Mises stress} = ((\sigma_1-\sigma_2)^2+(\sigma_2-\sigma_3)^2+(\sigma_3-\sigma_1)^2)^{1/2}$$

where σ_1, σ_2, and σ_3 indicate the principal stresses in three dimensions.

It is noted that in the analysis the maximum stress values were selected considering the direction of the horizontal load, i.e., the worse condition in case of the triangular and Y-shaped cross-sections. For instance, the triangular cross-section experienced the minimum soil minor principal stress of -6,003.4 psf for the horizontal load of 4,000,000 lbs when the load was applied toward a corner of the triangle, whereas that of -5323.6 psf at the same level of load resulted when the load was applied away from a corner of the triangle. Therefore, -6,003.4 psf was selected as the minimum soil minor principal stress associated with the triangular cross-section.

3.4.1 Behaviors under horizontal loads

1) Pile displacements

The maximum total pile displacement and maximum horizontal pile displacement under different horizontal loads at any point within the pile were compared first. The maximum total pile displacement represents the absolute, largest pile displacement generated at any node along any direction. Therefore, this displacement is the resultant of the horizontal and vertical displacements. The maximum horizontal pile displacement

represents the maximum pile displacement at any point along the loading direction. The maximum pile total and horizontal displacements due to the various horizontal loads applied at the center of the pile cap always occurred at the top of the pile along the loading direction, whereas the minimum pile displacement occurred at the bottom of the pile. Figure-16 shows one such example output. It is also noted from the figure that the pile was experiencing horizontal translational movement as well as rotational movement, as evidenced from the difference in pile movements along the vertical direction.

As shown in Figures-17 and 18, both maximum total and maximum horizontal pile displacements show a similar pattern against the applied horizontal load. The displacements varied linearly due to the elastic behavior under relatively small horizontal loads. As the horizontal load increased, the displacements showed a nonlinear behavior due to the inclusion of the plastic soil behavior. The variations of the curves are more or less hyperbolic shaped; hence, it is expected that the horizontal load will eventually approach the ultimate value. However, the ultimate horizontal load could not be obtained due to the non-convergence problem. As can be seen from the figures, the circular cross-section generated the smallest displacements at all loads in both comparisons. The largest displacements were always generated with the triangular cross-section at any given load. It is noted that the differences in displacements among different cross-sections increased with the increase in horizontal load, i.e., the effect of the cross-sectional shape is pronounced at relatively larger horizontal loads. The results of the finite element analyses are summarized in Table-11.

2) Minimum soil minor principal stresses

The minimum soil minor principal stress describes the absolute maximum soil compressive stress. Yielding of the soil starts within the highly stressed element when the largest principal stress within that element reaches the yield stress.

The maximum soil minor principal stress at any given horizontal load was always generated at the top of the advancing side of the pile after the geostatic stress was overcome. On the other hand, as the horizontal load increased, the receding side of the pile experienced relatively small tensile stresses due to the nature of kinematic hardening in the plastic analysis as shown in Figure-19.

The calculated minimum soil minor principal stresses associated with the circular cross-section are shown in Table-12. When the horizontal load was less than 2 million lbs, the triangular cross-section experienced the smallest minimum soil minor principal stress, while the circular cross-section became the most effective for load magnitudes above 3 million lbs. The difference in stress magnitudes among three cross-sections at horizontal loads below 2 million lbs are, however, very small, indicating that the circular cross-section is in general the most effective in terms of the soil stress under horizontal loads.

Figure-20 shows the relationship between the minimum soil minor principal stress and the applied horizontal load. Almost identical stresses were observed under relatively small horizontal loads. This is because the stresses generated by the applied load were not large enough. However, once the geostatic stresses were overcome, the minimum soil minor principal stresses increased nonlinearly with the increase in the horizontal load. The rate of the stress increase increased with the increase in load. The effect of the cross-section became more significant at higher horizontal loads.

3) Maximum pile von Mises stresses

The maximum pile von Mises stresses developed within the pile were studied in this section. As described previously, the von Mises stress can be used to effectively describe the failure of ductile materials, such as structural steel. The maximum pile von Mises stress was always generated near the loading point at the center of pile cap as can be seen in Figure-21. The maximum pile von Mises stress was selected considering the stresses developed on both the outer and the inner surface of the pile. Table-13 indicates the magnitude of such stress for all cross-sections considered in the study.

The relationship between the maximum pile von Mises stress and the applied horizontal load is shown in Figure-22. The maximum pile von Mises stress was almost proportional to the applied load. The smallest maximum pile von Mises stress was generated within the Y-shaped cross-section at all horizontal loads, whereas the largest stress was resulted with the triangular cross section. This is because the Y-shaped cross-section has the largest moment of inertia and the smallest cross-sectional area with the same contact area between the soil and the pile. The differences in the stresses between different cross-sections increased with the increase in horizontal load.

4) Relationship between displacements and stresses

As shown in Figure-23, the minimum soil minor principal stress increased almost linearly with the increase in the maximum total displacement after the geostatic stresses were overcome. At a given maximum total displacement, the circular cross-section

generated the smallest minimum soil minor principal stress. The largest minimum soil minor stress was associated with the triangular cross-section.

The relationship between the maximum pile von Mises stress and the maximum horizontal displacement shows a hyperbolic-shaped variation as shown in Figure-24. The smallest maximum pile von Mises stress was obtained with the Y-shaped cross-section for a given maximum total displacement. As mentioned previously, this is primarily because the moment of inertia is largest and the area of the pile top of the Y-shaped cross-section is smallest among the cross-sections studied with the same contact area between the soil and the pile. Therefore, the Y-shaped cross section is the most effective in terms of the developed pile stress.

3.4.2 Behaviors under vertical loads

1) Maximum pile vertical displacements

As mentioned previously, the maximum pile vertical displacement obtained from the finite element analysis was approximately the same as the maximum soil vertical displacement because the stiffness of the pile was assumed to be very large. With relatively large stiffness, the suction pile moved along the direction parallel to the loading direction with almost no relative deformation of the pile (Figure-25). The vertical displacements of the three selected cross-sections at various vertical loads are summarized in Table-14.

Figure-26 shows the distribution of the pile vertical displacements for the selected cross-sections at different vertical loads applied at the center of the pile top. The

relationship between the maximum vertical displacement and the vertical load shows the typical elasto-plastic behavior, i.e., a linear behavior at relatively low loads, followed by a nonlinear behavior due to the effect of the soil plasticity at relatively high loads. The smallest maximum vertical displacement at a given load was obtained with the circular cross-section, similar to the study results of suction piles under horizontal loads. The differences in displacements due to different cross-sections at the same vertical load increased with the increase in load. The maximum vertical displacements associated with the triangular and Y-shaped cross-sections were almost the same at relatively low loads. The elastic limit was observed to be approximately at a displacement of 0.06 ft for all cross-sections.

2) Minimum soil minor principal stresses

The minimum soil minor principal stresses, i.e., the absolute maximum soil compressive stresses, due to various vertical loads were generated around the pile as expected (Figure-27). The complete results of the analysis are summarized in Table-15.

The relationship between the minimum soil minor principal stress and the vertical load is shown in Figure-28. Before the developed stresses within the soil overcame the geostatic stresses, almost identical soil stresses were observed for all cross-sections studied. However, once the soil started to yield, the minimum soil minor principal stress increased rapidly. Circular and triangular cross-sections were equally effective in terms of the minimum soil minor principal stress against the vertical loads.

3) Maximum pile von Mises stresses

As expected, the maximum pile von Mises stress, i.e., the maximum mean pile stress, always occurred at the point of loading (Figure-29). The results of the finite element analyses are summarized in Table-16. Figure-30 shows the relationship between the maximum pile von Mises stress and the applied vertical load.

As shown in Figure-31, the maximum pile von Mises stress was almost directly proportional to the applied vertical load. This is because the pile was modeled by a linear elastic constitutive relationship. The maximum pile von Mises stress at a given load was the smallest for the Y-shaped cross-section, similar to the results of the study of the pile responses due to horizontal loads. Hence, the Y-shaped cross-section is considered to be the most effective in terms of the developed pile stress under the vertical load.

3.4.3 Behaviors under inclined loads

The load inclination angle of 45 degree to the horizontal was chosen to study the behaviors of suction piles under inclined loads.

1) Maximum pile displacements

The largest maximum horizontal displacement of the pile was always observed at the top of the pile, whereas the smallest maximum horizontal displacement of the pile occurred at the bottom of the pile. The pile experienced translational as well as rotational movements as expected. The displacements associated with the three selected cross-sections for various 45-degree inclined loads are summarized in Table-17.

Figures-31 and 32 show the distribution of the pile displacements for the selected cross-sections at different inclined loads applied at the center of the pile top. As the load increased, the displacement gradually approached to the limiting value. Due to the effect of the soil plasticity, the increase was linear at lower loads, followed by a nonlinear behavior at higher loads, both for the maximum total displacement and the maximum horizontal displacement. The smallest vertical displacement at a given load was obtained with the circular cross-section, as was the case with horizontal loads. The differences in displacements with different cross-sections at the same load increased with the increase in load.

2) Minimum soil minor principal stresses

The minimum soil minor principal stresses due to the 45-degree inclined loads were calculated around the pile and the results are summarized in Table-18.

The relationship between the minimum soil minor principal stress and the 45-degree inclined load is shown in Figure-33. With the increase in load, an elastic behavior followed by plastic behavior was observed. The smallest minimum soil minor principal stress at a given load was observed with the circular cross-section. The circular cross-section is therefore considered the most effective in terms of the soil stress under 45-degree inclined loads.

3) Maximum pile von Mises stresses

As expected, the maximum pile von Mises stress always occurred at the point of loading. The results of the finite element analyses are summarized in Table-19.

As shown in Figure-34, the maximum pile von Mises stress was directly proportional to the applied inclined load. The stress at a given inclined load was smallest with the Y-shaped cross-section, as observed in the study of the pile responses due to horizontal loads.

3.4.4 Additional results

The appendix of this report (figure numbers starting with "B") includes some of the typical results from the finite element analyses of suction piles in sand with circular, triangular, and Y-shape cross-sections under horizontal, vertical, and inclined loads. The results include: (1) soil displacements, (2) soil displacements on a vertical plane, (3) pile total displacements, (4) soil minor principal stresses, (5) soil minor principal stresses on a vertical plane, (6) pile normal stresses on the pile surface, (7) pile von Mises stresses on the pile surface.

3.5 Summary

3.5.1 General conclusions

From the results of the finite element analyses, it is evident that the effect of the soil plasticity is highly significant for large load magnitudes. There also exist general trends in terms of the overall responses of the pile under different applied loads. In general, the horizontal pile displacement due to the horizontal or 45-degree inclined loads

applied at the center of the pile cap varies almost linearly under very low loads but becomes nonlinear under high loads for all selected cross-sections. The variation is more or less hyperbolic-shaped and approaches to an ultimate value. On the other hand, the vertical pile displacement due to the vertical load applied at the center of the pile cap exhibits a sudden yielding behavior at displacement of approximately 0.06 ft for all cross-sections. The smallest displacement always occurs with the circular cross-section. The minimum soil minor principal stresses due to the horizontal or 45-degree inclined load applied at the center of the pile cap is dominated by the geostatic stress condition under low loads. However, as the geostatic stresses are gradually overcome, the minimum soil minor principal stresses develop at the top of the advancing side of the pile. The minimum soil minor principal stresses due to the vertical loads applied at the center of the pile cap are observed within the lower half of the pile. The smallest minimum soil minor principal stress is seen with the circular cross-section. The maximum pile von Mises stresses vary almost linearly with the increase in loads mainly because the pile is modeled by a linear elastic material. This modeling of the pile material behavior does not seem unrealistic, since the calculated pile stresses are much lower than its yield stress even at loads near failure. The smallest maximum pile von Mises stress is observed with the Y-shaped cross-section.

3.5.2 Pile failure loads

3.5.2.1 Pile failure based on horizontal displacement

Bang and Kim (4) attempted to describe the limiting deformation corresponding to the initial passive state of a pile experiencing rotational movements. Based on their study, the magnitude of the horizontal pile deformation that creates the initial passive state in loose sands was found to be 0.1642 ft. The horizontal and 45-degree inclined loads corresponding to the lateral deformation of 0.1642 ft are summarized in Table-20, where the loads have been determined by a linear interpolation method.

As can be seen from Table-20, the circular cross-section allows the largest horizontal load of 4,859,223 lbs before the initial passive state develops. The circular cross-section has already been identified to be the most effective shape of the suction pile in terms of the maximum horizontal pile displacement under horizontal and 45-degree inclined loads. It is noted that the loads described above do not necessarily represent the ultimate resistance of the pile. They indicate the loads at which the initial passive state develops, i.e., at one point within the entire soil mass the stress reaches its maximum passive earth pressure. The ultimate resistance of the pile occurs when enough soil elements reach the passive state so that the failure of the pile is imminent. Table-20 shows that the circular cross-section can resist approximately 7.5% and 5.2% more horizontal load than the triangular and Y-shaped cross-sections, respectively, at the initial passive state.

3.5.2.2 Pile failure load based on vertical displacement

As described previously, the displacement pattern of the suction pile under vertical loads applied at the center of the pile cap shows an apparent yield pattern.

Therefore, the loads corresponding to this apparent yield displacement have been compared for various cross-sections to identify their relative significance. The yield displacement was found to be approximately 0.06 ft for all selected cross-sections, which agrees very well with the model test results by Iskander et. al (6). The vertical loads corresponding to the yield displacement of 0.06 ft are summarized in Table-21. Again, the loads have been determined by a linear interpolation method.

Table-21 indicates that the pile failure load against the vertical load is 5,155,405 lbs for the circular cross-section, indicating that it is 7.1% and 5.1% higher than those of the triangular and Y-shaped cross-sections, respectively.

3.5.3 Soil minor principal stresses

To quantitatively compare the minimum soil minor principal stress for the selected cross-sections, the stress values corresponding to the failure loads described in previous section have been calculated and are summarized in Table-22.

The smallest absolute value of the minimum soil minor principal stress is observed with the circular cross-section under both the horizontal and 45-degree inclined loads. Under vertical loads, all three cross-sections produce virtually the same magnitude of stresses, indicating that the circular cross-section yields the smallest minimum soil minor principal stress under all loading conditions. The maximum difference in the developed soil stresses is 18.5% between the circular and triangular cross-sections under the horizontal load. Virtually identical minimum soil minor principal stresses under the vertical load are due to the fact that the soil starts to yield completely under the vertical

load before the geostatic stresses are overcome and thus geostatic stresses dominate the global behavior.

3.5.4 Pile von Mises stresses

Table-23 summarizes the maximum pile von Mises stresses with the selected cross-sections corresponding to the failure loads described previously.

As can be seen from the table, the Y-shaped cross-section generated the smallest maximum pile von Mises stress under a given loading situation. This becomes more apparent under the vertical loads where the difference in stresses between the circular and Y-shaped cross-sections exceeds 230%. However, the magnitude of stresses developed within the pile are very small when compared to the yield stress of the pile material. This indicates that the predominant factor governing the suction pile capacity is the failure of the soil, leading to the conclusion that the circular cross-section is the most effective shape of the suction pile.

It is noted that the vertical pile resistance embedded in sand is much smaller than the lateral resistance. Typically the pile resistance decreases in the order of horizontal, inclined, and vertical loads. This observation, however, has been obtained from the static finite element analyses of suction piles. It is well understood that due to the development of the negative pore water pressure the vertical pile resistance increases significantly under undrained conditions when the vertical load is applied very rapidly. This phenomenon has not been studied in detail to date, but is thought to be a function of the soil permeability and the rate of load application. Therefore, a systematic study,

including extensive laboratory tests, needs to be conducted to characterize the development of the negative pore water pressure underneath the suction pile before the increase in vertical capacity of suction piles can be safely included in the design.

3.5.5 Analysis with unsymmetrical global stiffness matrix

To ensure the accuracy of the plasticity analysis solutions described above, an additional attempt was made to extend the results beyond the normal range. This was done by allowing the global stiffness matrix to be unsymmetric during computation. Such results are shown in Figures-35 to 37, showing the behaviors of suction piles with three different cross-sections under various horizontal loads. Previous analysis was terminated at the horizontal load of about 7,000,000 lbs due to the non-convergence problem. However, with this provision allowing the matrix being unsymmetric, the solution extended further to the horizontal load of about 9,500,000 lbs. The results are continuing extension of the previous solutions with no major deviation.

4. PERFORMANCE STUDY OF SUCTION PILES IN CLAY WITH ELASTO-PLASTIC SOIL PROPERTIES

The purpose of this study is to investigate the detailed behaviors of the suction piles embedded in clay and subjected to various loading conditions. The behavior of the clay was characterized with elasto-perfectly plastic material properties.

Three different cross-sections selected from the linear elastic study were also used in this study. The selected cross-sections include 1) circular, 2) Y-shaped, and 3) triangular cross-sections. The loads were applied along the horizontal direction, vertical direction, and direction inclined at 45 degrees to the horizontal. All loads were applied at the center of the pile cap. All other conditions remained the same as for the study of suction piles in sand.

The initial linear elastic behavior of the clay soil was described by Young's modulus (E) and Poisson's ratio (υ), whereas the subsequent plastic behavior was modeled by the extended Drucker-Prager plasticity model based on the hyperbolic failure criterion. In addition, maximum tensile strength is prescribed by a tension cut-off in the hyperbolic extended Drucker-Prager plasticity model.

The main objective of this study is to identify the most efficient suction pile cross-section through quantitative comparisons of the responses of the selected suction pile cross-sections with elasto-perfectly plastic clay properties under three different loading conditions. The load was increased incrementally and the behaviors of suction piles were observed in detail at various load levels for the different loading directions. As was the case in the previous finite element analyses, the stiffness of the pile was assumed to be very large to eliminate the relative deformation of the pile itself near the point of loading.

Exactly the same details of the finite element models as used for the previous study with sand were directly utilized without any change except the material properties.

4.1 Extended Hyperbolic Drucker-Prager Plasticity

Several plasticity constitutive models are available in ABAQUS version 5.7 to model the behavior of frictional materials, e.g., granular soils and rock which exhibit the stress-dependent yield behavior (the material becomes stronger as the stress increases). The plasticity constitutive models for granular materials available in ABAQUS version 5.7 are: 1) extended Drucker-Prager (linear, hyperbolic, and exponential failure criteria) model, 2) Mohr-Coulomb model, and 3) Modified Drucker-Prager (Cap) model. These models can be used to model the behavior of granular materials in which the tensile and compressive yield strengths are significantly different. The models other than the Cap model are intended to simulate the material responses under essentially monotonic loading.

For the description of soil behaviors with relatively high friction angles under monotonic loading condition, the linear extended Drucker-Prager model would be appropriate, since significant tension would not develop due to the relatively steep slope angle (β). The linear extended Drucker-Prager model, however, is not suitable to model the behaviors of clayey soils having relatively low friction angles.

The hyperbolic yield criterion is assumed in both the hyperbolic extended Drucker-Prager and the Mohr-Coulomb models. The hyperbolic Drucker-Prager model is a continuous combination of the maximum Rankine tensile stress condition (tension cut-

off) and the linear Drucker-Prager condition at high confining stresses. The tension cut-off defined in the hyperbolic extended Drucker-Prager model is intended to reduce any potential error associated with the tension in the analysis with linear constitutive models. The hyperbolic model utilizes a linear assumption at high confining pressures but it provides a nonlinear relationship between the deviatoric and mean confining stress at low confining pressures. As shown in Figure-38, the hyperbolic flow potential function approaches the linear Drucker-Prager flow potential asymptotically at high confining pressures and intersects the hydrostatic pressure axis (p) at 90 degrees.

Since this study would include a clay soil with relatively lower friction angle, either the hyperbolic extended Drucker-Prager plasticity model or the Mohr-Coulomb model could be used to simulate its behaviors. However, the hyperbolic extended Drucker-Prager model was chosen in order to be consistent with the study with sand.

Typical soil parameters, such as the soil friction angle and cohesion, can be converted to equivalent Drucker-Prager parameters. The following shows how the linear extended Drucker-Prager model (or hyperbolic extended Drucker-Prager model at high confining pressures) parameters for soils with low friction angles are obtained to duplicate the same failure definition as in triaxial compression and tension.

Slope Angle (β) = $\tan^{-1}[6\sin\phi/(3-\sin\phi)]$

Initial compressive yield stress ($\sigma_{c|o}$) = $2C \times \cos\phi/(1-\sin\phi)$

4.2 Material and Loading Parameters

It was assumed that the clayey soil was homogeneous and isotropic. Its linear elastic behaviors under relatively smaller loads were described completely by two parameters, Young's modulus (E) and Poisson's ratio (ν). As described in the previous section, the hyperbolic extended Drucker-Prager plasticity model was utilized to simulate its plastic behaviors under relatively larger loads. At higher stress levels, the model is completely defined by two parameters, the slope angle and the dilation angle. When the values of the angle of dilation and slope angle are equal, the state of non-associated flow prevails ,i.e., the global stiffness matrix becomes symmetric. In addition, the yield stresses in tension and compression are defined to simulate the perfectly plastic behaviors of the clay. The following clayey seafloor soil properties were quoted from reference (9) and evaluated with information from references (1,3,7).

Fundamental Soil Parameters

Soil Classification = Organic Silty Clay of High Plasticity

Water Content (w) = 110 -160 %

Liquid Limit (LL) = 117 -142

Liquidity Index (LI) = 0.88 - 1.65

Total Unit Weight (γ_t) = 86.0 pcf

Sea-water Unit Weight (γ_b) = 64.0 pcf

Buoyant Unit Weight (γ_b) = 22.0 pcf

Initial Void Ratio (e_o) = 3.7

Cohesion (C) = 150.0 psf

Friction Angle (ϕ) = 5.0 deg (corresponding to slope angle of 10.2 deg in hyperbolic extended Drucker-Prager model)

Lateral Earth Pressure Coefficient (K_o) = 1-sinϕ = 0.91

Linear Elastic Soil Parameters

Young's Modulus (E) = 30,000 psf (200 times the soil cohesion)

Poisson's Ratio (υ) = 0.499 (undrained condition)

Extended Drucker-Prager Plasticity Soil Parameters

Slope Angle (β) = 10.2°

Angle of Dilation (φ) = 10.2°

Yield Stress in Compression ($\sigma_{c|o}$) = 327.4 psf

Initial Hydraulic Tension Strength (Tension cut-off) = 150.0 psf

The loads were applied at the center of the pile cap along the horizontal, vertical, or 45-degree inclined direction. As described previously in Chapter 3, the inclined load was applied by a combination of the horizontal and vertical loads. The loads were increased until the solutions approached the ultimate values.

4.3 Example Input Data

The following input data file was prepared for ABAQUS version 5.7 to simulate the elasto-perfectly plastic clayey soil behaviors due to the load applied at the center of

the pile cap. Data for nodes and elements generation, boundary conditions creation, output control, etc. are not included below. Any command preceded by ** is ignored by ABAQUS, i.e., it is "commented out." Initial field geostatic stress condition was also established by the command of "*STEP."

```
** GROUP nodes and elements----------------------------------------------------------------
*NSET,NSET=ALL,GENERATE
1,2140,1                    (all nodes are named by ALL)
*ELSET,ELSET=SOIL,GENERATE
1,3228,1                    (all soil elements are named by SOIL)
** FEAMAP Material 1 : AISI 4340 Steel-----------------------------------------------------
*MATERIAL, NAME=M1          (begin the definition of a material named M1)
*ELASTIC,TYPE=ISO           (specify elastic properties)
4.176E+9,0.32               (Young's Modulus=4.176E+9 psf, Poisson's ratio=0.32)
** FEAMAP Material 2 : Soil Properties-----------------------------------------------------
*MATERIAL, NAME=M2          (begin the definition of a material named M2)
*ELASTIC                    (specify elastic properties)
30000.,0.499                (modulus of elasticity = 30,000 psf, Poisson's ratio =0.499)
*DRUCKER PRAGER,SHEAR CRITERION=HYPERBOLIC      (specify extended
                            Drucker-Prager plasticity model with hyperbolic failure
                            criterion)
10.2,150., ,10.2            (slope angle = 10.2 deg., tensile cut-off = 150 psf., angle of
                            dilation = 10.2 deg., associated flow)
```

*DRUCKER PRAGER HARDENING,TYPE=COMPRESSION (specify hardening or yield behavior in compression for Drucker-Prager material)

327.4,0. (elasto-perfectly plastic behavior specified, residual stress = 327.4 psf for all strain)

*INITIAL CONDITIONS, TYPE=RATIO (specify initial void ratio)

ALL,3.7 (all node points are assigned an initial value of 3.7)

*INITIAL CONDITIONS, TYPE=STRESS,GEOSTATIC (specify initial geostatic stress condition)

SOIL, 0.,0.,-22.,-1.,0.91,0.91 (all soil elements are assigned initial effective stresses by linear interpolation between two points, (depth, stress) =(0.ft,0.psf) and (-1ft, -22.0psf), and lateral stress coefficient at rest (k_o) = 0.91)

** GEOSTATIC STEP----------

*STEP (set up equilibrium for geostatic condition)

*GEOSTATIC

*BOUNDARY

14,1 (node=14, x-direction is constrained)

(all boundaries are specified continuously)

*DLOAD

SOIL, BZ,-22.0 (body force =-22.0pcf in z-direction for all soil elements)

*END STEP

**LOAD STEP----------

*STEP,INC=1000 (start analysis with a concentration load)

*STATIC

*CLOAD,OP=NEW

2100,1,100000. (horizontal load=100,000lbs applied at node=2100)

*END STEP

4.4 Description of Pile Cross-Sections

The same suction pile cross-sections used in the analysis with sand were utilized in this study without any change. The detailed dimensions of each pile cross-section were determined based on the constant pile-soil contact area. A circular pile of 30 feet in diameter and 30 feet in length was selected as the standard pile. It is noted that two different directional loads were analyzed for triangular and Y-shaped cross-sections because the different loading directions resulted in different behaviors of the suction pile.

4.5 Results

To simulate the in-situ field conditions, the geostatic state satisfying the prescribed boundary conditions was established first by the *GEOSTATIC step before the external loads were applied. The gravity load, due to the soil buoyant unit weight of 22.0 pcf, was applied as a distributed body force. Loads and prescribed initial stresses were in exact equilibrium and produce zero deformations under the geostatic stress condition. Figures-39 and 40 show the established field states under the geostatic stress condition.

It is noted that in the analysis the maximum stress values were selected considering the direction of the horizontal load, i.e., the worse condition in case of the triangular and Y-shaped cross-sections.

4.5.1 Behaviors under horizontal loads

1) Pile displacements

The maximum total pile displacement and the maximum horizontal pile displacement under different horizontal loads at any point within the pile were compared first. The maximum total and horizontal pile displacements due to the various horizontal loads applied at the center of the pile cap always occurred at the top of the pile along the loading direction, whereas the minimum pile displacement occurred at the bottom of the pile. Figure-41 shows one such example output. It is also noted from the figure that the pile was experiencing horizontal translational movements as well as rotational movements, as evidenced from the difference in pile movements along the vertical direction.

Figure-42 shows a typical load vs. displacement behavior under various horizontal loads. As expected, the load increased very rapidly at small displacements, followed by the plastic behavior. The ultimate load of a circular suction pile embedded in the clay soil whose properties were described previously was found to be approximately 2,000,000 lbs.

Almost identical displacements under various horizontal loads were observed with the circular and Y-shaped cross-sections when the loads were less than 1,600,000 lbs, as shown in Table-24. Generally, the circular cross-section generated the smallest maximum total and horizontal displacements under the loads of up to 1,100,000 lbs. Beyond this load, the Y-shaped cross-section yielded the smallest displacements. The triangular cross-section generated the largest displacements for the entire rage of the

applied horizontal loads. The effect of the cross-sectional shape became very pronounced at relatively larger horizontal loads near the failure.

As shown in Figures-43 and 44, both the maximum total and maximum horizontal pile displacements associated with three cross-sections show a similar pattern against the applied horizontal load. The displacements varied almost linearly due to the elastic behavior under relatively small horizontal loads. As the horizontal load increased, the displacements showed a nonlinear behavior due to the inclusion of the plastic soil behavior. Finally, the horizontal loads gradually approached the ultimate values. The variations of the curves are hyperbolic shaped. The ultimate horizontal loads were observed approximately to be 2,000,000 lbs for the circular and Y-shaped cross-sections, and 1,800,000 lbs for the triangular cross-section. The largest displacements were always generated with the triangular cross-section at any given load.

2) Minimum soil minor principal stresses

The minimum soil minor principal stress at any given horizontal load was always generated near the bottom of the advancing side of the pile. The receding side of the pile experienced relatively small stresses due to the nature of kinematic hardening in the plastic analysis as shown in Figure-45.

The calculated minimum soil minor principal stresses associated with the selected cross-sections are shown in Table-25. The most effective cross-section in terms of the minimum soil minor principal stress depended on the applied load level. Almost identical minimum soil minor principal stresses for all cross-sections were observed under the horizontal load of 100,000 lbs, mainly because the developed stresses were not

large enough to overcome the geostatic stresses. When the horizontal load was less than 700,000 lbs, the Y-shaped cross-section experienced the smallest minimum soil minor principal stress, whereas the circular cross-section became the most effective for load magnitudes from 700,000 lbs to 1,700,000 lbs. Beyond the horizontal load of 1,700,000 lbs, the Y-shaped cross-section again became the most effective. However, the difference in stress magnitudes between the circular and Y-shaped cross-sections were relatively small for loads less than 1,8000,000 lbs, except near the load of 1,500,000 lbs where the difference exceeded 30%. The largest minimum soil minor principal stresses were always generated with the triangular cross-section.

Figure-46 shows the relationship between the minimum soil minor principal stress and the applied horizontal load. Once the geostatic stresses were overcome, the minimum soil minor principal stresses increased following various patterns. The patterns are not consistent as can be seen from the figure. This is mainly because the minimum soil minor principal stress did not occur within the same element as the horizontal load increased, which was most evident for the Y-shaped cross-section. To validate this reasoning, an additional plot was made for stresses at a given element.

Figure-47 shows the relationship between the horizontal load and the soil minor principal stress of the element at the top of the advancing side of the pile. The seemingly inconsistent behavior of the Y-shaped cross-section as observed in Figure-46 is not evident in Figure-47. Initial geostatic stress at the geometric center of the selected element was -825.0 psf. As the horizontal load increased, the soil minor principal stresses increased linearly and then subsequent yielding and hardening processes occurred. As can be seen from the figure, the variations of the minimum soil minor

principal stresses were similar for the circular and Y-shaped cross-sections. The rate of the soil stress increase with the increase in load for the triangular cross-section was much lower than the others. This is probably due to the stress concentration near the corners. The effect of the cross-section on the soil stress development became more significant at higher horizontal loads. The Y-shaped cross-section is the most effective in terms of the minimum soil minor principal stress.

3) Maximum pile von Mises stresses

The maximum pile von Mises stresses developed within the pile were studied in this section. The maximum pile von Mises stress for the circular (and Y-shaped cross-sections) was generated near the loading point at the center of the pile cap, whereas the stress for the triangular cross section was observed clearly at the corner of the advancing side of the pile due to the stress concentration (Figures-48 and 49). Table-26 indicates the magnitudes of such stress for all cross-sections considered in the study.

The relationship between the maximum pile von Mises stress and the applied horizontal load is shown in Figure-50. The maximum pile von Mises stress was almost proportional to the applied load. The smallest maximum pile von Mises stress was generated within the Y-shaped cross-section at all horizontal loads, whereas the largest stress was resulted with the triangular cross-section. The differences in the stresses between different cross-sections increased with the increase in horizontal load.

4) Relationship between displacements and stresses

As shown in Figures-51, the minimum soil minor principal stress increased following different patterns with the increase in the maximum horizontal displacement after the maximum geostatic stresses of -1,155.0 psf were overcome. At a given maximum horizontal displacement, the Y-shaped cross-section generated the smallest minimum soil minor principal stress. The largest minimum soil minor principal stress was associated with the triangular cross-section.

The relationship between the maximum pile von Mises stress and the maximum horizontal displacement shows a hyperbolic-shaped variation as shown in Figure-52. It is expected that the maximum pile von Mises stresses would approach the ultimate values, indicating the state of complete soil yield. The smallest maximum pile von Mises stress was obtained with the Y-shaped cross-section for a given maximum horizontal displacement as expected. Y-shaped cross section is therefore the most effective in terms of the developed pile stress.

4.5.2 Behaviors under vertical loads

1) Maximum pile vertical displacements

As mentioned previously, the maximum pile vertical displacement obtained from the finite element analysis was approximately the same as the maximum soil vertical displacement because of the large stiffness of the pile. With the relatively large stiffness, the suction pile moved along the direction parallel to the loading direction with almost no relative deformation of the pile (Figure-53). The vertical displacements of the three selected cross-sections at various vertical load levels are summarized in Table-27.

Figure-54 shows the distribution of the pile vertical displacements for the selected cross-sections at different vertical loads applied at the center of the pile top. The relationship between the maximum vertical displacement and the vertical load shows the typical elasto-plastic behavior, i.e., a linear behavior at relatively low loads, followed by a nonlinear behavior due to the effect of the soil plasticity at relatively high loads. The smallest maximum vertical displacement at a given load was obtained with the circular cross-section. The largest maximum vertical displacement at a given load was generated with the triangular cross-section. The difference in displacements between the circular and Y-shaped cross-sections was insignificant before the yield occurred. However, the differences in displacements due to different cross-sections at the same vertical load increased with the increase in load. It is specially evident after the elastic yield occurred. The elastic limit was observed to be approximately at the displacement of 0.6 ft for all cross-sections.

2) Minimum soil minor principal stresses

As expected, the minimum soil minor principal stresses, i.e., the absolute maximum soil compressive stress, due to various vertical loads were generated near the lower half around the pile (Figures-55 and 56). For triangular and Y-shaped cross-sections, the minimum soil minor principal stresses due to the vertical loads were generated near the corners within the lower half of the pile due to the stress concentration.

The complete results of the analysis are summarized in Table-28. Smallest minimum soil minor principal stresses due to vertical loads less than 1,700,000 lbs were generated with either the triangular (between 1,000,000 lbs and 1,700,000 lbs) or Y-

shaped cross sections (between 100,000 lbs and 1,000,000 lbs). For vertical loads beyond 1,700,000 lbs, the minimum soil minor principal stresses for all cross-sections increased rapidly with no apparent pattern. The vertical load of 1,700,000 lbs corresponded approximately to the load associated with the elastic limit of the displacements (0.6 ft).

The relationship between the minimum soil minor principal stress and the vertical load is shown in Figure-57. The irregular variations of the stresses may have resulted for various reasons, including 1) numerical errors due to the relatively large displacements within each load increment, and 2) difference in locations of elements where the minimum soil minor principal stresses occurred. Figure-58 shows the relationship between the minimum soil minor principal stress and the applied vertical load at an element located near the lower half of the pile. The yielding and hardening processes of the soil in compression are clearly seen in the figure.

3) Maximum pile von Mises stresses

As expected, the maximum pile von Mises stress due to the vertical loads always occurred at the point of loading (Figure-59). The results of the finite element analyses are summarized in Table-29.

Figure-60 shows the relationship between the maximum pile von Mises stress and the applied vertical load. The maximum pile von Mises stress was almost directly proportional to the applied vertical load at almost all loads. The maximum pile von Mises stress at a given load was the smallest for the Y-shaped cross-section, similar to the results of the study of the pile responses due to horizontal loads. Hence, the Y-shaped

cross- section is considered to be the most effective in terms of the developed pile stress under vertical loads.

4.5.3 Behaviors under inclined loads

The load inclination angle of 45 degree to the horizontal was chosen to study the behaviors of suction piles under inclined loads.

1) Maximum pile displacements

The maximum pile displacements always occurred at the top of the pile. As expected, the pile experienced translational as well as rotational movements. The displacements associated with the three selected cross-sections for various 45-degree inclined loads are summarized in Table-30. Almost identical displacements were generated for the circular and Y-shaped cross-sections in both comparisons of the maximum total and maximum horizontal displacements as was observed in the analysis for the horizontal loads.

Figures-61 and 62 show the distributions of the pile displacements for the selected cross-sections at different inclined loads applied at the center of the pile top. As the load increased, the displacements gradually approached the limiting values. The relationship is linear at lower loads, followed by a nonlinear behavior at higher loads, both for the maximum total displacement and the maximum horizontal displacement, due to the effect of the soil plasticity. The smallest vertical displacement at a given load was obtained with either the circular or the Y-shape cross-section, as was the case with horizontal

loads. The differences in displacements with different cross-sections at a given load increased with the increase in load.

2) Minimum soil minor principal stresses

The minimum soil minor principal stresses due to the 45-degree inclined loads were calculated around the pile and the results are summarized in Table-31. The relationship between the minimum soil minor principal stress and the 45-degree inclined load is shown in Figure-63. With the increase in load, the stresses showed irregular variations. The smallest minimum soil minor principal stress for loads less than 1,300,000 lbs was observed with the triangular cross-section.

3) Maximum pile von Mises stresses

The results of the finite element analyses of the maximum pile von Mises stresses are summarized in Table-32. The smallest maximum pile von Mises stress was observed with the circular cross-section when the loads were less than 200,000 lbs. For loads greater than 200,000 lbs, the Y-shaped cross-section generated the smallest maximum pile von Mises stress with the circular cross-section yielding the largest.

As shown in Figure-64, the maximum pile von Mises stress was directly proportional to the applied inclined load greater than 600,000 lbs. For loads less than 600,000 lbs, the maximum pile von Mises stresses varied nonlinearly for the triangular and Y-shaped cross-sections.

4.5.4 Additional results

The appendix of this report (figure numbers starting with "C") includes some of the typical results from the finite element analyses of suction piles in clay with circular, triangular, and Y-shape cross-sections under horizontal, vertical, and inclined loads. The results include: (1) soil displacements, (2) soil displacements on a vertical plane, (3) pile displacements, (4) soil minor principal stresses on a vertical plane, (5) soil minor principal stresses on the pile surface, (6) pile normal stresses on the pile surface, and (7) pile von Mises stresses on the pile surface.

4.6 Summary

4.6.1 General conclusions

It is evident that the effect of the soil plasticity is highly significant for large load magnitudes, as was observed from the study of suction piles embedded in sand. There also exist general trends in terms of the overall responses of the pile under different applied loads. In general, the horizontal pile displacement due to the horizontal or 45-degree inclined loads applied at the center of the pile cap varies almost linearly under very low loads but becomes nonlinear under high loads for all selected cross-sections. The variation is apparently hyperbolic-shaped and gradually approaches to an ultimate value. The smallest pile displacement due to the horizontal or 45-degree inclined loads occurs with either the circular or the Y-shaped cross-section, depending upon the magnitude and direction of the applied load. On the other hand, the vertical pile

displacement due to the vertical load applied at the center of the pile cap exhibits a sudden yielding behavior at displacement of approximately 0.6 ft for all cross-sections. The smallest displacement due to the vertical loads occurs always with the circular cross-section.

The minimum soil minor principal stresses due to the horizontal or 45-degree inclined loads applied at the center of the pile cap are dominated by the geostatic stress condition under low loads. However, as the geostatic stresses are gradually overcome, the minimum soil minor principal stresses due to the horizontal or 45-degree inclined loads develop at the bottom of the advancing side of the pile. This is different from that of sand, where the minimum soil minor principal stresses were observed near the top of the advancing side of the pile. The minimum soil minor principal stresses due to the vertical loads applied at the center of the pile cap are observed within the lower half of the pile. The smallest minimum soil minor principal stress depends on the direction and magnitude of the load. Under horizontal loads, the Y-shaped cross-section yielded the smallest stresses while the triangular cross-section generated the smallest stresses under inclined loads. When vertical loads are applied, the smallest stresses developed with the triangular and Y-shaped cross-section under smaller loads and higher loads, respectively.

The maximum pile von Mises stresses vary almost linearly with the increase in loads. However, the nonlinear variation is observed with the triangular and Y-shaped cross-sections for relatively low vertical and 45-degree inclined loads. The smallest maximum pile von Mises stress is always observed with the Y-shaped cross-section.

4.6.2 Pile failure loads

4.6.2.1 Pile failure based on horizontal displacement

Anderson et al. (2) suggested from their model test results that the pile would fail against the lateral load when the pile experiences the rotation of 0.04 ~ 0.06 radians. For 30 ft. long pile, the lateral displacement corresponding to this rotation is found to be 1.2 ~ 1.8 ft. Using the average value of 1.5 ft as the limiting lateral displacement of the pile, the horizontal and 45-degree inclined loads corresponding to the lateral displacement of 1.5 ft are summarized in Table-33, where the loads have been determined by a linear interpolation method.

As can be seen from Table-33, the Y-shaped cross-section allows the largest horizontal load of 1,484,100 lbs before the pile displacement reaches the limiting value. While the circular cross-section exhibits the largest resistance of 1,619,970 lbs against the 45-degree inclined load, the difference in failure loads between the circular and the Y-shaped cross-section is very small (less than 0.8%). Table-33 also shows that the circular and Y-shaped cross-sections can resist approximately 5.1% and 5.8% more horizontal and 45-degree inclined loads than the triangular cross-section, respectively.

4.6.2.2 Pile failure based on vertical displacement

As described previously, the displacement pattern of the suction pile under vertical loads applied at the center of the pile cap shows an abrupt yield pattern. The yield displacement is approximately 0.6 ft for all cross-sections. The loads corresponding

to the displacement of 0.6 ft are 1,910,000 lbs for the circular cross-section, 1,850,000 lbs for the Y-shaped cross-section, and 1,720,000 lbs for the triangular cross-section, respectively, indicating that the circular cross-section can provide the highest resistance against the vertical pull-out.

5. ADDITIONAL PERFORMANCE STUDY OF SUCTION PILES

The purpose of this study is to investigate behaviors of suction piles with additional parameters that may influence the overall performance. The parameters selected for this study include the width of the flange at the top of the pile, the point of mooring line attachment (loading point), the pile diameter change, and the layered soil condition. This study utilized the same soils (clay and sand) whose detailed properties were described in the previous chapters.

This study only considered the circular cross-section. A suction pile with a diameter of 30 ft. and a length of 30 ft. was chosen again as the standard pile in this study. Under a given loading condition, responses of the standard pile were compared with those of the suction piles with selected parameters.

The initial linear elastic behaviors of the soils were described by Young's modulus (E) and Poisson's ratio (υ), whereas the subsequent plastic behaviors were modeled by the extended Drucker-Prager plasticity model based on the linear (sand) or hyperbolic (clay) failure criteria.

The objective of this study is to investigate the effects of the various parameters described above through quantitative comparisons of the responses of the suction pile and the soil. The loads were increased incrementally and the behaviors were observed in detail at various load levels.

5.1 Description of Parameters

The parameters selected for the study are the width of the flange, the pile diameter change, the layered soil condition, and the loading point. These parameters varied as described below to investigate their effects on the overall behavior of the suction pile system.

5.1.1 Width of flange

It is conceivable that the suction pile can provide additional resistance against the lateral load if a flange whose diameter is larger than that of the pile is attached at the top of the pile. The purpose is to take advantage of the soil bearing pressure under the flange as the pile rotates. Flange widths of 5, 10, and 15 ft. beyond the pile outside diameter were chosen to investigate its effect. Figure-65 shows a schematic finite element grid of a suction pile with a flange.

5.1.2 Loading point

It is well known that the behavior of a laterally loaded pile is significantly influenced by the point where the lateral load is applied, since it dictates the mode of the pile movement. To investigate the effect of the loading point, three different locations were selected as shown in Figure-66, i.e., at the top, at the mid-height, and at the tip of the pile.

5.1.3 Pile diameter change

In anticipation of the soil volume increase due to the applied suction inside the pile, suction piles with a slightly larger diameter for the upper half have been used. The diameters of the telescopic piles included in the study were selected to have the same contact area between the soil and the pile as that of the standard circular pile, which in essence kept the amount of pile material the same. The telescopic pile would have smooth transition between two sections with different diameters, such as a 45^{o} wedge. However, the finite element simulation of the telescopic pile had a sharp, 90^{o} sudden transition between the upper and lower halves of the pile due to the difficulties in three dimensional finite element mesh generation. This discrepancy would result in concentration of the soil and pile stresses near the sharp corners. However, the resulting pile and soil displacements would not be affected much. The dimensions of the selected telescopic pile had diameters of 32 ft. for the upper half and 28 ft. for the lower half with a total length of 30 ft., as shown in Figure-67.

5.1.4 Layered soil condition

The seafloor typically consists of soil layers with different properties or a single homogeneous soil whose strength varies with depth. To investigate the effect of varying soil properties, six different soil layer combinations were selected for the study. The selected soil layer combinations included two general conditions, i.e., one with a strong sandy soil layer beneath a weak clayey soil layer, and the other with a weak clayey soil layer overlying a strong sandy soil layer. These two conditions were further divided into

eight cases, having different upper and lower soil layer thicknesses, as shown in Figure-68. The thickness of the upper soil layer therefore varied from zero to 30 ft. with an increment of 7.5 ft.

5.2 Material and Loading Parameters

It was assumed that the soils were homogeneous and isotropic. Their linear elastic behaviors under relatively smaller loads were described completely by two parameters, Young's modulus (E) and Poisson's ratio (ν). The hyperbolic (clay) and linear (sand) extended Drucker-Prager plasticity models were utilized to simulate its plastic behaviors under relatively larger loads. At higher stress levels, the plasticity model is completely defined by two parameters, the slope angle and the dilation angle. The soil properties used in previous chapters were directly quoted in this study.

The loads were applied along the horizontal or 45-degree inclined direction. The loads were increased until the solutions approached the ultimate values.

5.3 Results

5.3.1 Effect of flange

To investigate the effect of the flange attached at the top of the pile, three different widths of a circular flange were selected. The flange width was measured from the edge of the pile to the outer boundary of the flange. The selected widths of the flange were 5,

10, and 15 feet. The pile was loaded at the center of the pile cap. The flange was modeled by shell elements but those elements were flat geometrically.

5.3.1.1 Behaviors of suction piles in sand

1) Pile displacements

As shown in Figure-69, the maximum total and horizontal pile displacements due to various horizontal loads applied at the center of the pile cap with a flange always occurred at the top of pile along the loading direction, whereas the minimum pile displacement occurred at the bottom of the pile. It is also noted from the figure that the pile was experiencing horizontal translational movements as well as rotational movements. Even though the stiffness of the pile was assumed to be very large, small deformations of the pile were observed near the middle of the pile under relatively large loads.

The maximum displacements under various horizontal loads decreased with the increase in the width of the flange, as shown in Tables-34 and 35. This is primarily due to the compressive resistance of the soil under the flange of the advancing side of the pile. The effect of the flange width became more pronounced at relatively larger horizontal loads near the failure. Similarly, the effect of the flange width decreased as the flange width increased.

Figures-70 and 71 show typical load vs. displacement behaviors under various horizontal loads. Both the maximum total and maximum horizontal pile displacements associated with different flange widths show a similar pattern against the applied

horizontal load. The displacements varied almost linearly due to the elastic behavior under relatively small horizontal loads. As the horizontal load increased, the displacements showed a nonlinear behavior due to the inclusion of the plastic soil behavior. The variations of the curves are hyperbolic shaped, with horizontal loads gradually approaching the ultimate values. The suction pile with a wider flange is more effective in terms of the maximum displacement of the pile embedded in sand.

2) Minimum soil minor principal stresses

The minimum soil minor principal stress at any given horizontal load was always generated beneath the outer edge of the flange of the advancing side of the pile. The soil elements under the receding side of the pile experienced relatively small tensile stress due to the nature of kinematic hardening in the plastic analysis, as shown in Figure-72.

The calculated minimum soil minor principal stresses associated with the selected widths of the flange are shown in Table-36. At the beginning of the analysis, identical geostatic stress conditions were established for all piles with different flange widths. As the load increased, the geostatic stresses were finally overcome and the elastic soil behavior started. As can be seen in Figure-73, the elastic behavior was characterized by a steep rise in horizontal load with respect to the minimum soil minor principal stress. The elastic soil behavior eventually ceased at horizontal loads of approximately 3,000,000 lbs for the pile with no flange, 3,500,000 lbs for the pile with a 5 ft. wide flange, 4,000,000 lbs for the pile with a 10 ft. wide flange, and 4,500,000 lbs for the pile with a 15 ft. wide flange. Plastic soil behavior then followed. For a given load, the minimum soil minor

principal stresses decreased with the increase in the flange width. The rate of decrease, however, decreased as the flange width increased.

It is clearly seen from Figure-74 that the suction pile with a wider flange generated smaller minimum soil minor principal stresses, indicating that the widest flange is the most effective in terms of the minimum soil minor principal stress. The difference in minimum soil minor principal stresses for a given load increased with the increase in load due to the effect of plasticity.

3) Maximum pile von Mises stresses

The maximum pile von Mises stress was generated near the loading point at the center of the pile cap, as shown in Figures-74. In addition, relatively higher maximum pile von Mises stresses were observed on the flange of advancing side of the pile due to the larger compressive reaction of the soil. The maximum pile von Mises stress was determined considering both the outer and the inner surfaces of the pile. Table-37 indicates the magnitudes of such stress for all flange widths considered in the study. The largest maximum pile von Mises stress was generated with the pile having no flange up to the horizontal load of 8,000,000 lbs, indicating that the attachment of a flange would reduce the maximum pile von Mises stress. The reduction in maximum pile von Mises stress for piles with flanges was, however, very small. It is noted that in this study the flange was assumed to be very stiff. Therefore, the results may not be applicable if the flange is not sufficiently reinforced.

The relationship between the maximum pile von Mises stress and the applied horizontal load is shown in Figure-75. The maximum pile von Mises stress was almost

proportional to the applied load. Almost identical stresses were observed for all selected flange widths.

5.3.1.2 Behaviors of suction piles in clay

1) Pile displacements

The maximum total and horizontal pile displacements due to various horizontal loads applied at the center of the pile cap always occurred at the top of the pile along the loading direction, whereas the minimum pile displacement occurred at the bottom of the pile as was observed in the analyses with sand. Figure-76 shows one such example output. The pile was experiencing horizontal translational movements as well as rotational movements, as can be seen from the figure.

Tables-38 and 39 show that smaller maximum displacements were observed under various horizontal loads with the increase in the flange width, mainly due to the soil resistance beneath the flange as the pile rotated. The effect of the flange width became much more significant at relatively larger horizontal loads near the failure due to the effect of the soil plasticity. Again, the effect of the flange width diminished as the flange width increased.

Figures-77 and 78 show typical load vs. displacement behaviors due to various horizontal loads. Both the maximum total and horizontal pile displacements associated with different flange widths show a similar pattern against the applied horizontal load. The displacements varied almost linearly under relatively small horizontal loads. As the horizontal load increased, the displacements showed a nonlinear behavior. Finally, the

horizontal loads approached the ultimate values. The ultimate loads were approximately 1,900,000 lbs for the pile without flange, 2,300,000 lbs for the pile with a 5 ft. flange, 2,800,000 lbs for the pile with a 10 ft. flange, and 3,600,000 lbs for the pile with a 15 ft. flange. The ultimate load increased by almost 190% when the flange width increased from 0 ft to 15 ft. In other words, the suction pile with a 15-ft flange may exhibit twice the ultimate resistance than that of the pile without a flange. Consequently, the suction pile with a wider flange is more effective in terms of the maximum displacements of the pile in clay.

2) Minimum soil minor principal stresses

The minimum soil minor principal stress at any given horizontal load was always generated at the bottom of the advancing side of the pile. Note that in sand the minimum soil minor principal stress was generated under the outer edge of the flange of the advancing side of the pile. Relatively large stresses were also observed within the soil under the outer edge of the flange of the advancing side of the pile due to the rotational movement of the pile. The soil under the receding side of the pile experienced relatively small tensile stress due to the nature of kinematic hardening in the plastic analysis, as shown in Figure-79.

The calculated minimum soil minor principal stresses associated with the selected widths of the flange are shown in Table-40. Identical maximum geostatic stresses of -1,155 psf were established at the beginning of the analysis for piles with all flange widths. Below the horizontal load of 300,000 lbs, almost identical minimum soil minor principal stresses for all piles with different flange widths were observed. This is primarily

because the developed stresses were not large enough to overcome the geostatic stresses. When the horizontal load was less than 900,000 lbs, the minimum soil minor principal stress decreased with the increase in the flange width. Above that load, there was no general trend in solutions, partly due to the numerical instability.

Figure-80 shows the relationship between the minimum soil minor principal stress and the applied horizontal load. Once the geostatic stresses were overcome, the minimum soil minor principal stresses increased nonlinearly. The patterns were not completely consistent as can be seen from the figure. As was discussed in the previous study with clay, this is mainly because the minimum soil minor principal stress did not occur within the same element as the horizontal load increased,. However, the variations of the minimum soil minor principal stresses are roughly hyperbolic shaped, i.e., the loads would gradually approach the ultimate values. Generally, the pile with a wider flange generated the smaller minimum soil principal stress, indicating that the wider flange is more effective in terms of the minimum soil minor principal stress. The difference in the minimum soil minor principal stress for a given load increased with the increase in load due to the effect of plasticity.

3) Maximum pile von Mises stresses

The maximum pile von Mises stress was generated near the loading point under relatively small loads (Figure-81), whereas the maximum stress was observed near the intersection between the flange and the pile along the loading direction (Figure-82). The location of the maximum pile von Mises stress shifted from the loading point to the intersection between the pile and the flange as the load increased. Generally, relatively

higher maximum pile von Mises stresses were observed within the flange of the advancing side of the pile due to the large compressive soil stress caused by the rotational movement of the pile. Table-41 indicates the magnitudes of such stress for all flange widths considered in the study.

The relationship between the maximum pile von Mises stress and the applied horizontal load is shown in Figure-83. The maximum pile von Mises stress was almost proportional to the applied load except for the pile with a 15 ft. flange. Almost identical stresses were observed for the flange widths less than 15 ft. The largest maximum pile von Mises stress was always generated within the pile with a 15 ft. flange.

5.3.1.3 Additional results

The appendix of this report (figure numbers starting with "D") includes some of the typical results from the finite element analyses of suction piles with different flange widths under horizontal loads. The results include: (1) soil displacements, (2) soil displacements on a vertical plane, (3) pile displacements, (4) soil minor principal stresses on a vertical plane, (5) soil minor principal stresses on the pile surface, and (6) pile von Mises stresses on the pile surface.

5.3.2 Effect of loading point

The standard pile, 30 ft. in diameter and 30 ft. in length, was loaded at different points to identify the effect of the loading point under horizontal and 45-degree inclined

loads. As can be seen in Figure-66, the selected loading points were the center of the pile cap, the mid-height of the pile, and the toe of the pile.

5.3.2.1 Behaviors of suction piles in sand

5.3.2.1.1 Behaviors under horizontal loads

1) Pile displacements

The maximum total and horizontal pile displacements due to various horizontal loads applied at the mid-height of the pile always occurred at the top of the pile along the loading direction, whereas the minimum pile displacement occurred at the bottom of the pile, as was seen in the analyses with the load applied at the center of the pile cap. This is because the geostatic stresses of the upper half of the pile were much smaller than those of the lower half of the pile due to the difference in depth. Figure-84 shows one such example output. The pile was experiencing horizontal translational movements as well as rotational movements.

The maximum total and horizontal pile displacements due to various horizontal loads applied at the toe of the pile occurred always at the bottom of the pile along the loading direction, whereas the minimum pile displacement occurred at the top of the pile, as shown in Figure-85. As can be seen from the figure, the pile was experiencing horizontal translational movements as well as rotational movements. The pile rotation was along the opposite direction to the cases when the pile was loaded at the top or at the mid-height.

The largest maximum displacements due to various horizontal loads were always observed when the load was applied at the center of the pile cap, as shown in Table-42. The smallest maximum displacements were generated with the horizontal loads applied at the mid-height of the pile up to the load of 17,000,000 lbs, beyond which the maximum displacements were associated with the loads applied at the toe of the pile. The difference in maximum displacements between the load applied at the mid-height of the pile and the load applied at the toe of the pile was very small for loads less than 17,000,000 lbs. However, the difference in maximum displacements for a given load became very much pronounced at relatively larger loads, i.e., near the failure, due to the effect of plasticity.

Figures-86 and 87 show typical load vs. displacement behaviors under various horizontal loads. Both the maximum total and maximum horizontal pile displacements associated with different loading points show a similar pattern against the applied horizontal load. The displacements varied almost linearly due to the elastic behavior under relatively small horizontal loads, followed by a nonlinear behavior under relatively large loads. The variations of the curves are hyperbolic shaped, gradually approaching the ultimate values.

2) Minimum soil minor principal stresses

The minimum soil minor principal stress at any given horizontal load was generated at the advancing side of the pile when the load was applied at the middle of the pile (Figure-88), whereas the minimum soil minor principal stress at any given horizontal load was observed at the lower half of the advancing side of the pile when the horizontal load was applied at the toe of the pile (Figure-89). When the horizontal load was applied

at the toe of the pile, the soil elements below the heel of the pile experienced relatively higher stresses due to the downward movement of the pile resulting from the counterclockwise rotational movement of the pile (Figure-89). The soil elements behind the receding side of the pile experienced relatively small tensile stress as can be seen from the figure. The calculated minimum soil minor principal stresses associated with the different loading points are shown in Table-43. Identical maximum geostatic stresses of -2,499.0 psf were established for all cases at the beginning of the analysis. The elastic behaviors were overcome completely at the load of approximately 3,000,000 lbs for the cases with the load at the center of the pile cap and at the toe of the pile, and 5,0000,000 lbs for the case with the load at the mid-height of the pile (Figure-90) Once the elastic behavior was overcome the minimum soil minor principal stress started to increase with a nonlinear variation. The minimum soil minor principal stress at any given horizontal load was generated at the advancing side of the pile when the load was applied at the middle of the pile (Figure-88), whereas the minimum soil minor principal stress at any given horizontal load was observed at the lower half of the advancing side of the pile when the horizontal load was applied at the toe of the pile (Figure-89). Figure-90 shows the relationship between the minimum soil minor principal stress and the applied horizontal load. The minimum soil minor principal stresses associated with the loads applied at the center of the pile cap were much greater than other cases. The difference in minimum soil minor principal stresses for a given load increased with the increase in load due to the effect of plasticity.

3) Maximum pile von Mises stresses

As expected, the maximum pile von Mises stress was generated at the top of the advancing side of the pile when the load was applied at the mid-height of the pile, whereas the maximum pile von Mises stress was observed at the lower half of the advancing side of the pile (near the loading point) when the load was applied at the toe of the pile, as can be seen in Figures-91 and 92.

Table-44 indicates the magnitudes of such stress for all loading points considered in the study. The magnitude of the maximum pile von Mises stress for a given load approximately was doubled when the load shifted from the top to the mid-height and again from the mid-height to the bottom, i.e., the stress associated with the load applied at the toe of the pile was approximately four times greater than that associated with the load applied at the top of the pile cap.

The relationship between the maximum pile von Mises stress and the applied horizontal load is shown in Figure-93. The maximum pile von Mises stress was directly proportional to the applied load. The smallest maximum pile von Mises stress for a given load was generated with the load applied at the center of the pile cap, indicating that the most effective loading point is the center of the pile cap in terms of the pile stress.

5.3.2.1.2 Behaviors under 45-degree inclined loads

1) Maximum pile displacements

The maximum pile displacements due to 45-degree inclined loads applied at the mid-height of the pile always occurred at the top of the pile, whereas the maximum pile displacements associated with the load applied at the toe of the pile were always observed

at the bottom of the pile. Same results were observed from the analysis with horizontal loads. The pile experienced translational as well as rotational movements as expected. The displacements associated with different loading points for various 45-degree inclined loads are summarized in Table-45.

Figures-94 and 95 show the distributions of the pile displacements due to different inclined loads applied at various loading points. As the load increased, the displacements gradually approached the limiting values. The relationship is linear at smaller loads, followed by a nonlinear behavior at higher loads, for both the maximum total displacement and the maximum horizontal displacement due to the effect of the soil plasticity. The smallest displacement at a given load was obtained with the load applied at the mid-height of the pile, indicating that the most effective loading point is near the middle of the pile in terms of the pile displacement. The difference in maximum displacements associated with different loading points at a given load increased with the increase in load.

2) Minimum soil minor principal stresses

The minimum soil minor principal stresses associated with different loading points due to the 45-degree inclined loads were calculated and the results are summarized in Table-46. The elastic behaviors were overcome at the load of 3,500,000 lbs for both the cases with the load at the center of the pile cap and at the mid-height of the pile, and 2,000,000 lbs for the case with the load at the bottom of the pile (Figure-96). Once the elastic behavior was overcome, the stresses increased rapidly with a nonlinear variation. The smallest minimum soil minor principal stress at all load levels was observed with the

load applied at the mid-height of the pile, indicating that the most effective loading point is near the mid-height of the pile in terms of the soil stress.

3) Maximum pile von Mises stresses

The results of the finite element analyses of the maximum pile von Mises stresses are summarized in Table-47. The smallest maximum pile von Mises stress was observed with the load applied at the mid-height of the pile at all loads. When the load was applied at the toe of the pile, the stress became the largest. The most effective loading point is the mid-height of the pile in terms of the pile stress. It is noted that the most effective loading point with respect to the horizontal load was found to be the center of the pile cap.

As shown in Figure-97, the maximum pile von Mises stress was almost proportional to the applied inclined load. With the increase in load the difference in stresses increased.

5.3.2.2 Behaviors of suction piles in clay

5.3.2.2.1 Behaviors under horizontal loads

1) Pile displacements

The maximum total and horizontal pile displacements due to various horizontal loads applied at the mid-height of the pile always occurred at the top of the pile along the loading direction, whereas the minimum pile displacement occurred at the bottom of the

pile. The maximum total and horizontal pile displacements due to various horizontal loads applied at the toe of the pile occurred always at the bottom of the pile along the loading direction, whereas the minimum pile displacement occurred at the top of the pile. These rotational movements are similar to those observed in the analysis with sand.

The smallest maximum displacements due to various horizontal loads were observed with the load applied at the mid-height of the pile, as shown in Table-48. However, the difference in maximum displacements between the cases with the loads applied at the mid-height and at the toe of the pile was small. The maximum displacement associated with the load applied at the center of the pile cap was much greater than the others. The effect of the loading point became much more pronounced at relatively larger horizontal loads, i.e., near the failure.

Figures-98 and 99 show typical load vs. displacement behaviors under various horizontal loads. Both the maximum total and maximum horizontal pile displacements associated with different loading points show a similar pattern. The displacements varied almost linearly under relatively small horizontal loads due to the elastic behavior. As the horizontal load increased, the displacements showed a nonlinear behavior. The variations of the curves are hyperbolic shaped, gradually approaching the ultimate values. It is clearly seen from the figures that the suction pile loaded at the center of the pile cap generated much larger maximum displacements at a given load than the others.

2) Minimum soil minor principal stresses

The minimum soil minor principal stress at any given horizontal load was always generated at the lower half of the advancing side of the pile and under the pile toe when

the load was applied at the mid-height of the pile, whereas the minimum soil minor principal stress at any given horizontal load was observed at the lower half of the advancing side of the pile when the horizontal load was applied at the toe of the pile. As was the analysis with sand, the soil under the pile heel experienced relatively higher stresses due to the downward movement of the pile resulted from the rotation of the pile when the horizontal load was applied at the toe of the pile. The soil behind the receding side of the pile experienced relatively small tensile stress as shown in Figures-100 and 101. The calculated minimum soil minor principal stresses associated with different loading points are shown in Table-49.

For a given load, the smallest minimum soil minor principal stresses were associated with the load applied at the mid-height of the pile, indicating that the most effective loading point with respect to the horizontal load is near the mid-height of the pile in terms of the soil stress.

Figure-102 shows the relationship between the minimum soil minor principal stress and the applied horizontal load. The difference in minimum soil minor principal stresses for a given load increased with the increase in load due to the effect of plasticity. As was discussed in the previous study with clay, the irregular variations of the relationship might be due to the shift of the elements which generated the minimum soil minor principal stresses as the load increased. The largest minimum soil minor principal stresses were associated with the load applied at the toe of the pile.

3) Maximum pile von Mises stresses

The maximum pile von Mises stress was generated at the top of the advancing side of the pile when the load was applied at the mid-height of the pile, whereas the maximum pile von Mises stress was observed at the lower half of the advancing side of the pile when the load was applied at the toe of the pile, as was the case in the analyses with sand. Table-50 indicates the magnitudes of such stress for all loading points considered in the study. The magnitude of the maximum pile von Mises stress for a given load approximately was doubled when the load shifted from the top to the mid-height and again from the mid-height to the bottom, i.e., the stress associated with the load applied at the bottom of the pile is approximately four times greater than that associated with the load applied at the center the pile cap.

The relationship between the maximum pile von Mises stress and the applied of horizontal load is shown in Figure-103. The maximum pile von Mises stress was directly proportional to the applied load. The largest maximum pile von Mises stress for a given load was generated with the load applied at the toe of the pile.

5.3.2.2.2 Behaviors under 45-degree inclined loads

1) Maximum pile displacements

The maximum pile displacements with respect to the 45-degree inclined load applied at the mid-height of the pile always occurred at the top of the pile, whereas the maximum pile displacements associated with the load applied at the toe of the pile were always observed at the bottom of the pile, as was observed in the analysis with horizontal loads. As expected, the pile experienced translational as well as rotational movements.

The displacements associated with different loading points for various 45-degree inclined loads are summarized in Table-51.

Figures-104 and 105 show the distributions of the pile displacements for different loading points. As the load increased, the displacements gradually approached the limiting values. The relationship was linear at lower loads, followed by a nonlinear behavior at higher loads, both for the maximum total and the maximum horizontal displacements. The most effective loading point is the mid-height of the pile in terms of the pile displacements. The difference in displacements with different loading points at a given load increased with the increase in load.

2) Minimum soil minor principal stresses

The minimum soil minor principal stresses associated with different loading points due to the 45-degree inclined loads were calculated around the pile, and the results are summarized in Table-52. The relationship between the minimum soil minor principal stress and the 45-degree inclined load is shown in Figure-106. The variations of the stresses show irregular patterns. As described previously, this would be primarily due to the transition of elements associated with the minimum soil minor principal stresses. The smallest minimum soil minor principal stress for all load levels was observed with the load applied at the center of the pile cap, indicating that the most effective loading point is the center of the pile cap in terms of the soil stresses. The largest minimum soil minor principal stress was generated with the load applied at the toe of the pile.

3)Maximum pile von Mises stresses

The results of the finite element analyses of the maximum pile von Mises stresses are summarized in Table-53. The smallest maximum pile von Mises stress was observed with the load applied at the mid-height of the pile for all loads, with the load at the toe of the pile yielding the largest. The most effective loading point is the mid-height of the pile in terms of the pile stress.

As shown in Figure-107, the maximum pile von Mises stress was directly proportional to the applied inclined load. With the increase in load, the difference in stresses increased.

5.3.2.3. Additional results

The appendix of this report (figure numbers starting with "E") includes some of the typical results from the finite element analyses of suction piles with different loading points under various horizontal loads. The results include: (1) soil displacements on a vertical plane, (2) pile displacements, (3) soil minor principal stresses on a vertical plane, (4) soil minor principal stresses on the pile surface, and (5) pile von Mises stresses on the pile surface.

5.3.3 Effect of pile diameter change

A telescopic suction pile was analyzed to investigate the effect of the variation in the pile diameter along depth. The results of the analysis on the telescopic pile were compared with those of the prismatic standard pile that were available from the previous

analyses. Prismatic pile is defined as a pile with a constant cross-section along its entire length. In order to keep the same contact area of the pile with the soil, the diameters of the telescopic pile were chosen to be 32 ft. for the upper half of the pile and 28 ft. for the lower half. The average diameter of the telescopic pile was therefore 30 ft., which is the same as that of the standard pile. The length of the telescopic pile remained as 30 ft., i.e., the same as that of the prismatic standard pile. The horizontal loads were applied at the center of the pile cap.

5.3.3.1 Behaviors of telescopic piles in sand

1) Pile displacements

The maximum total and horizontal pile displacements due to various horizontal loads applied at the center of the pile cap occurred always at the top of the pile along the loading direction, whereas the minimum pile displacement occurred at the bottom of the pile. Figure-108 shows one such example output. The pile was experiencing horizontal translational movements as well as rotational movements.

The maximum displacements of the telescopic pile due to various horizontal loads were lower than those of the prismatic standard pile at smaller loads but became higher at higher loads, as shown in Table-54. The difference in maximum displacements was within 5 % up to the load of 5,000,000 lbs. The difference became larger as the load increased, resulting in approximately 23% at a load of 9,500,000 lbs. This is primarily due to the effect of the soil plasticity. Results indicate that the prismatic pile is more effective in terms of the maximum pile displacement.

Figures-109 and 110 show typical load vs. displacement behaviors under various horizontal loads. Both the maximum total and maximum horizontal pile displacements associated with the telescopic and prismatic piles show a similar pattern against the applied horizontal load. The displacements varied almost linearly due to the elastic behavior under relatively small horizontal loads. As the horizontal load increased, the displacements showed a nonlinear behavior due to the inclusion of the plastic soil behavior. The variations of the curves are hyperbolic shaped, gradually approaching the ultimate values.

2) Minimum soil minor principal stresses

The minimum soil minor principal stress at any given horizontal load was always generated at the upper half of the advancing side of the pile. The soil behind the receding side of the pile experienced relatively small tensile stress, as shown in Figure-111. The soil behind the lower half of the pile experienced relatively large compressive stress due to the rotational movement of the pile.

The calculated minimum soil minor principal stresses associated with the telescopic and prismatic piles are shown in Table-55. The maximum geostatic stresses of -2,499 psf for the prismatic pile and –2,677.5 psf for the telescopic pile were established at the beginning of the finite element analyses. The difference in maximum geostatic stresses was due to the difference in element sizes of the finite element mesh generated for the analyses along the vertical direction, although the solution domains remained the same for both cases. The elastic behaviors were overcome completely at the load of approximately 3,000,000 lbs for both cases (Figure-112). Once the elastic behavior was

overcome, the minimum soil minor principal stress increased rapidly. Figure-112 clearly shows that the telescopic suction pile generated the larger minimum soil minor principal stresses, indicating that the prismatic pile is more effective in terms of the minimum soil minor principal stress. The difference in minimum soil minor principal stresses for a given load increased with the increase in load due to the effect of the soil plasticity.

3) Maximum pile von Mises stresses

The maximum pile von Mises stress was generated near the loading point at the center of the pile cap, as can be seen in Figures-113. Table-56 indicates the magnitudes of such stress for all type of the pile considered in the study

The relationship between the maximum pile von Mises stress and the applied horizontal load is shown in Figure-114. The maximum pile von Mises stress was almost proportional to the applied load. Almost identical stresses were observed at relatively smaller loads for both piles, whereas slightly larger maximum pile von Mises stresses were generated under relatively larger loads with the telescopic pile. The difference in stresses became more significant with the increase in load. The telescopic pile is more effective in terms of the pile stress.

5.3.3.2 Behaviors of telescopic suction piles in clay

1) Pile displacements

The maximum total and horizontal pile displacements due to various horizontal loads applied at the center of the pile cap always occurred at the top of the pile along the

loading direction, whereas the minimum pile displacement occurred at the bottom of the pile, as was the case in the analyses with sand. Figure-115 shows one such example output. It is also noted from the figure that the pile was experiencing horizontal translational movements as well as rotational movements.

Table-57 shows that the maximum displacements of the telescopic pile under various horizontal loads were smaller than those of the prismatic standard pile for almost the entire range of loads, except near the maximum load where the trend reversed. The difference in maximum total and horizontal pile displacements was within 2 % and 4 % up to the load of 1,400,000 lbs, respectively, indicating that the prismatic and telescopic piles are equally effective for working loads in terms of the pile displacements.

Figures-116 and 117 show typical load vs. displacement behaviors under various horizontal loads. Both the maximum total and maximum horizontal pile displacements associated with the telescopic and prismatic piles show a similar pattern against the applied horizontal load. The displacements varied almost linearly under relatively small horizontal loads. As the horizontal load increased, the displacements showed a nonlinear behavior. The variations of the curves are hyperbolic shaped, gradually approaching the ultimate values. The ultimate loads were found to be approximately 1,900,000 lbs for both piles.

2) Minimum soil minor principal stresses

The minimum soil minor principal stress at any given horizontal load was always generated below the bottom edge of the upper half of the pile in the loading direction. This is the location where the transition in pile diameter takes place. Soil elements at the

receding side of the pile experienced relatively small tensile stress as shown in Figure-118.

The calculated minimum soil minor principal stresses associated are shown in Table-58. The maximum geostatic stresses of -1,155.0 psf for the prismatic pile and -1,237.5 psf for the telescopic pile were established at the beginning of the analyses. The difference in maximum geostatic stresses resulted from the difference in the element sizes of the finite element mesh generated for the analyses along the vertical direction. For horizontal loads less than 300,000 lbs, the difference in minimum soil minor principal stresses for both piles was resulted from the different initial geostatic stresses. The telescopic pile became more effective for load magnitudes from 300,000 lbs to 700,000 lbs. Beyond the horizontal load of 800,000 lbs, the prismatic pile became more effective.

Figure-119 shows the relationship between the minimum soil minor principal stress and the applied horizontal load. The minimum soil minor principal stresses increased following various patterns. As can be seen from the figure, the patterns are not consistent. This is mainly because the minimum soil minor principal stress did not occur within the same element as the horizontal load increased. However, the variations of the minimum soil minor principal stresses are roughly hyperbolic shaped, gradually approaching the ultimate values. The difference in minimum soil minor principal stresses for a given load increased with the increase in load due to the effect of the soil plasticity.

3) Maximum pile von Mises stresses

As expected, the maximum pile von Mises stress was generated near the loading point (Figure-120). Table-59 indicates the magnitudes of such stress for the two types of

the pile considered in the study. Slightly smaller maximum stresses were observed with the telescopic pile. The difference in maximum pile stresses with respect to the horizontal load applied at the center of the pile cap was very small and negligible (less than 6.0 %). However, the difference in maximum pile stresses increased with the increase in load.

The relationship between the maximum pile von Mises stress and the applied horizontal load is shown in Figure-121. The maximum pile von Mises stress was almost proportional to the applied load. It is observed that slightly larger maximum pile von Mises stresses were generated within the prismatic pile, indicating that the telescopic pile is more effective in terms of the developed pile stress against the horizontal load applied at the center of the pile cap.

5.3.3.3. Additional results

The appendix of this report (figure numbers starting with "F") includes some of the typical results from the finite element analyses of suction piles with a telescopic diameter change under horizontal load. The results include: (1) soil displacements, (2) soil displacements on a vertical plane, (3) pile displacements, (4) soil minor principal stresses on a vertical plane, (5) soil minor principal stresses on the pile surface, and (6) pile von Mises stresses on the pile surface.

5.3.4 Effect of layered soil condition

To investigate the responses of a suction pile embedded in layered soils, eight different layered soil conditions were chosen for the study. The layered soil condition was classified by two groups. The first group (Group-I) indicated the soil condition with the strong soil (sand) above a weak soil (clay) and the second group (Group-II) represented the reverse situation. Further, each group was divided into four conditions according to the thickness of the each soil layer, i.e., the thickness of the upper soil layer varied from 0.0 ft. to 22.5 ft. with an increment of 7.5 ft. The elasto-plastic sandy soil properties modeled by the linear extended Drucker-Prager plasticity represented the strong soil, whereas the elasto-plastic clayey soil properties modeled by the hyperbolic extended Drucker-Prager plasticity represented the weak soil. The dimension of the standard pile was used in this study, and the horizontal load applied at the center of the pile cap was increased incrementally. Same solution domain, including the finite element mesh, was used for the analyses except the layered soil condition.

5.3.4.1 Suction piles with group-I soil conditions

Group-I included four different layered soil conditions, namely, Layered Soil-1, 2, 3, and 4 as defined in Figure-68. Layered Soil-1 represents the soil stratum consisting of only clayey soil. Layered Soil-2, 3, and 4 represent the soil strata having the thickness of the upper sandy soil layer of 7.5, 15.0, and 22.5 ft, respectively.

1) Pile displacements

The maximum total and horizontal pile displacements due to various horizontal loads applied at the center of the pile cap always occurred at the top of the pile along the loading direction, whereas the minimum pile displacement occurred at the bottom of the pile. Figure-122 shows one such example output. It is also noted from the figure that the pile was experiencing horizontal translational movements as well as rotational movements.

Smaller maximum displacements under various horizontal loads were observed with the increase in the thickness of the upper strong sand layer, as shown in Tables-60 and 28. The effect of the thickness of the upper strong soil layer became very pronounced at relatively larger horizontal loads.

Figures-123 and 124 show typical load vs. displacement behaviors under various horizontal loads. Both the maximum total and maximum horizontal pile displacements associated with the thickness of the upper strong soil layer showed a similar pattern against the applied horizontal load. As the horizontal load increased, the displacements showed a nonlinear behavior. The variations of the curves were hyperbolic shaped, gradually approaching the ultimate values. The suction pile in the soil strata with the thickest upper strong soil layer generated the smaller displacements as expected.

2) Minimum soil minor principal stresses

The minimum soil minor principal stress at any given horizontal load was always generated within the strong soil layer located near the top of the advancing side of the pile as expected. As shown in Figure-125, the soil at the receding side of the pile experienced relatively small tensile stresses due to the nature of kinematic hardening in the plastic

analysis. The calculated minimum soil minor principal stresses associated with the selected thickness of the upper strong soil layer are shown in Table-62. Different maximum geostatic stresses in four cases were obtained due to the nature of different soil layer conditions. For a given load, the minimum soil minor principal stresses decreased with the increase in the thickness of the upper strong soil layer after the geostatic stresses were overcome.

Figure-126 shows the relationship between the minimum soil minor principal stress and the applied horizontal load. Once the elastic behaviors were overcome, the stress increased with a nonlinear variation due to the effect of the soil plasticity. It is clearly seen from the figure that the suction pile in the soil condition with the thickest upper strong soil layer generated the smallest minimum soil minor principal stress for a given load. The difference in minimum soil minor principal stresses for a given load increased with the increase in load due to the effect of plasticity.

3) Maximum pile von Mises stresses

The maximum pile von Mises stress was generated near the loading point at the center of the pile cap, as can be seen in Figure-127. Table-63 indicates the magnitudes of such stress for all soil conditions considered in the study. The generated maximum stresses for all soil conditions were almost the same, with the difference being within 3%.

The relationship between the maximum pile von Mises stress and the applied horizontal load is shown in Figure-128. The maximum pile von Mises stress was directly proportional to the applied load. It is clearly seen that almost identical stresses were generated for all layered soil conditions.

5.3.4.2 Suction piles with group-II soil conditions

Group-II includes four different layered soil conditions, namely, Layered Soil-5, 6, 7, and 8 as defined in Figure-68. Layered Soil-5 represents the soil stratum consisting of only the sandy soil. Layered Soil-6, 7, and 8 represent the soil strata having the thickness of the upper weak clayey soil layer of 7.5, 15.0, and 22.5 ft, respectively.

1) Pile displacements

The maximum total and horizontal pile displacements due to various horizontal loads applied at the center of the pile cap always occurred at the top of the pile along the loading direction, whereas the minimum pile displacement occurred at the bottom of the pile. Figure-129 shows one such example output. The pile was experiencing horizontal translational movements as well as rotational movements as expected. Larger maximum displacements under various horizontal loads were observed with the increase in the thickness of the upper weak clay layer, as shown in Tables-64 and 65. The effect of the thickness of the upper weak clay layer became very much pronounced at relatively larger horizontal loads.

Figures-130 and 131 show typical load vs. displacement behaviors under various horizontal loads. Both the maximum total and horizontal pile displacements associated with the thickness of the upper weak soil layer show a similar pattern against the applied horizontal load. As the horizontal load increased, the displacements showed a nonlinear behavior. The variations of the curves are hyperbolic shaped, gradually approaching the

ultimate values. The suction pile in the soil condition with the thickest upper weak soil layer generated the largest displacements as expected.

2) Minimum soil minor principal stresses

The minimum soil minor principal stress at any given horizontal load was always generated within the lower two thirds of the lower strong soil layer on the advancing side of the pile as expected. Relatively larger minimum soil principal stresses were also observed within the sand layer near the toe of the pile due to the rotational movement of the pile along the loading direction. The soil near the top of the receding side of the pile experienced relatively small tensile stress as shown in Figure-132. The calculated minimum soil minor principal stresses associated with different layered soil conditions are shown in Table-66. Different initial geostatic stress conditions were due to the different soil layer conditions. The elastic behaviors were completely overcome at the horizontal load of 2,000,000 lbs for Layered Soil-5 and 6, and 1,000,000 lbs for Layered Soil-7 and 8 (Figure-133). For a given load, the minimum soil minor principal stress increased with the increase in the thickness of the upper weak soil layer after the geostatic stresses were overcome.

It is clearly seen from the figure that the suction pile in the layered soil condition with the thickest upper weak soil layer generated the largest minimum soil minor principal stress at a given load. Once the elastic behaviors were overcome, the stresses varied rapidly with a nonlinear variation. The difference in minimum soil minor principal stresses for a given load increased with the increase in load.

3) Maximum pile von Mises stresses

The maximum pile von Mises stress was generated near the loading point at the center of the pile cap as can be seen in Figures-134. Relatively larger stresses generated near the toe and heel of the pile were due to the strong reaction from the lower strong sandy soil. Table-67 indicates the magnitudes of such stress for all soil conditions considered in the study. For a given load, almost identical stresses were generated, as was observed previously.

The relationship between the maximum pile von Mises stress and the applied horizontal load is shown in Figure-135. The maximum pile von Mises stress was directly proportional to the applied load.

5.3.4.3. Additional results

The appendix of this report (figure numbers starting with "G") includes some of the typical results from the finite element analyses of suction piles with layered soil conditions under various horizontal loads. The results include: (1) soil displacements, (2) soil displacements on a vertical plane, (3) pile displacements, (4) soil minor principal stresses on a vertical plane, (5) soil minor principal stresses on the pile surface, and (6) pile von Mises stress on the pile surface.

5.4 Summary

5.4.1 General conclusions

In general, the horizontal pile displacement due to the horizontal and 45-degree inclined loads varies almost linearly under very low loads but becomes nonlinear under high loads for all conditions considered. The pile experiences translational horizontal movements as well as rotational movements along the loading direction. As the elastic behavior is gradually overcome, the minimum soil minor principal stresses increase with a nonlinear variation due to the effect of the soil plasticity. The maximum pile von Mises stresses vary almost linearly with the increase in loads mainly because the pile is modeled by a linear elastic material. This modeling of the pile material behavior may not be unrealistic, since the calculated pile stresses are much lower than the yield stress even at loads near failure. The general conclusions obtained from the analyses of each parameter are described below.

5.4.1.1 Flange width

In general, the attachment of the flange reduces the displacements of the pile in both sand and clay resulting from the load applied at the center of the pile cap. The wider the flange width, the smaller the displacement. The minimum soil minor principal stress is generated within the soil beneath the outer edge of the flange of the advancing side of the pile in sand, whereas the minimum soil stress is observed under the toe of the pile in clay. The attachment of the flange also reduces the minimum soil minor principal stress in both sand and clay. The minimum soil stress of the sand for a given load decreases with the increase in flange width. The maximum pile von Mises stress due to the load

applied at the center of the pile cap is generated near the loading point. Almost identical stress is observed in the analyses with sand, whereas the largest maximum pile stress is observed with the largest flange width with clay. The capacity of a suction pile embedded in clay is increased by 100% if a 15 ft. wide flange is added on top of the 30 ft. long pile.

5.4.1.2 Loading point

Smallest maximum displacements of the pile in both sand and clay are generated due to the either horizontal or 45-degree inclined load applied at the mid-height of the pile. The largest pile displacement is always observed with the load applied at the center of the pile cap. The difference in maximum displacements due to horizontal loads applied at the mid-height and the toe of the pile is relatively small in the analysis with both clay and sand, whereas the difference in displacements due to the 45-degree inclined loads applied at the center of the pile cap and the toe of the pile is relatively small in the analysis with both sand and clay. The minimum soil minor principal stress due to the applied loads is generated within the soil located at the advancing side of the pile in sand as expected. The smallest minimum soil minor principal stress of both sand and clay due to horizontal loads is associated with the load applied at the mid-height of the pile in general. The smallest minimum soil minor principal stress with sand due to 45-degree inclined loads is associated with the load applied at the mid-height of the pile. However, the smallest stress in analyses with clay is generated due to 45-degree inclined loads applied at the center of the pile cap. These results are in general agreement with previous

studies which indicate that the optimum loading point for horizontal loads is between 1/2 and 2/3 of the pile length from the top. The precise point is approximately near the point where the resulting pile displacement is purely translational.

The maximum pile von Mises stress is generated at the upper half of the pile when the load is applied at the mid-height of the pile and at the lower half of the pile when the load is applied at the toe of the pile. The smallest maximum pile von Mises stress is associated with the horizontal load applied at the center of the pile cap and the 45-degree inclined load at the mid-height of the pile in both analyses with sand and clay. In both clay and sand, pile stresses are approximately doubled when the loading point moves from the top to the mid-height, and again when it moves from the mid-height to the bottom of the pile.

5.4.1.3 Diameter change

In sand, the telescopic pile always generates larger displacements due to horizontal loads applied at the center of the pile cap than the prismatic pile. In clay, the prismatic pile generates slightly larger displacements under smaller loads but much smaller displacements under larger loads than the telescopic pile. However, the difference in displacements is not significant under small loads. The minimum soil minor principal stress of both clay and sand due to horizontal loads is generated within the soil under the edge of the upper half of the telescopic pile along the loading direction. As noted in the previous analyses of standard suction piles, the minimum soil minor principal stress against the horizontal load applied at the center of the pile cap is

generated near the top of the advancing side of the prismatic pile in sand and near the toe of the prismatic pile in clay. Smaller minimum soil minor principal stress is always generated with the prismatic pile under relatively large loads. The maximum pile von Mises stress due to the horizontal load applied at the center of the pile cap is generated near the loading point. Slightly smaller maximum pile von Mises stress due to the applied load is always generated with the telescopic pile.

5.4.1.4 Layered soil condition

The soil condition with the strong soil layer lying above the weak soil layer generates less pile displacements and soil stresses. As the thickness of the upper strong soil layer increases, they decrease further. The soil condition with the weak soil layer lying above the strong soil layer generates the opposite behavior. The minimum soil minor principal stress develops within the strong soil layer. Identical von Mises pile stresses are generated for all soil conditions considered in the study.

5.4.2 Pile failure loads

From the results of the analyses, it is observed that the load vs. displacement behavior of suction piles embedded in clay is almost elasto-perfectly plastic. For suction piles in sand, however, definite failure loads cannot be defined. Instead, the load continuously increases as the pile deformation increases. Therefore, it is concluded that a suction pile embedded in clay will fail when the applied load reaches the ultimate value.

However, a suction pile embedded in sand tends to fail when the pile experiences enough displacements to create an unstable state. These are applicable for horizontal and 45-degree inclined loads applied at any point along the entire length of the pile.

6. CONCLUSIONS

Table-68 shows a summary of the best suction pile cross-sections under various loading conditions and criteria. The results of the finite element analyses have led to the following general conclusions on the performance of suction piles under various conditions. In summary, the circular cross-section provides the best performance when the primary concern is the failure of the soil, i.e., for relatively weak seafloor soil conditions. On the other hand, the Y-shaped cross-section becomes the most efficient against the failure of the pile, i.e., for relatively strong seafloor soil conditions.

6.1 Linear Elastic Analysis

The results of the linear elastic analyses on suction piles indicate that the cross-sectional shape of the pile has a significant effect on the overall performance of the pile. The horizontal pile displacement due to the horizontal load applied at the top of the pile generally decreases with the increase in the face width of the pile. Also the soil and pile stresses increase with the increase in the horizontal displacement. The critical response of the pile under the vertical load is concentrated near the point of loading.

The results of the linear elastic analysis indicate that circle, Y-shape with 1:1 ratio of the branch width vs. length, and triangle cross-sections are the most effective in terms of providing resistance against both horizontal and vertical loads.

6.2 Elasto-Plastic Analysis with Sand

From the results of the finite element analyses with elasto-plastic soil properties, it is evident that the effect of the soil plasticity is highly significant for large load magnitudes. In general, the horizontal pile displacement due to the horizontal or 45-degree inclined loads applied at the center of the pile cap varies almost linearly under very low loads but becomes nonlinear under high loads for all cross-sections considered. The variation is more or less hyperbolic-shaped and approaches to an ultimate value. The vertical pile displacement due to the vertical load applied at the center of the pile cap however exhibits a sudden yielding behavior at displacement of approximately 0.06 ft for all cross-sections considered. The smallest displacement always occurs with the circular cross-section.

The minimum soil minor principal stresses due to the horizontal or 45-degree inclined load applied at the center of the pile cap is dominated by the geostatic stress condition under low loads. As the geostatic stresses are gradually overcome, the minimum soil minor principal stresses develop at the top of the advancing side of the pile. The minimum soil minor principal stresses due to the vertical loads develop within the lower half of the pile. The smallest absolute value of the minimum soil minor principal stress is observed with the circular cross-section under both the horizontal and

45-degree inclined loads. Under vertical loads, all cross-sections produce virtually the same magnitude of stresses, leading to the conclusion that the circular cross-section yields the smallest minimum soil minor principal stress under all loading conditions.

Y-shaped cross-section generates the smallest maximum pile von Mises stress under a given loading situation. This becomes more apparent under the vertical loads. The magnitude of stresses developed within the pile are, however, very small when compared to the yield stress of the pile material. This indicates that the predominant factor governing the suction pile capacity is the failure of the soil, leading to the conclusion that the circular cross-section is the most effective shape of the suction pile.

The vertical pile resistance embedded in sand is much smaller than the lateral resistance. Typically the pile resistance decreases in the order of horizontal, inclined, and vertical.

6.3 Elasto-Plastic Analysis with Clay

In general, the horizontal pile displacement due to the horizontal or 45-degree inclined loads applied at the center of the pile cap varies almost linearly under very low loads but becomes nonlinear under high loads for all cross-sections considered. The variation is hyperbolic-shaped with an ultimate asymptote. The smallest pile displacement due to the horizontal or 45-degree inclined loads occurs with either the circular or the Y-shaped cross-section. On the other hand, the vertical pile displacement due to the vertical load exhibits a sudden yielding behavior at displacement of

approximately 0.6 ft for all cross-sections. The smallest displacement due to the vertical loads occurs always with the circular cross-section.

The minimum soil minor principal stresses due to the horizontal or 45-degree inclined loads applied at the center of the pile cap are dominated by the geostatic stress condition under low loads. As the geostatic stresses are gradually overcome, the minimum soil minor principal stresses due to the horizontal or 45-degree inclined loads develop at the bottom of the advancing side of the pile. This is different from that of sand, where the minimum soil minor principal stresses are observed near the top of the advancing side of the pile. The minimum soil minor principal stresses due to the vertical loads are observed within the lower half of the pile. The smallest minimum soil minor principal stress depends on the direction and magnitude of the load. Under horizontal loads, the circular cross-section yielded the smallest stresses while the triangular cross-section generated the smallest stresses under inclined loads. When vertical loads are applied, the smallest stresses developed with the triangular and Y-shaped cross-section under smaller loads and higher loads, respectively.

The maximum pile von Mises stresses vary almost linearly with the increase in loads. However, the nonlinear variation is observed with the triangular and Y-shaped cross-sections for relatively low vertical and 45-degree inclined loads. The smallest maximum pile von Mises stress is always observed with the Y-shaped cross-section.

6.4 Effects of Additional Parameters

6.4.1 Flange width

The attachment of a flange reduces the displacements of the pile in both sand and clay resulting from the load applied at the center of the pile cap. The wider the flange width is, the smaller the displacement becomes. The minimum soil minor principal stress is generated within the soil beneath the outer edge of the flange of the advancing side of the pile in sand, whereas the minimum soil stress is observed under the toe of the pile in clay. The attachment of a flange also reduces the minimum soil minor principal stress in both sand and clay. The minimum soil stress of the sand for a given load decreases with the increase in flange width.

The maximum pile von Mises stress due to the load applied at the center of the pile cap is generated near the loading point. Almost identical stress is observed in the analyses with sand, whereas the largest maximum pile stress is observed with the largest flange width with clay. The capacity of a suction pile embedded in clay is increased by 100% if a 15 ft. wide flange is added on top of the 30 ft. long pile.

6.4.2 Loading point

The smallest maximum displacements of the pile in both sand and clay are generated due to the either horizontal or 45-degree inclined load applied at the mid-height of the pile. The largest pile displacement is always observed with the load applied at the center of the pile cap. The difference in maximum displacements due to horizontal loads applied at the mid-height and the toe of the pile is relatively small in the analysis with both clay and sand, whereas the difference in displacements due to the 45-degree inclined

loads applied at the center of the pile cap and the toe of the pile is relatively small in the analysis with both sand and clay.

The minimum soil minor principal stress due to the applied loads is generated within the soil located at the advancing side of the pile in sand. The smallest minimum soil minor principal stress of both sand and clay due to horizontal loads is associated with the load applied at the mid-height of the pile. The smallest minimum soil minor principal stress with sand due to 45-degree inclined loads is associated with the load applied at the mid-height of the pile. The smallest stress in analyses with clay is, however, generated with the 45-degree inclined loads applied at the center of the pile cap.

The maximum pile von Mises stress is generated at the upper half of the pile when the load is applied at the mid-height of the pile and at the lower half of the pile when the load is applied at the toe of the pile. The smallest maximum pile von Mises stress is associated with the horizontal load applied at the center of the pile cap and the 45-degree inclined load at the mid-height of the pile in both analyses with sand and clay. In both clay and sand, pile stresses are approximately doubled when the loading point moves from the top to the mid-height, and again when it moves from the mid-height to the bottom of the pile.

6.4.3 Diameter change

In sand, the telescopic pile generates larger displacements due to horizontal loads applied at the center of the pile cap than the prismatic pile. In clay, the prismatic pile generates slightly larger displacements under smaller loads but much smaller

displacements under larger loads than the telescopic pile. However, the difference in displacements is not significant under small loads.

The minimum soil minor principal stress of both clay and sand due to horizontal loads is generated within the soil under the edge of the upper half of the telescopic pile along the loading direction. It is noted that the minimum soil minor principal stress against the horizontal load applied at the center of the pile cap is generated near the top of the advancing side of the prismatic pile in sand and near the toe of the prismatic pile in clay. Smaller minimum soil minor principal stress is always generated with the prismatic pile under relatively large loads.

The maximum pile von Mises stress due to the horizontal load applied at the center of the pile cap is generated near the loading point. Slightly smaller maximum pile von Mises stress due to the applied load is always generated with the telescopic pile.

6.4.4 Layered soil condition

The soil condition with the strong soil layer lying above the weak soil layer generates less pile displacements and soil stresses. As the thickness of the upper strong soil layer increases, they decrease further. The soil condition with the weak soil layer lying above the strong soil layer generates the opposite behavior. The minimum soil minor principal stress develops within the strong soil layer.

7. REFERENCES

1) ABAQUS/Standard User's Manual, Version 5.7, Hibbit, Karlsson & Sorensen, Inc., 1998.

2) Anderson, K.H., R. Dyvik, and K. Schroder, "Pullout Capacity Analysis of Suction Anchors for Tension Leg Platforms," Boss-92, Vol.2, pp 1311-1322, 1992.

3) Atkinson, J.H. and P.L. Bransby, *The Mechanics of Soils*, MaGRAW-HILL, London, 1978.

4) Bang, S. and H. Kim, "Passive Lateral Earth Pressure Development behind Rigid Wall," Transportation Research Record 1129, pp 66-67, 1988.

5) FEMAP User's Manual, version 4.5.1, Enterprise Software Products, Inc., 1997.

6) Iskander, M.G., R. E. Olsen, and R. W. Pavlicek, "Behavior of Suction Piles in Sand," (ASCE) Design and Performance of Deep Foundations: Piles and Piers in Soil and Soft Rock, Geotechnical Special Publication No. 38, 1993.

7) Lade, P.V. and K.L. Lee, "Engineering Properties of Soils," UCLA Report No., UCLA-ENG-7652, May, 1976.

8) Shugar, T.A., "Numerical Modeling of Steady-State Plow/Soil Interaction," Technical Report TR-2081-SHR, Naval Facilities Engineering Service Center, August 1997.

9) Taylor, R.J., "Drag Embedded Anchor Tests in Sand and Mud," TN N-1635, Naval Civil Engineering Laboratory, Port Huenemo, CA, June, 1982

FIGURES AND TABLES

Figure - 1 Selected Cross-sectional Shapes of Pile

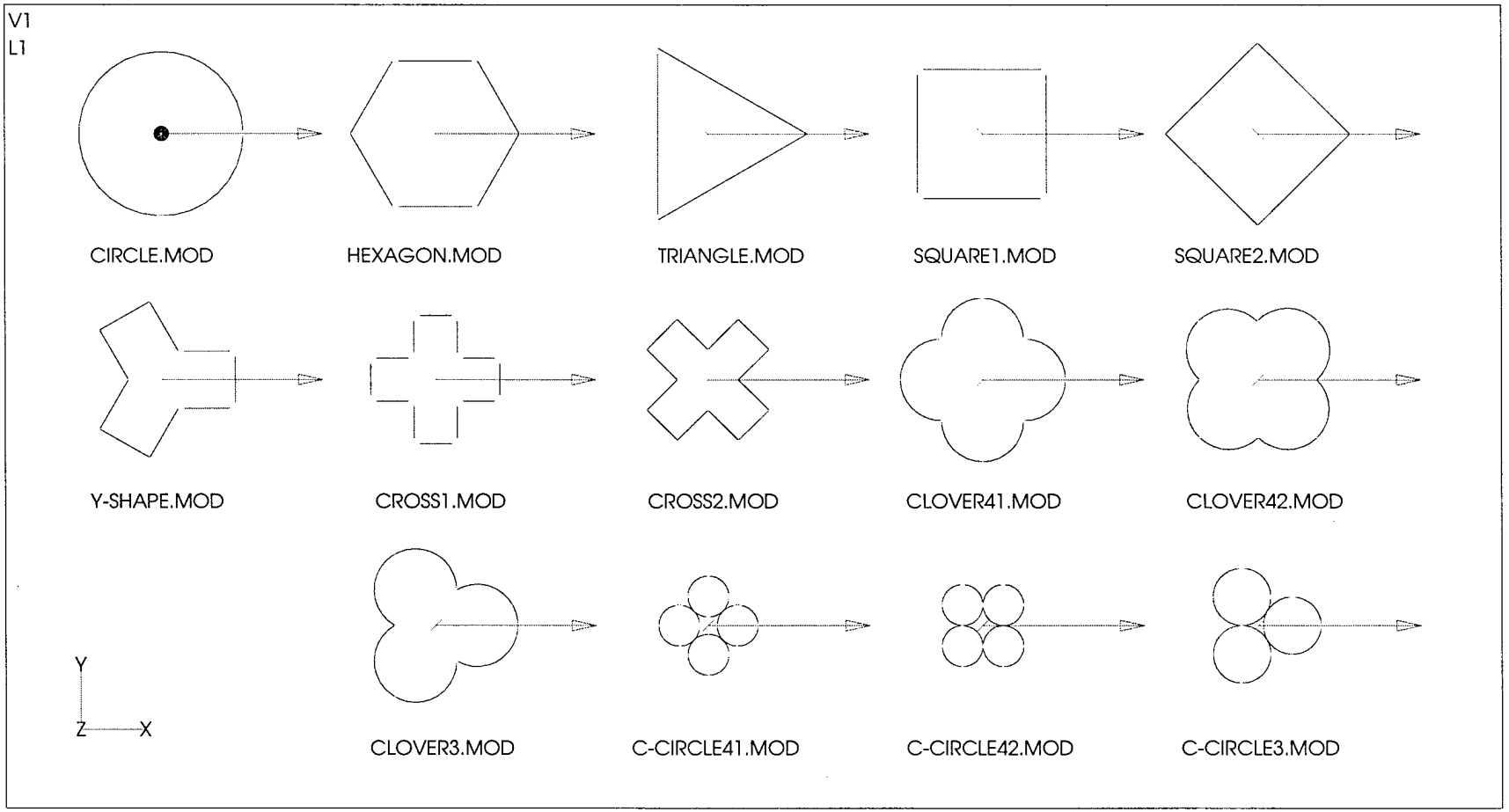

Figure 2. Nodal Arrangement of Circular Pile

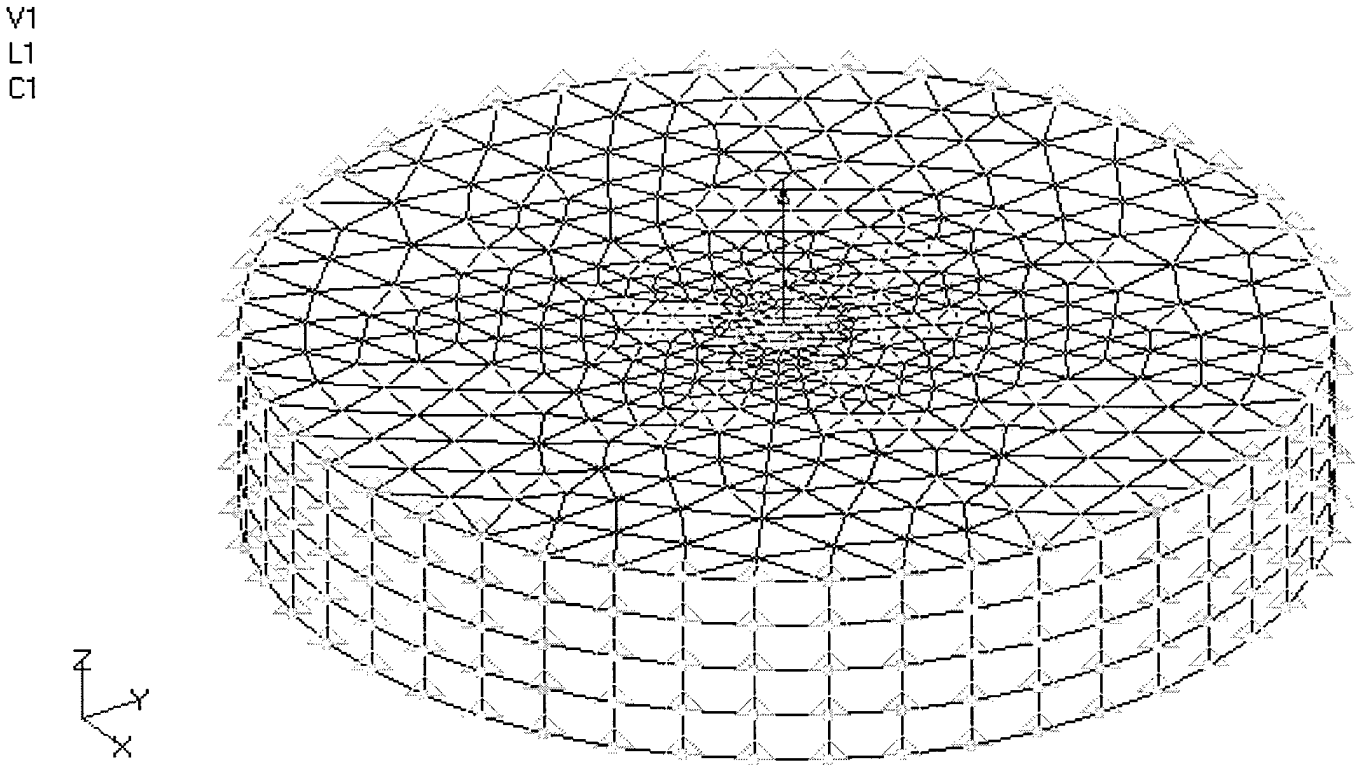

Figure - 3 Definition of Pile Cross-Section Dimensions

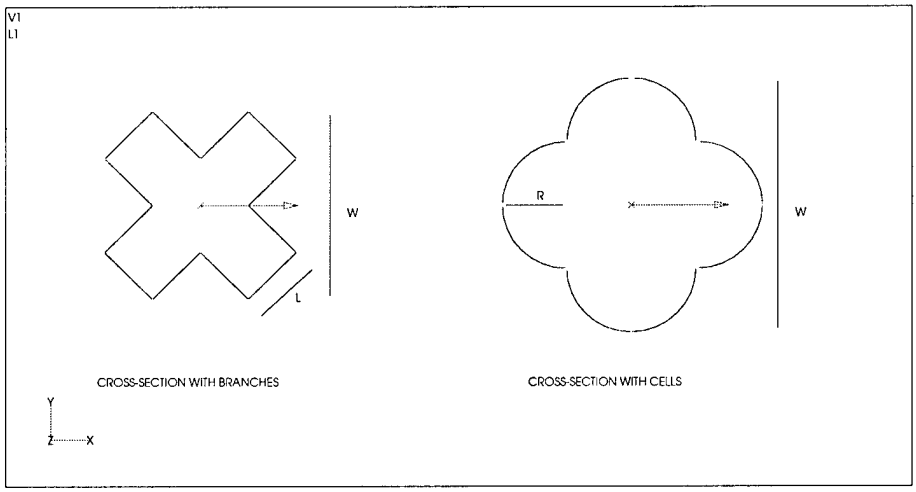

Note;

1. L = constant width of the pile cell
2. W = face width or largest width of the pile
3. R = radius of circular cell

Figure 4. X-directional Displacement of Soil for Circular Pile

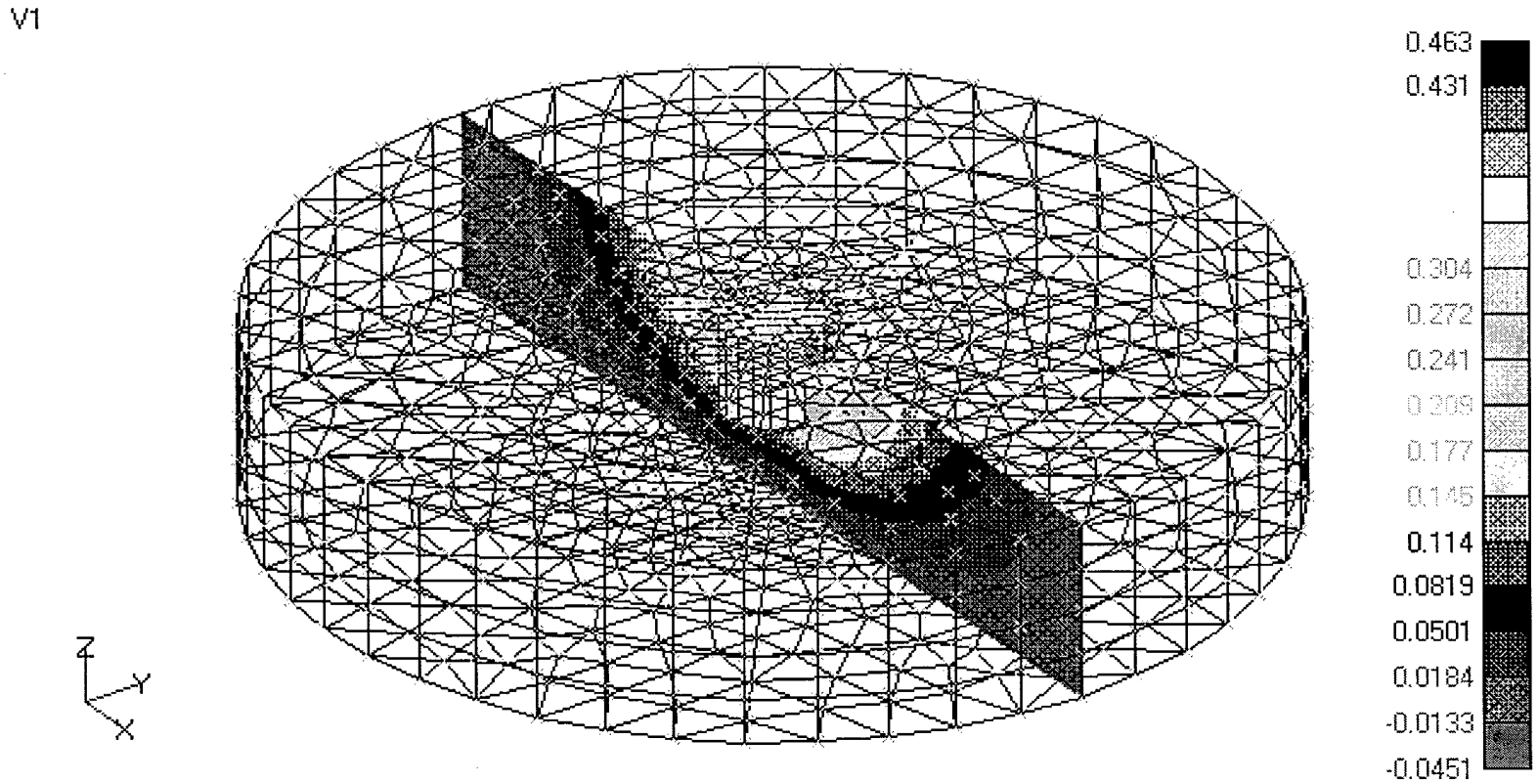

Horizontal Load = 300,000 lbs
Linear Elastic Soil, E = 5,000psf, $\nu = 0.499$
AISI 4340 Steel Pile

Figure 5. X-directional Displacements of Pile for Circular Pile

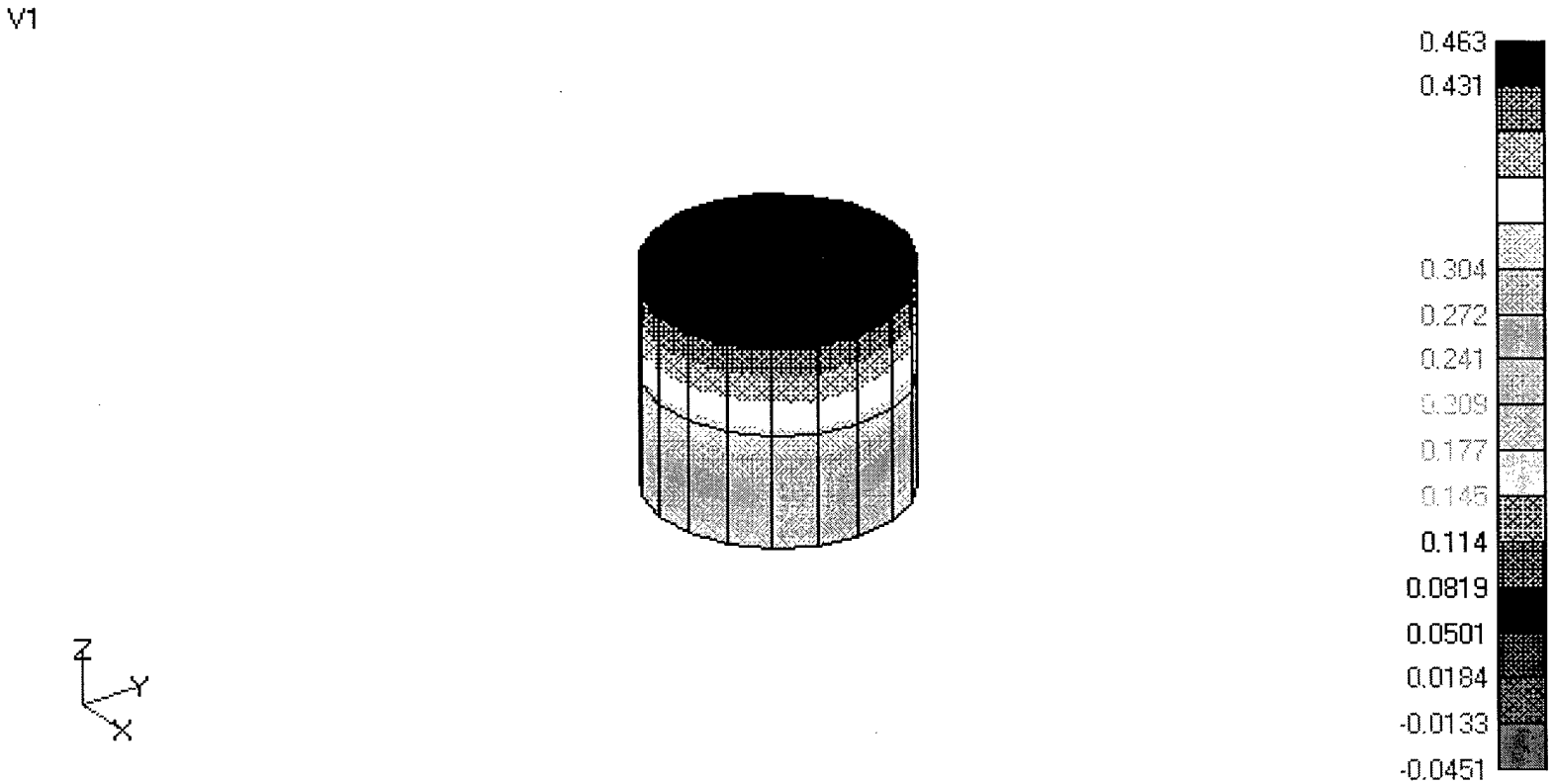

Horizontal Load = 300,000 lbs
Linear Elastic Soil, E = 5,000psf, $\nu = 0.499$
AISI 4340 Steel Pile

Figure - 6. Face Width of Pile vs. Maximum Horizontal Displacement

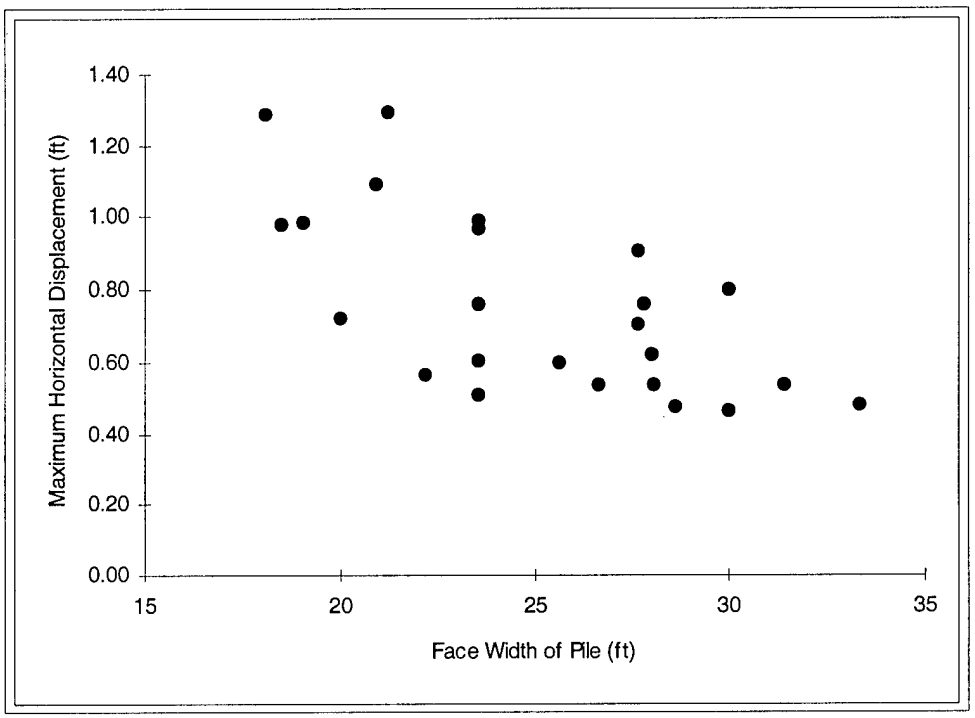

Figure - 7 Maximum Horizontal Normal Soil Compressive Stress vs. Maximum Horizontal Soil Displacement

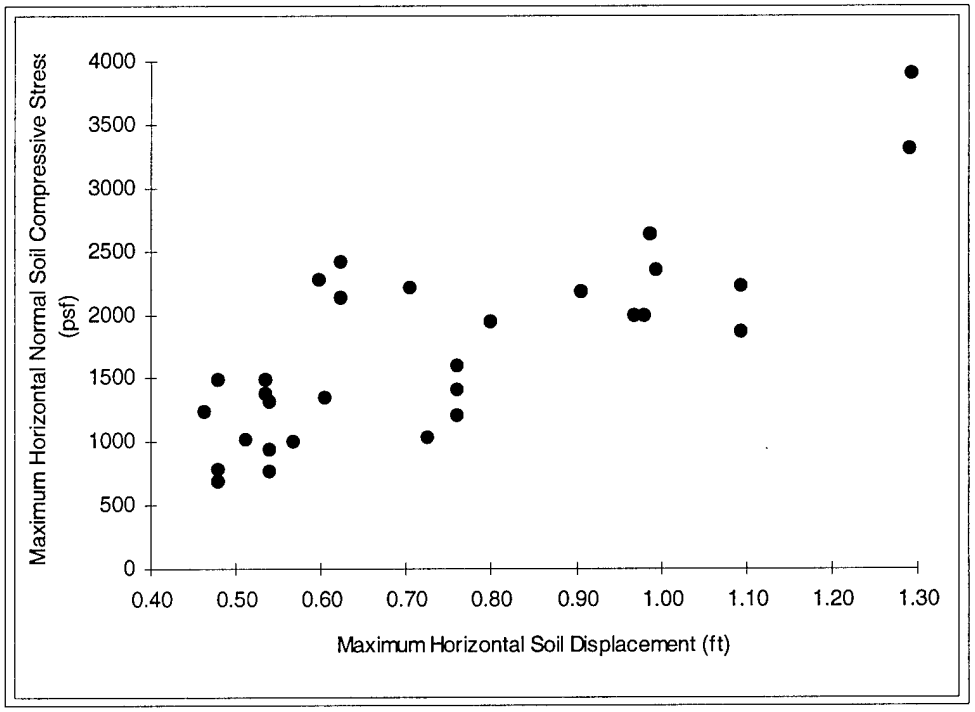

Figure - 8 Minimum Soil Minor Principal Stress vs. Maximum Horizontal Soil Displacement

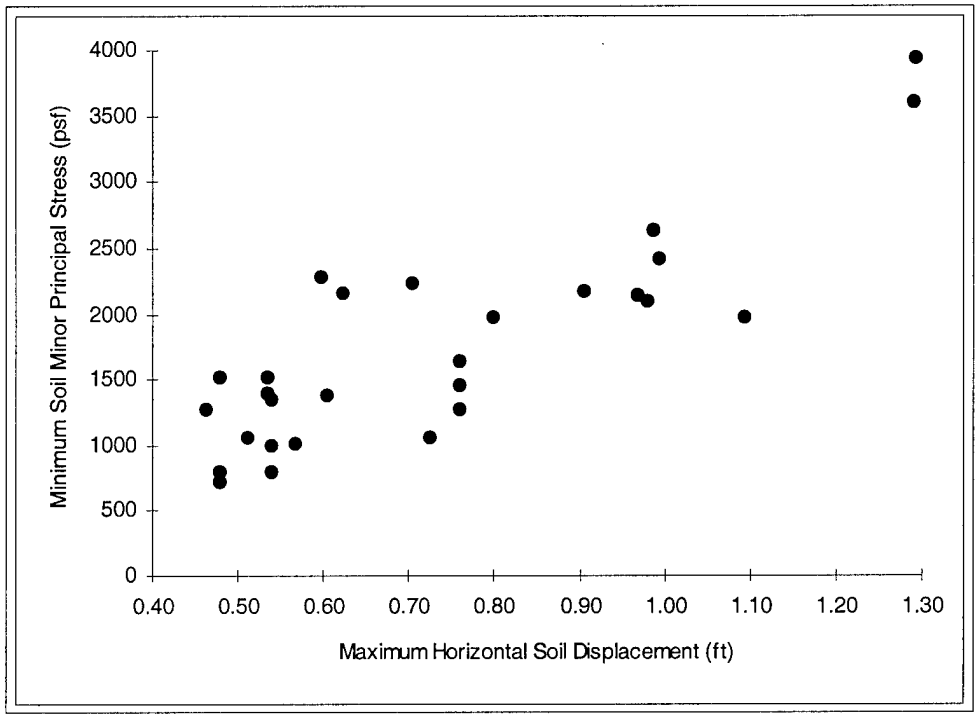

Figure - 9 Maximum Horizontal Normal Pile Tensile Stresses vs. Maximum Horizontal Pile Displacement

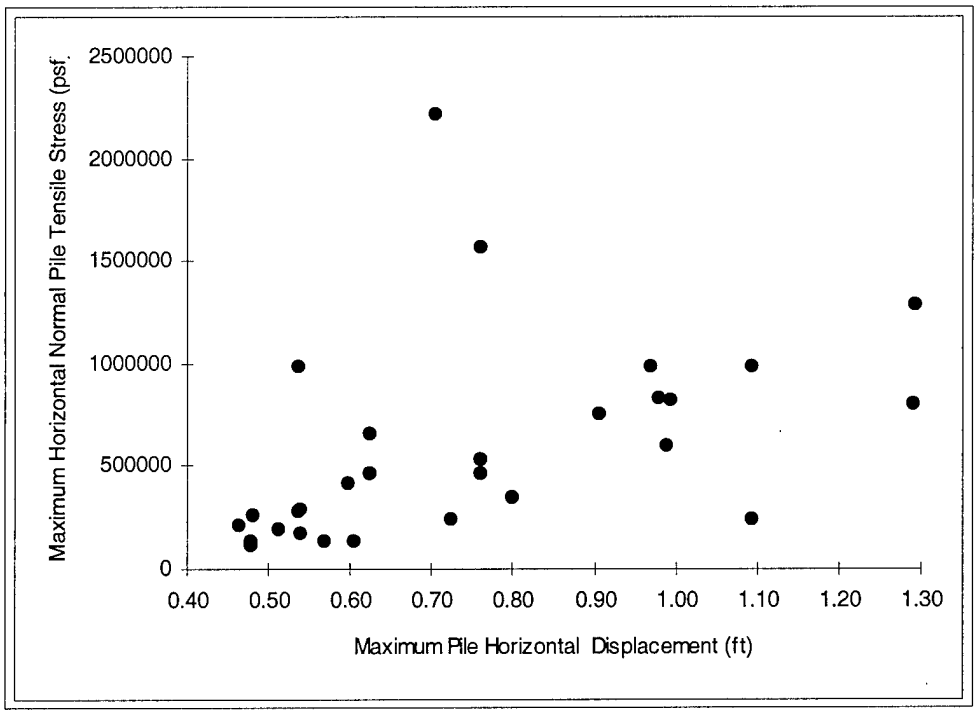

Figure - 10 Maximum Pile Major Principal Stress vs. Maximum Pile Horizontal Displacement

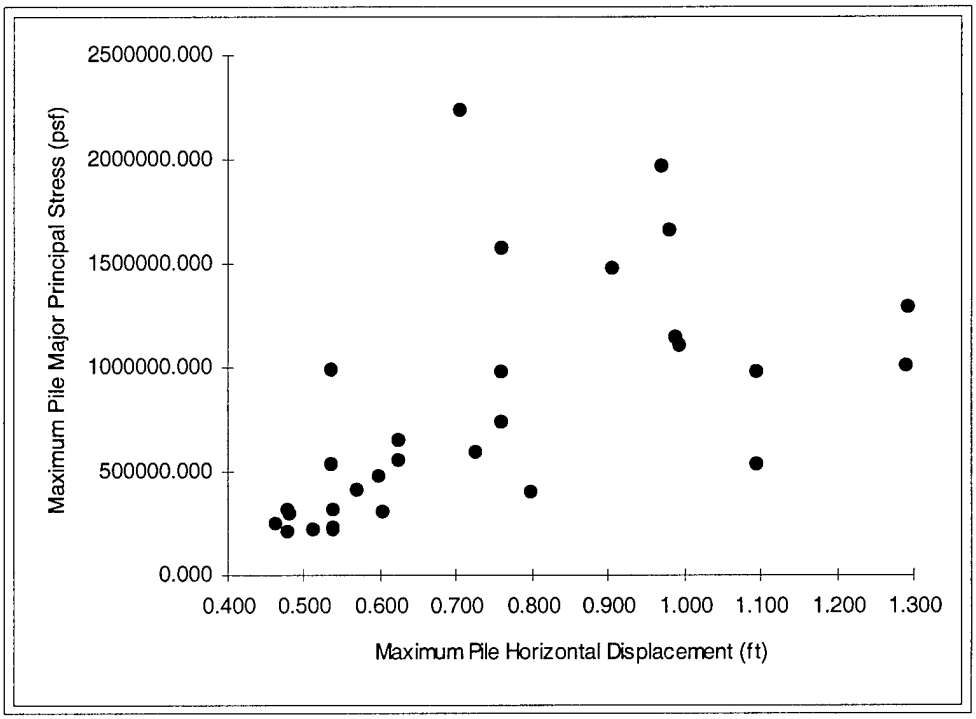

Figure - 11 Maximum Horizontal Pile Tensile Stress vs. Maximum Horizontal Normal Soil Compressive Stress

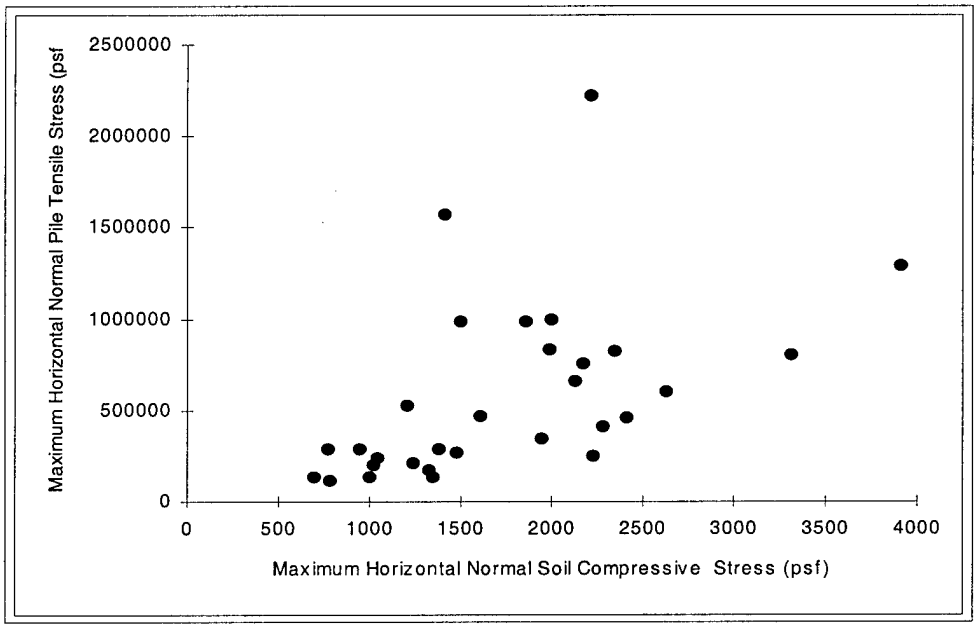

Figure - 12 Maximum Pile Major Principal Stress vs. Minimum Soil Minor Principal Stress

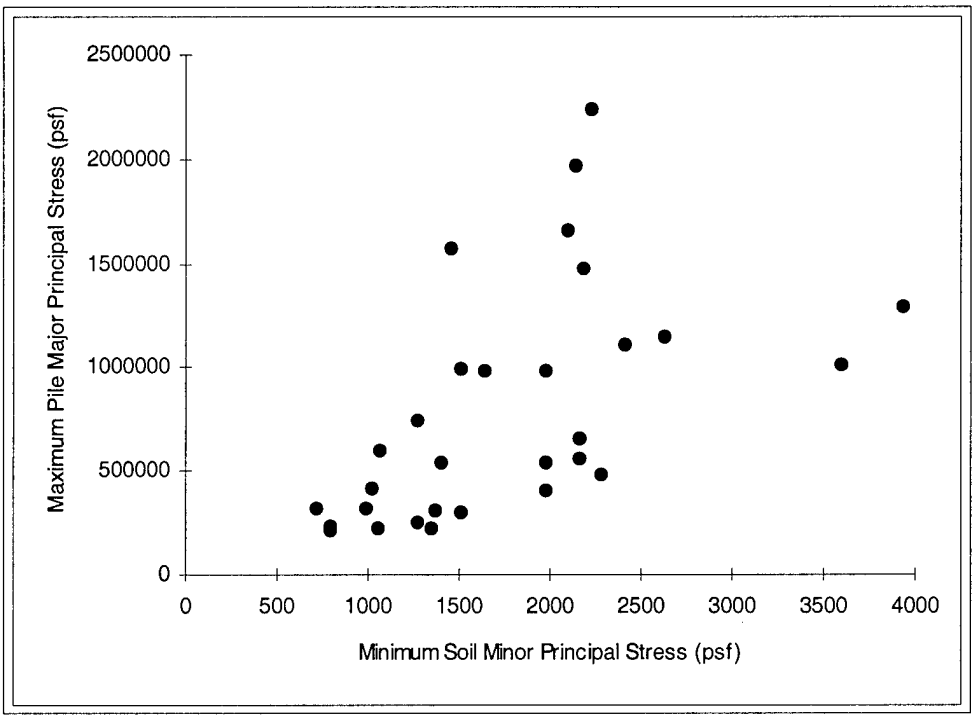

Figure 13. Vertical Displacements of Pile for Circular Pile

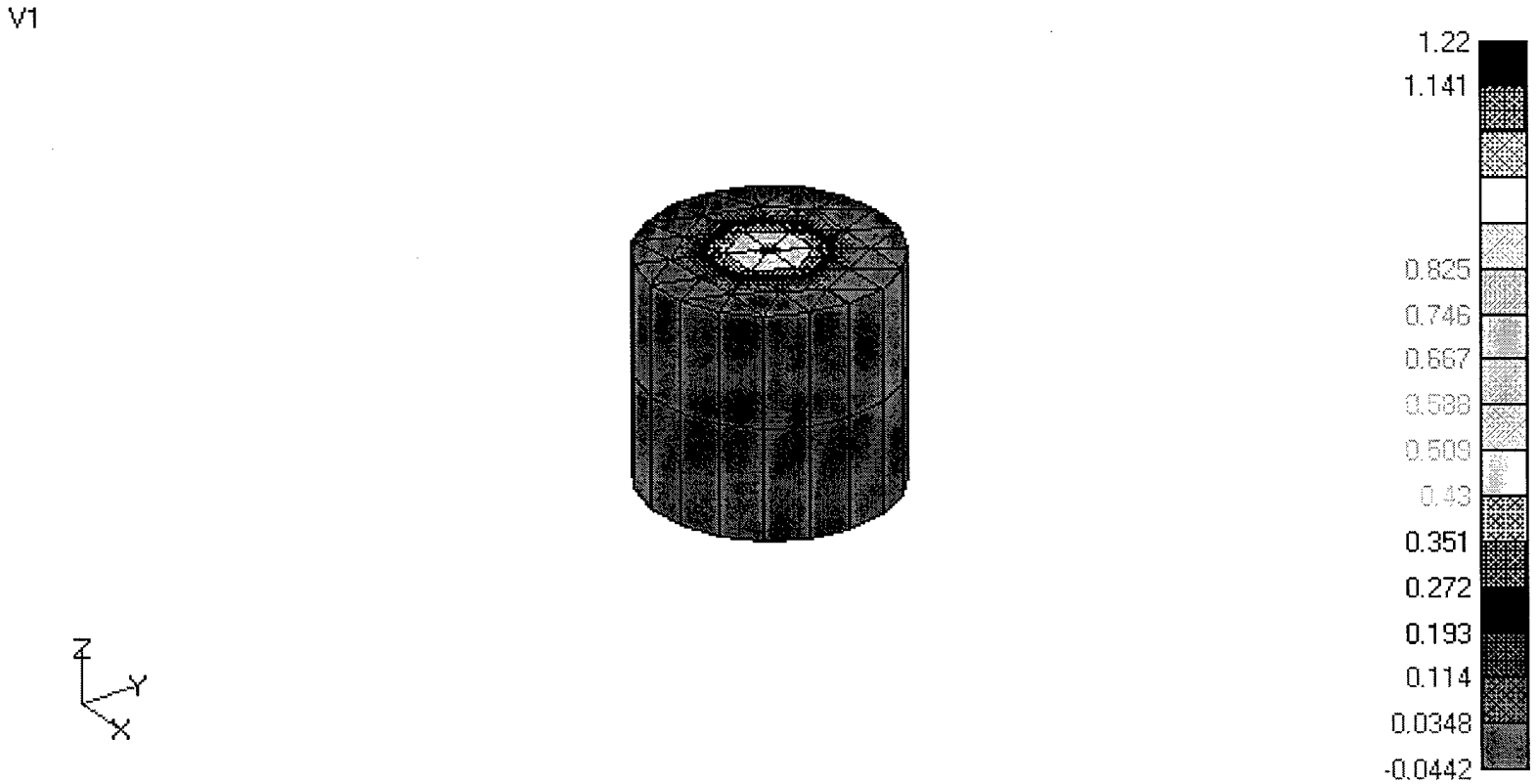

Vertical Load = 300,000 lbs
Linear Elastic Soil, E = 5,000psf, $\nu = 0.499$
AISI 4340 Steel Pile

Figure - 14 Cross Sectional Profiles

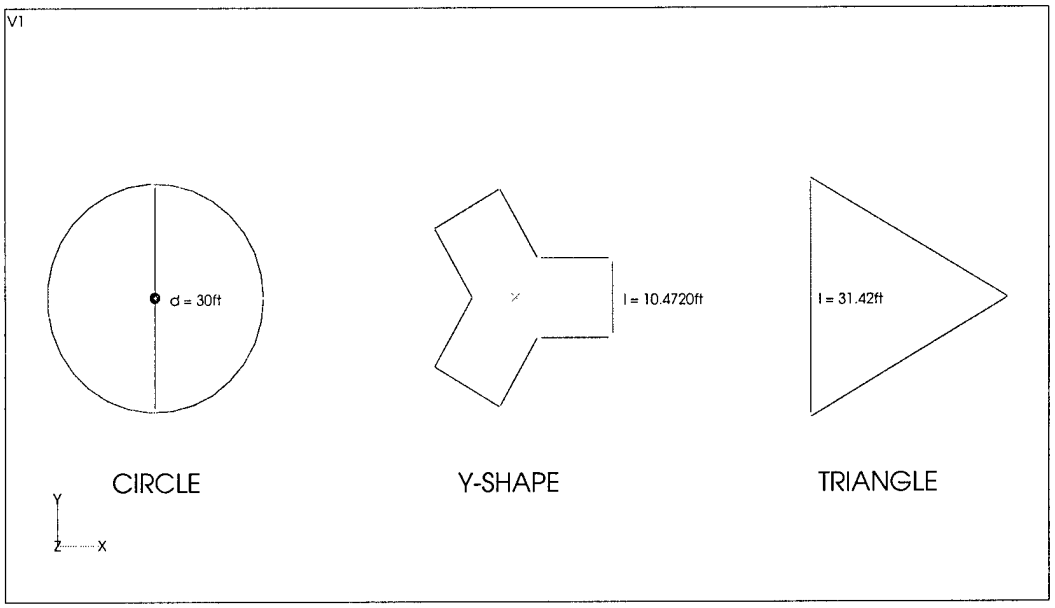

Note; 1. d indicates the diameter of circle.
2. l represents the length of a edge of the cells in Y-shape and a edge in triangle.

Figure - 15 Horizontal Soil Normal Stresses vs. Horizontal Load for Circular Cross-Section

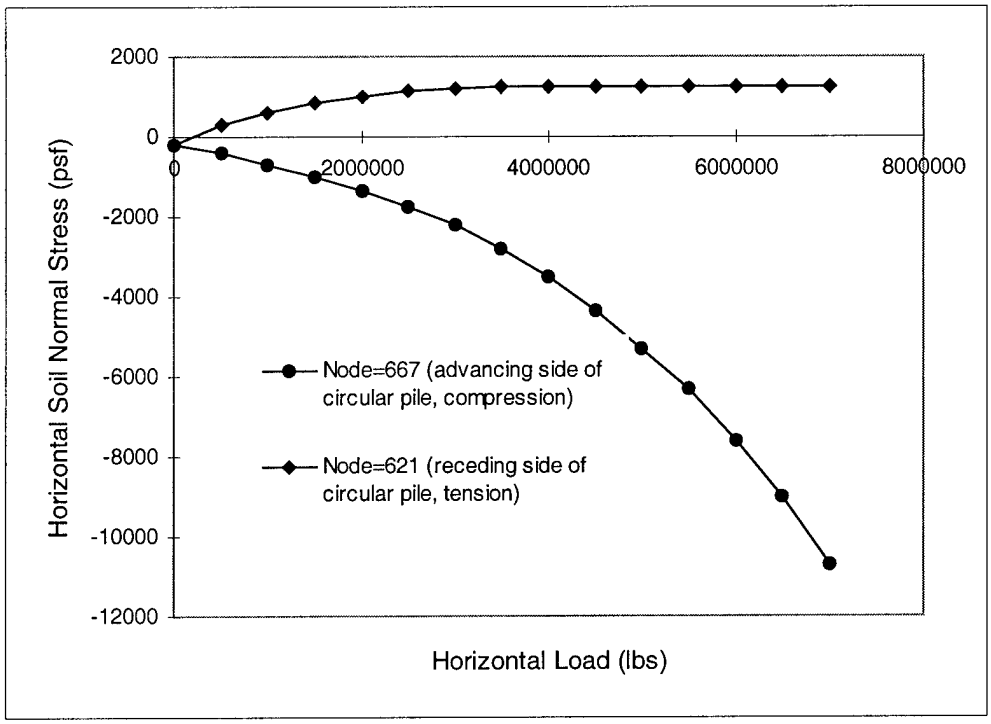

Figure - 16 Pile Total Displacements for Circular Pile

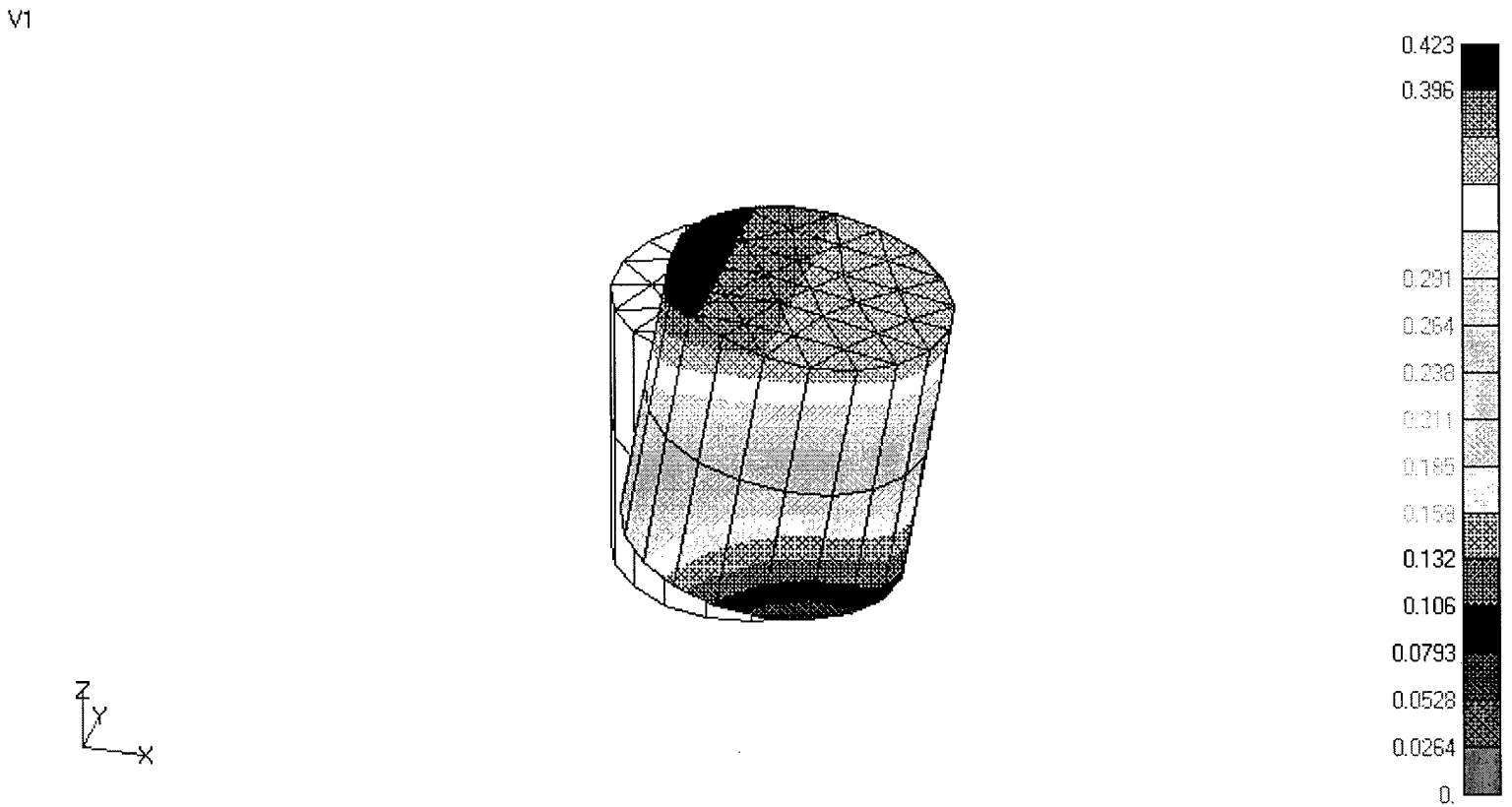

Horizontal Load = 7,000,000 lbs
Linear Elastic-Perfectly Plastic Sandy Soil (Linear Extended Drucker-Prager)
E = 864,000 psf, $\upsilon = 0.3$, Slope Angle = 42.6°, Dilation Angle = 21.5°
Pile, AISI 4340 Steel

Figure - 17 Horizontal Load vs. Maximum Total Pile Displacements

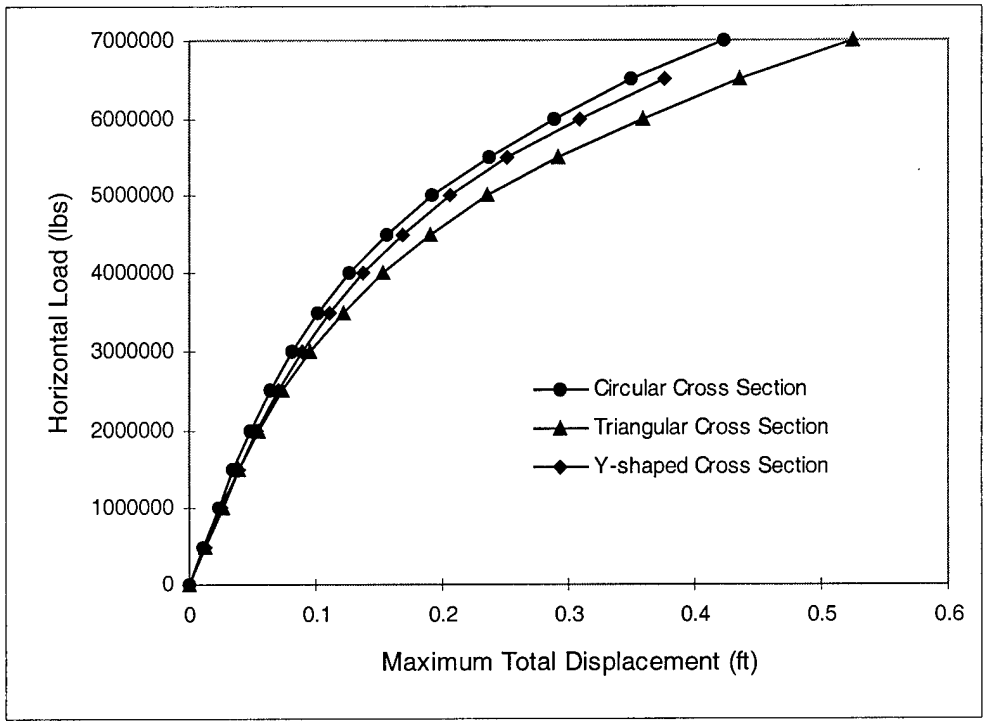

Figure - 18 Relationship of Horizontal Loads vs. Maximum Horizontal Pile Displacements

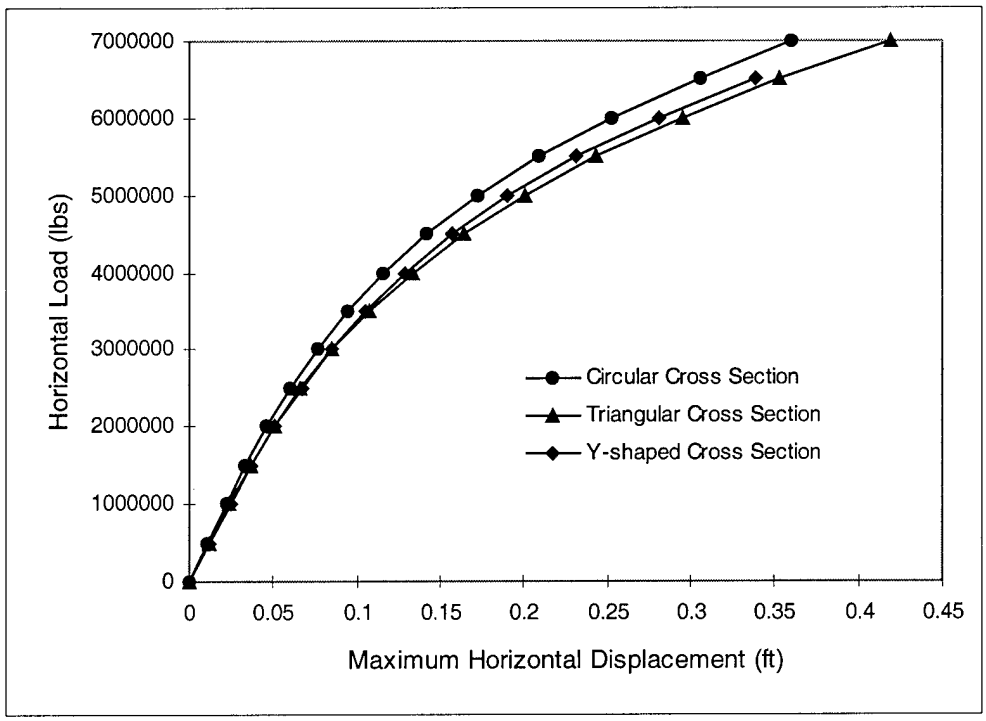

Figure - 19 Soil Minor Principal Stresses on a Vertical Plane along Load Direction for Circular Pile

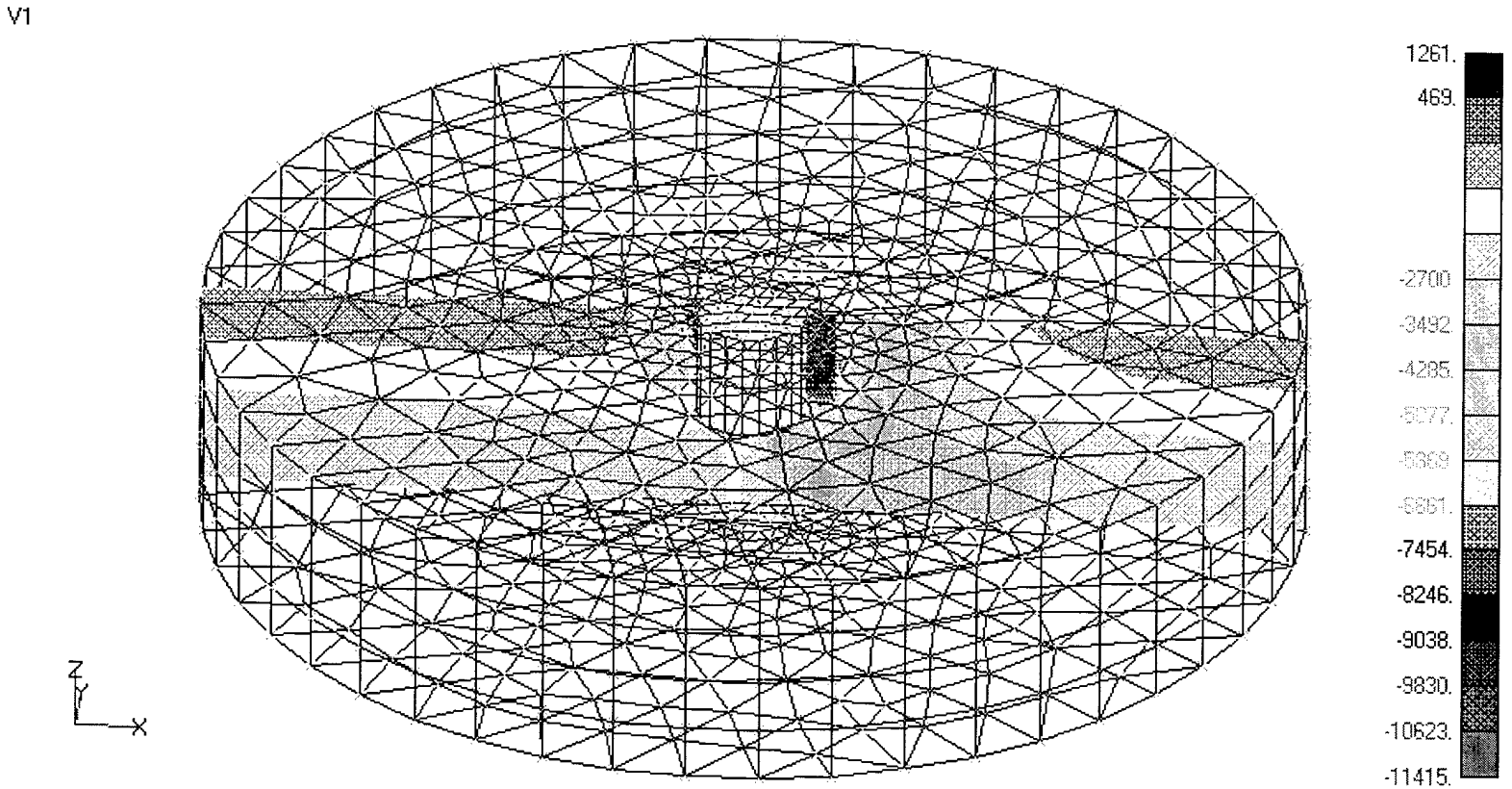

Horizontal Load = 7,000,000 lbs
Linear Elastic-Perfectly Plastic Sandy Soil (Linear Extended Drucker-Prager)
E = 864,000 psf, υ = 0.3, Slope Angle = 42.6°, Dilation Angle = 21.5°
Pile, AISI 4340 Steel

Figure - 20 Minimum Soil Minor Principal Stress vs. Horizontal Load

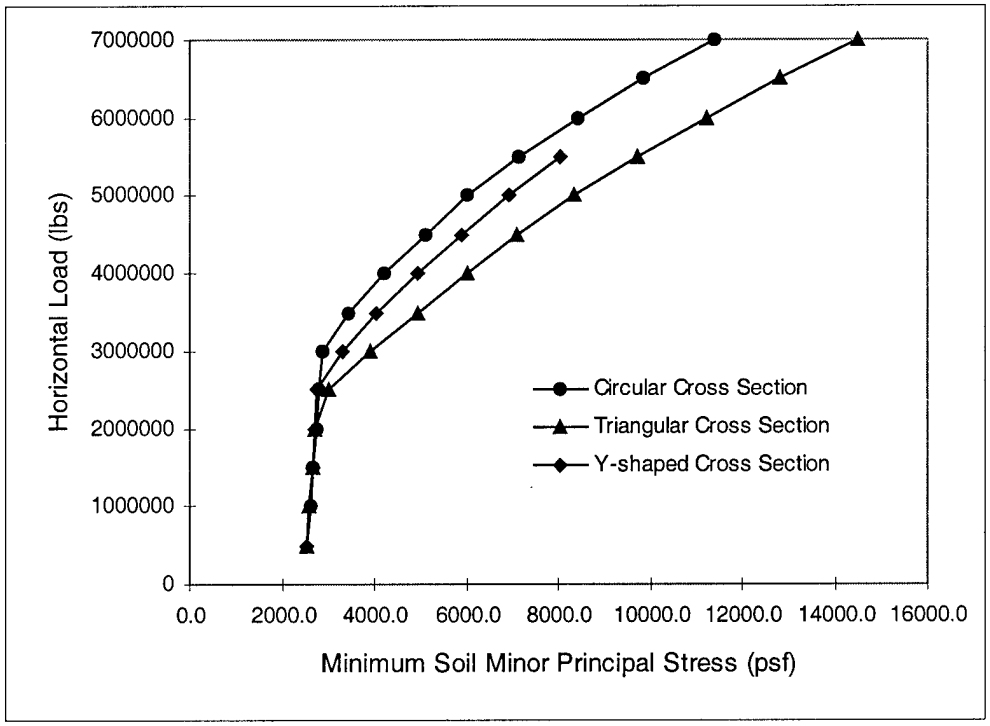

Figure - 21 Pile von Mises Stresses on the Pile Surface for Circular Pile

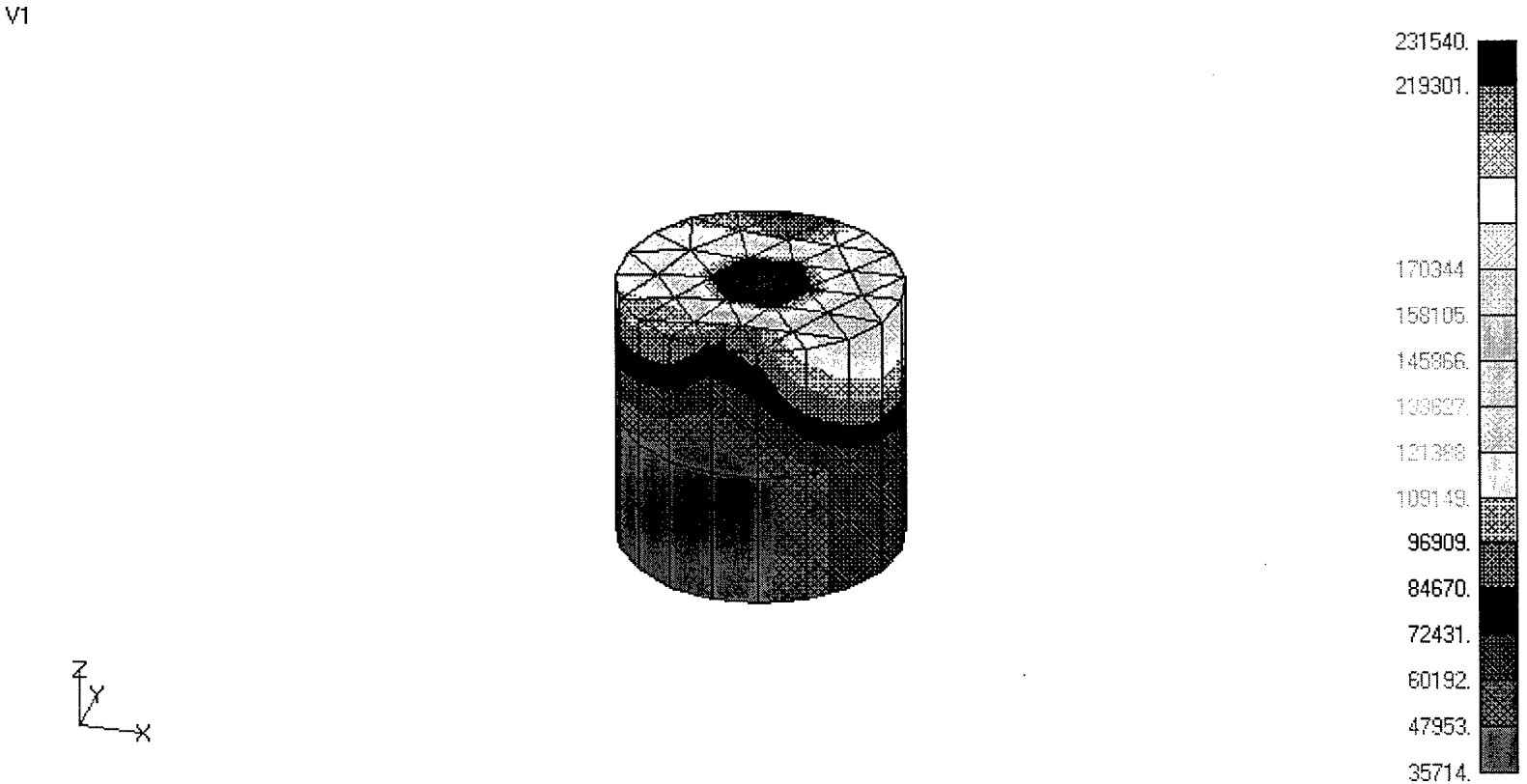

Horizontal Load = 7,000,000 lbs
Linear Elastic-Perfectly Plastic Sandy Soil (Linear Extended Drucker-Prager)
E = 864,000 psf, $\upsilon = 0.3$, Slope Angle = 42.6°, Dilation Angle = 21.5°
Pile, AISI 4340 Steel

Figure – 22 Maximum Pile von Mises Stress vs. Horizontal Load

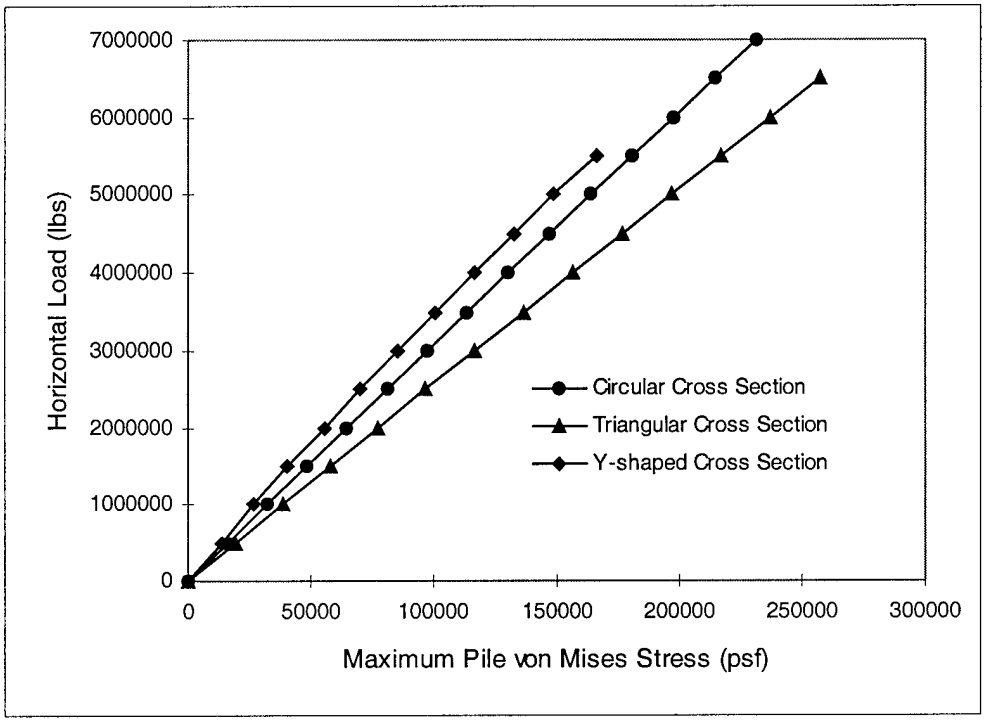

Figure - 23 Minimum Soil Minor Principal Stress vs. Maximum Total Displacement due to Horizontal Load

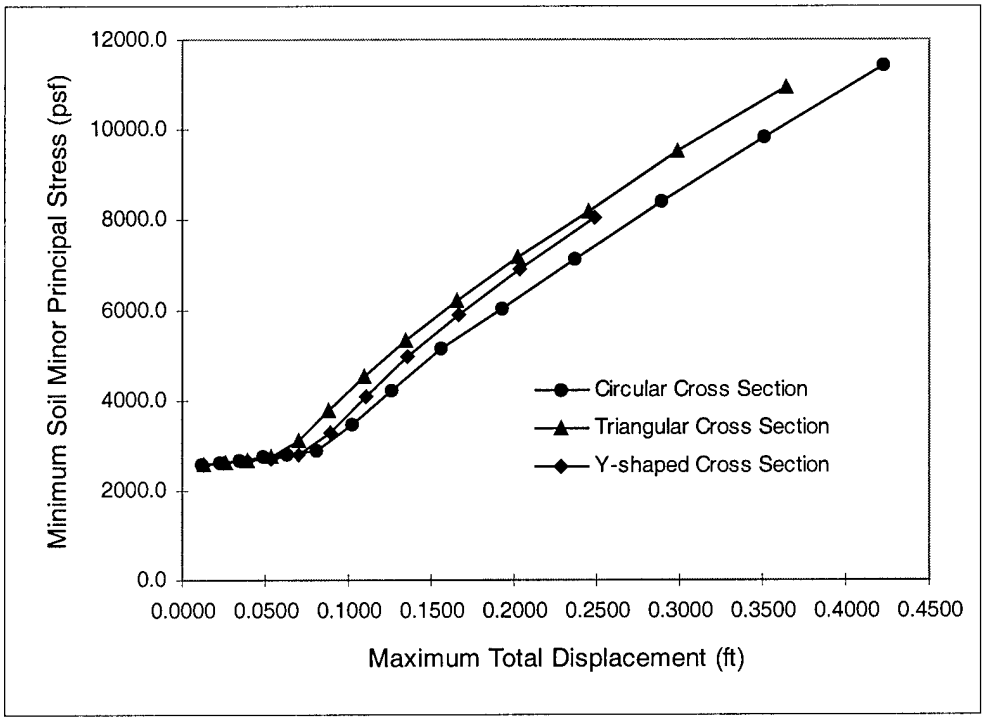

Figure - 24 Maximum Pile von Mises Stress vs. Maximum Horizontal Displacement due to Horizontal Load

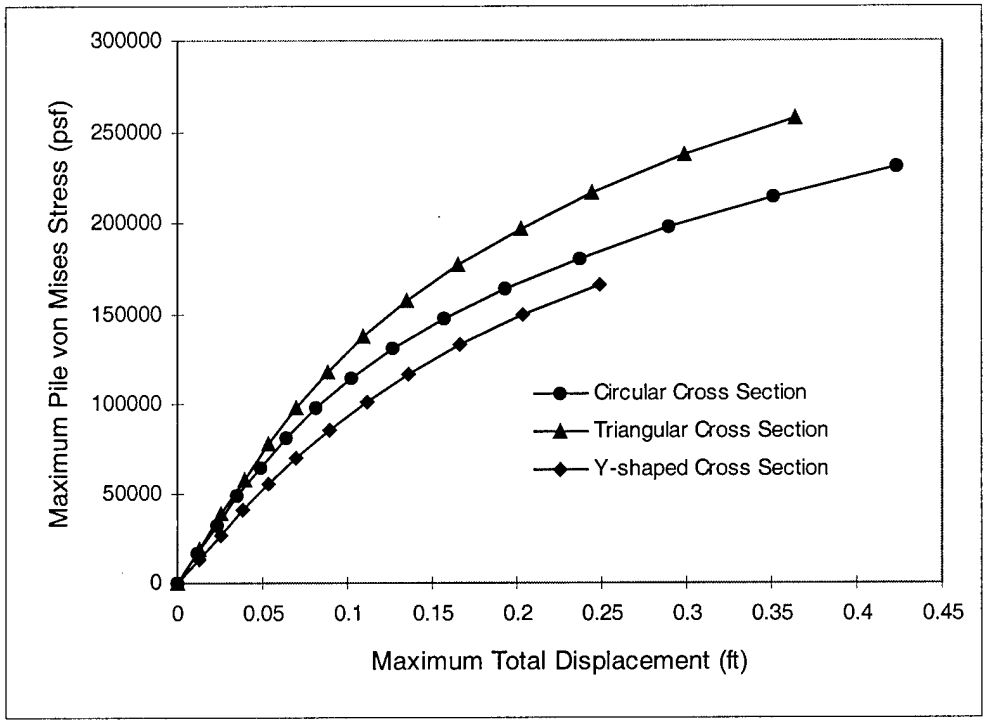

Figure - 25 Pile Total Displacements for Circular Pile

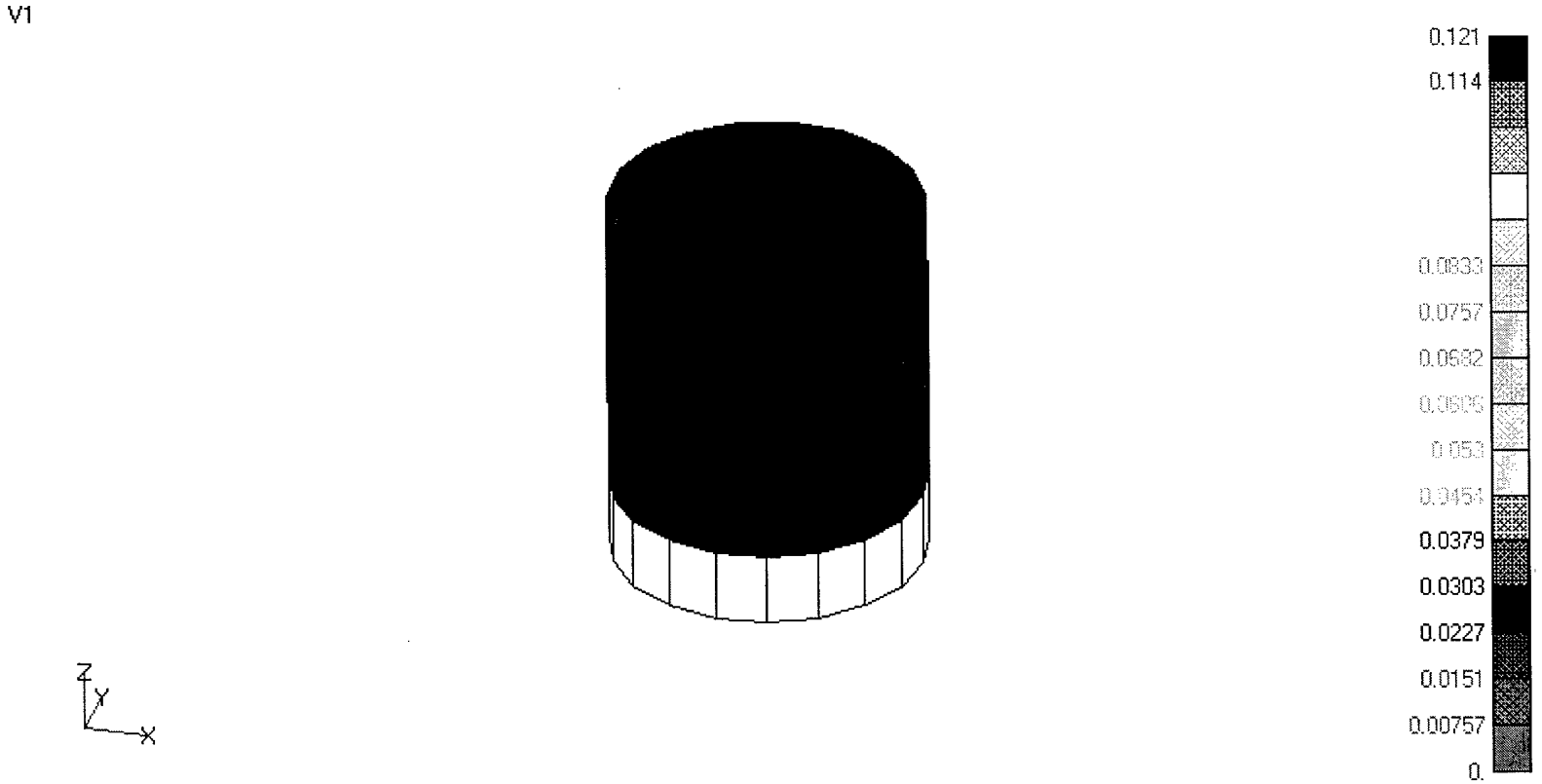

Vertical Load = 7,000,000 lbs
Linear Elastic-Perfectly Plastic Sandy Soil (Linear Extended Drucker-Prager)
E = 864,000 psf, $\upsilon = 0.3$, Slope Angle = 42.6°, Dilation Angle = 21.5°
Pile, AISI 4340 Steel

Figure - 26 Maximum Vertical Displacement vs. Vertical Load

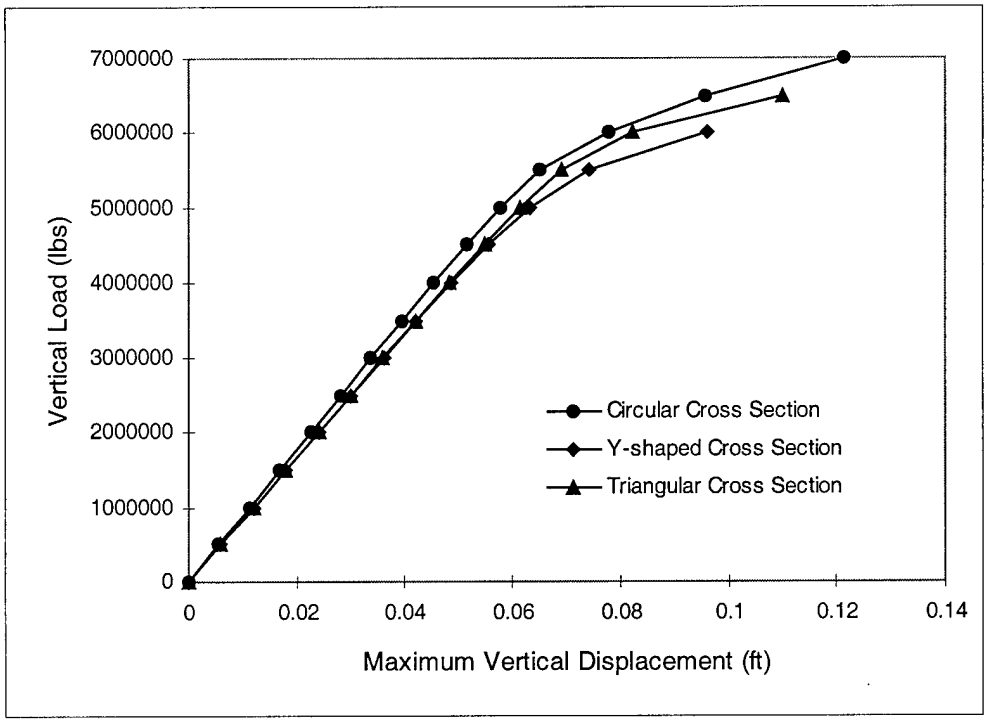

Figure - 27 Soil Minor Principal Stresses on a Vertical Plane for Circular Pile

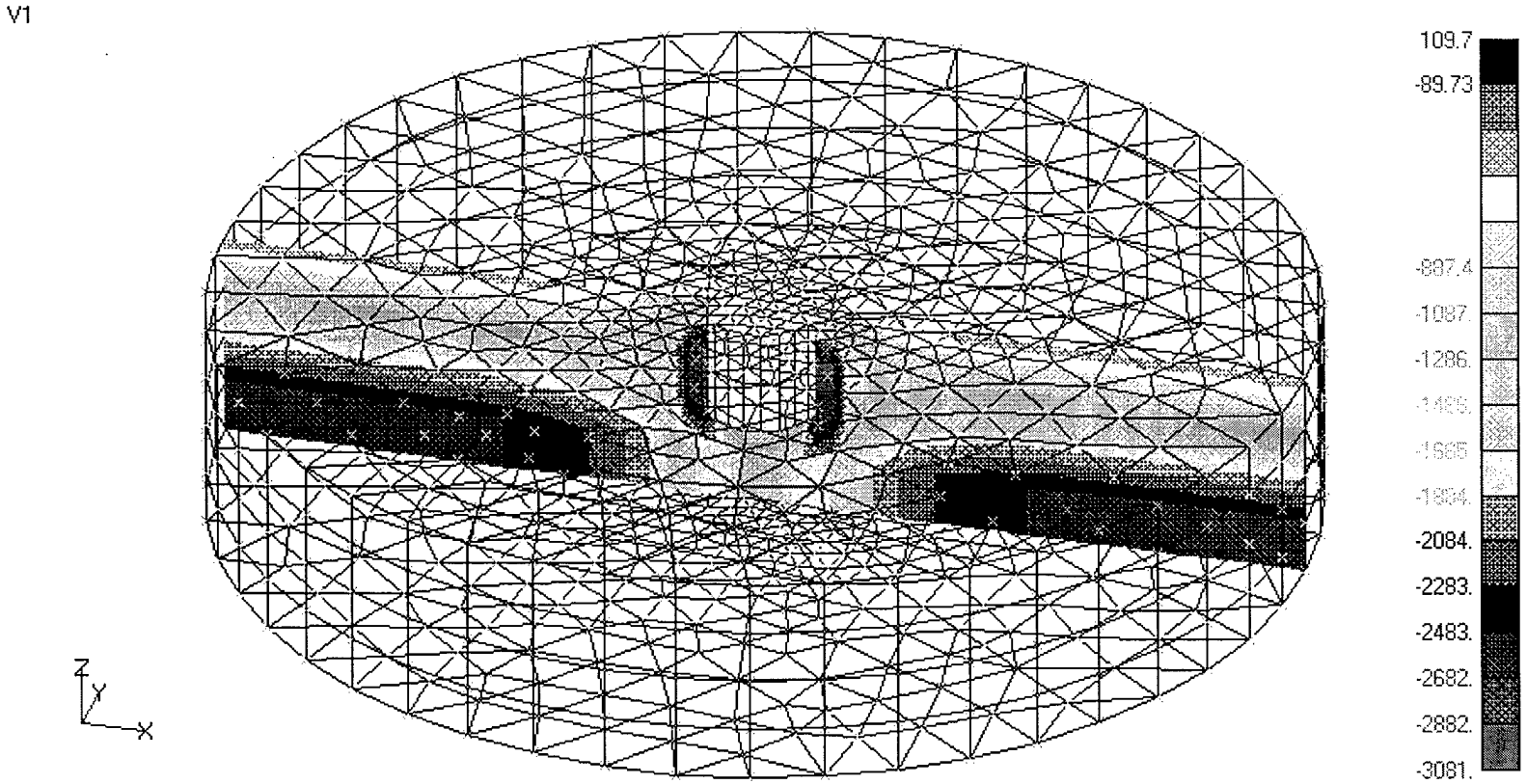

Vertical Load = 7,000,000 lbs
Linear Elastic-Perfectly Plastic Sandy Soil (Linear Extended Drucker-Prager)
E = 864,000 psf, $\upsilon = 0.3$, Slope Angle = 42.6°, Dilation Angle = 21.5°
Pile, AISI 4340 Steel

Figure - 28 Minimum Soil Minor Principal Stress vs. Vertical Load

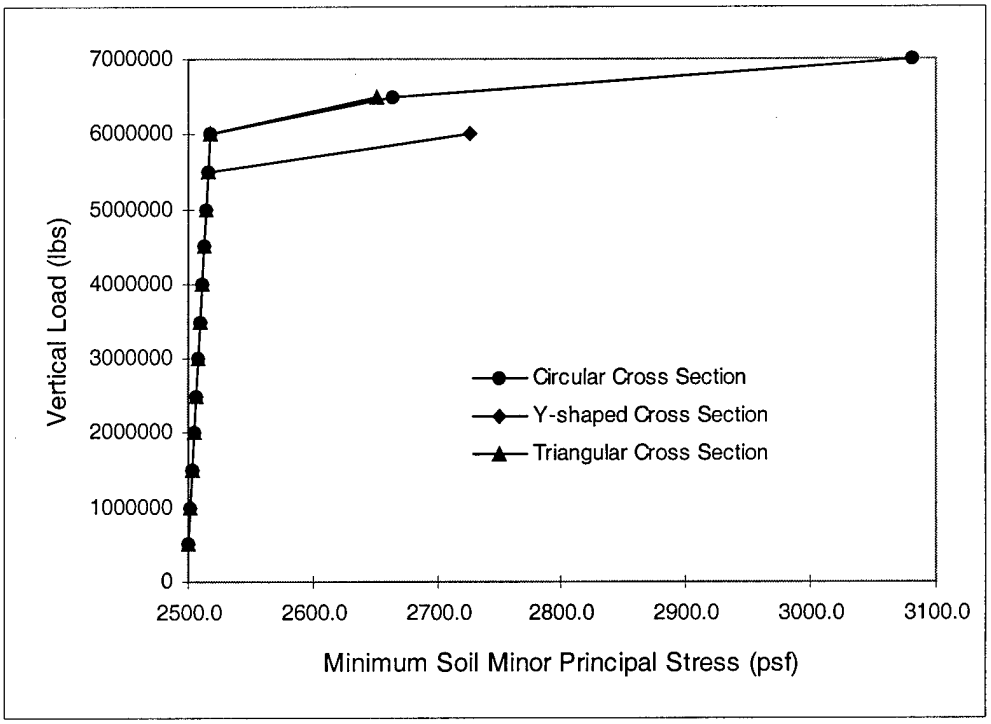

Figure - 29 Pile von Mises Stresses on the Pile Surface for Circular Pile

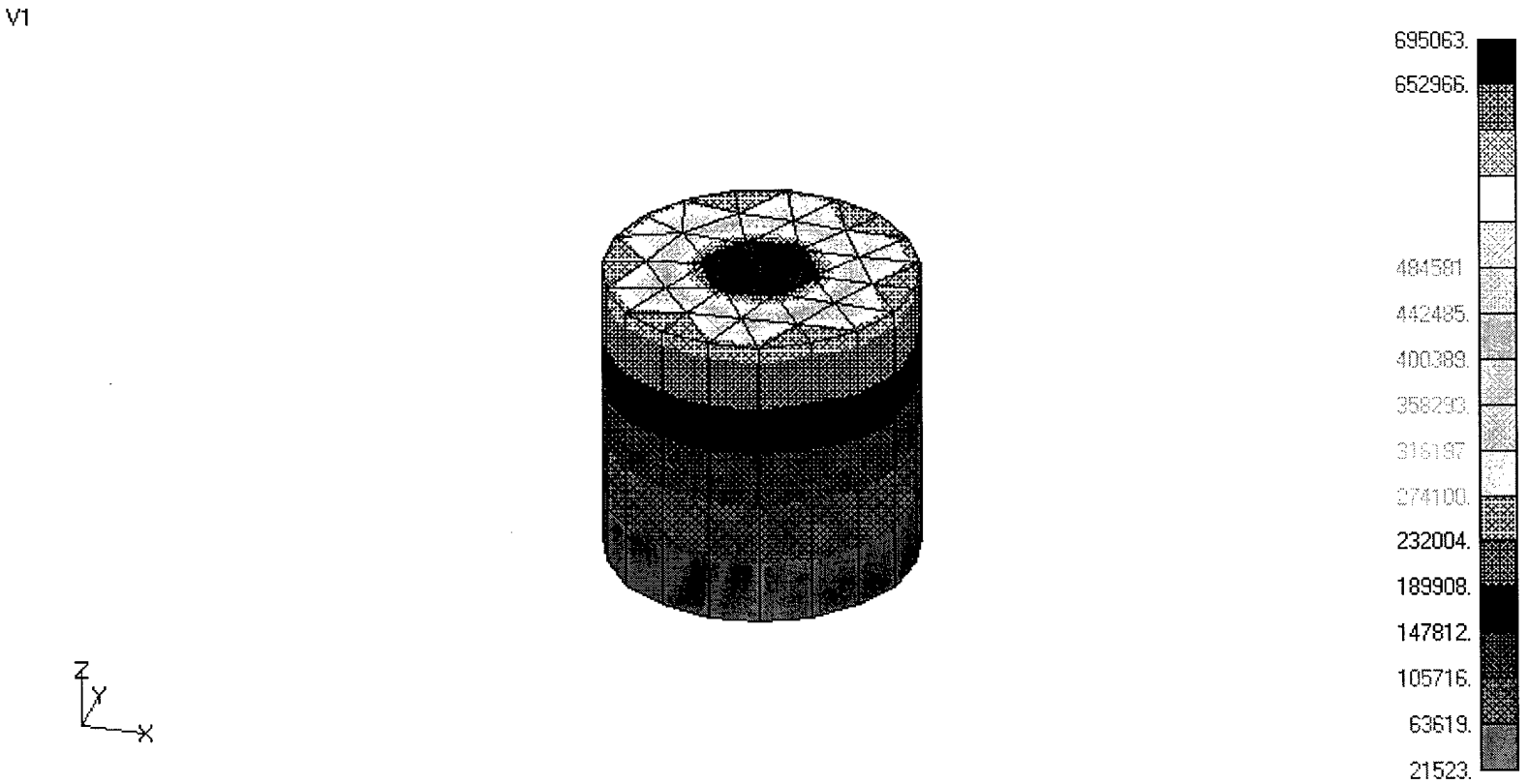

Vertical Load = 7,000,000 lbs
Linear Elastic-Perfectly Plastic Sandy Soil (Linear Extended Drucker-Prager)
E = 864,000 psf, υ = 0.3, Slope Angle = 42.6°, Dilation Angle = 21.5°
Pile, AISI 4340 Steel

Figure - 30 Maximum Pile von Mises Stress vs. Vertical Load

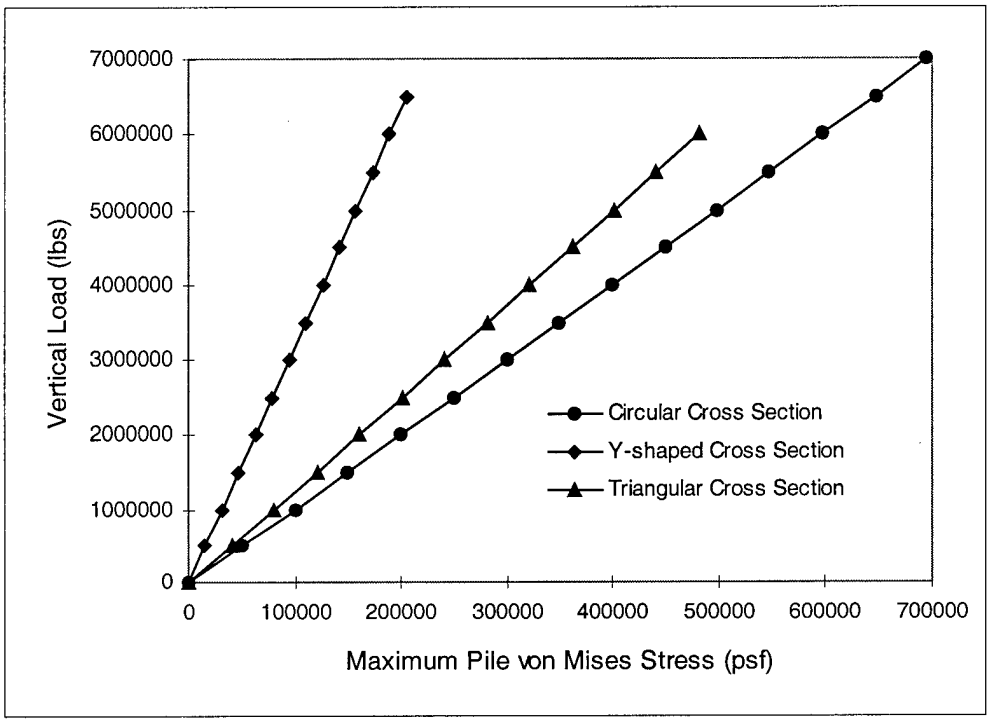

Figure - 31 Maximum Total Displacement vs. 45-Degree Inclined Load

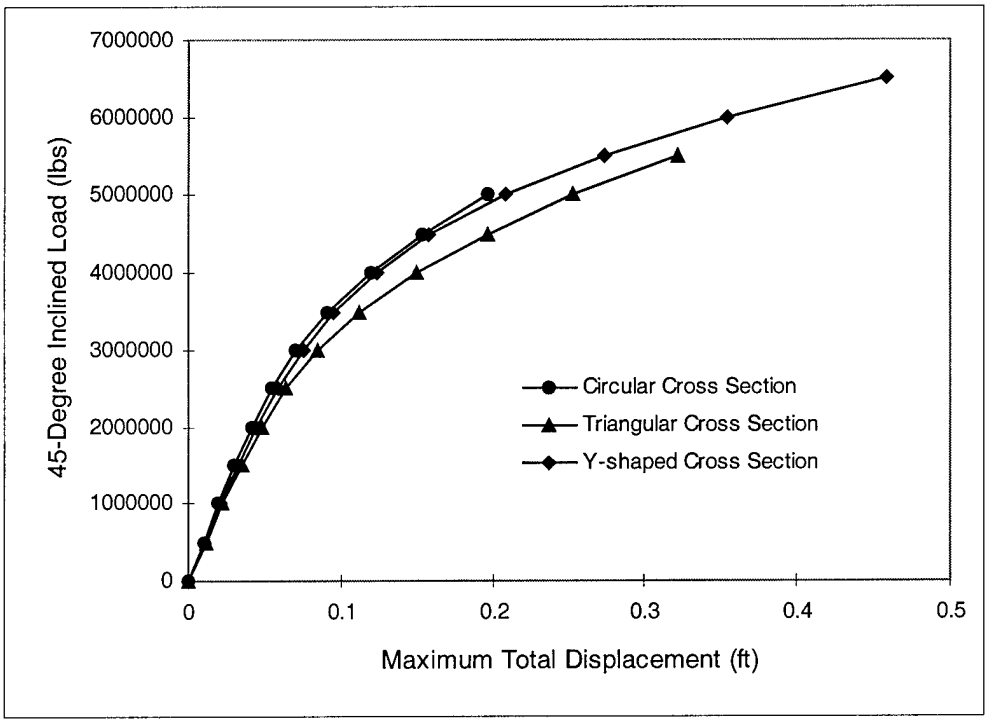

Figure - 32 Maximum Horizontal Displacement vs. 45-Degree Inclined Load

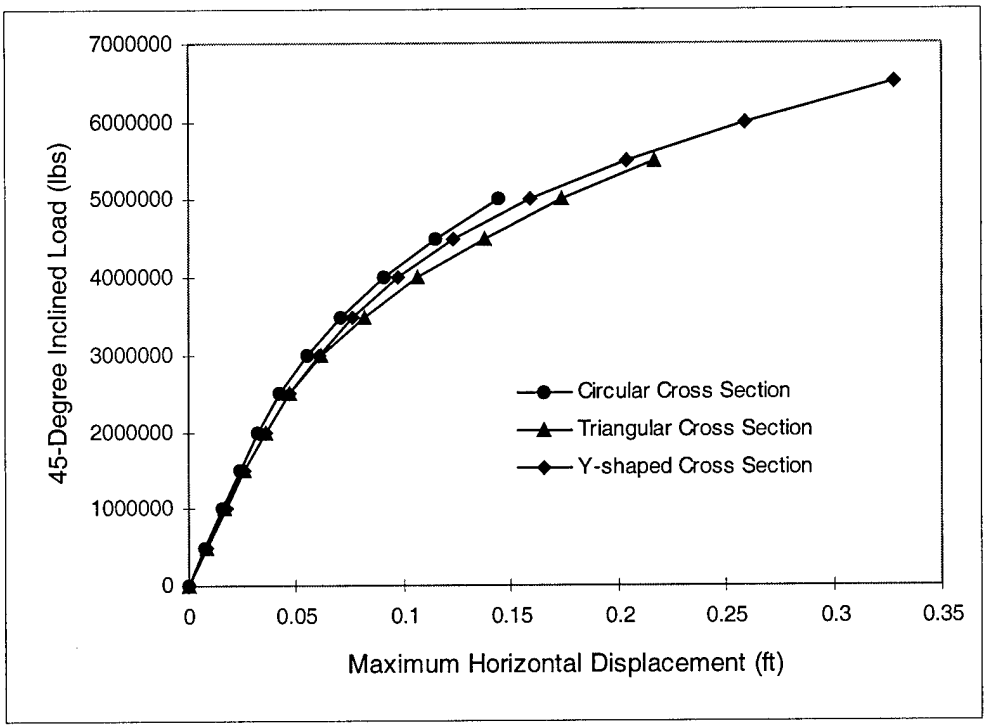

Figure - 33 Minimum Soil Minor Principal Stress vs. 45-Degree Inclined Load

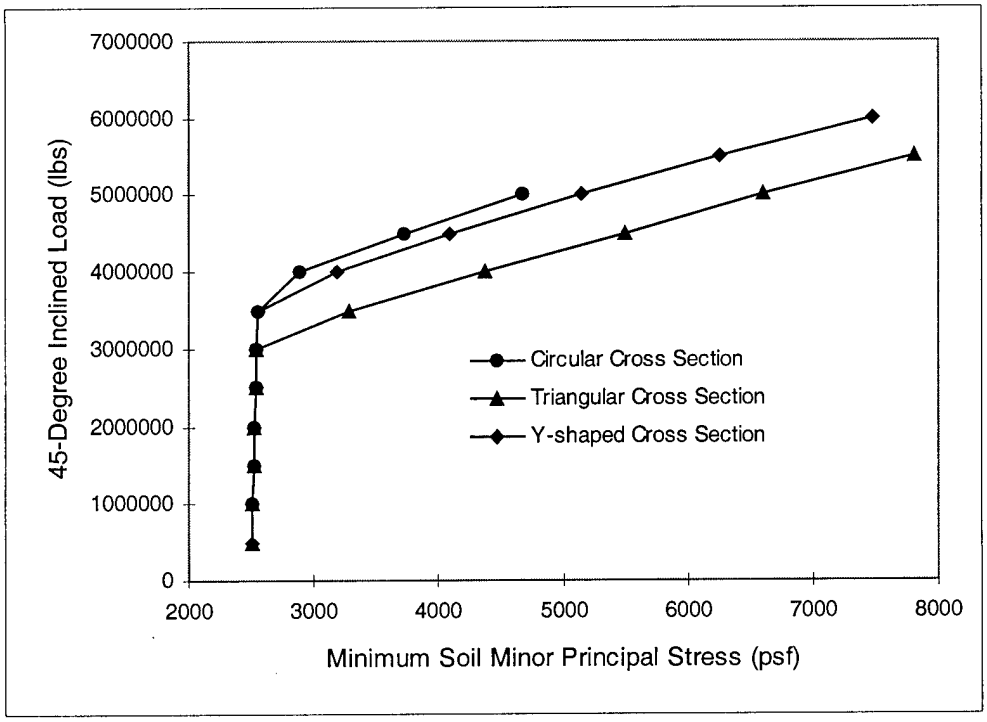

Figure - 34 Maximum Pile von Mises Stress vs. 45-Degree Inclined Load

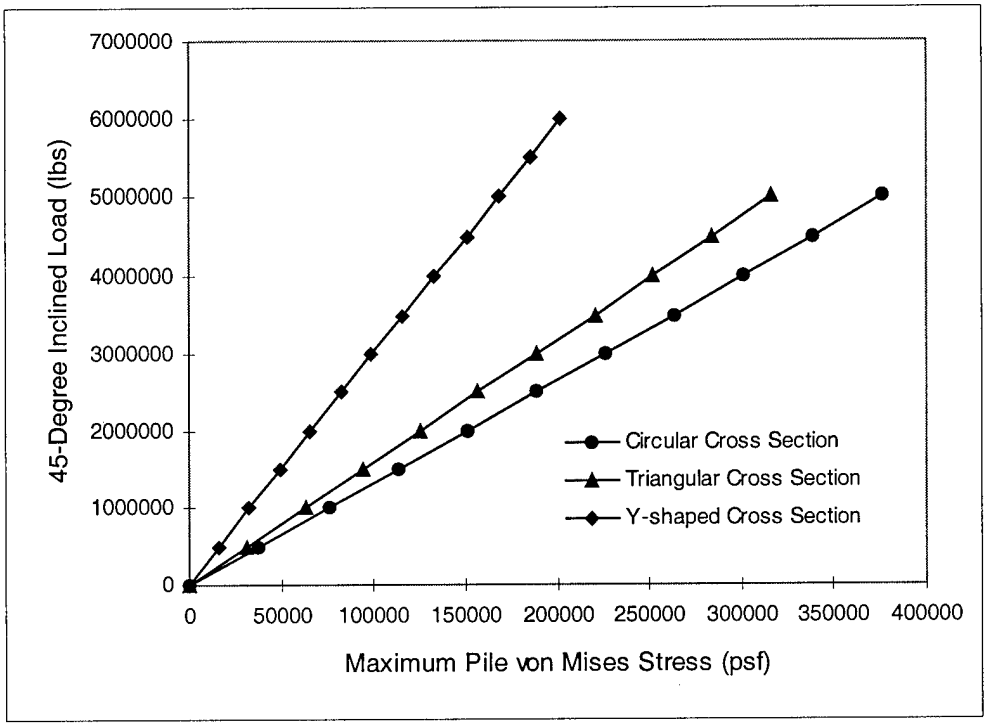

Figure - 35 Maximum Horizontal Displacement vs. Horizontal Load

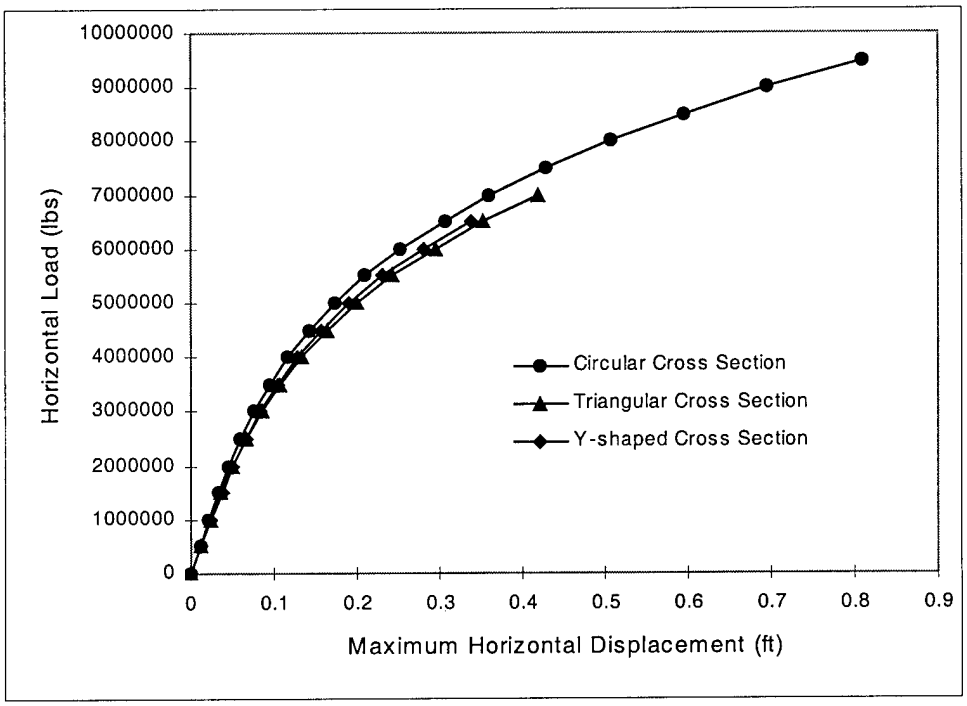

Figure - 36 Minimum Soil Minor Principal Stress vs. Horizontal Load

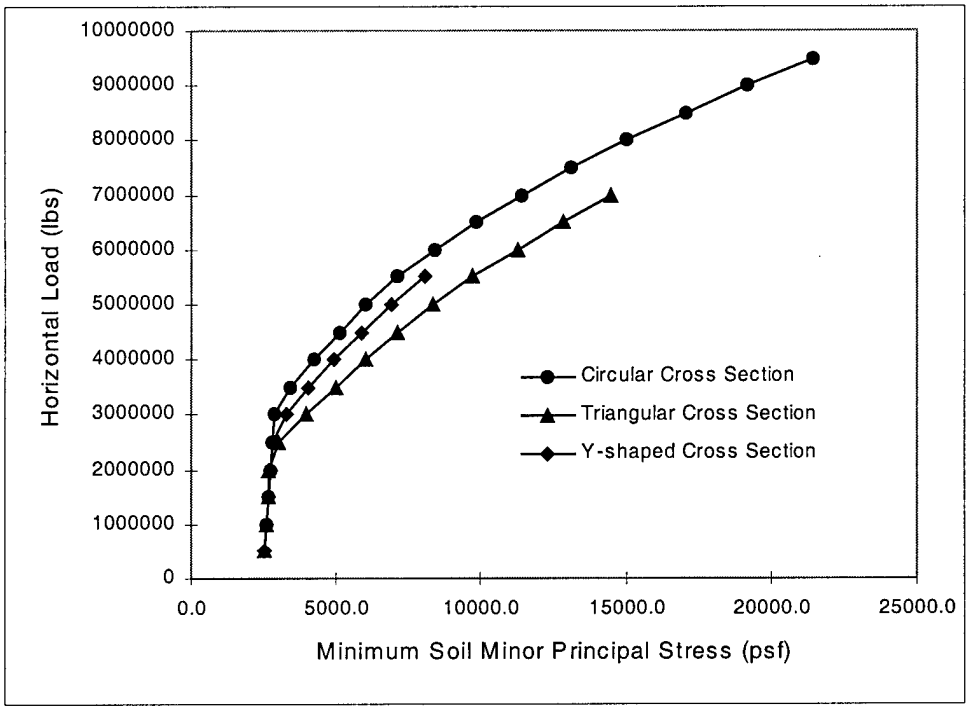

Figure - 37 Maximum Pile von Mises Stress vs. Horizontal Load

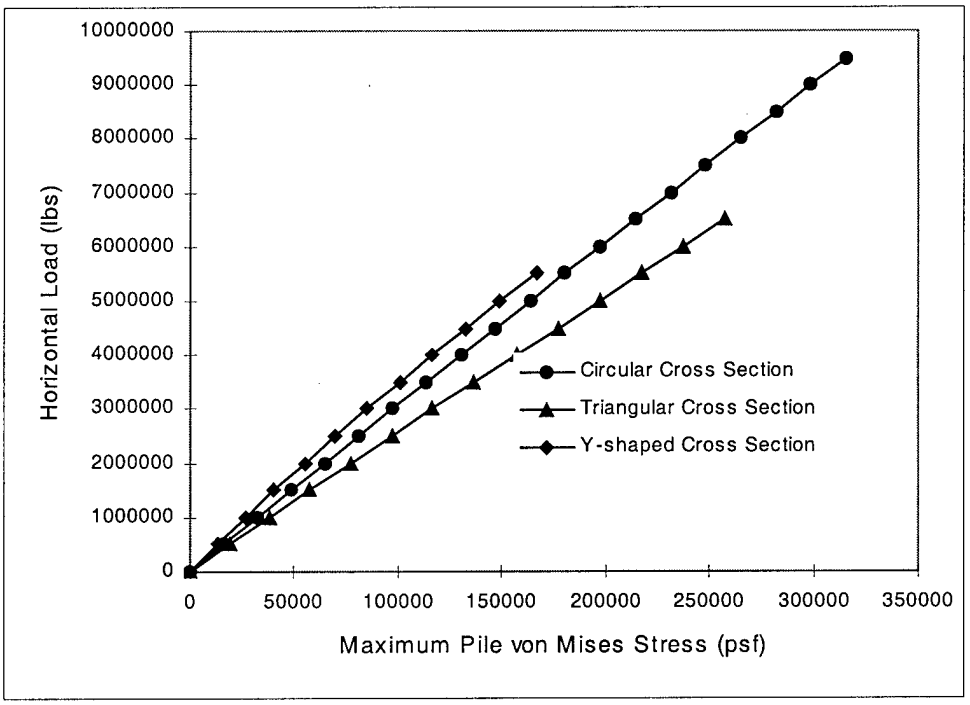

Figure -38 Hyperbolic Model: Yield Surface and Hardening Behavior in the p-q Plane

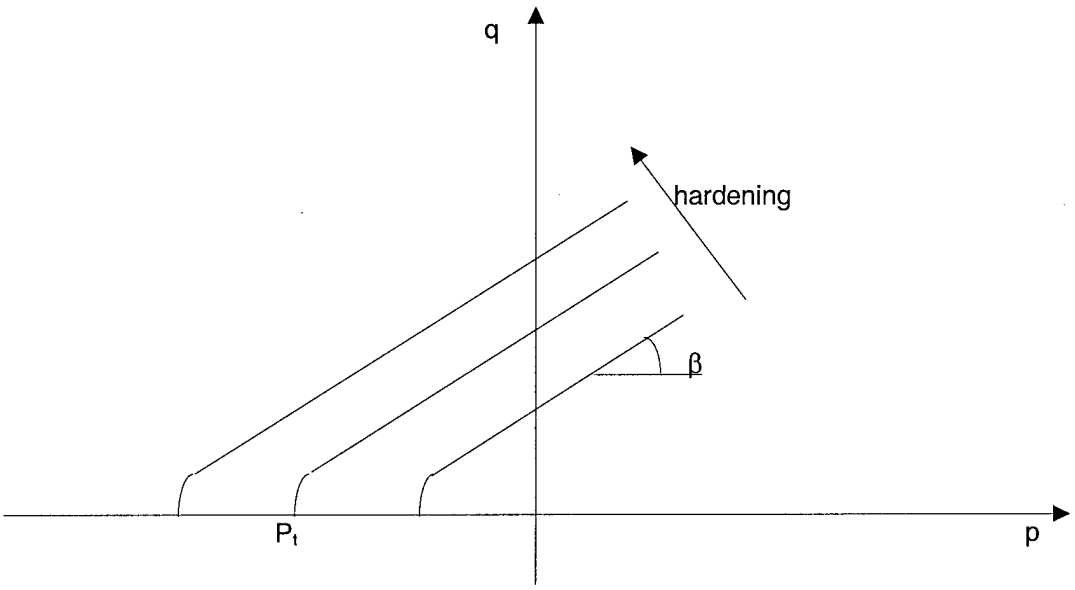

Figure - 39 Soil Minor Principal Stress Distribution under Geostatic Stress Condition

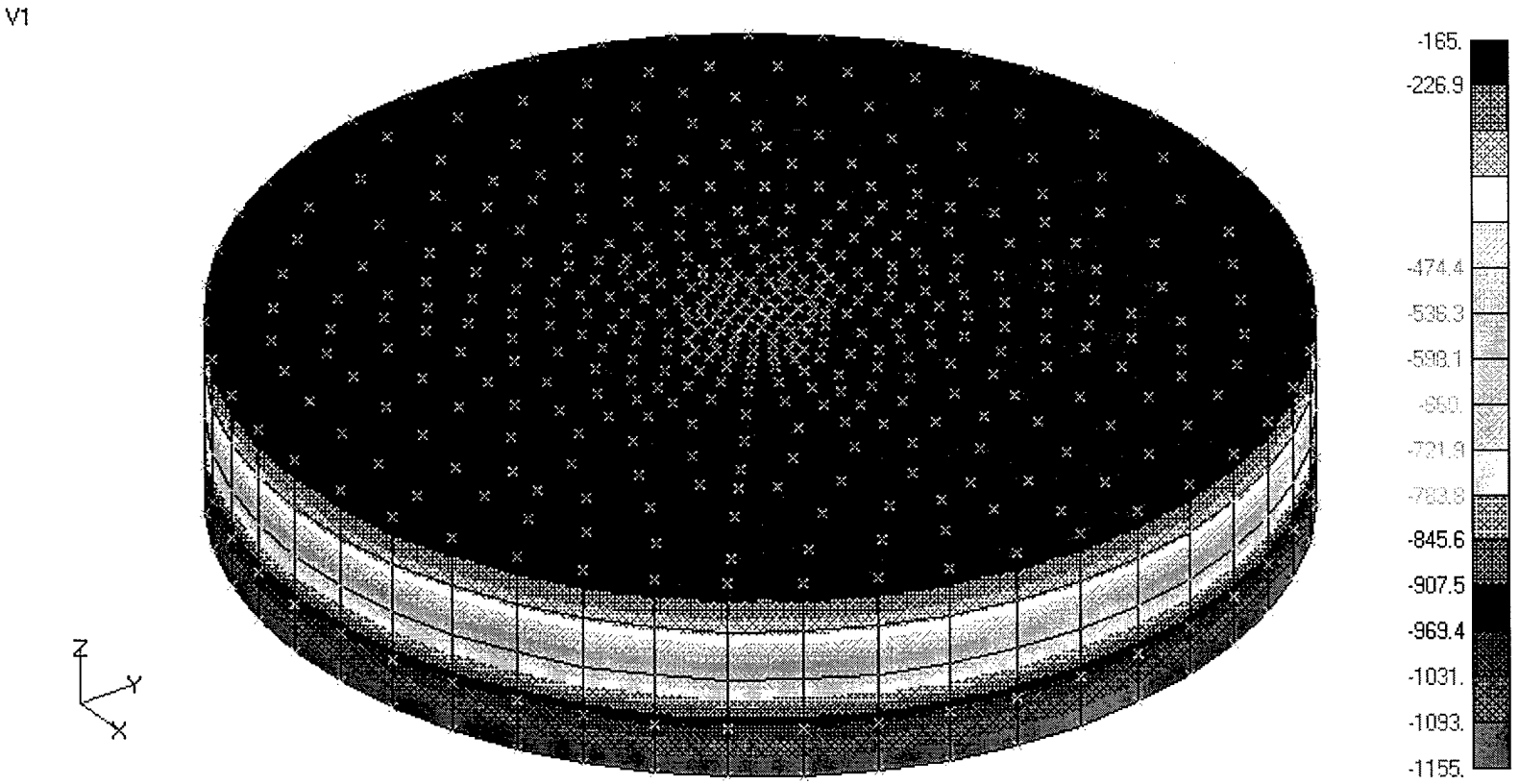

Figure - 40 Zero Displacement under Geostatic Stress Condition

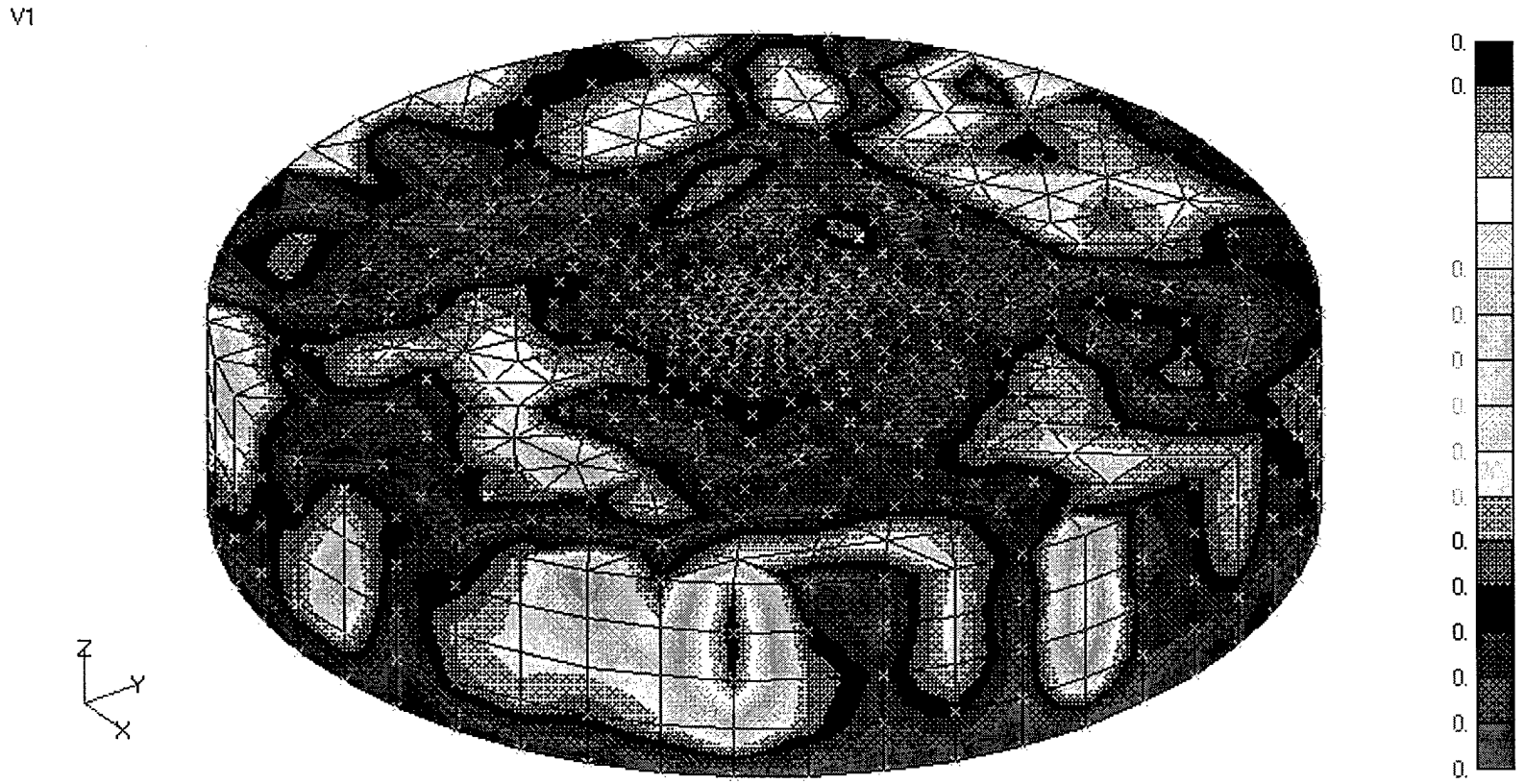
V1
0.
0.
0.
0.
0.
0.
0.
0.
0.
0.
0.
Z
Y
X

Figure - 41 Pile Total Displacements (Circular Section)

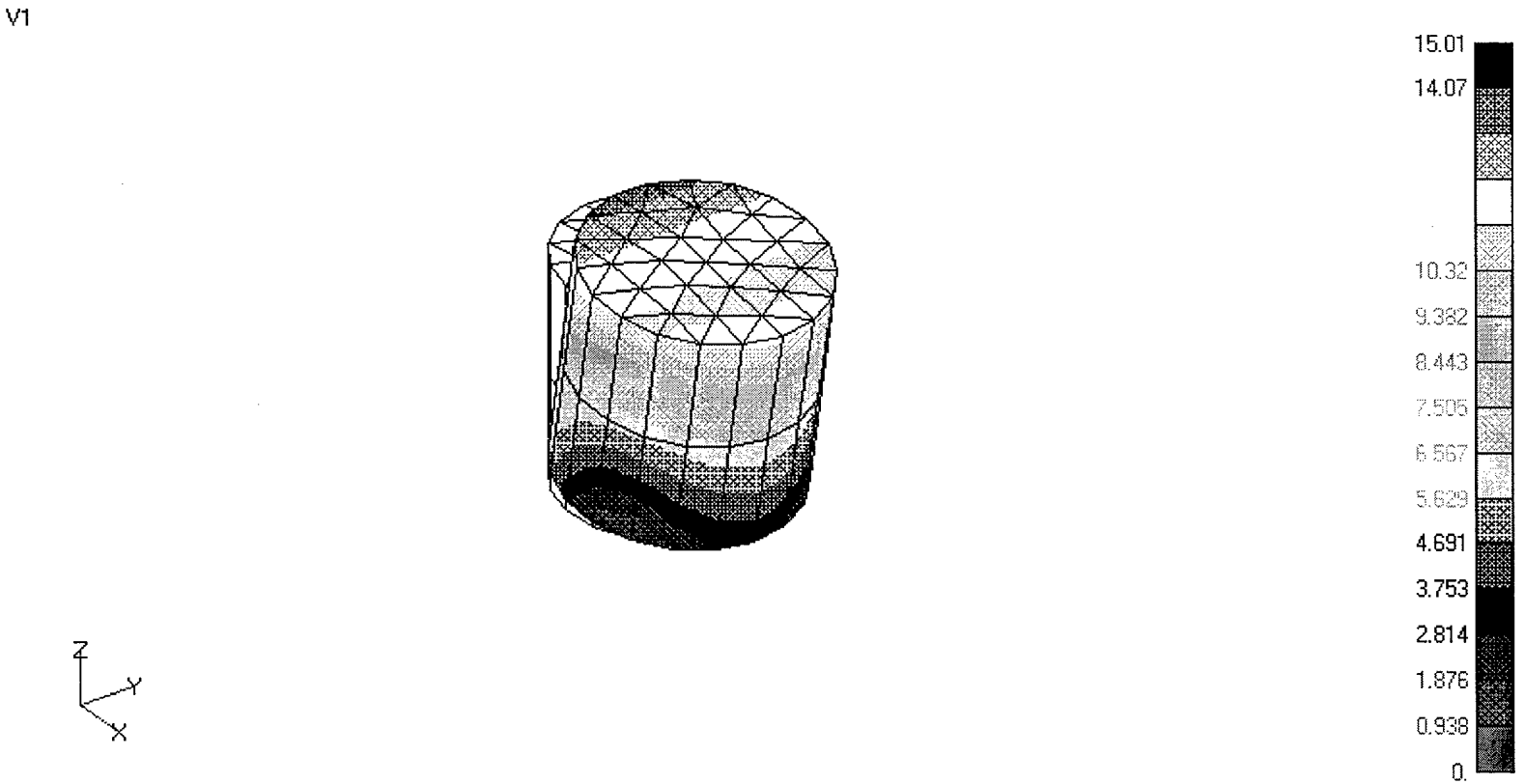

Horizontal Load = 1,900,000 lbs
Linear Elastic-Perfectly Plastic Clayey Soil (Hyperbolic Extended Drucker-Prager)
E = 30,000 psf, $\upsilon = 0.499$, Slope Angle = 10.2^{o}, Dilation Angle = 10.2^{o}
Pile, AISI 4340 Steel

Figure - 42 Maximum Total Pile Displacement vs. Horizontal Load for Circular Pile

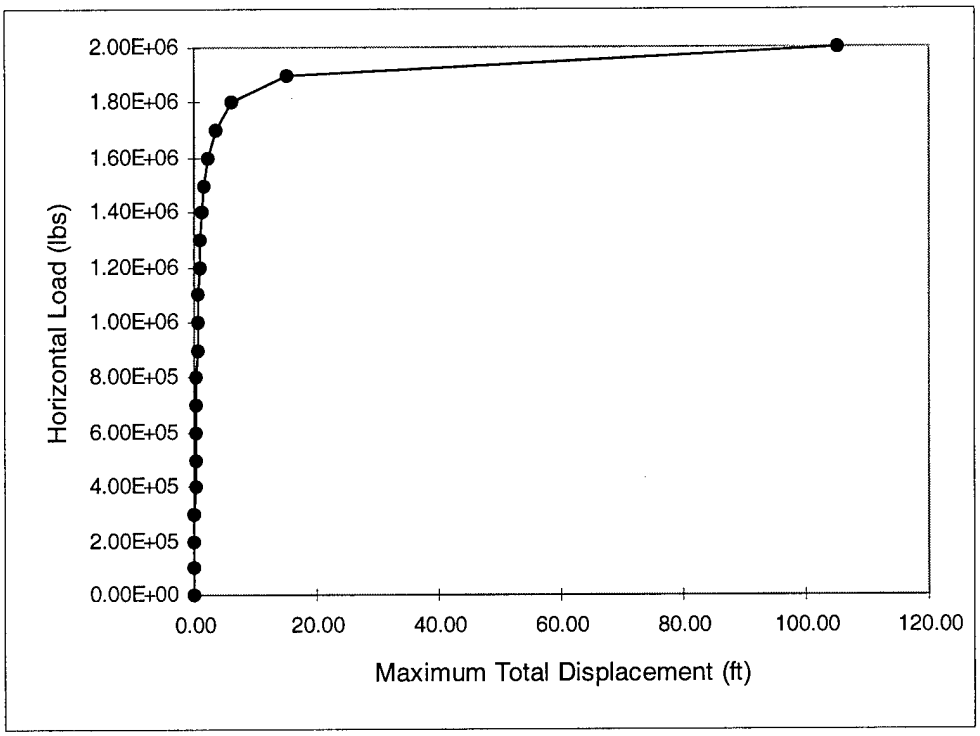

Figure - 43 Maximum Total Pile Displacement vs. Horizontal Load

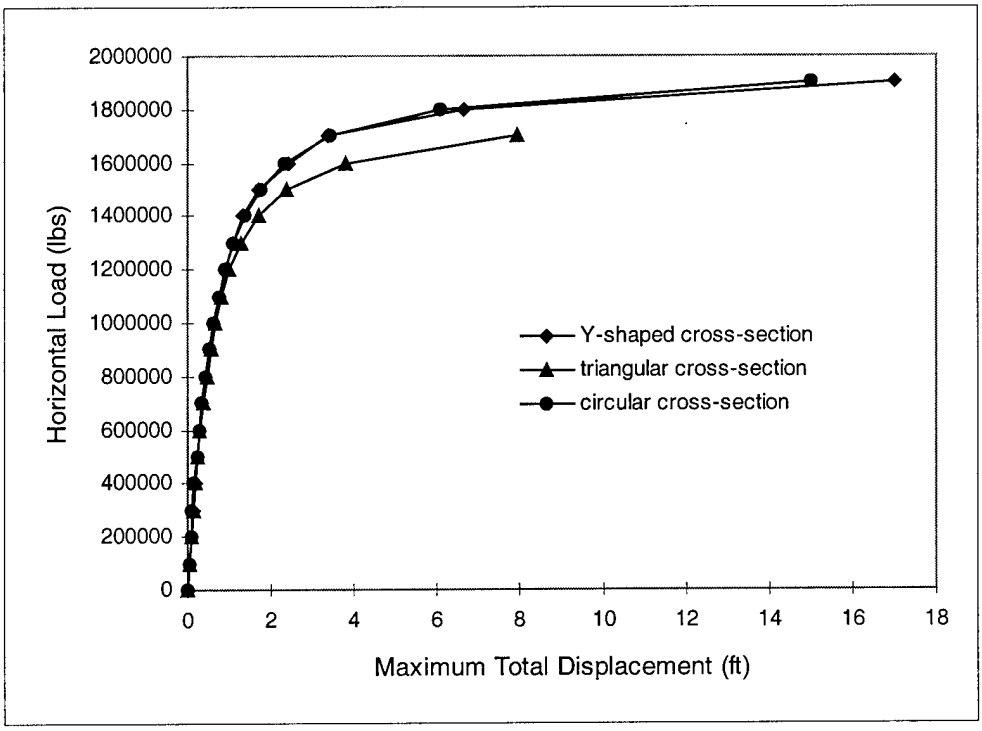

Figure - 44 Maximum Horizontal Pile Displacement vs. Horizontal Load

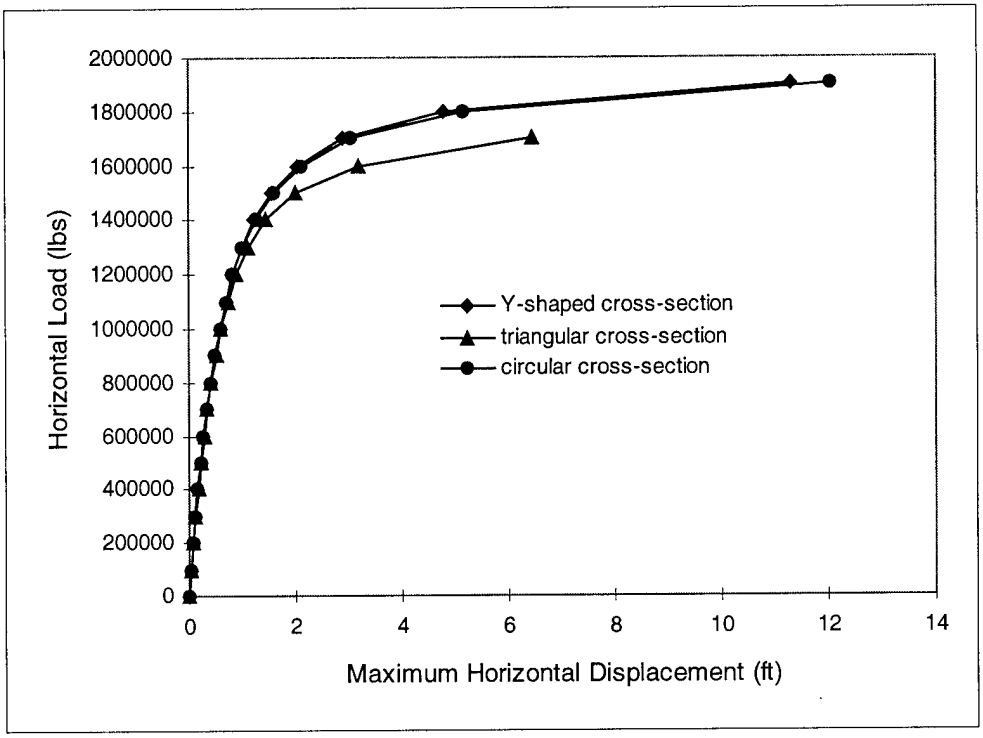

Figure - 45 Soil Minor Principal Stresses for Circular Pile on a Vertical Plane along Horizontal Load Direction (Circular Section)

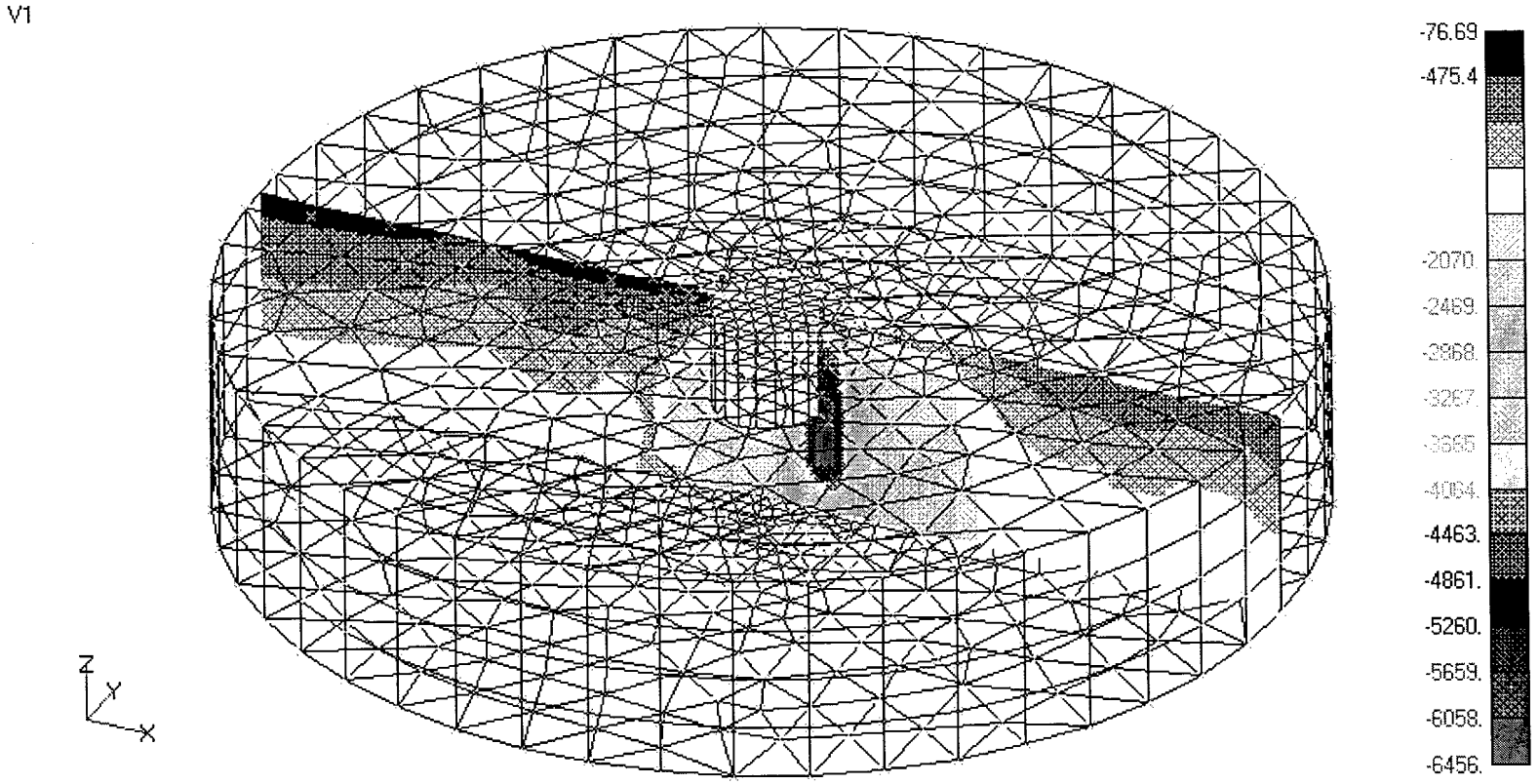

Horizontal Load = 1,900,000 lbs
Linear Elastic-Perfectly Plastic Clayey Soil (Hyperbolic Extended Drucker-Prager)
E = 30,000 psf, $\upsilon = 0.499$, Slope Angle = 10.2^{o}, Dilation Angle = 10.2^{o}
Pile, AISI 4340 Steel

Figure – 46 Minimum Soil Minor Principal Stress vs. Horizontal Load

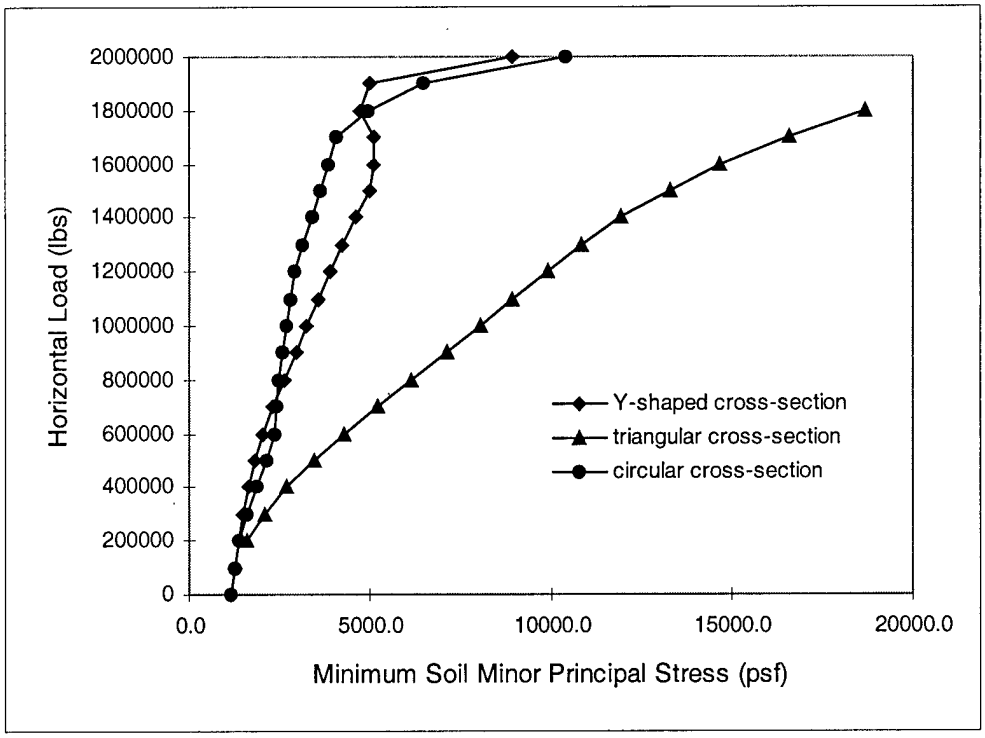

Figure - 47 Horizontal Load vs. Soil Minor Principal Stress of Element near the Top of the Advancing Side of the Pile

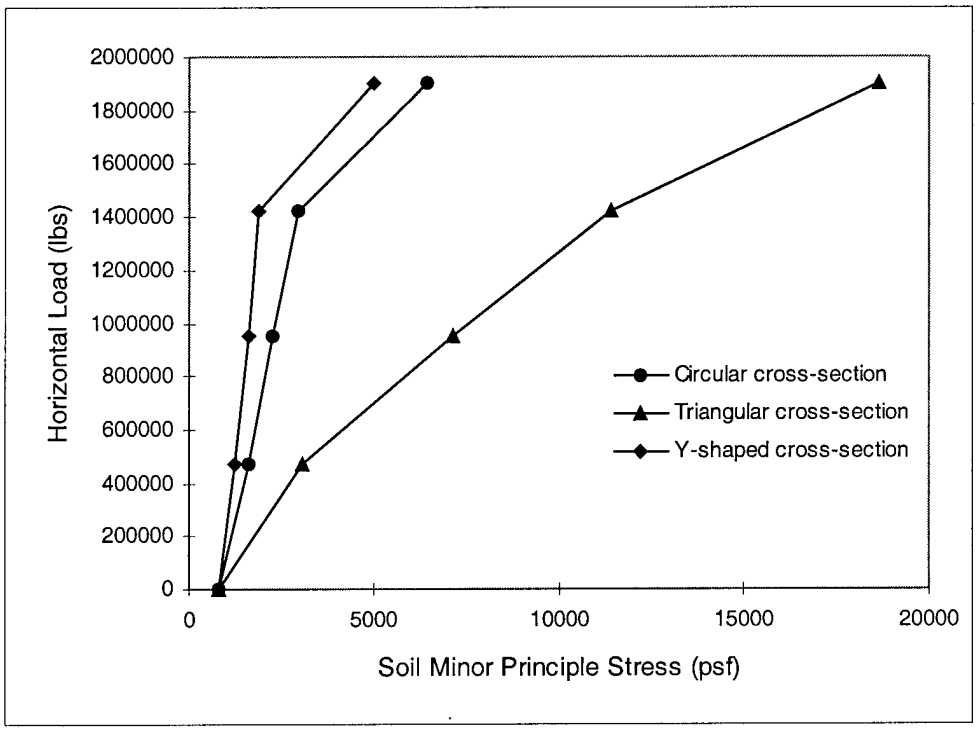

Figure - 48 Pile von Mises Stresses on the Pile Surface (Circular Section)

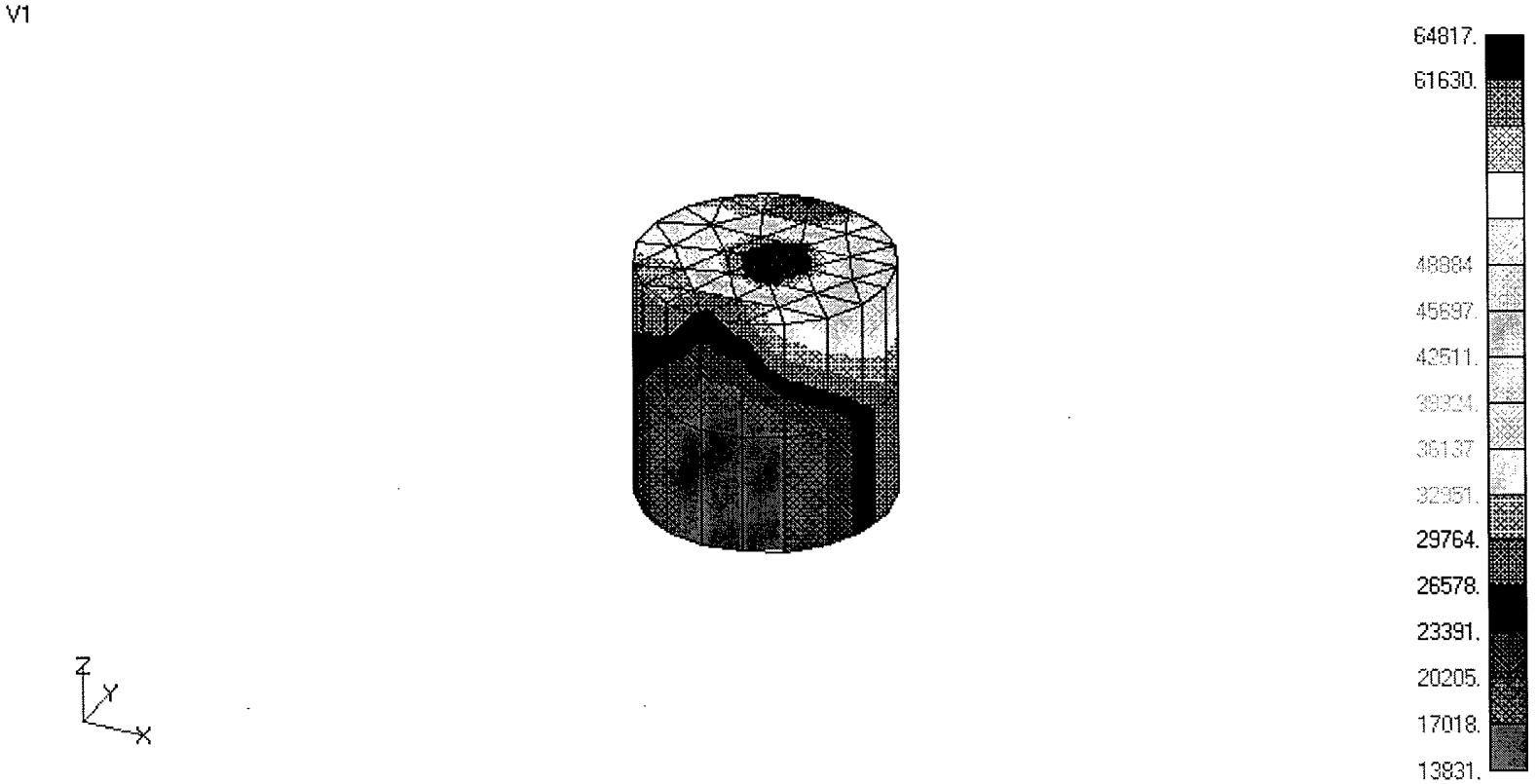

Horizontal Load = 1,900,000 lbs
Linear Elastic-Perfectly Plastic Clayey Soil (Hyperbolic Extended Drucker-Prager)
E = 30,000 psf, υ = 0.499, Slope Angle = 10.2°, Dilation Angle = 10.2°
Pile, AISI 4340 Steel

Figure - 49 Pile von Mises Stresses on the Pile Surface (Triangular Section)

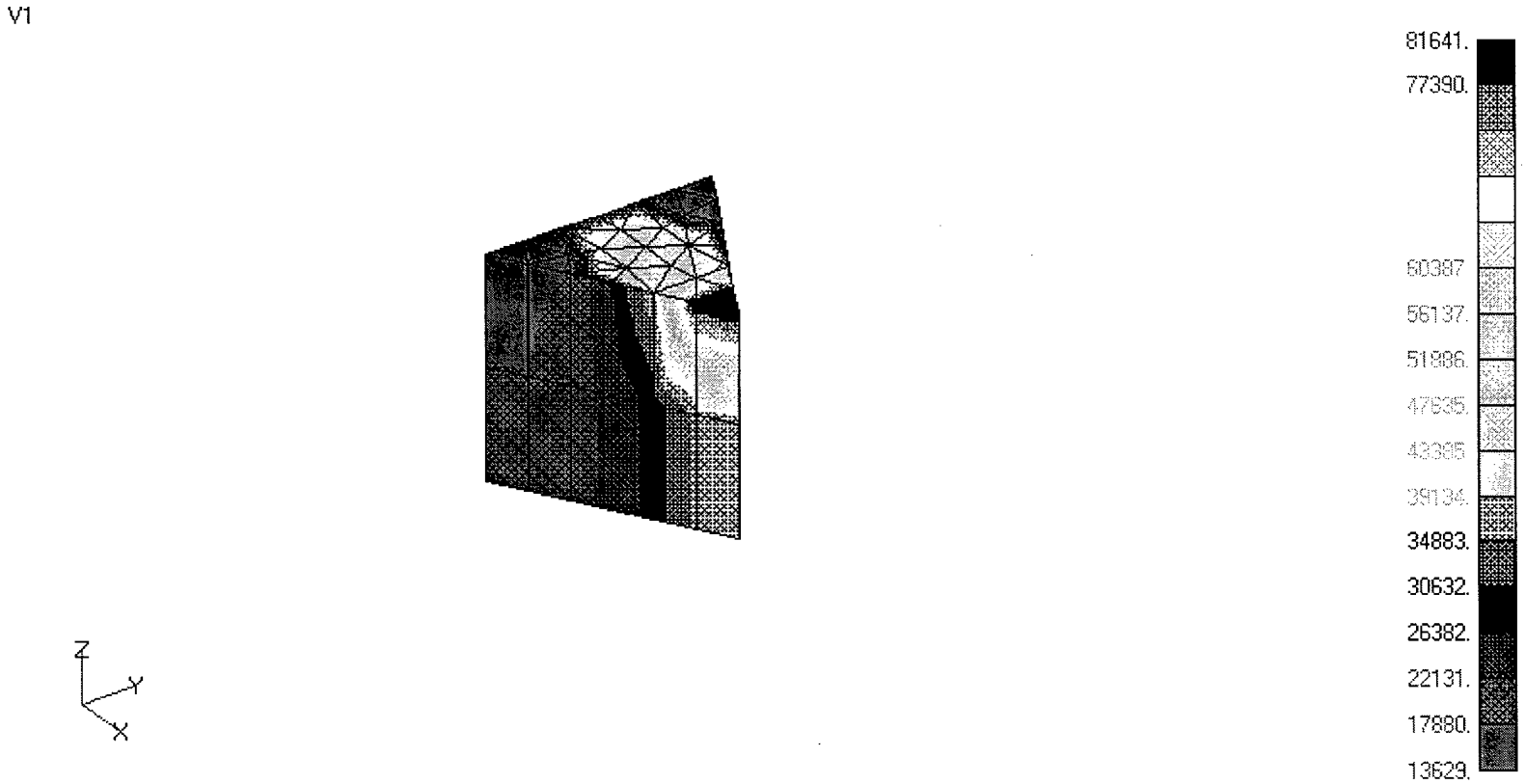

Horizontal Load = 1,900,000 lbs
Linear Elastic-Perfectly Plastic Clayey Soil (Hyperbolic Extended Drucker-Prager)
E = 30,000 psf, $\upsilon = 0.499$, Slope Angle = 10.2°, Dilation Angle = 10.2°
Pile, AISI 4340 Steel

Figure - 50 Maximum Pile von Mises Stress vs. Horizontal Load

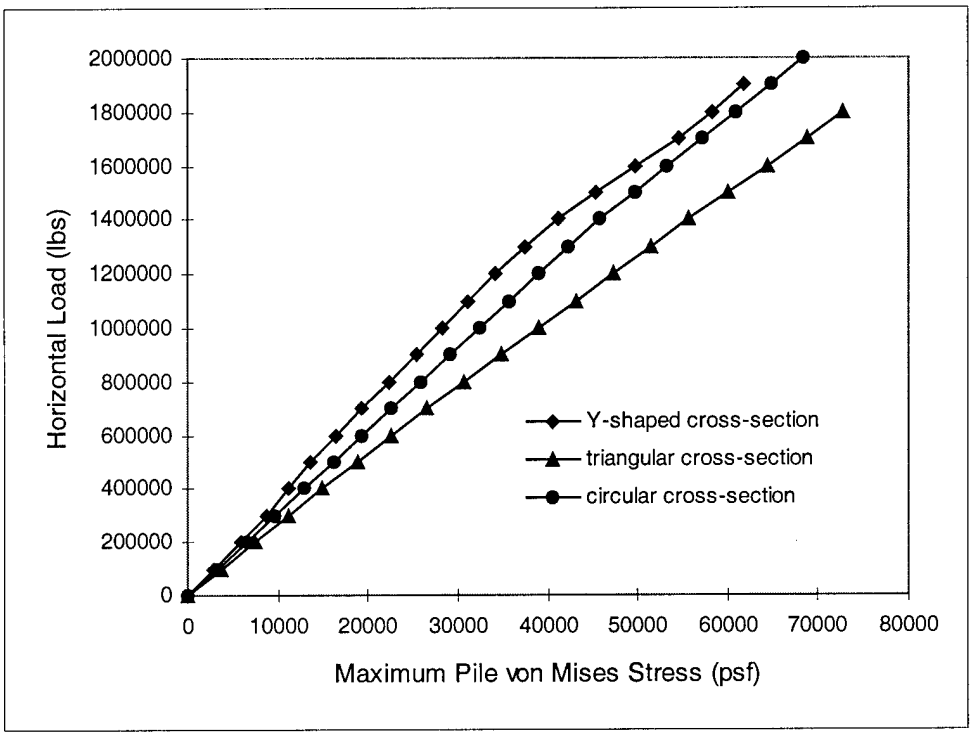

Figure - 51 Minimum Soil Minor Principal Stress vs. Maximum Horizontal Displacement due to Horizontal Load

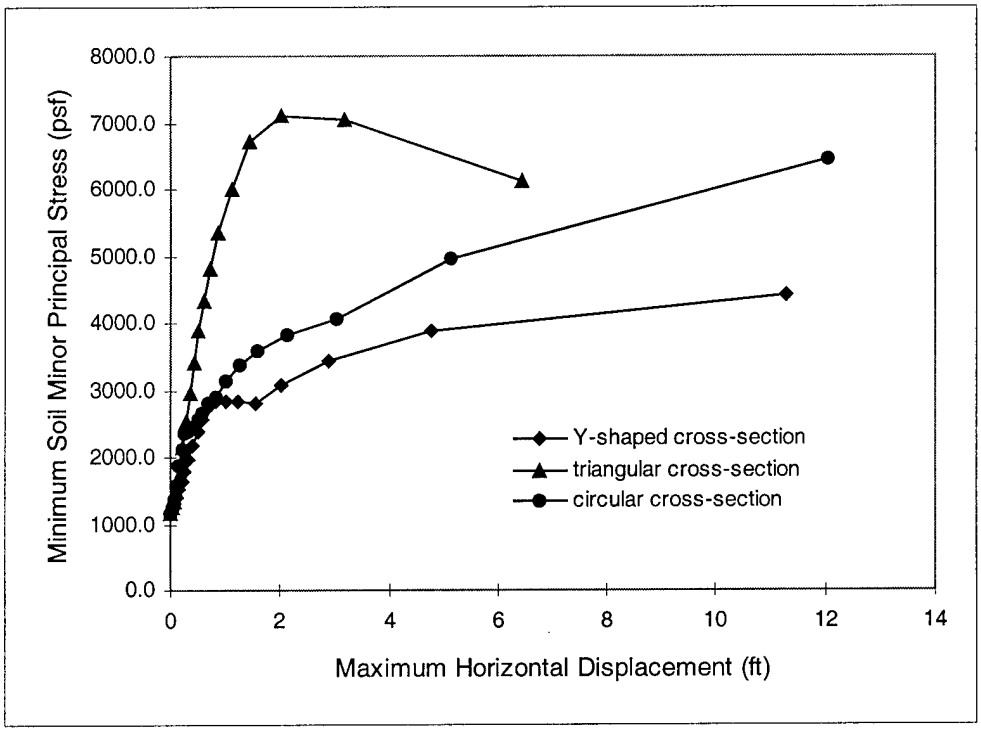

Figure - 52 Maximum Pile von Mises Stress vs. Maximum Horizontal Displacement due to Horizontal Load

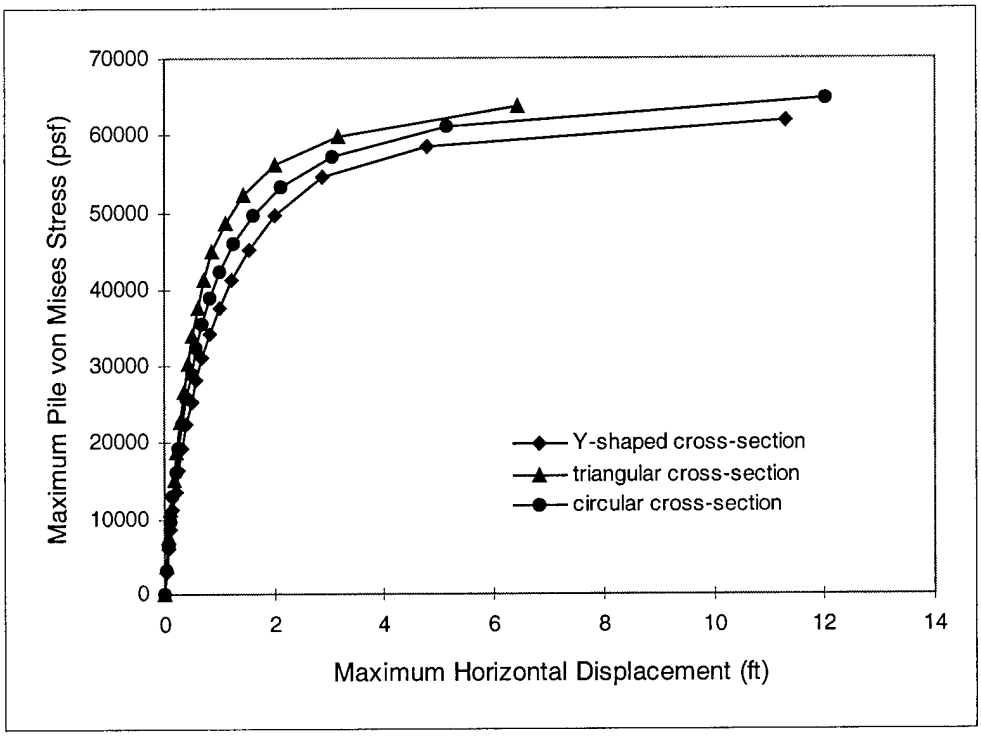

Figure - 53 Pile Vertical Displacements (Circular Section)

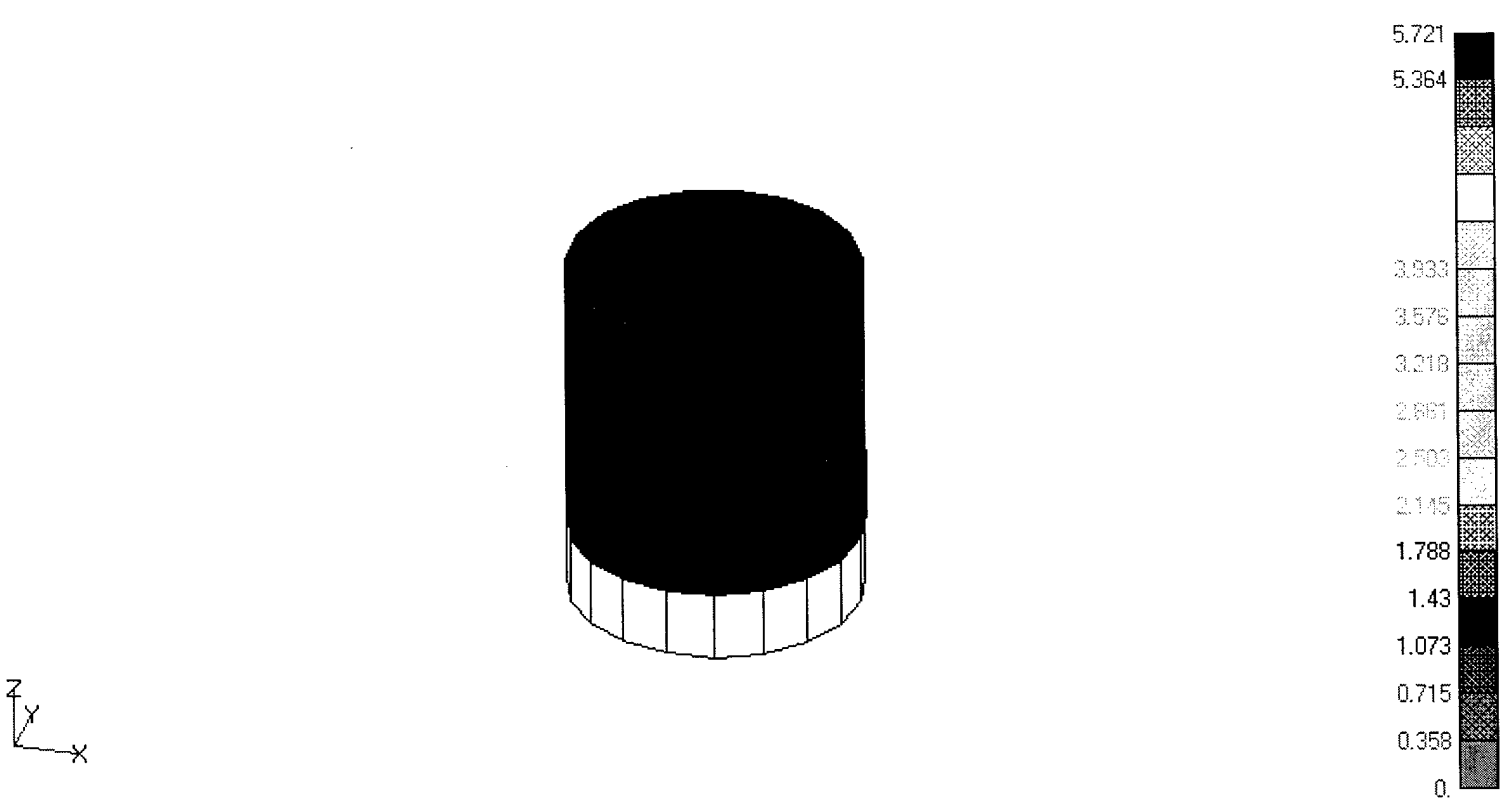

Vertical Load = 2,300,000 lbs
Linear Elastic-Perfectly Plastic Clayey Soil (Hyperbolic Extended Drucker-Prager)
E = 30,000 psf, υ = 0.499, Slope Angle = 10.2°, Dilation Angle = 10.2°
Pile, AISI 4340 Steel

Figure - 54 Maximum Pile Vertical Displacement vs. Vertical Load

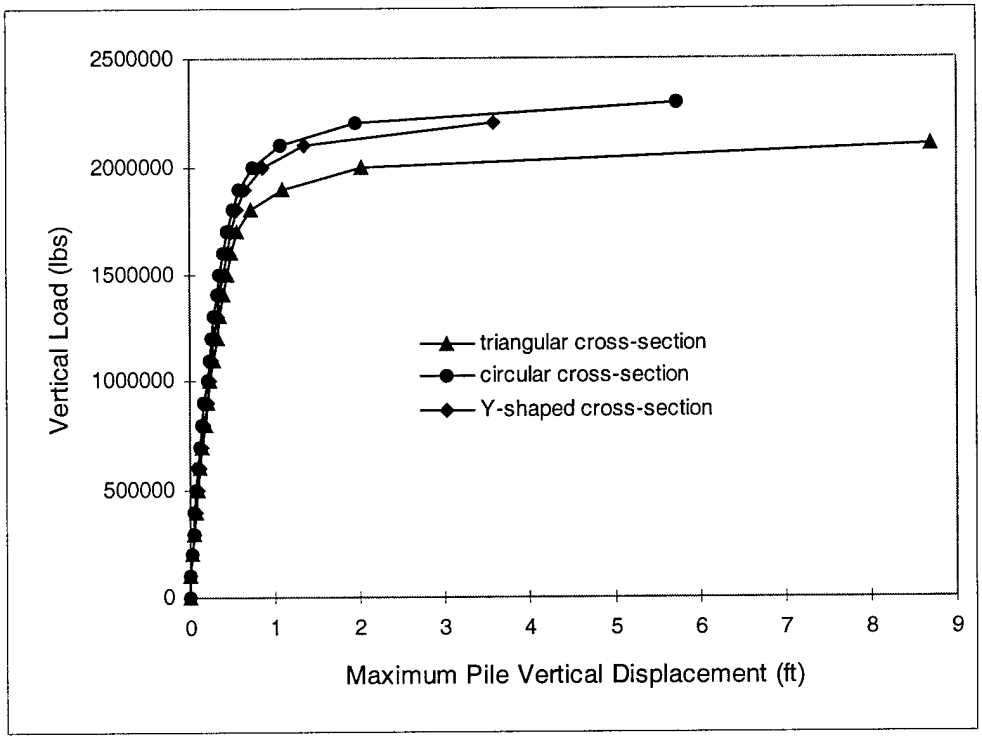

Figure - 55 Soil Minor Principal Stresses on the Pile Surface (Circular Section)

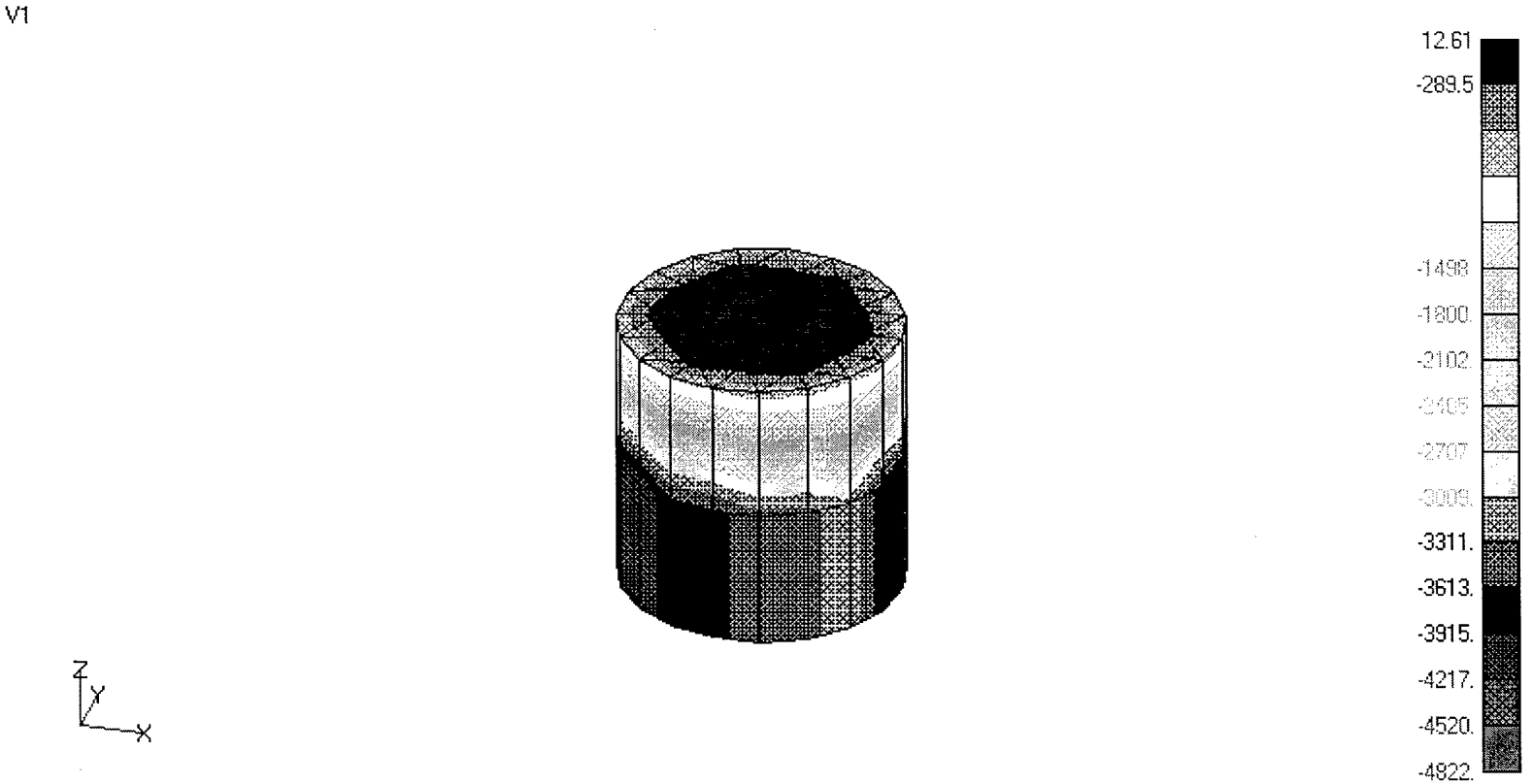

Vertical Load = 2,300,000 lbs
Linear Elastic-Perfectly Plastic Clayey Soil (Hyperbolic Extended Drucker-Prager)
E = 30,000 psf, $\upsilon = 0.499$, Slope Angle = 10.2^{o}, Dilation Angle = 10.2^{o}
Pile, AISI 4340 Steel

Figure - 56 Soil Minor Principal Stresses on the Pile Surface (Triangular Section)

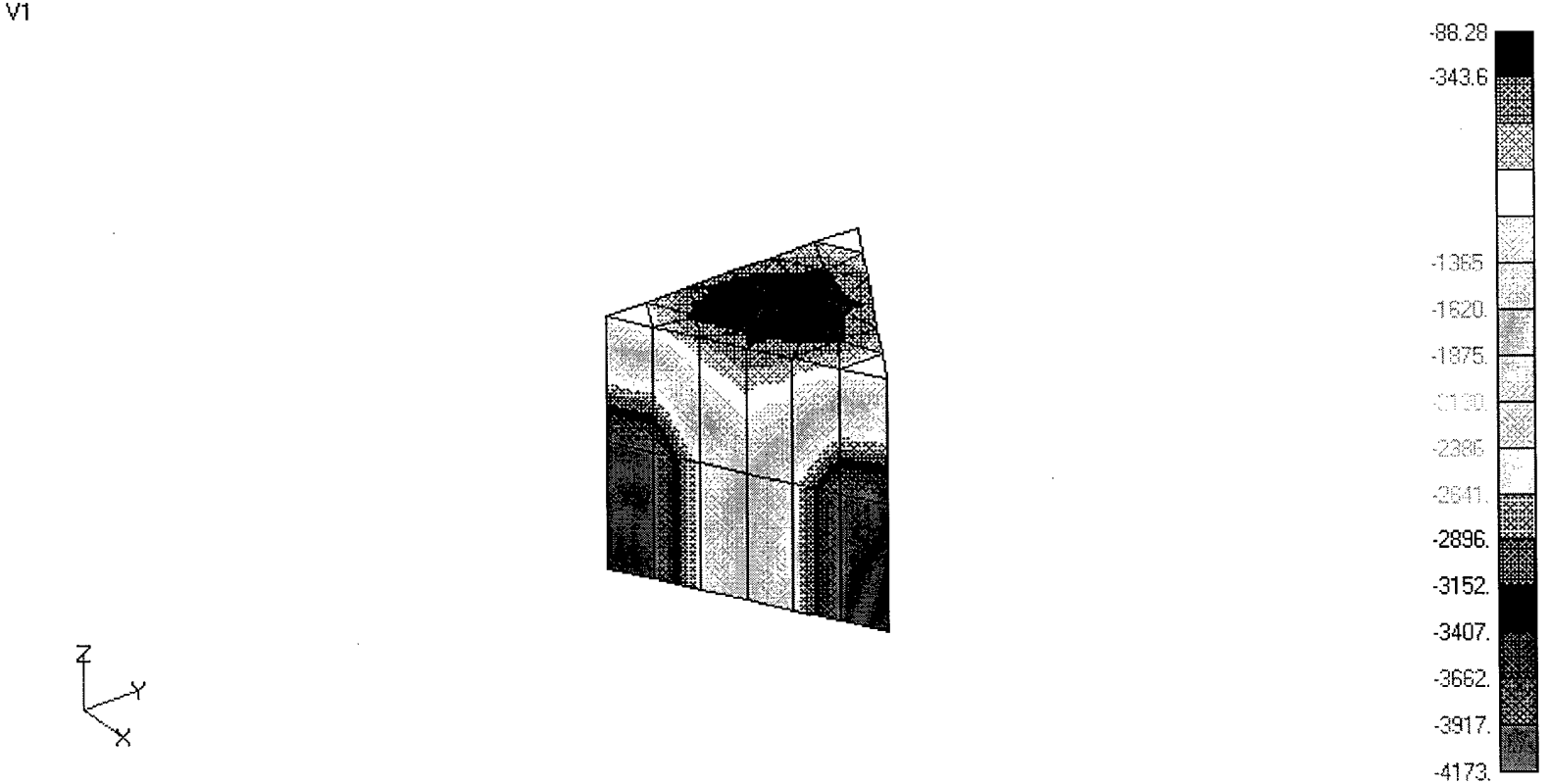

Vertical Load = 2,100,000 lbs
Linear Elastic-Perfectly Plastic Clayey Soil (Hyperbolic Extended Drucker-Prager)
E = 30,000 psf, $\upsilon = 0.499$, Slope Angle = 10.2°, Dilation Angle = 10.2°
Pile, AISI 4340 Steel

Figure - 57 Minimum Soil Minor Principal Stress vs. Vertical Load

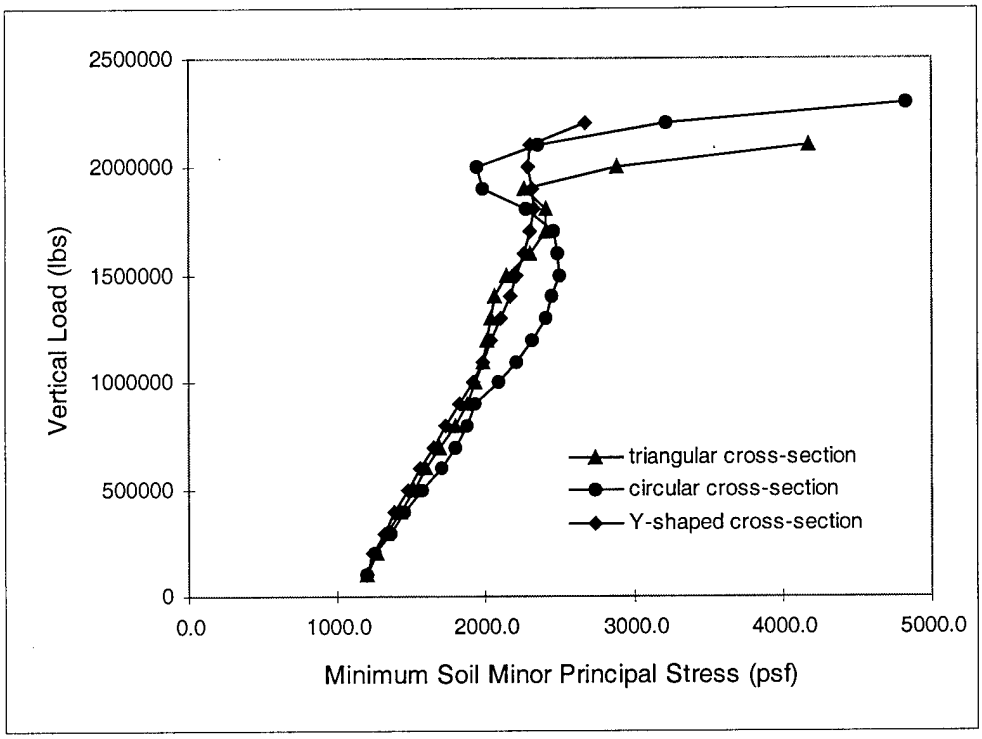

Figure - 58 Soil Minor Principal Stress vs. Vertical Load, at Element 1244 of Circular Cross-Section

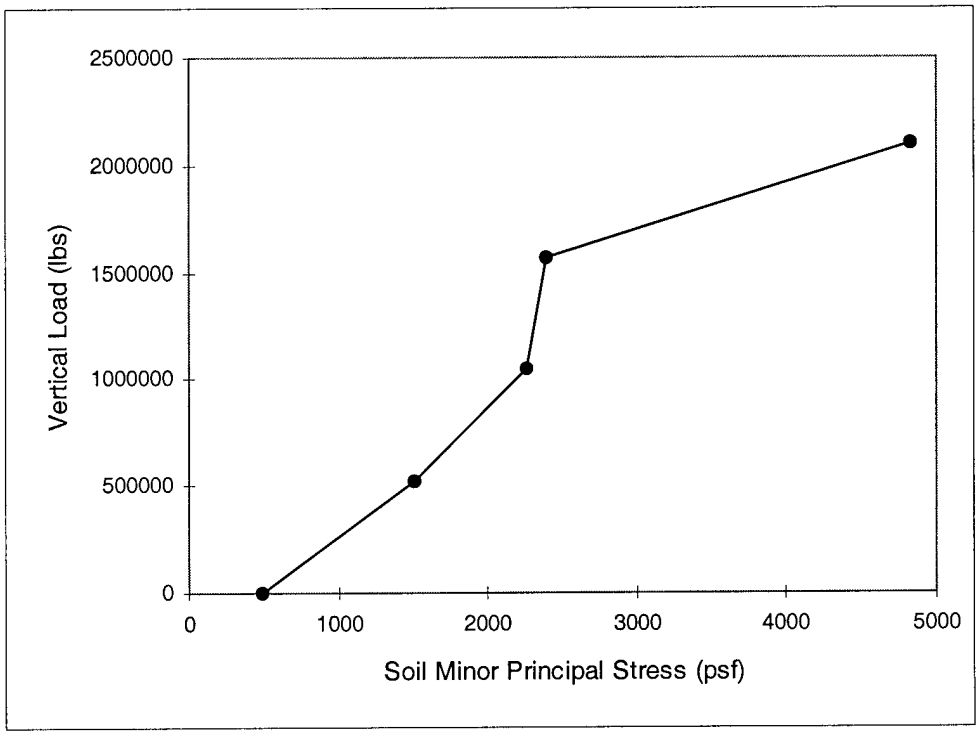

Figure - 59 Pile von Mises Stresses on the Pile Surface (Circular Section)

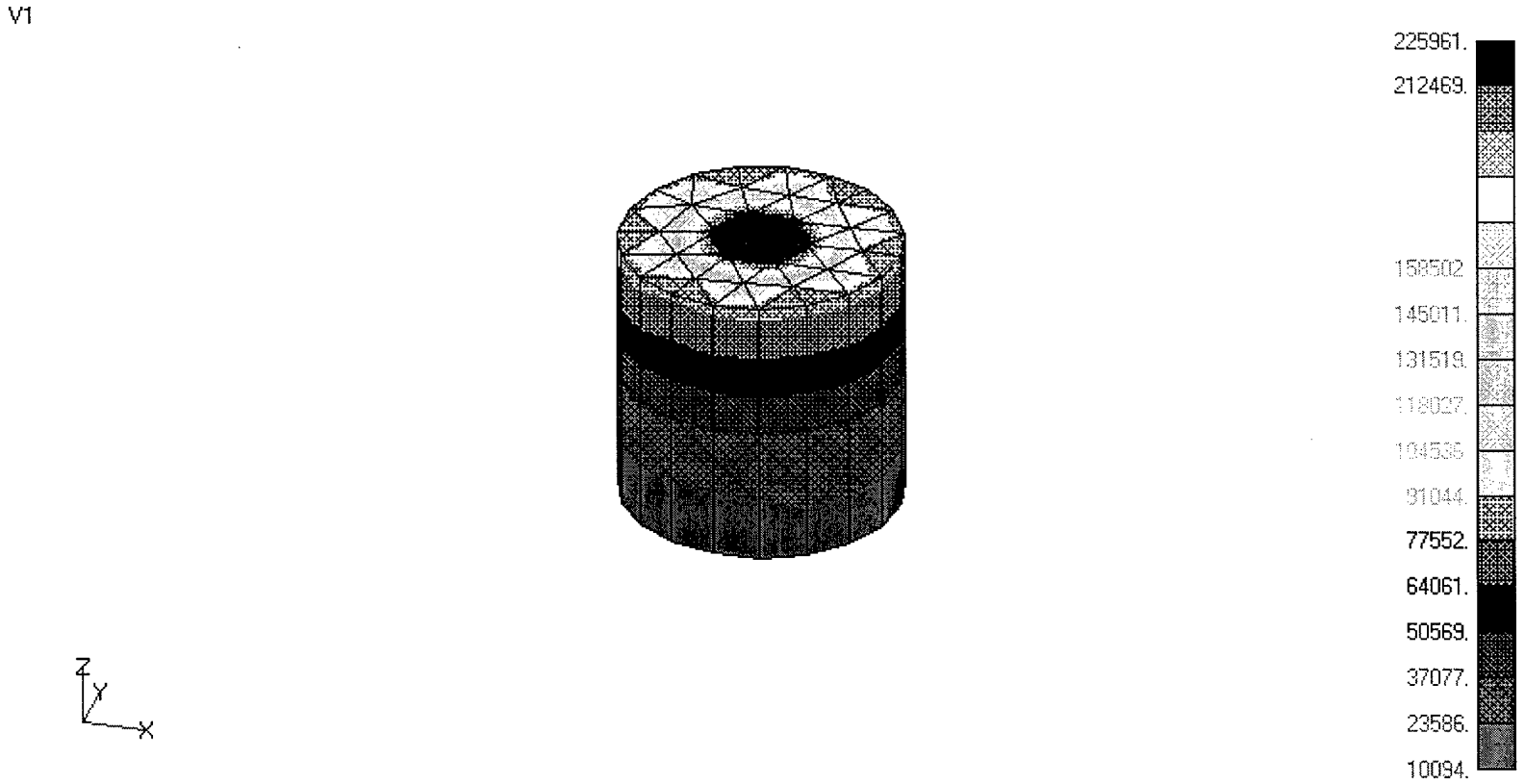

Vertical Load = 2,300,000 lbs
Linear Elastic-Perfectly Plastic Clayey Soil (Hyperbolic Extended Drucker-Prager)
E = 30,000 psf, υ = 0.499, Slope Angle = 10.2°, Dilation Angle = 10.2°
Pile, AISI 4340 Steel

Figure - 60 Maximum Pile von Mises Stress vs. Vertical Load

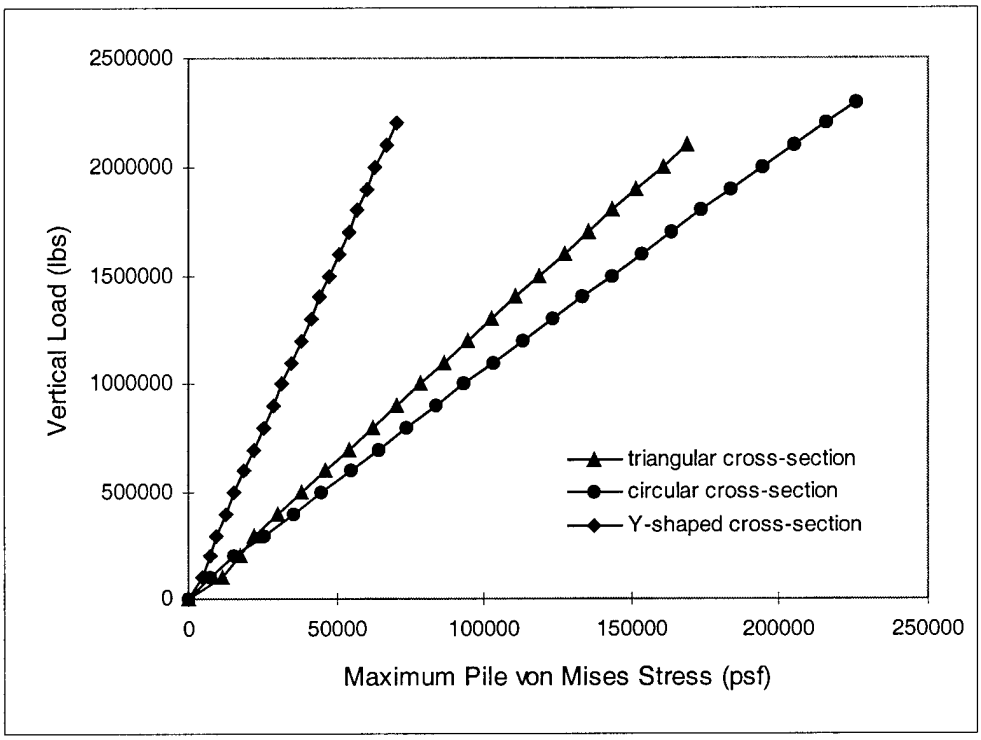

Figure - 61 Maximum Total Pile Displacement vs. 45-Degree Inclined Load

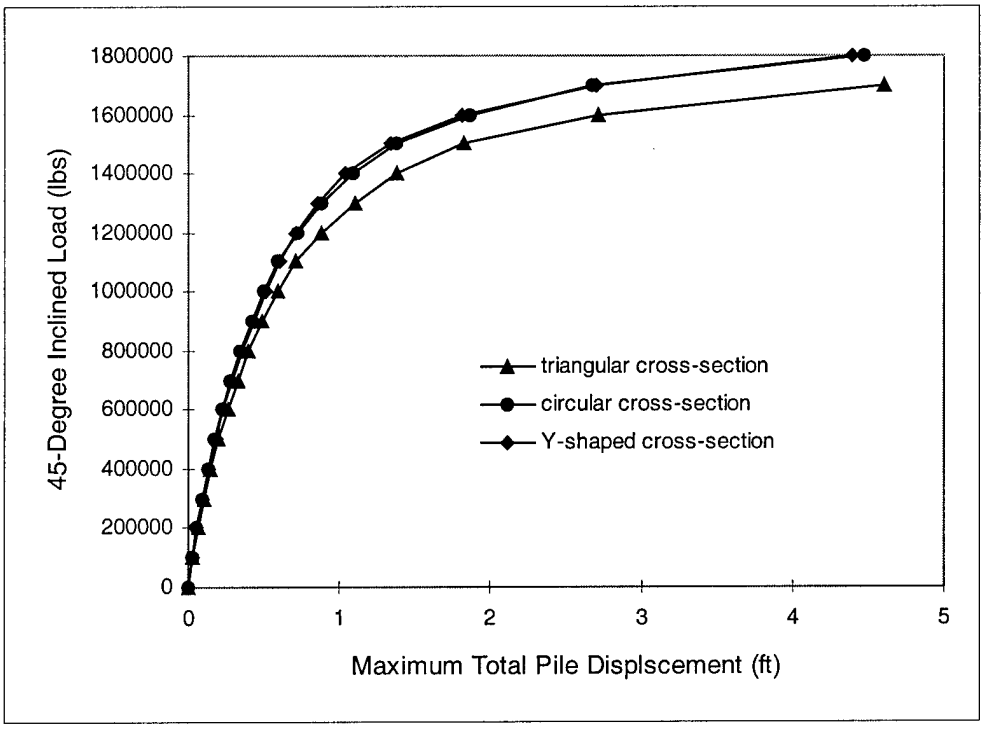

Figure - 62 Maximum Horizontal Pile Displacement vs. 45-Degree Inclined Load

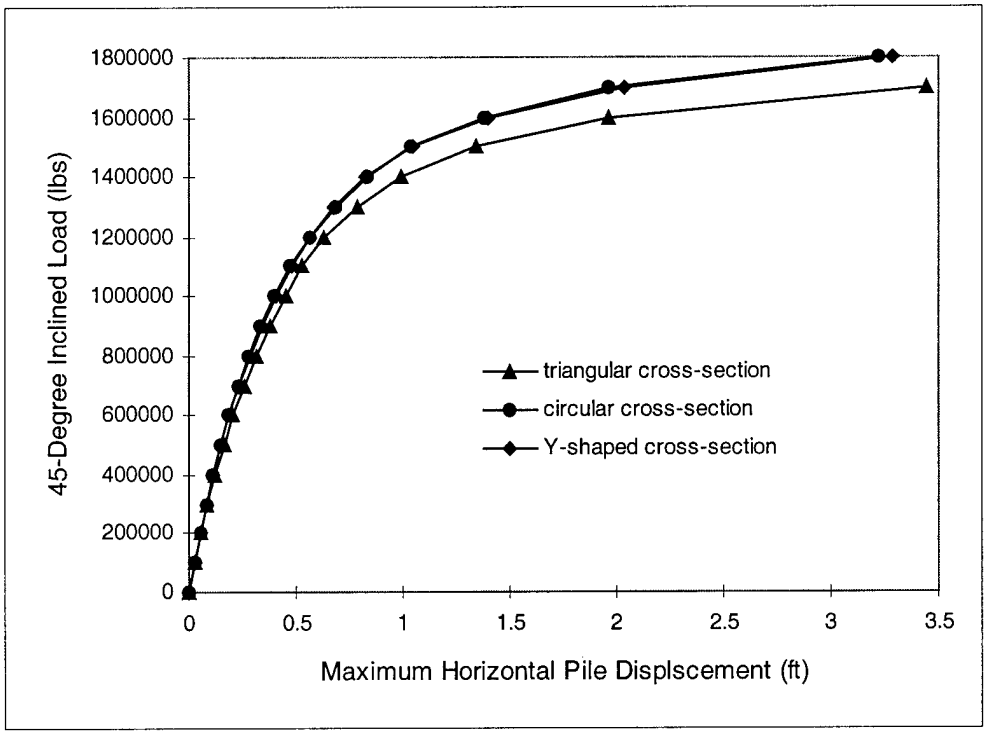

Figure - 63 Minimum Soil Minor Principal Stress vs. 45-Degree Inclined Load

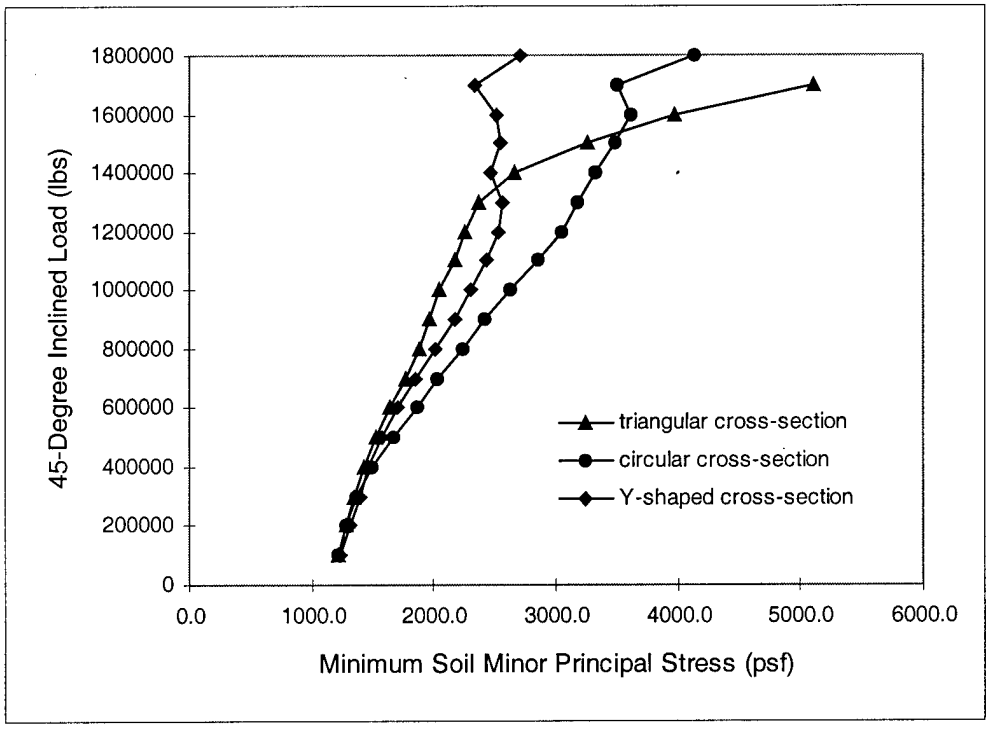

Figure - 64 Maximum Pile von Mises Stress vs. 45-Degree Inclined Load

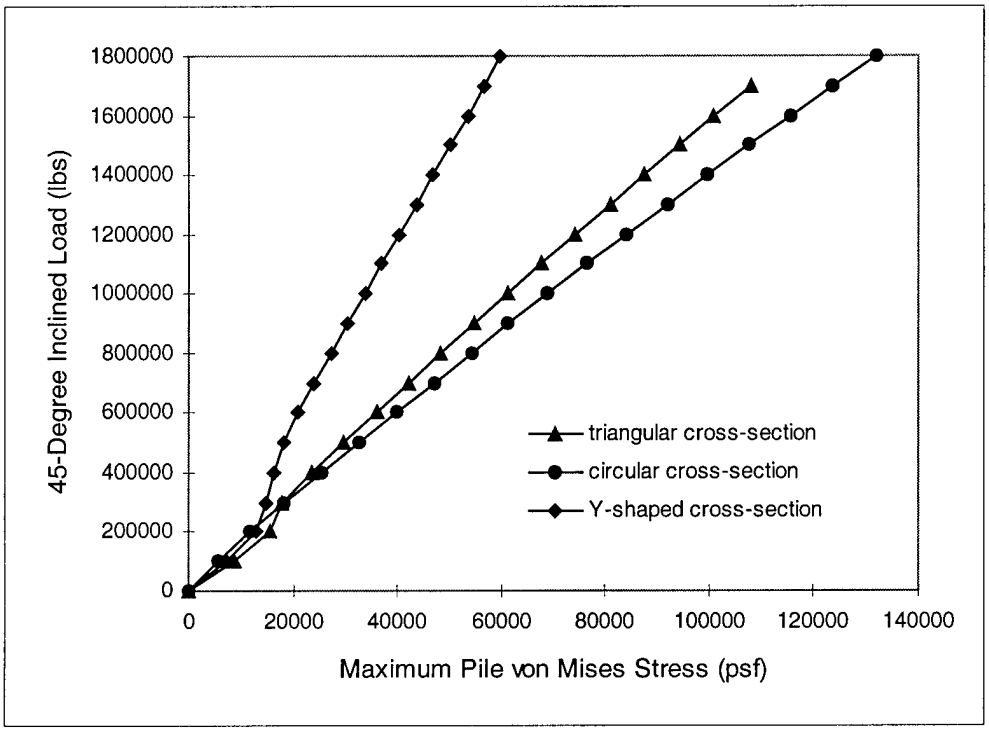

Figure - 65 Schematic of Suction Pile with Flange

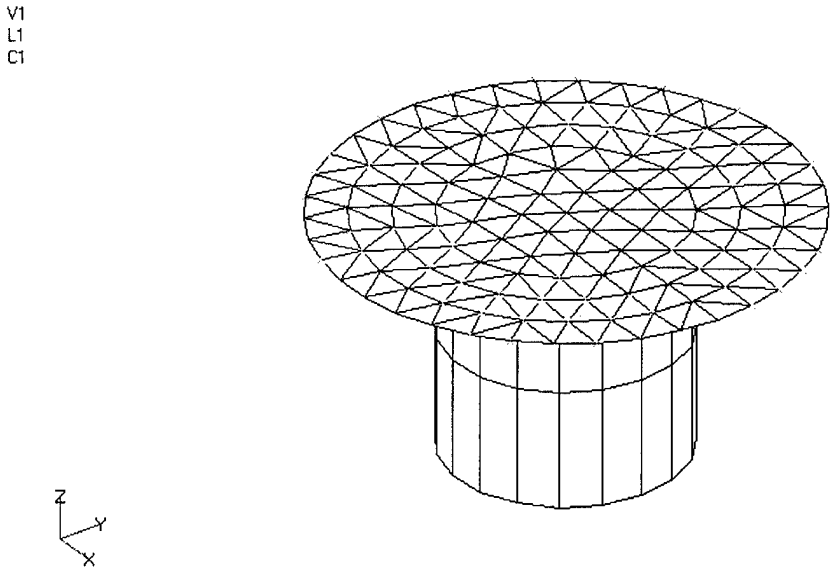

Figure - 66 Selected Loading Points

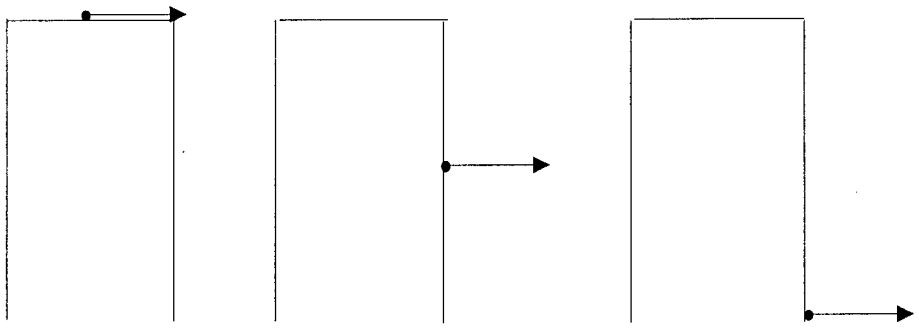

Figure - 67 Schematic of the Telescopic Pile

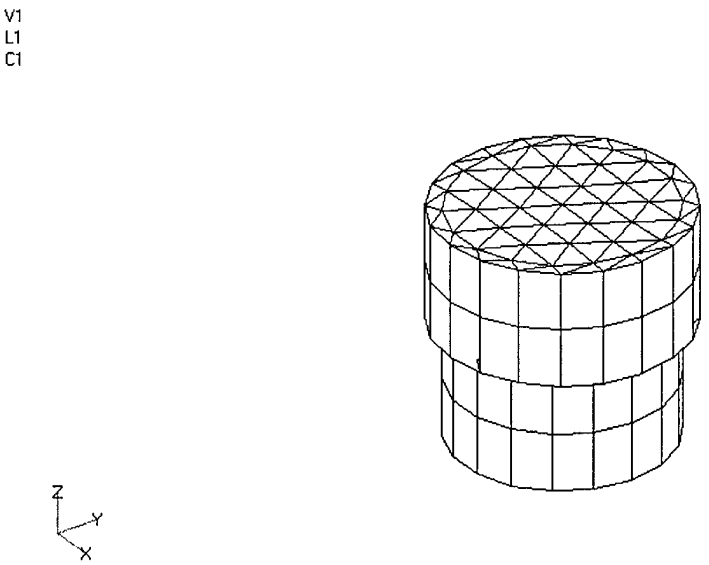

Figure - 68 Layered Soil Conditions

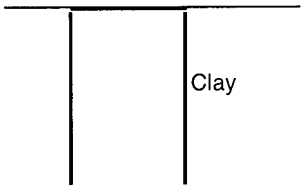

Layered Soil - 1

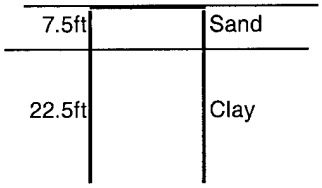

Layered Soil - 2

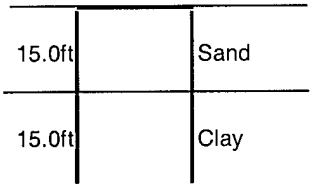

Layered Soil - 3

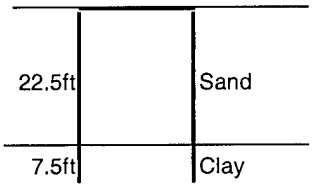

Layered Soil - 4

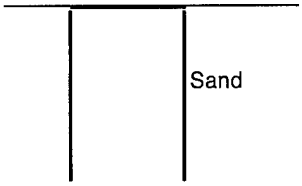

Layered Soil - 5

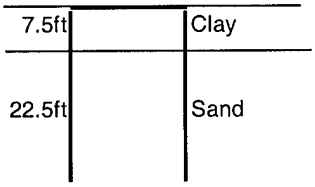

Layered Soil - 6

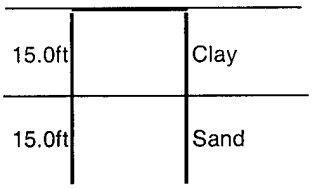

Layered Soil - 7

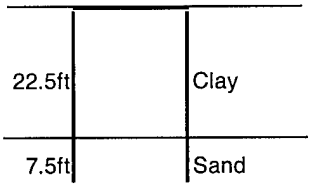

Layered Soil - 8

Figure - 69 Pile Total Displacements (Circular Section)

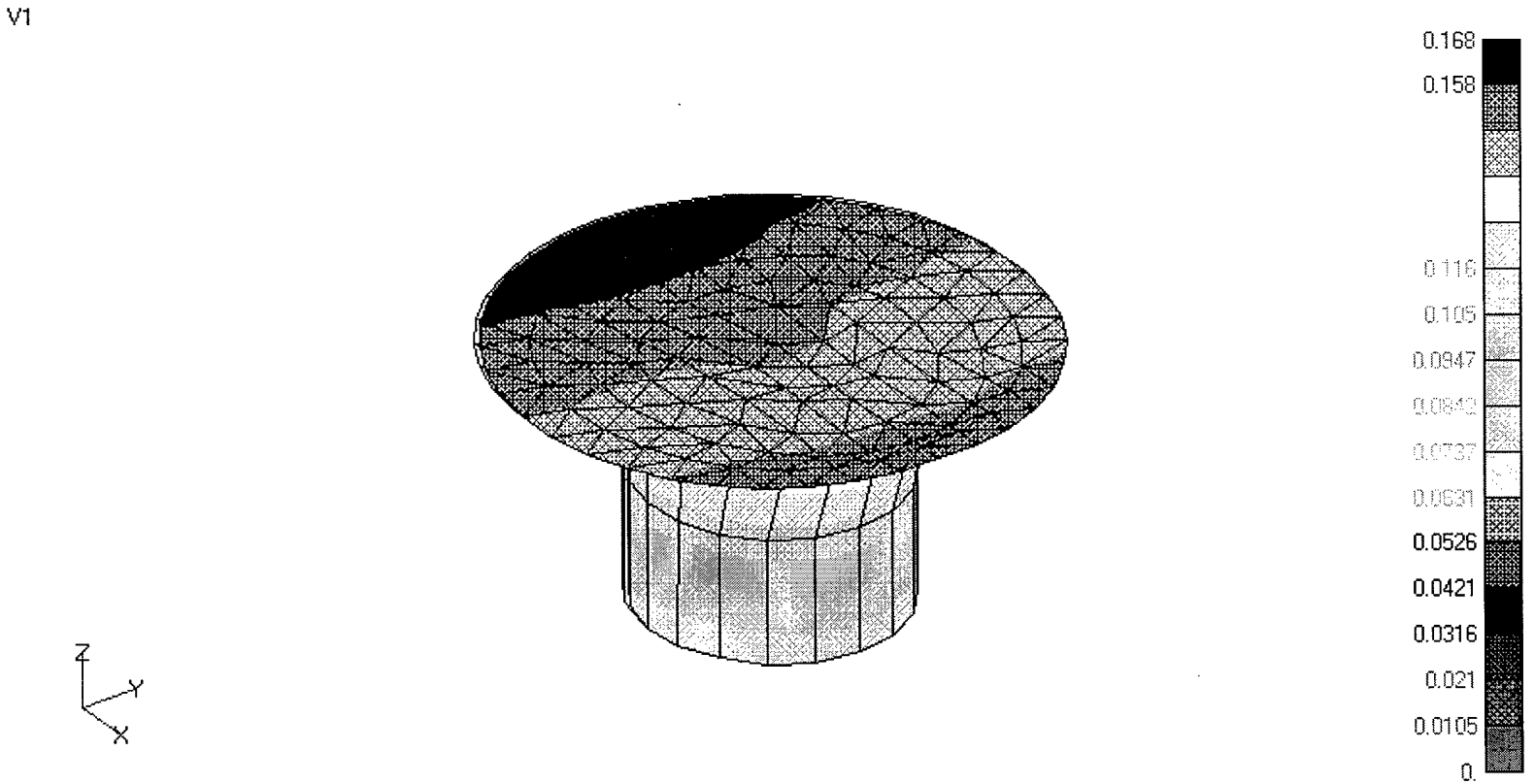

Horizontal Load = 8,000,000 lbs
Linear Elastic-Perfectly Plastic Sandy Soil (Linear Extended Drucker-Prager)
E = 864,000 psf, $\upsilon = 0.3$, Slope Angle = 46.2°, Dilation Angle = 21.5°
Pile, AISI 4340 Steel

Figure - 70 Maximum Total Pile Displacement vs. Horizontal Load

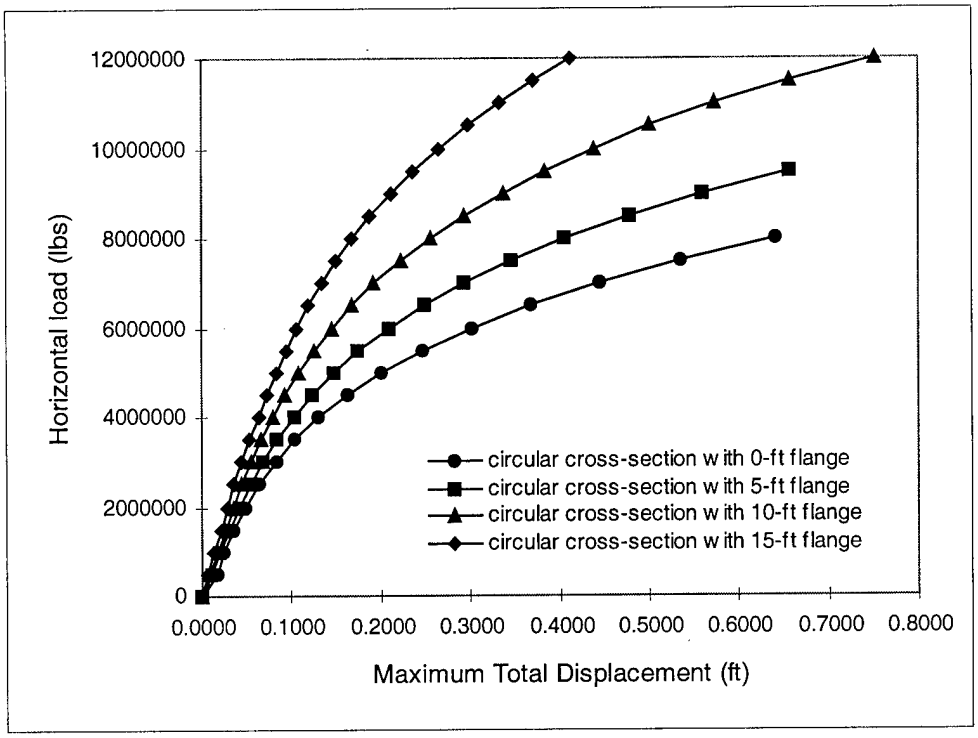

Figure - 71 Maximum Horizontal Pile Displacement vs. Horizontal Load

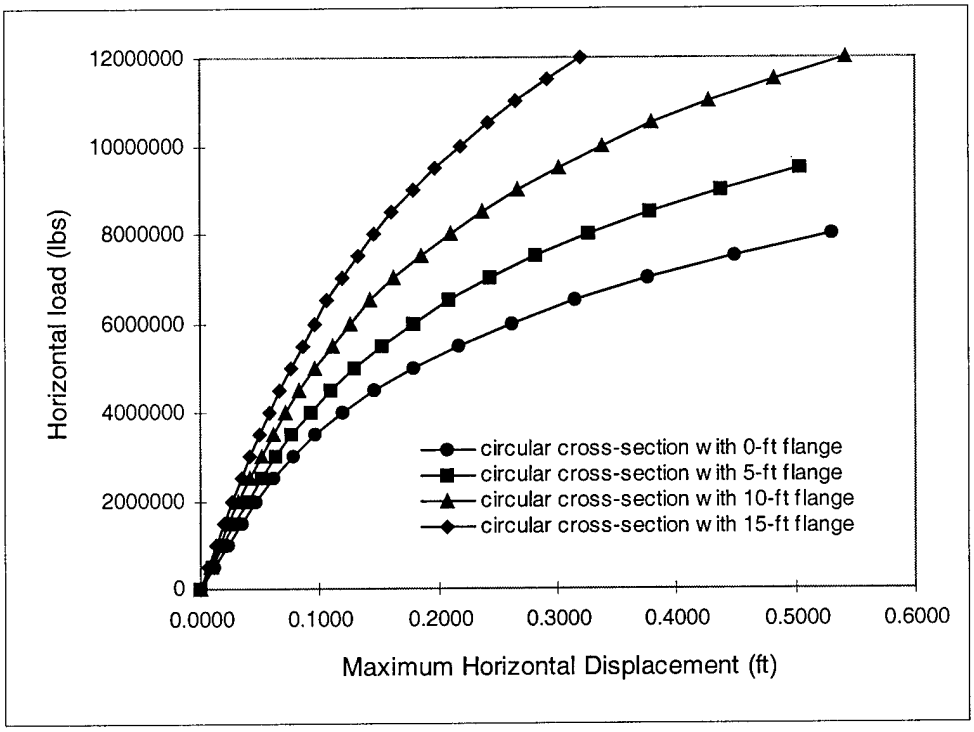

Figure - 72 Soil Minor Principal Stresses on a Vertical Plane along Horizontal Load Direction (Circular Pile with 15-ft flange)

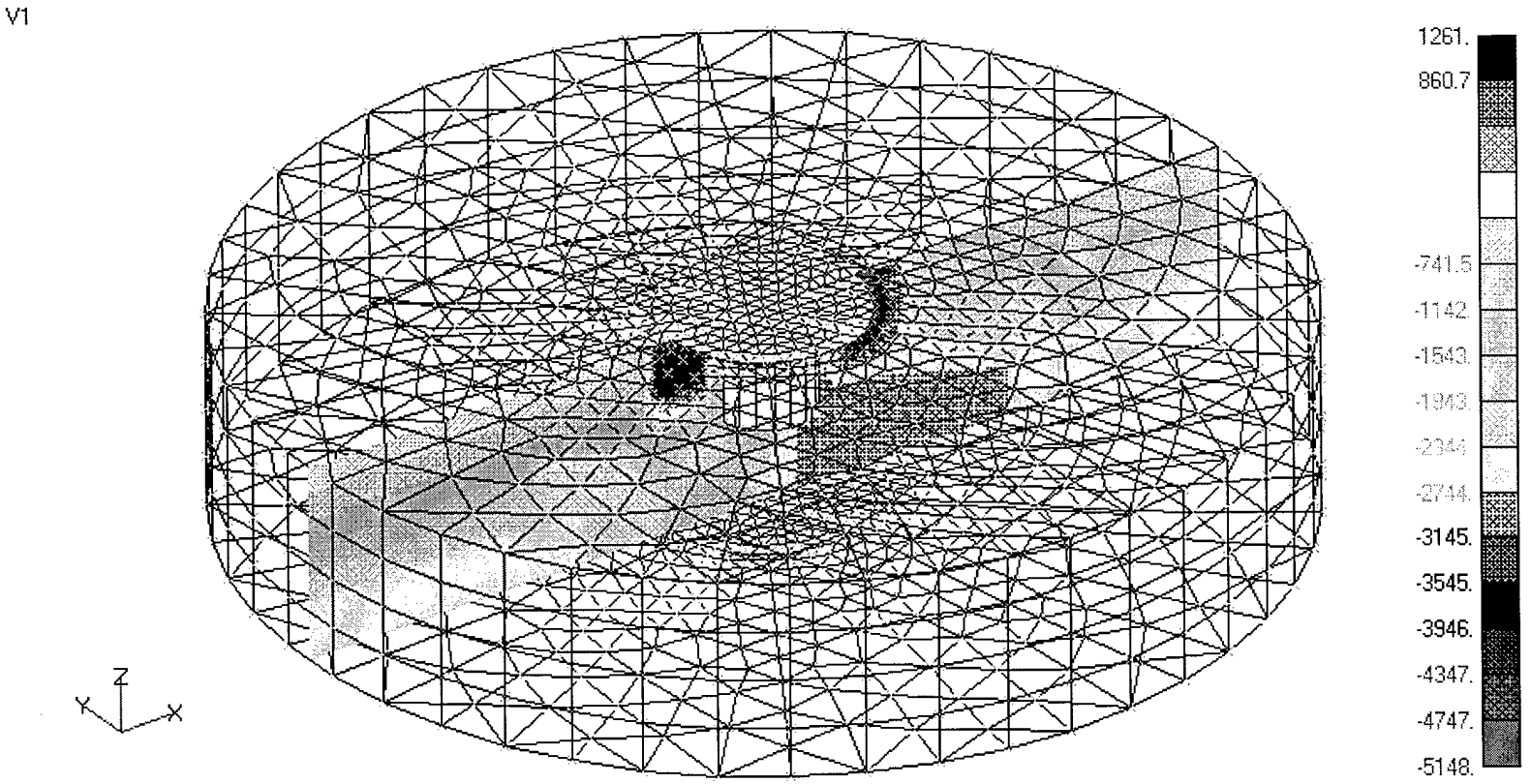

Horizontal Load = 8,000,000 lbs
Linear Elastic-Perfectly Plastic Sandy Soil (Linear Extended Drucker-Prager)
E = 864,000 psf, υ = 0.3, Slope Angle = 46.2°, Dilation Angle = 21.5°
Pile, AISI 4340 Steel

Figure - 73 Minimum Soil Minor Principal Stress vs. Horizontal Load

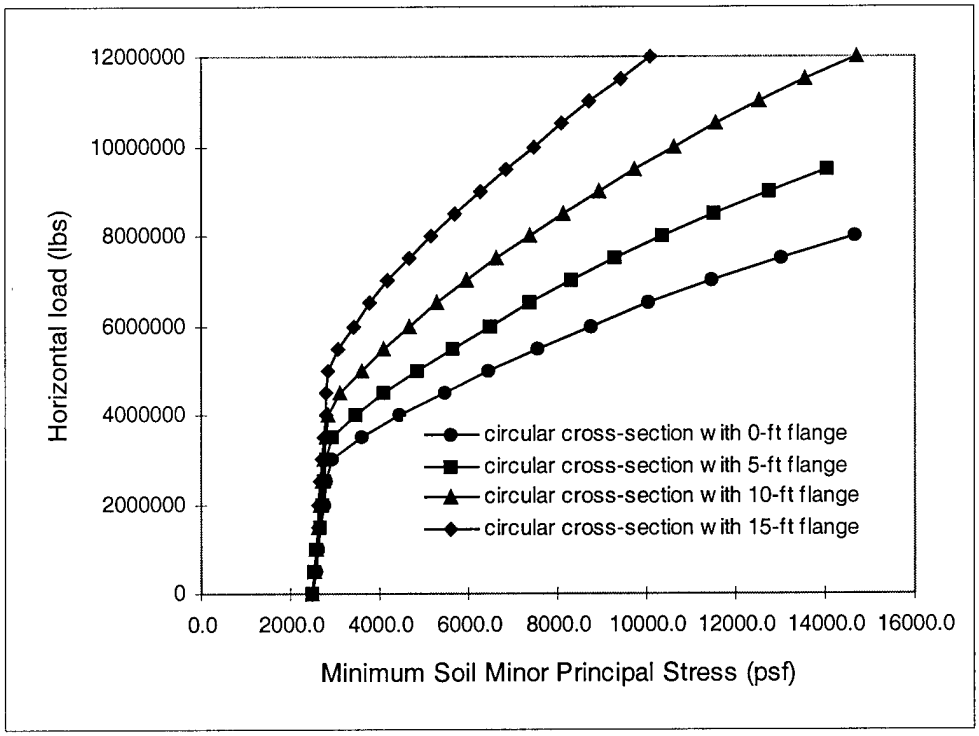

Figure - 74 Pile von Mises Stresses on the Pile Surface (Circular Pile with 15-ft Flange)

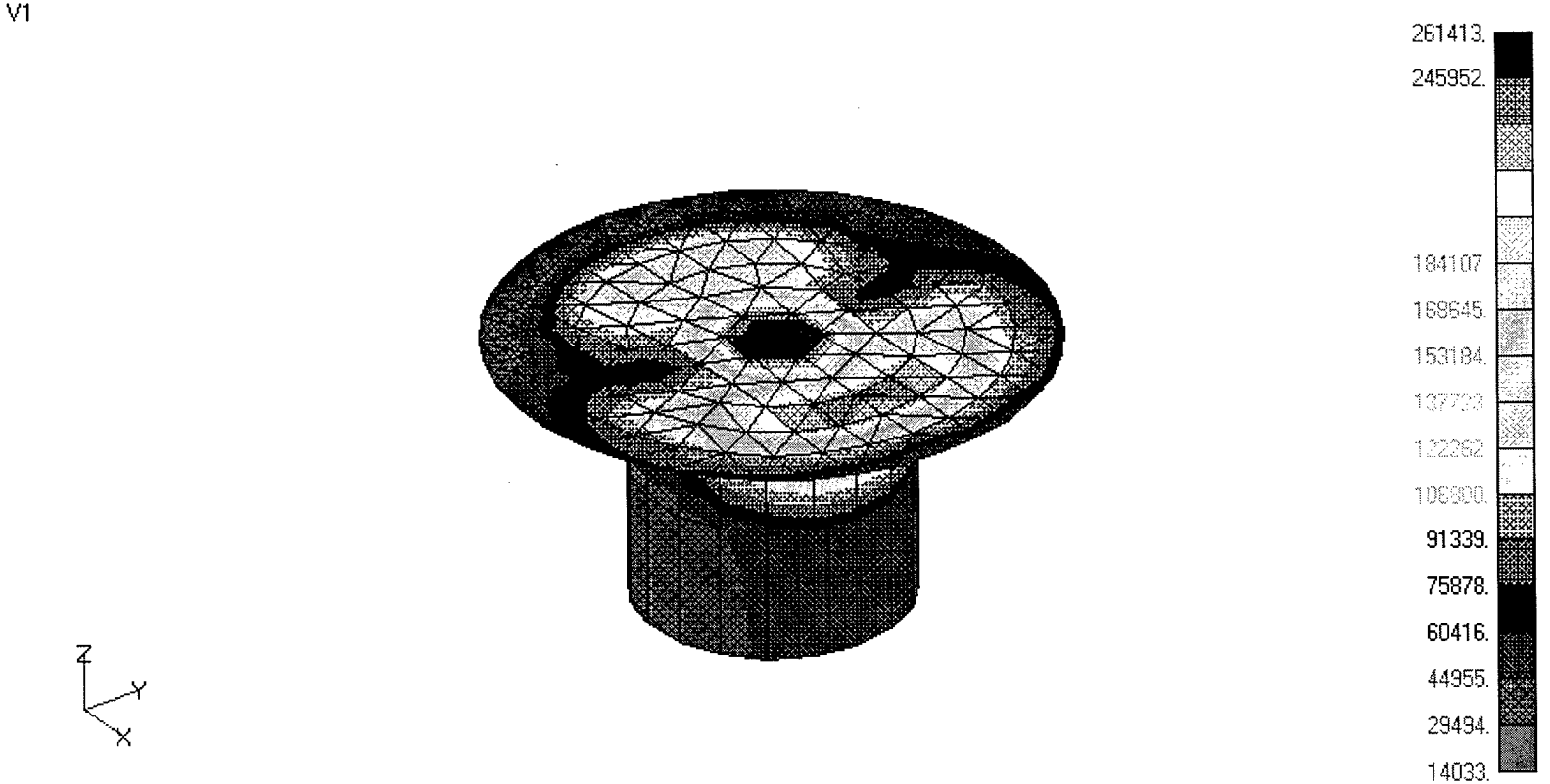

Horizontal Load = 8,000,000 lbs
Linear Elastic-Perfectly Plastic Sandy Soil (Linear Extended Drucker-Prager)
E = 864,000 psf, $\upsilon = 0.3$, Slope Angle = 46.2°, Dilation Angle = 21.5°
Pile, AISI 4340 Steel

Figure - 75 Maximum Pile von Mises Stress vs. Horizontal Load

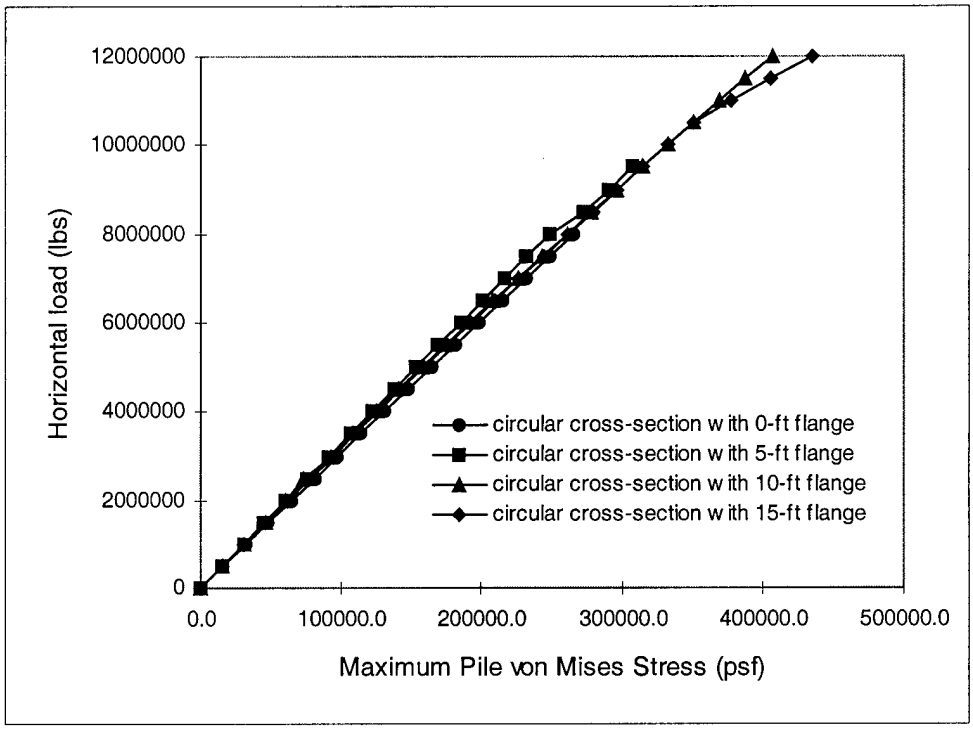

Figure – 76 Pile Total Displacements (Circular Pile with 15-ft Flange)

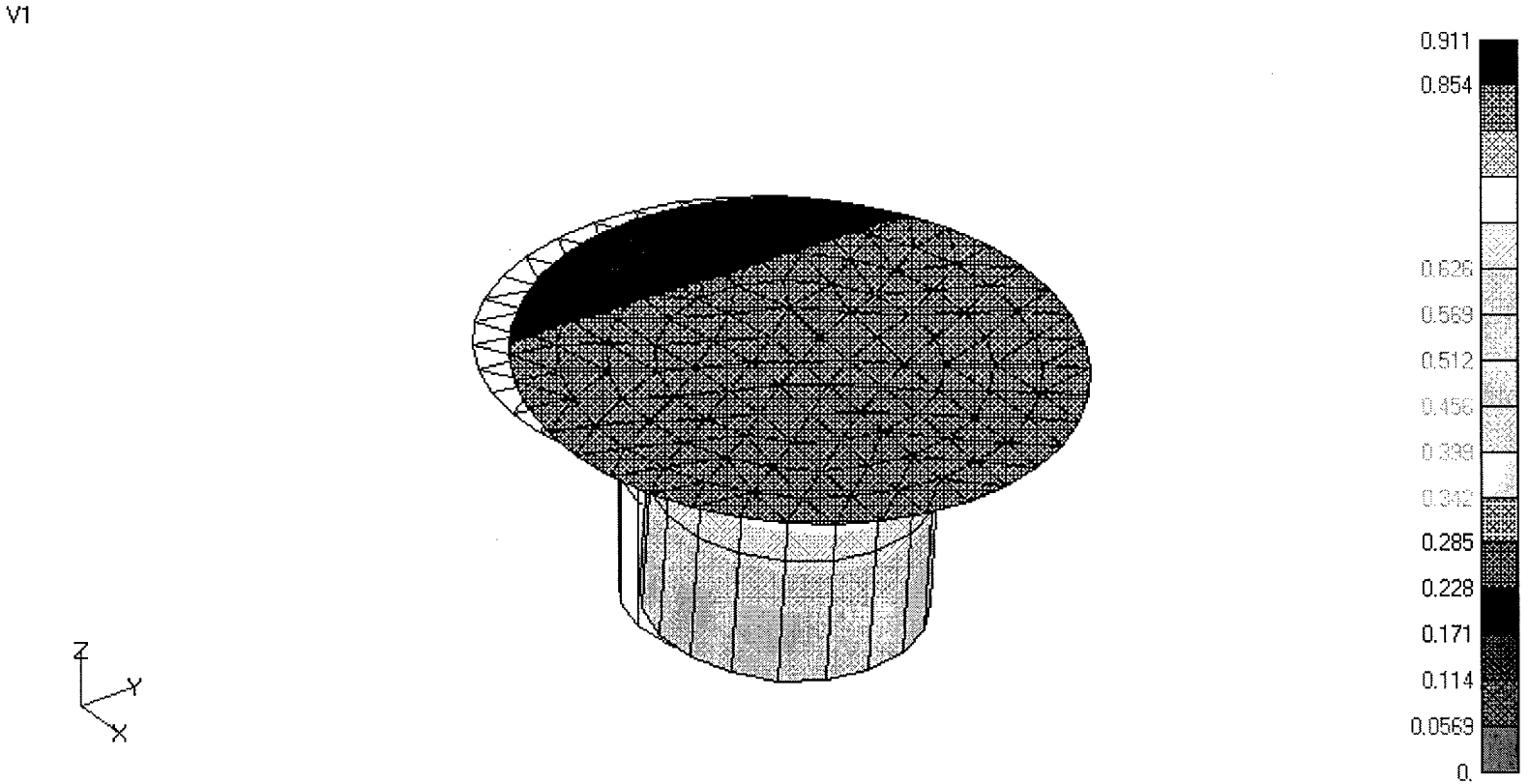

Horizontal Load = 2,100,000 lbs
Linear Elastic-Perfectly Plastic Clayey Soil (Hyperbolic Extended Drucker-Prager)
E = 30,000 psf, υ = 0.499, Slope Angle = 10.2°, Dilation Angle = 10.2°
Pile, AISI 4340 Steel

Figure - 77 Maximum Total Pile Displacement vs. Horizontal Load

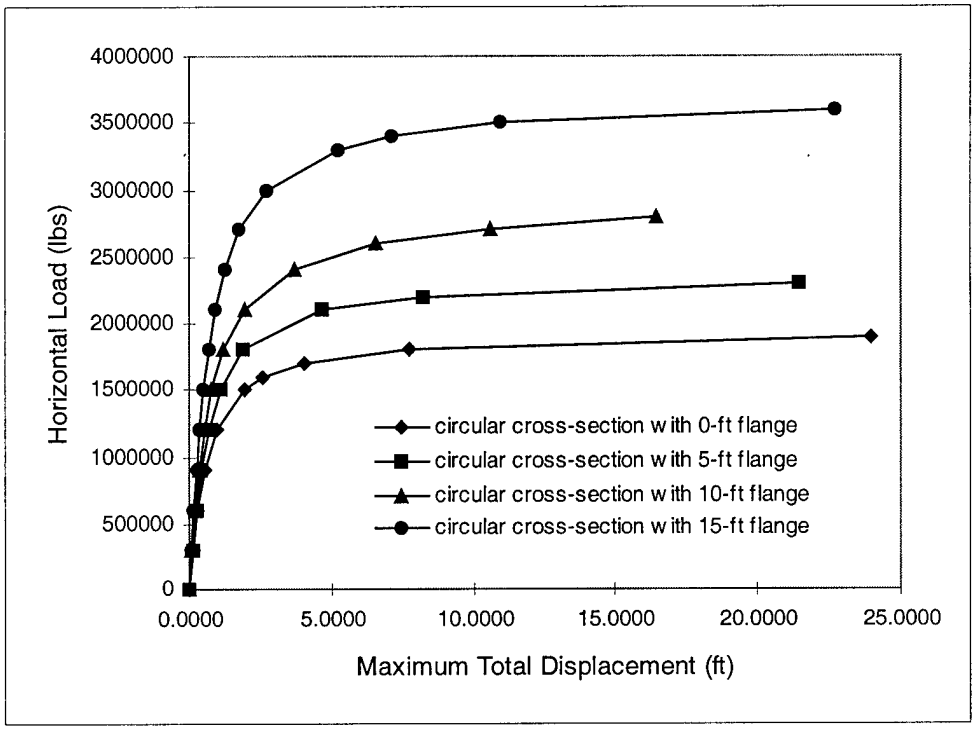

Figure - 78 Maximum Horizontal Pile Displacement vs. Horizontal Load

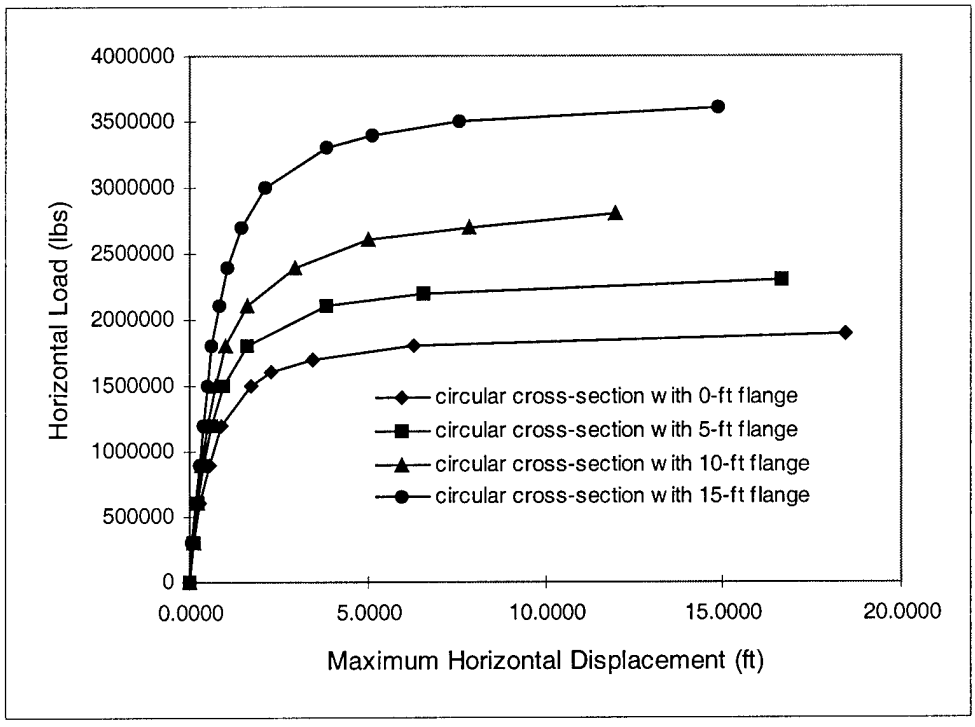

Figure - 79 Soil Minor Principal Stresses on a Vertical Plane along Horizontal Load Direction (Circular Pile with 15-ft flange)

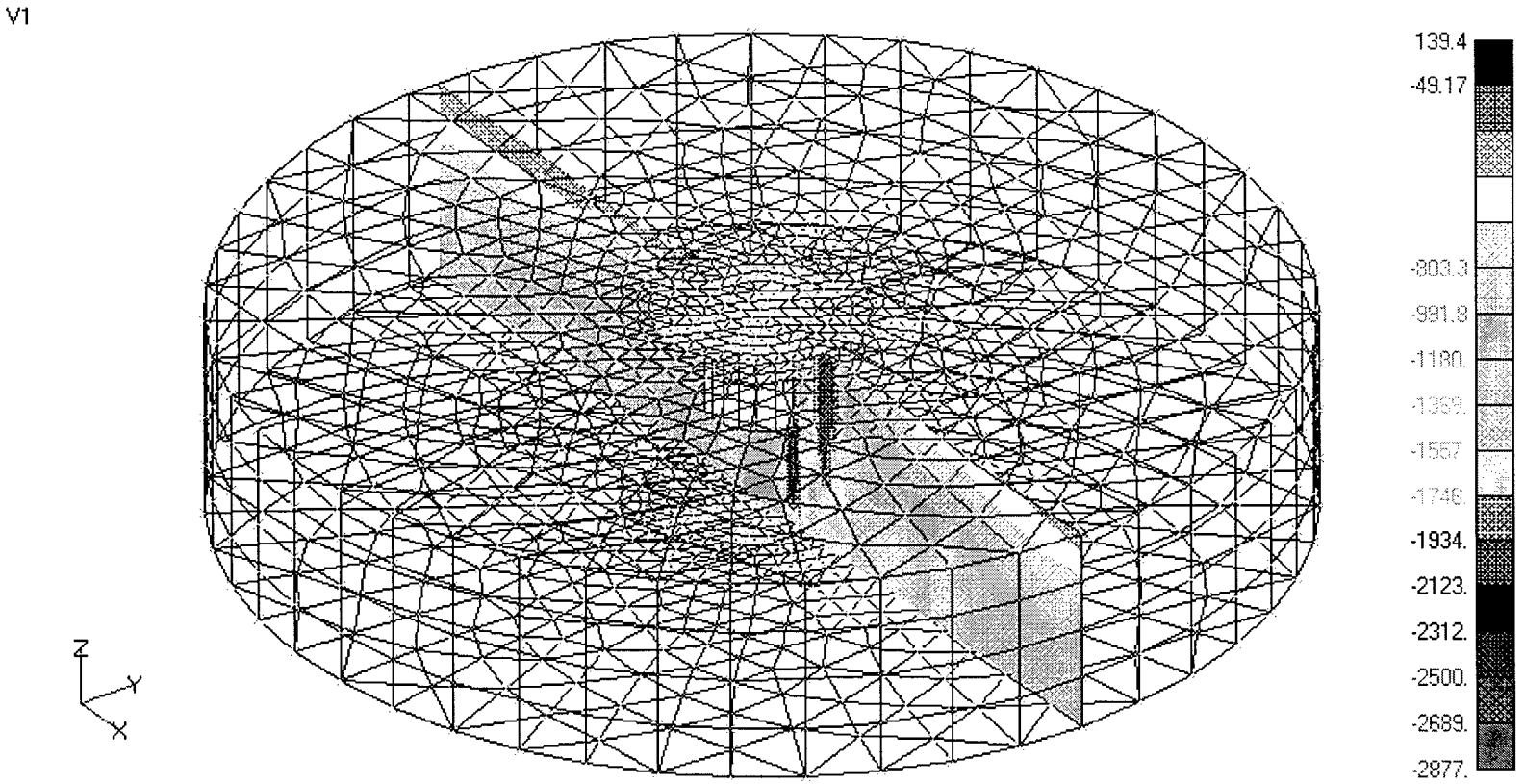

Horizontal Load = 2,100,000 lbs
Linear Elastic-Perfectly Plastic Clayey Soil (Hyperbolic Extended Drucker-Prager)
E = 30,000 psf, υ = 0.499, Slope Angle = 10.2°, Dilation Angle = 10.2°
Pile, AISI 4340 Steel

Figure - 80 Minimum Soil Minor Principal Stress vs. Horizontal Load

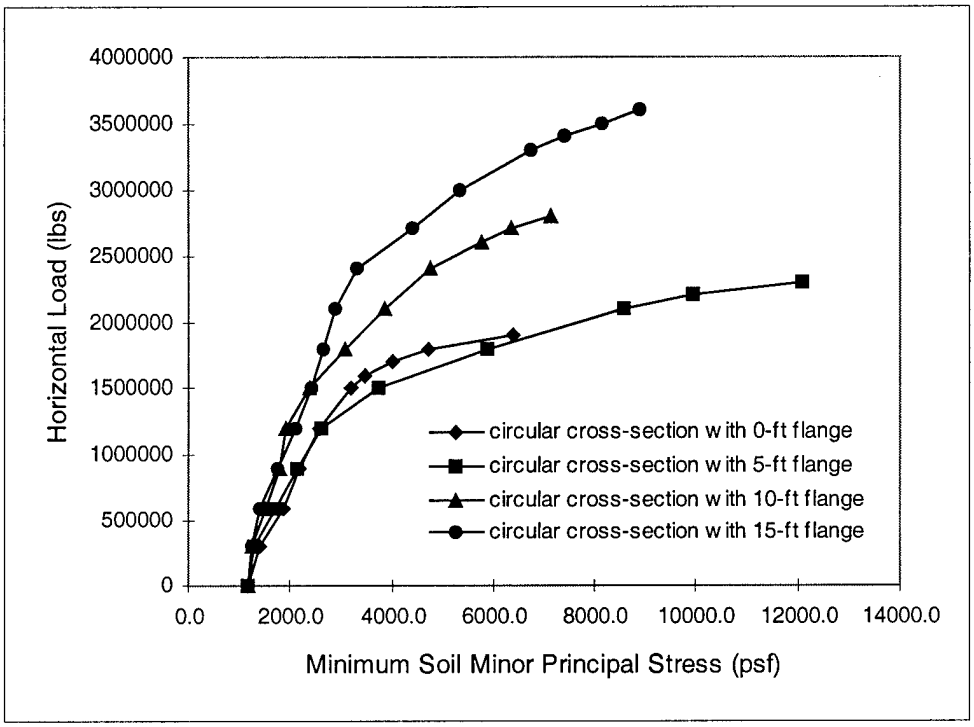

Figure - 81 Pile von Mises Stresses on the Pile Surface (Circular Pile with 15-ft Flange)

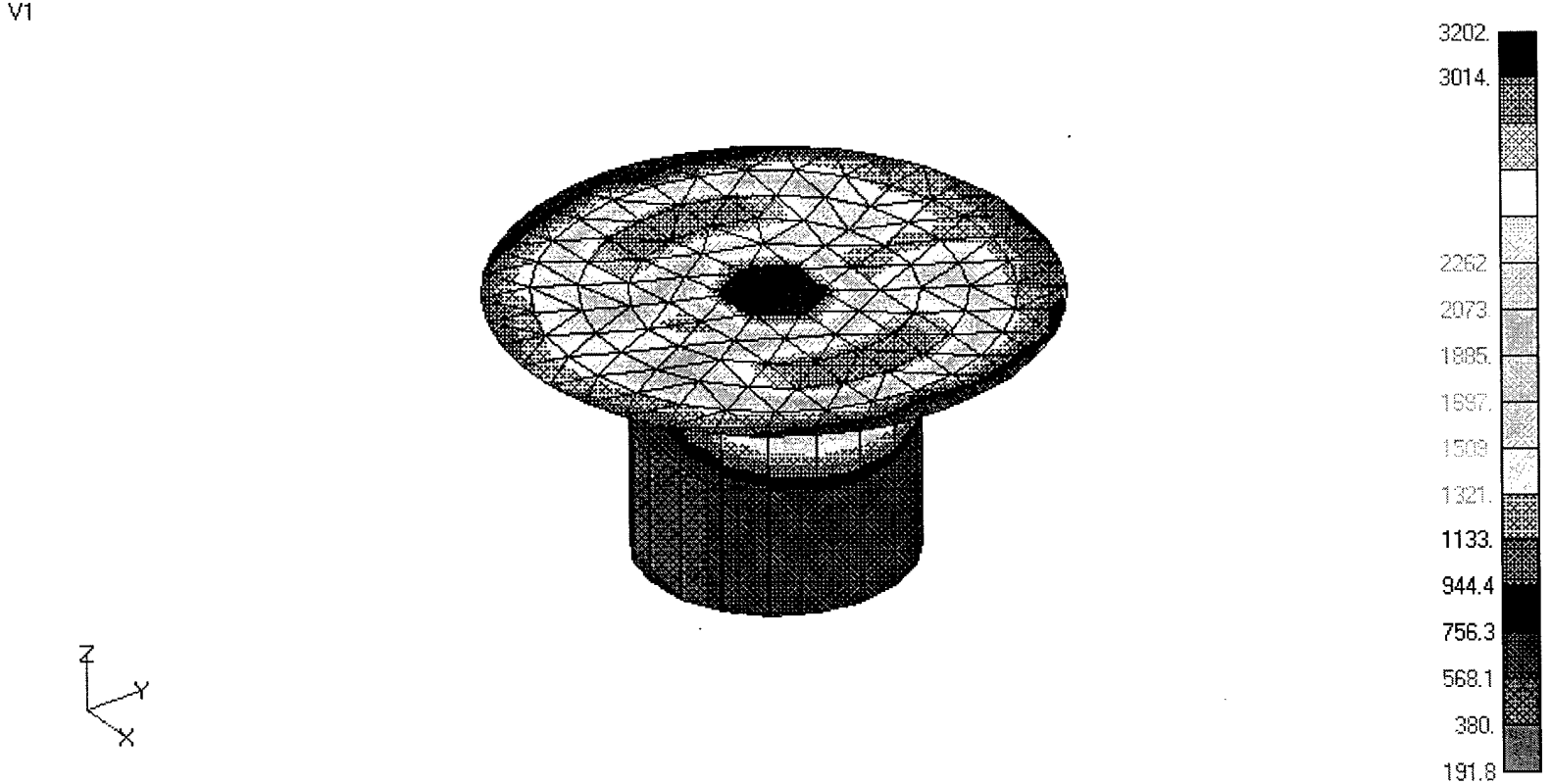

Horizontal Load = 100,000 lbs
Linear Elastic-Perfectly Plastic Clayey Soil (Hyperbolic Extended Drucker-Prager)
E = 30,000 psf, υ = 0.499, Slope Angle = 10.2°, Dilation Angle = 10.2°
Pile, AISI 4340 Steel

Figure - 82 Pile von Mises Stresses on the Pile Surface (Circular Pile with 15-ft Flange)

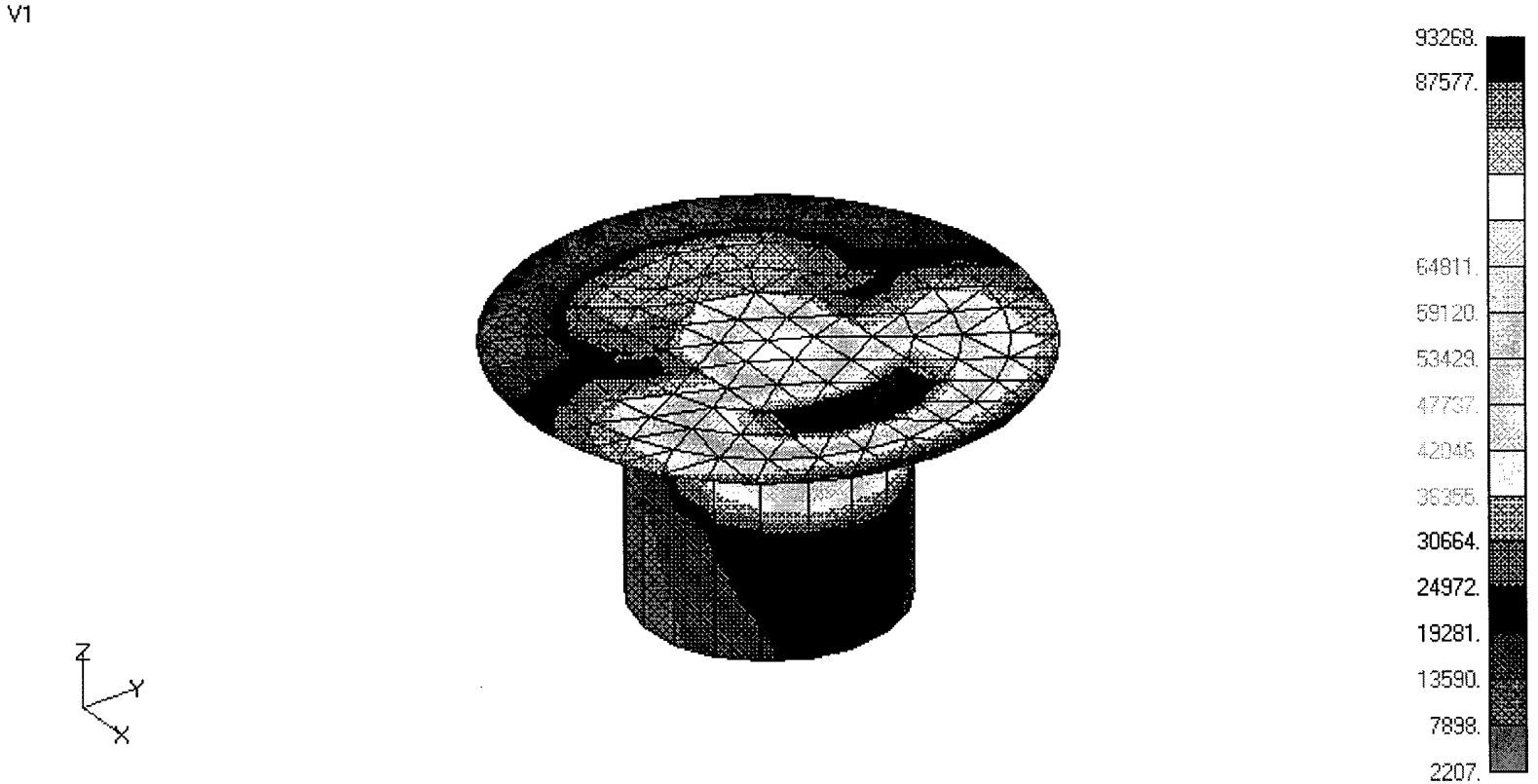

Horizontal Load = 2,100,000 lbs
Linear Elastic-Perfectly Plastic Clayey Soil (Hyperbolic Extended Drucker-Prager)
E = 30,000 psf, $\upsilon = 0.499$, Slope Angle = 10.2°, Dilation Angle = 10.2°
Pile, AISI 4340 Steel

Figure - 83 Maximum Pile von Mises Stress vs. Horizontal Load

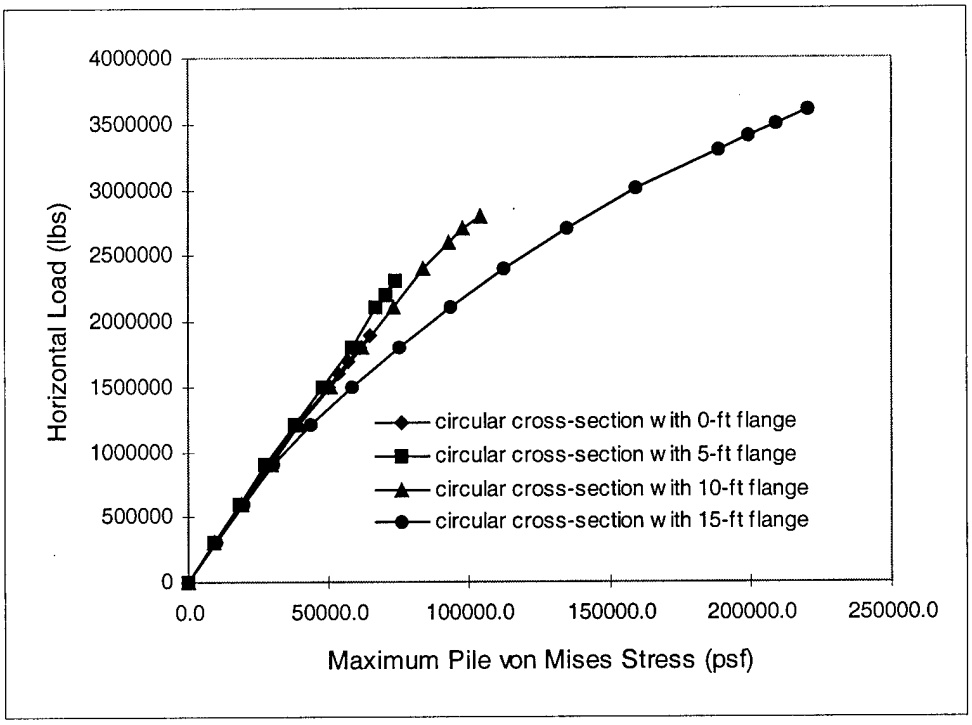

Figure - 84 Pile Total Displacements (Circular Section)

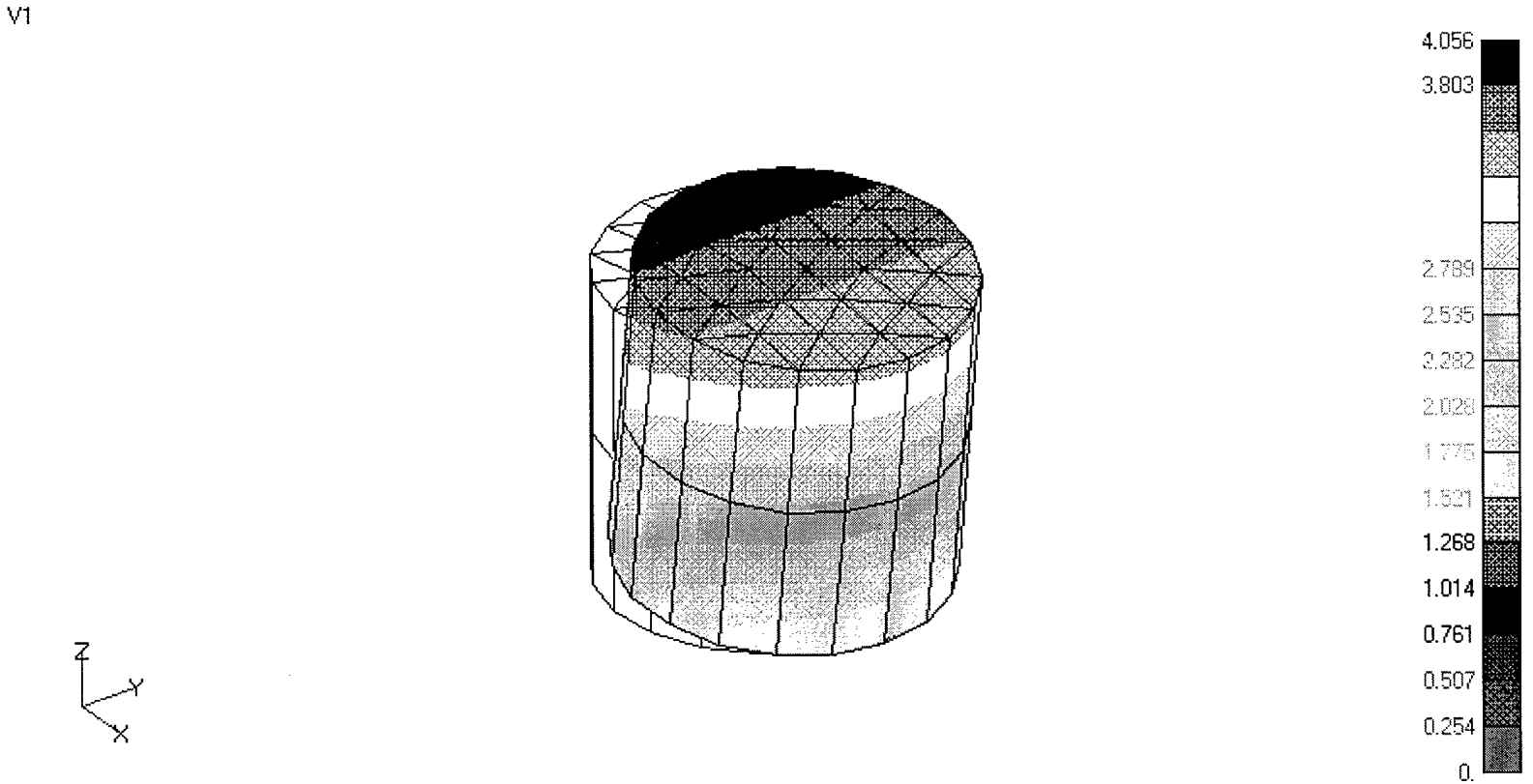

Horizontal Load at the Middle Depth of the Pile = 24,000,000 lbs
Linear Elastic-Perfectly Plastic Sandy Soil (Linear Extended Drucker-Prager)
E = 864,000 psf, υ = 0.3, Slope Angle = 46.2°, Dilation Angle = 21.5°
Pile, AISI 4340 Steel

Figure - 85 Pile Total Displacements (Circular Section)

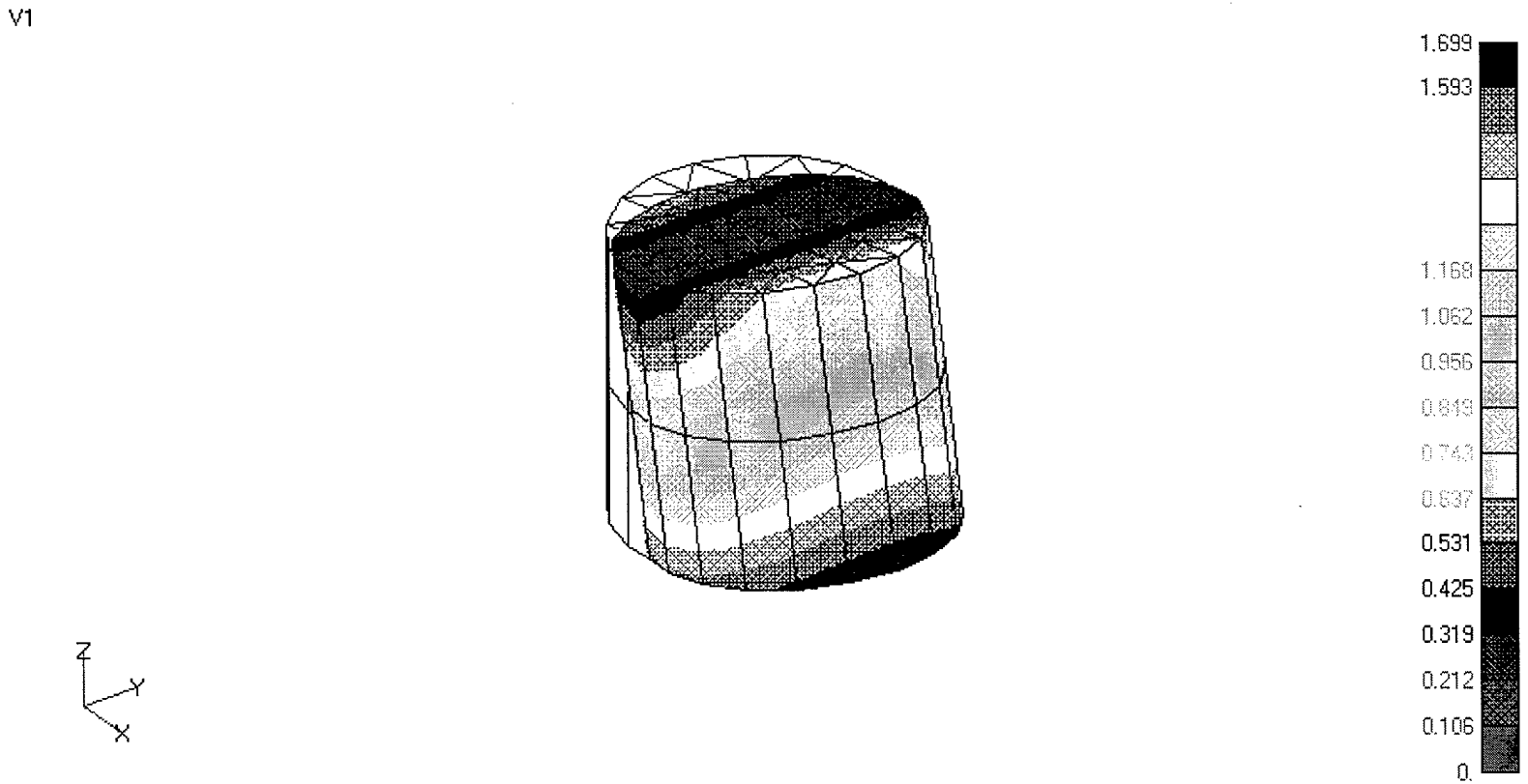

Horizontal Load at the Bottom of the Pile = 20,000,000 lbs
Linear Elastic-Perfectly Plastic Sandy Soil (Linear Extended Drucker-Prager)
E = 864,000 psf, $\upsilon = 0.3$, Slope Angle = 46.2°, Dilation Angle = 21.5°
Pile, AISI 4340 Steel

Figure - 86 Maximum Total Pile Displacement vs. Horizontal Load

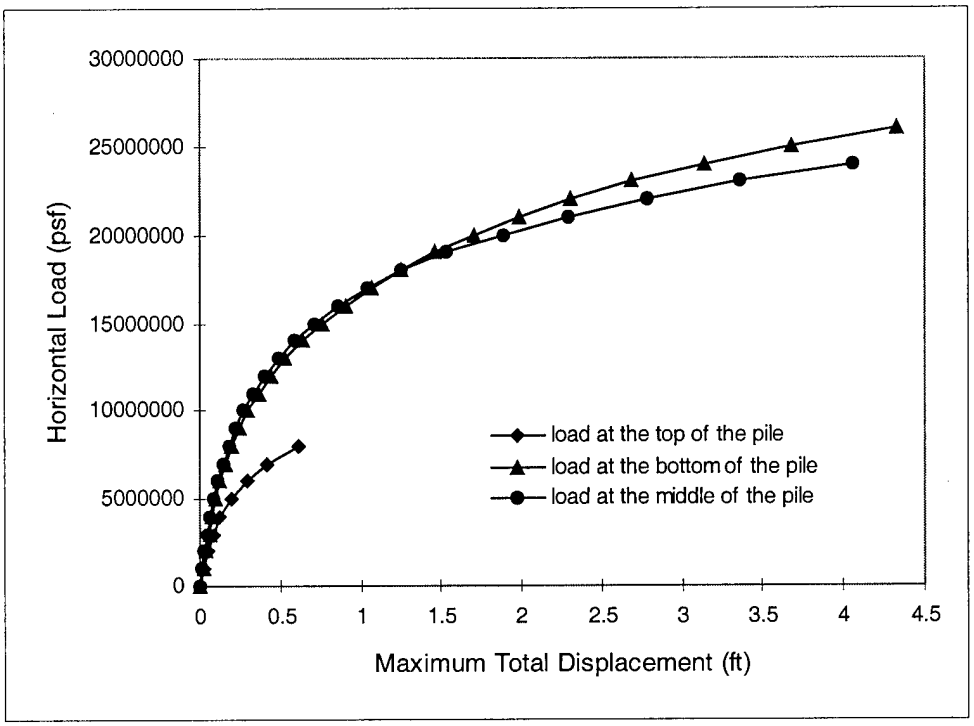

Figure - 87 Maximum Horizontal Pile Displacement vs. Horizontal Load

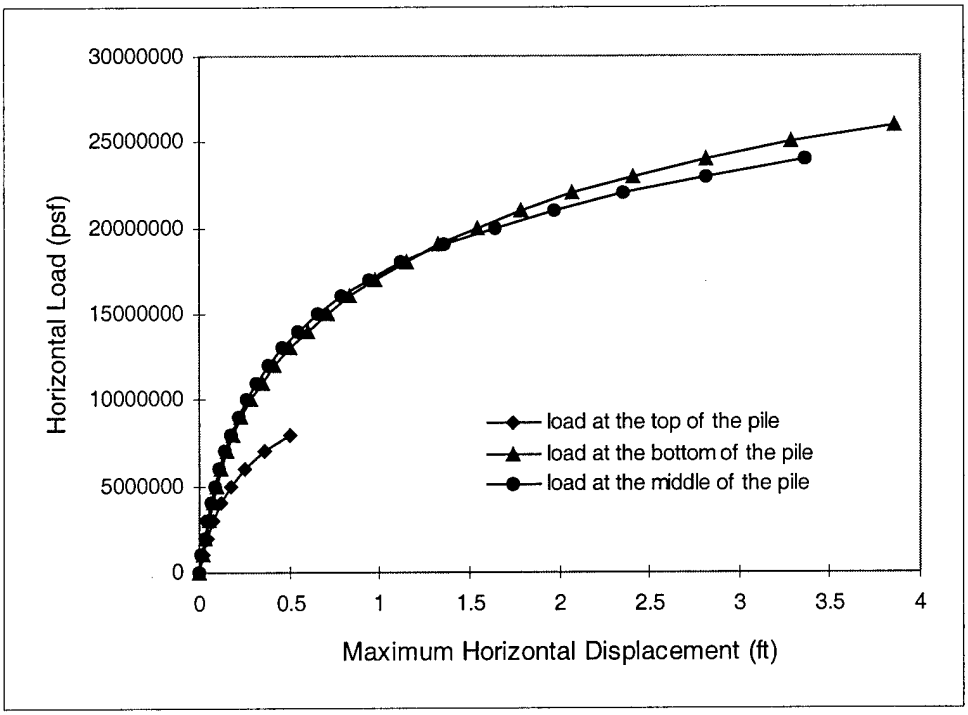

Figure - 88 Soil Minor Principal Stresses on a Vertical Plane along Horizontal Load Direction (Circular Pile with 15-ft flange)

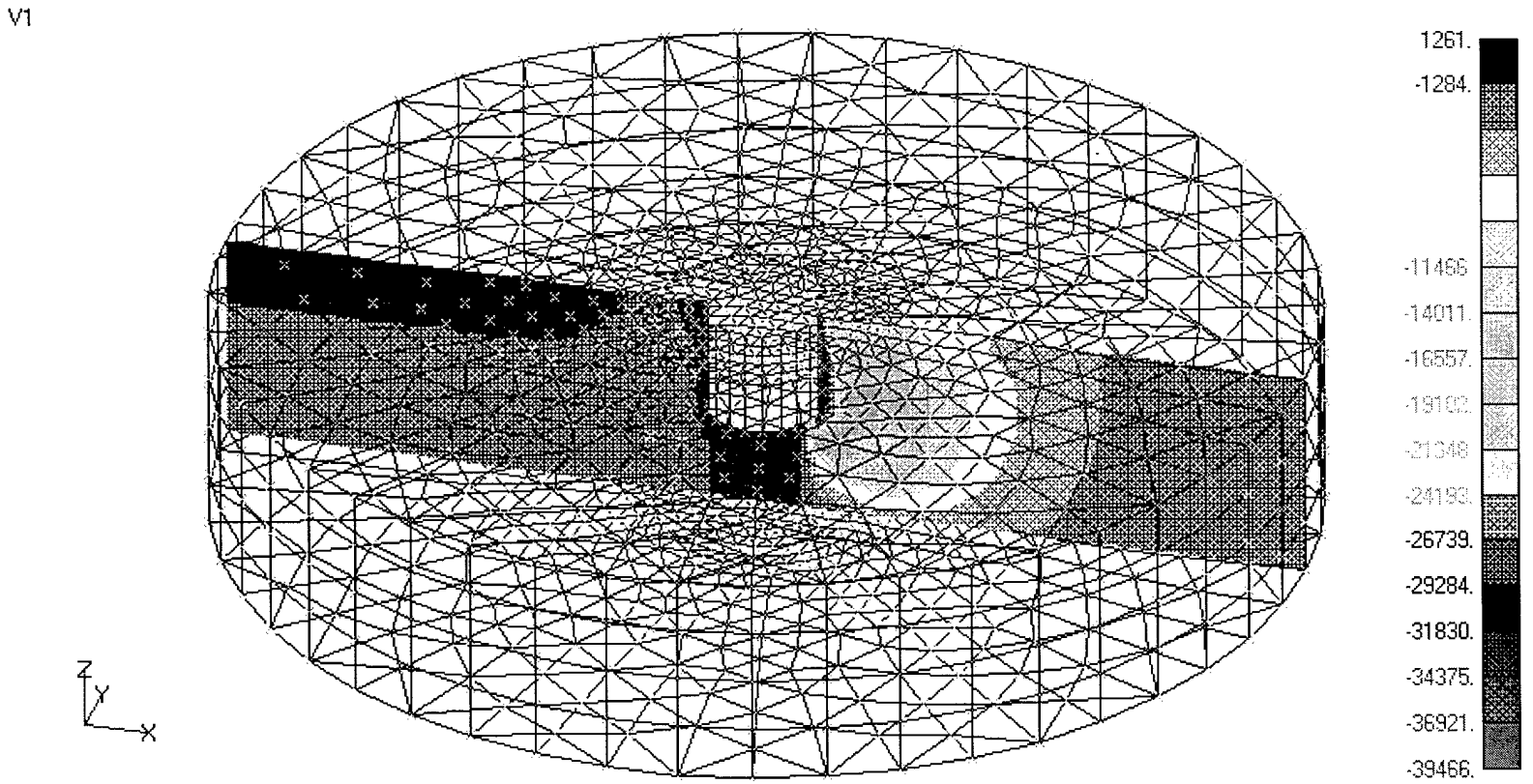

Horizontal Load at the Middle of the Pile = 24,000,000 lbs
Linear Elastic-Perfectly Plastic Sandy Soil (Linear Extended Drucker-Prager)
E = 864,000 psf, υ = 0.3, Slope Angle = 46.2°, Dilation Angle = 21.5°
Pile, AISI 4340 Steel

Figure - 89 Soil Minor Principal Stresses on a Vertical Plane along Horizontal Load Direction (Circular Pile with 15-ft flange)

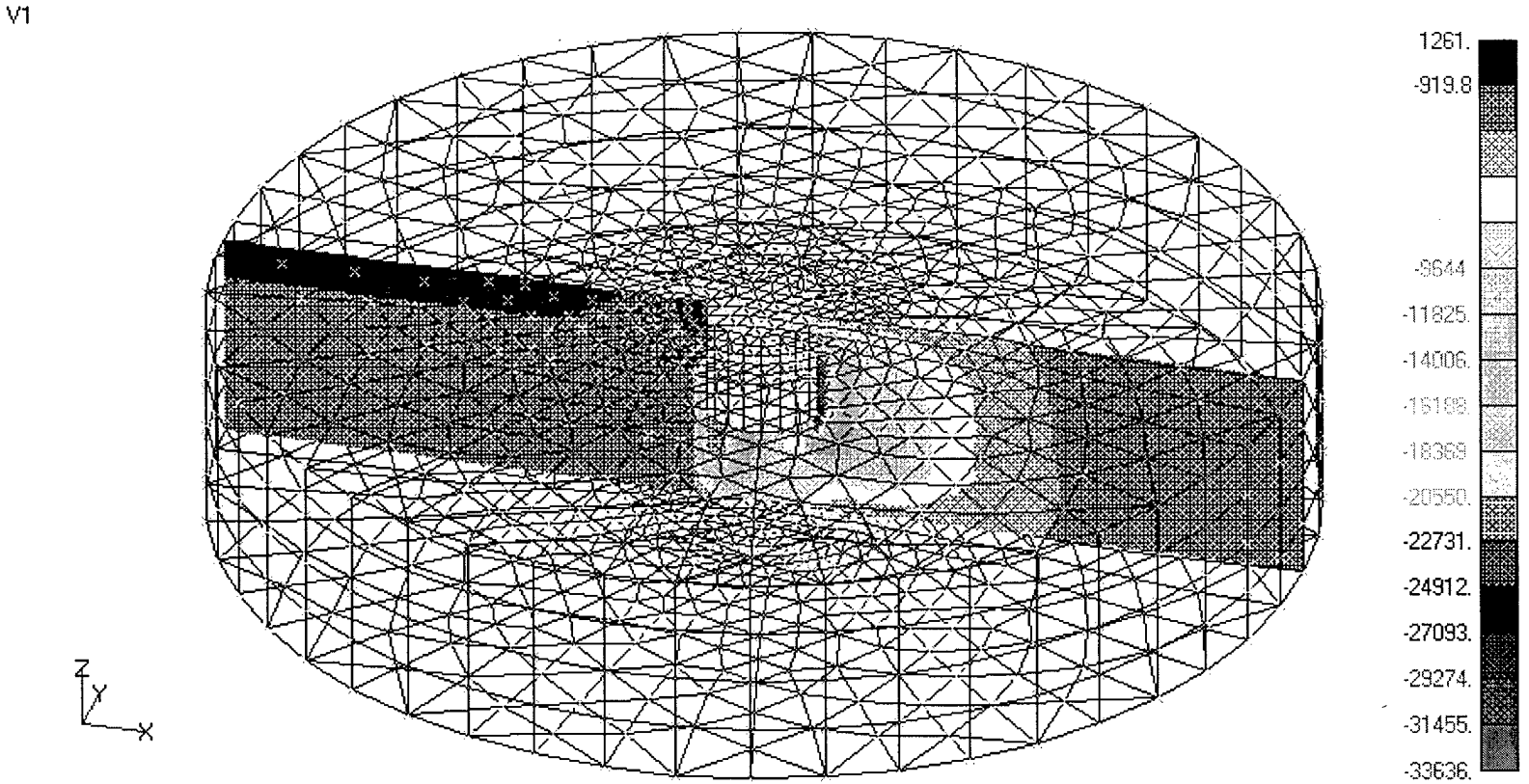

Horizontal Load at the Bottom of the Pile = 20,000,000 lbs
Linear Elastic-Perfectly Plastic Sandy Soil (Linear Extended Drucker-Prager)
E = 864,000 psf, υ = 0.3, Slope Angle = 46.2°, Dilation Angle = 21.5°
Pile, AISI 4340 Steel

Figure - 90 Minimum Soil Minor Principal Stress vs. Horizontal Load

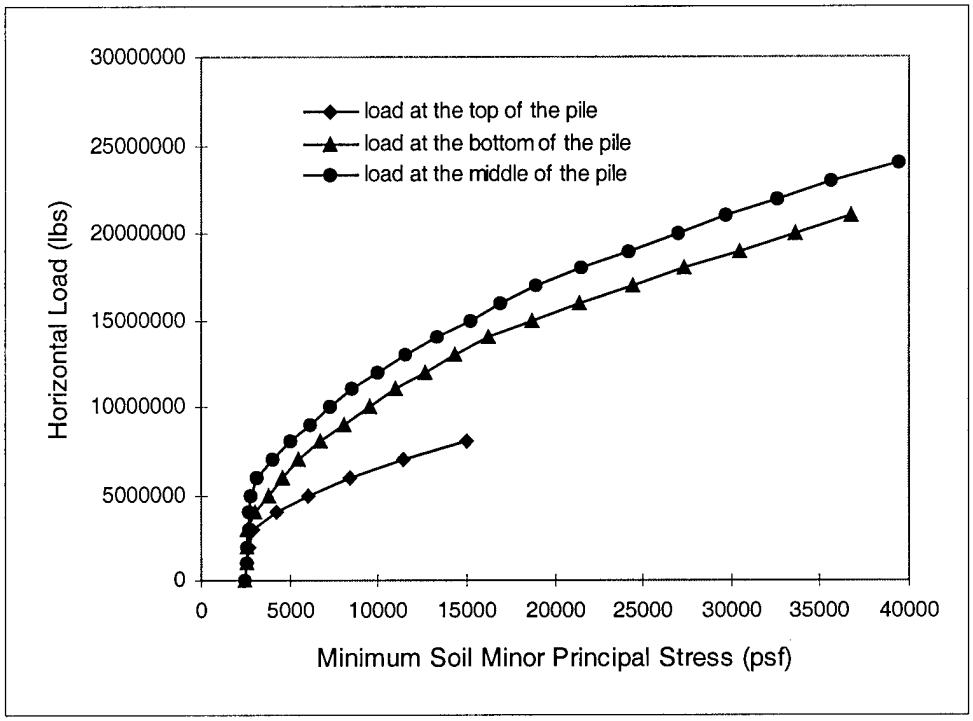

Figure - 91 Pile von Mises Stresses on the Pile Surface (Circular Pile)

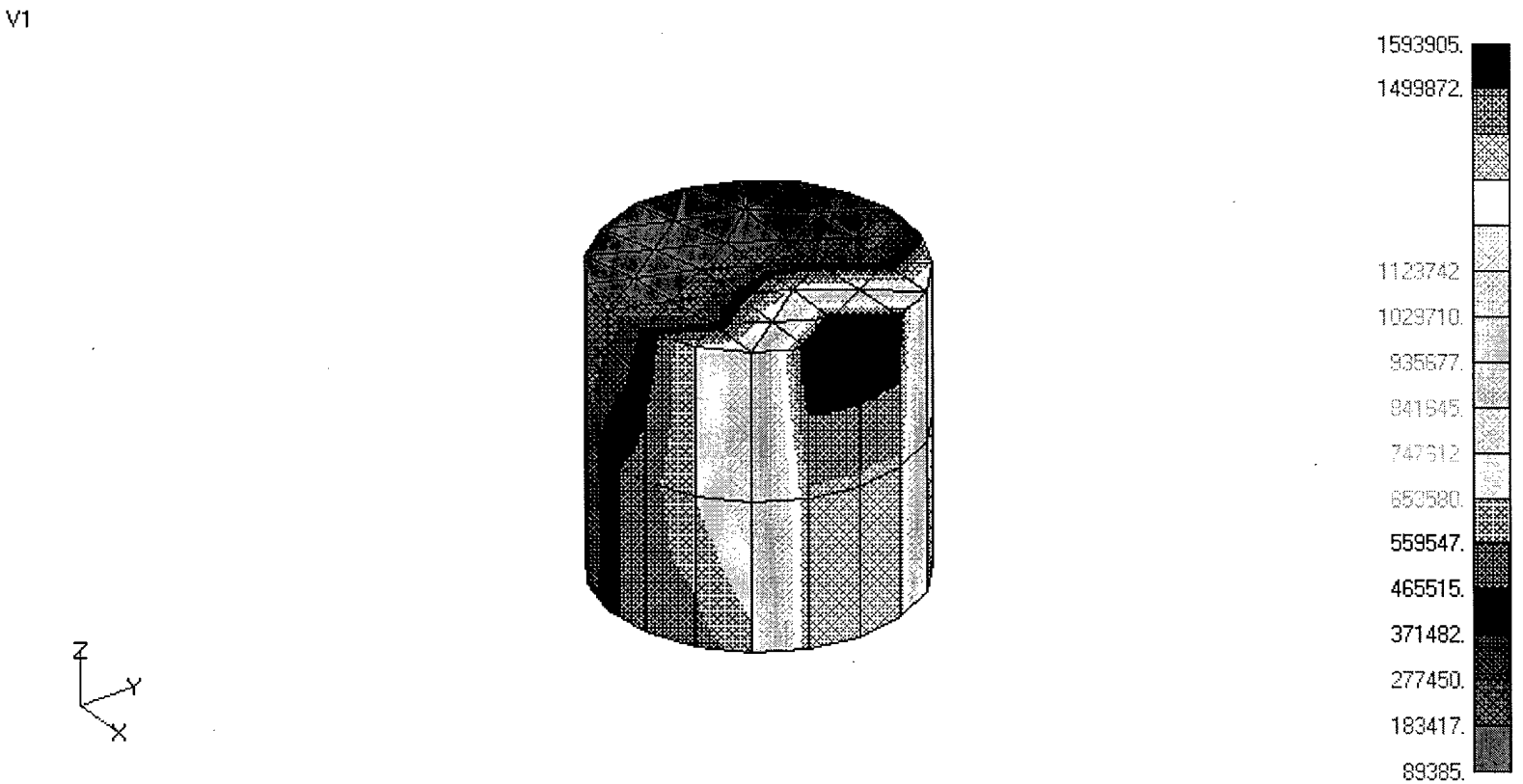

Horizontal Load at the Middle of the Pile = 24,000,000 lbs
Linear Elastic-Perfectly Plastic Sandy Soil (Linear Extended Drucker-Prager)
E = 864,000 psf, $\upsilon = 0.3$, Slope Angle = 46.2°, Dilation Angle = 21.5°
Pile, AISI 4340 Steel

Figure - 92 Pile von Mises Stresses on the Pile Surface (Circular Pile)

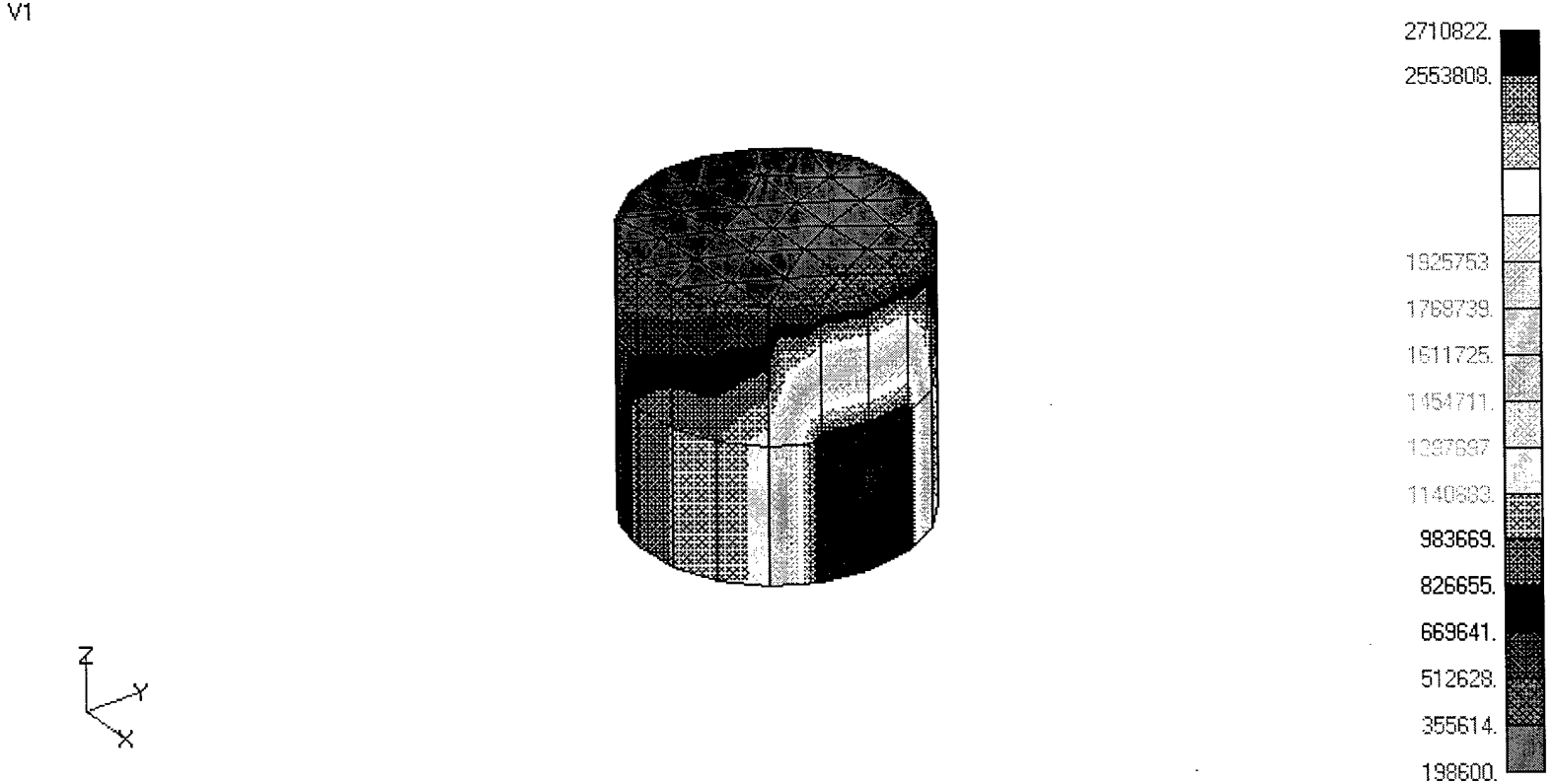

Horizontal Load at the Bottom of the Pile = 20,000,000 lbs
Linear Elastic-Perfectly Plastic Sandy Soil (Linear Extended Drucker-Prager)
E = 864,000 psf, υ = 0.3, Slope Angle = 46.2°, Dilation Angle = 21.5°
Pile, AISI 4340 Steel

Figure - 93 Maximum Pile von Mises Stress vs. Horizontal Load

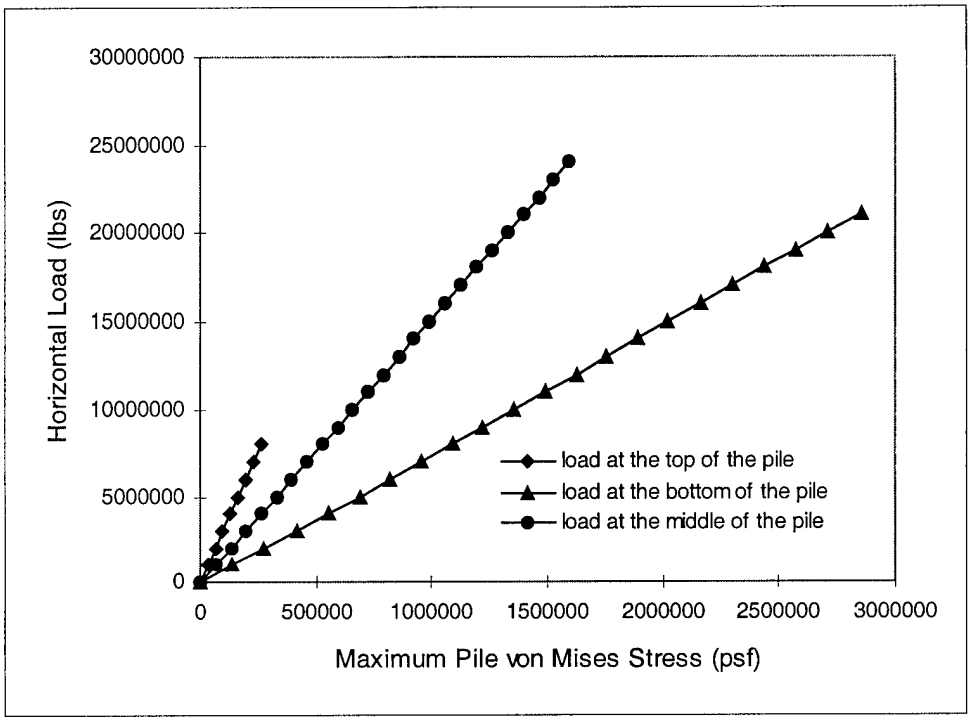

Figure - 94 Maximum Total Pile Displacement vs. 45-Degree Inclined Load

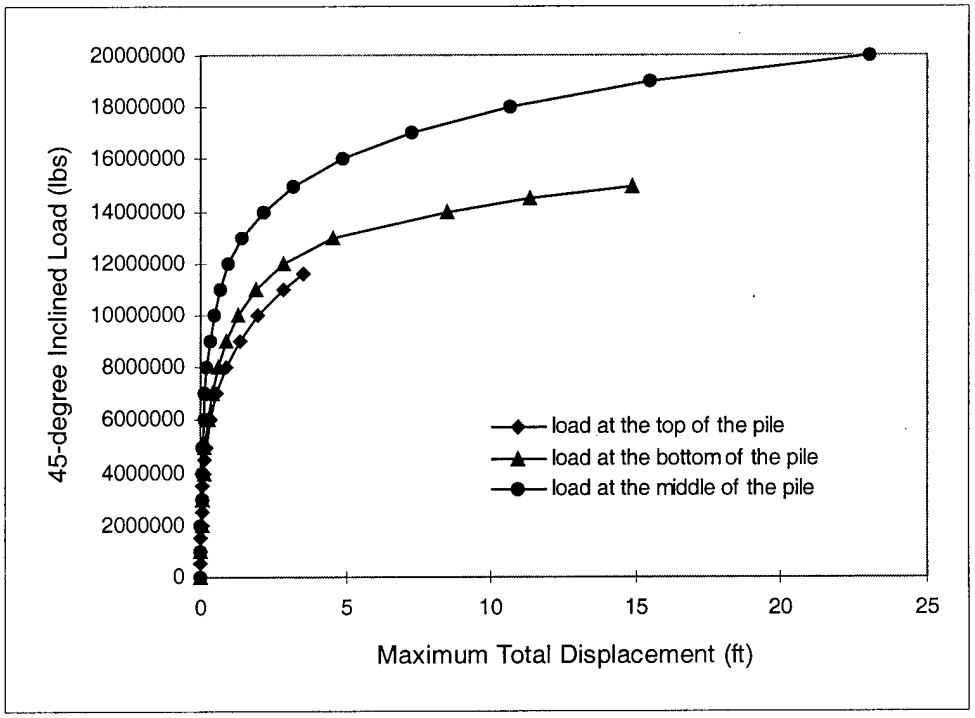

Figure - 95 Maximum Horizontal Pile Displacement vs. 45-Degree Inclined Load

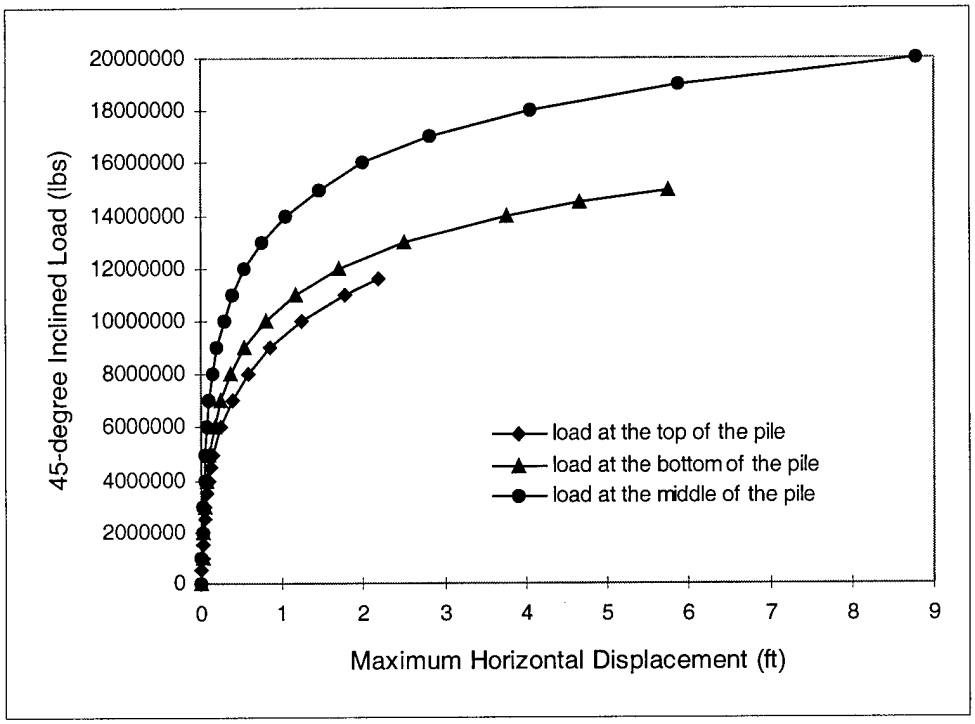

Figure - 96 Minimum Soil Minor Principal Stress vs. 45-Degree Inclined Load

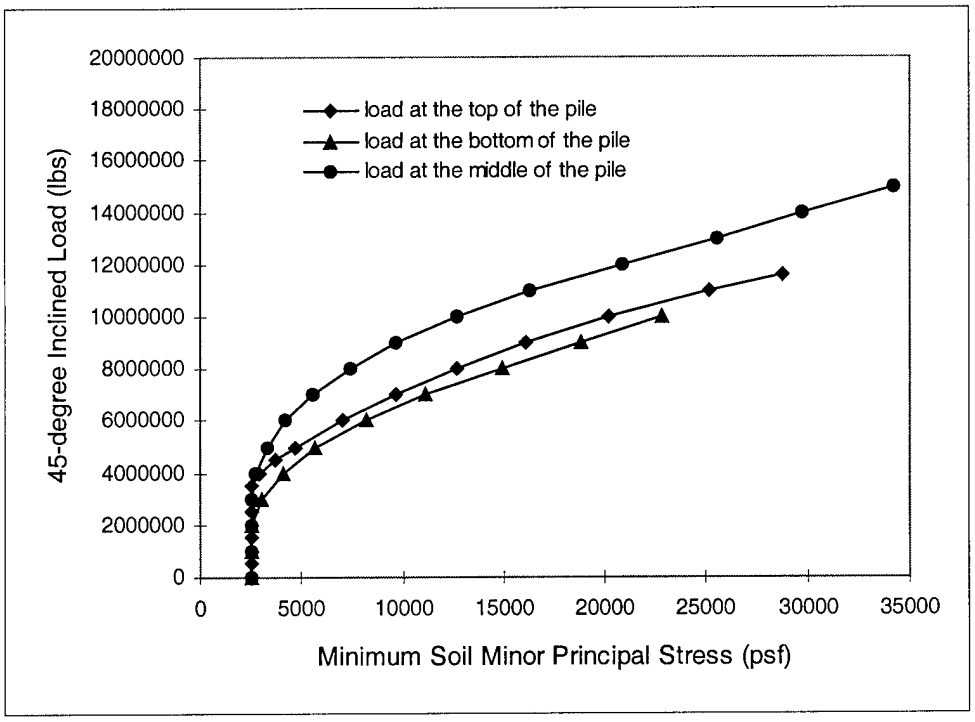

Figure - 97 Maximum Pile von Mises Stress vs. 45-Degree Inclined Load

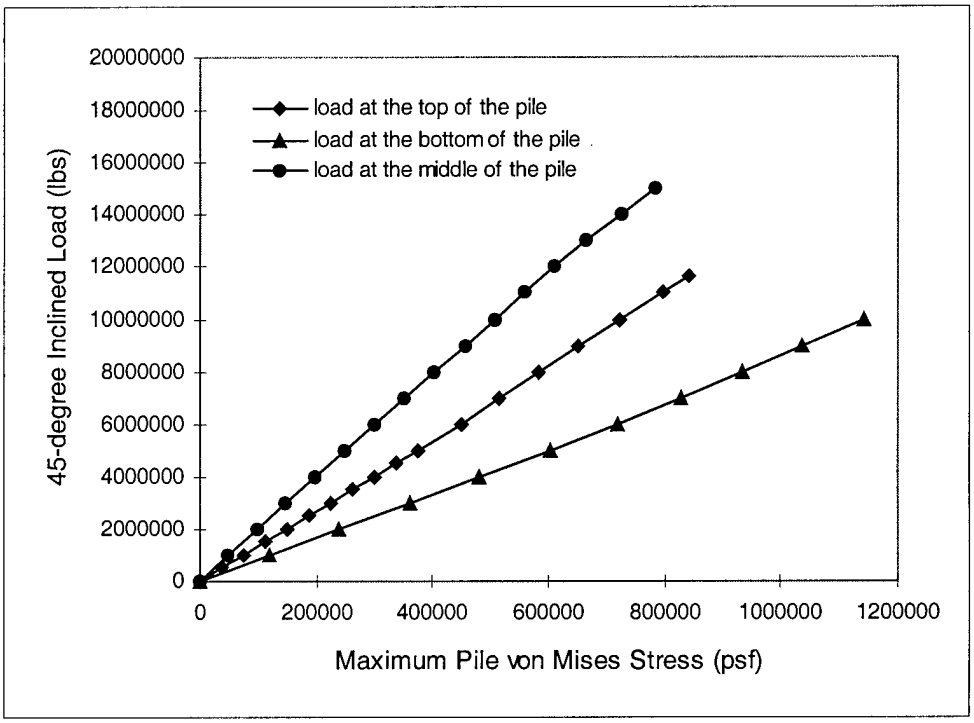

Figure - 98 Maximum Total Pile Displacement vs. Horizontal Load

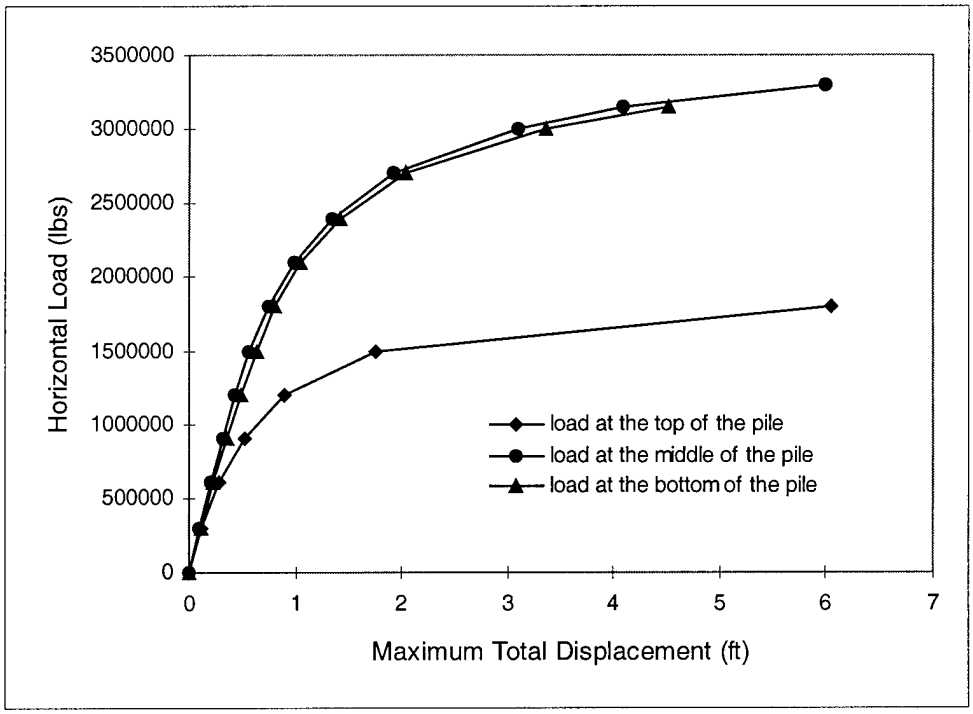

Figure - 99 Maximum Horizontal Pile Displacement vs. Horizontal Load

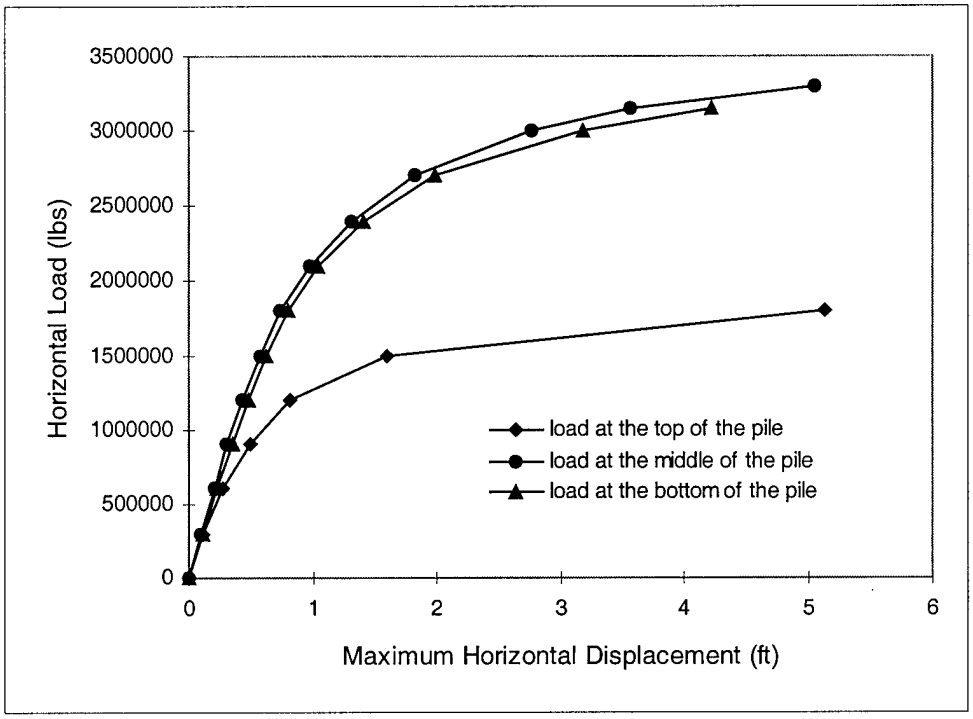

Figure - 100 Soil Minor Principal Stresses on a Vertical Plane along Horizontal Load Direction (Circular Pile)

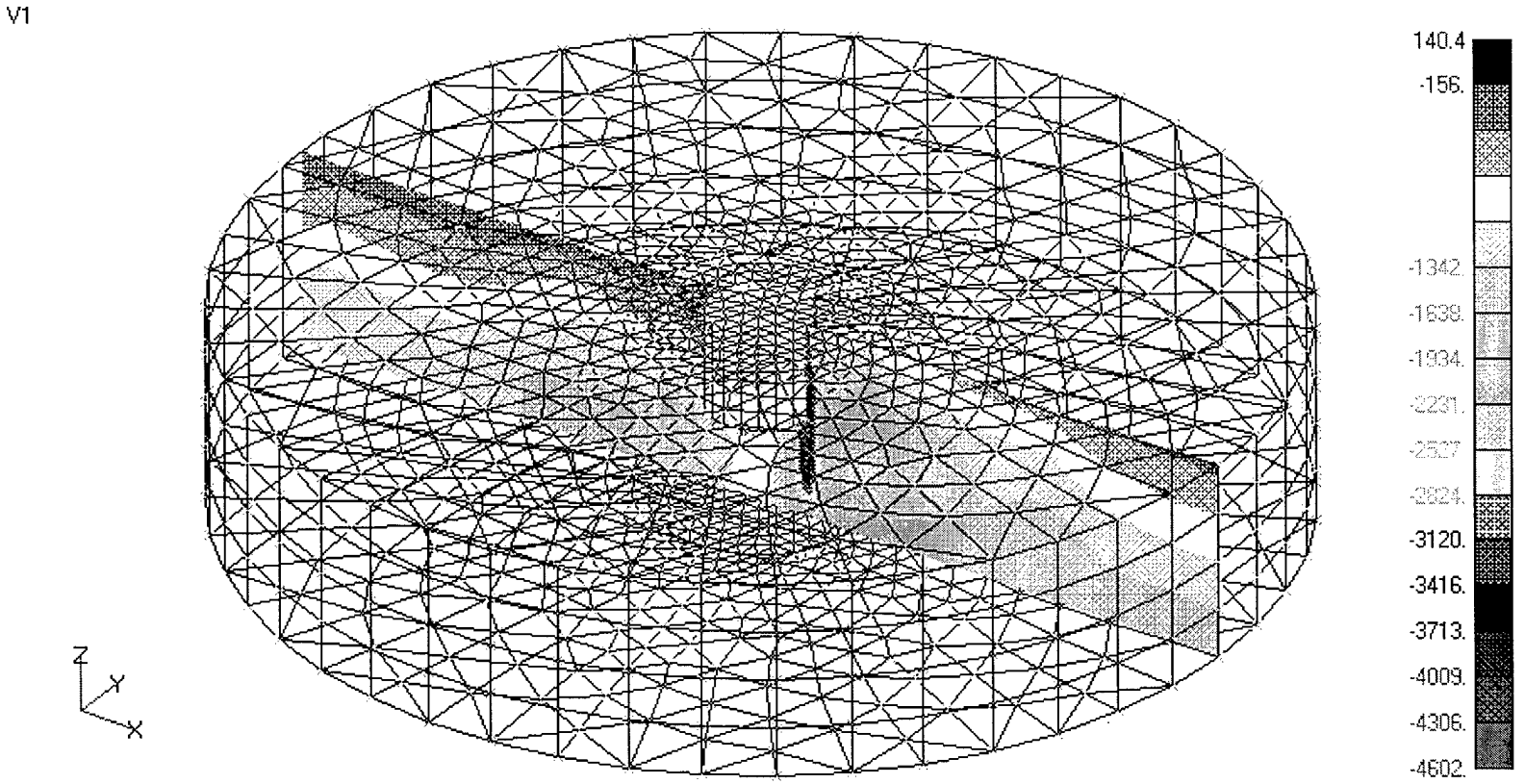

Horizontal Load at the Middle of the Pile = 3,000,000 lbs
Linear Elastic-Perfectly Plastic Clayey Soil (Hyperbolic Extended Drucker-Prager)
E = 30,000 psf, $\upsilon = 0.499$, Slope Angle = 10.2°, Dilation Angle = 10.2°
Pile, AISI 4340 Steel

Figure - 101 Soil Minor Principal Stresses on a Vertical Plane along Horizontal Load Direction (Circular Pile)

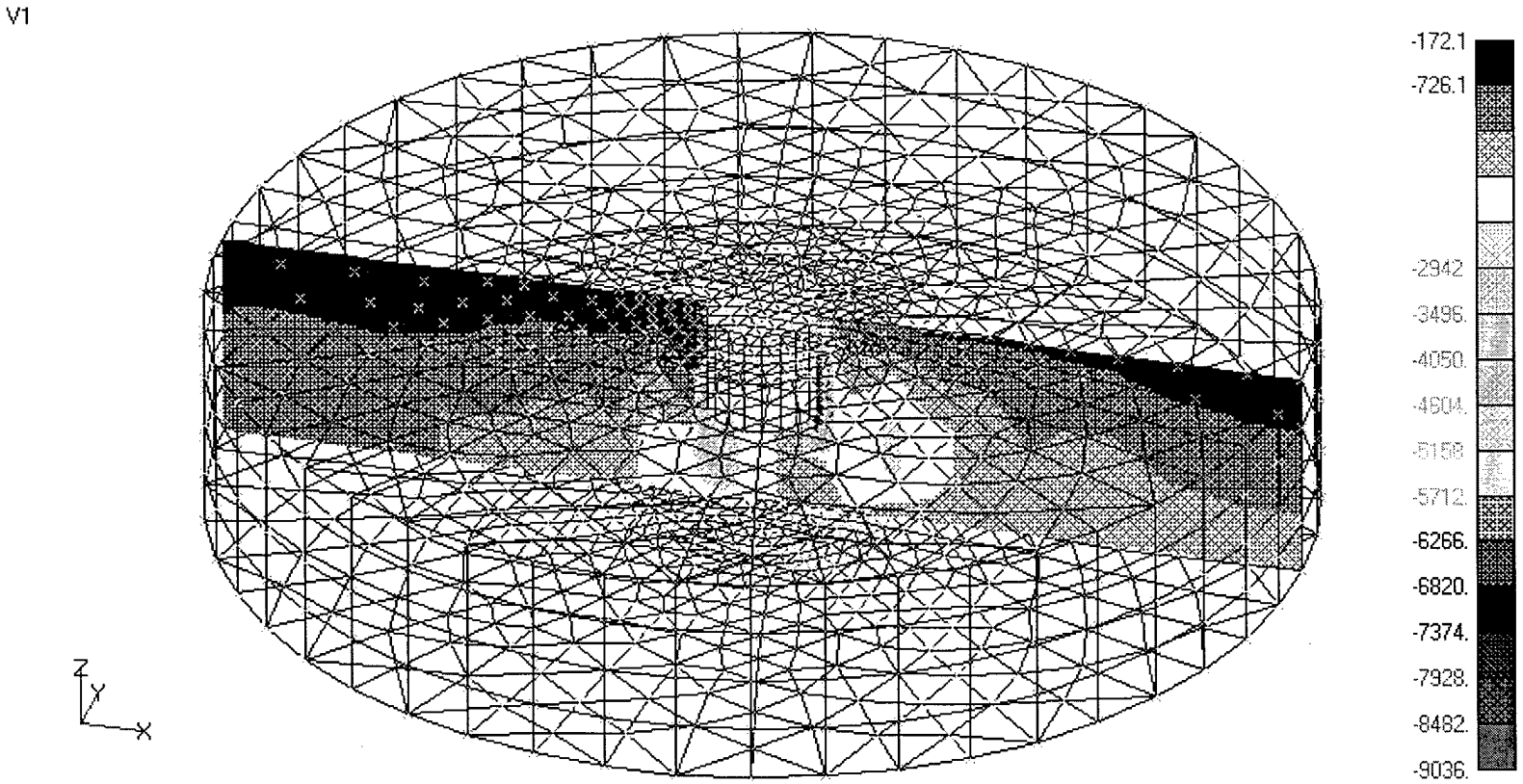

Horizontal Load at the Bottom of the Pile = 3,000,000 lbs
Linear Elastic-Perfectly Plastic Clayey Soil (Hyperbolic Extended Drucker-Prager)
E = 30,000 psf, υ = 0.499, Slope Angle = 10.2°, Dilation Angle = 10.2°
Pile, AISI 4340 Steel

Figure - 102 Minimum Soil Minor Principal Stress vs. Horizontal Load

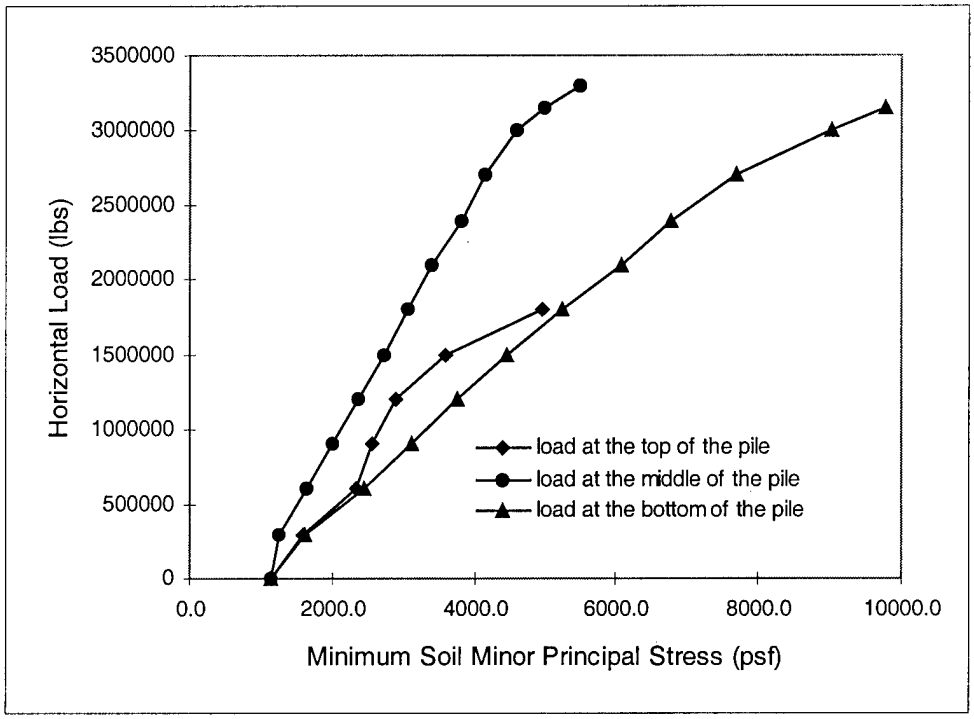

Figure - 103 Maximum Pile von Mises Stress vs. Horizontal Load

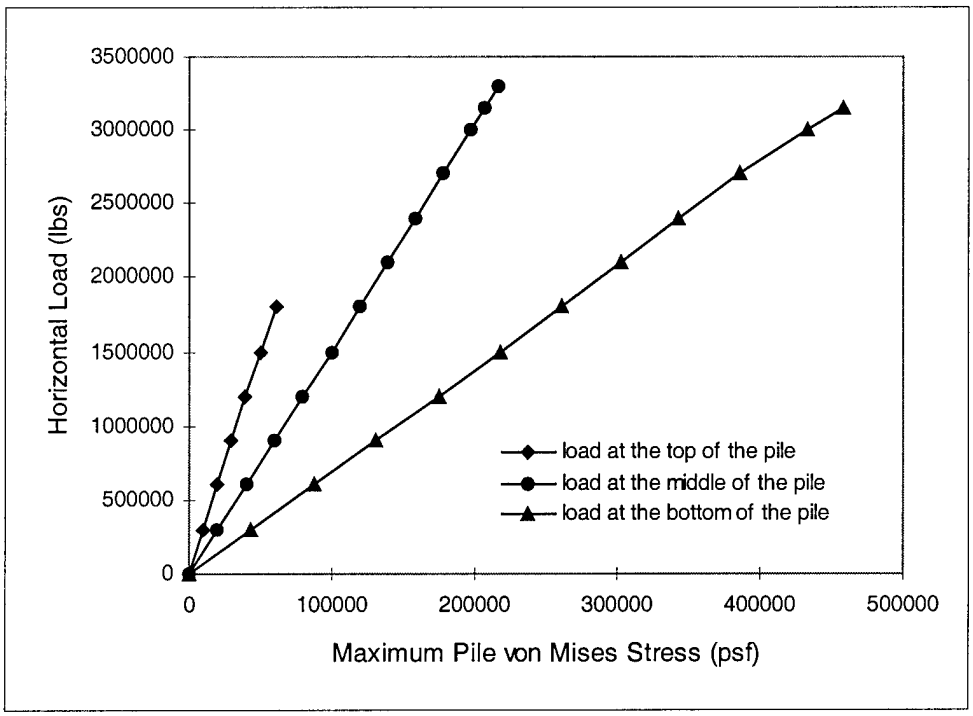

Figure - 104 Maximum Total Pile Displacement vs. 45-Degree Inclined Load

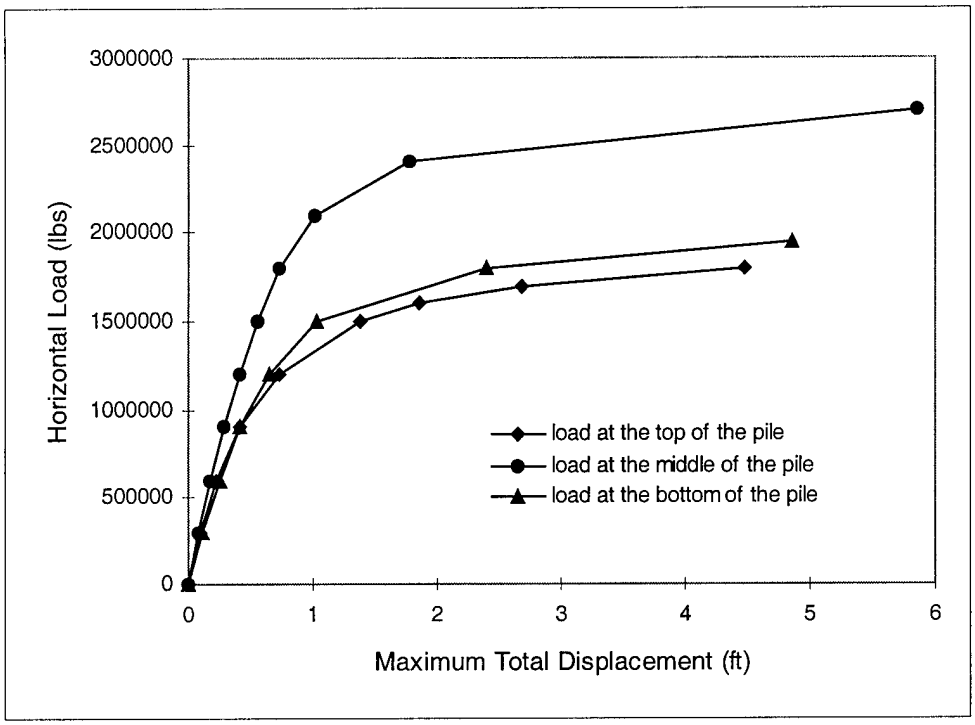

Figure - 105 Maximum Horizontal Pile Displacement vs. 45-Degree Inclined Load

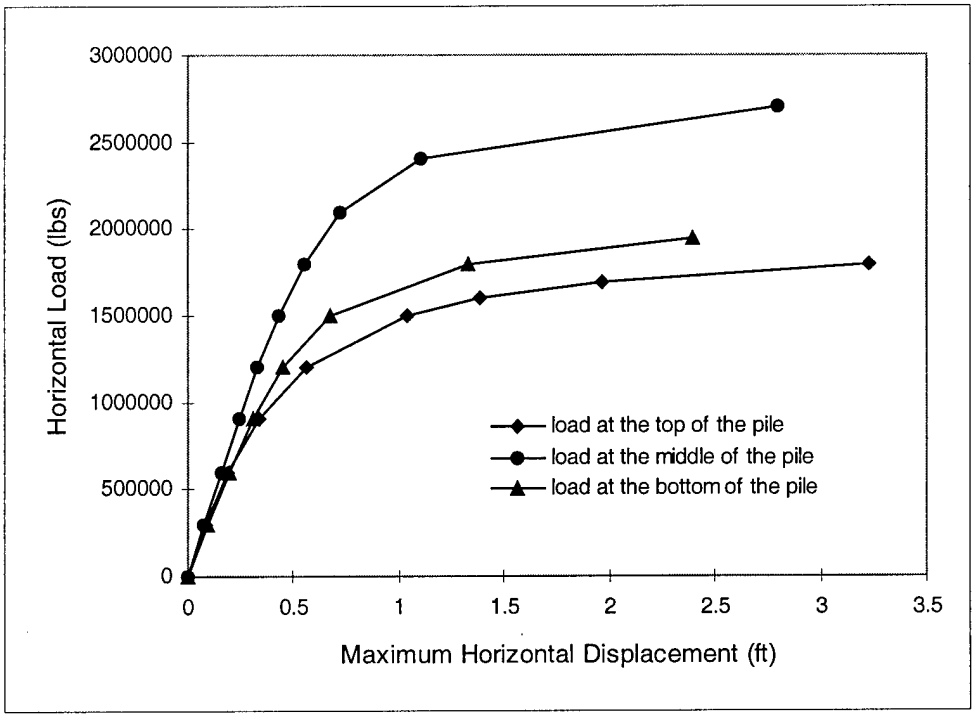

Figure - 106 Minimum Soil Minor Principal Stress vs. 45-Degree Inclined Load

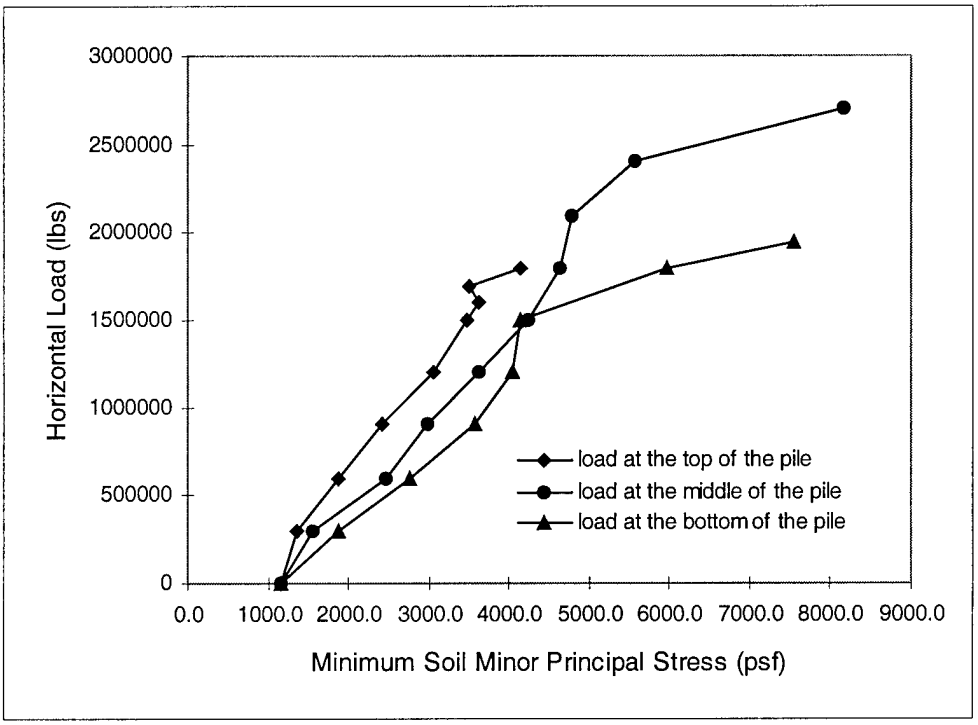

Figure - 107 Maximum Pile von Mises Stress vs. 45-Degree Inclined Load

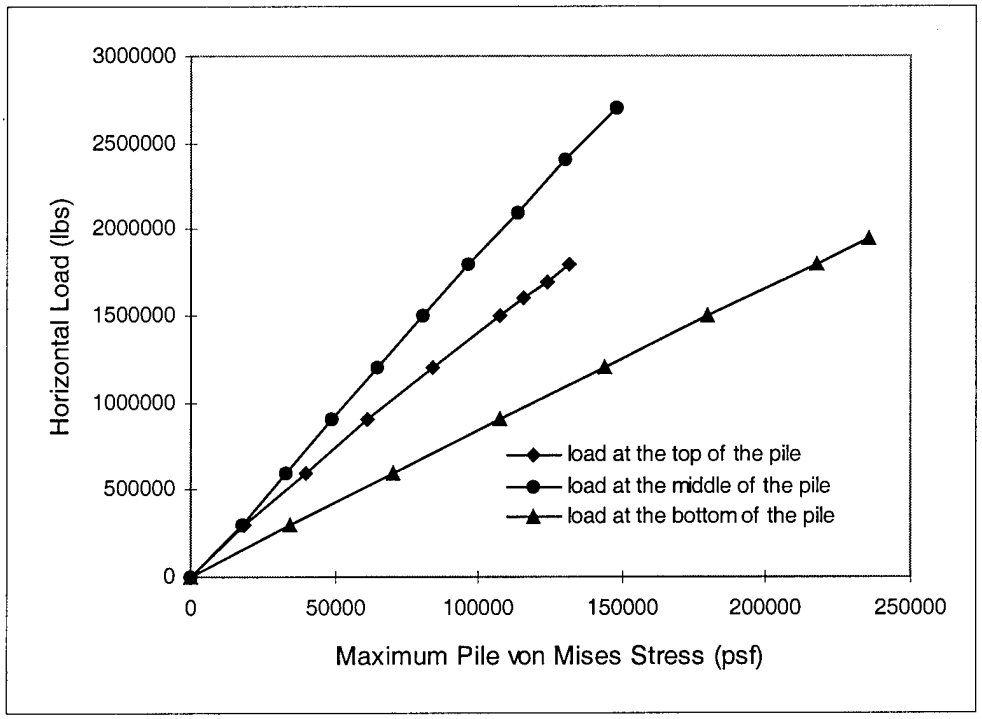

Figure - 108 Pile Total Displacements (Telescopic Pile)

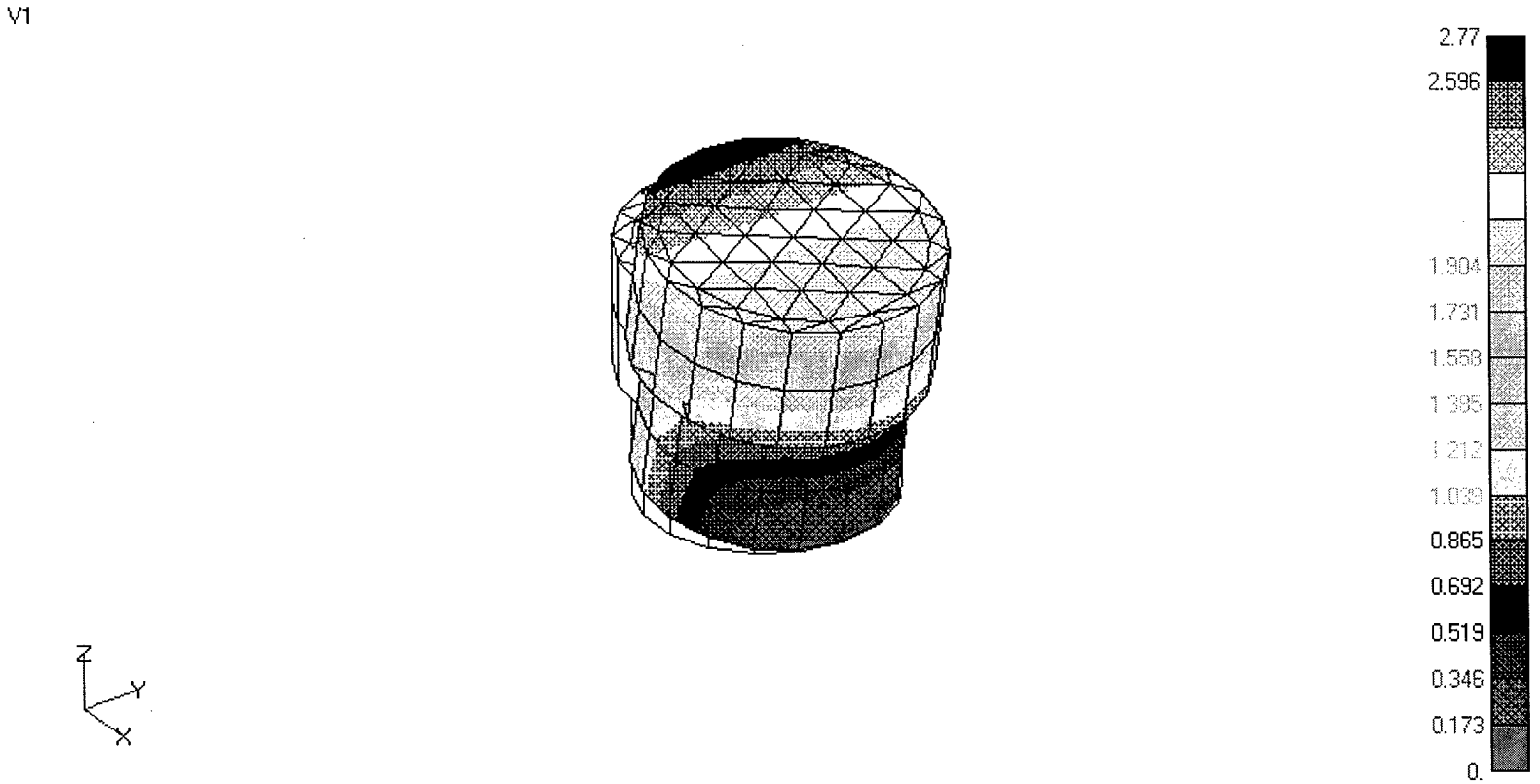

Horizontal Load = 12,000,000 lbs
Linear Elastic-Perfectly Plastic Sandy Soil (Linear Extended Drucker-Prager)
E = 864,000 psf, υ = 0.3, Slope Angle = 46.2°, Dilation Angle = 21.5°
Pile, AISI 4340 Steel

Figure - 109 Maximum Total Pile Displacement vs. Horizontal Load

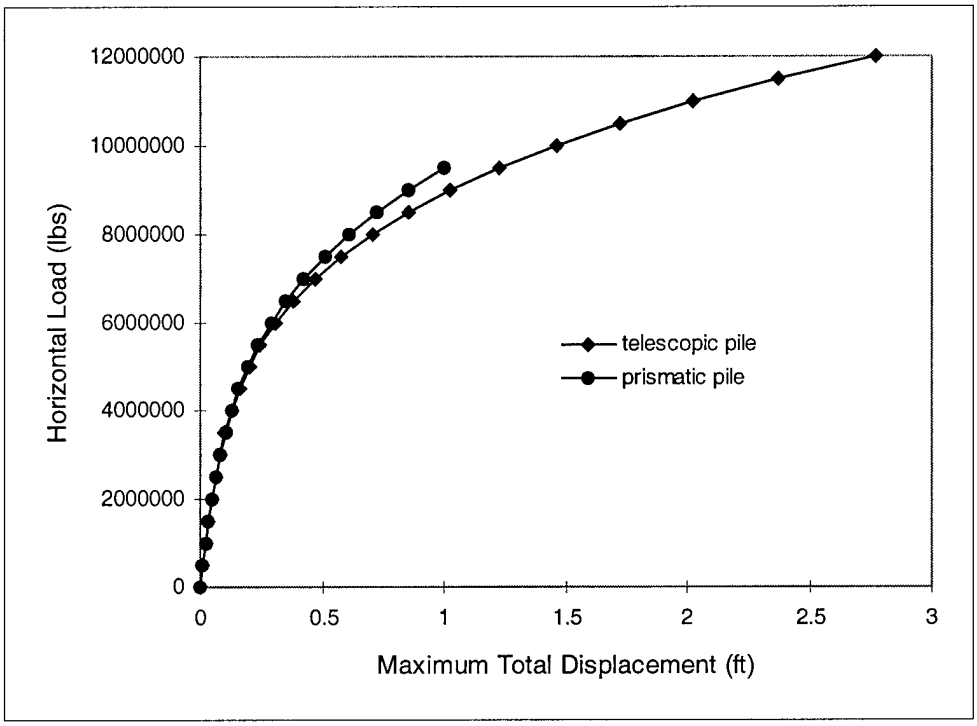

Figure - 110 Maximum Horizontal Pile Displacement vs. Horizontal Load

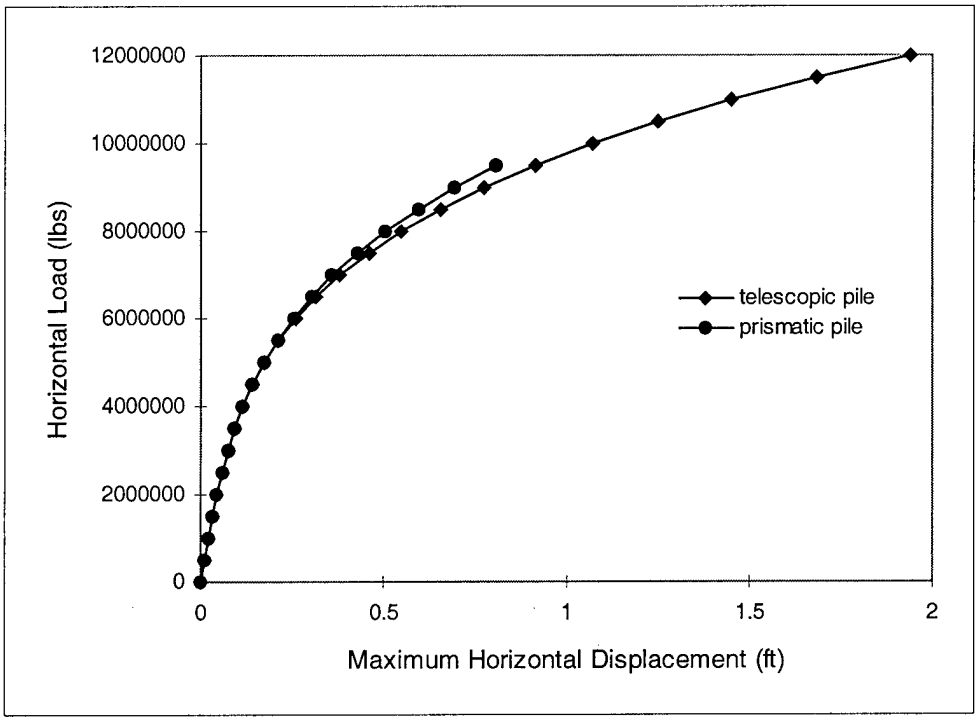

Figure - 111 Soil Minor Principal Stresses on a Vertical Plane along Horizontal Load Direction (Telescopic Pile)

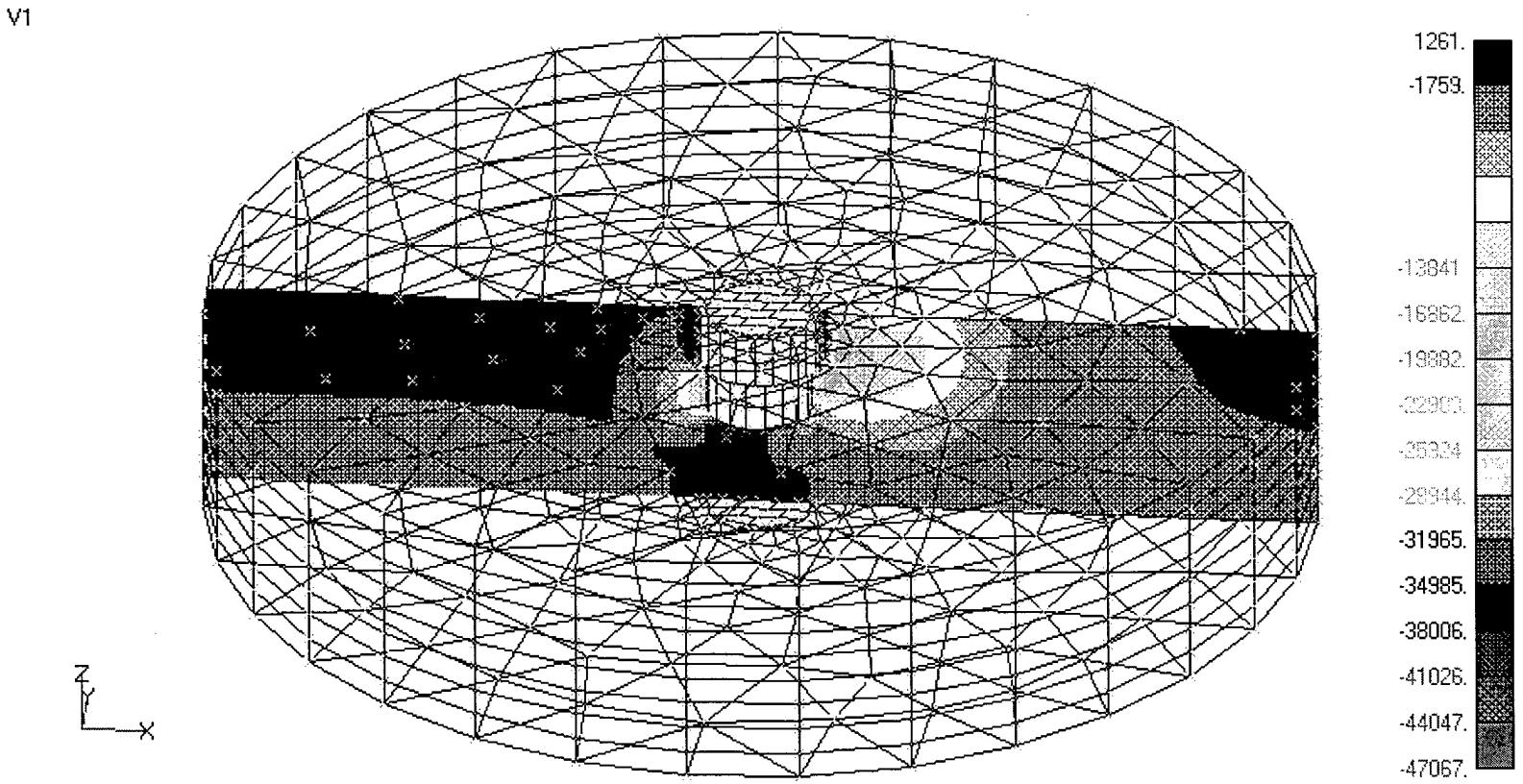

Horizontal Load = 12,000,000 lbs
Linear Elastic-Perfectly Plastic Sandy Soil (Linear Extended Drucker-Prager)
E = 864,000 psf, $\upsilon = 0.3$, Slope Angle = 46.2°, Dilation Angle = 21.5°
Pile, AISI 4340 Steel

Figure - 112 Minimum Soil Minor Principal Stress vs. Horizontal Load

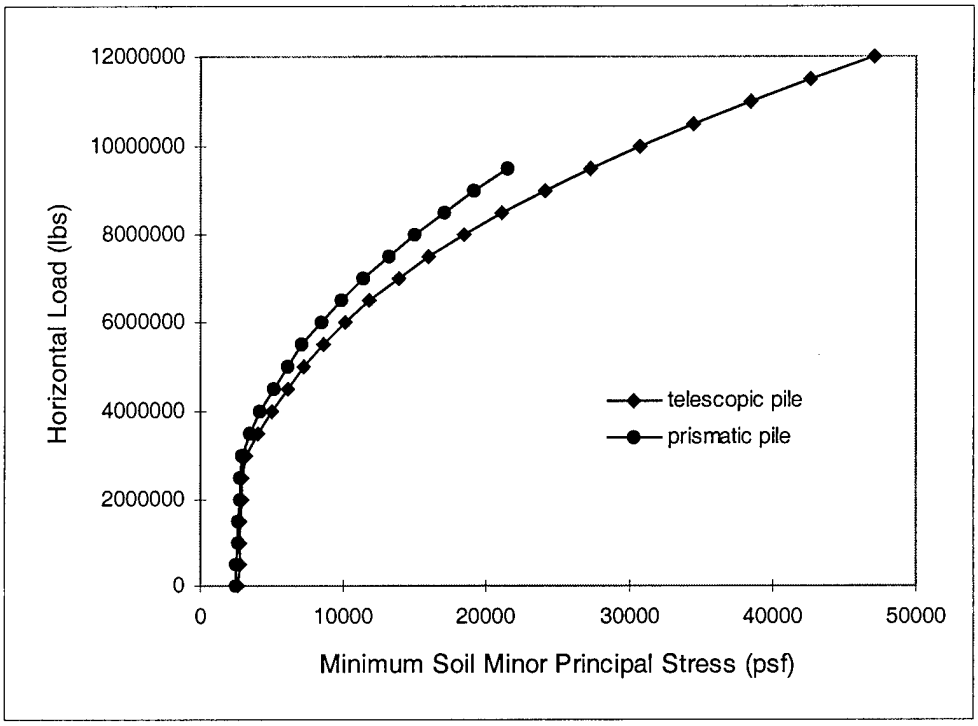

Figure - 113 Pile von Mises Stresses on the Pile Surface (Telescopic Pile)

Horizontal Load = 12,000,000 lbs
Linear Elastic-Perfectly Plastic Sandy Soil (Linear Extended Drucker-Prager)
E = 864,000 psf, υ = 0.3, Slope Angle = 46.2°, Dilation Angle = 21.5°
Pile, AISI 4340 Steel

Figure - 114 Maximum Pile von Mises Stress vs. Horizontal Load

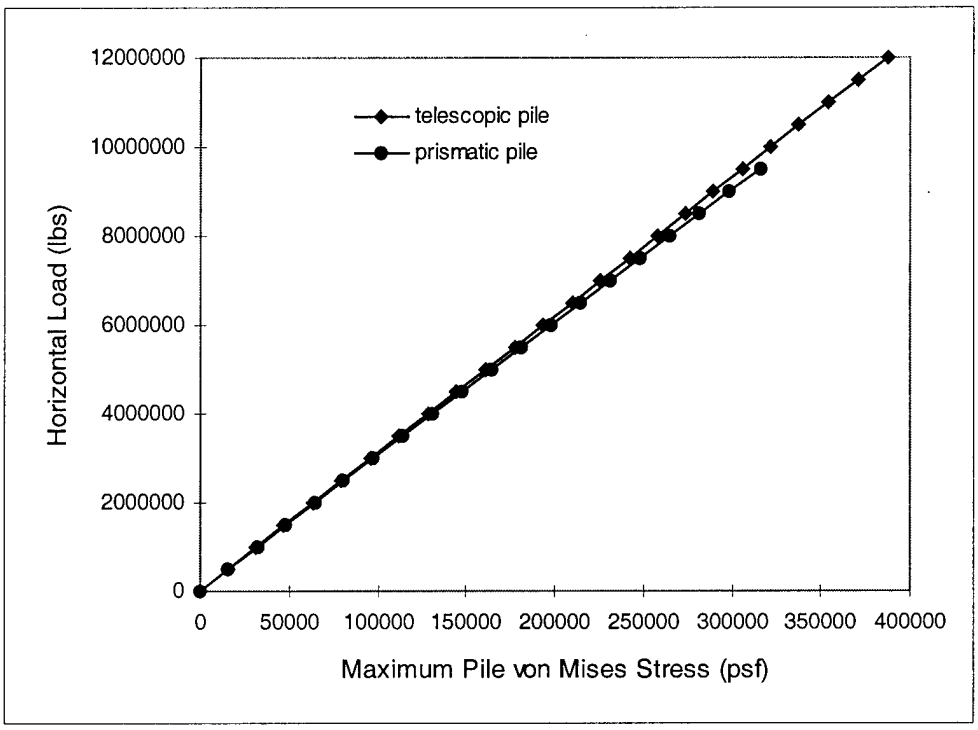

Figure - 115 Pile Total Displacements (Telescopic Pile)

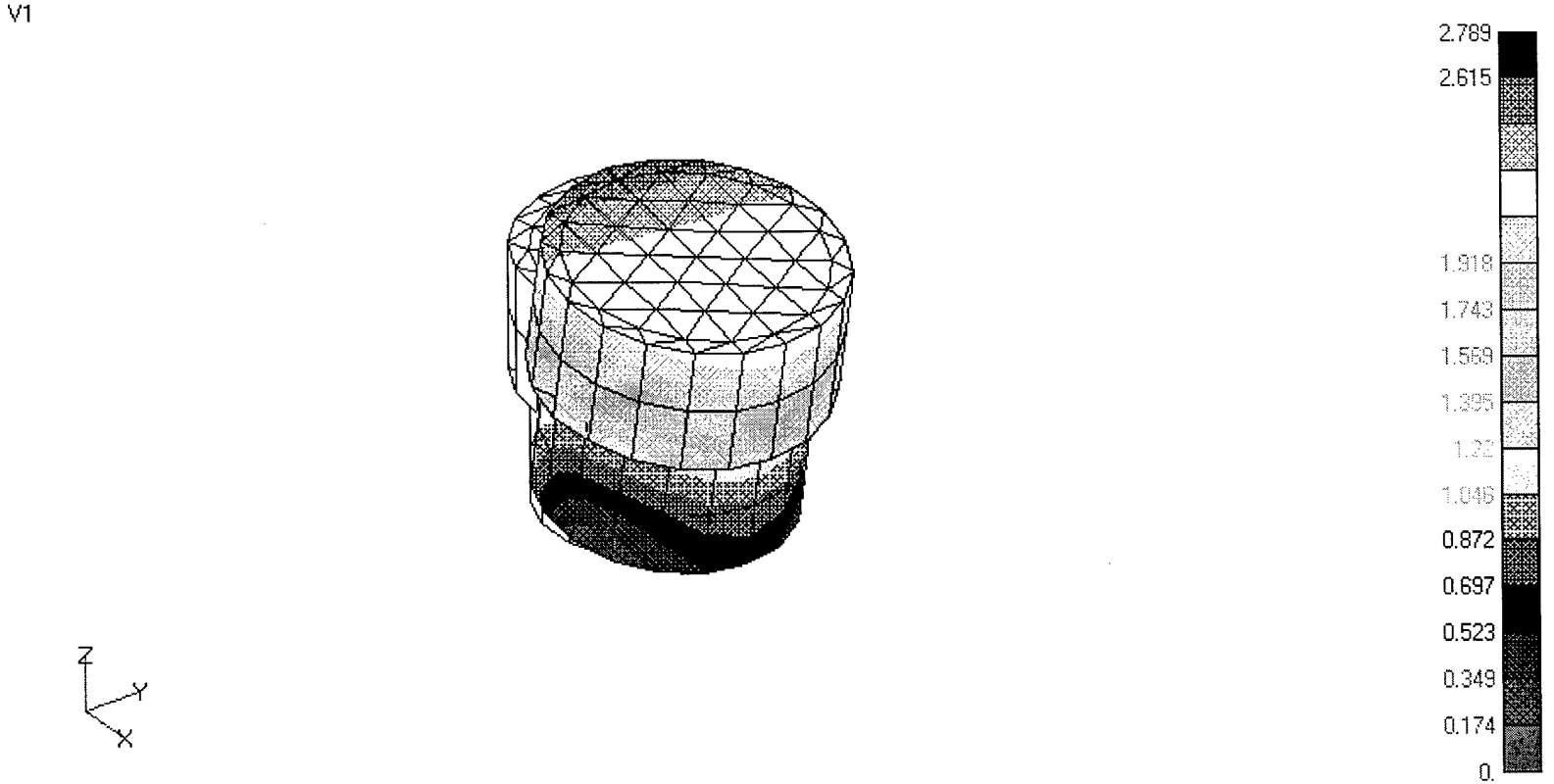

Horizontal Load = 16,000,000 lbs
Linear Elastic-Perfectly Plastic Clayey Soil (Hyperbolic Extended Drucker-Prager)
E = 30,000 psf, υ = 0.499, Slope Angle = 10.2°, Dilation Angle = 10.2°
Pile, AISI 4340 Steel

Figure - 116 Maximum Total Pile Displacement vs. Horizontal Load

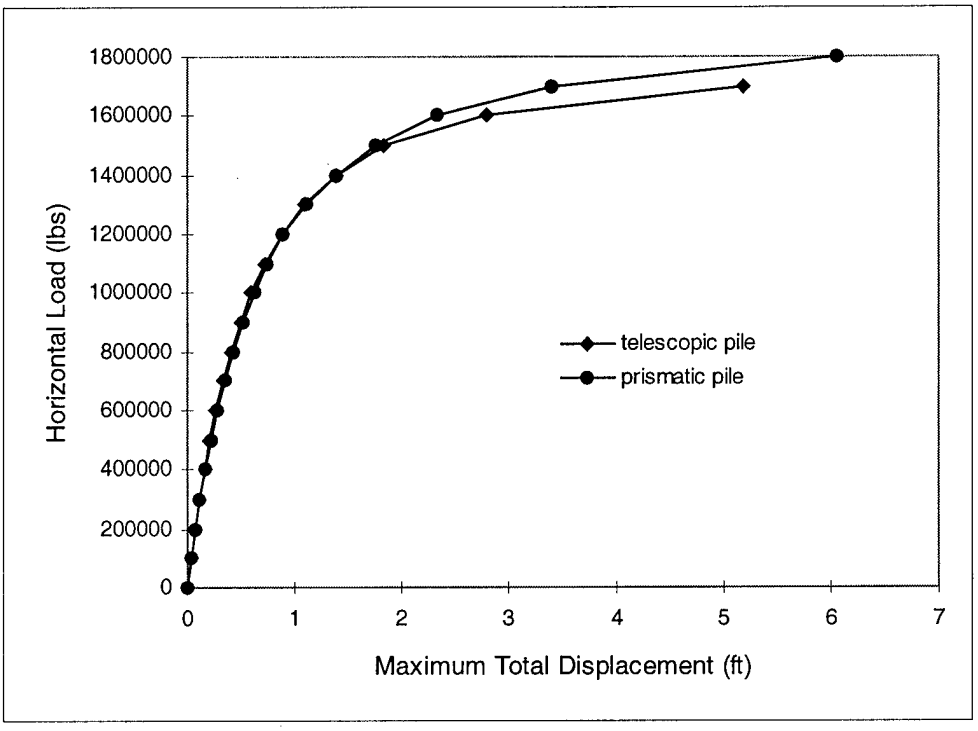

Figure - 117 Maximum Horizontal Pile Displacement vs. Horizontal Load

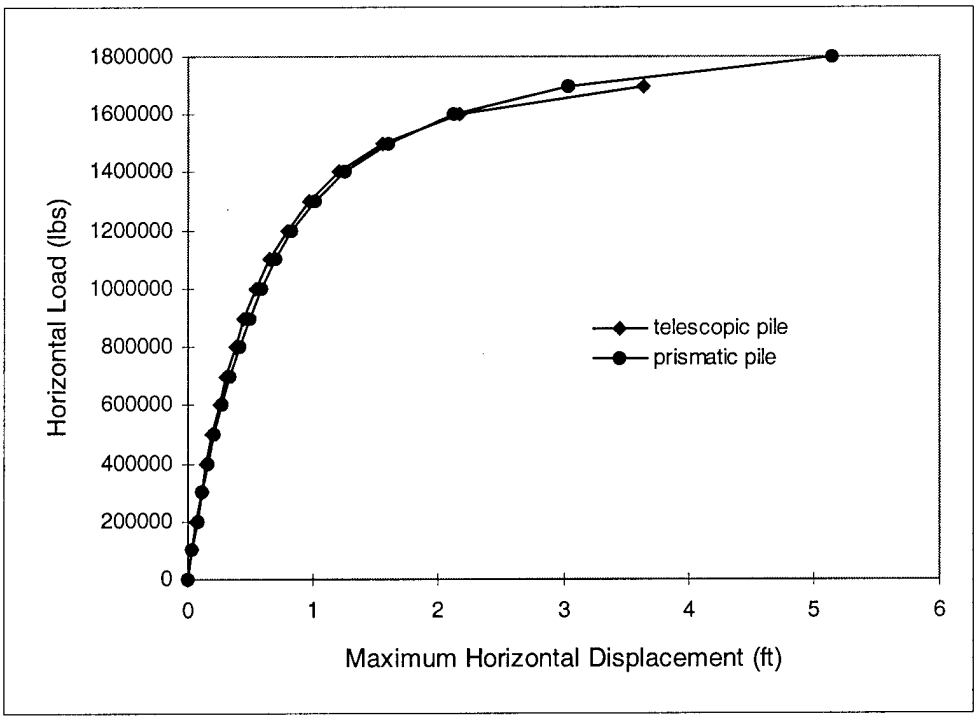

Figure - 118 Soil Minor Principal Stresses on a Vertical Plane along Horizontal Load Direction (Telescopic Pile)

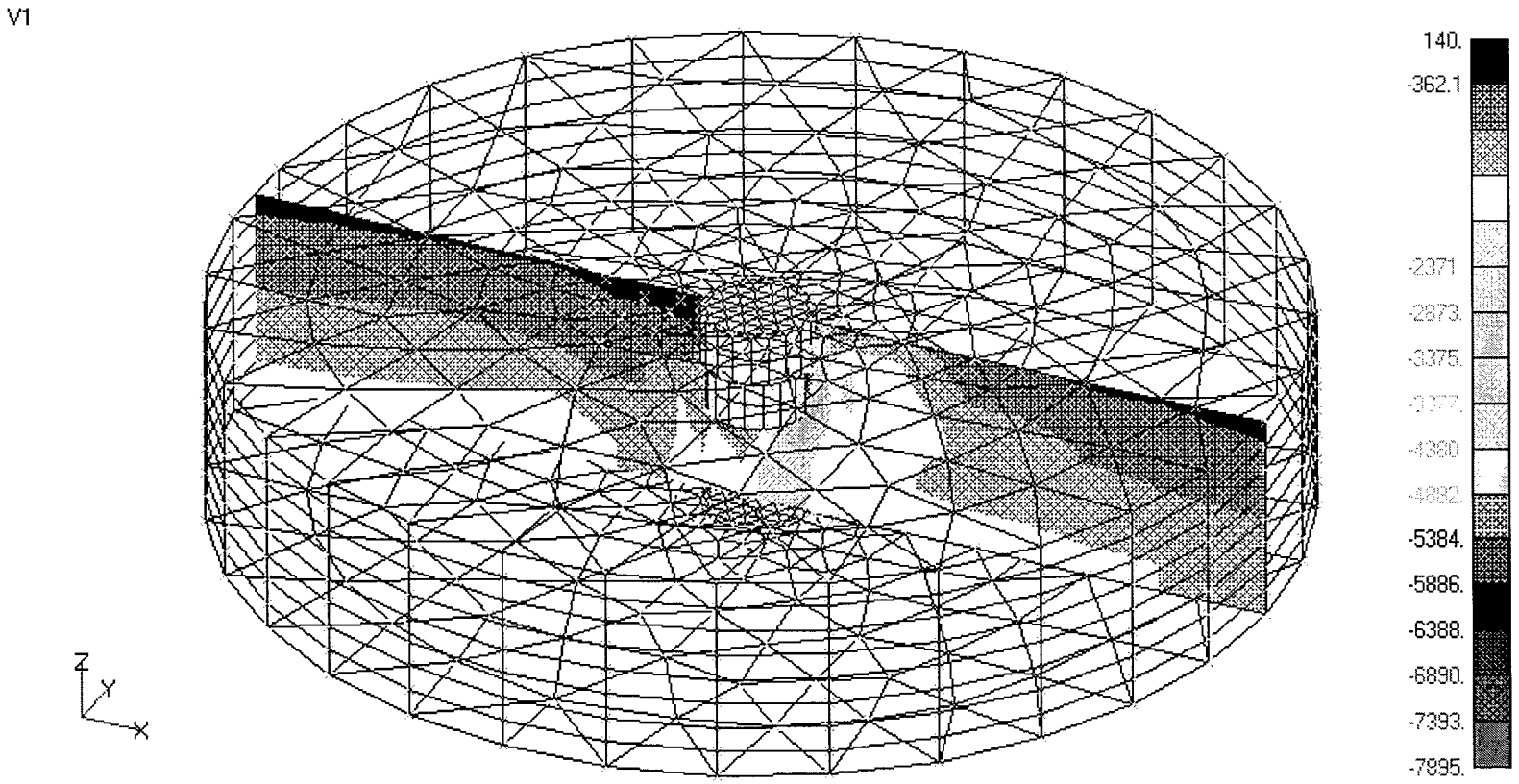

Horizontal Load = 16,000,000 lbs
Linear Elastic-Perfectly Plastic Clayey Soil (Hyperbolic Extended Drucker-Prager)
E = 30,000 psf, υ = 0.499, Slope Angle = 10.2°, Dilation Angle = 10.2°
Pile, AISI 4340 Steel

Figure - 119 Minimum Soil Minor Principal Stress vs. Horizontal Load

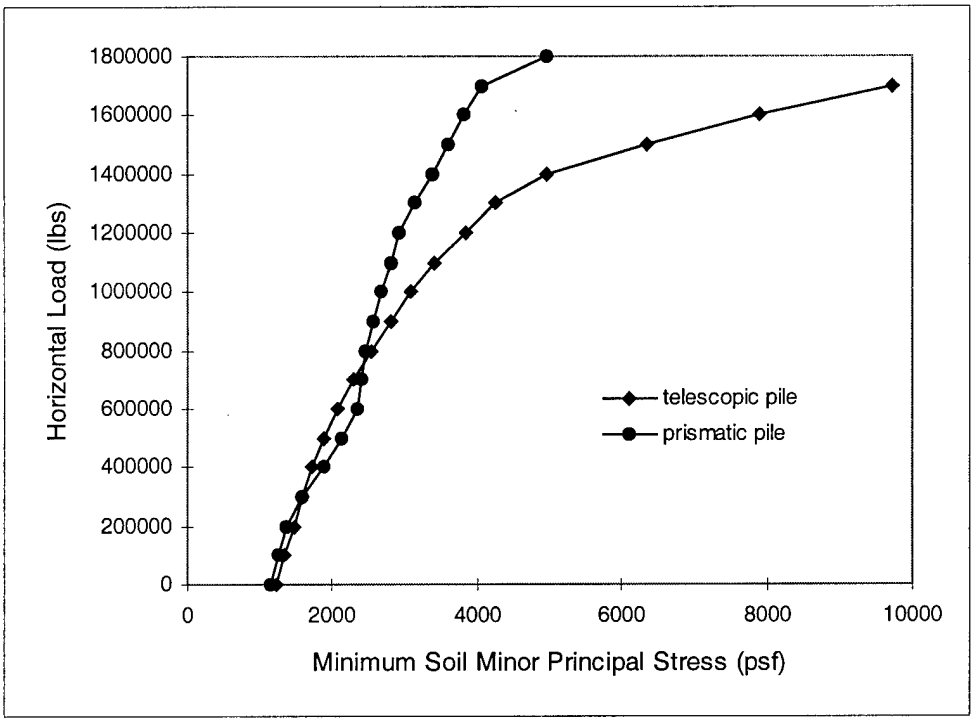

Figure - 120 Pile von Mises Stresses on the Pile Surface (Telescopic Pile)

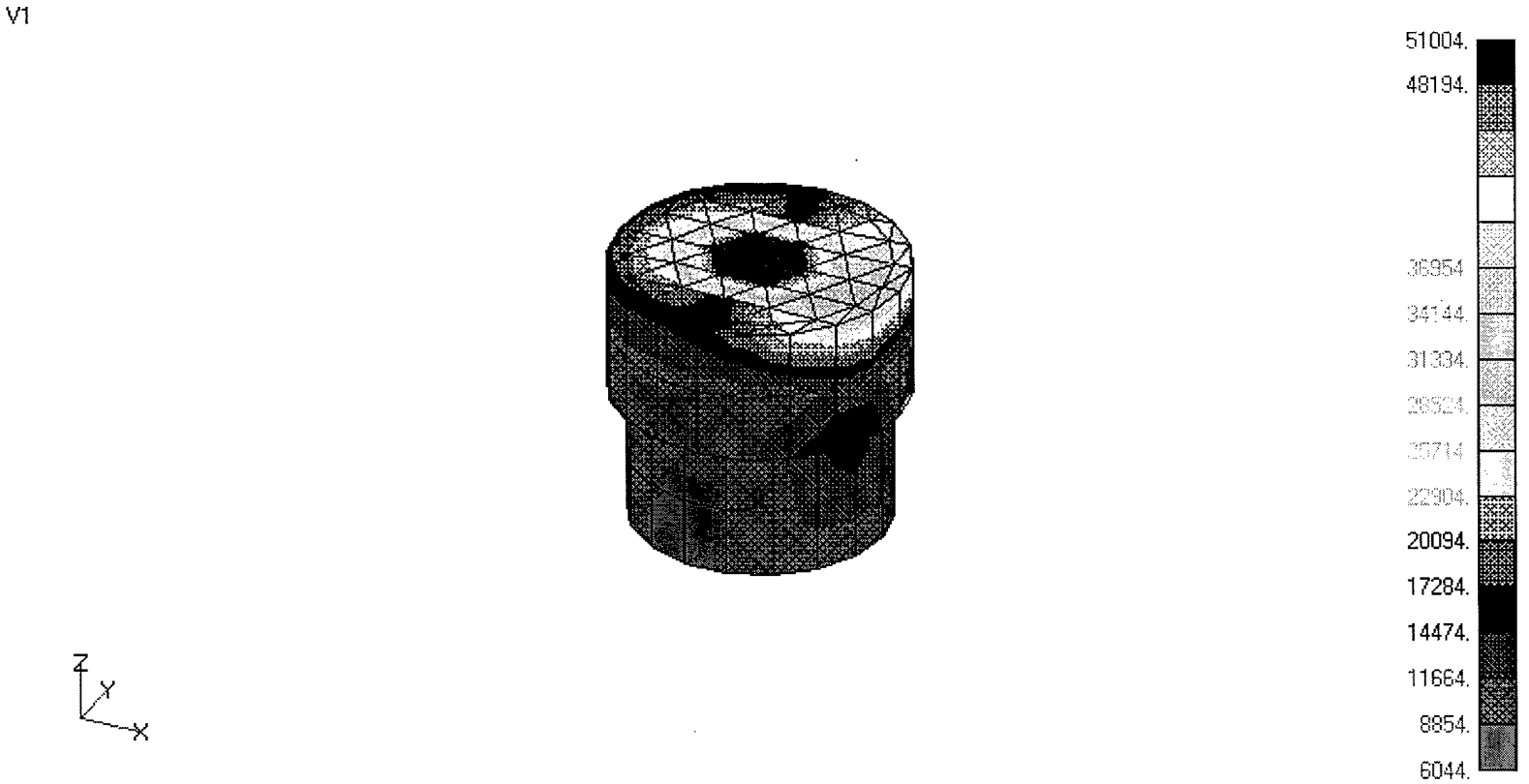

Horizontal Load = 16,000,000 lbs
Linear Elastic-Perfectly Plastic Clayey Soil (Hyperbolic Extended Drucker-Prager)
E = 30,000 psf, υ = 0.499, Slope Angle = 10.2°, Dilation Angle = 10.2°
Pile, AISI 4340 Steel

Figure – 121 Maximum Pile von Mises Stress vs. Horizontal Load

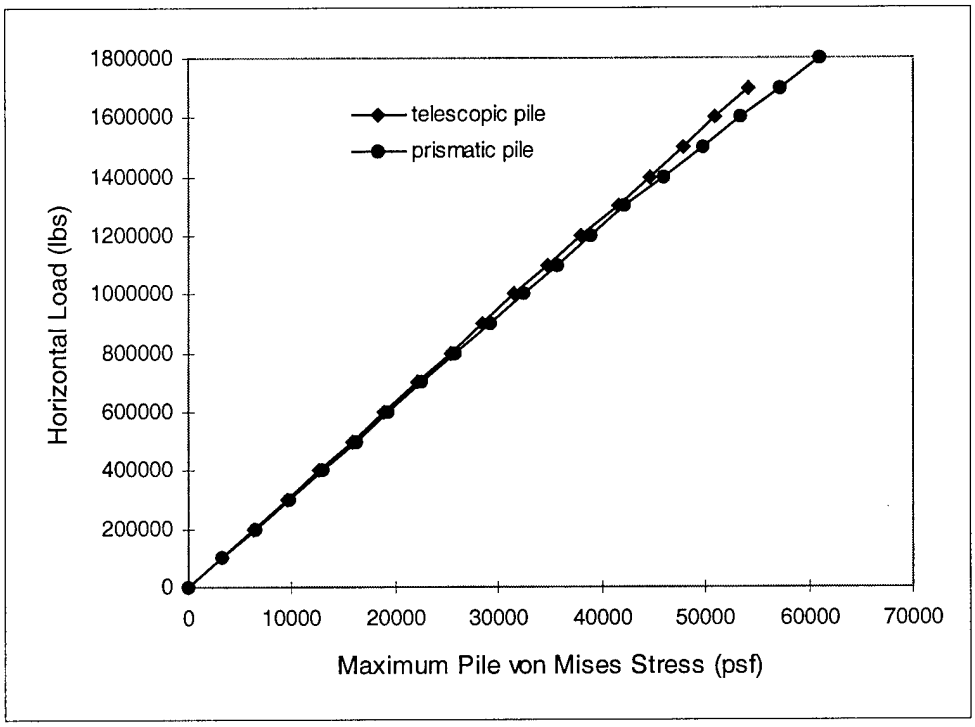

Figure - 122 Pile Total Displacements (Circular Pile in Layered Soil-2)

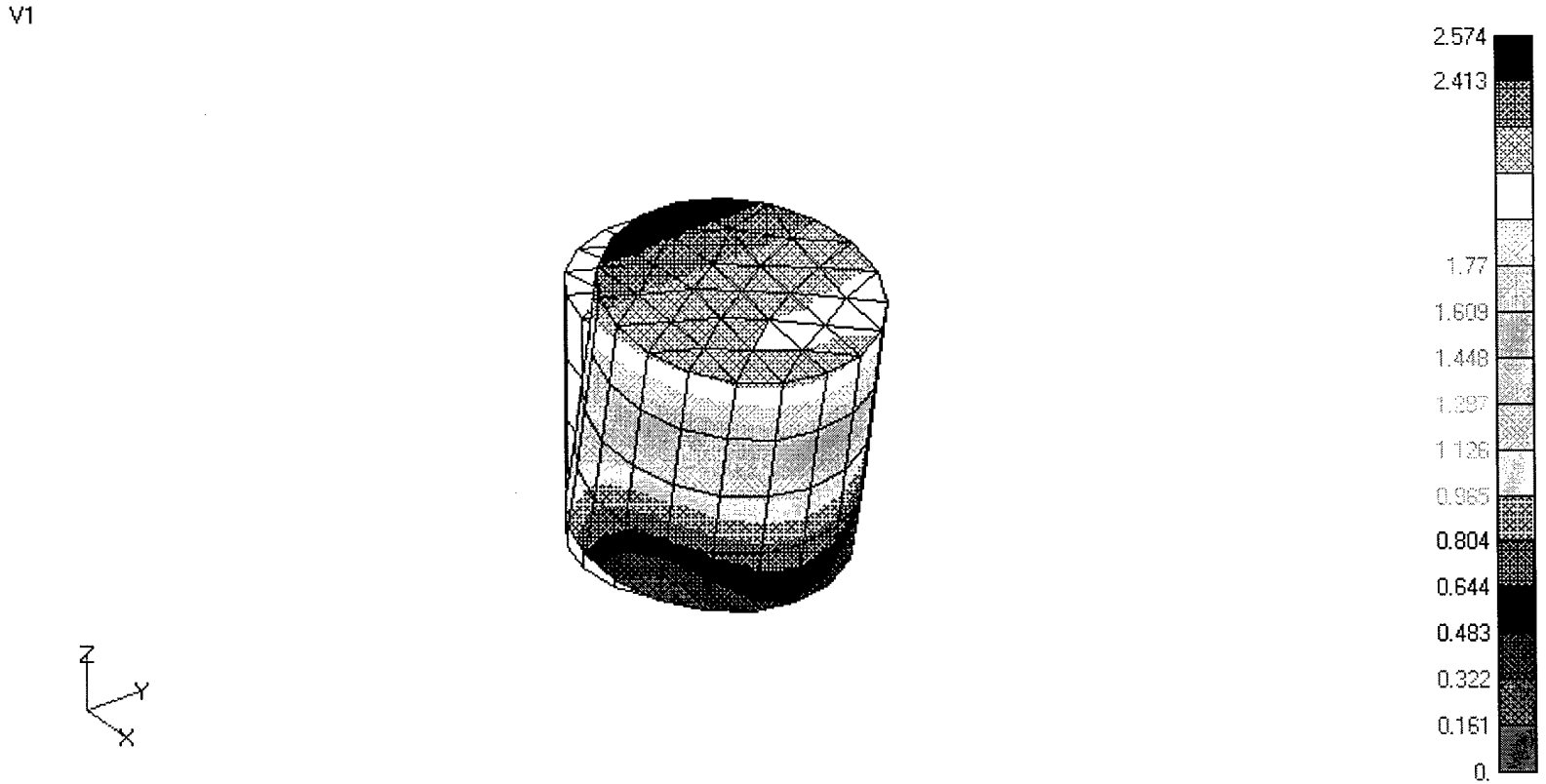

Horizontal Load = 5,000,000 lbs
Linear Elastic-Perfectly Plastic Clayey Soil (Hyperbolic Extended Drucker-Prager)
E = 30,000 psf, υ = 0.499, Slope Angle = 10.2°, Dilation Angle = 10.2°
Linear Elastic-Perfectly Plastic Sandy Soil (Linear Extended Drucker-Prager)
E = 864,000 psf, υ = 0.3, Slope Angle = 46.2°, Dilation Angle = 21.5°
Pile, AISI 4340 Steel

Figure - 123 Maximum Total Pile Displacement vs. Horizontal Load

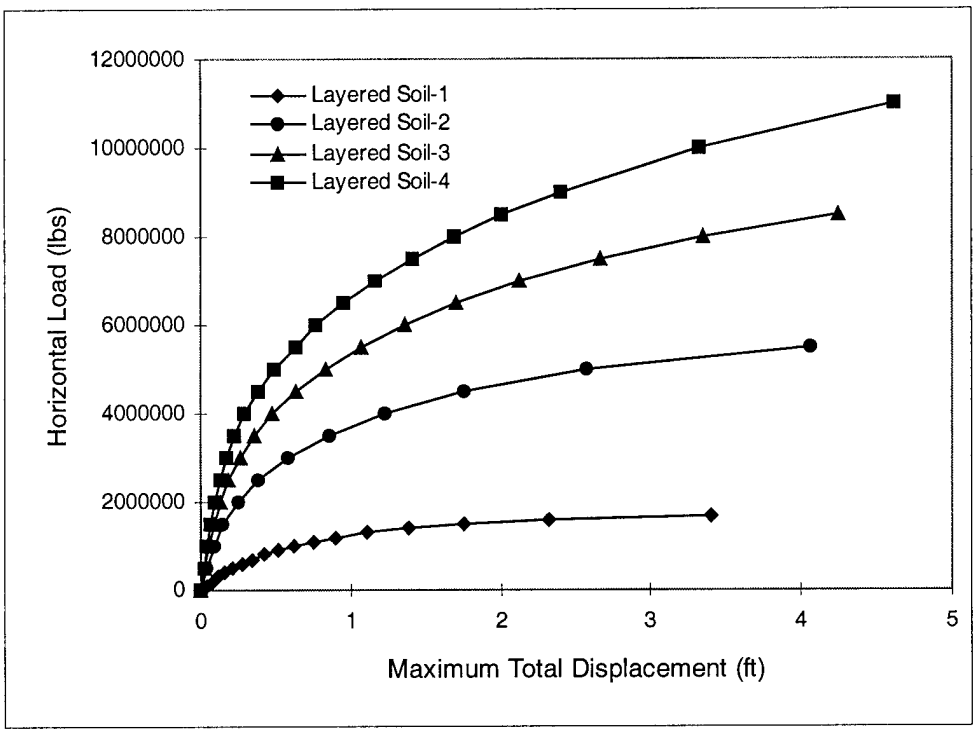

Figure - 124 Maximum Horizontal Pile Displacement vs. Horizontal Load

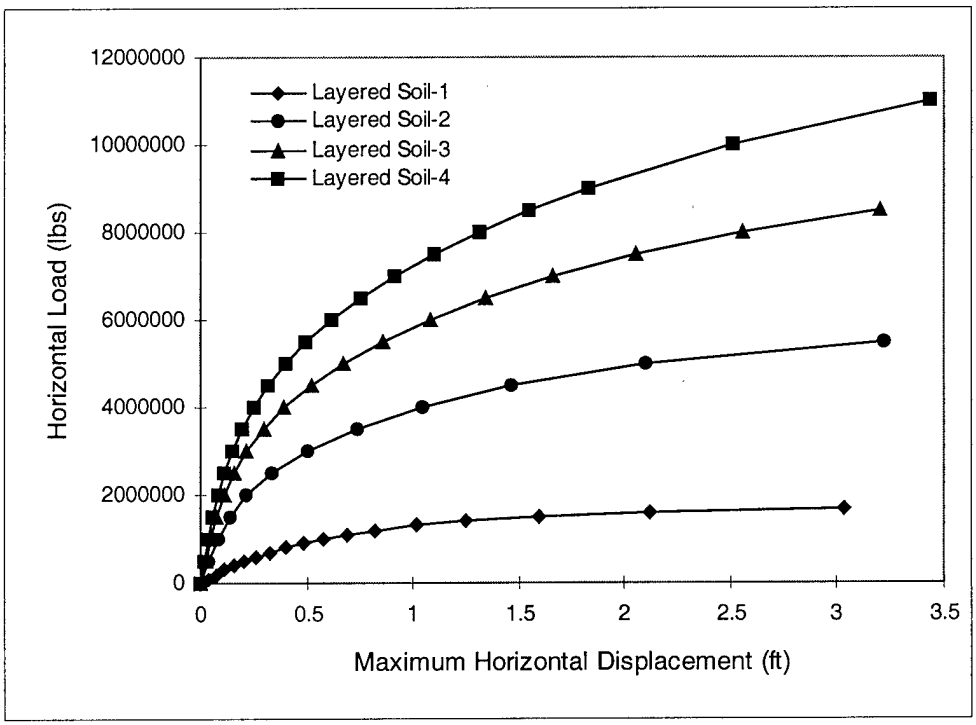

Figure - 125 Soil Minor Principal Stresses on a Vertical Plane along Horizontal Load Direction (Circular Pile in Layered Soil-2)

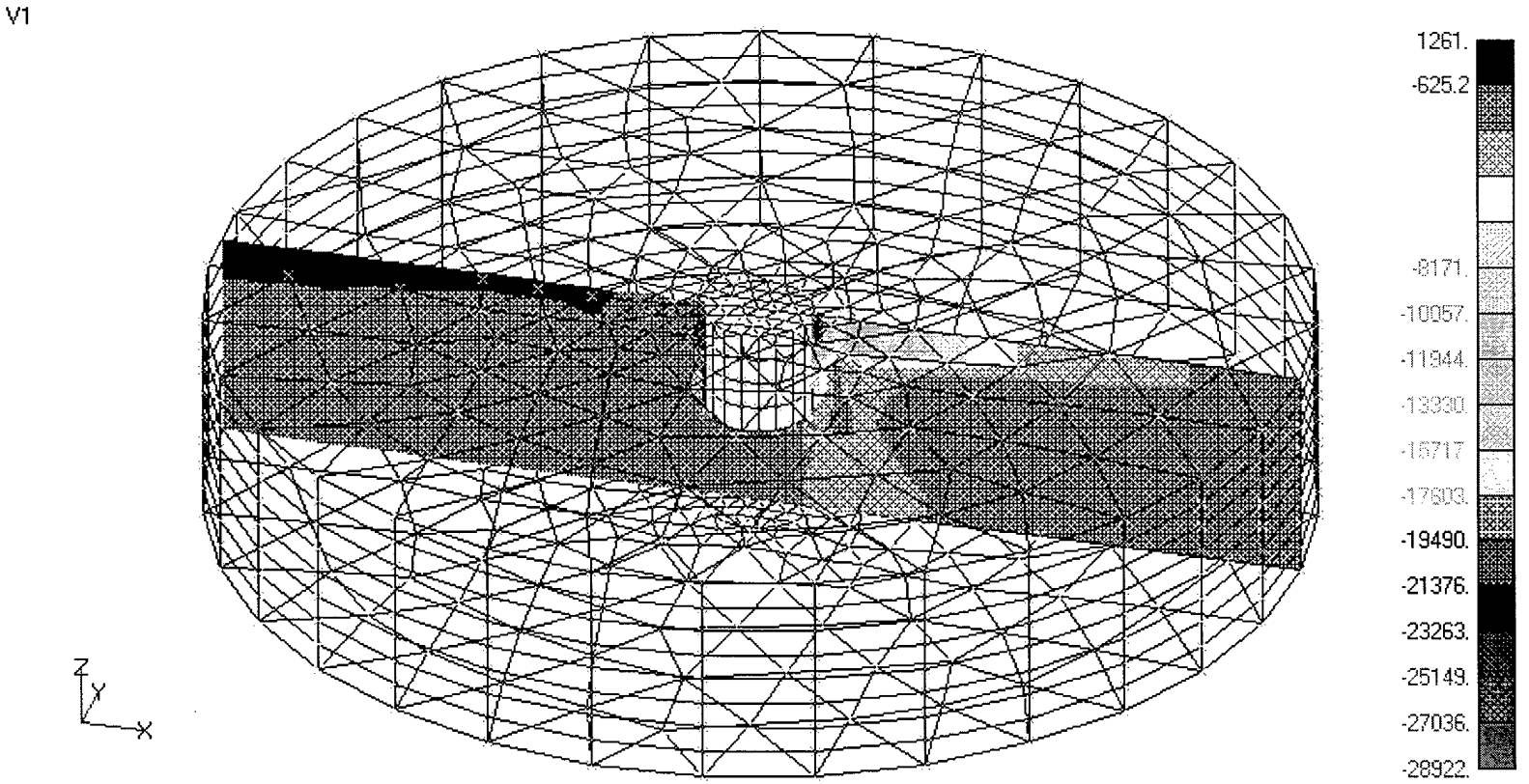

Horizontal Load = 5,000,000 lbs
Linear Elastic-Perfectly Plastic Clayey Soil (Hyperbolic Extended Drucker-Prager)
E = 30,000 psf, υ = 0.499, Slope Angle = 10.2°, Dilation Angle = 10.2°
Linear Elastic-Perfectly Plastic Sandy Soil (Linear Extended Drucker-Prager)
E = 864,000 psf, υ = 0.3, Slope Angle = 46.2°, Dilation Angle = 21.5°
Pile, AISI 4340 Steel

Figure - 126 Minimum Soil Minor Principal Stress vs. Horizontal Load

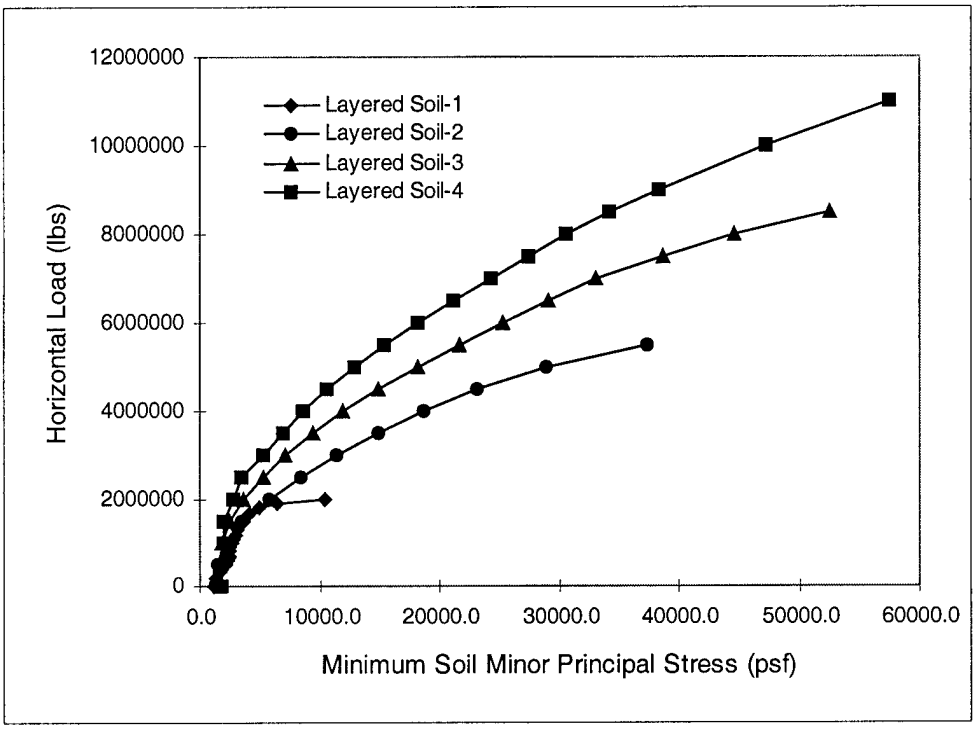

Figure - 127 Pile von Mises Stresses on the Pile Surface (Circular Pile in Layered Soil-2)

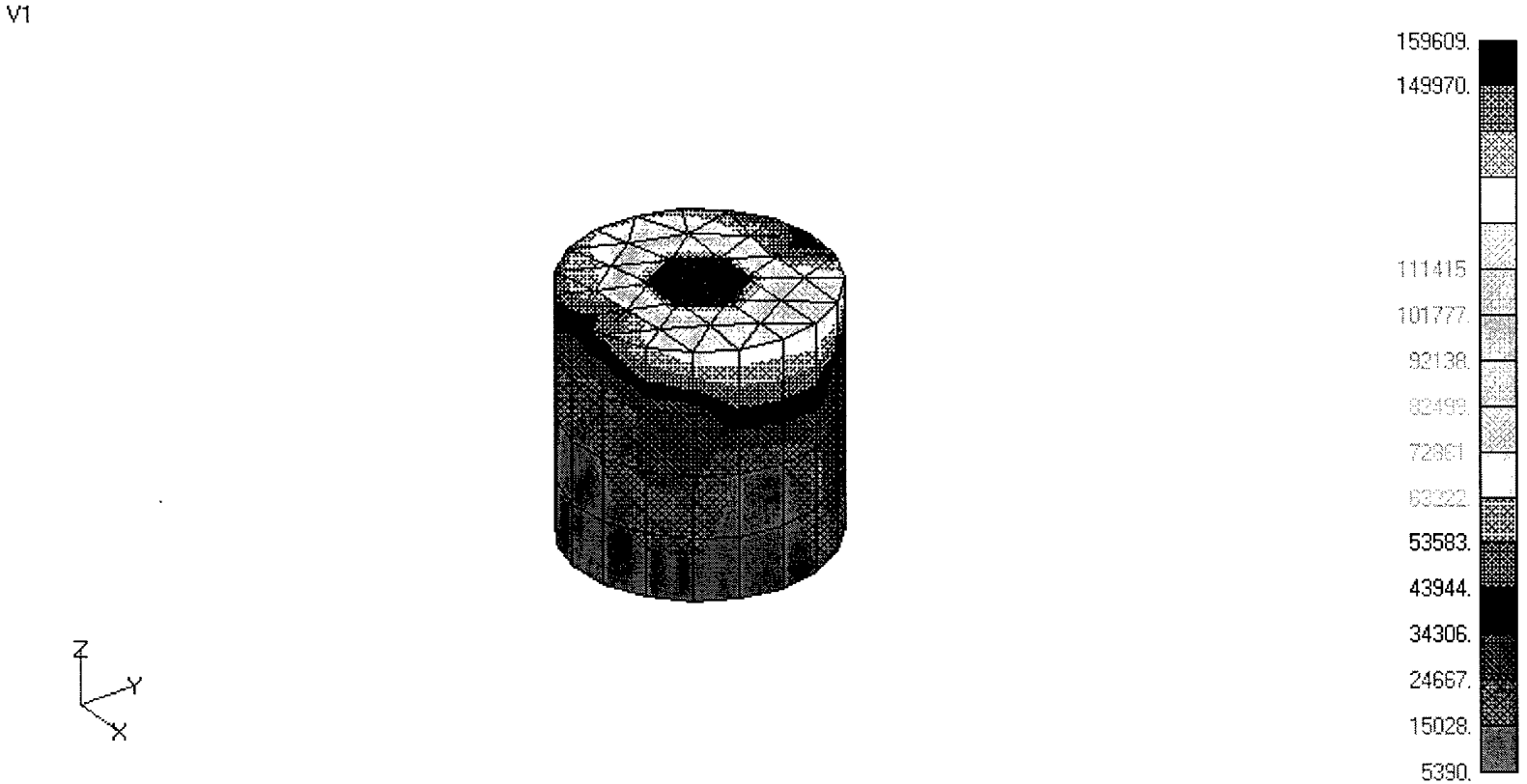

Horizontal Load = 5,000,000 lbs
Linear Elastic-Perfectly Plastic Clayey Soil (Hyperbolic Extended Drucker-Prager)
E = 30,000 psf, υ = 0.499, Slope Angle = 10.2°, Dilation Angle = 10.2°
Linear Elastic-Perfectly Plastic Sandy Soil (Linear Extended Drucker-Prager)
E = 864,000 psf, υ = 0.3, Slope Angle = 46.2°, Dilation Angle = 21.5°
Pile, AISI 4340 Steel

Figure - 128 Maximum Pile von Mises Stress vs. Horizontal Load

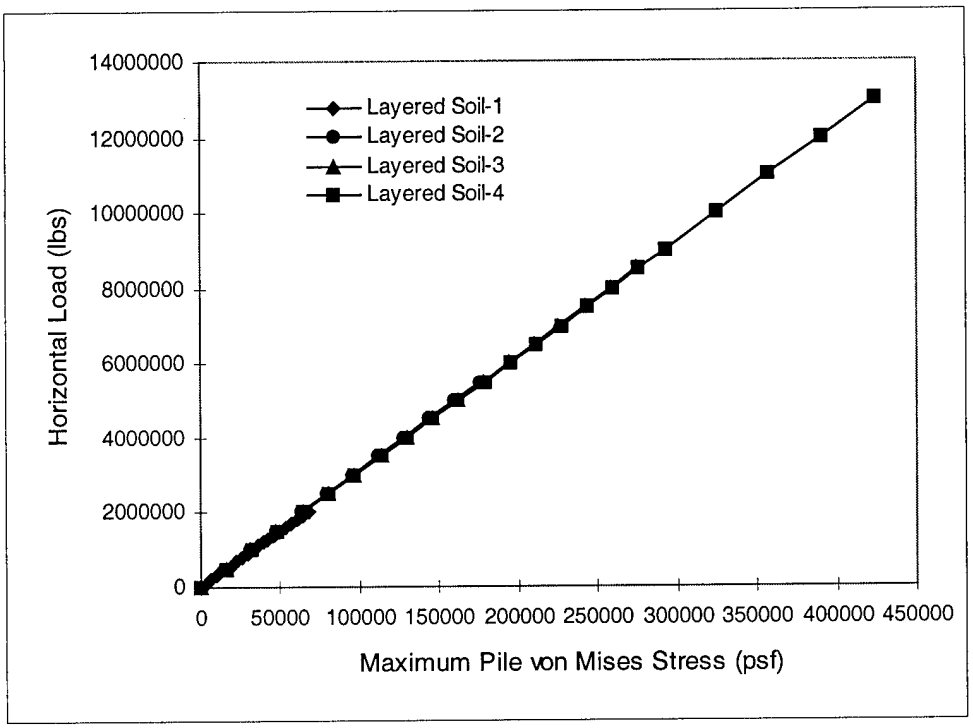

Figure - 129 Pile Total Displacements (Circular Pile in Layered Soil-6)

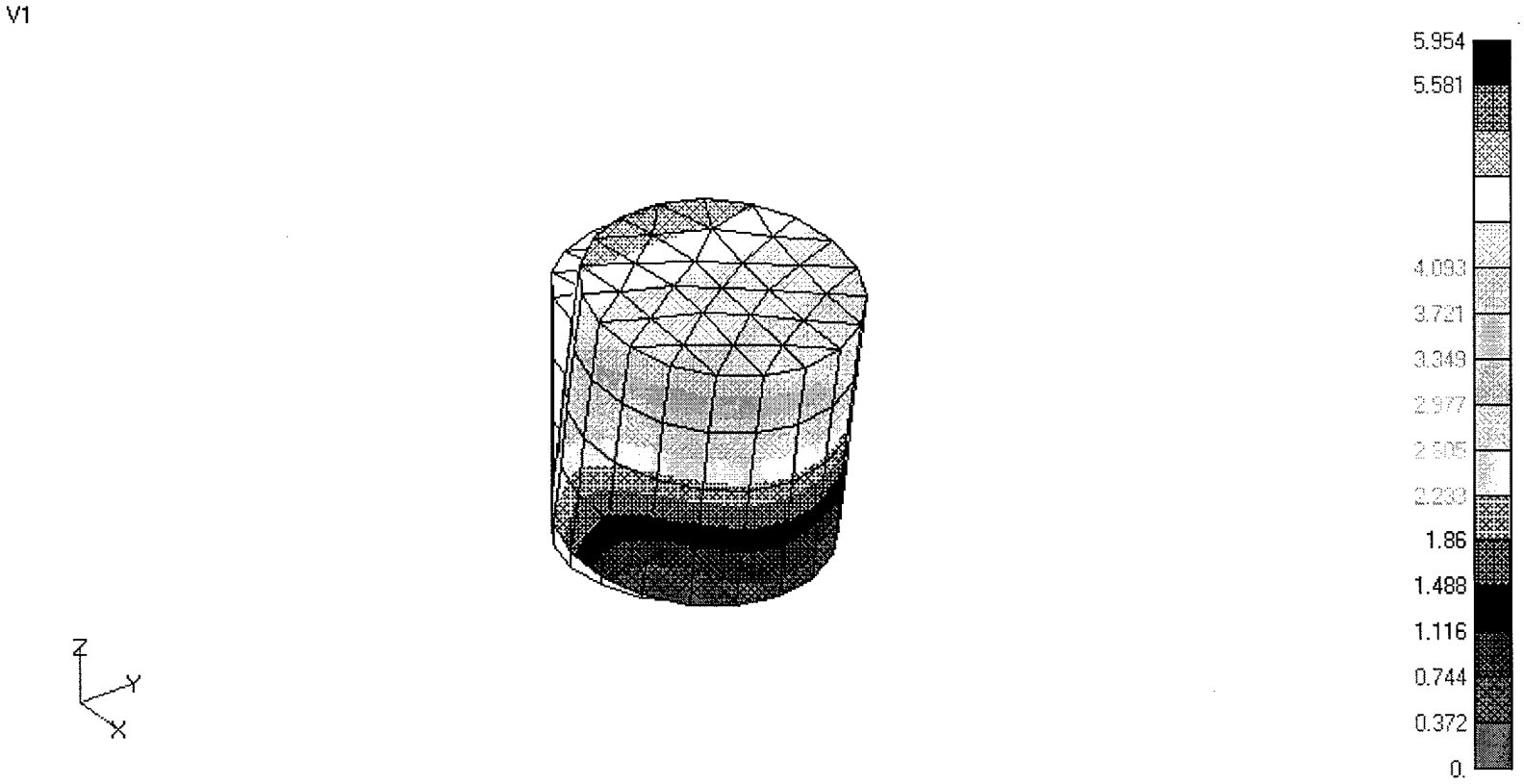

Horizontal Load = 5,000,000 lbs
Linear Elastic-Perfectly Plastic Clayey Soil (Hyperbolic Extended Drucker-Prager)
E = 30,000 psf, υ = 0.499, Slope Angle = 10.2°, Dilation Angle = 10.2°
Linear Elastic-Perfectly Plastic Sandy Soil (Linear Extended Drucker-Prager)
E = 864,000 psf, υ = 0.3, Slope Angle = 46.2°, Dilation Angle = 21.5°
Pile, AISI 4340 Steel

Figure - 130 Maximum Total Pile Displacement vs. Horizontal Load

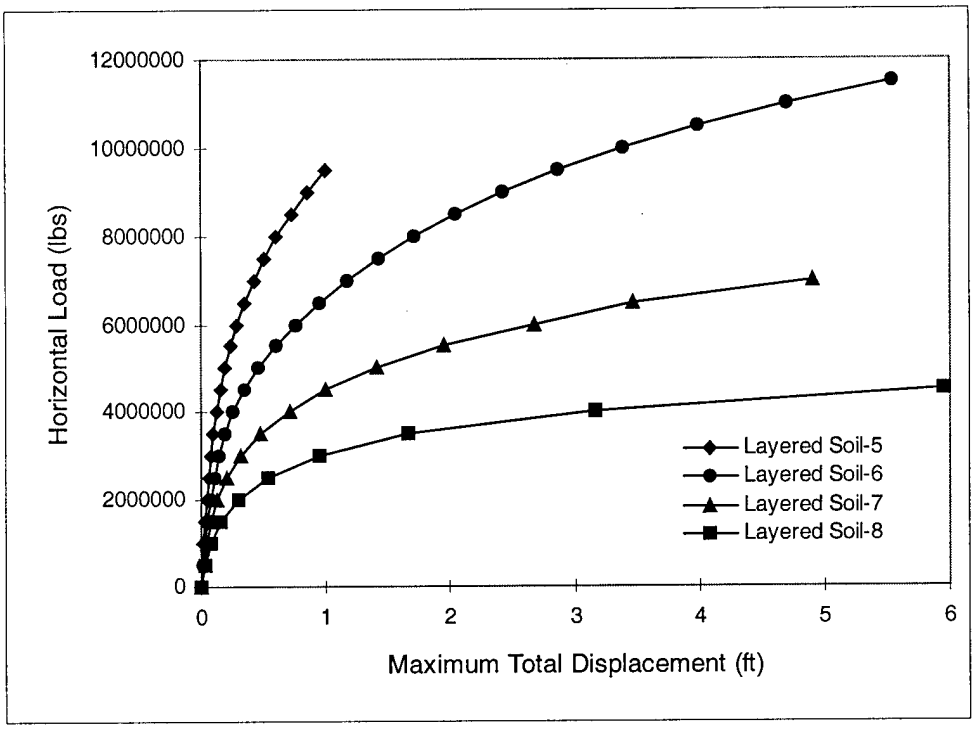

Figure - 131 Maximum Horizontal Pile Displacement vs. Horizontal Load

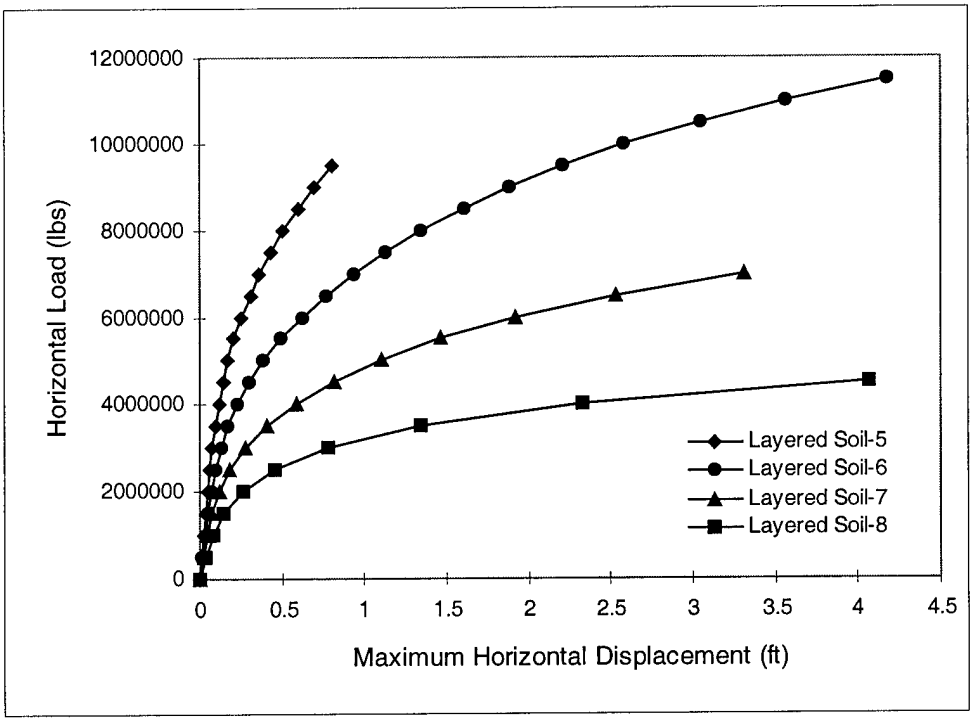

Figure - 132 Soil Minor Principal Stresses on a Vertical Plane along Horizontal Load Direction (Circular Pile in Layered Soil-5)

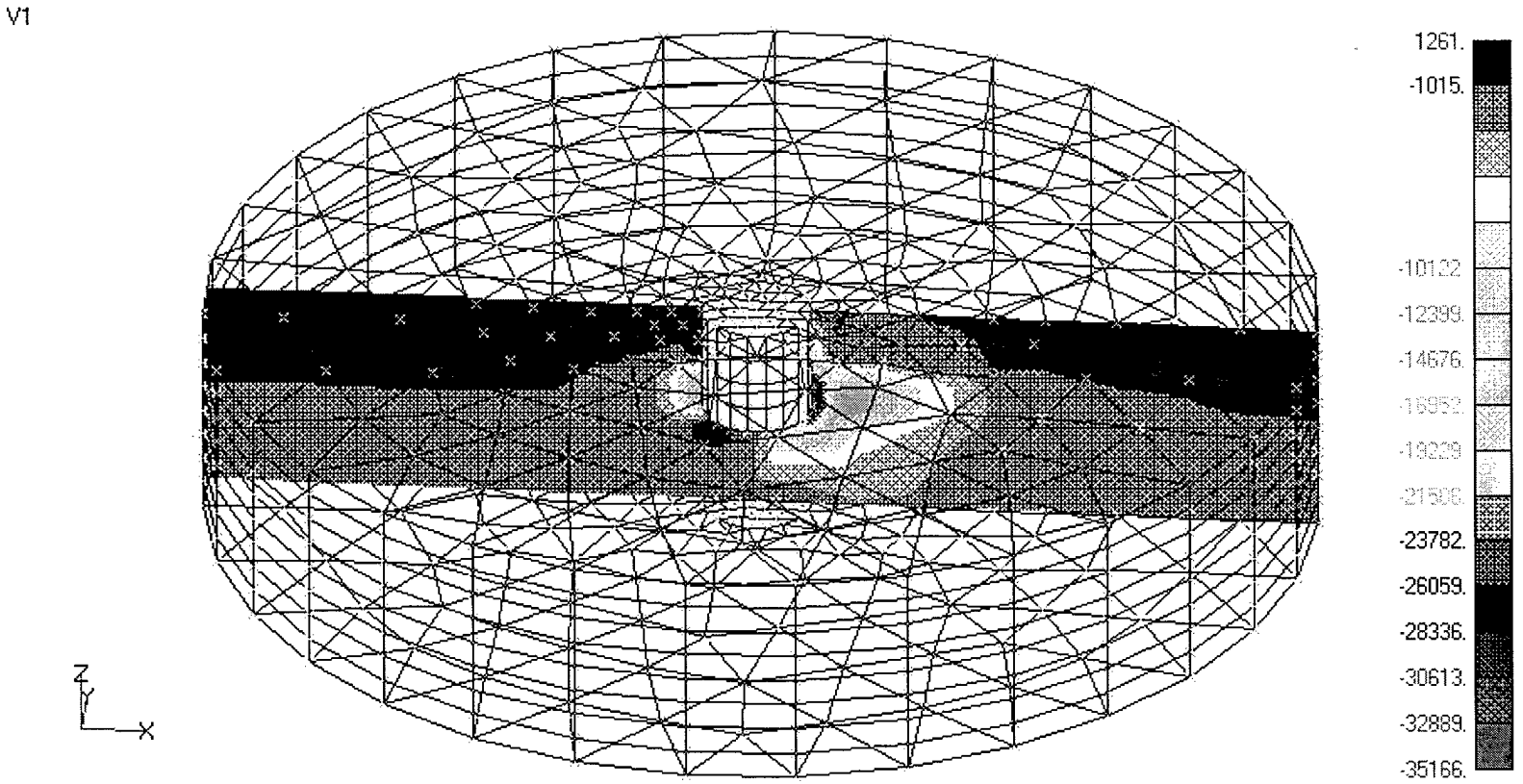

Horizontal Load = 5,000,000 lbs
Linear Elastic-Perfectly Plastic Clayey Soil (Hyperbolic Extended Drucker-Prager)
E = 30,000 psf, υ = 0.499, Slope Angle = 10.2°, Dilation Angle = 10.2°
Linear Elastic-Perfectly Plastic Sandy Soil (Linear Extended Drucker-Prager)
E = 864,000 psf, υ = 0.3, Slope Angle = 46.2°, Dilation Angle = 21.5°
Pile, AISI 4340 Steel

Figure - 133 Minimum Soil Minor Principal Stress vs. Horizontal Load

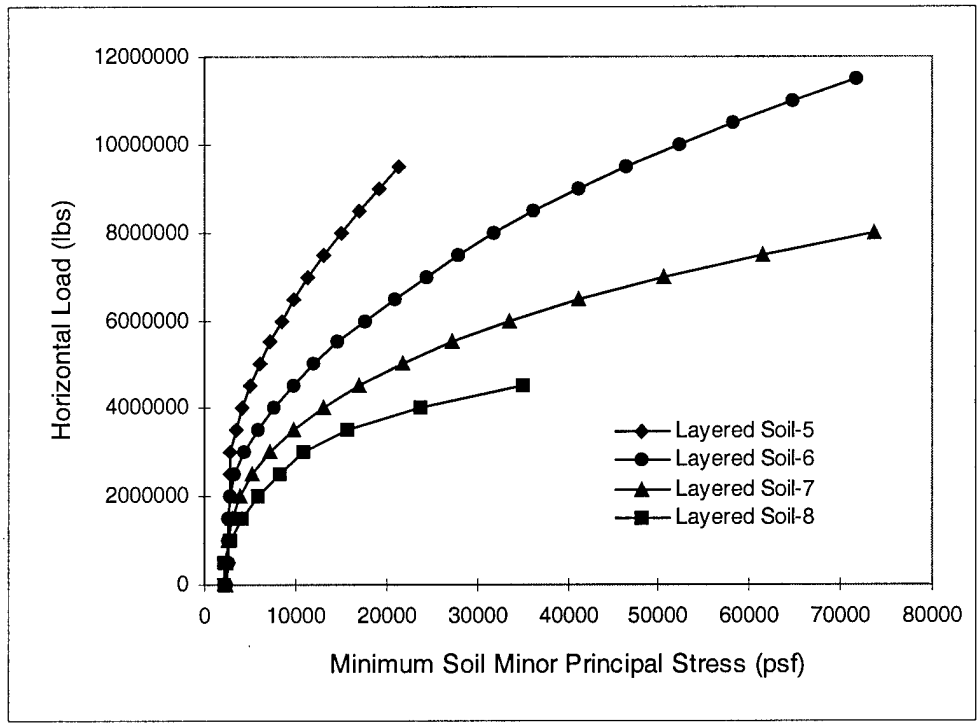

Figure - 134 Pile von Mises Stresses on the Pile Surface (Circular Pile in Layered Soil-2)

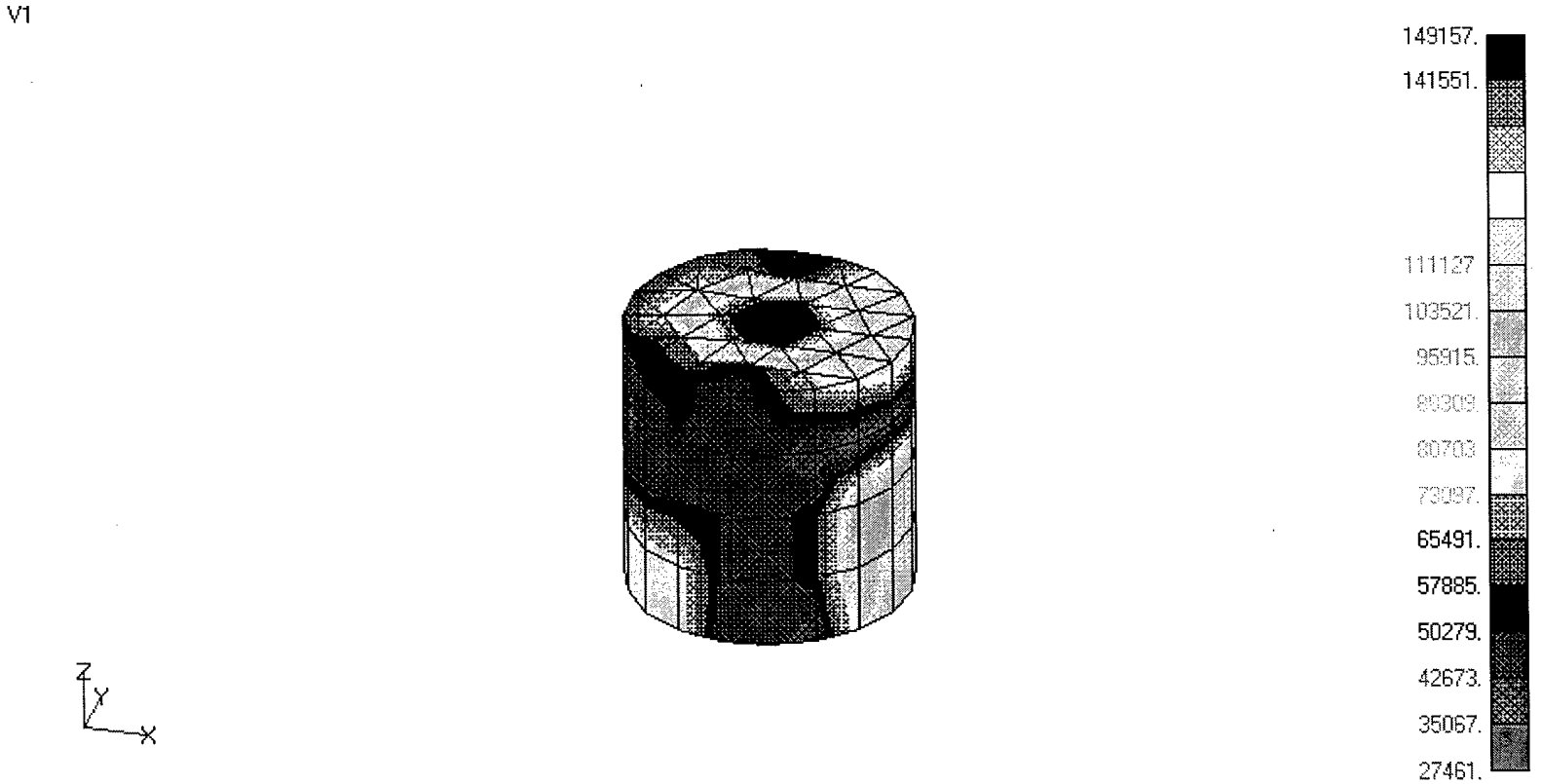

Horizontal Load = 5,000,000 lbs
Linear Elastic-Perfectly Plastic Clayey Soil (Hyperbolic Extended Drucker-Prager)
E = 30,000 psf, υ = 0.499, Slope Angle = 10.2°, Dilation Angle = 10.2°
Linear Elastic-Perfectly Plastic Sandy Soil (Linear Extended Drucker-Prager)
E = 864,000 psf, υ = 0.3, Slope Angle = 46.2°, Dilation Angle = 21.5°
Pile, AISI 4340 Steel

Figure - 135 Maximum Pile von Mises Stress vs. Horizontal Load

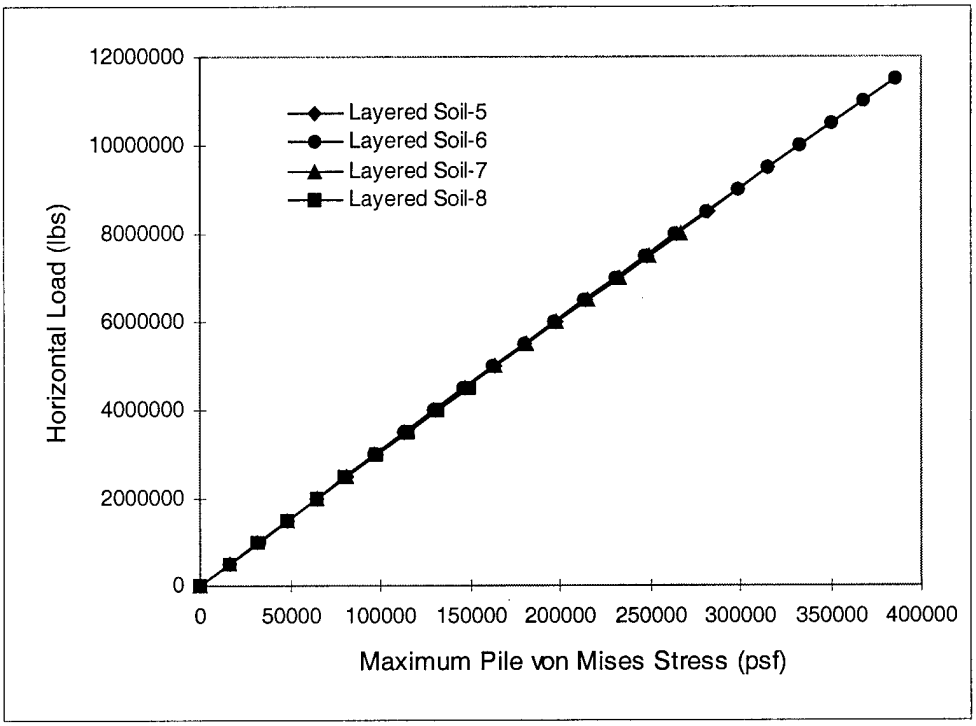

Table - 1 Dimensions of Pile Cells

Types of Pile	Dimension (R or L, ft)	Face Width (W, ft)	Types of Pile	Dimension (R or L, ft)	Face Width (W, ft)
Circle	R = 15.00	30.00	Cross2 (1:2)	L = 4.71	19.99
Hexagon	L = 15.38	26.64	Cross1 (1:3)	L = 3.37	23.56
Triangle	L = 31.42	31.42	Cross2 (1:3)	L = 3.37	19.04
Square1	L = 23.56	23.56	Cross1 (1:4)	L = 2.62	23.56
Square2	L = 23.56	33.32	Cross2 (1:4)	L = 2.62	18.51
Y-shape (1:1)	L = 10.47	28.60	Clover41	R = 7.50	30.00
Y-shape (1:2)	L = 6.28	28.05	Clover42	R = 7.50	25.61
Y-shape (1:3)	L = 4.49	27.81	Clover3	R = 7.50	27.99
Y-shape (1:4)	L = 3.49	27.68	C-circle41	R = 3.75	18.11
Cross1 (1:1)	L = 7.85	23.55	C-circle42	R = 3.75	21.21
Cross2 (1:1)	L = 7.85	22.20	C-circle3	R = 5.24	20.94
Cross1 (1:2)	L = 4.71	23.56			

Note;

1. C-circle indicates cross-section width clustered circles
2. Clover-shaped cross-sections with four leaves consist of half-circles.
3. Clover-shaped cross-section with three leaves consists of circles with circumference of 0.75 times the full circle.
4. Cross1 indicates the cross-shaped cross section with the horizontal load applied along the centerline of its branch (Figure-1)
5. Cross2 indicates the cross-shaped cross section with the horizontal load applied between the branches (Figure-1)
6. Clover41 indicates the clover-shaped cross-section with the horizontal load applied through the centerline of its cell.
7. Clover42 indicates the clover-shaped cross-section with the horizontal load applied between the cells.
8. C-circle41 indicates the clustered circles cross-section with the horizontal load applied through the centerline of its cell.
9. C-circle42 indicates the clustered circles cross-section with the horizontal load applied between cells.

Table - 2 Pile Responses due to Horizontal Load

No	Cross-section	Load, P_x (lbs)	$\delta_{horizon}$ (ft)	Soil		Pile	
				$\sigma_{x\text{-normal}}$ (psf)	$\sigma_{1\text{-principal}}$ (psf)	$\sigma_{x\text{-normal}}$ (psf)	$\sigma_{3\text{-principal}}$ (psf)
1	Circle	30,0000	0.463	-1,234.1	-1,271.9	213,362.2	251,974.1
2	Hexagon	〃	0.539	-769.0	-795.4	290,178.7	228,297.2
3	Triangle	〃	0.539	-1,321.7	-1,347.5	176,514.6	222,626.7
4		-300,000	0.539	-949.0	-992.9	290,069.4	319,693.9
5	Square1	300,000	0.511	-1,016.5	-1,057.6	197,061.7	225,329.4
6	Square2	〃	0.480	-1,483.5	-1,511.8	265,100.4	299,000.6
7	Y-shape (1:1)	〃	0.478	-777.2	-792.1	114,214.0	209,738.3
8		-300,000	0.478	-692.8	-713.0	136,891.4	315,212.2
9	Y-shape (1:2)	300,000	0.535	-1,497.7	-1,510.6	986,449.4	991,839.4
10		-300,000	0.535	-1,377.7	-1,400.3	283,259.7	539,419.2
11	Y-shape (1:3)	300,000	0.759	-1,408.0	-1,461.3	1,566,514.0	1,577,371.0
12		-300,000	0.759	-1,604.7	-1,638.1	467,600.3	988,001.2
13	Y-shape (1:4)	300,000	0.905	-2,214.6	-2,233.1	2,219,640.0	2,241,384.0
14		-300,000	0.905	-2,179.0	-2,182.2	757,703.6	1,473,907.0
15	Cross1 (1:1)	300,000	0.604	-1,346.6	-1,374.6	137,658.0	308,256.0
16	Cross2 (1:1)	〃	0.568	-997.6	-1,017.6	133,674.5	410,489.4
17	Cross1 (1:2)	〃	0.759	-1,201.4	-1,272.9	528,851.4	738,552.4
18	Cross2 (1:2)	〃	0.724	-1,038.5	-1,061.2	240,806.1	600,118.5
19	Cross1 (1:3)	〃	0.994	-2,351.6	-2,416.1	825,200.9	1,113,784.0
20	Cross2 (1:3)	〃	0.988	-2,632.4	-2,634.4	600,587.3	1,146,139.0
21	Cross1 (1:4)	〃	0.969	-1,997.9	-2,145.5	991,921.8	1,967,976.0
22	Cross2 (1:4)	〃	0.979	-1,989.2	-2,101.4	834,382.8	1,662,154.0
23	Clover41	〃	0.799	-1,945.5	-1,979.4	346,083.9	401,336.8
24	Clover42	〃	0.598	-2,280.5	-2,284.3	412,957.7	481,922.6
25	Clover3	〃	0.623	-2,407.9	-2,475.9	463,357.1	463.358.0
26		-300,000	0.623	-2,129.2	-2,166.2	658,110.3	658,112.7
27	C-circle41	300,000	1.290	-3,311.8	-3,595.0	803,725.9	1,009,618.0
28	C-circle42	〃	1.293	-3,910.1	-3,936.5	1,292,378.0	1,292,402.0
29	C-circle3	〃	1.094	-2,233.2	-2,262.2	245,431.6	540,225.5
30		-300,000	1.094	-1,860.2	-1983.2	985,818.2	985,890.3

Note:

1. $\sigma_{1\text{-principal}}$ is the minimum soil minor principal stress
2. $\sigma_{3\text{-principal}}$ is the maximum pile major principal stress

Table - 3 Five Cross-Sections with Smallest Maximum Horizontal Displacements

Order	Cross-Section	Maximum Displacement (ft)
1	Circle	0.463
2	Y-shape (1:1)	0.478
3	Square	0.511
4	Y-shape (1:2)	0.535
5	Triangle or Hexagon	0.539

Table - 4 Five Cross-sections with Smallest Maximum Horizontal Normal Soil Compressive Stresses

Order	Cross-Section	Maximum horizontal normal compressive stresses (psf)
1	Hexagon	-769.0
2	Y-shape (1:1)	-777.2
3	Cross (1:2)	-1,201.4
4	Circle	-1,234.1
5	Triangle	-1,321.7

Table - 5 Five Cross-Sections with Smallest Minimum Soil Minor Principal Stress

Order	Cross-Section	Minimum soil minor principal stress (psf)
1	Y-shape (1:1)	-792.1
2	Hexagon	-795.4
3	Circle	-1,271.9
4	Cross (1:2)	-1,272.9
5	Triangle	-1,347.5

Table - 6 Five Cross-Sections with Smallest Maximum Horizontal Normal Pile Tensile Stress

Order	Types of Pile	Maximum horizontal normal pile tensile stress (psf)
1	Y-shape (1:1)	136,891.4
2	Cross (1:1)	137,658.0
3	Circle	213,362.2
4	Square	265,100.4
5	Triangle	290,069.4

Table - 7 Five Cross-Sections with Smallest Maximum Pile Major Principal Stress

Order	Cross-section	Maximum pile major principal stress (psf)
1	Hexagon	228,297.2
2	Circle	251,974.1
3	Square	299,000.6
4	Y-shape (1:1)	315,212.2
5	Triangle	319,693.6

Table - 8 Pile Responses due to Vertical Load

No.	Type of Pile	Max. $\delta_{vertical}$ (ft)	Soil	Pile
			$\sigma_{1\text{-principal}}$ (psf)	$\sigma_{3\text{-principal}}$ (psf)
1	Circle	1.220	-714.0	1,235,627.0
2	Hexagon	1.408	-1,533.7	12,694,291.0
3	Triangle	1.575	-1,064.4	13,605,085.0
4	Square	1.469	-2,824.1	13,559,383.0
5	Y-shape (1:1)	0.514	-879.2	2,494,272.0
6	Y-shape (1:2)	0.733	-1,797.6	16,801,791.0
7	Y-shape (1:3)	0.536	-1,310.4	17,704,726.0
8	Y-shape (1:4)	0.510	-1,147.2	16,565,421.0
9	Cross (1:1)	0.470	-1,091.4	2,340,180.0
10	Cross (1:2)	0.585	-1,826.1	11,746,705.0
11	Cross (1:3)	0.535	-1,436.6	4,5089,08.0
12	Cross (1:4)	0.469	-1,852.0	12,620,515.0
13	Clover4	1.711	-2,080.2	24,602,413.0
14	Clover3	1.475	-1,722.8	25,767,137.0
15	C-circle4	0.482	-1,222.2	13,017,584.0
16	C-circle3	0.684	-860.9	12,153,883.0

Note:

1 $\sigma_{1\text{-principal}}$ is the minimum soil minor principal stress

2 $\sigma_{3\text{-principal}}$ is the maximum pile major principal stress

Table - 9 Five Cross-Sections with Smallest Minimum Soil Minor Principal Stress

Order	Cross-section	Minimum soil minor principal stress (psf)
1	Circle	-714.0
2	C-circle3	-860.9
3	Y-shape (1:1)	-879.2
4	Triangle	-1,064.6
5	Cross (1:1)	-1,091.4

Table - 10 Five Cross-Sections with Smallest Maximum Pile Major Principal Stress

Order	Cross-section	Maximum pile major principal stress (psf)
1	Circle	1,235,627.0
2	Cross (1:1)	2,340,180.0
3	Y-shape (1:1)	2,494,272.9
4	Cross (1:3)	4,508,908.0
5	Cross (1:2)	11,746,883.0

Table - 11 Maximum Displacements of Suction Piles at Various Horizontal Loads

No	Horizontal Load (lbs)	Max. Total Displacement (ft)			Max. Hor. Displacement(ft)		
		Circle	Triangle	Y-shape	Circle	Triangl	Y-shape
1	500,000	0.0116	0.0129	0.0127	0.0111	0.0119	0.0122
2	1,000,000	0.0232	0.0258	0.0255	0.0221	0.0239	0.0244
3	1,500,000	0.0350	0.0394	0.0387	0.0334	0.0364	0.0370
4	2,000,000	0.0484	0.0547	0.0533	0.0460	0.0502	0.0510
5	2,500,000	0.0636	0.0730	0.0697	0.0600	0.0664	0.0668
6	3,000,000	0.0814	0.0949	0.0886	0.0762	0.0854	0.0845
7	3,500,000	0.1021	0.1215	0.1107	0.0947	0.1079	0.1049
8	4,000,000	0.1266	0.1532	0.1369	0.1163	0.1340	0.1289
9	4,500,000	0.1564	0.1911	0.1682	0.1420	0.1646	0.1572
10	5,000,000	0.1929	0.2363	0.2068	0.1729	0.2003	0.1907
11	5,500,000	0.2368	0.2918	0.2520	0.2095	0.2443	0.2312
12	6,000,000	0.2891	0.3592	0.3097	0.2525	0.2947	0.2812
13	6,500,000	0.3506	0.4365	0.3772	0.3062	0.3529	0.3386
14	7,000,000	0.4227	0.5254		0.3604	0.4193	

Table - 12 Minimum Soil Minor Principal Stresses of Suction Piles at Various Horizontal Loads

No	Horizontal Load (lbs)	Minimum Soil Minor Principal Stress (psf)		
		Circle	Triangle	Y-shape
1	500,000	-2,557.1	-2,548.4	-2,551.7
2	1,000,000	-2,615.5	-2,597.9	-2,604.7
3	1,500,000	-2,674.4	-2,647.2	-2,658.3
4	2,000,000	-2,735.2	-2,696.8	-2,712.9
5	2,500,000	-2,798.1	-2,998.3	-2,768.7
6	3,000,000	-2,862.7	-3,935.2	-3,295.2
7	3,500,000	-3,444.9	-4,962.9	-4,063.7
8	4,000,000	-4,208.8	-6,003.4	-4,949.0
9	4,500,000	-5,117.9	-7,110.5	-5,878.1
10	5,000,000	-6,042.6	-8,359.2	-6,915.7
11	5,500,000	-7,130.5	-9,733.5	-8,041.5
12	6,000,000	-8,408.9	-11,239.1	
13	6,500,000	-9,845.9	-12,832.4	
14	7,000,000	-11,415.0	-14,513.0	

Table - 13 Maximum Pile Von Mises Stresses of Suction Piles at Various Horizontal Loads

No	Horizontal Load (lbs)	Maximum Pile Von Mimes Stress (psf)		
		Circle	Triangle	Y-shape
1	500,000	16,071.5	19,198.8	13,329.6
2	1,000,000	32,142.9	38,397.1	26,659.2
3	1,500,000	48,192.9	57,575.9	40,500.4
4	2,000,000	64,459.6	77,095.8	55,119.9
5	2,500,000	80,946.8	96,864.4	70,070.3
6	3,000,000	97,312.9	116,790.0	85,271.0
7	3,500,000	113,685.9	136,839.2	100,851.4
8	4,000,000	130,283.5	156,974.2	116,570.9
9	4,500,000	146,984.5	177,161.2	132,540.5
10	5,000,000	163,761.0	197,303.4	149,086.1
11	5,500,000	180,684.9	217,409.5	166,593.1
12	6,000,000	197,681.1	237,527.2	
13	6,500,000	214,625.9	257,608.7	
14	7,000,000	231,540.1		

Table - 14 Maximum Vertical Displacements of Suction Piles due to Various Vertical Loads

No	Vertical Load (lbs)	Maximum Vertical Displacement (ft)		
		Circle	Triangle	Y-shape
1	500,000	0.0056	0.0060	0.0060
2	1,000,000	0.0113	0.0120	0.0120
3	1,500,000	0.0169	0.0180	0.0180
4	2,000,000	0.0225	0.0240	0.0240
5	2,500,000	0.0282	0.0300	0.0300
6	3,000,000	0.0338	0.0361	0.0360
7	3,500,000	0.0396	0.0422	0.0421
8	4,000,000	0.0454	0.0486	0.0483
9	4,500,000	0.0515	0.0555	0.0548
10	5,000,000	0.0577	0.0633	0.0614
11	5,500,000	0.0651	0.0741	0.0691
12	6,000,000	0.0779	0.0962	0.0823
13	6,500,000	0.0958		0.1100
14	7,000,000	0.1212		

Table - 15 Minimum Soil Minor Principal Stresses of Suction Piles due to Various Vertical Loads

No	Vertical Load (lbs)	Minimum Soil Minor Principal Stress (psf)		
		Circle	Triangle	Y-shape
1	500,000	2,500.5	2,500.5	2,500.5
2	1,000,000	2,502.0	2,502.0	2,502.0
3	1,500,000	2,503.6	2,503.5	2,503.4
4	2,000,000	2,505.1	2,505.1	2,504.9
5	2,500,000	2,506.6	2,506.6	2,506.4
6	3,000,000	2,508.1	2,508.1	2,507.9
7	3,500,000	2,509.7	2,509.6	2,509.4
8	4,000,000	2,511.2	2,511.2	2,511.0
9	4,500,000	2,512.9	2,512.9	2,512.6
10	5,000,000	2,514.5	2,514.6	2,514.2
11	5,500,000	2,516.3	2,516.5	2,516.0
12	6,000,000	2,518.3	2,726.4	2,518.3
13	6,500,000	2,663.8		2,650.8
14	7,000,000	3,081.0		

Table - 16 Maximum Pile von Mises Stresses of Suction Piles due to Various Vertical Loads

No	Vertical Load (lbs)	Maximum Pile von Mises Stress (psf)		
		Circle	Triangle	Y-shape
1	500,000	49,978.3	40,231.1	15,849.1
2	1,000,000	99,958.7	80,462.1	31,698.1
3	1,500,000	149,938.0	120,693.2	47,547.2
4	2,000,000	199,917.3	160,924.2	63,396.2
5	2,500,000	249,896.7	201,155.3	79,245.3
6	3,000,000	299,876.0	241,355.1	95,113.4
7	3,500,000	349,674.0	281,529.4	110,938.3
8	4,000,000	399,471.9	321,492.9	126,526.9
9	4,500,000	449,067.0	361,264.2	142,083.1
10	5,000,000	498,589.9	400,928.0	157,556.2
11	5,500,000	547,853.6	440,569.9	173,137.0
12	6,000,000	597,507.1	481,166.3	188,946.3
13	6,500,000	646,945.2		205,011.8
14	7,000,000	695,062.5		

Table - 17 Maximum Displacements of Suction Piles due to Various 45-Degree Inclined Loads

No	45-Deg. I. Load (lbs)	Max. Total Displacement			Max. Hor. Displacement(ft)		
		Circle	Triangl	Y-shape	Circle	Triangl	Y-shape
1	500,000	0.0100	0.0113	0.0107	0.0078	0.0084	0.0086
2	1,000,000	0.0200	0.0227	0.0214	0.0156	0.0169	0.0172
3	1,500,000	0.0301	0.0346	0.0325	0.0236	0.0257	0.0260
4	2,000,000	0.0417	0.0479	0.0448	0.0325	0.0355	0.0359
5	2,500,000	0.0547	0.0639	0.0590	0.0427	0.0472	0.0473
6	3,000,000	0.0707	0.0844	0.0757	0.0549	0.0620	0.0606
7	3,500,000	0.0915	0.1122	0.0957	0.0705	0.0815	0.0764
8	4,000,000	0.1193	0.1499	0.1231	0.0905	0.1070	0.0972
9	4,500,000	0.1536	0.1971	0.1582	0.1147	0.1379	0.1232
10	5,000,000	0.1967	0.2526	0.2083	0.1442	0.1735	0.1587
11	5,500,000		0.3221	0.2734		0.2166	0.2039
12	6,000,000			0.3545			0.2592
13	6,500,000			0.4581			0.3280

Table - 18 Minimum Soil Minor Principal Stresses of Suction Piles due to Various 45-Degree inclined Loads

No	45-Deg. Inclined Load (lbs)	Minimum Soil Minor Principal Stress (psf)		
		Circle	Triangle	Y-shape
1	500,000	2,504.2	2,504.3	2,504.3
2	1,000,000	2,509.5	2,509.6	2,509.7
3	1,500,000	2,514.9	2,515.3	2,515.5
4	2,000,000	2,521.9	2,522.2	2,522.4
5	2,500,000	2,530.4	2,531.4	2,531.0
6	3,000,000	2,541.4	2,543.9	2,542.0
7	3,500,000	2,555.9	3,281.4	2,555.4
8	4,000,000	2,879.3	4,372.1	3,190.0
9	4,500,000	3,722.4	5,499.5	4,085.8
10	5,000,000	4,679.1	6,607.6	5,147.0
11	5,500,000		7,812.0	6,265.3
12	6,000,000			7,475.6

Table - 19 Maximum Pile von Mises Stresses of Suction Piles due to Various 45-Degree Inclined Loads

No	45-Deg. Inclined Load (lbs)	Minimum Soil Minor Principal Stress (psf)		
		Circle	Triangle	Y-shape
1	500,000	38,022.2	31,413.6	16,296.3
2	1,000,000	76,044.4	62,827.2	32,592.6
3	1,500,000	113,990.7	94,162.6	48,982.6
4	2,000,000	151,382.5	125,493.1	65,636.8
5	2,500,000	188,475.5	156,847.2	82,059.3
6	3,000,000	225,909.1	188,483.6	98,898.7
7	3,500,000	263,738.8	220,486.6	116,007.3
8	4,000,000	301,530.6	252,441.6	133,477.1
9	4,500,000	339,085.7	284,489.1	151,028.2
10	5,000,000	375,985.2	316,620.3	168,346.3
11	5,500,000			185,003.8
12	6,000,000			202,077.2

Table - 20 Failure Loads Corresponding to the Displacement of Initial Passive State

Horizontal Load			45-Degree Inclined Load		
Circle	Triangle	Y-shape	Circle	Triangle	Y-shape
4,859,223	4,493,464	4,604,478	*	4,869,382	5,060,840

Note: * indicates that the solution did not converge but greater than 5,060,840 lbs.

Table - 21 Failure Loads Corresponding to the Yield Displacement under Vertical Load

Shape	Circle	Triangle	Y-shape
Load (lbs)	5,155,405	4,788,462	4,893,939

Table - 22 Minimum Soil Minor Principal Stresses at Pile Failure Loads

Load Direction	Minimum Soil Minor Principal Stress (psf)		
	Circle	Triangle	Y-shape
Horizontal Load	-5,782.2	-7,096.0	-6,094.9
45-Degree Inclined Load	*	-6318.1	-5,283.1
Vertical Load	-2,515.1	-2,513.9	-2,513.9

Note: * indicates that the solution did not converge but greater than -5,283.1 psf.

Table - 23 Maximum Pile von Mises Stresses at Failure Loads

Load Direction	Maximum Pile von Mises Stress (psf)		
	Circle	Triangle	Y-shape
Horizontal Load	159,037.5	176,493.6	135,997.8
45-Degree Inclined Load	*	308,226.5	170,373.2
Vertical Load	513,901.6	384,147.2	154,274.0

Note: * indicates that the solution did not converge but greater than 170,373.2 psf and smaller than 308,226.5 psf.

Table - 24 Maximum Displacements at Various Horizontal Loads

N	Horizont	Max. Total Displacement (ft)			Max. Hor. Displacement(ft)		
	Load	Circle	Triangle	Y-shape	Circle	Triangle	Y-shape
1	100,000	0.0370	0.0416	0.0372	0.0360	0.0397	0.0361
2	200,000	0.0761	0.0850	0.0765	0.0738	0.0809	0.0742
3	300,000	0.1183	0.1312	0.1193	0.1146	0.1244	0.1153
4	400,000	0.1649	0.1824	0.1670	0.1592	0.1721	0.1609
5	500,000	0.2172	0.2392	0.2199	0.2088	0.2243	0.2110
6	600,000	0.2774	0.3044	0.2819	0.2654	0.2832	0.2688
7	700,000	0.3476	0.3793	0.3524	0.3308	0.3497	0.3340
8	800,000	0.4285	0.4609	0.4318	0.4052	0.4214	0.4071
9	900,000	0.5204	0.5595	0.5242	0.4888	0.5068	0.4914
10	1,000,00	0.6242	0.6798	0.6289	0.5823	0.6095	0.5861
11	1,100,00	0.7463	0.8193	0.7492	0.6921	0.7271	0.6943
12	1,200,00	0.8919	1.0008	0.8882	0.8221	0.8782	0.8185
13	1,300,00	1.1105	1.2778	1.0949	1.0135	1.1037	1.0006
14	1,400,00	1.3836	1.7058	1.3503	1.2526	1.4537	1.2239
15	1,500,00	1.7578	2.3785	1.7295	1.5991	2.0149	1.5522
16	1,600,00	2.3235	3.7760	2.4148	2.1174	3.1767	2.0256
17	1,700,00	3.4062	7.9464	3.3745	3.0356	6.4430	2.8893
18	1,800,00	6.0573	52.2462	6.6464	5.1410	39.0819	4.7829
19	1,900,00	15.0104		17.0219	12.0427		11.3005
20	2,000,00	105.227			80.6334		

Table - 25 Minimum Soil Minor Principal Stresses at Various Horizontal Loads

No	Horizontal Load (lbs)	Minimum Soil Minor Principal Stress (psf)		
		Circle	Triangle	Y-shape
1	100,000	-1,255.3	-1,242.9	-1,264.0
2	200,000	-1,363.3	-1,567.2	-1,381.7
3	300,000	-1,588.3	-2,056.2	-1,506.3
4	400,000	-1,872.3	-2,678.4	-1,639.1
5	500,000	-2,127.0	-3,464.6	-1,808.4
6	600,000	-2,350.5	-4,297.0	-2,001.0
7	700,000	-2,398.0	-5,187.2	-2,296.0
8	800,000	-2,456.6	-6,154.5	-2,631.5
9	900,000	-2,553.8	-7,130.2	-2,934.6
10	1,000,000	-2,665.9	-8,033.8	-3,231.3
11	1,100,000	-2,798.0	-8,909.9	-3,554.8
12	1,200,000	-2,908.0	-9,912.1	-3,884.0
13	1,300,000	-3,144.8	-10,871.0	-4,197.8
14	1,400,000	-3,371.5	-11,960.6	-4,599.8
15	1,500,000	-3,593.0	-13,288.5	-4,978.5
16	1,600,000	-3,822.7	-14,689.2	-5,087.0
17	1,700,000	-4,072.4	-16,618.1	-5,083.1
18	1,800,000	-4,946.3	-18,671.9	-4,728.7
19	1,900,000	-6,456.4		-4,982.7
20	2,000,000	-10,412.0		-8,931.4

Table - 26 Maximum Pile Von Mises Stresses at Various Horizontal Loads

No	Horizontal Load (lbs)	Maximum Pile Von Mises Stress (psf)		
		Circle	Triangle	Y-shape
1	100,000	3,243.9	3,770.8	2,940.5
2	200,000	6,481.3	7,518.8	5,963.0
3	300,000	9,736.1	11,243.2	8,678.0
4	400,000	12,975.1	14,990.3	11,256.5
5	500,000	16,139.1	18,749.5	13,620.9
6	600,000	19,325.0	22,621.0	16,375.5
7	700,000	22,528.6	26,611.7	19,357.5
8	800,000	25,768.3	30,726.5	22,410.8
9	900,000	29,089.9	34,853.9	25,352.1
10	1,000,000	32,356.0	38,962.9	28,291.8
11	1,100,000	35,635.1	43,082.9	31,168.2
12	1,200,000	38,945.9	47,272.1	34,141.4
13	1,300,000	42,247.5	51,429.0	37,487.5
14	1,400,000	45,911.9	55,669.3	41,207.4
15	1,500,000	49,699.9	60,019.6	45,288.8
16	1,600,000	53,355.7	64,404.3	49,678.2
17	1,700,000	57,148.6	68,751.0	54,578.8
18	1,800,000	61,025.6	72,859.9	58,395.0
19	1,900,000	64,816.5		61,901.5
20	2,000,000	68,382.6		

Table - 27 Maximum Vertical Displacements due to Various Vertical Loads

No	Vertical Load (lbs)	Maximum Vertical Displacement (ft)		
		Circle	Triangle	Y-shape
1	100,000	0.0078	0.0106	0.0106
2	200,000	0.0166	0.0256	0.0250
3	300,000	0.0350	0.0474	0.0449
4	400,000	0.0548	0.0710	0.0675
5	500,000	0.0765	0.0865	0.0908
6	600,000	0.0991	0.1226	0.1163
7	700,000	0.1223	0.1502	0.1425
8	800,000	0.1471	0.1794	0.1701
9	900,000	0.1731	0.2102	0.1986
10	1,000,000	0.2003	0.2428	0.2276
11	1,100,000	0.2289	0.2774	0.2574
12	1,200,000	0.2586	0.3141	0.2886
13	1,300,000	0.2898	0.3533	0.3210
14	1,400,000	0.3223	0.3957	0.3556
15	1,500,000	0.3582	0.4402	0.3939
16	1,600,000	0.3998	0.4967	0.4363
17	1,700,000	0.4483	0.5666	0.4879
18	1,800,000	0.5109	0.7282	0.5525
19	1,900,000	0.5837	1.0933	0.6426
20	2,000,000	0.7479	2.0137	0.8497
21	2,100,000	1.0702	8.7076	1.3516
22	2,200,000	1.9548		3.5824
23	2,300,000	5.7212		

Table - 28 Minimum Soil Minor Principal Stresses due to Various Vertical Loads

No	Vertical Load (lbs)	Minimum Soil Minor Principal Stress (psf)		
		Circle	Triangle	Y-shape
1	100,000	-1,203.2	-1,195.8	-1,195.7
2	200,000	-1,256.1	-1,257.0	-1,243.3
3	300,000	-1,359.0	-1,336.1	-1,311.8
4	400,000	-1,446.1	-1,421.8	-1,387.9
5	500,000	-1,570.5	-1,510.5	-1,469.5
6	600,000	-1,702.2	-1,600.4	-1,556.0
7	700,000	-1,792.4	-1,692.3	-1,643.5
8	800,000	-1,873.4	-1,789.4	-1,733.9
9	900,000	-1,934.1	-1,878.2	-1,826.6
10	1,000,000	-2,082.3	-1,931.9	-1,916.2
11	1,100,000	-2,209.5	-1,974.8	-1,981.2
12	1,200,000	-2,316.8	-2,007.7	-2,039.4
13	1,300,000	-2,403.2	-2,037.0	-2,104.0
14	1,400,000	-2,452.2	-2,067.8	-2,161.3
15	1,500,000	-2,498.1	-2,135.1	-2,205.8
16	1,600,000	-2,485.2	-2,305.9	-2,255.7
17	1,700,000	-2,461.1	-2,402.1	-2,296.1
18	1,800,000	-2,280.0	-2,407.3	-2,324.3
19	1,900,000	-1,981.7	-2,259.4	-2,309.7
20	2,000,000	-1,945.4	-2,884.3	-2,289.8
21	2,100,000	-2,359.0	-4,172.7	-2,298.7
22	2,200,000	-3,228.8		-2,670.3
23	2,300,000	-4,821.7		

Table - 29 Maximum Pile von Mises Stresses due to Various Vertical Loads

No	Vertical Load (lbs)	Maximum Pile von Mises Stress (psf)		
		Circle	Triangle	Y-shape
1	100,000	7,696.7	11,454.9	4,683.1
2	200,000	15,588.7	17,510.8	7,446.1
3	300,000	25,398.4	22,371.9	9,538.8
4	400,000	35,214.7	30,278.8	12,630.5
5	500,000	44,974.4	38,279.9	15,688.0
6	600,000	54,697.6	46,318.8	18,790.3
7	700,000	64,377.6	54,293.8	22,022.5
8	800,000	73,976.4	62,322.4	25,326.0
9	900,000	83,551.8	70,370.3	28,510.7
10	1,000,000	93,464.6	78,421.2	31,676.1
11	1,100,000	103,439.0	86,510.0	34,849.0
12	1,200,000	113,434.9	94,605.1	38,040.9
13	1,300,000	123,450.7	102,689.5	41,261.8
14	1,400,000	133,459.3	110,797.2	44,427.0
15	1,500,000	143,517.2	118,929.4	47,628.3
16	1,600,000	153,663.2	127,030.3	50,901.2
17	1,700,000	163,734.9	135,186.8	54,124.2
18	1,800,000	173,798.4	143,393.3	57,127.2
19	1,900,000	183,918.2	151,693.5	60,130.7
20	2,000,000	194,464.3	160,579.9	63,272.3
21	2,100,000	205,295.6	169,020.2	66,883.7
22	2,200,000	215,864.0		70,519.8
23	2,300,000	225,960.7		

Table - 30 Maximum Displacements due to Various 45-Degree Inclined Loads

No	45-Deg. I. Load (lbs)	Max. Total Displacement (ft)			Max. Hor. Displacement(ft)		
		Circle	Triangle	Y-shape	Circle	Triangl	Y-shape
1	100,000	0.0277	0.0326	0.0282	0.0253	0.0280	0.0254
2	200,000	0.0568	0.0672	0.0584	0.0516	0.0569	0.0522
3	300,000	0.0906	0.1069	0.0930	0.0806	0.0878	0.0814
4	400,000	0.1292	0.1507	0.1328	0.1121	0.1227	0.1136
5	500,000	0.1728	0.2004	0.1790	0.1467	0.1624	0.1498
6	600,000	0.2224	0.2571	0.2294	0.1855	0.2081	0.1892
7	700,000	0.2794	0.3229	0.2861	0.2295	0.2584	0.2337
8	800,000	0.3439	0.3986	0.3532	0.2789	0.3166	0.2861
9	900,000	0.4186	0.4835	0.4293	0.3360	0.3816	0.3458
10	1,000,000	0.5015	0.5874	0.5117	0.3992	0.4512	0.4103
11	1,100,000	0.5961	0.7152	0.6041	0.4705	0.5296	0.4830
12	1,200,000	0.7225	0.8807	0.7087	0.5639	0.6331	0.5655
13	1,300,000	0.8850	1.1003	0.8478	0.6831	0.7878	0.6734
14	1,400,000	1.0931	1.3830	1.0407	0.8340	0.9917	0.8210
15	1,500,000	1.3812	1.8299	1.3417	1.0414	1.3450	1.0469
16	1,600,000	1.8603	2.7163	1.8149	1.3842	1.9585	1.3962
17	1,700,000	2.6802	4.6112	2.6987	1.9641	3.4410	2.0390
18	1,800,000	4.4695	14.4655	4.3947	3.2247	12.2746	3.2825
19	1,900,000	11.0873		12.8929	7.9236		9.2997

Table - 31 Minimum Soil Minor Principal Stresses due to Various 45-Degree inclined Loads

No	45-Deg. Inclined Load (lbs)	Minimum Soil Minor Principal Stress (psf)		
		Circle	Triangle	Y-shape
1	100,000	-1,216.8	-1,219.7	-1,235.0
2	200,000	-1,282.9	-1,278.9	-1,313.8
3	300,000	-1,360.9	-1,350.0	-1,392.4
4	400,000	-1,487.0	-1,432.3	-1,467.2
5	500,000	-1,667.4	-1,523.2	-1,573.5
6	600,000	-1,864.0	-1,635.7	-1,702.6
7	700,000	-2,025.9	-1,759.9	-1,848.3
8	800,000	-2,241.6	-1,882.7	-2,015.0
9	900,000	-2,417.0	-1,968.2	-2,177.2
10	1,000,000	-2,627.1	-2,039.4	-2,308.6
11	1,100,000	-2,853.5	-2,178.3	-2,426.0
12	1,200,000	-3,047.5	-2,261.9	-2,522.0
13	1,300,000	-3,185.3	-2,361.3	-2,562.3
14	1,400,000	-3,317.2	-2,662.4	-2,464.7
15	1,500,000	-3,478.9	-3,258.7	-2,545.7
16	1,600,000	-3,618.8	-3,979.0	-2,510.4
17	1,700,000	-3,504.0	-5,107.2	-2,331.8
18	1,800,000	-4,131.7	-6,356.3	-2,706.7
19	1,900,000	-5,246.5		-3,393.5

Table - 32 Maximum Pile von Mises Stresses due to Various 45-Degree Inclined Loads

No	45-Deg. Inclined Load (lbs)	Maximum Pile von Mises Stress (psf)		
		Circle	Triangle	Y-shape
1	100,000	5,885.4	8,573.9	7,223.4
2	200,000	11,821.4	15,608.8	12,789.5
3	300,000	18,385.2	17,926.8	14,965.1
4	400,000	25,626.4	23,713.2	16,509.3
5	500,000	32,827.7	29,853.7	18,310.6
6	600,000	39,996.3	36,044.7	20,834.3
7	700,000	47,132.2	42,204.6	24,043.4
8	800,000	54,228.4	48,338.6	27,335.5
9	900,000	61,288.2	54,743.0	30,611.6
10	1,000,000	68,684.8	61,162.8	33,868.0
11	1,100,000	76,390.9	67,672.2	37,077.5
12	1,200,000	84,152.7	74,279.1	40,325.3
13	1,300,000	91,946.0	80,955.9	43,652.9
14	1,400,000	99,660.6	87,664.9	46,809.7
15	1,500,000	107,622.6	94,237.5	50,334.2
16	1,600,000	115,691.4	100,931.7	53,511.9
17	1,700,000	123,825.0	107,854.6	56,555.7
18	1,800,000	131,880.1	114,087.6	59,849.0
19	1,900,000	139,062.4		63,041.7

Table - 33 Load Comparison at Horizontal Displacement of 1.5 ft

Horizontal Load (lbs)			45-Degree Inclined Load (lbs)		
Circle	Triangle	Y-shape	Circle	Triangle	Y-shape
1,471,400	1,408,250	1,484,100	1,619,970	1,525,265	1,616,148

Table - 34 Maximum Total Displacements at Various Horizontal Loads

No.	Horizontal Load (lbs)	Maximum Total Displacement (ft)			
		Flange Width = 0 ft	5 ft	10 ft	15 ft
1	500,000	0.0166	0.0102	0.0086	0.0072
2	1,000,000	0.0232	0.0204	0.0183	0.0143
3	1,500,000	0.0355	0.0310	0.0258	0.0215
4	2,000,000	0.0491	0.0421	0.0345	0.0286
5	2,500,000	0.0641	0.0547	0.0446	0.0363
6	3,000,000	0.0831	0.0688	0.0554	0.0447
7	3,500,000	0.1045	0.0847	0.0671	0.0535
8	4,000,000	0.1304	0.1025	0.0796	0.0629
9	4,500,000	0.1621	0.1229	0.0934	0.0729
10	5,000,000	0.2009	0.1469	0.1086	0.0834
11	5,500,000	0.2469	0.1749	0.1255	0.0946
12	6,000,000	0.3022	0.2090	0.1447	0.1068
13	6,500,000	0.3677	0.2485	0.1667	0.1199
14	7,000,000	0.4453	0.2935	0.1919	0.1343
15	7,500,000	0.6408	0.3456	0.2217	0.1505
16	8,000,000		0.4058	0.2555	0.1684
17	8,500,000		0.4779	0.2935	0.1883
18	9,000,000		0.5605	0.3373	0.2110
19	9,500,000		0.6561	0.3835	0.2366
20	10,000,000			0.4380	0.2654
21	10,500,000			0.5008	0.2970
22	11,000,000			0.5731	0.3317
23	11,500,000			0.6568	0.3698
24	12,000,000			0.7519	0.4115

Table - 35 Maximum Horizontal Displacements at Various Horizontal Loads

No.	Horizontal Load (lbs)	Maximum Horizontal Displacement (ft)			
		Flange Width = 0 ft	5 ft	10 ft	15 ft
1	500,000	0.0117	0.0095	0.0080	0.0068
2	1,000,000	0.0233	0.0190	0.0160	0.0136
3	1,500,000	0.0350	0.0286	0.0240	0.0204
4	2,000,000	0.0466	0.0392	0.0322	0.0272
5	2,500,000	0.0609	0.0506	0.0414	0.0343
6	3,000,000	0.0777	0.0631	0.0509	0.0420
7	3,500,000	0.0968	0.0769	0.0611	0.0499
8	4,000,000	0.1194	0.0923	0.0719	0.0582
9	4,500,000	0.1465	0.1095	0.0836	0.0669
10	5,000,000	0.1791	0.1292	0.0964	0.0760
11	5,500,000	0.2172	0.1519	0.1104	0.0856
12	6,000,000	0.2625	0.1787	0.1259	0.0959
13	6,500,000	0.3152	0.2092	0.1432	0.1068
14	7,000,000	0.3769	0.2434	0.1627	0.1187
15	7,500,000	0.4486	0.2834	0.1851	0.1318
16	8,000,000	0.5298	0.3266	0.2101	0.1460
17	8,500,000		0.3266	0.2376	0.1615
18	9,000,000		0.3786	0.2676	0.1789
19	9,500,000		0.4373	0.3009	0.1980
20	10,000,000		0.5044	0.3381	0.2190
21	10,500,000			0.3802	0.2415
22	11,000,000			0.4278	0.2660
23	11,500,000			0.4818	0.2922
24	12,000,000			0.5423	0.3206

Table - 36 Minimum Soil Minor Principal Stresses at Various Horizontal Loads

No.	Horizontal Load (lbs)	Minimum Soil Minor Principal Stress (psf)			
		Flange Width	5 ft	10 ft	15 ft
1	Geostatic	-2,499.0	-2,499.0	-2,499.0	-2,499.0
2	500,000	-2,559.1	-2,548.7	-2,540.3	-2,533.4
3	1,000,000	-2,619.1	-2,598.7	-2,581.8	-2,567.9
4	1,500,000	-2,679.2	-2,648.9	-2,623.5	-2,602.5
5	2,000,000	-2,739.2	-2,700.1	-2,665.4	-2,637.2
6	2,500,000	-2,803.3	-2,752.1	-2,707.8	-2,672.6
7	3,000,000	-2,918.3	-2,805.0	-2,750.6	-2,709.0
8	3,500,000	-3,604.5	-2,936.6	-2,793.7	-2,746.0
9	4,000,000	-4,454.5	-3,484.7	-2,837.6	-2,783.8
10	4,500,000	-5,446.1	-4,110.6	-3,132.0	-2,822.2
11	5,000,000	-6,457.9	-4,827.1	-3,585.6	-2,861.6
12	5,500,000	-7,550.5	-5,649.4	-4,084.6	-3,058.3
13	6,000,000	-8,756.1	-6,493.8	-4,645.8	-3,411.8
14	6,500,000	-10,054.4	-7,373.2	-5,267.6	-3,789.7
15	7,000,000	-11,476.3	-8,312.4	-5,957.4	-4,198.3
16	7,500,000	-13,016.6	-9,309.2	-6,644.3	-4,652.4
17	8,000,000	-14,659.0	-10,356.7	-7,365.6	-5,147.8
18	8,500,000		-11,502.7	-8,126.1	-5,694.7
19	9,000,000		-12,736.8	-8,915.0	-6,280.8
20	9,500,000		-14,056.2	-9,743.5	-6,853.2
21	10,000,000			-10,614.3	-7,451.6
22	10,500,000			-11,534.6	-8,074.5
23	11,000,000			-12,515.0	-8,728.8
24	11,500,000			-13,573.1	-9,409.0
25	12,000,000			-14,696.0	-10,105.7

Table - 37 Maximum Pile Von Mises Stresses at Various Horizontal Loads

No.	Horizontal Load (lbs)	Maximum Pile Von Mises Stress (psf)			
		Flange Width = 0 ft	5 ft	10 ft	15 ft
1	500,000	16,125.2	15,187.3	15,315.5	15,597.7
2	1,000,000	32,250.3	30,374.9	30,631.1	31,195.4
3	1,500,000	48,375.5	45,554.4	45,946.6	46,793.0
4	2,000,000	64,500.6	60,832.9	60,979.4	62,390.7
5	2,500,000	80,945.5	76,265.4	73,231.0	77,687.5
6	3,000,000	97,281.8	91,618.2	92,442.2	93,523.4
7	3,500,000	113,666.6	106,947.1	108,484.1	109,548.6
8	4,000,000	130,351.3	122,398.0	124,725.3	125,751.6
9	4,500,000	147,096.9	137,936.5	141,132.1	142,155.7
10	5,000,000	163,949.0	153,569.4	157,703.0	158,713.0
11	5,500,000	180,929.6	169,229.1	174,465.2	175,478.3
12	6,000,000	197,963.0	184,940.3	191,371.7	192,378.1
13	6,500,000	215,001.3	200,715.4	208,445.9	209,421.8
14	7,000,000	232,039.6	216,477.8	225,707.6	226,622.8
15	7,500,000	249,077.9	232,225.1	243,114.4	243,945.9
16	8,000,000	266,035.5	247,894.3	260,693.0	261,413.2
17	8,500,000		272,931.7	278,459.2	279,074.0
18	9,000,000		290,038.1	296,340.1	296,950.0
19	9,500,000		307,494.6	314,364.5	314,877.3
20	10,000,000			332,583.1	333,116.2
21	10,500,000			350,877.6	351,543.2
22	11,000,000			369,290.0	378,163.1
23	11,500,000			388,110.0	406,204.4
24	12,000,000			407,308.9	434,788.1

Table - 38 Maximum Total Displacements at Various Horizontal Loads

No.	Horizontal Load (lbs)	Maximum Total Displacement (ft)			
		Flange Width = 0 ft	5 ft	10 ft	15 ft
1	300,000	0.1361	0.1169	0.0978	0.0801
2	600,000	0.3099	0.2545	0.2113	0.1668
3	900,000	0.5656	0.4374	0.356	0.2633
4	1,200,000	0.9795	0.6898	0.5461	0.3789
5	1,500,000	1.9402	1.0913	0.7971	0.5129
6	1,600,000	2.5966	*	*	*
7	1,700,000	4.0121	*	*	*
8	1,800,000	7.7404	1.9020	1.1950	0.6844
9	1,900,000	23.9522	*	*	*
10	2,100,000		4.6852	1.9199	0.9110
11	2,200,000		8.2147	*	*
12	2,300,000		21.4302	*	*
13	2,400,000			3.6999	1.2216
14	2,600,000			6.5729	*
15	2,700,000			10.5831	1.7313
16	2,800,000			16.4371	*
17	3,000,000				2.6843
18	3,300,000				5.2190
19	3,400,000				7.1210
20	3,500,000				10.9431
21	3,600,000				22.7240

Note that typical load increment was 300,000 lbs. Smaller increments were used when solutions varied much.

Table - 39 Maximum Horizontal Displacements at Various Horizontal Loads

No.	Horizontal Load (lbs)	Maximum Horizontal Displacement (ft)			
		Flange Width = 0 ft	5 ft	10 ft	15 ft
1	300,000	0.1327	0.1127	0.0949	0.0797
2	600,000	0.2977	0.2431	0.2034	0.1638
3	900,000	0.5325	0.4091	0.3356	0.2560
4	1,200,000	0.9035	0.6295	0.5012	0.3646
5	1,500,000	1.7352	0.9662	0.7092	0.4859
6	1,600,000	2.2908	*	*	*
7	1,700,000	3.4397	*	*	*
8	1,800,000	6.3109	1.6244	1.0242	0.6310
9	1,900,000	18.4483	*	*	*
10	2,100,000		3.8436	1.5915	0.8138
11	2,200,000		6.5812	*	*
12	2,300,000		16.6405	*	*
13	2,400,000			2.9435	1.0610
14	2,600,000			5.0397	*
15	2,700,000			7.8595	1.4436
16	2,800,000			11.9592	*
17	3,000,000				2.1366
18	3,300,000				3.8490
19	3,400,000				5.1006
20	3,500,000				7.5581
21	3,600,000				14.8775

Note that typical load increment was 300,000 lbs. Smaller increments were used when solutions varied much.

Table - 40 Minimum Soil Minor Principal Stresses at Various Horizontal Loads

No.	Horizontal Load (lbs)	Minimum Soil Minor Principal Stress (psf)			
		Flange Width = 0 ft	5 ft	10 ft	15 ft
1	Geostatic	-1,155.0	-1,155.0	-1,155.0	-1,155.0
2	300,000	-1,409.3	-1,273.2	-1,249.4	-1,236.4
3	600,000	-1,879.8	-1,732.2	-1,510.2	-1,394.7
4	900,000	-2,171.3	-2,137.3	-1,776.3	-1,747.5
5	1,200,000	-2,571.8	-2,630.3	-1,923.1	-2,086.4
6	1,500,000	-3,204.6	-3,742.0	-2,363.4	-2,408.6
7	1,600,000	-3,460.8	*	*	*
8	1,700,000	-4,007.0	*	*	*
9	1,800,000	-4,699.8	-5,898.7	-3,080.7	-2,657.2
10	1,900,000	-6,382.1	*	*	*
11	2,100,000		-8,561.7	-3,879.2	-2,877.1
12	2,200,000		-9,943.6	*	*
13	2,300,000		-12,088.0	*	*
14	2,400,000			-4,746.4	-3,320.6
15	2,600,000			-5,762.8	*
16	2,700,000			-6,365.8	-4,421.1
17	2,800,000			-7,126.3	*
18	3,000,000				-5,346.0
19	3,300,000				-6,738.8
20	3,400,000				-7,396.9
21	3,500,000				-8,138.3
22	3,600,000				-8,888.5

Note that typical load increment was 300,000 lbs. Smaller increments were used when solutions varied much.

Table - 41 Maximum Pile Von Mises Stresses at Various Horizontal Loads

No.	Horizontal Load (lbs)	Maximum Pile Von Mises Stress (psf)			
		Flange Width = 0 ft	5 ft	10 ft	15 ft
1	300,000	9,524.4	8,991.5	9,460.6	9,617.0
2	600,000	19,044.0	18,110.8	19,075.4	19,591.4
3	900,000	29,056.9	27,598.4	29,227.3	30,526.7
4	1,200,000	38,916.8	37,842.7	39,672.4	43,565.0
5	1,500,000	49,581.3	47,743.0	50,497.8	58,203.0
6	1,600,000	53,238.8	*	*	*
7	1,700,000	57,100.7	*	*	*
8	1,800,000	61,019.6	58,086.8	61,851.2	75,114.1
9	1,900,000	64,884.5	*	*	*
10	2,100,000		66,997.0	72,953.6	93,267.8
11	2,200,000		70,127.6	*	*
12	2,300,000		73,849.9	*	*
13	2,400,000			83,632.2	112,638.8
14	2,600,000			92,580.9	*
15	2,700,000			97,788.8	134,978.2
16	2,800,000			103,583.7	*
17	3,000,000				159,355.0
18	3,300,000				188,646.1
19	3,400,000				199,112.8
20	3,500,000				209,467.4
21	3,600,000				220,439.5

Note that typical load increment was 300,000 lbs. Smaller increments were used when solutions varied much.

Table - 42 Maximum Displacements at Various Horizontal Loads

No.	Horizontal Load (lbs)	Max. Total Displacement (ft)			Max. Hor. Displacement (ft)		
		Loaded at Top	Middle	Bottom	Top	Middle	Bottom
1	1,000,000	0.0232	0.0151	0.0187	0.0221	0.0150	0.0182
2	2,000,000	0.0484	0.0301	0.0374	0.0460	0.300	0.0364
3	3,000,000	0.0814	0.0452	0.0563	0.0762	0.0451	0.0547
4	4,000,000	0.1266	0.0626	0.0766	0.1163	0.0622	0.0744
5	5,000,000	0.1929	0.0834	0.1011	0.1729	0.0826	0.0983
6	6,000,000	0.2891	0.1100	0.1266	0.2525	0.1083	0.1230
7	7,000,000	0.4227	0.1417	0.1574	0.3604	0.1382	0.1528
8	8,000,000	0.6084	0.1787	0.1958	0.5066	0.1729	0.1897
9	9,000,000	0.8524	0.2226	0.2427	0.6956	0.2137	0.2342
10	10,000,000	1.0002	0.2736	0.2986	0.8091	0.2604	0.2868
11	11,000,000		0.3350	0.3650		0.3163	0.3486
12	12,000,000		0.4076	0.4428		0.3818	0.4205
13	13,000,000		0.4922	0.5331		0.4583	0.5031
14	14,000,000		0.5934	0.6386		0.5489	0.5990
15	15,000,000		0.7142	0.7605		0.6559	0.7086
16	16,000,000		0.8604	0.9015		0.7839	0.8347
17	17,000,000		1.0396	1.0632		0.9385	0.9781
18	18,000,000		1.2560	1.2479		1.1222	1.1483
19	19,000,000		1.5342	1.4592		1.3537	1.3312
20	20,000,000		1.8840	1.6987		1.6390	1.5427
21	21,000,000		2.2933	1.9806		1.9685	1.7899
22	22,000,000		2.7832	2.3091		2.3598	2.0762
23	23,000,000		3.3553	2.6821		2.8132	2.4098
24	24,000,000		4.0560	3.1332		3.3637	2.8123
25	25,000,000			3.6752			3.2862
26	26,000,000			4.3301			3.8620

Table - 43 Minimum Soil Minor Principal Stresses at Various Horizontal Loads

No.	Horizontal Load (lbs)	Minimum Soil Minor Principal Stress (psf)		
		Loaded at Top	Middle	Bottom
1	Geostatic	-2,499.0	-2,499.0	-2,499.0
2	1,000,000	-2,615.5	-2,577.0	-2,532.3
3	2,000,000	-2,735.2	-2,615.0	-2,569.5
4	3,000,000	-2,862.7	-2,675.0	-2,624.4
5	4,000,000	-4,208.8	-2,740.6	-3,065.3
6	5,000,000	-6,042.6	-2,812.0	-3,791.2
7	6,000,000	-8,408.9	-3,146.7	-4,557.9
8	7,000,000	-11,415.0	-4,014.0	-5,470.5
9	8,000,000	-15,015.8	-5,028.0	-6,676.1
10	9,000,000	-19,176.6	-6,123.7	-8,075.8
11	10,000,000	-21,429.3	-7,242.6	-9,494.0
12	11,000,000		-8,538.3	-10,999.1
13	12,000,000		-9,996.9	-12,633.4
14	13,000,000		-11,591.3	-14,384.8
15	14,000,000		-13,333.2	-16,216.9
16	15,000,000		-15,206.2	-18,676.2
17	16,000,000		-16,898.4	-21,435.8
18	17,000,000		-18,954.4	-24,376.1
19	18,000,000		-21,472.0	-27,367.2
20	19,000,000		-24,149.0	-30,482.6
21	20,000,000		-26,948.5	-33,636.5
22	21,000,000		-29,737.4	-36,780.8
23	22,000,000		-32,604.0	
24	23,000,000		-35,617.6	
25	24,000,000		-39,466.0	

Table - 44 Maximum Pile Von Mises Stresses at Various Horizontal Loads

No.	Horizontal Load (lbs)	Maximum Pile Von Mises Stress (psf)		
		Loaded at Top	Middle	Bottom
1	1,000,000	32,142.9	66,112.2	137,971.8
2	2,000,000	64,459.6	132,224.4	275,943.6
3	3,000,000	97,312.9	198,320.1	413,603.5
4	4,000,000	130,283.5	264,115.0	550,705.9
5	5,000,000	163,761.0	329,928.9	686,346.1
6	6,000,000	197,681.1	395,805.7	822,179.0
7	7,000,000	231,540.1	461,636.7	956,999.0
8	8,000,000	265,289.1	527,243.8	1,089,876.5
9	9,000,000	298,846.3	592,607.3	1,222,911.7
10	10,000,000	315,762.2	657,911.9	1,357,238.2
11	11,000,000		724,240.5	1,491,396.3
12	12,000,000		790,589.8	1,625,567.3
13	13,000,000		857,128.8	1,759,415.2
14	14,000,000		923,863.9	1,893,299.4
15	15,000,000		990,944.6	2,024,006.0
16	16,000,000		1,058,406.5	2,163,214.9
17	17,000,000		1,126,070.3	2,299,177.3
18	18,000,000		1,193,225.0	2,435,846.0
19	19,000,000		1,262,883.0	2,573,496.0
20	20,000,000		1,332,500.0	2,710,822.0
21	21,000,000		1,396,864.0	2,852,132.0
22	22,000,000		1,462,286.0	
23	23,000,000		1,526,982.0	
24	24,000,000		1,593,905.0	

Table - 45 Maximum Displacements due to Various 45-Degree Inclined Loads

No.	45-deg. I. Load (lbs)	Max. Total Displacement (ft)			Max. Hor. Displacement (ft)		
		Loaded at Top	Middle	Bottom	Top	Middle	Bottom
1	1,000,000	0.0200	0.0159	0.0219	0.0156	0.0118	0.0160
2	2,000,000	0.0417	0.0317	0.0440	0.0325	0.0236	0.0320
3	3,000,000	0.0707	0.0476	0.0679	0.0549	0.0354	0.0487
4	4,000,000	0.1193	0.0639	0.1027	0.0905	0.0474	0.0711
5	5,000,000	0.1967	0.0821	0.1592	0.1442	0.0605	0.1052
6	6,000,000	0.3479	0.1067	0.2530	0.2441	0.0774	0.1620
7	7,000,000	0.5586	0.1478	0.3884	0.3782	0.1032	0.2417
8	8,000,000	0.8785	0.2145	0.5931	0.5772	0.1448	0.3628
9	9,000,000	1.3250	0.3103	0.8887	0.8522	0.2030	0.5438
10	10,000,000	1.9439	0.4506	1.3195	1.2301	0.2839	0.8023
11	11,000,000	2.8272	0.6591	1.9149	1.7644	0.3929	1.1579
12	12,000,000		0.9795	2.8387		0.5437	1.6868
13	13,000,000		1.4559	4.5235		0.7563	2.4933
14	14,000,000		2.1698	8.4657		1.0514	3.7644
15	15,000,000		3.2260			1.4464	
16	16,000,000		4.8935			1.9860	
17	17,000,000		7.2910			2.8085	
18	18,000,000		10.6439			4.0430	

Table - 46 Minimum Soil Minor Principal Stresses due to Various 45-Degree inclined Loads

No.	45-deg. I. Load (lbs)	Minimum Soil Minor Principal Stress (psf)		
		Loaded at Top	Middle	Bottom
1	Geostatic	-2,499.0	-2,499.0	-2,499.0
2	1,000,000	-2,509.5	-2,501.8	-2,504.8
3	2,000,000	-2,521.9	-2,504.6	-2,510.9
4	3,000,000	-2,541.4	-2,507.3	-2,980.9
5	4,000,000	-2,879.3	-2,704.7	-4,058.4
6	5,000,000	-4,679.1	-3,282.0	-5,695.8
7	6,000,000	-7,028.3	-4,205.5	-8,146.0
8	7,000,000	-9,700.0	-5,518.5	-11,137.8
9	8,000,000	-12,685.0	-7,380.0	-14,905.2
10	9,000,000	-16,072.0	-9,692.7	-18,808.6
11	10,000,000	-20,144.0	-12,633.5	-22,824.7
12	11,000,000	-25,174.0	-16,306.4	
13	12,000,000		-20,831.1	
14	13,000,000		-25,506.6	
15	14,000,000		-29,755.1	
16	15,000,000		-34,246.3	

Table - 47 Maximum Pile von Mises Stresses due to Various 45-Degree inclined Loads

No.	45-deg. I. Load (lbs)	Maximum Pile von Mises Stress (psf)		
		Loaded at Top	Middle	Bottom
1	1,000,000	76,044.4	49,202.6	119,326.8
2	2,000,000	151,382.5	98,405.2	238,587.1
3	3,000,000	225,909.1	147,607.8	359,720.7
4	4,000,000	301,530.6	197,441.3	482,012.7
5	5,000,000	375,985.2	247,643.5	604,256.0
6	6,000,000	449,263.1	299,104.7	719,754.5
7	7,000,000	516,225.0	352,361.0	826,923.8
8	8,000,000	583,190.2	403,324.1	934,098.6
9	9,000,000	651,755.0	455,193.8	1,037,339.0
10	10,000,000	723,882.0	506,258.1	1,141,569.0
11	11,000,000	796,846.0	557,452.4	
12	12,000,000		610,212.7	
13	13,000,000		666,317.8	
14	14,000,000		725,899.0	
15	15,000,000		785,469.4	

Table - 48 Maximum Displacements at Various Horizontal Loads

No.	Horizontal Load (lbs)	Max. Total Displacement (ft)			Max. Hor. Displacement (ft)		
		Loaded at Top	Middle	Bottom	Top	Middle	Bottom
1	300,000	0.1183	0.0969	0.1084	0.1146	0.0969	0.1084
2	600,000	0.2774	0.2002	0.2236	0.2654	0.2002	0.2236
3	900,000	0.5204	0.3088	0.3476	0.4888	0.3088	0.3475
4	1,200,000	0.8919	0.4267	0.4817	0.8221	0.4267	0.4811
5	1,500,000	1.7578	0.5693	0.6330	1.5991	0.5685	0.6314
6	1,800,000	6.0573	0.7467	0.8076	5.1410	0.7418	0.8046
7	2,100,000		0.9833	1.0508		0.9696	1.0458
8	2,400,000		1.3354	1.4213		1.3045	1.4041
9	2,700,000		1.9249	2.0411		1.8265	1.9826
10	3,000,000		3.1015	3.3649		2.7726	3.1861
11	3,300,000		5.9877			5.0619	

Table - 49 Minimum Soil Minor Principal Stresses at Various Horizontal Loads

No.	Horizontal Load (lbs)	Minimum Soil Minor Principal Stress (psf)		
		Loaded at Top	Middle	Bottom
1	Geostatic	-1,155.0	-1,155.0	-1,155.0
2	300,000	-1,588.3	-1,251.9	-1,616.0
3	600,000	-2,350.5	-1,646.0	-2,437.9
4	900,000	-2,553.8	-2,003.2	-3,133.1
5	1,200,000	-2,908.0	-2,358.4	-3,773.4
6	1,500,000	-3,593.0	-2,733.2	-4,453.5
7	1,800,000	-4,946.3	-3,052.3	-5,232.5
8	2,100,000		-3,404.2	-6,075.5
9	2,400,000		-3,808.2	-6,773.2
10	2,700,000		-4,139.2	-7,674.2
11	3,000,000		-4,602.0	-9,036.0
12	3,300,000		-5,495.4	

Table - 50 Maximum Pile Von Mises Stresses at Various Horizontal Loads

No.	Horizontal Load (lbs)	Maximum Pile Von Mises Stress (psf)		
		Loaded at Top	Middle	Bottom
1	300,000	9,736.1	19,777.0	43,351.9
2	600,000	19,325.0	39,605.2	86,871.0
3	900,000	29,089.9	59,562.6	13,066.3
4	1,200,000	38,945.9	79,440.8	174,318.9
5	1,500,000	49,699.9	99,326.7	217,416.7
6	1,800,000	61,025.6	119,425.6	260,463.4
7	2,100,000		139,271.0	302,380.1
8	2,400,000		158,586.3	343,479.9
9	2,700,000		177,832.8	386,711.7
10	3,000,000		197,246.0	433,903.9
11	3,300,000		217,327.5	

Table - 51 Maximum Displacements due to Various 45-Degree Inclined Loads

No.	45-deg. I. Load (lbs)	Max. Total Displacement (ft)			Max. Hor. Displacement (ft)		
		Loaded at Top	Middle	Bottom	Top	Middle	Bottom
1	300,000	0.0906	0.0824	0.1073	0.0806	0.0751	0.0931
2	600,000	0.2224	0.1812	0.2463	0.1855	0.1548	0.1941
3	900,000	0.4186	0.2925	0.4169	0.3360	0.2402	0.3108
4	1,200,000	0.7225	0.4158	0.6499	0.5639	0.3313	0.4538
5	1,500,000	1.3812	0.5572	1.0324	1.0414	0.4311	0.6692
6	1,700,000	2.6802	*	*	1.9641	*	*
7	1,800,000	4.4695	0.7330	2.3959	3.2247	0.5475	1.3298
8	1,950,000		*	4.8597		*	2.3957
9	2,100,000		1.0205			0.7185	
10	2,400,000		1.7780			1.1084	
11	2,700,000		5.8634			2.7970	

Note that typical load increment was 300,000 lbs. Smaller increments were used when solutions varied much.

Table - 52 Minimum Soil Minor Principal Stresses due to Various 45-Degree inclined Loads

No.	Horizontal Load (lbs)	Minimum Soil Minor Principal Stress (psf)		
		Loaded at Top	Middle	Bottom
1	Geostatic	-1,155.0	1155.0	1155.0
2	300,000	-1,360.9	1564.8	1883.3
3	600,000	-1,864.0	2462.6	2760.6
4	900,000	-2,417.0	2986.8	3573.8
5	1,200,000	-3,047.5	3615.5	4055.1
6	1,500,000	-3,478.9	4235.0	4152.0
7	1,700,000	-3,504.0	*	*
8	1,800,000	-4,131.7	4645.3	5970.3
9	1,950,000		*	7542.5
10	2,100,000		4786.2	
11	2,400,000		5580.9	
12	2,700,000		8172.7	

Note that typical load increment was 300,000 lbs. Smaller increments were used when solutions varied much.

Table - 53 Maximum Pile von Mises Stresses due to Various 45-Degree inclined Loads

No.	Horizontal Load (lbs)	Maximum Pile Von Mises Stress (psf)		
		Loaded at Top	Middle	Bottom
1	300,000	18,385.2	17,787.1	34,375.3
2	600,000	39,996.3	32,901.3	70,440.7
3	900,000	61,288.2	48,849.6	107,476.4
4	1,200,000	84,152.7	64,947.4	144,095.4
5	1,500,000	107,622.6	80,824.8	179,757.7
6	1,700,000	123,825.0	*	*
7	1,800,000	131,880.1	96,458.2	217,546.2
8	1,950,000		*	235,854.1
9	2,100,000		113,489.2	
10	2,400,000		130,486.2	
11	2,700,000		148,391.8	

Note that typical load increment was 300,000 lbs. Smaller increments were used when solutions varied much.

Table - 54 Maximum Displacements at Various Horizontal Loads

No.	Horizontal Load (lbs)	Max. T. Displacement (ft)		Max. Hor. Displacement (ft)	
		Diameter: Prismatic	Telescopic	Prismatic	Telescopic
1	5000,000	0.0116	0.0113	0.0111	0.0107
2	1,000,000	0.0232	0.0225	0.0221	0.0213
3	1,500,000	0.0350	0.0342	0.0334	0.0323
4	2,000,000	0.0484	0.0469	0.0460	0.0442
5	2,500,000	0.0636	0.0618	0.0600	0.0577
6	3,000,000	0.0814	0.0792	0.0762	0.0733
7	3,500,000	0.1021	0.1005	0.0947	0.0917
8	4,000,000	0.1266	0.1268	0.1163	0.1139
9	4,500,000	0.1564	0.1594	0.1420	0.1408
10	5,000,000	0.1929	0.1996	0.1729	0.1732
11	5,500,000	0.2368	0.2477	0.2095	0.2115
12	6,000,000	0.2891	0.3078	0.2525	0.2580
13	6,500,000	0.3506	0.3809	0.3062	0.3136
14	7,000,000	0.4227	0.4711	0.3604	0.3807
15	7,500,000	0.5087	0.5776	0.4284	0.4582
16	8,000,000	0.6084	0.7038	0.5066	0.5495
17	8,500,000	0.7226	0.8521	0.5964	0.6546
18	9,000,000	0.8524	1.0264	0.6956	0.7761
19	9,500,000	1.0002	1.2282	0.8091	0.9149
20	10,000,000		1.4600		1.0725
21	10,500,000		1.7234		1.2497
22	11,000,000		2.0269		1.4524
23	11,500,000		2.3750		1.6830
24	12,000,000		2.7696		1.9426

Table - 55 Minimum Soil Minor Principal Stresses at Various Horizontal Loads

No.	Horizontal Load (lbs)	Minimum Soil Minor Principal Stress (psf)	
		Diameter:	Telescopic
1	Geostatic	-2,499.0	-2,677.5
2	5000,000	-2,557.1	-2,723.0
3	1,000,000	-2,615.5	-2,768.6
4	1,500,000	-2,674.4	-2,814.4
5	2,000,000	-2,735.2	-2,861.4
6	2,500,000	-2,798.1	-2,909.6
7	3,000,000	-2,862.7	-3,200.7
8	3,500,000	-3,444.9	-4,046.6
9	4,000,000	-4,208.8	-5,053.4
10	4,500,000	-5,117.9	-6,050.8
11	5,000,000	-6,042.6	-7,238.6
12	5,500,000	-7,130.5	-8,542.0
13	6,000,000	-5,408.9	-10,077.9
14	6,500,000	-9,845.9	-11,817.6
15	7,000,000	-11,415.0	-13,802.3
16	7,500,000	-13,132.0	-15,995.5
17	8,000,000	-15,015.8	-18,438.1
18	8,500,000	-17,049.1	-21,118.0
19	9,000,000	-19,176.6	-24,050.5
20	9,500,000	-21,429.3	-27,264.2
21	10,000,000		-30,764.1
22	10,500,000		-34,525.3
23	11,000,000		-38,560.3
24	11,500,000		-42,726.2
25	12,000,000		-47,067.2

Table - 56 Maximum Pile Von Mises Stresses at Various Horizontal Loads

No.	Horizontal Load (lbs)	Maximum Pile Von Mises Stress (psf)	
		Diameter: Prismatic	Telescopic
1	5000,000	16,071.5	15,742.9
2	1,000,000	32,142.9	31,485.9
3	1,500,000	48,192.9	47,347.5
4	2,000,000	64,459.6	63,371.2
5	2,500,000	80,946.8	79,464.8
6	3,000,000	97,312.9	95,634.6
7	3,500,000	113,685.9	111,920.9
8	4,000,000	130,283.5	128,241.5
9	4,500,000	146,984.5	144,625.1
10	5,000,000	163,761.0	160,994.2
11	5,500,000	180,684.9	177,220.7
12	6,000,000	197,681.1	193,396.8
13	6,500,000	214,625.9	209,500.0
14	7,000,000	231,540.1	225,765.3
15	7,500,000	248,421.0	241,940.2
16	8,000,000	265,289.1	258,023.1
17	8,500,000	282,014.9	274,063.0
18	9,000,000	298,846.3	289,897.5
19	9,500,000	315,762.2	306,319.3
20	10,000,000		321,915.1
21	10,500,000		337,653.1
22	11,000,000		353,941.1
23	11,500,000		370,832.6
24	12,000,000		387,853.3

Table - 57 Maximum Displacements at Various Horizontal Loads

No.	Horizontal Load (lbs)	Max. T. Displacement (ft)		Max. Hor. Displacement (ft)	
		Diameter: Prismatic	Telescopic	Prismatic	Telescopic
1	100,000	0.0370	0.0345	0.0360	0.0329
2	200,000	0.0761	0.0721	0.0738	0.0684
3	300,000	0.1183	0.1135	0.1146	0.1074
4	400,000	0.1649	0.1592	0.1592	0.1501
5	500,000	0.2172	0.2094	0.2088	0.1965
6	600,000	0.2774	0.2657	0.2654	0.2477
7	700,000	0.3476	0.3323	0.3308	0.3075
8	800,000	0.4285	0.4064	0.4052	0.3734
9	900,000	0.5204	0.4940	0.4888	0.4506
10	1,000,000	0.6242	0.5941	0.5823	0.5383
11	1,100,000	0.7463	0.7145	0.6921	0.6421
12	1,200,000	0.8919	0.8822	0.8221	0.7858
13	1,300,000	1.1105	1.0976	1.0135	0.9669
14	1,400,000	1.3836	1.3813	1.2526	1.2018
15	1,500,000	1.7578	1.8290	1.5991	1.5559
16	1,600,000	2.3235	2.7894	2.1174	2.1706
17	1,700,000	3.4062	5.1834	3.0356	3.6448

Table - 58 Minimum Soil Minor Principal Stresses at Various Horizontal Loads

No.	Horizontal Load (lbs)	Minimum Soil Minor Principal Stress (psf)	
		Diameter: Prismatic	Telescopic
1	Geostatic	-1,155.0	-1,237.5
2	100,000	-1,255.3	-1,343.4
3	200,000	-1,363.3	-1,461.8
4	300,000	-1,588.3	-1,589.3
5	400,000	-1,872.3	-1,728.6
6	500,000	-2,127.0	-1,874.6
7	600,000	-2,350.5	-2,061.4
8	700,000	-2,398.0	-2,285.7
9	800,000	-2,456.6	-2,546.3
10	900,000	-2,553.8	-2,807.7
11	1,000,000	-2,665.9	-3,081.4
12	1,100,000	-2,798.0	-3,401.3
13	1,200,000	-2,908.0	-3,582.7
14	1,300,000	-3,144.8	-4,240.2
15	1,400,000	-3,371.5	-4,946.3
16	1,500,000	-3,593.0	-6,354.3
17	1,600,000	-3,822.7	-7,894.8
18	1,700,000	-4,072.4	-9,720.0

Table - 59 Maximum Pile Von Mises Stresses at Various Horizontal Loads

No.	Horizontal Load (lbs)	Maximum Pile Von Mises Stress (psf)	
		Diameter: Prismatic	Telescopic
1	100,000	3,243.9	3,162.4
2	200,000	6,481.3	6,315.8
3	300,000	9,736.1	9,452.6
4	400,000	12,975.1	12,591.3
5	500,000	16,139.1	15,745.5
6	600,000	19,325.0	18,899.5
7	700,000	22,528.6	22,088.5
8	800,000	25,768.3	25,274.6
9	900,000	29,089.9	28,428.9
10	1,000,000	32,356.0	31,556.3
11	1,100,000	35,635.1	34,676.3
12	1,200,000	38,945.9	38,036.7
13	1,300,000	42,247.5	41,488.8
14	1,400,000	45,911.9	44,726.5
15	1,500,000	49,699.9	47,876.1
16	1,600,000	53,355.7	51,003.8
17	1,700,000	57,148.6	54,118.2

Table - 60 Maximum Total Displacements at Various Horizontal Loads

No.	Horizontal Load (lbs)	Maximum Total Displacement (ft)			
		Lay. Soil-1	Lay. Soil-2	Lay. Soil-3	Lay. Soil-4
1	500,000	0.2172	0.0398	0.0257	0.0198
2	1,000,000	0.6242	0.0867	0.0530	0.0400
3	1,500,000	1.7578	0.1515	0.0876	0.0633
4	1,600,000	2.3235	*	*	*
5	1,700,000	3.4062	*	*	*
6	2,000,000		0.2444	0.1308	0.0920
7	2,500,000		0.3816	0.1854	0.1277
8	3,000,000		0.5809	0.2588	0.1703
9	3,500,000		0.8567	0.3566	0.2268
10	4,000,000		1.2327	0.4813	0.2965
11	4,500,000		1.7534	0.6367	0.3829
12	5,000,000		2.5740	0.8331	0.4902
13	5,500,000		4.0591	1.0708	0.6195
14	6,000,000			1.3571	0.7707
15	6,500,000			1.6994	0.9548
16	7,000,000			2.1274	1.1624
17	7,500,000			2.6604	1.4078
18	8,000,000			3.3452	1.6869
19	8,500,000			4.2466	2.0085
20	9,000,000				2.3981
21	10,000,000				3.3217
22	11,000,000				4.6141

Note that typical load increment was 500,000 lbs. Smaller increments were used when solutions varied much.

Table - 61 Maximum Horizontal Displacements at Various Horizontal Loads

No.	Horizontal Load (lbs)	Maximum Horizontal Displacement (ft)			
		Lay. Soil-1	Lay. Soil-2	Lay. Soil-3	Lay. Soil-4
1	500,000	0.2088	0.0375	0.0238	0.0185
2	1,000,000	0.5823	0.0802	0.0488	0.0372
3	1,500,000	1.5991	0.1374	0.0789	0.0582
4	1,600,000	2.1174	*	*	*
5	1,700,000	3.0356	*	*	*
6	2,000,000		0.2178	0.1151	0.0831
7	2,500,000		0.3357	0.1592	0.1132
8	3,000,000		0.5060	0.2179	0.1482
9	3,500,000		0.7377	0.2959	0.1930
10	4,000,000		1.0466	0.3955	0.2476
11	4,500,000		1.4645	0.5191	0.3148
12	5,000,000		2.1025	0.6740	0.3981
13	5,500,000		3.2209	0.8593	0.4988
14	6,000,000			1.0808	0.6161
15	6,500,000			1.3423	0.7576
16	7,000,000			1.6635	0.9160
17	7,500,000			2.0578	1.1018
18	8,000,000			2.5560	1.3116
19	8,500,000			3.2008	1.5503
20	9,000,000				1.8291
21	10,000,000				2.5084
22	11,000,000				3.4308

Note that typical load increment was 500,000 lbs. Smaller increments were used when solutions varied much.

Table - 62 Minimum Soil Minor Principal Stresses at Various Horizontal Loads

No.	Horizontal Load (lbs)	Minimum Soil Minor Principal Stress (psf)			
		Lay. Soil-1	Lay. Soil-2	Lay. Soil-3	Lay. Soil-4
1	Geostatic	-1,155.0	-1,429.5	-1,621.5	-1,813.5
2	500,000	-2,127.0	-1,551.7	-1,705.3	-1,877.7
3	1,000,000	-2,665.9	-1,933.3	-1,795.1	-1,943.7
4	1,500,000	-3,593.0	*	*	*
5	1,600,000	-3,822.7	*	*	*
6	1,700,000	-4,072.4	-3,521.3	-2,491.0	-2,020.0
7	2,000,000		-5,747.2	-3,715.3	-2,874.5
8	2,500,000		-8,368.5	-5,288.4	-3,396.3
9	3,000,000		-11,362.6	-7,186.0	-5,344.3
10	3,500,000		-14,842.0	-9,418.2	-6,925.8
11	4,000,000		-18,736.5	-11,978.5	-8,600.1
12	4,500,000		-23,079.4	-14,881.5	-10,551.2
13	5,000,000		-28,922.0	-18,132.6	-12,847.2
14	5,500,000		-37,317.9	-21,605.4	-15,430.3
15	6,000,000			-25,308.6	-18,210.4
16	6,500,000			-29,025.1	-21,180.0
17	7,000,000			-33,126.9	-24,217.0
18	7,500,000			-38,605.9	-27,398.5
19	8,000,000			-44,694.1	-30,586.0
20	8,500,000			-52,513.1	-34,288.4
21	9,000,000				-38,380.0
22	10,000,000				-47,225.0
23	11,000,000				-57,516.7

Note that typical load increment was 500,000 lbs. Smaller increments were used when solutions varied much.

Table - 63 Maximum Pile Von Mises Stresses at Various Horizontal Loads

No.	Horizontal Load (lbs)	Maximum Pile Von Mises Stress (psf)			
		Lay. Soil-1	Lay. Soil-2	Lay. Soil-3	Lay. Soil-4
1	500,000	16,139.1	15,522.7	15,706.8	15,815.0
2	1,000,000	32,356.0	31,110.5	31,461.3	31,621.5
3	1,500,000	49,699.9	47,166.2	47,536.4	47,678.0
4	1,600,000	53,355.7	*	*	*
5	1,700,000	57,148.6	*	*	*
6	2,000,000		63,538.2	63,767.0	63,918.5
7	2,500,000		79,674.1	80,143.4	80,343.1
8	3,000,000		95,747.8	96,640.1	96,714.8
9	3,500,000		111,838.4	113,160.9	113,198.0
10	4,000,000		127,742.9	129,547.3	129,601.2
11	4,500,000		143,720.8	145,877.1	145,870.7
12	5,000,000		159,608.8	162,076.9	162,419.8
13	5,500,000		175,210.3	178,171.1	179,131.3
14	6,000,000			194,133.7	195,464.7
15	6,500,000			210,070.9	211,932.8
16	7,000,000			225,531.3	227,591.9
17	7,500,000			242,289.8	243,902.3
18	8,000,000			258,299.0	260,232.6
19	8,500,000			274,249.0	276,259.2
20	9,000,000				292,376.5
21	10,000,000				324,782.3
22	11,000,000				357,429.3

Note that typical load increment was 500,000 lbs. Smaller increments were used when solutions varied much.

Table - 64 Maximum Total Displacements at Various Horizontal Loads

No.	Horizontal Load (lbs)	Maximum Total Displacement (ft)			
		Lay. Soil-5	Lay. Soil-6	Lay. Soil-7	Lay. Soil-8
1	500,000	0.0116	0.0208	0.0250	0.0393
2	1,000,000	0.0232	0.0370	0.0514	0.0850
3	1,500,000	0.0350	0.0551	0.0839	0.1593
4	2,000,000	0.0484	0.0765	0.1314	0.2946
5	2,500,000	0.0636	0.1032	0.2056	0.5453
6	3,000,000	0.0814	0.1386	0.3166	0.9556
7	3,500,000	0.1021	0.1908	0.4823	1.6680
8	4,000,000	0.1266	0.2585	0.7054	3.1725
9	4,500,000	0.1564	0.3481	1.0013	5.9536
10	5,000,000	0.1929	0.4596	1.4161	
11	5,500,000	0.2368	0.5971	1.9506	
12	6,000,000	0.2891	0.7615	2.6733	
13	6,500,000	0.3506	0.9510	3.4653	
14	7,000,000	0.4227	1.1710	4.9070	
15	7,500,000	0.5087	1.4240		
16	8,000,000	0.6084	1.7097		
17	8,500,000	0.7226	2.0472		
18	9,000,000	0.8524	2.4293		
19	9,500,000	1.0002	2.8634		
20	10,000,000		3.3810		
21	10,500,000		3.9874		
22	11,000,000		4.6977		
23	11,500,000		5.5359		

Table - 65 Maximum Horizontal Displacements at Various Horizontal Loads

No.	Horizontal Load (lbs)	Maximum Horizontal Displacement (ft)			
		Lay. Soil-5	Lay. Soil-6	Lay. Soil-7	Lay. Soil-8
1	500,000	0.0111	0.0156	0.0234	0.0367
2	1,000,000	0.0221	0.0315	0.0480	0.0789
3	1,500,000	0.0334	0.0489	0.0777	0.1445
4	2,000,000	0.0460	0.0695	0.1195	0.2584
5	2,500,000	0.0600	0.0954	0.1825	0.4611
6	3,000,000	0.0762	0.1282	0.2739	0.7781
7	3,500,000	0.0947	0.1722	0.4066	1.3429
8	4,000,000	0.1163	0.2280	0.5831	2.3329
9	4,500,000	0.1420	0.3003	0.8149	4.0715
10	5,000,000	0.1729	0.3887	1.1035	
11	5,500,000	0.2095	0.4960	1.4604	
12	6,000,000	0.2525	0.6236	1.9217	
13	6,500,000	0.3062	0.7694	2.5279	
14	7,000,000	0.3604	0.9381	3.3088	
15	7,500,000	0.4284	1.1311		
16	8,000,000	0.5066	1.3481		
17	8,500,000	0.5954	1.6027		
18	9,000,000	0.6956	1.8894		
19	9,500,000	0.8091	1.2132		
20	10,000,000		2.5792		
21	10,500,000		3.0440		
22	11,000,000		3.5636		
23	11,500,000		4.1724		

Table - 66 Minimum Soil Minor Principal Stresses at Various Horizontal Loads

No.	Horizontal Load (lbs)	Minimum Soil Minor Principal Stress (psf)			
		Lay. Soil-5	Lay. Soil-6	Lay. Soil-7	Lay. Soil-8
1	Geostatic	-2,499.0	-2,490.8	-2,293.5	-2,101.5
2	500,000	-2,557.1	-2,560.5	-2,404.4	-2,269.7
3	1,000,000	-2,615.5	-2,634.7	-2,518.9	-2,778.3
4	1,500,000	-2,674.4	-2,711.6	-3,018.0	-4,227.2
5	2,000,000	-2,735.2	-2,792.6	-3,937.7	-5,873.5
6	2,500,000	-2,798.1	-3,366.4	-5,287.6	-8,235.9
7	3,000,000	-2,862.7	-4,459.4	-7,146.0	-10,898.8
8	3,500,000	-3,444.9	-5,965.2	-9,779.7	-15,659.6
9	4,000,000	-4,208.8	-7,664.4	-13,040.0	-23,736.5
10	4,500,000	-5,117.9	-9,707.5	-17,088.2	-35,165.9
11	5,000,000	-6,042.6	-12,055.8	-21,732.3	
12	5,500,000	-7,130.5	-14,691.5	-27,163.7	
13	6,000,000	-8,408.9	-17,674.0	-33,521.5	
14	6,500,000	-9,845.9	-20,888.7	-41,251.2	
15	7,000,000	-11,415.0	-24,307.6	-50,581.4	
16	7,500,000	-13,132.0	-27,815.7		
17	8,000,000	-15,015.8	-31,718.2		
18	8,500,000	-17,049.1	-36,262.0		
19	9,000,000	-19,176.6	-41,157.8		
20	9,500,000	-21,429.3	-46,432.6		
21	10,000,000		-52,310.8		
22	10,500,000		-58,290.9		
23	11,000,000		-64,718.0		
24	11,500,000		-71,681.9		

Table - 67 Maximum Pile Von Mises Stresses at Various Horizontal Loads

No.	Horizontal Load (lbs)	Maximum Pile Von Mises Stress (psf)			
		Lay. Soil-5	Lay. Soil-6	Lay. Soil-7	Lay. Soil-8
1	500,000	16,071.5	16,454.3	16,105.7	16,033.4
2	1,000,000	32,142.9	32,630.2	32,194.9	32,099.4
3	1,500,000	48,192.9	48,697.1	48,314.2	48,706.3
4	2,000,000	64,459.6	64,687.7	64,643.8	64,380.1
5	2,500,000	80,946.8	80,744.2	80,994.8	80,278.6
6	3,000,000	97,312.9	96,786.1	96,694.8	97,621.6
7	3,500,000	113,685.9	112,992.0	112,657.3	115,118.5
8	4,000,000	130,283.5	129,512.5	129,530.0	132,098.3
9	4,500,000	146,984.5	146,408.0	146,747.3	149,157.2
10	5,000,000	163,761.0	163,006.1	163,747.9	
11	5,500,000	180,684.9	179,852.4	180,902.2	
12	6,000,000	197,681.1	196,715.8	198,087.9	
13	6,500,000	214,625.9	213,566.1	215,353.1	
14	7,000,000	231,540.1	230,524.9	232,555.3	
15	7,500,000	248,421.0	247,508.1		
16	8,000,000	265,289.1	264,224.2		
17	8,500,000	282,014.9	281,582.0		
18	9,000,000	298,846.3	298,754.5		
19	9,500,000	315,762.2	315,856.2		
20	10,000,000		333,298.4		
21	10,500,000		350,667.3		
22	11,000,000		367,914.4		
23	11,500,000		385,308.8		

Table – 68 Best Suction Pile Cross-Sections with Elasto-Plastic Soil Properties

	Sand			Clay		
	Hor. Load	Vert. Load	Incl. Load	Hor.Load	Vert. Load	Incl. Load
Horz. def.	C	NA	C	C,Y	NA	C,Y
Soil stress	C	C,T,Y	C	C	T,Y	T
Pile stress	Y	Y	Y	Y	Y	Y

Note: C: Circular section
T: Triangular section
Y: Y-shaped section
NA: Not applicable

USE OF SUCTION PILES FOR MOORING OF MOBILE OFFSHORE BASES

(ONR Grant No. N00014-97-1-0887)

Task 2 Completion Report: Analytical Performance Study

(July 1, 1997 – Sep. 30, 1998)

APPENDIX: Results of Analysis

Submitted to

Naval Facilities Engineering Service Center
Port Hueneme, CA

by

Sangchul Bang and Yeongki Cho

Department of Civil and Environmental Engineering
South Dakota School of Mines and Technology
Rapid City, SD 57701

Mar., 1999

TABLE OF FIGURES

Figure-A1	Horizontal Displacements (Circular Section)
Figure-A2	Horizontal Displacements on a Vertical Plane along the Horizontal Load Direction (Circular Section)
Figure-A3	Horizontal Normal Pile Stresses on the Pile Surface (Circular Section)
Figure-A4	Horizontal Normal Soil Stresses on the Pile Surface (Circular Section)
Figure-A5	Pile Major Principal Stresses on the Pile Surface (Circular Section)
Figure-A6	Soil Minor Principal Stresses on the Pile Surface (Circular Section)
Figure-A7	Horizontal displacements (Y-shape)
Figure-A8	Horizontal Displacements on a Vertical Plane along the Horizontal Load Direction (Y-shape)
Figure-A9	Horizontal Normal Pile Stresses on the Pile Surface (Y-shape)
Figure-A10	Horizontal Normal Soil Stresses on the Pile Surface (Y-shape)
Figure-A11	Pile Major Principal Stresses on the Pile Surface (Y-shape)
Figure-A12	Soil Minor Principal Stresses on the Pile Surface (Y-shape)
Figure-A13	Horizontal displacements (Clover-shape with three cells)
Figure-A14	Horizontal Displacements on a Vertical Plane along the Horizontal Load Direction (Clover-shape with three cells)
Figure-A15	Horizontal Normal Pile Stresses on the Pile Surface (Clover-shape with three cells)
Figure -A16	Horizontal Normal Soil Stresses on the Pile Surface (Clover-shape with three cells)
Figure-A17	Pile Major Principal Stresses on the Pile Surface (Clover-shape with three cells)

Figure-A18 Soil Minor Principal Stresses on the Pile Surface (Clover-shape with three cells)

Figure-A19 Horizontal Displacements (Clustered circle with four cells)

Figure-A20 Horizontal Displacements on a Vertical Plane along the Horizontal Load Direction (Clustered circle with four cells)

Figure-A21 Horizontal Normal Pile Stresses on the Pile Surface (Clustered circle with four cells)

Figure-A22 Horizontal Normal Soil Stresses on the Pile Surface (Clustered circle with four cells)

Figure-A23 Pile Major Principal Stresses on the Pile Surface (Clustered circle with four cells)

Figure-A24 Soil Minor Principal Stresses on the Pile Surface (Clustered circle with four cells)

Figure-B1 Horizontal Displacements (Circular Section)

Figure-B2 Horizontal Displacements on a Vertical Plane along the Horizontal Load Direction (Circular Section)

Figure-B3 Pile Total Displacements (Circular Section)

Figure-B4 Soil Minor Principal Stresses (Circular Section)

Figure-B5 Soil Minor Principal Stresses on a Vertical Plane along the Horizontal Load Direction (Circular Section)

Figure-B6 Horizontal Normal Pile Stresses on the Pile Surface (Circular Section)

Figure-B7 Pile von Mises Stresses on the Pile Surface (Circular Section)

Figure-B8 Vertical Displacements (Circular Section)

Figure-B9 Vertical Displacements on a Vertical Plane (Circular Section)

Figure-B10 Pile Vertical Displacements (Circular Section)

Figure-B11 Soil Minor Principal Stresses (Circular Section)

Figure-B12 Soil Minor Principal Stresses on a Vertical Plane (Circular Section)

Figure-B13 Pile von Mises Stresses on the Pile Surface (Circular Section)

Figure-B14 Horizontal Displacements (Triangular Section)

Figure-B15 Horizontal Displacements on a Vertical Plane along the Horizontal Load Direction (Triangular Section)

Figure-B16 Pile Total Displacements (Triangular Section)

Figure-B17 Soil Minor Principal Stresses (Triangular Section)

Figure-B18 Soil Minor Principal Stresses on a Vertical Plane along the Horizontal Load Direction (Triangular Section)

Figure-B19 Horizontal Normal Pile Stresses on the Pile Surface (Triangular Section)

Figure-B20 Pile von Mises Stresses on the Pile Surface (Triangular Section)

Figure-B21 Vertical Displacements (Triangular Section)

Figure-B22 Vertical Displacements on a Vertical Plane (Triangular Section)

Figure-B23 Pile Vertical Displacements (Triangular Section)

Figure-B24 Soil Minor Principal Stresses (Triangular Section)

Figure-B25 Soil Minor Principal Stresses on a Vertical Plane (Triangular Section)

Figure-B26 Pile von Mises Stresses on the Pile Surface (Triangular Section)

Figure-B27 Horizontal Displacements (Y-shaped Section)

Figure-B28 Horizontal Displacements on a Vertical Plane along the Horizontal Load Direction (Y-shaped Section)

Figure-B29 Pile Total Displacements (Y-shaped Section)

Figure-B30 Soil Minor Principal Stresses (Y-shaped Section)

Figure-B31 Soil Minor Principal Stresses on a Vertical Plane along the Horizontal Load Direction (Y-shaped Section)

Figure-B32 Horizontal Normal Pile Stresses on the Pile Surface (Y-shaped Section)

Figure-B33 Pile von Mises Stresses on the Pile Surface (Y-shaped Section)

Figure-B34 Vertical Displacements (Y-shaped Section)

Figure-B35 Vertical Displacements on a Vertical Plane (Y-shaped Section)

Figure-B36 Pile Vertical Displacements (Y-shaped Section)

Figure-B37 Soil Minor Principal Stresses (Y-shaped Section)

Figure-B38 Soil Minor Principal Stresses on a Vertical Plane (Y-shaped Section)

Figure-B39 Pile von Mises Stresses on the Pile Surface (Y-shaped Section)

Figure-C1 Horizontal Displacements (Circular Section)

Figure-C2 Horizontal Displacements on a Vertical Plane along the Horizontal Load Direction (Circular Section)

Figure-C3 Pile Total Displacements (Circular Section)

Figure-C4 Soil Minor Principal Stresses (Circular Section)

Figure-C5 Soil Minor Principal Stresses on a Vertical Plane along the Horizontal Load Direction (Circular Section)

Figure-C6 Horizontal Normal Pile Stresses on the Pile Surface (Circular Section)

Figure-C7 Pile von Mises Stresses on the Pile Surface (Circular Section)

Figure-C8 Vertical Displacements (Circular Section)

Figure-C9 Vertical Displacements on a Vertical Plane (Circular Section)

Figure-C10 Pile Vertical Displacements (Circular Section)

Figure-C11 Soil Minor Principal Stresses on a Vertical Plane (Circular Section)

Figure-C12 Soil Minor Principal Stresses on the Pile Surface (Circular Section)

Figure-C13 Pile von Mises Stresses on the Pile Surface (Circular Section)

Figure-C14 Horizontal Displacements (Triangular Section)

Figure-C15 Horizontal Displacements on a Vertical Plane along the Horizontal Load Direction (Triangular Section)

Figure-C16 Pile Total Displacements (Triangular Section)

Figure-C17 Soil Minor Principal Stresses (Triangular Section)

Figure-C18 Soil Minor Principal Stresses on a Vertical Plane along the Horizontal Load Direction (Triangular Section)

Figure-C19 Horizontal Normal Pile Stresses on the Pile Surface (Triangular Section)

Figure-C20 Pile von Mises Stresses on the Pile Surface (Triangular Section)

Figure-C21 Vertical Displacements (Triangular Section)

Figure-C22 Vertical Displacements on a Vertical Plane (Triangular Section)

Figure-C23 Pile Vertical Displacements (Triangular Section)

Figure-C24 Soil Minor Principal Stresses on a Vertical Plane (Triangular Section)

Figure-C25 Soil Minor Principal Stresses on the Pile Surface (Triangular Section)

Figure-C26 Pile von Mises Stresses on the Pile Surface (Triangular Section)

Figure-C27 Horizontal Displacements (Y-shaped Section)

Figure-C28 Horizontal Displacements on a Vertical Plane along the Horizontal Load Direction (Y-shaped Section)

Figure-C29 Pile Total Displacements (Y-shaped Section)

Figure-C30 Soil Minor Principal Stresses (Y-shaped Section)

Figure-C31 Soil Minor Principal Stresses on a Vertical Plane along the Horizontal Load Direction (Y-shaped Section)

Figure-C32 Horizontal Normal Pile Stresses on the Pile Surface (Y-shaped Section)

Figure-C33 Pile von Mises Stresses on the Pile Surface (Y-shaped Section)

Figure-C34 Vertical Displacements (Y-shaped Section)

Figure-C35 Vertical Displacements on a Vertical Plane (Y-shaped Section)

Figure-C36 Pile Vertical Displacements (Y-shaped Section)

Figure-C37 Soil Minor Principal Stresses a Vertical Plane (Y-shaped Section)

Figure-C38 Soil Minor Principal Stresses on the Pile Surface (Y-shaped Section)

Figure-C39 Pile von Mises Stresses on the Pile Surface (Y-shaped Section)

Figure-D1 Horizontal Displacements (Circular Pile with 15-ft Flange in Sand)

Figure-D2 Horizontal Displacements on a Vertical Plane along the Horizontal Load Direction (Circular Pile with 15-ft Flange in Sand)

Figure-D3 Pile Total Displacements (Circular Pile with 15-ft Flange in Sand)

Figure-D4 Soil Minor Principal Stresses on a Vertical Plane along the Horizontal Load Direction (Circular Pile with 15-ft Flange in Sand)

Figure-D5 Soil Minor Principal Stresses on the Pile Surface (Circular Pile with 15-ft Flange in Sand)

Figure-D6 Pile von Mises Stresses on the Pile Surface (Circular Pile with 15-ft Flange in Sand)

Figure-D7 Horizontal Displacements (Circular Pile with 15-ft Flange in Clay)

Figure-D8 Horizontal Displacements on a Vertical Plane along the Horizontal Load Direction (Circular Pile with 15-ft Flange in Clay)

Figure-D9 Pile Total Displacements (Circular Pile with 15-ft Flange in Clay)

Figure-D10 Soil Minor Principal Stresses on a Vertical Plane along the Horizontal Load Direction (Circular Pile with 15-ft Flange in Clay)

Figure-D11 Soil Minor Principal Stresses on the Pile Surface (Circular Pile with 15-ft Flange in Clay)

Figure-D12 Pile von Mises Stresses on the Pile Surface (Circular Pile with 15-ft Flange in Clay)

Figure-E1 Horizontal Displacements on a Vertical Plane along the Horizontal Load Direction (Load at the Middle of the Pile in Clay)

Figure-E2 Pile Total Displacements (Load at the Middle of the Pile in Clay)

Figure-E3 Soil Minor Principal Stresses on a Vertical Plane along the Horizontal Load Direction (Load at the Middle of the Pile in Clay)

Figure-E4 Soil Minor Principal Stresses on the Pile Surface (Load at the Middle of the Pile in Clay)

Figure-E5 Pile von Mises Stresses on the Pile Surface (Load at the Middle of the Pile in Clay)

Figure-E6 Horizontal Displacements on a Vertical Plane along the Horizontal Load Direction (Load at the Bottom of the Pile in Clay)

Figure-E7 Pile Total Displacements (Load at the Bottom of the Pile in Clay)

Figure-E8 Soil Minor Principal Stresses on a Vertical Plane along the Horizontal Load Direction (Load at the Bottom of the Pile in Clay)

Figure-E9 Soil Minor Principal Stresses on the Pile Surface (Load at the Bottom of the Pile in Clay)

Figure-E10 Pile von Mises Stresses on the Pile Surface (Load at the Bottom of the Pile in Clay)

Figure-E11 Horizontal Displacements on a Vertical Plane along the Horizontal Load Direction (Load at the Middle of the Pile in Sand)

Figure-E12 Pile Total Displacements (Load at the Middle of the Pile in Sand)

Figure-E13 Soil Minor Principal Stresses on a Vertical Plane along the Horizontal Load Direction (Load at the Middle of the Pile in Sand)

Figure-E14 Soil Minor Principal Stresses on the Pile Surface (Load at the Middle of the Pile in Sand)

Figure-E15 Pile von Mises Stresses on the Pile Surface (Load at the Middle of the Pile in Sand)

Figure-E16 Horizontal Displacements on a Vertical Plane along the Horizontal Load Direction (Load at the Bottom of the Pile in Sand)

Figure-E17 Pile Total Displacements (Load at the Bottom of the Pile in Sand)

Figure-E18 Soil Minor Principal Stresses on a Vertical Plane along the Horizontal Load Direction (Load at the Bottom of the Pile in Sand)

Figure-E19 Soil Minor Principal Stresses on the Pile Surface (Load at the Bottom of the Pile in Sand)

Figure-E20 Pile von Mises Stresses on the Pile Surface (Load at the Bottom of the Pile in Sand)

Figure-F1 Horizontal Displacements (Telescopic Pile in Sand)

Figure-F2 Horizontal Displacements on a Vertical Plane along the Horizontal Load Direction (Telescopic Pile in Sand)

Figure-F3 Pile Total Displacements (Telescopic Pile in Sand)

Figure-F4 Soil Minor Principal Stresses on a Vertical Plane along the Horizontal Load Direction (Telescopic Pile in Sand)

Figure-F5 Soil Minor Principal Stresses on the Pile Surface (Telescopic Pile in Sand)

Figure-F6 Pile von Mises Stresses on the Pile (Telescopic Pile in Sand)

Figure-F7 Horizontal Displacements (Telescopic Pile in Clay)

Figure-F8 Horizontal Displacements on a Vertical Plane along the Horizontal Load Direction (Telescopic Pile in Clay)

Figure-F9 Pile Total Displacements (Telescopic Pile in Clay)

Figure-F10 Soil Minor Principal Stresses on a Vertical Plane along the Horizontal Load Direction (Telescopic Pile in Clay)

Figure-F11 Soil Minor Principal Stresses on the Pile (Telescopic Pile in Clay)

Figure-F12 Pile von Mises Stresses on the Pile Surface (Telescopic Pile in Clay)

Figure-G1 Horizontal Displacements (Layered Soil-2)

Figure-G2 Horizontal Displacements on a Vertical Plane along the Horizontal Load Direction (Layered Soil-2)

Figure-G3 Pile Total Displacements (Layered Soil-2)

Figure-G4 Soil Minor Principal Stresses on a Vertical Plane along the Horizontal Load Direction (Layered Soil-2)

Figure-G5 Soil Minor Principal Stresses on the Pile Surface (Layered Soil-2)

Figure-G6 Pile von Mises Stresses on the Pile (Layered Soil-2)

Figure-G7 Horizontal Displacements (Layered Soil-6)

Figure-G8 Horizontal Displacements on a Vertical Plane along the Horizontal Load Direction (Layered Soil-6)

Figure-G9 Pile Total Displacements (Layered Soil-6)

Figure-G10 Soil Minor Principal Stresses on a Vertical Plane along the Horizontal Load Direction (Layered Soil-6)

Figure-G11 Soil Minor Principal Stresses on the Pile (Layered Soil-6)

Figure-G12 Pile von Mises Stresses on the Pile Surface (Layered Soil-6)

Figure-A1. Horizontal Displacements (Circular Section)

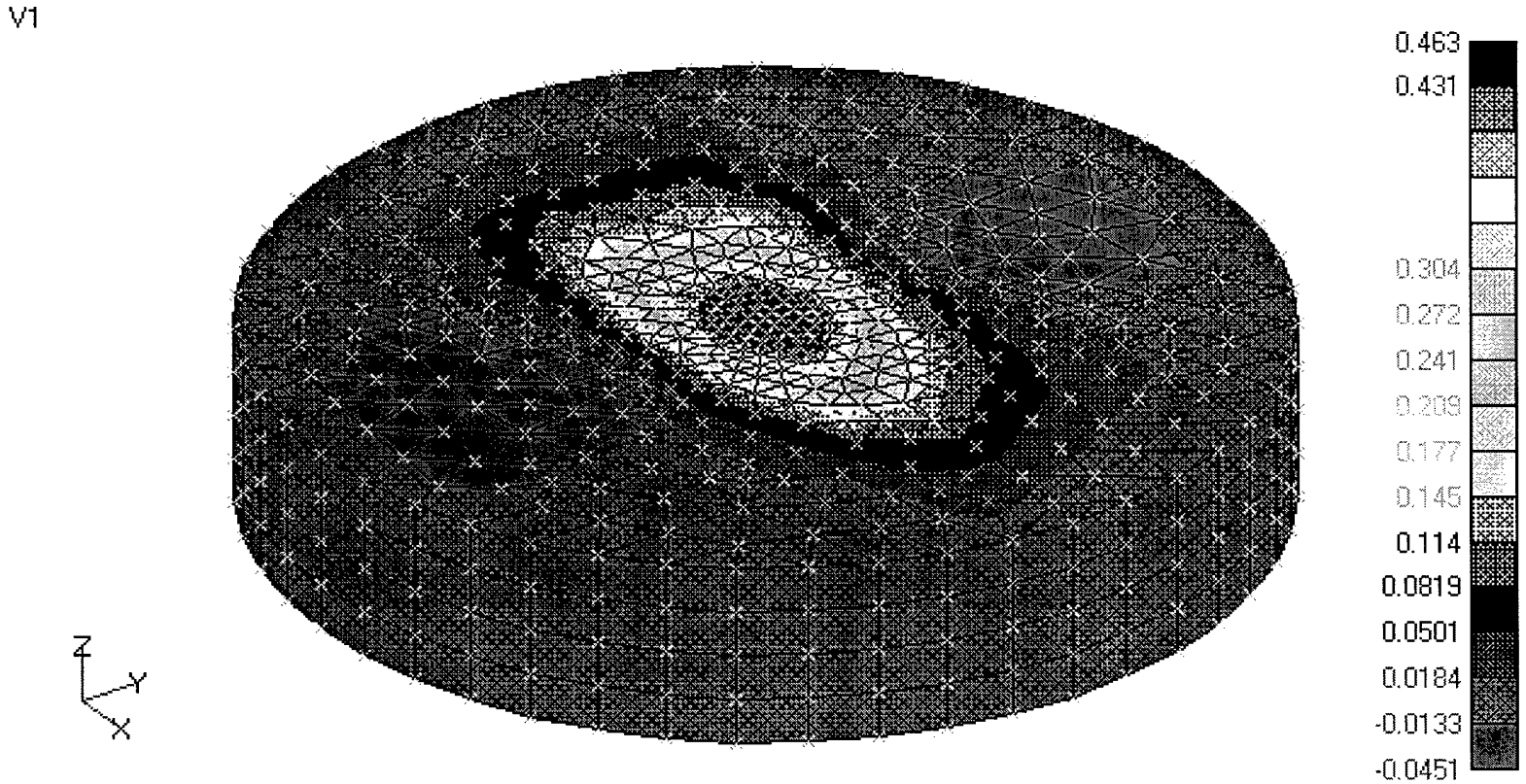

Horizontal Load = 300,000 lbs
Linear Elastic Soil, E = 5,000psf, $\nu = 0.499$
AISI 4340 Steel Pile

Figure-A2 Horizontal Displacements on a Vertical Plane along the Horizontal Load Direction (Circular Section)

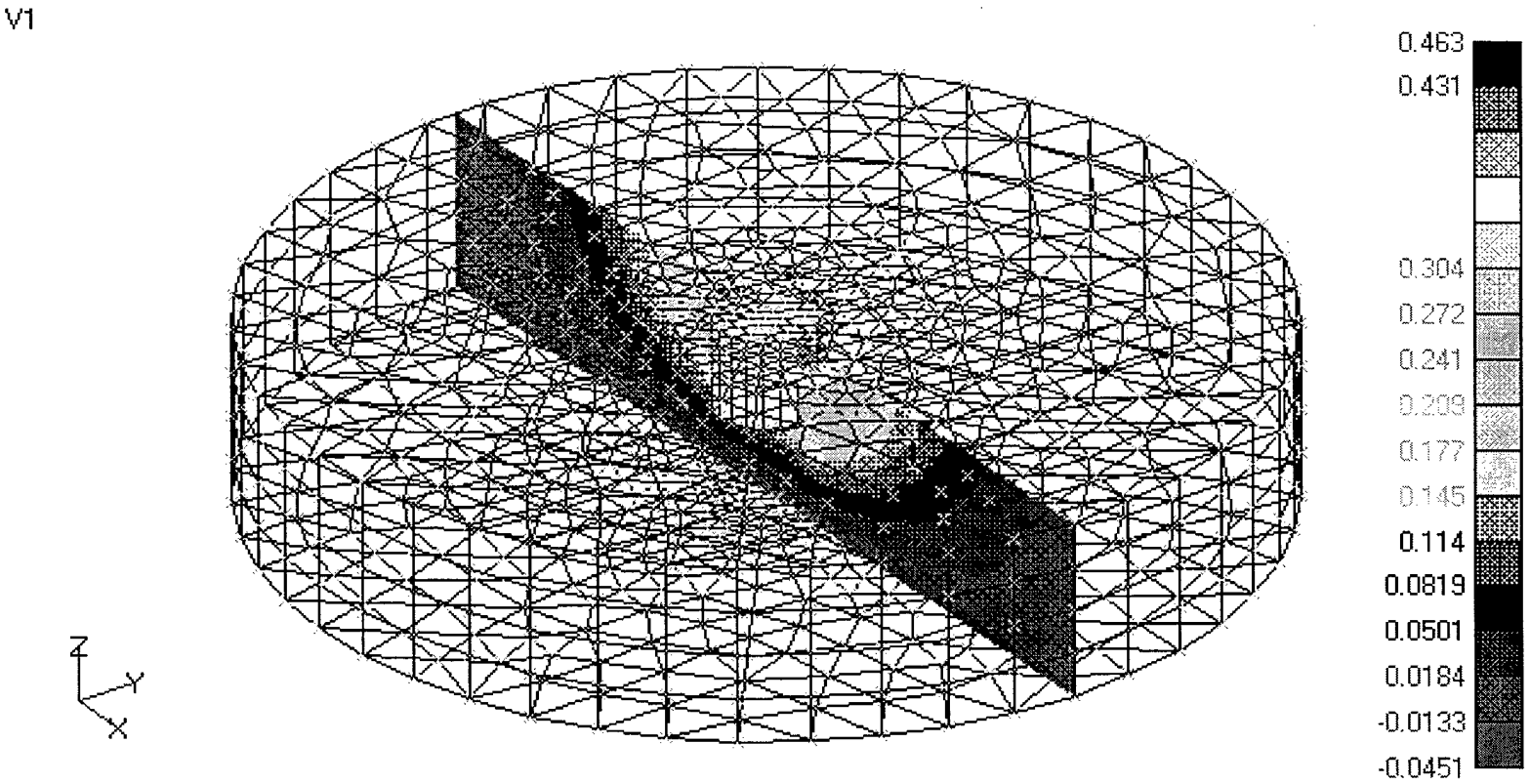

Horizontal Load = 300,000 lbs
Linear Elastic Soil, E = 5,000psf, $\nu = 0.499$
AISI 4340 Steel Pile

Figure-A3 Horizontal Normal Pile Stresses on the Pile Surface (Circular Pile)

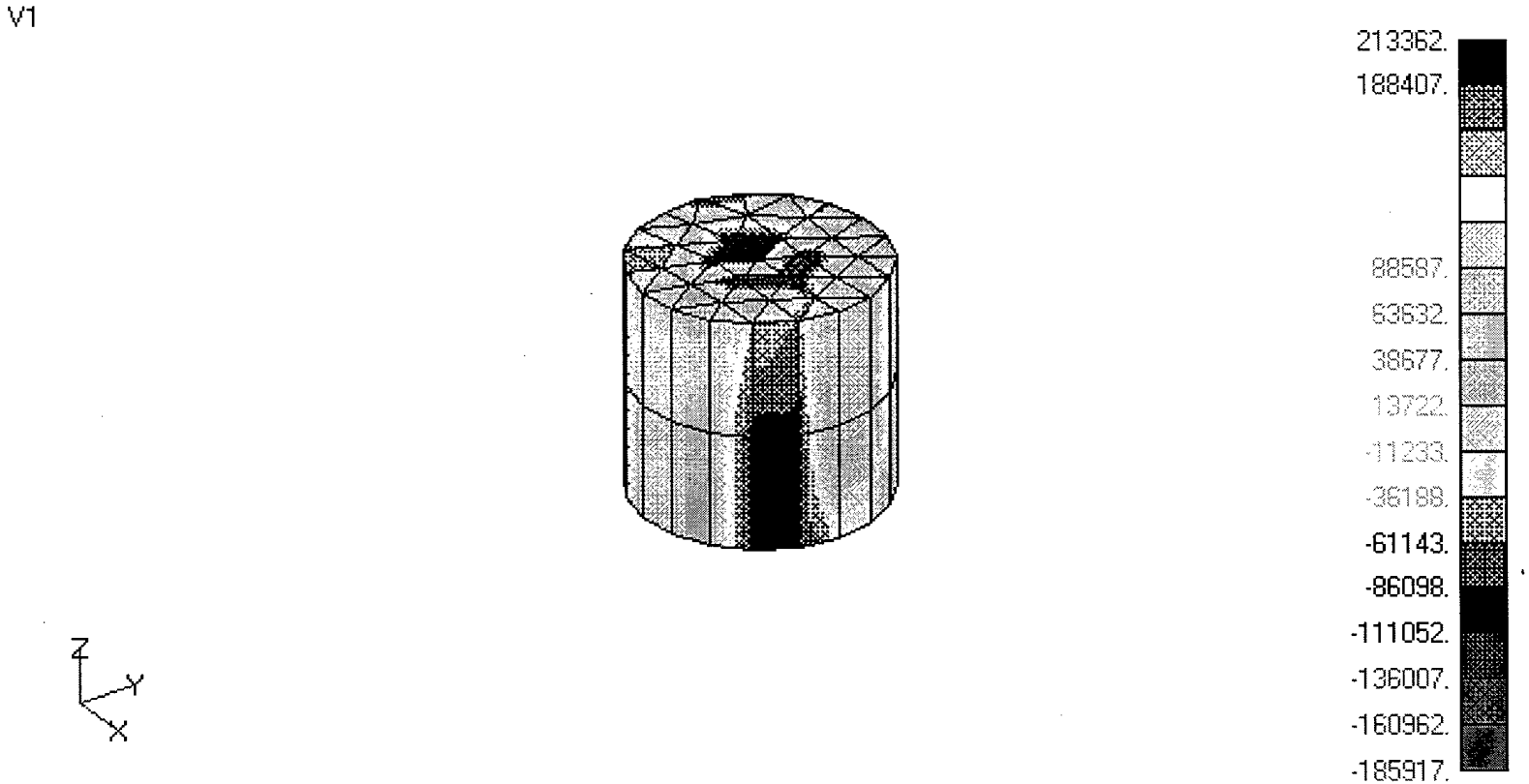

Horizontal Load = 300,000 lbs
Linear Elastic Soil, E = 5,000psf, $\nu = 0.499$
AISI 4340 Steel Pile

Figure-A4 Horizontal Normal Soil Stresses on the Pile Surface (Circular Section)

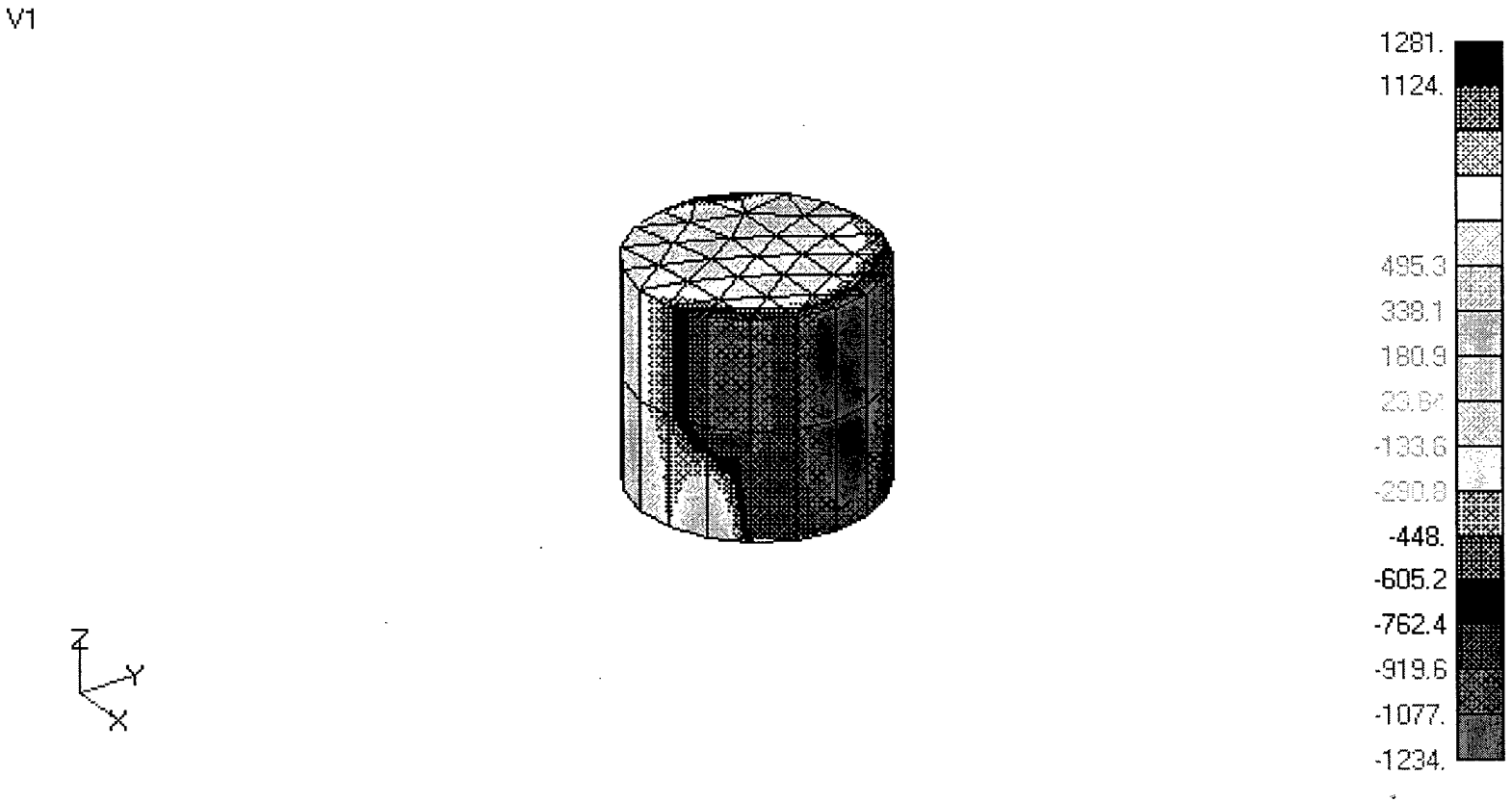

Horizontal Load = 300,000 lbs
Linear Elastic Soil, E = 5,000psf, ν = 0.499
AISI 4340 Steel Pile

Figure-A5 Pile Major Principal stresses on the Pile Surface (Circular Section)

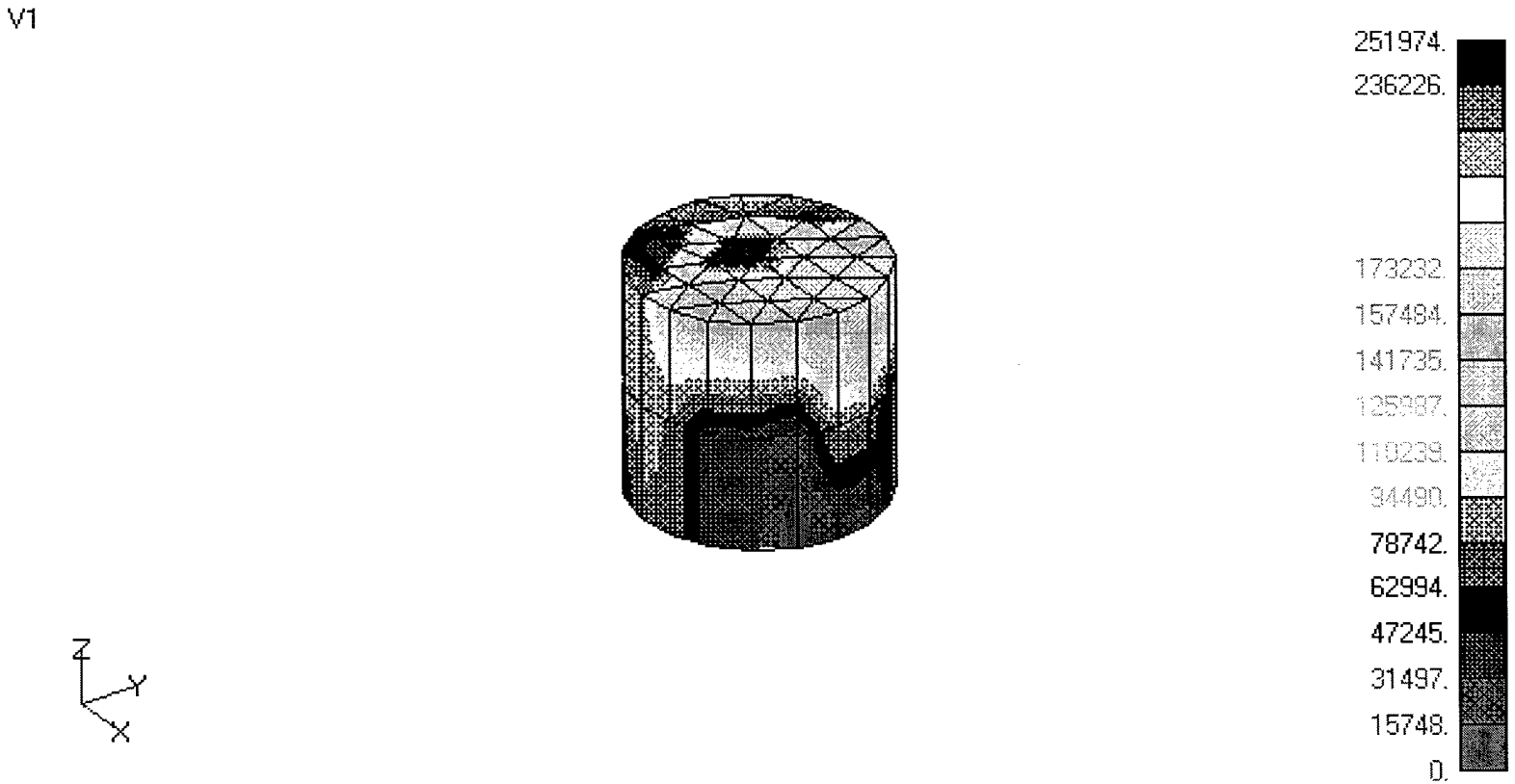

Horizontal Load = 300,000 lbs
Linear Elastic Soil, E = 5,000psf, ν = 0.499
AISI 4340 Steel Pile

Figure-A6 Soil Minor Principal Stresses on the Pile Surface (Circular Section)

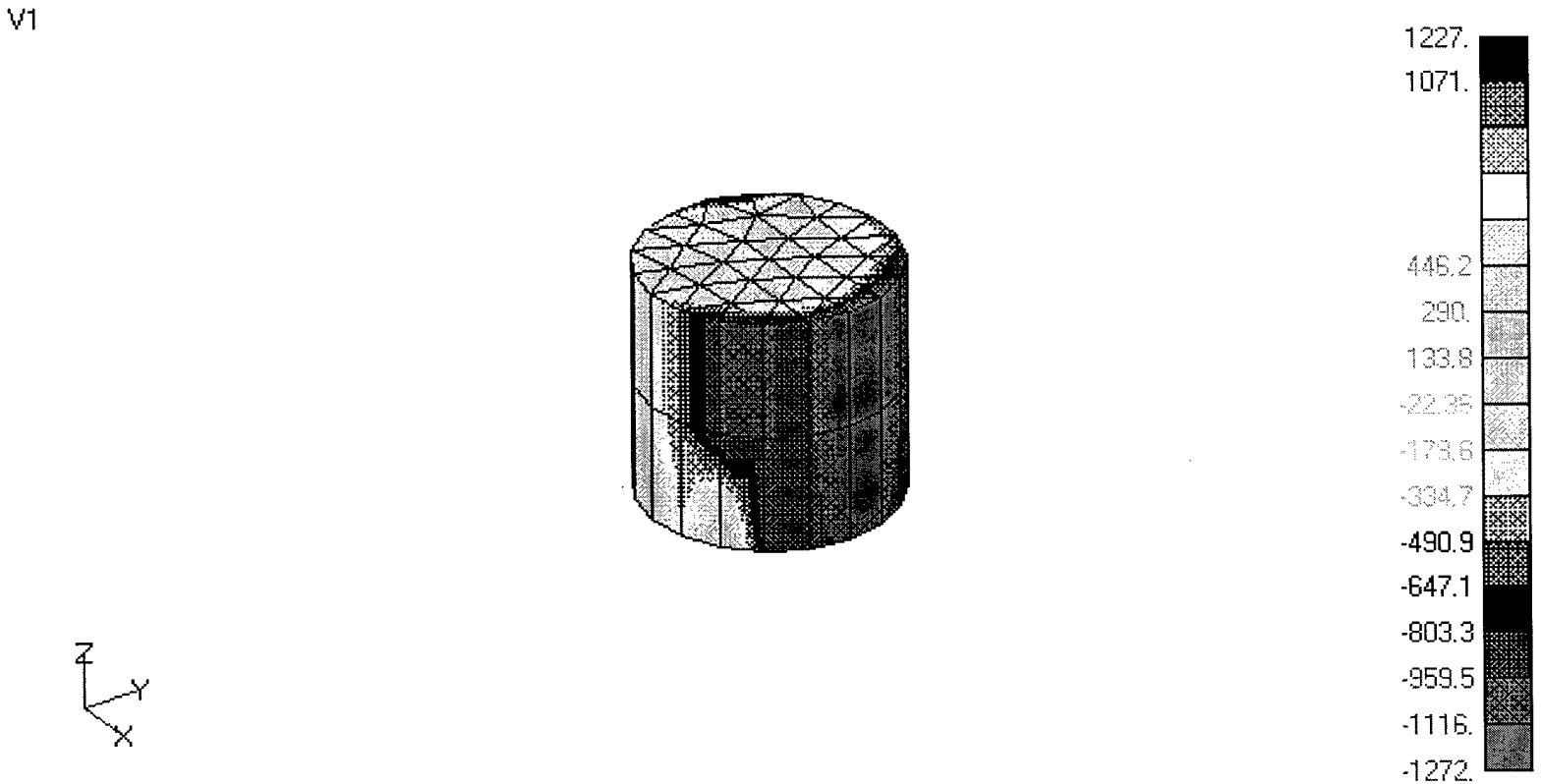

Horizontal Load = 300,000 lbs
Linear Elastic Soil, E = 5,000psf, $\nu = 0.499$
AISI 4340 Steel Pile

Figure-A7 Horizontal Displacements (Y-shape)

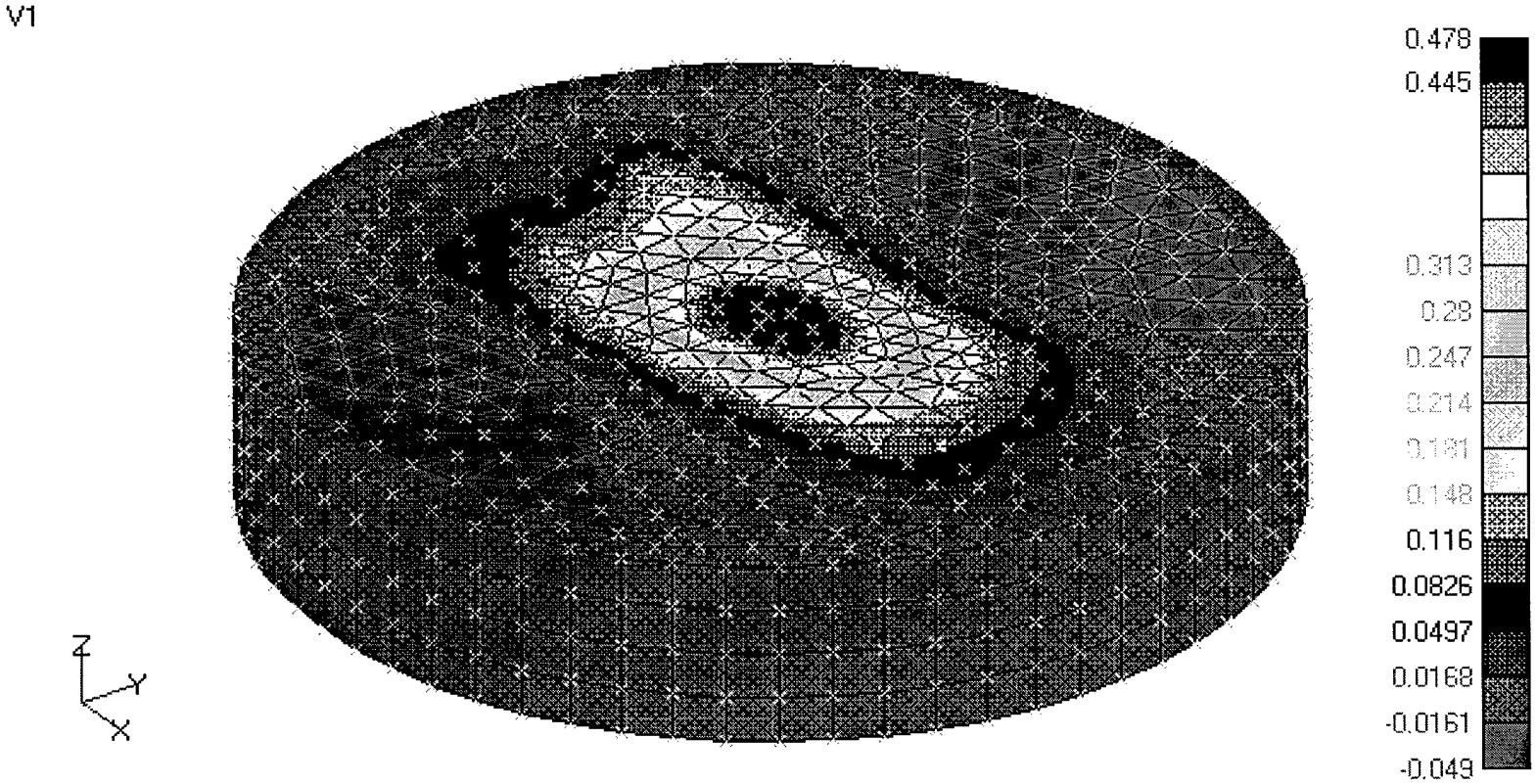

Horizontal Load = 300,000 lbs
Linear Elastic Soil, E = 5,000psf, $\nu = 0.499$
AISI 4340 Steel Pile

Figure-A8 Horizontal Displacements on a Vertical Plane along the Horizontal Load Direction (Y-shape)

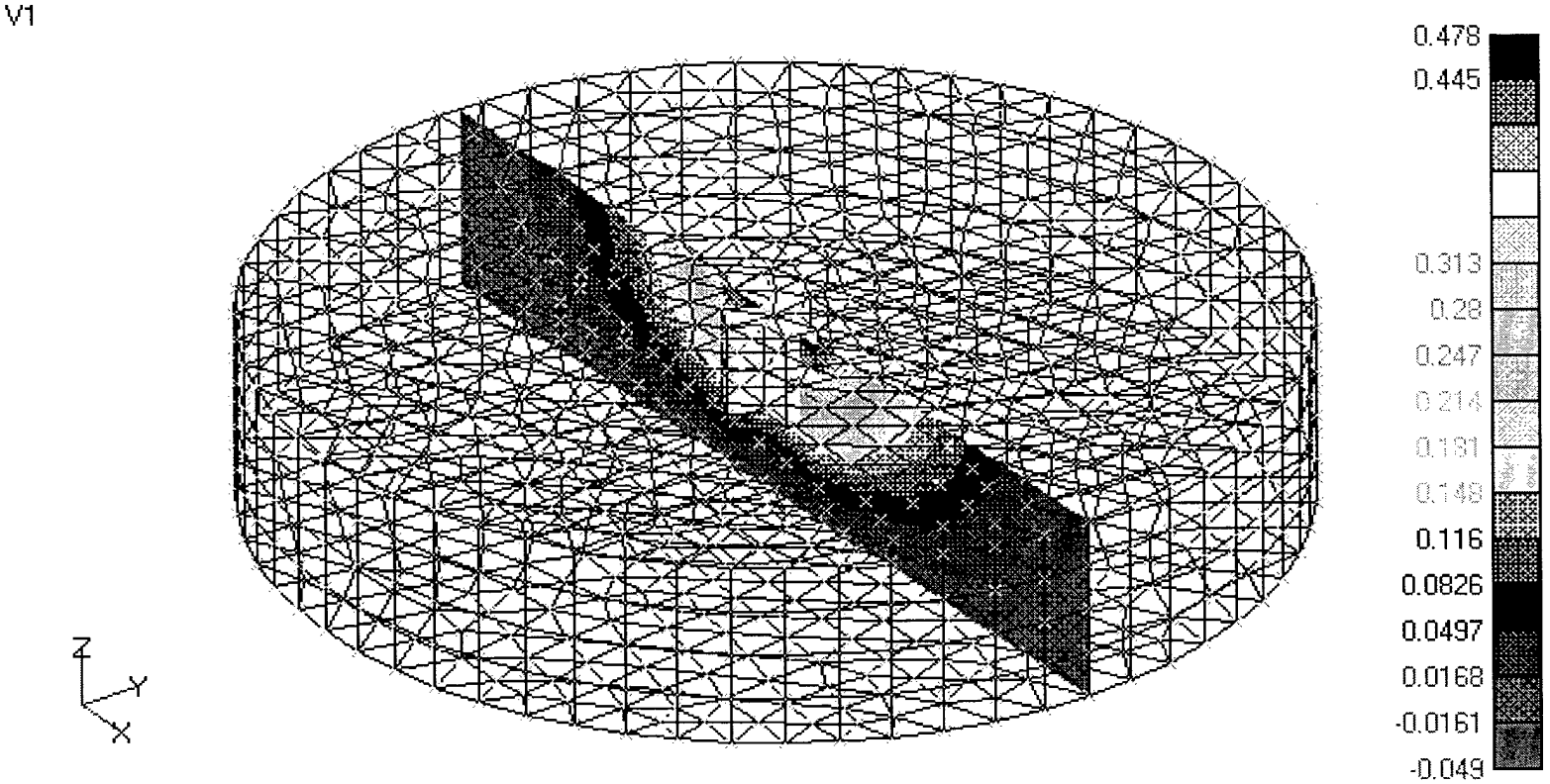

Horizontal Load = 300,000 lbs
Linear Elastic Soil, E = 5,000psf, $\nu = 0.499$
AISI 4340 Steel Pile

Figure-A9 Horizontal Normal Pile Stresses on the Pile Top Surface (Y-shape)

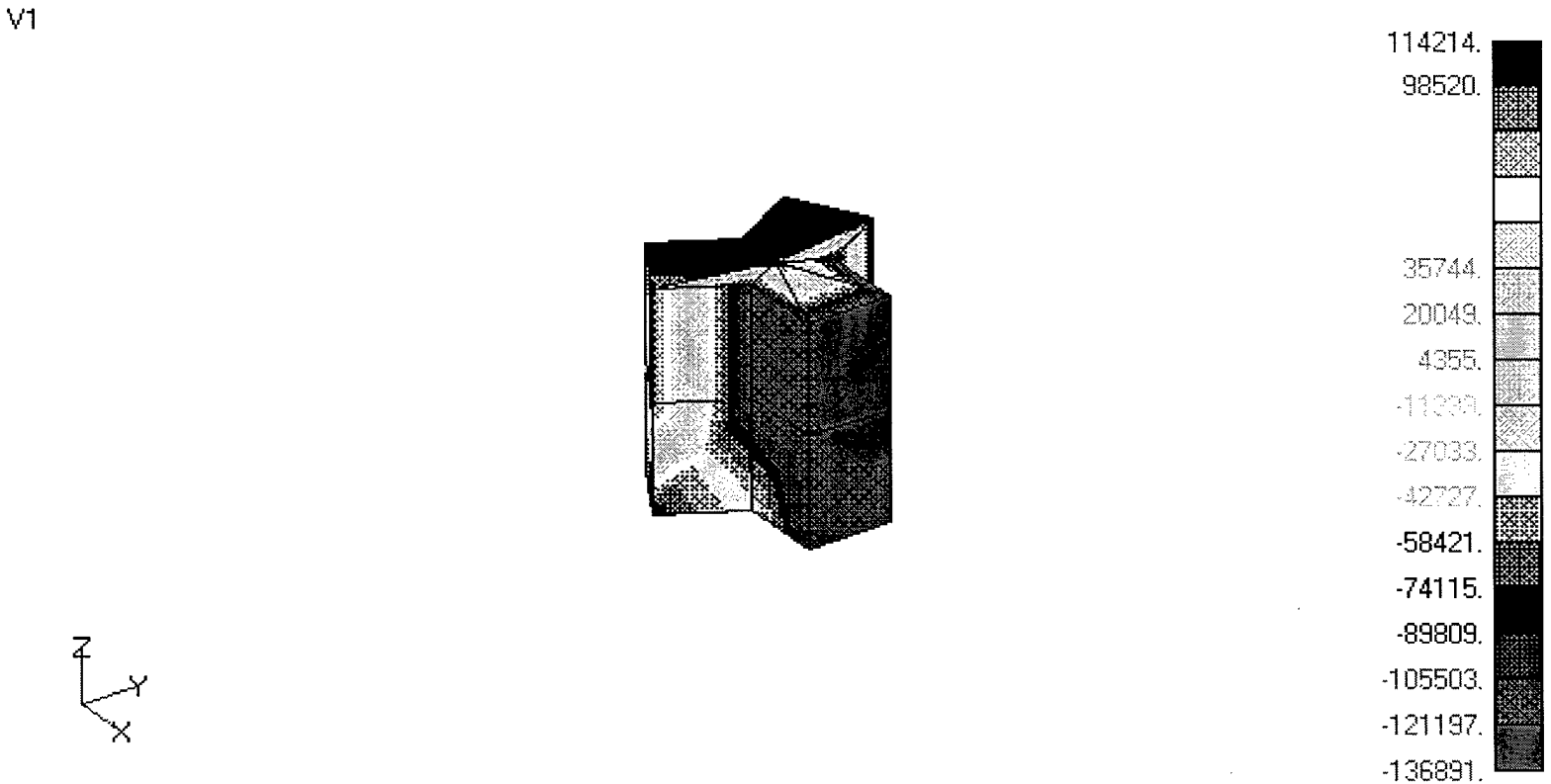

Horizontal Load = 300,000 lbs
Linear Elastic Soil, E = 5,000psf, ν = 0.499
AISI 4340 Steel Pile

Figure-A10 Horizontal Normal Soil Stresses on the Pile Top Surface (Y-shape)

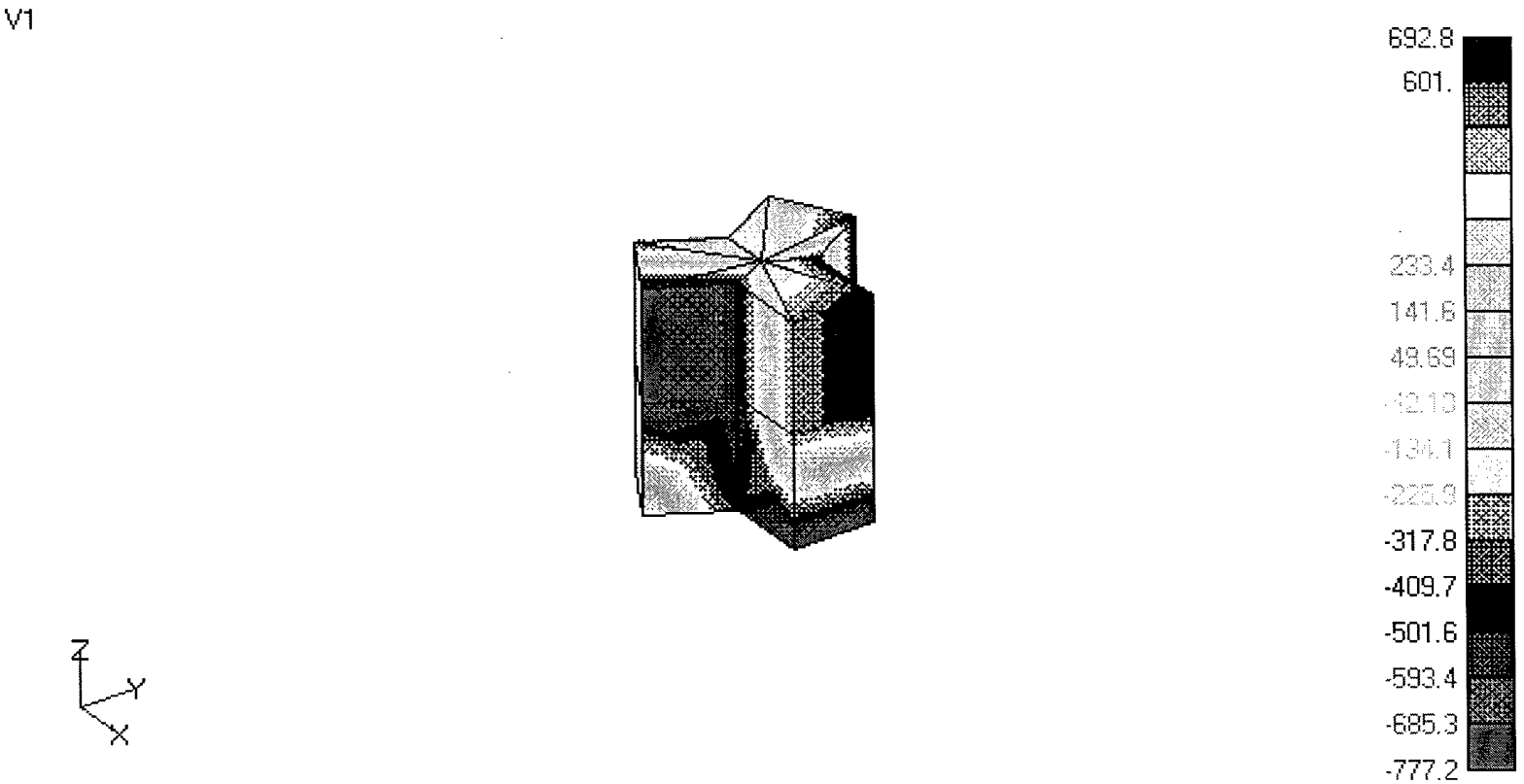

Horizontal Load = 300,000 lbs
Linear Elastic Soil, E = 5,000psf, ν = 0.499
AISI 4340 Steel Pile

Figure-A11 Pile Major Principal Stresses on the Pile Surface (Y-shape)

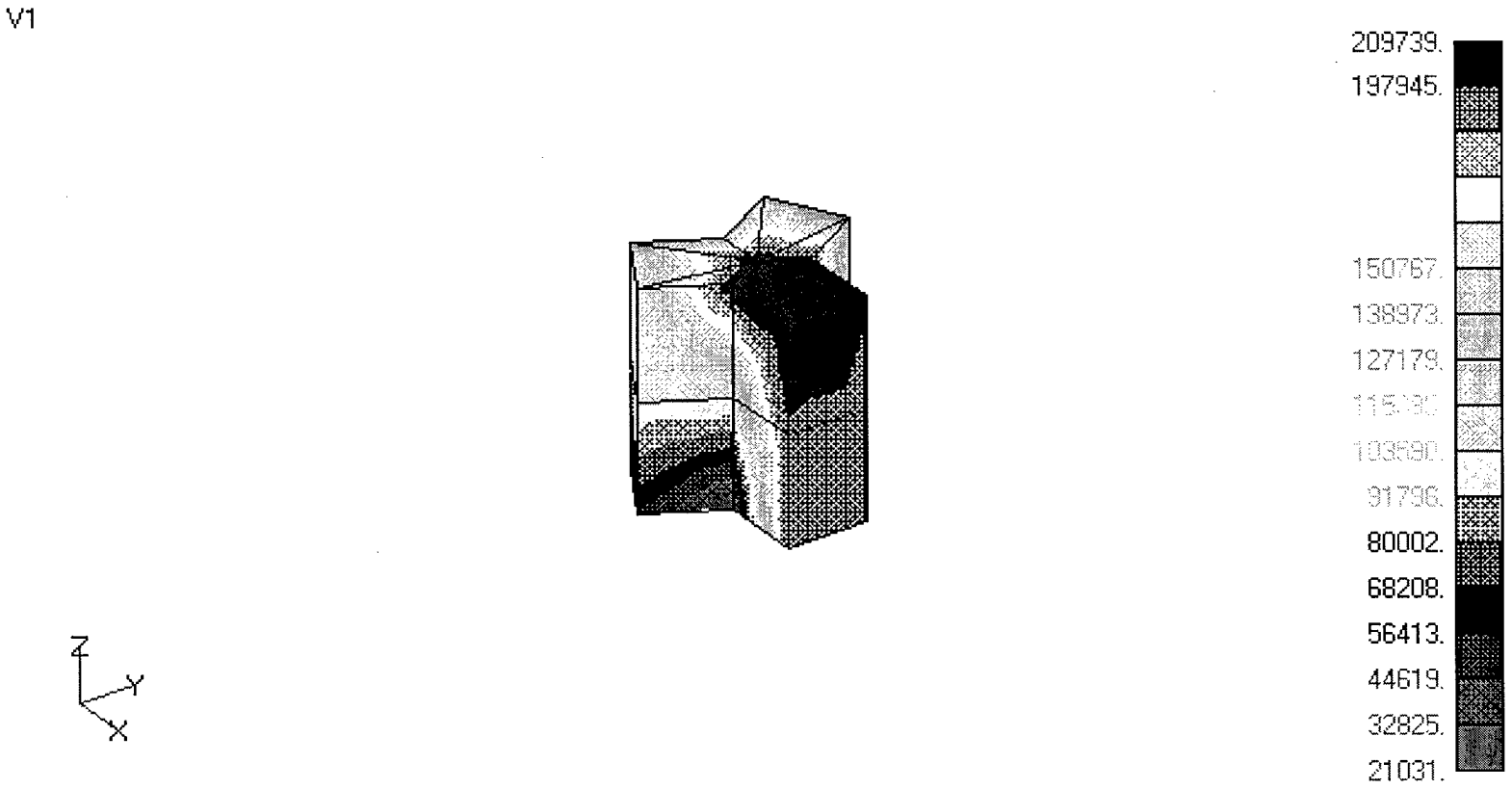

Horizontal Load = 300,000 lbs
Linear Elastic Soil, E = 5,000psf, ν = 0.499
AISI 4340 Steel Pile

Figure-A12 Soil Minor Principal Stresses on the Pile Surface (Y-shape)

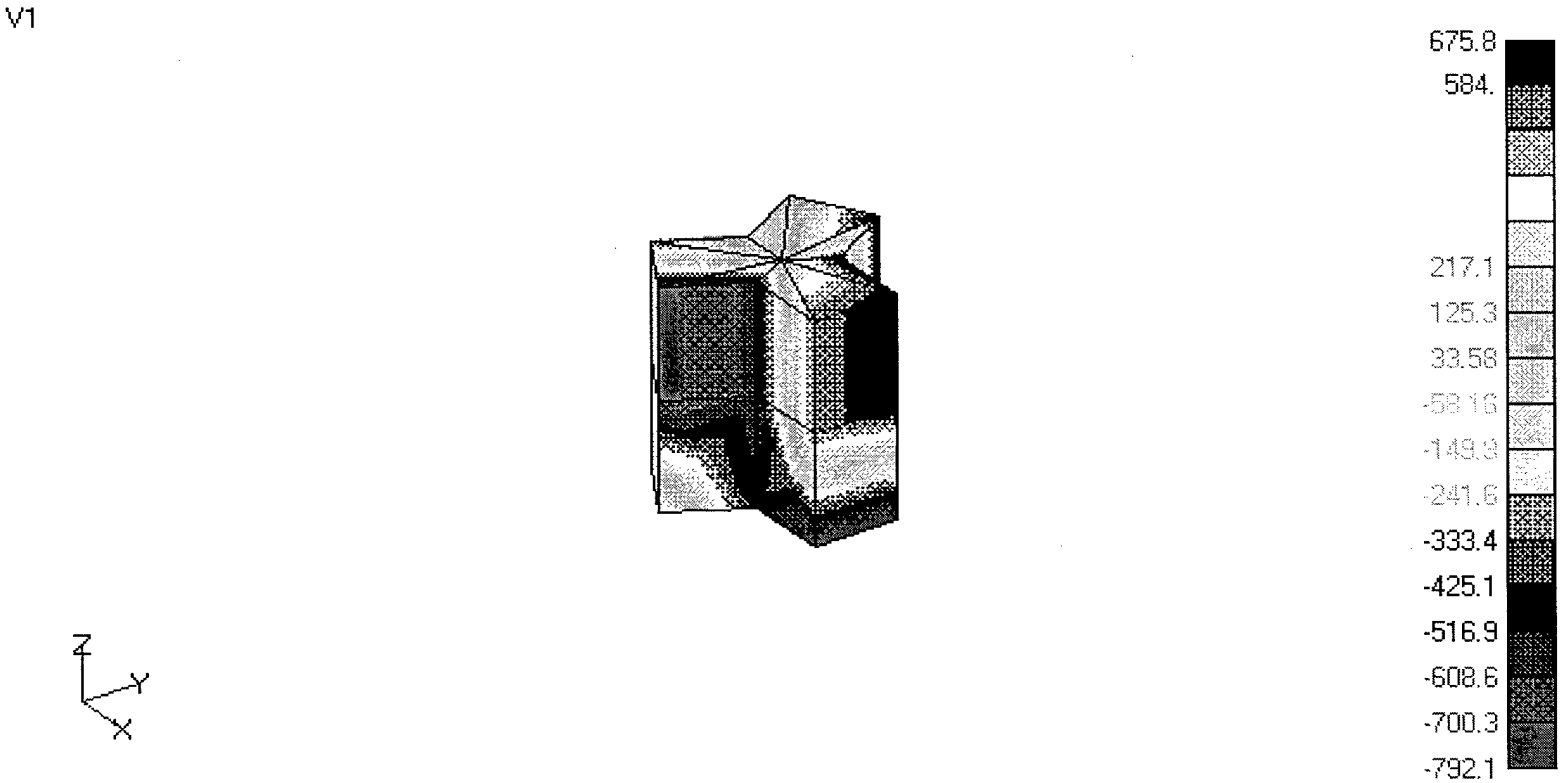

Horizontal Load = 300,000 lbs
Linear Elastic Soil, E = 5,000psf, $\nu = 0.499$
AISI 4340 Steel Pile

Figure-A13 Horizontal Displacements (Clover-shape with Three Leaves)

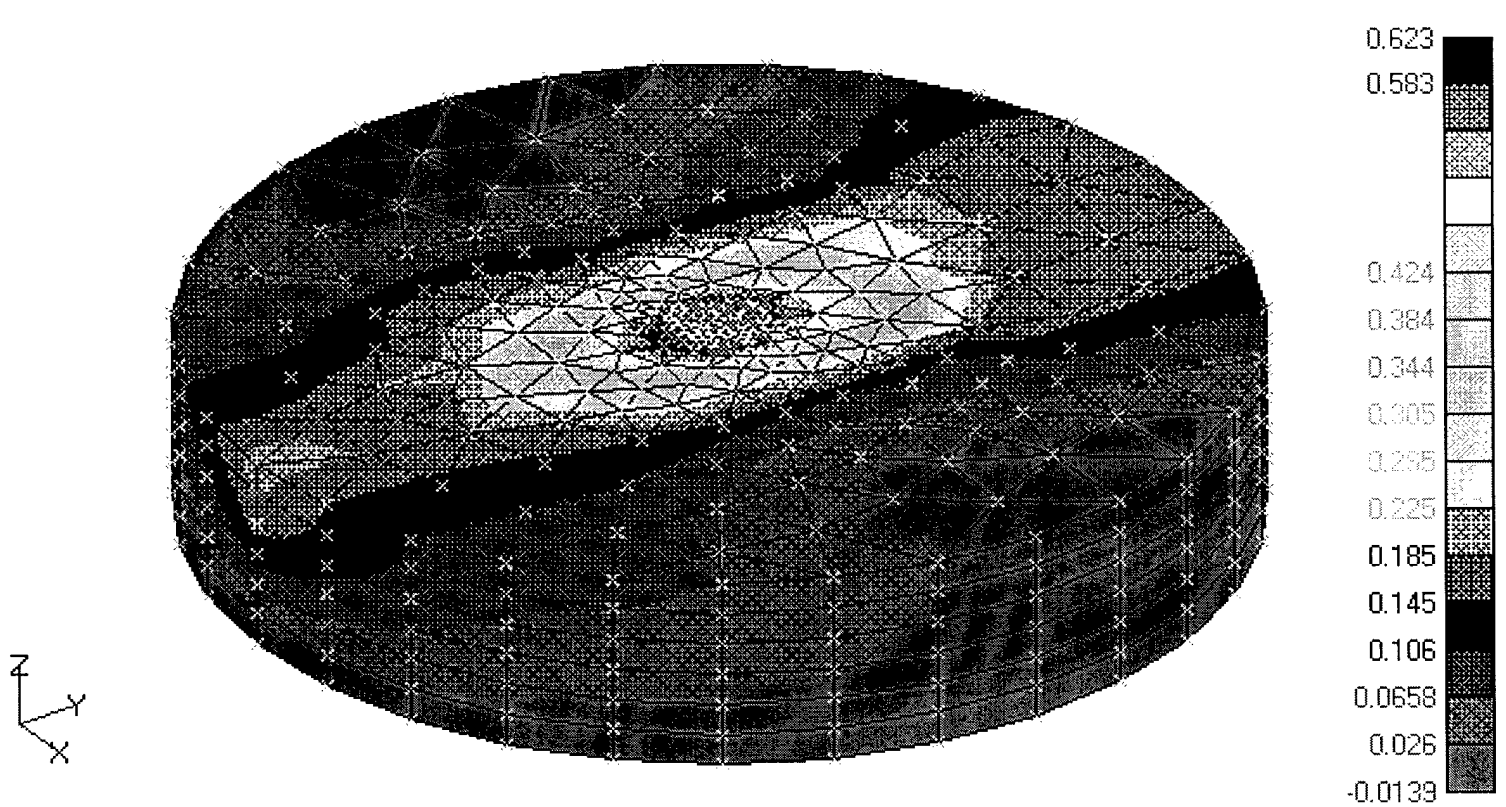

Horizontal Load = 300,000 lbs
Linear Elastic Soil, E = 5,000psf, ν = 0.499
AISI 4340 Steel Pile

Figure-A14 Horizontal Displacements on a Vertical Plane along the Horizontal Load Direction (Clover-shape with Three Leaves)

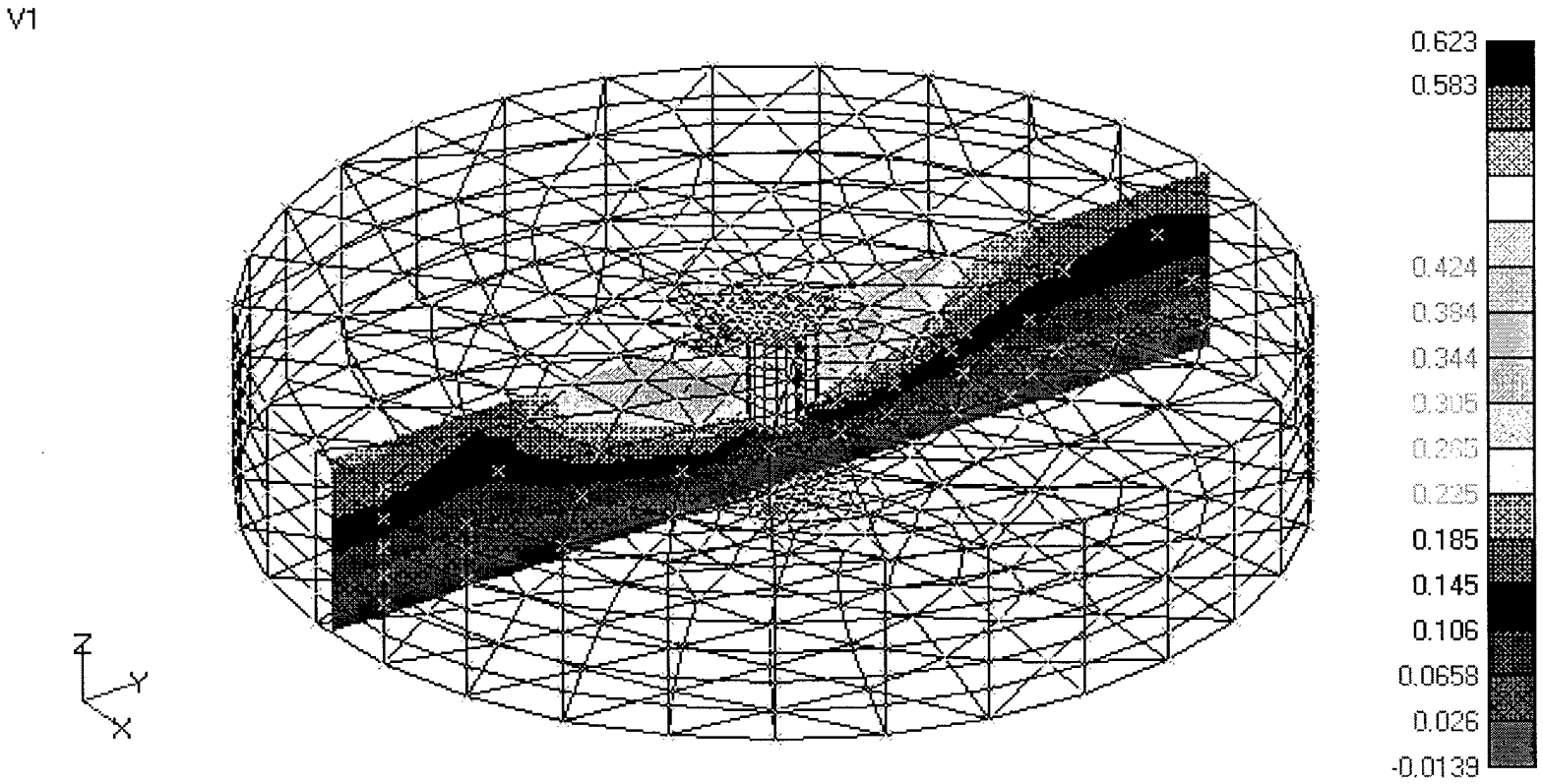

Horizontal Load = 300,000 lbs
Linear Elastic Soil, E = 5,000psf, $\nu = 0.499$
AISI 4340 Steel Pile

Figure-A15 Horizontal Normal Pile Stresses on the Pile Surface (Clover-shape with Three Leaves)

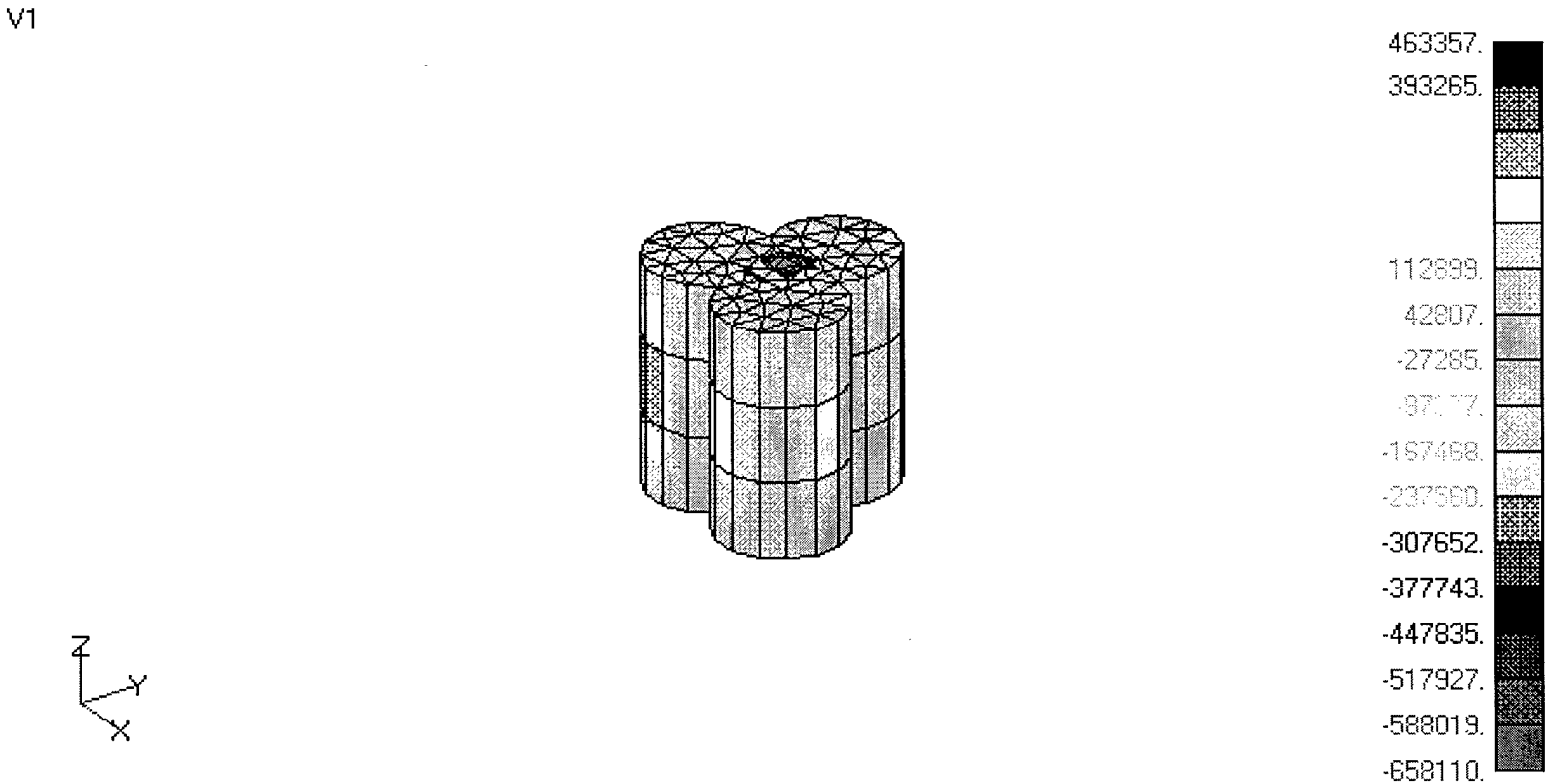

Horizontal Load = 300,000 lbs
Linear Elastic Soil, E = 5,000psf, ν = 0.499
AISI 4340 Steel Pile

Figure-A16 Horizontal Normal Soil Stresses on the Pile Surface (Clover-shape with Three Leaves)

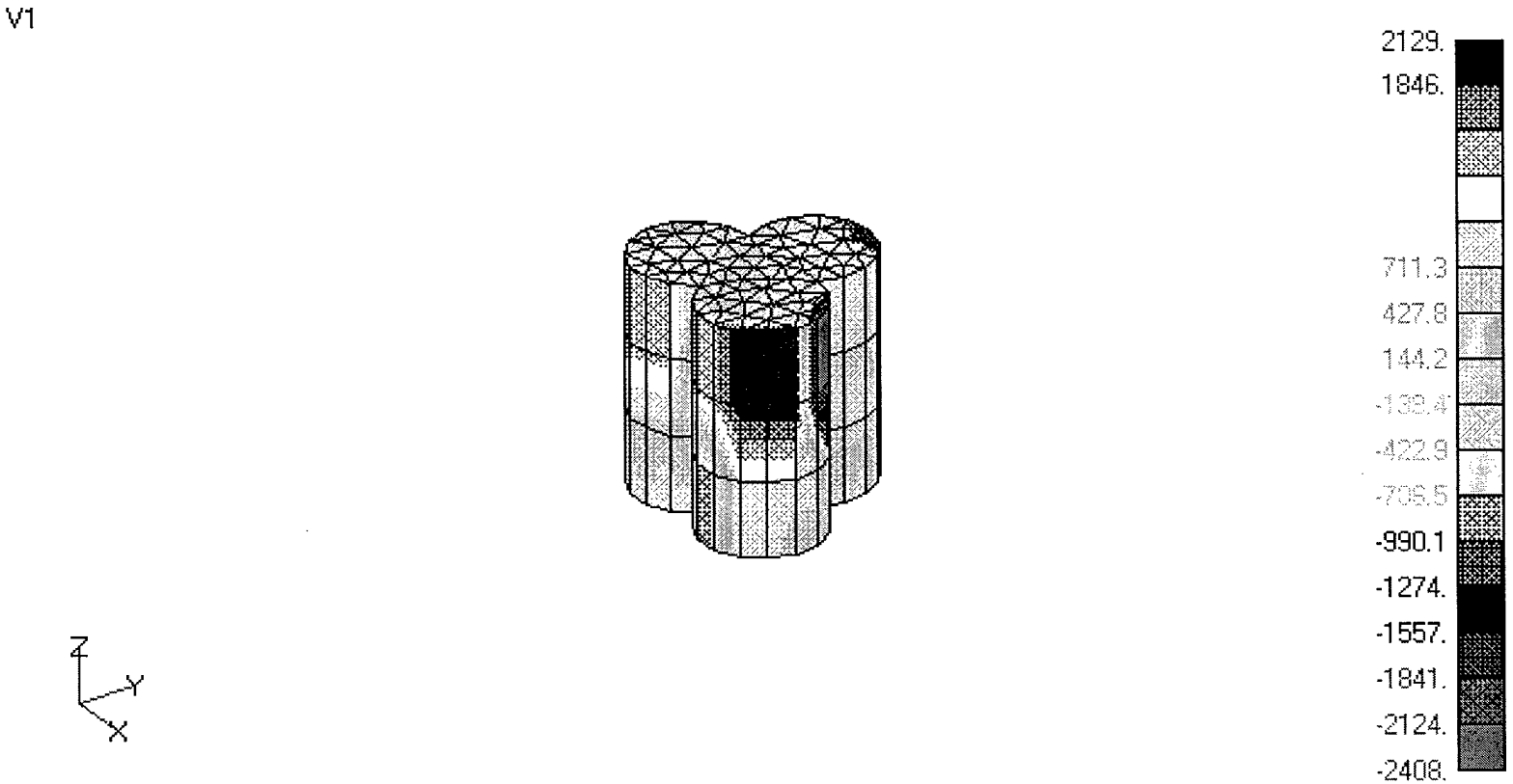

Horizontal Load = 300,000 lbs
Linear Elastic Soil, E = 5,000psf, ν = 0.499
AISI 4340 Steel Pile

Figure-A17 Pile Major Principal Stresses on the Pile Surface (Clover-shape with Three Leaves)

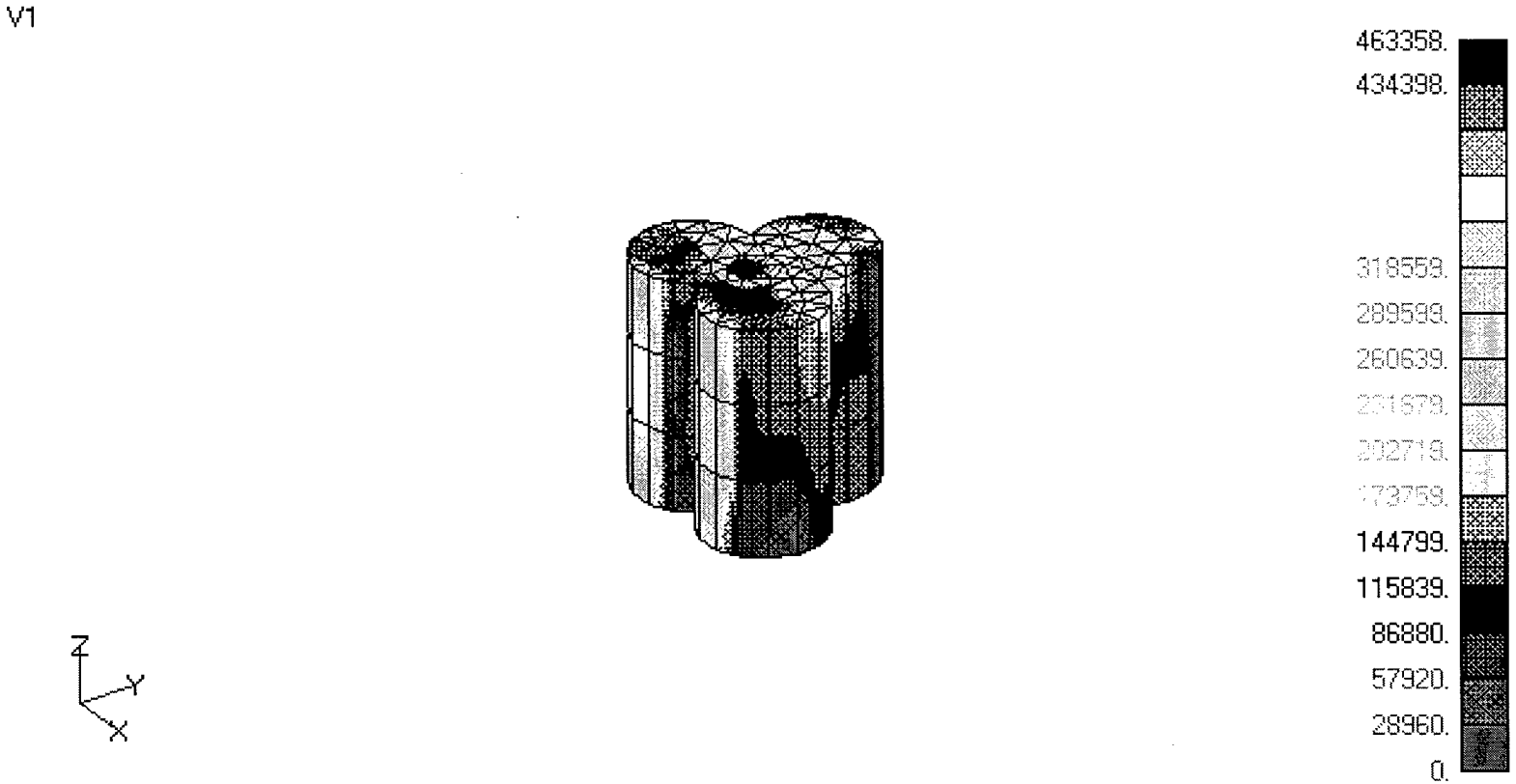

Horizontal Load = 300,000 lbs
Linear Elastic Soil, E = 5,000psf, ν = 0.499
AISI 4340 Steel Pile

Figure-A18 Soil Minor Principal Stresses on the Pile Surface (Clover-shape with Three Leaves)

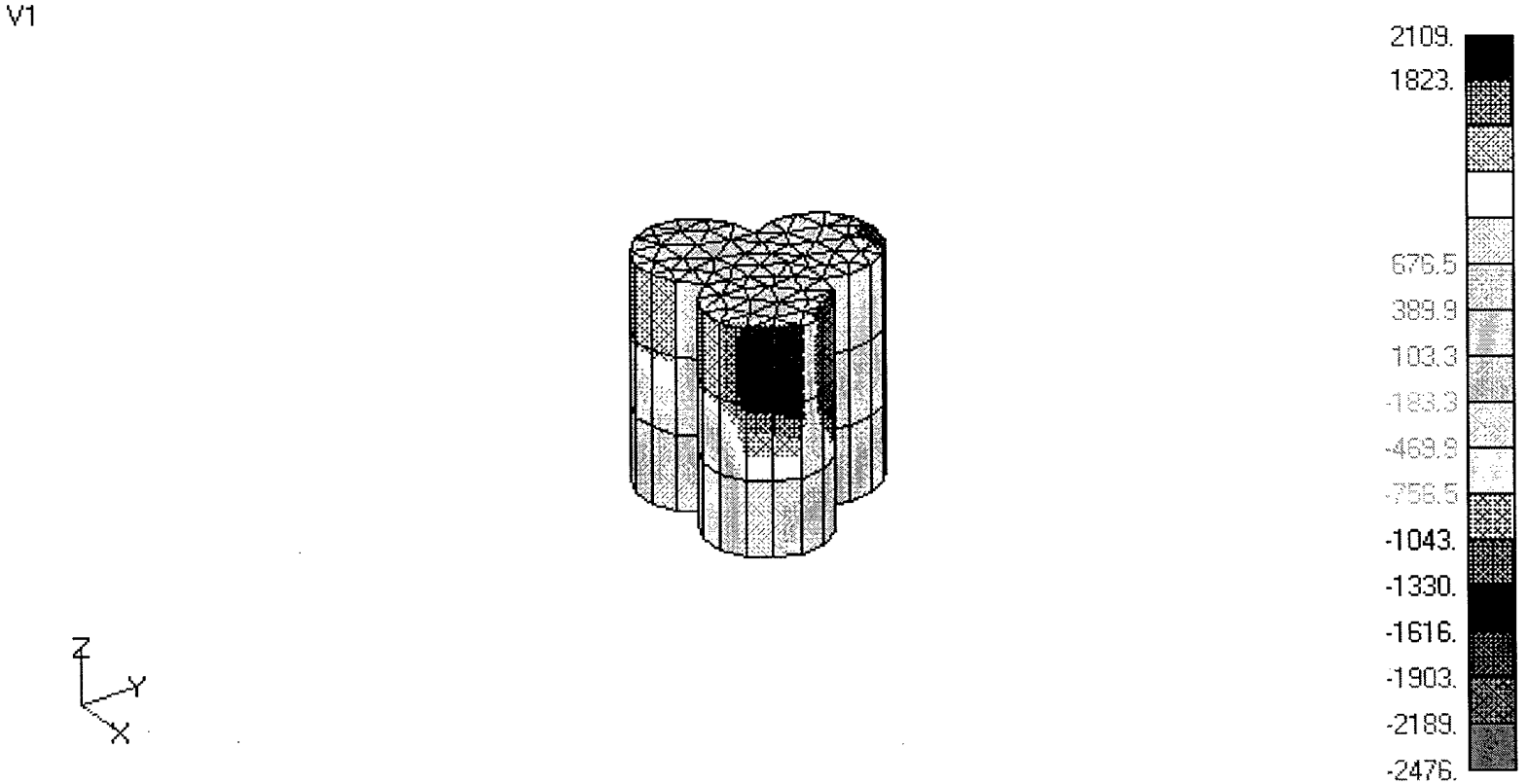

Horizontal Load = 300,000 lbs
Linear Elastic Soil, E = 5,000psf, $\nu = 0.499$
AISI 4340 Steel Pile

Figure-A19 Horizontal Displacements (Clustered Circle with Four Cells)

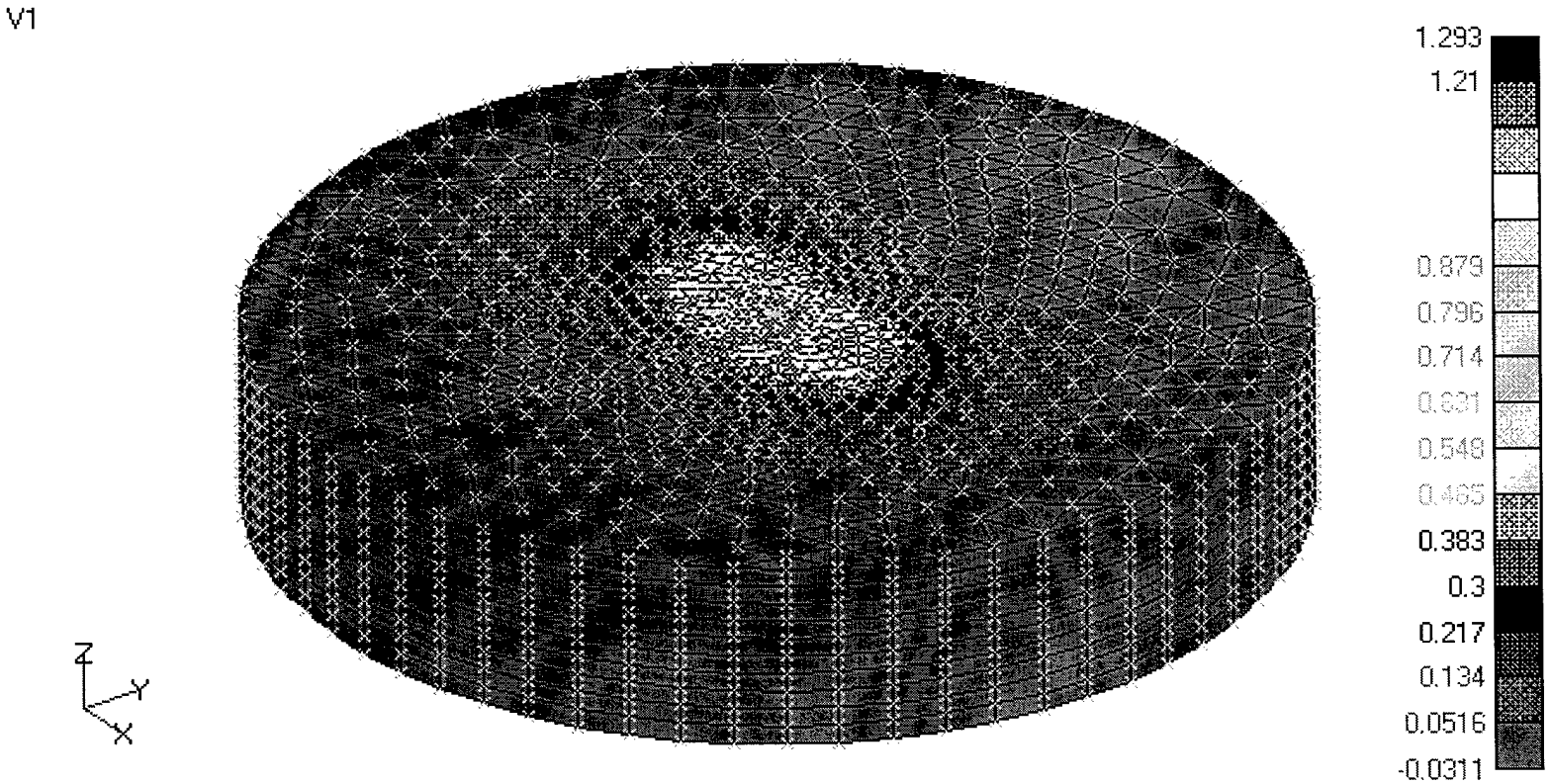

Horizontal Load = 300,000 lbs
Linear Elastic Soil, E = 5,000psf, $\nu = 0.499$
AISI 4340 Steel Pile

Figure-A20 Horizontal Displacements on a Vertical Plane along Horizontal Load Direction (Clustered Circle with Four Cells)

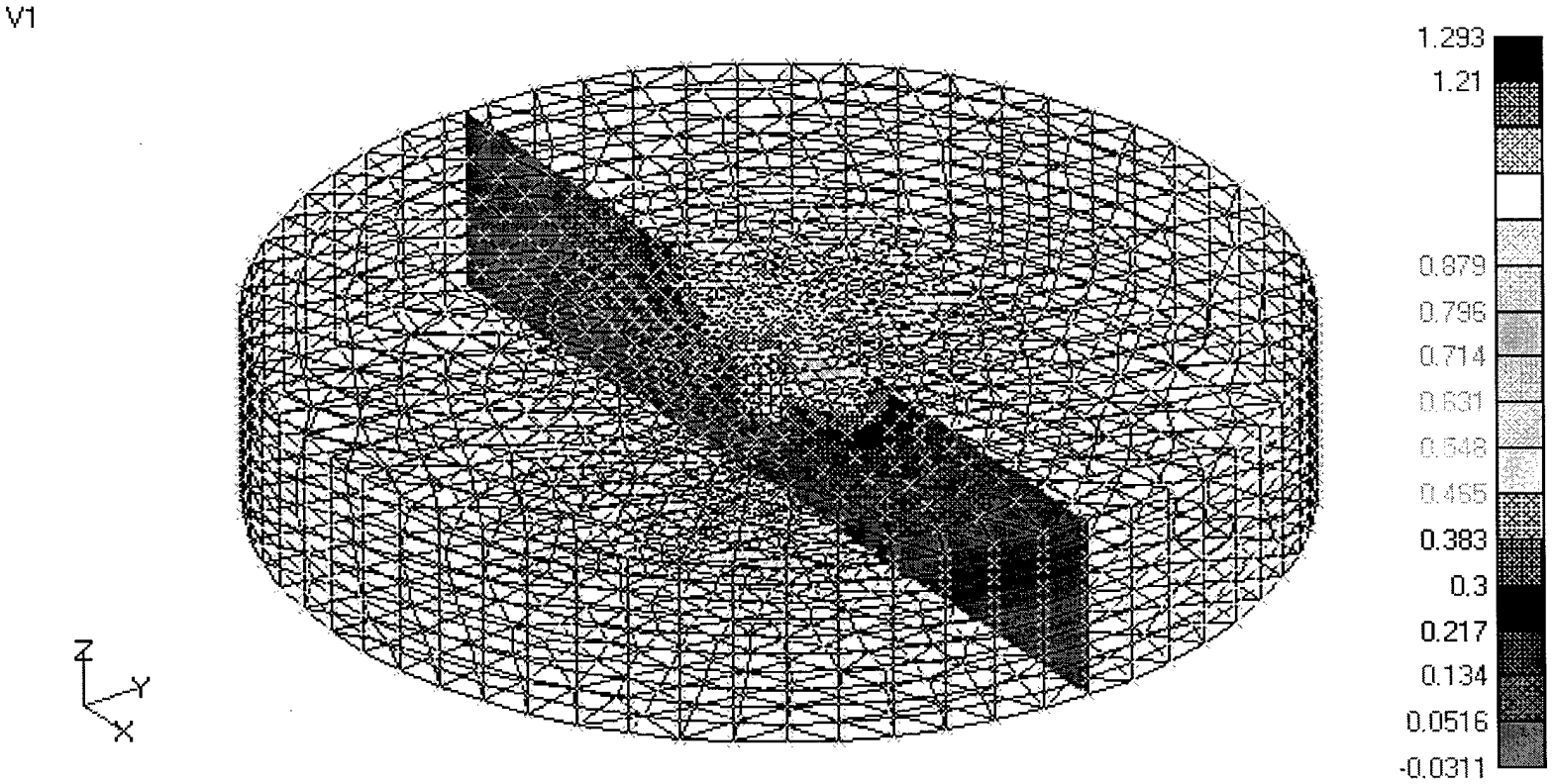

Horizontal Load = 300,000 lbs
Linear Elastic Soil, E = 5,000psf, ν = 0.499
AISI 4340 Steel Pile

Figure-A21 Horizontal Normal Pile Stresses on the Pile Surface (Clustered Circle with Four Cells)

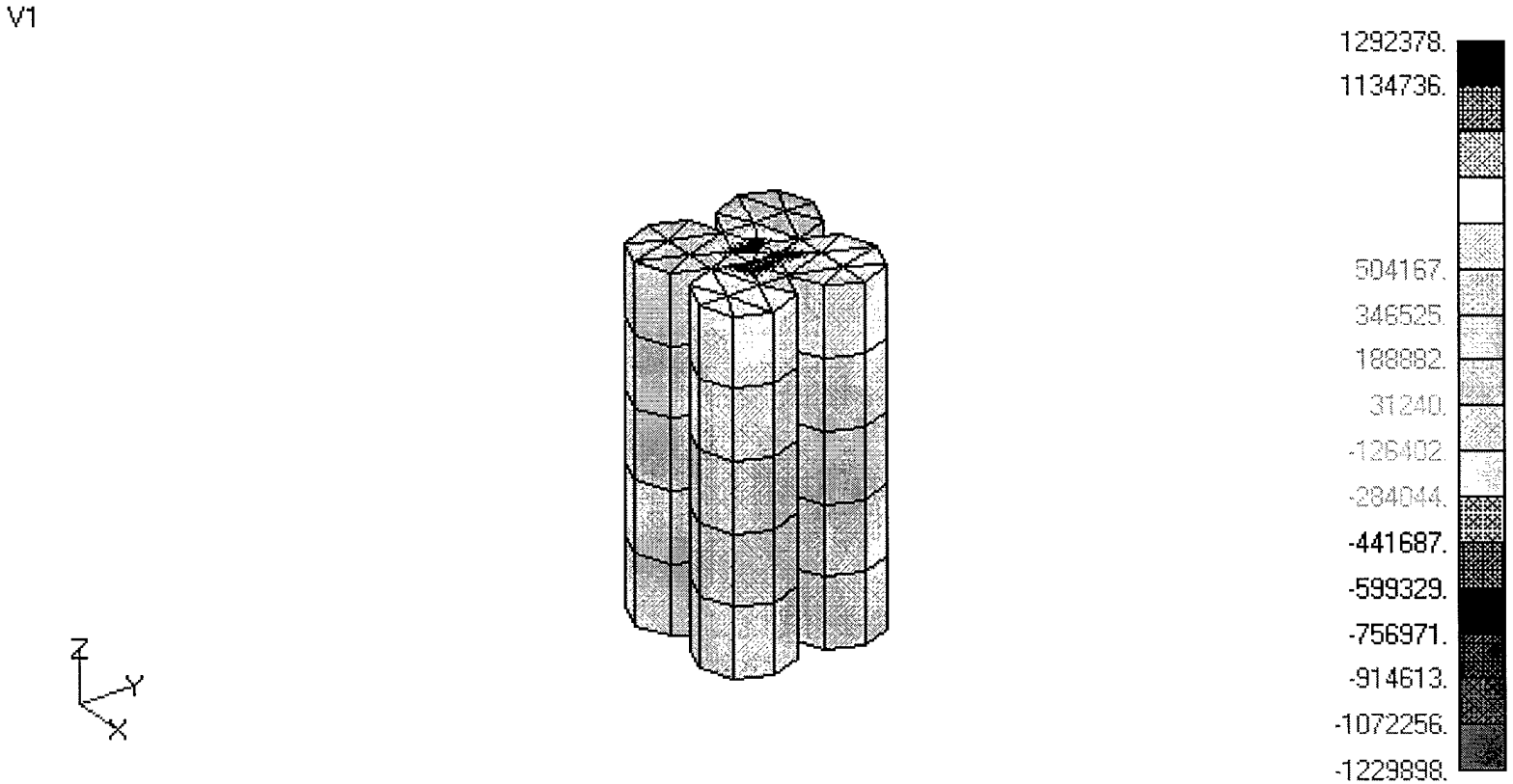

Horizontal Load = 300,000 lbs
Linear Elastic Soil, E = 5,000psf, $\nu = 0.499$
AISI 4340 Steel Pile

Figure-A22 Horizontal Normal Soil Stresses on the Pile Surface (Clustered Circle with Four Cells)

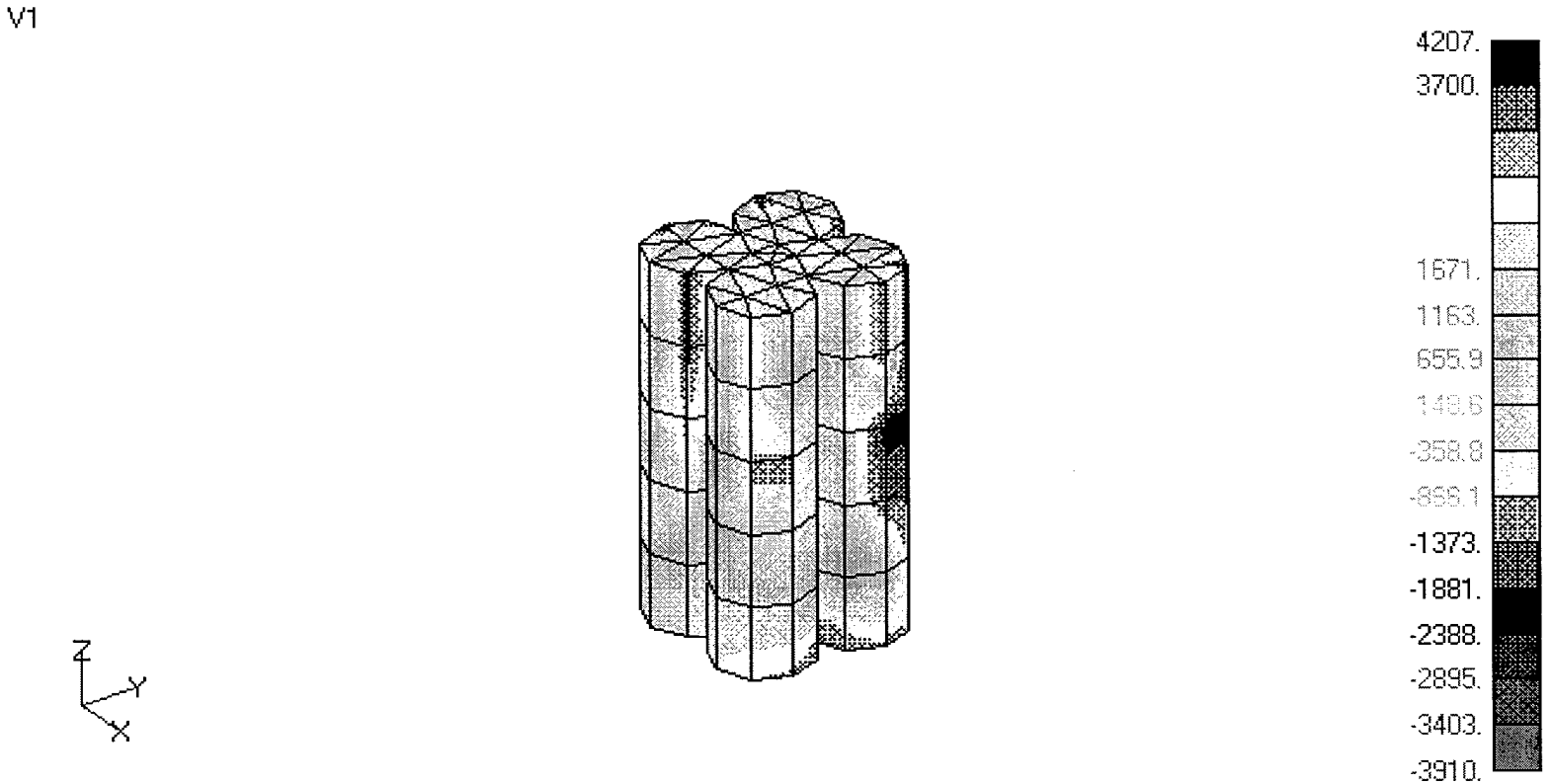

Horizontal Load = 300,000 lbs
Linear Elastic Soil, E = 5,000psf, ν = 0.499
AISI 4340 Steel Pile

Figure-A23 Pile Major Principal Stresses on the Pile Top Surface (Clustered Circle with Four Cells)

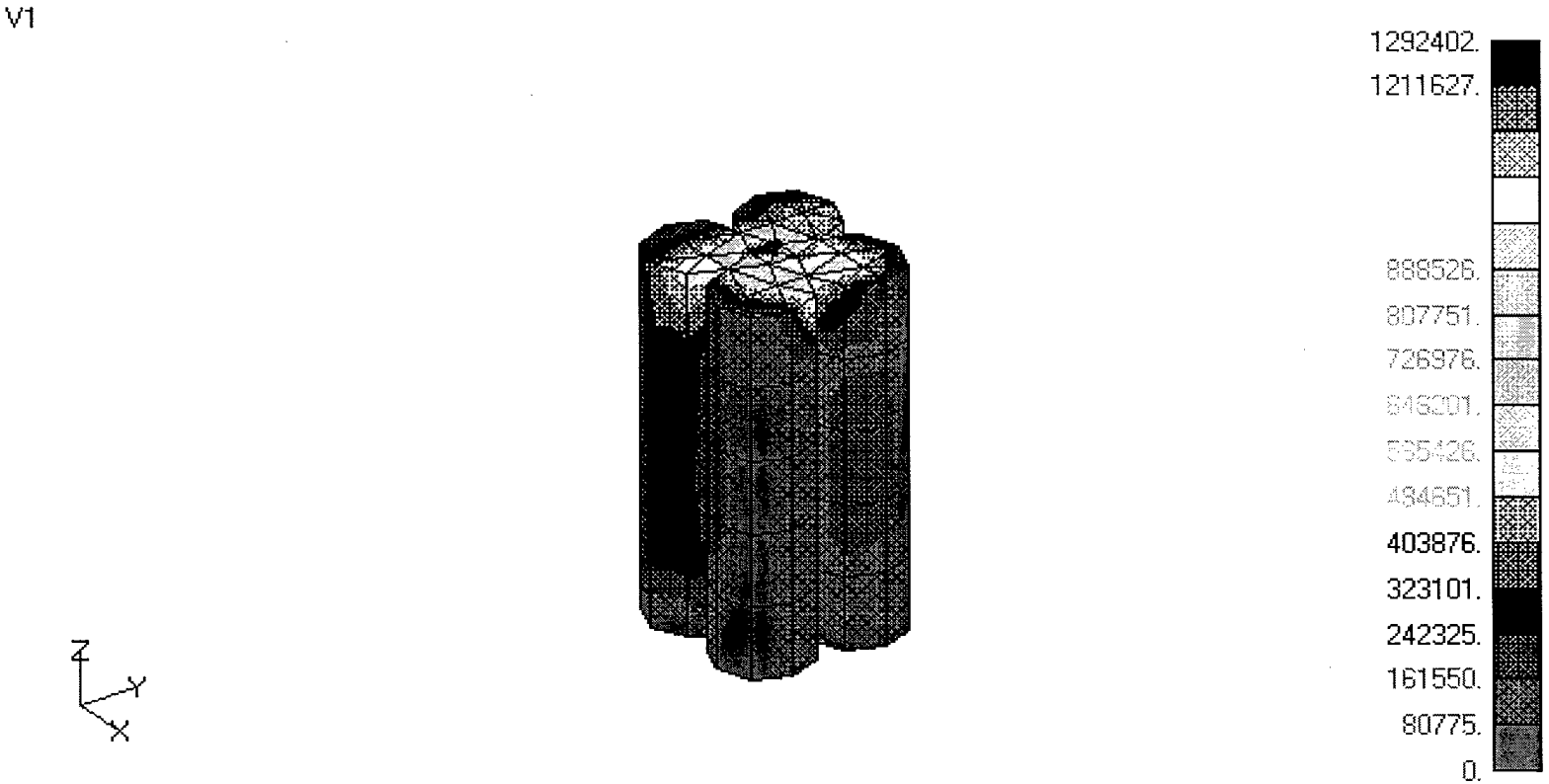

Horizontal Load = 300,000 lbs
Linear Elastic Soil, E = 5,000psf, ν = 0.499
AISI 4340 Steel Pile

Figure-A24 Soil Minor Principal Stresses on the Pile Surface (Clustered Circle with Four Cells)

V1

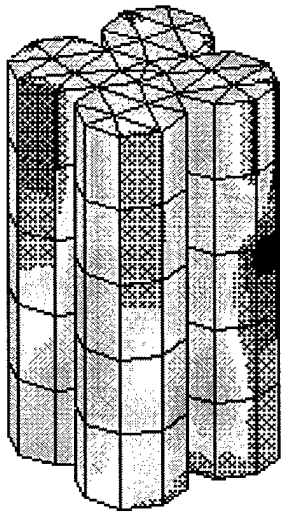

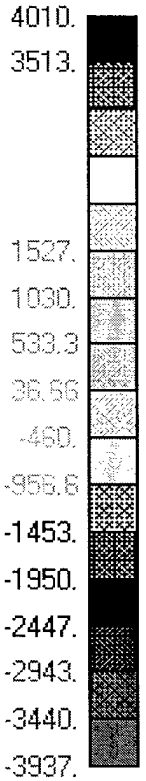

Horizontal Load = 300,000 lbs
Linear Elastic Soil, E = 5,000psf, ν = 0.499
AISI 4340 Steel Pile

Figure-B1. Horizontal Displacements (Circular Section)

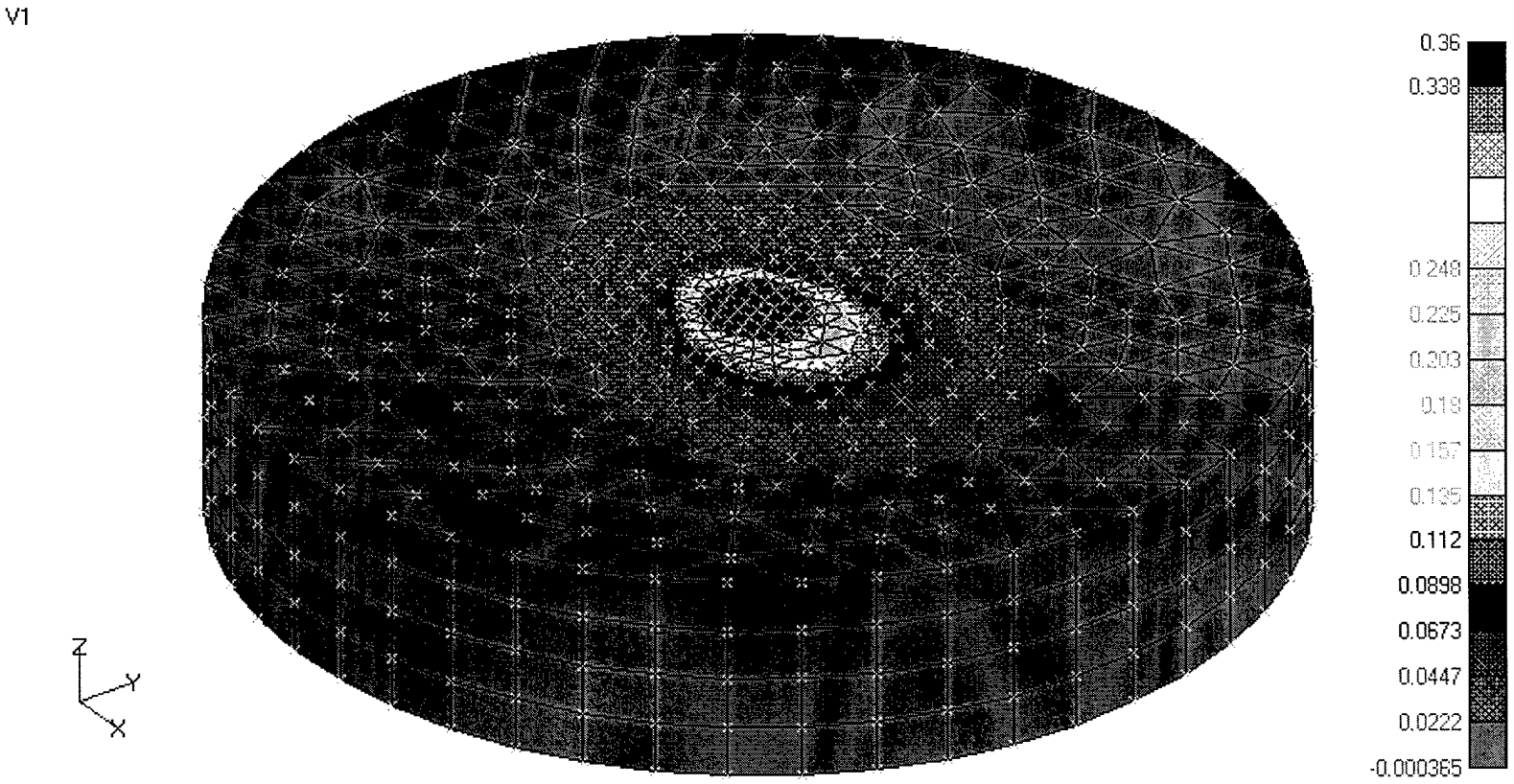

Horizontal Load = 7,000,000 lbs
Linear Elastic-Perfectly Plastic Sandy Soil (Linear Extended Drucker-Prager)
E = 864,000 psf, $\upsilon = 0.3$, Slope Angle = 42.6°, Dilation Angle = 21.5°
Pile, AISI 4340 Steel

Figure-B2. Horizontal Displacements on a Vertical Plane along the Horizontal Load Direction (Circular Section)

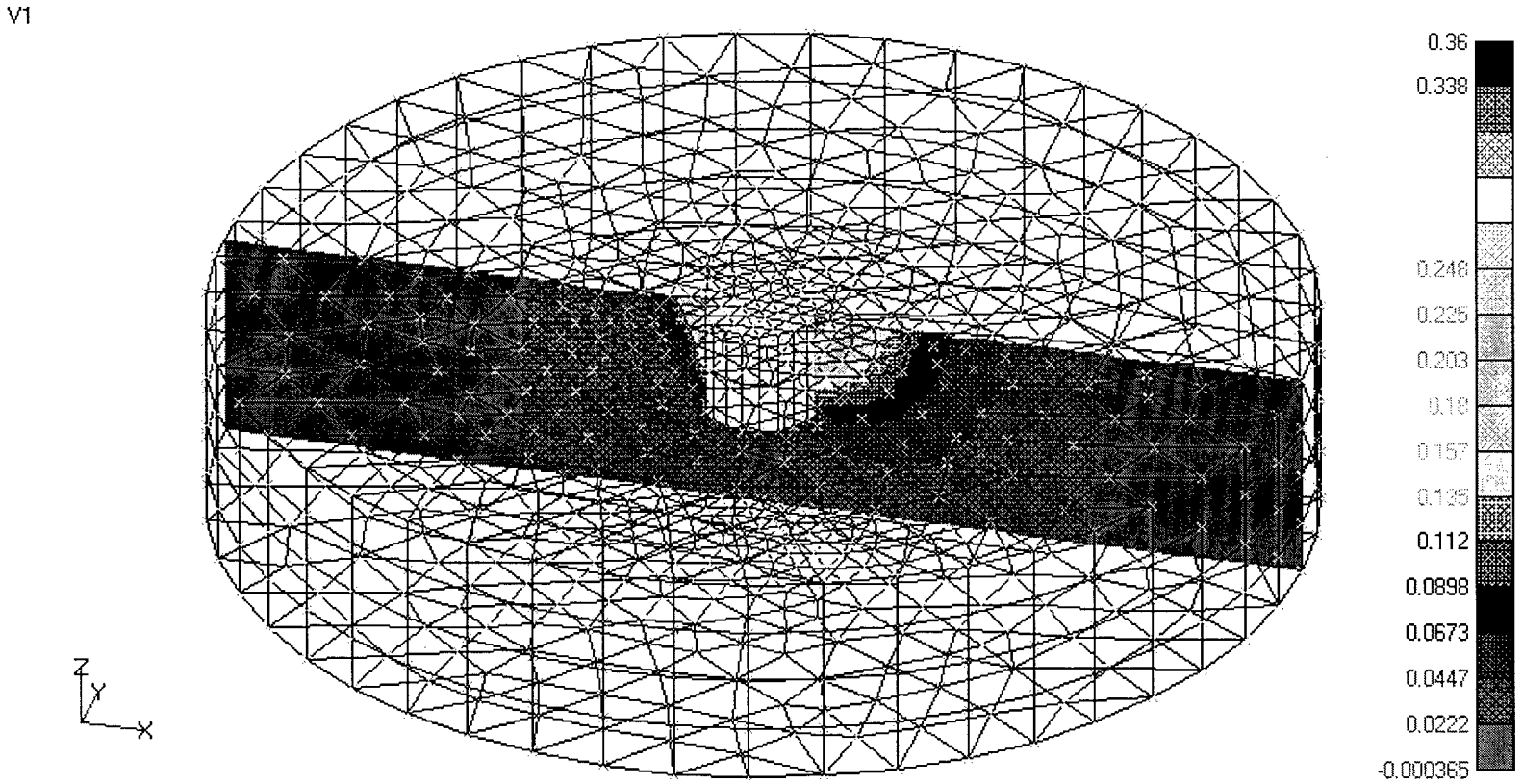

Horizontal Load = 7,000,000 lbs
Linear Elastic-Perfectly Plastic Sandy Soil (Linear Extended Drucker-Prager)
E = 864,000 psf, $\upsilon = 0.3$, Slope Angle = 42.6°, Dilation Angle = 21.5°
Pile, AISI 4340 Steel

Figure-B3. Pile Total Displacements (Circular Section)

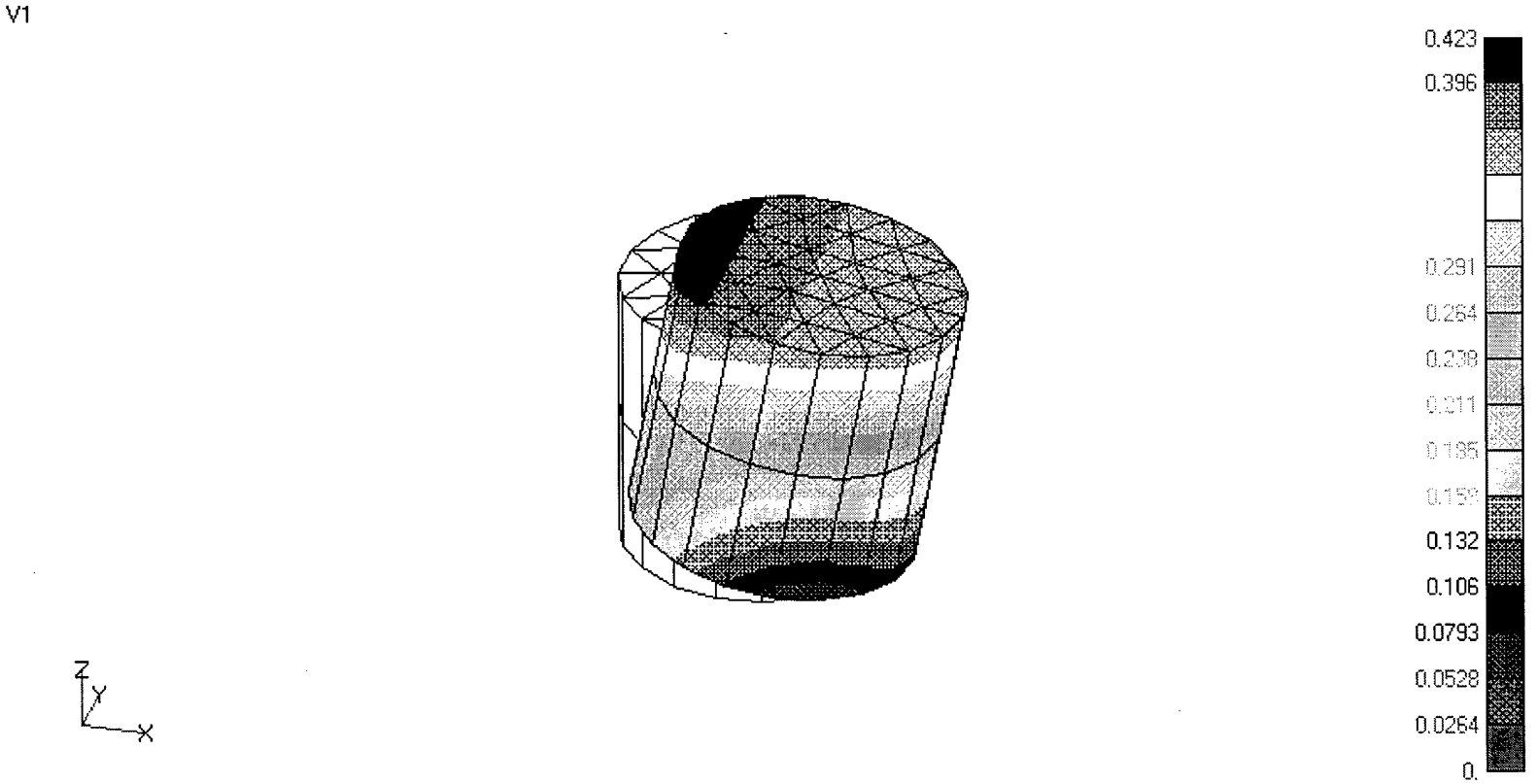

Horizontal Load = 7,000,000 lbs
Linear Elastic-Perfectly Plastic Sandy Soil (Linear Extended Drucker-Prager)
E = 864,000 psf, $\upsilon = 0.3$, Slope Angle = 42.6°, Dilation Angle = 21.5°
Pile, AISI 4340 Steel

Figure-B4. Soil Minor Principal Stresses (Circular Section)

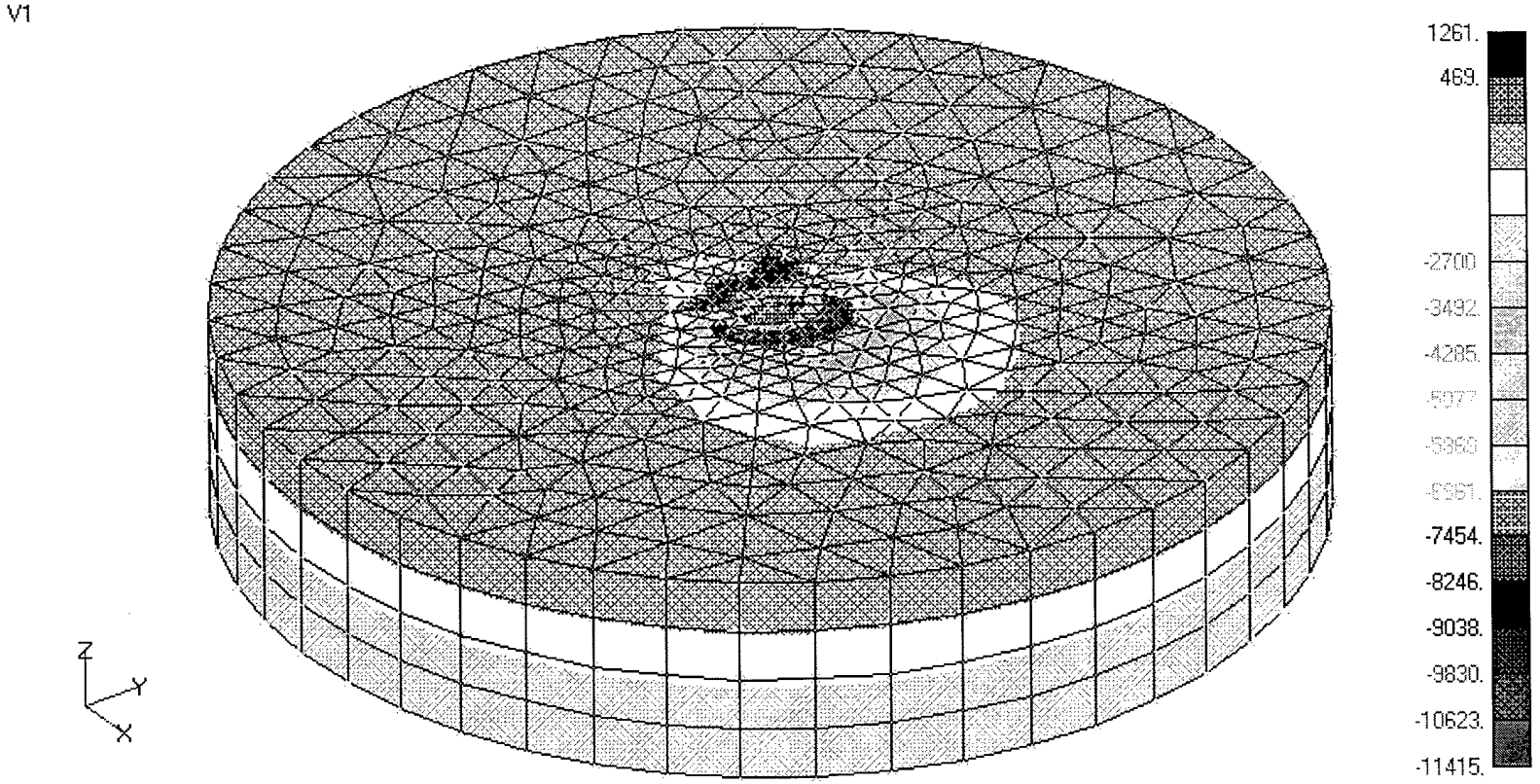

Horizontal Load = 7,000,000 lbs
Linear Elastic-Perfectly Plastic Sandy Soil (Linear Extended Drucker-Prager)
E = 864,000 psf, $\upsilon = 0.3$, Slope Angle = 42.6°, Dilation Angle = 21.5°
Pile, AISI 4340 Steel

Figure-B5. Soil Minor Principal Stresses on a Vertical Plane along the Horizontal Load Direction (Circular Section)

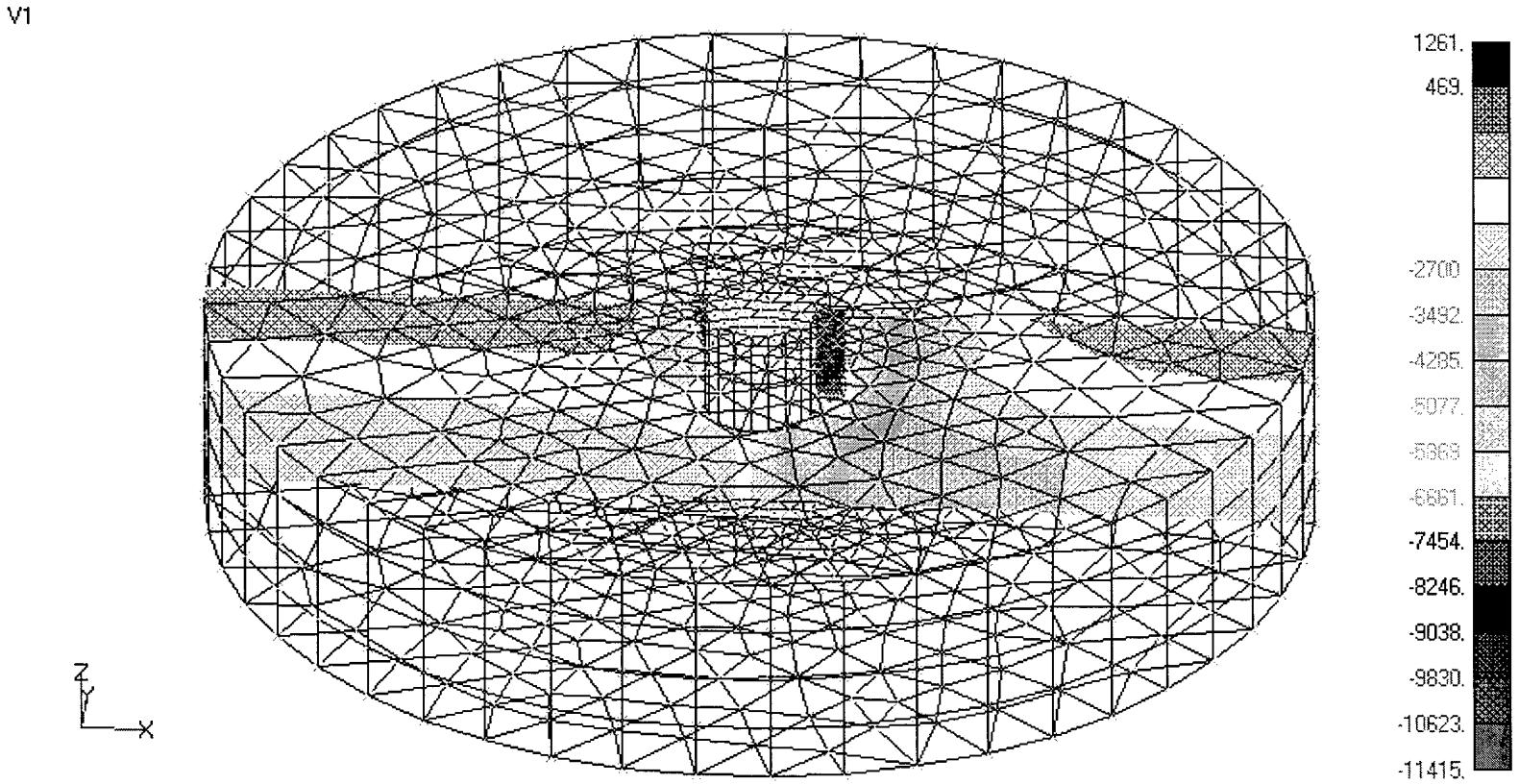

Horizontal Load = 7,000,000 lbs
Linear Elastic-Perfectly Plastic Sandy Soil (Linear Extended Drucker-Prager)
E = 864,000 psf, υ = 0.3, Slope Angle = 42.6°, Dilation Angle = 21.5°
Pile, AISI 4340 Steel

Figure-B6. Horizontal Normal Pile Stresses on the Pile Surface (Circular Section)

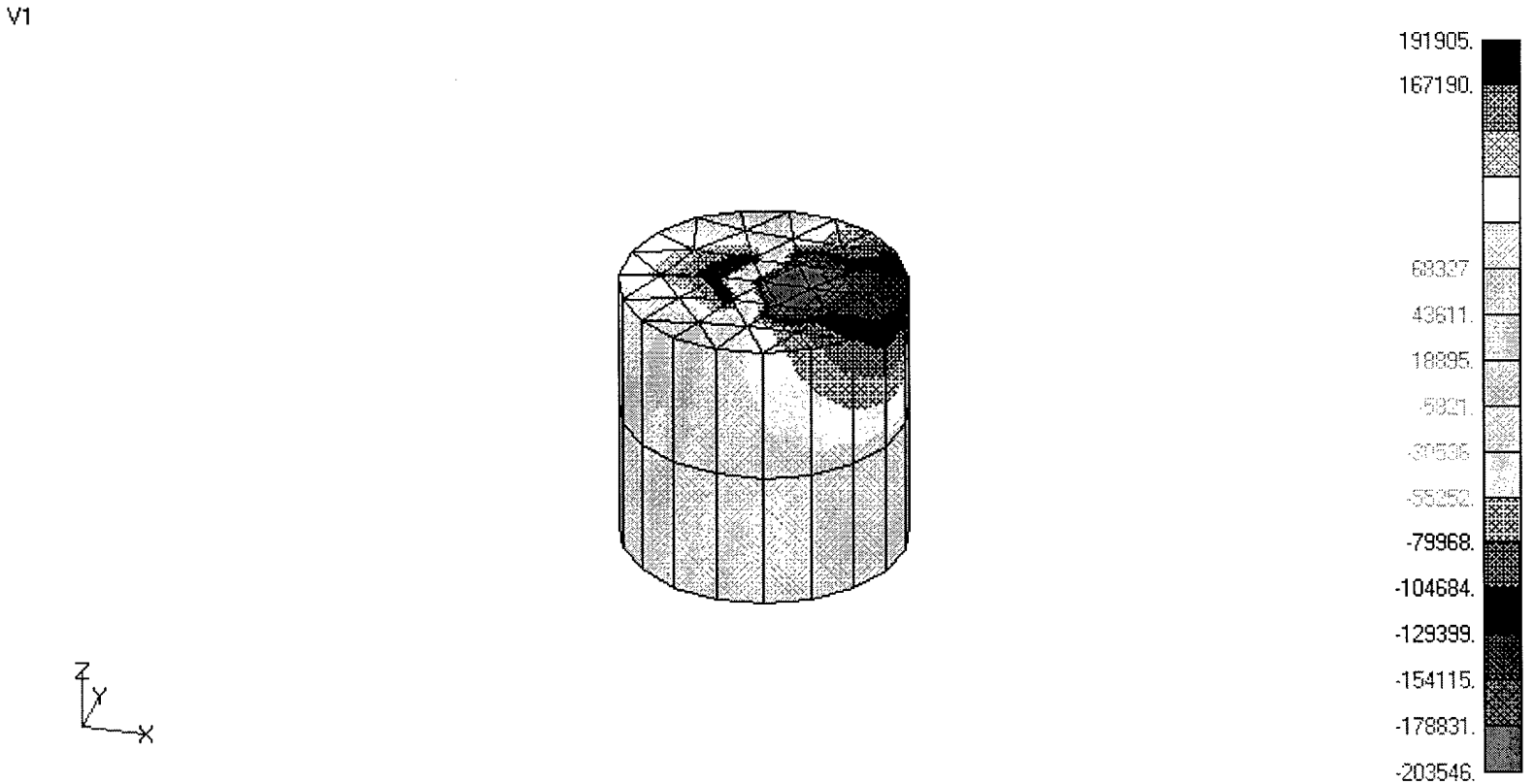

Horizontal Load = 7,000,000 lbs
Linear Elastic-Perfectly Plastic Sandy Soil (Linear Extended Drucker-Prager)
E = 864,000 psf, υ = 0.3, Slope Angle = 42.6°, Dilation Angle = 21.5°
Pile, AISI 4340 Steel

Figure-B7. Pile von Mises Stresses on the Pile Surface (Circular Section)

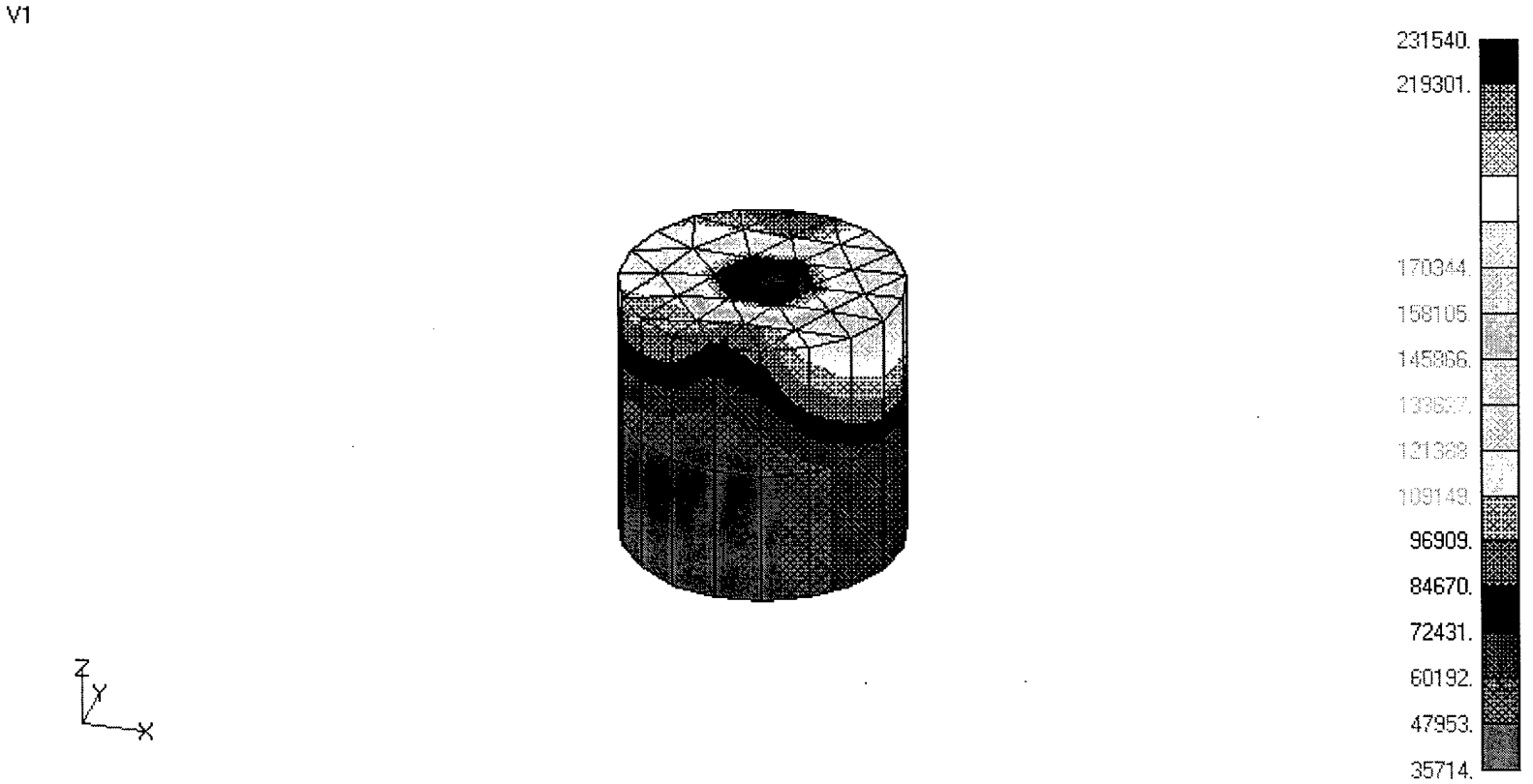

Horizontal Load = 7,000,000 lbs
Linear Elastic-Perfectly Plastic Sandy Soil (Linear Extended Drucker-Prager)
E = 864,000 psf, υ = 0.3, Slope Angle = 42.6°, Dilation Angle = 21.5°
Pile, AISI 4340 Steel

Figure-B8. Vertical Displacements (Circular Section)

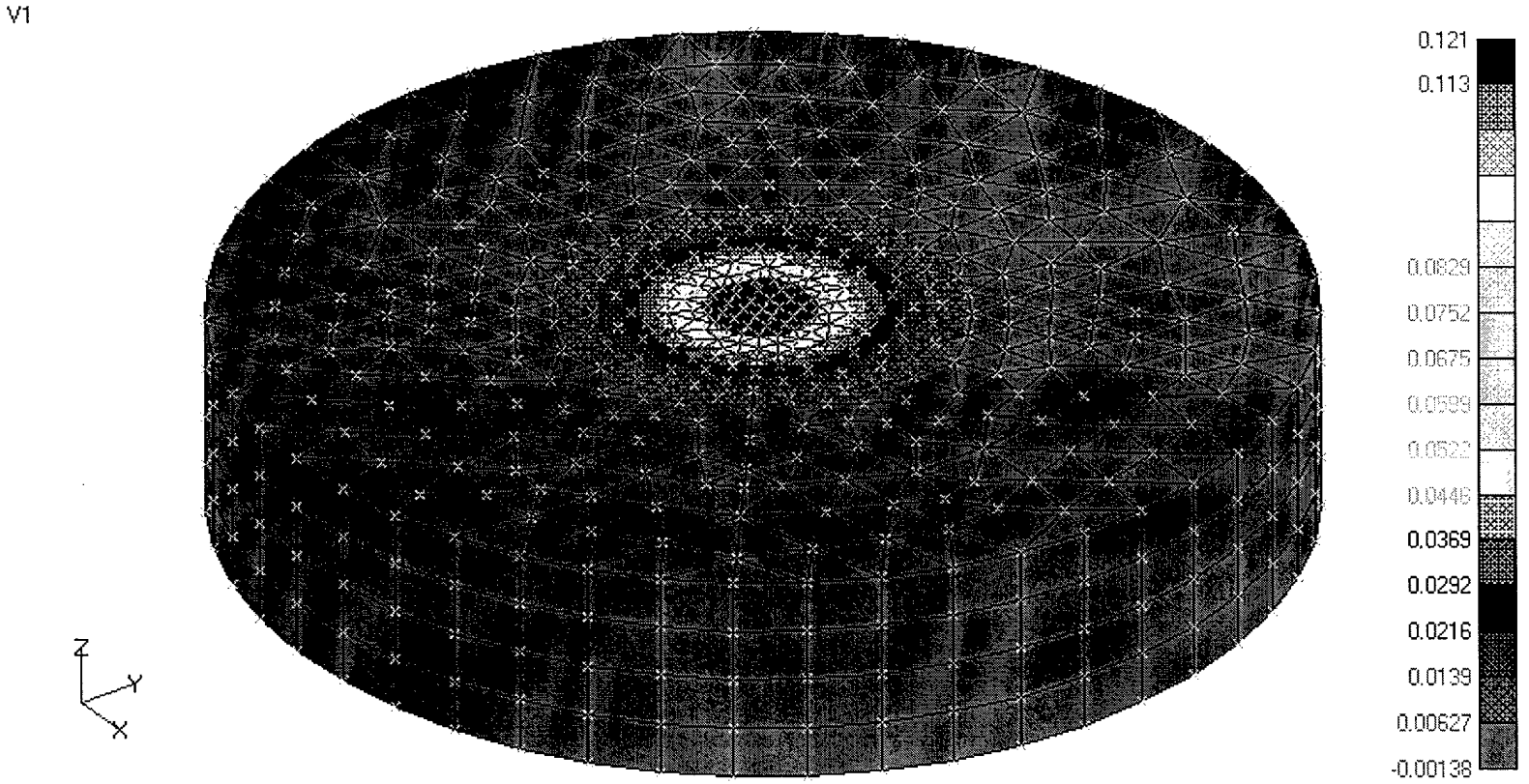

Vertical Load = 7,000,000 lbs
Linear Elastic-Perfectly Plastic Sandy Soil (Linear Extended Drucker-Prager)
E = 864,000 psf, $\upsilon = 0.3$, Slope Angle = 42.6°, Dilation Angle = 21.5°
Pile, AISI 4340 Steel

Figure-B9. Vertical Displacements on a Vertical Plane (Circular Section)

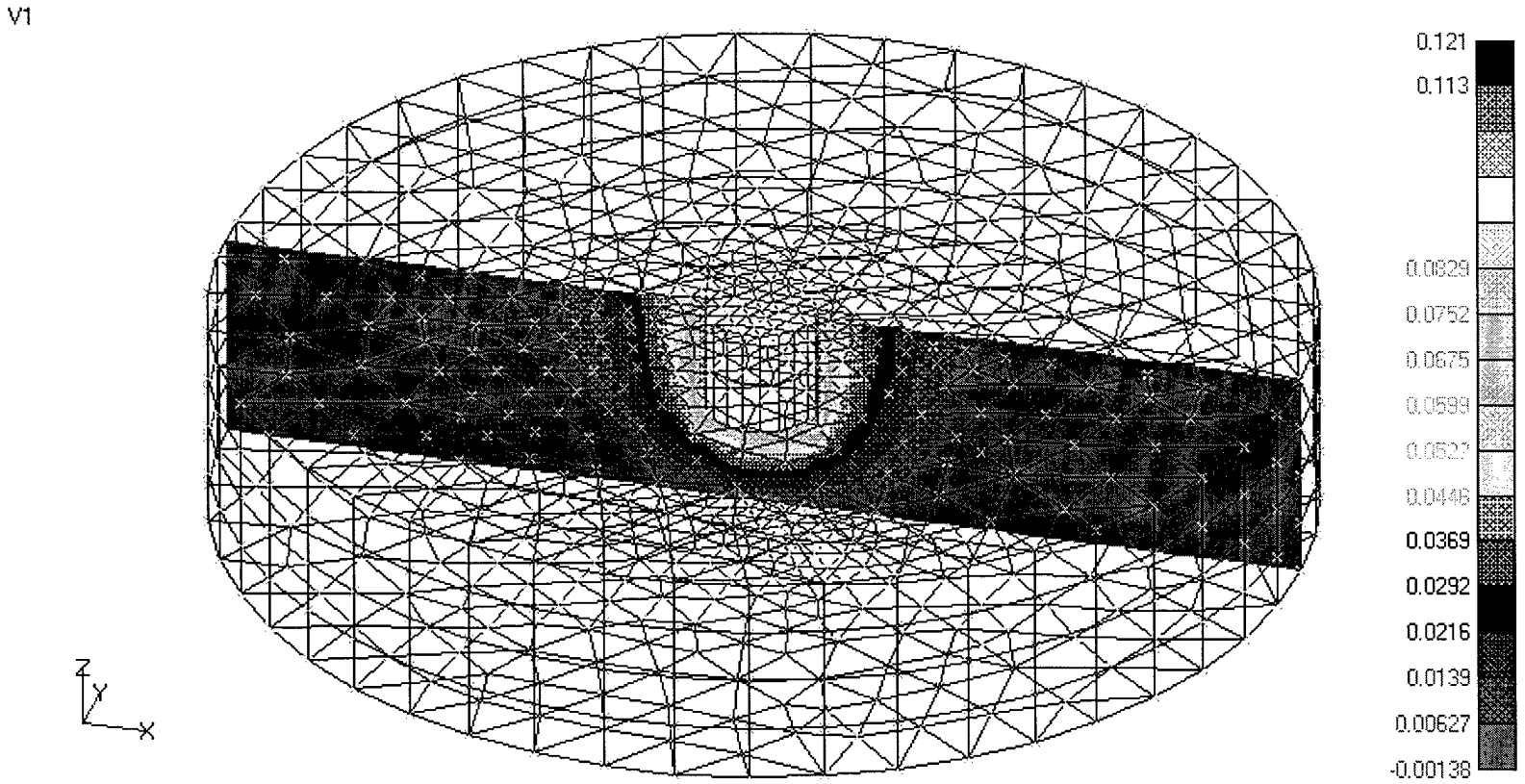

Vertical Load = 7,000,000 lbs
Linear Elastic-Perfectly Plastic Sandy Soil (Linear Extended Drucker-Prager)
E = 864,000 psf, $\upsilon = 0.3$, Slope Angle = 42.6°, Dilation Angle = 21.5°
Pile, AISI 4340 Steel

Figure-B10. Pile Vertical Displacements (Circular Section)

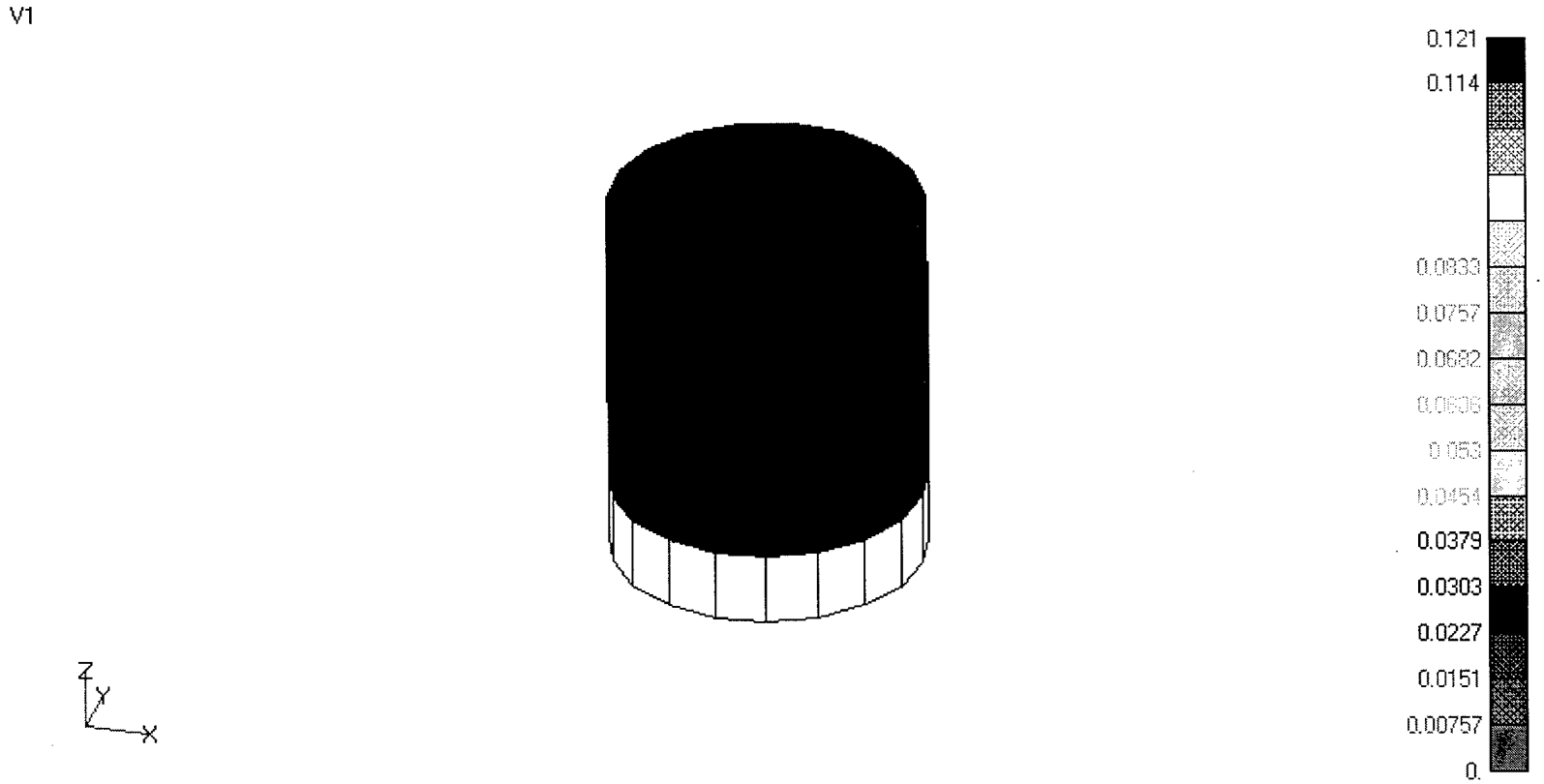

Vertical Load = 7,000,000 lbs
Linear Elastic-Perfectly Plastic Sandy Soil (Linear Extended Drucker-Prager)
E = 864,000 psf, $\upsilon = 0.3$, Slope Angle = 42.6°, Dilation Angle = 21.5°
Pile, AISI 4340 Steel

Figure-B11. Soil Minor Principal Stresses (Circular Section)

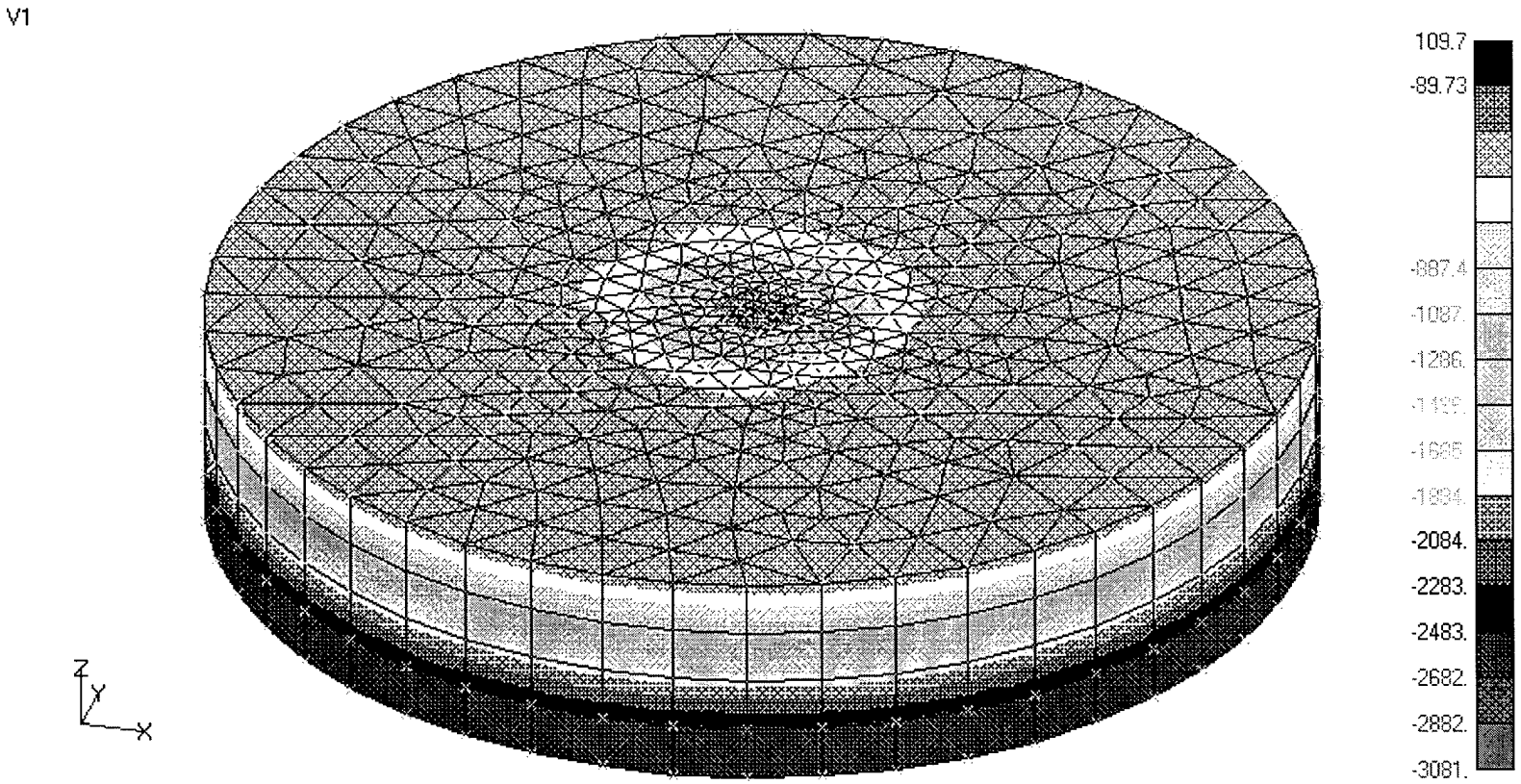

Vertical Load = 7,000,000 lbs
Linear Elastic-Perfectly Plastic Sandy Soil (Linear Extended Drucker-Prager)
E = 864,000 psf, $\upsilon = 0.3$, Slope Angle = 42.6°, Dilation Angle = 21.5°
Pile, AISI 4340 Steel

Figure-B12. Soil Minor Principal Stresses on a Vertical Plane (Circular Section)

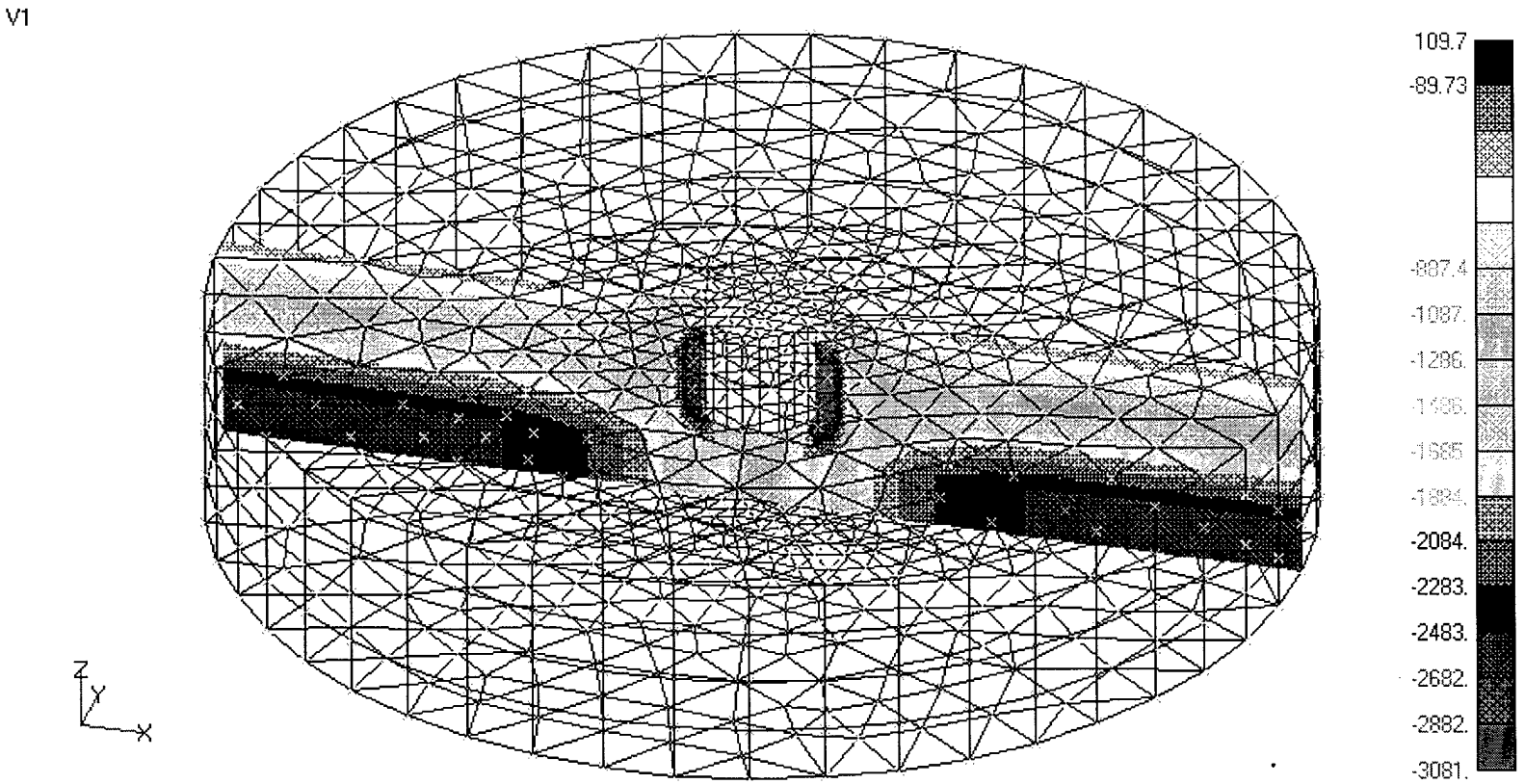

Vertical Load = 7,000,000 lbs
Linear Elastic-Perfectly Plastic Sandy Soil (Linear Extended Drucker-Prager)
E = 864,000 psf, $\upsilon = 0.3$, Slope Angle = 42.6°, Dilation Angle = 21.5°
Pile, AISI 4340 Steel

Figure-B13. Pile von Mises Stresses on the Pile Surface (Circular Section)

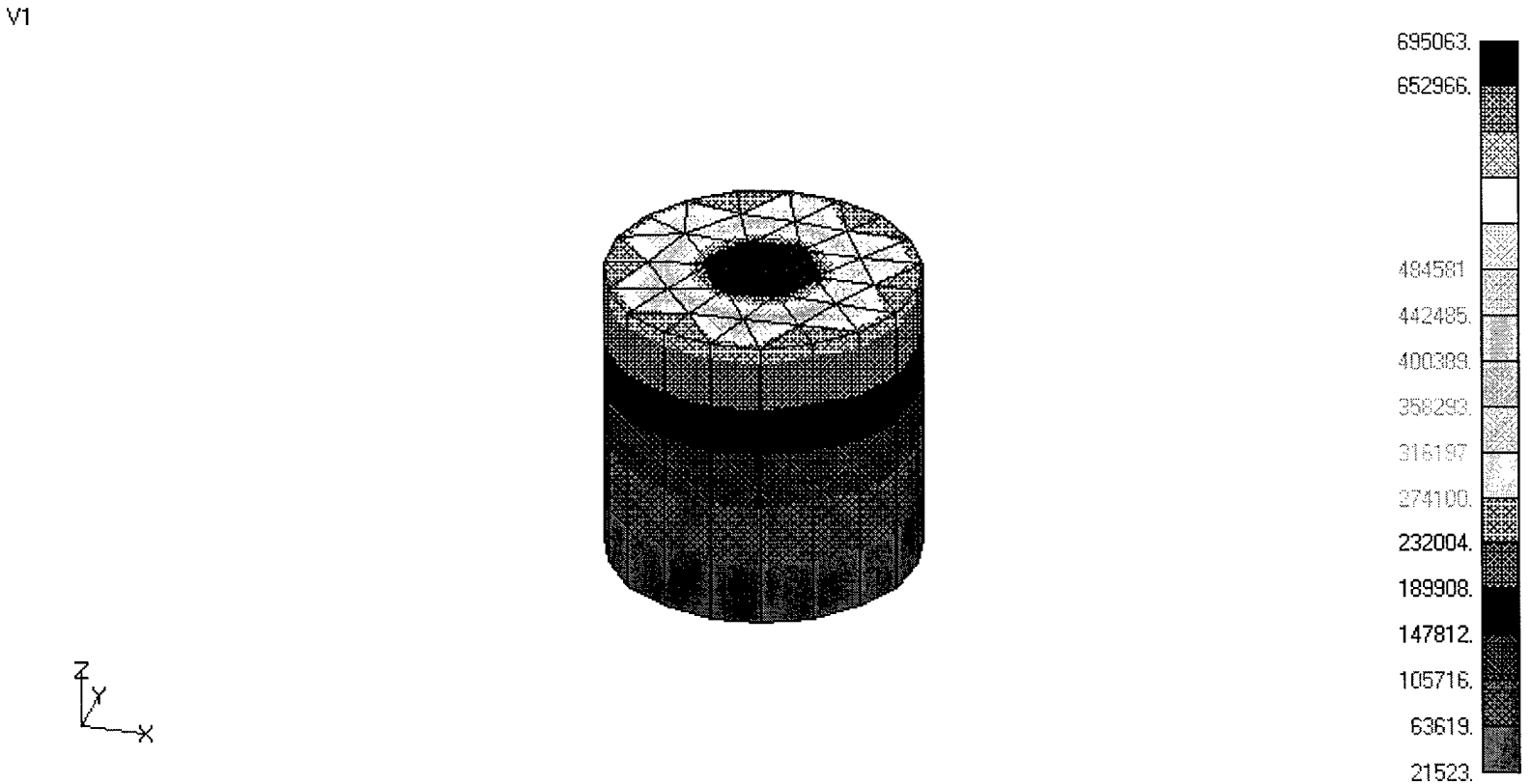

Vertical Load = 7,000,000 lbs
Linear Elastic-Perfectly Plastic Sandy Soil (Linear Extended Drucker-Prager)
E = 864,000 psf, $\upsilon = 0.3$, Slope Angle = 42.6°, Dilation Angle = 21.5°
Pile, AISI 4340 Steel

Figure-B14. Horizontal Displacements (Triangular Section)

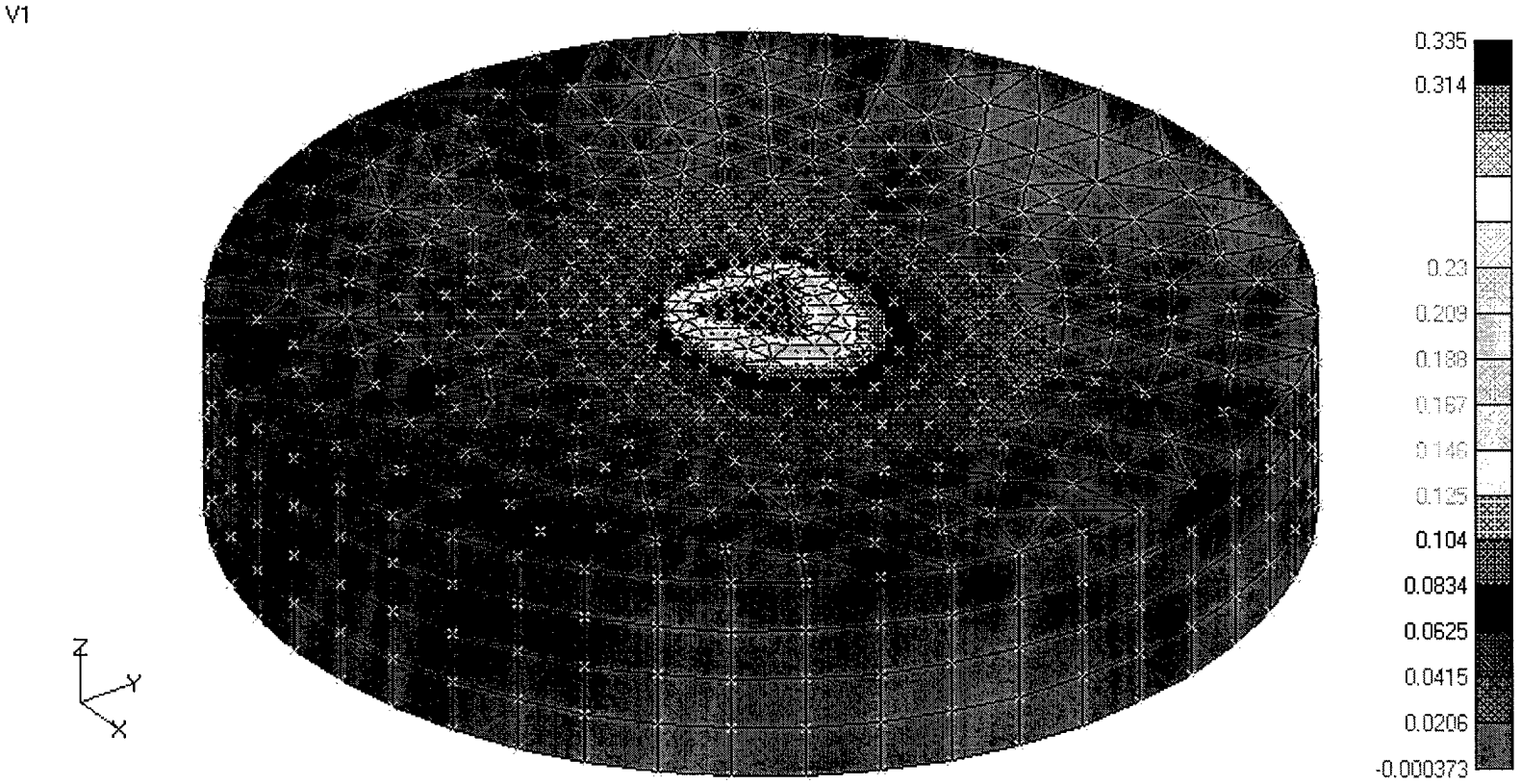

Horizontal Load = 6,500,000 lbs
Linear Elastic-Perfectly Plastic Sandy Soil (Linear Extended Drucker-Prager)
E = 864,000 psf, υ = 0.3, Slope Angle = 42.6°, Dilation Angle = 21.5°
Pile, AISI 4340 Steel

Figure-B15. Horizontal Displacements on a Vertical Plane along the Horizontal Load Direction (Triangular Section)

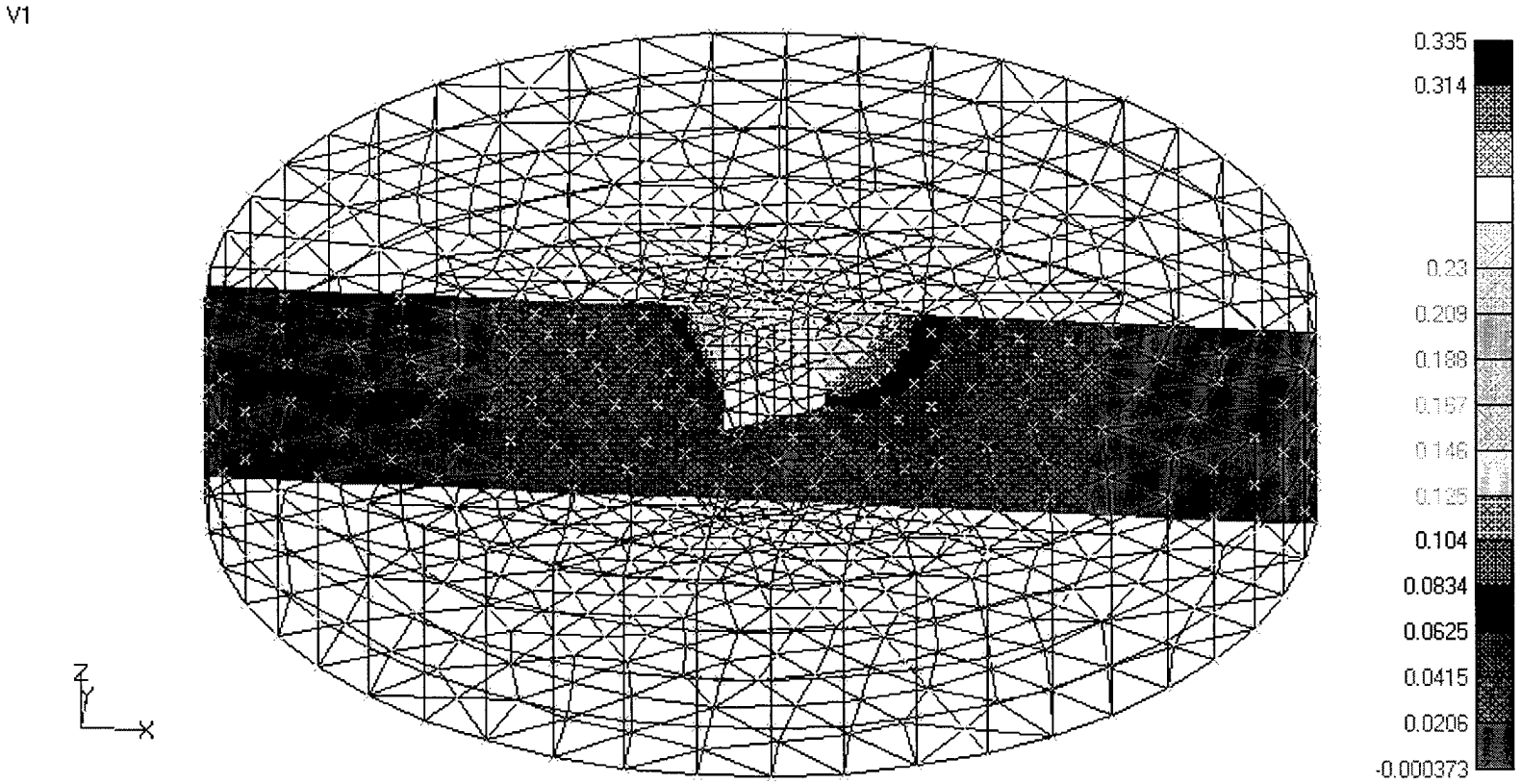

Horizontal Load = 6,500,000 lbs
Linear Elastic-Perfectly Plastic Sandy Soil (Linear Extended Drucker-Prager)
E = 864,000 psf, $\upsilon = 0.3$, Slope Angle = 42.6°, Dilation Angle = 21.5°
Pile, AISI 4340 Steel

Figure-B16. Pile Total Displacements (Triangular Section)

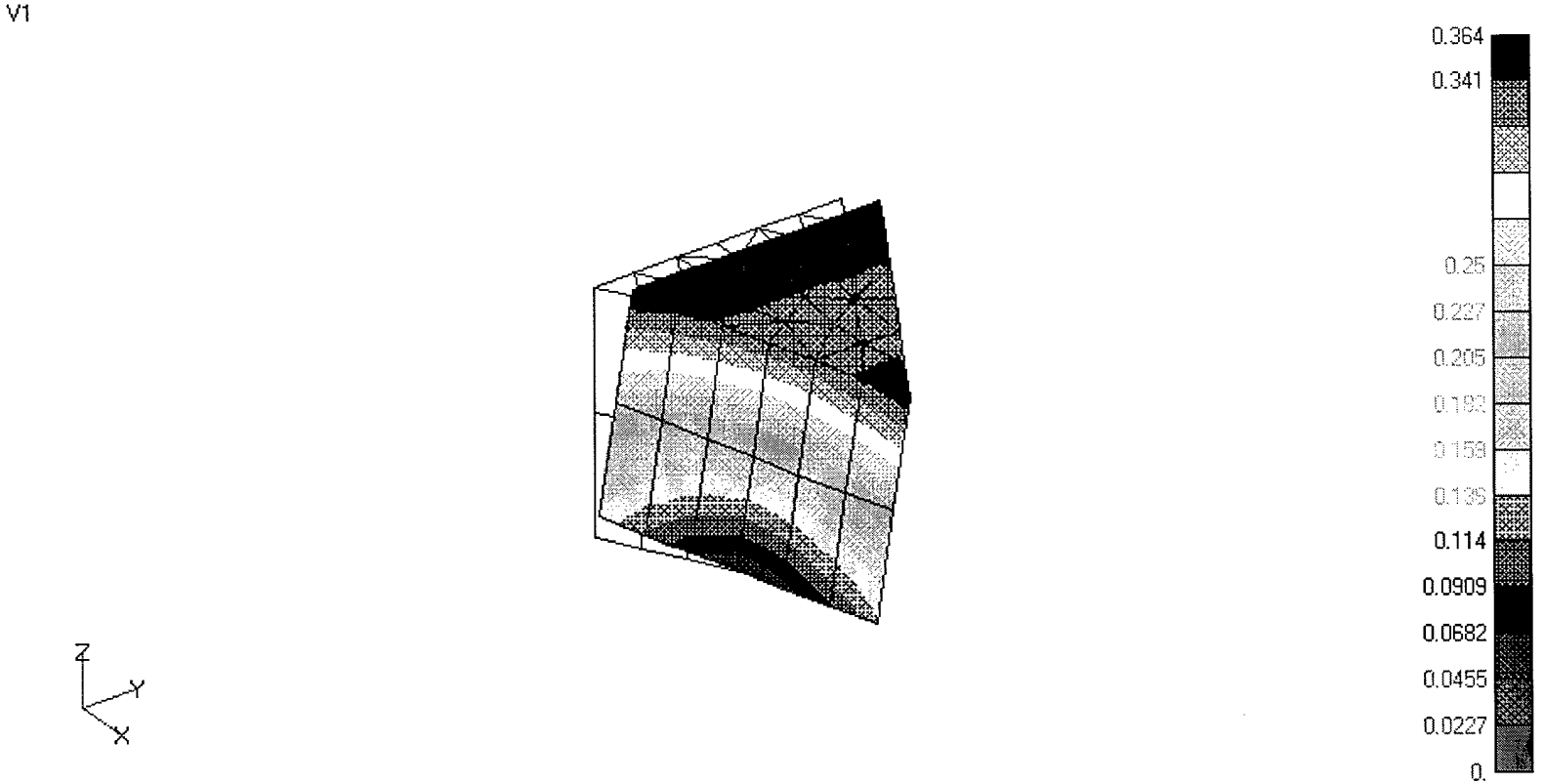

Horizontal Load = 6,500,000 lbs
Linear Elastic-Perfectly Plastic Sandy Soil (Linear Extended Drucker-Prager)
E = 864,000 psf, $\upsilon = 0.3$, Slope Angle = 42.6°, Dilation Angle = 21.5°
Pile, AISI 4340 Steel

Figure-B17. Soil Minor Principal Stresses (Triangular Section)

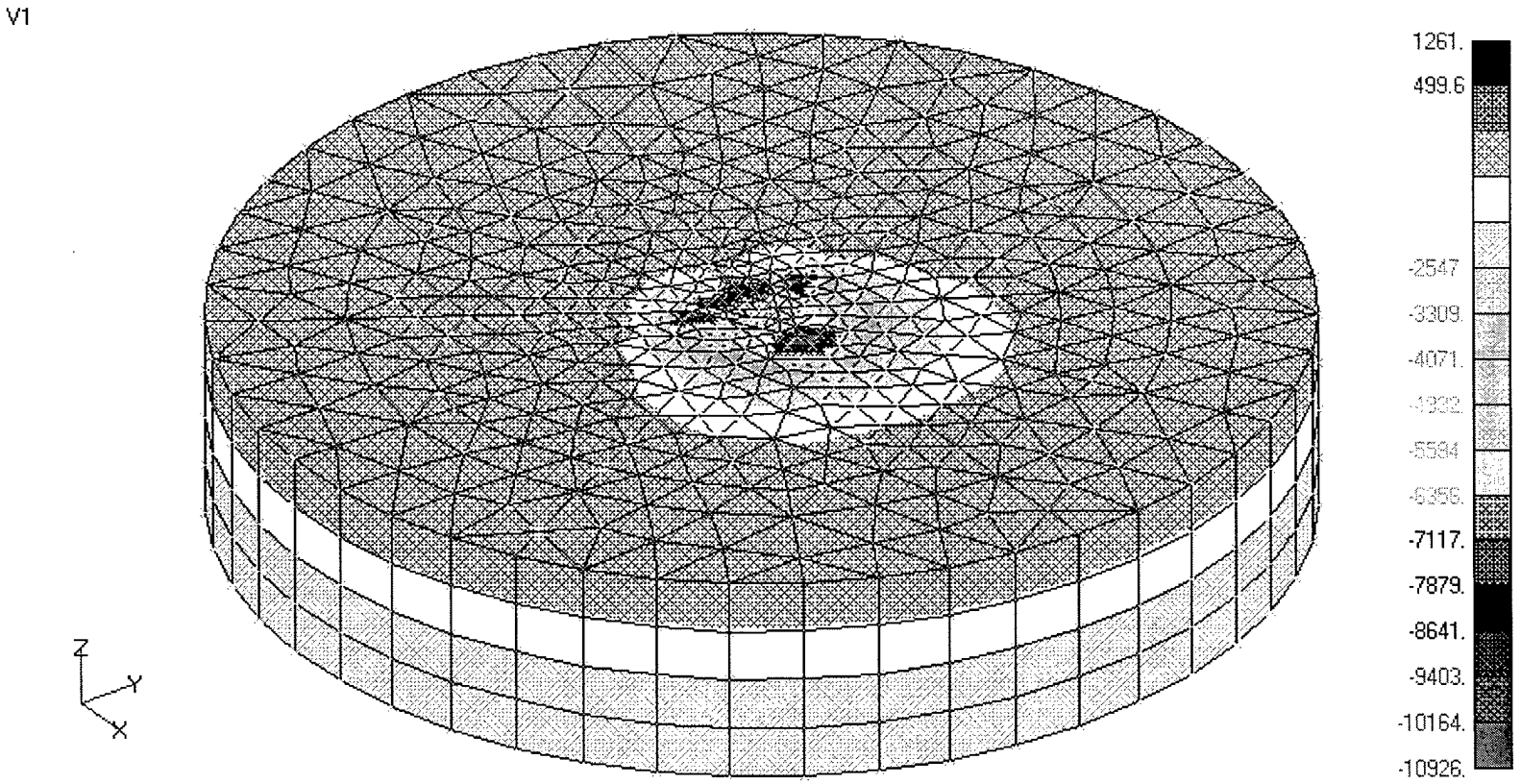

Horizontal Load = 6,500,000 lbs
Linear Elastic-Perfectly Plastic Sandy Soil (Linear Extended Drucker-Prager)
E = 864,000 psf, $\upsilon = 0.3$, Slope Angle = 42.6°, Dilation Angle = 21.5°
Pile, AISI 4340 Steel

Figure-B18. Soil Minor Principal Stresses on a Vertical Plane along the Horizontal Load Direction (Triangular Section)

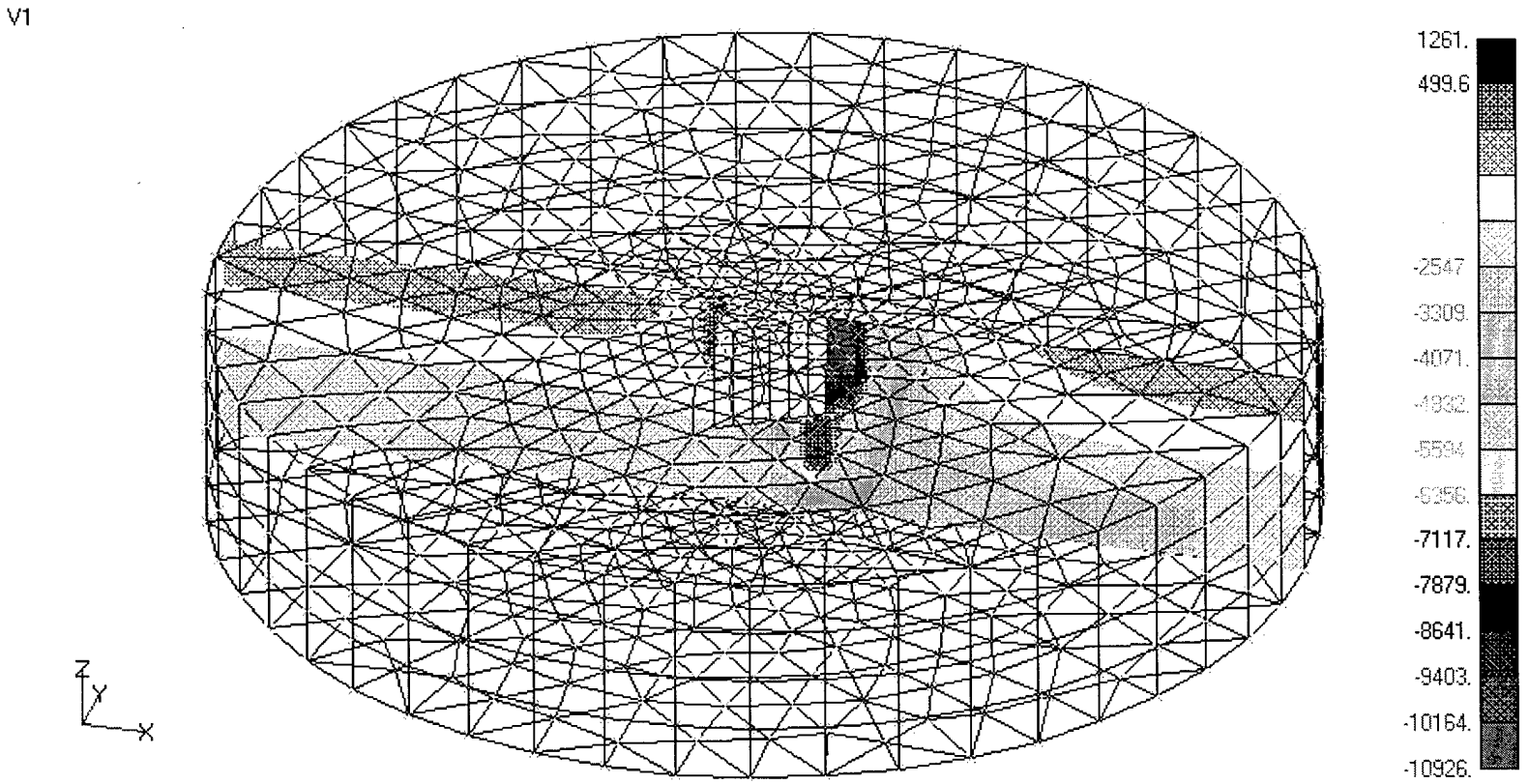

Horizontal Load = 6,500,000 lbs
Linear Elastic-Perfectly Plastic Sandy Soil (Linear Extended Drucker-Prager)
E = 864,000 psf, $\upsilon = 0.3$, Slope Angle = 42.6°, Dilation Angle = 21.5°
Pile, AISI 4340 Steel

Figure-B19. Horizontal Normal Pile Stresses on the Pile Surface (Triangular Section)

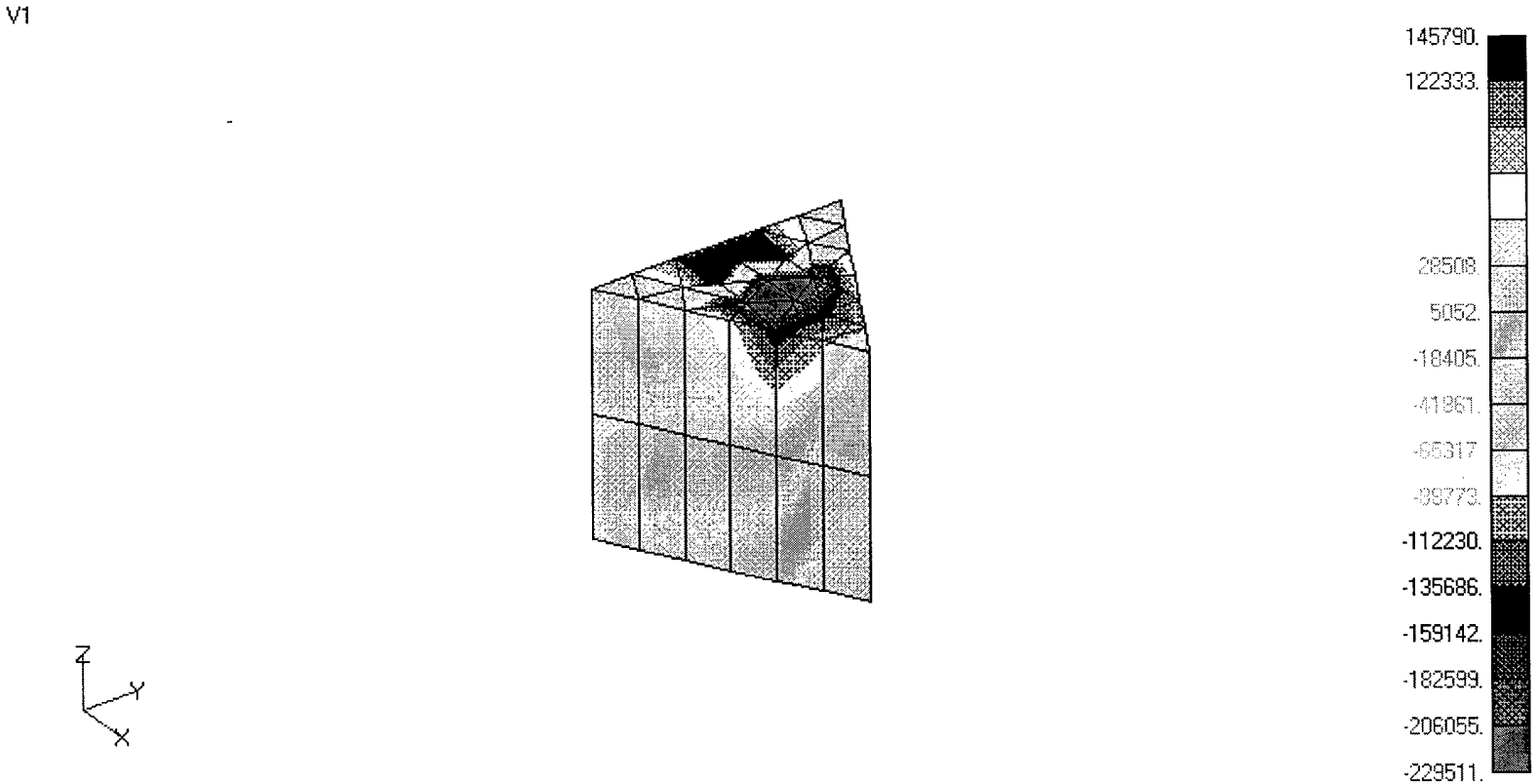

Horizontal Load = 6,500,000 lbs
Linear Elastic-Perfectly Plastic Sandy Soil (Linear Extended Drucker-Prager)
E = 864,000 psf, υ = 0.3, Slope Angle = 42.6°, Dilation Angle = 21.5°
Pile, AISI 4340 Steel

Figure-B20. Pile von Mises Stresses on the Pile Surface (Triangular Section)

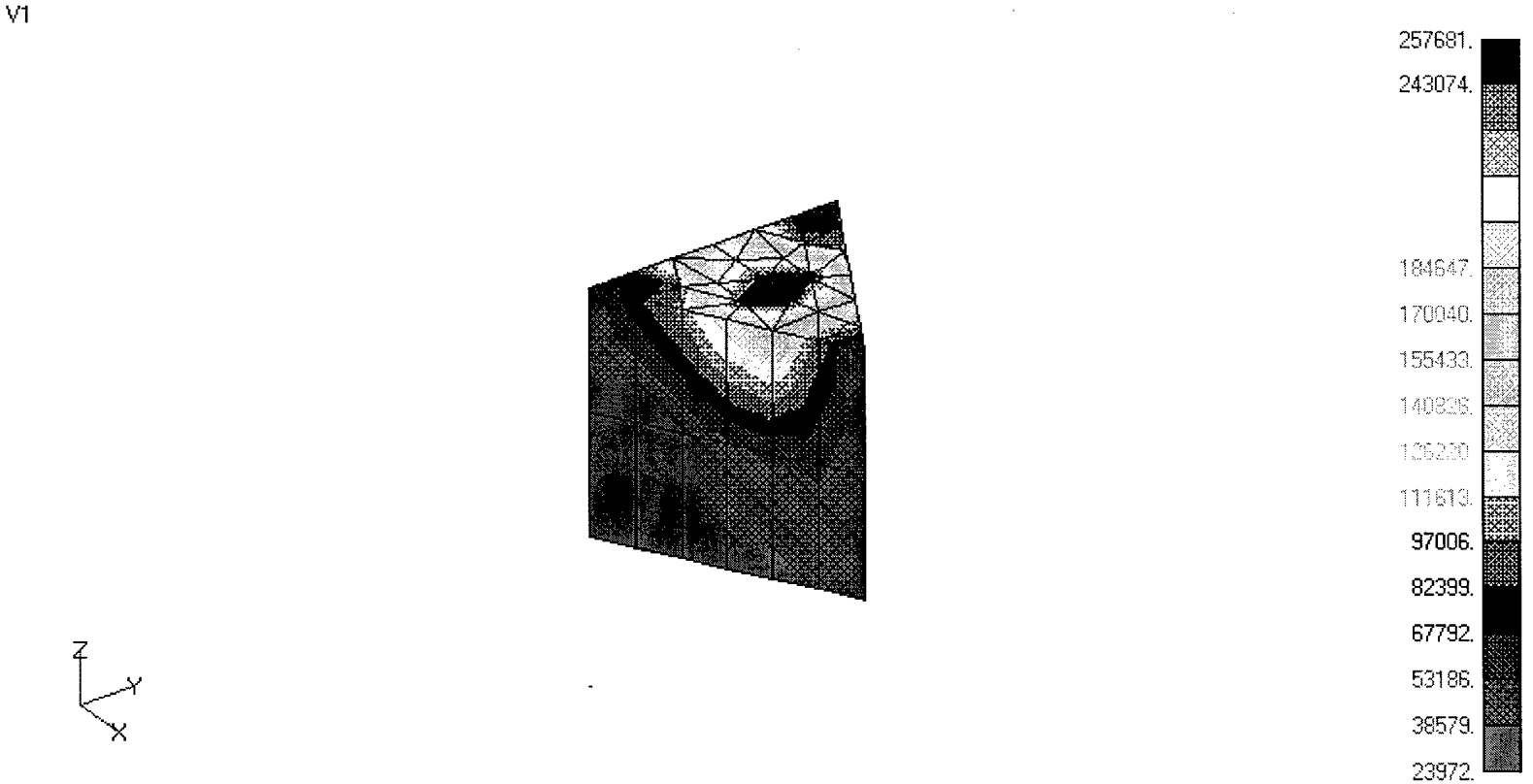

Horizontal Load = 6,500,000 lbs
Linear Elastic-Perfectly Plastic Sandy Soil (Linear Extended Drucker-Prager)
E = 864,000 psf, $\upsilon = 0.3$, Slope Angle = 42.6°, Dilation Angle = 21.5°
Pile, AISI 4340 Steel

Figure-B21. Vertical Displacements (Triangular Section)

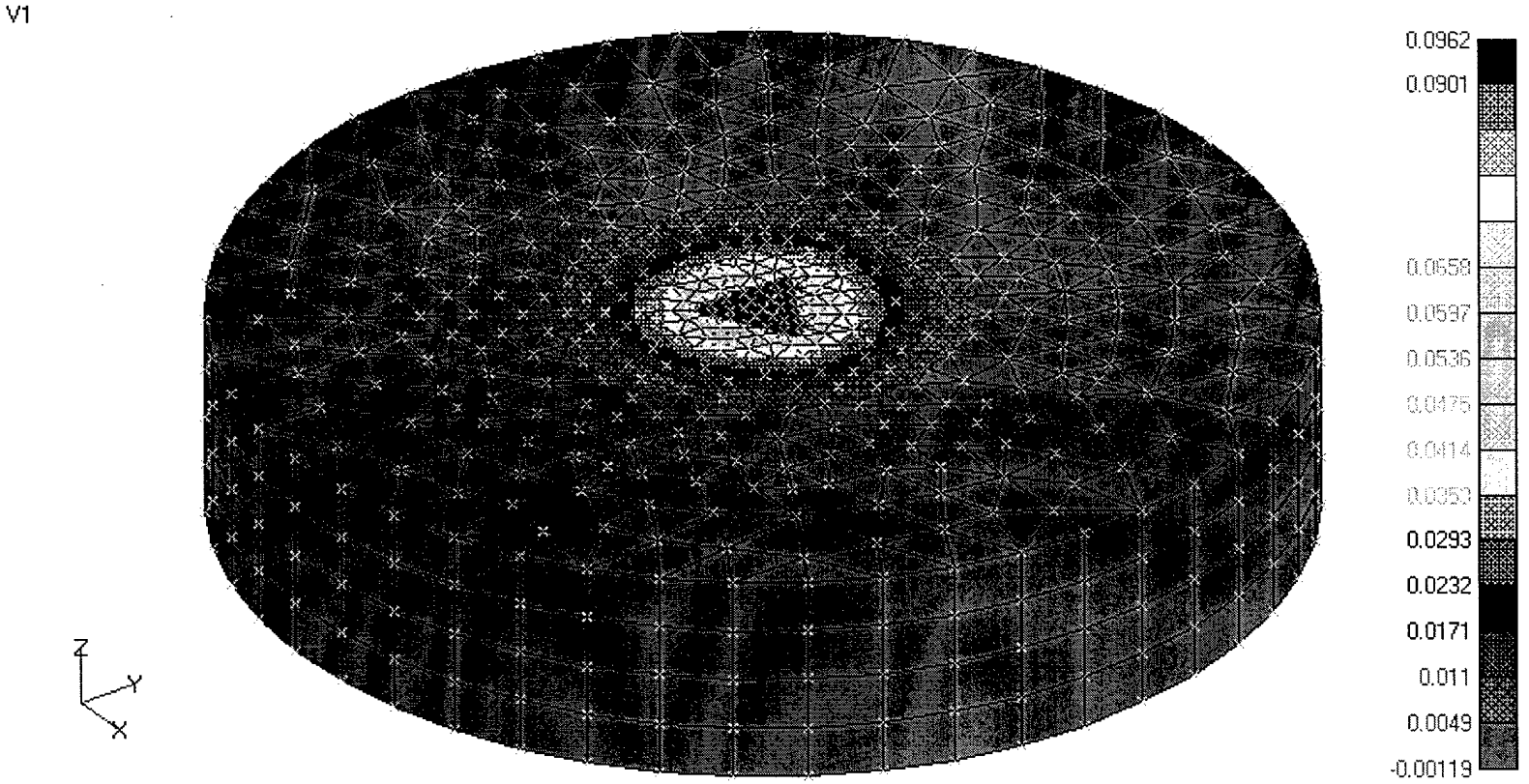

Vertical Load = 6,000,000 lbs
Linear Elastic-Perfectly Plastic Sandy Soil (Linear Extended Drucker-Prager)
E = 864,000 psf, $\upsilon = 0.3$, Slope Angle = 42.6°, Dilation Angle = 21.5°
Pile, AISI 4340 Steel

Figure-B22. Vertical Displacements on a Vertical Plane (Triangular Section)

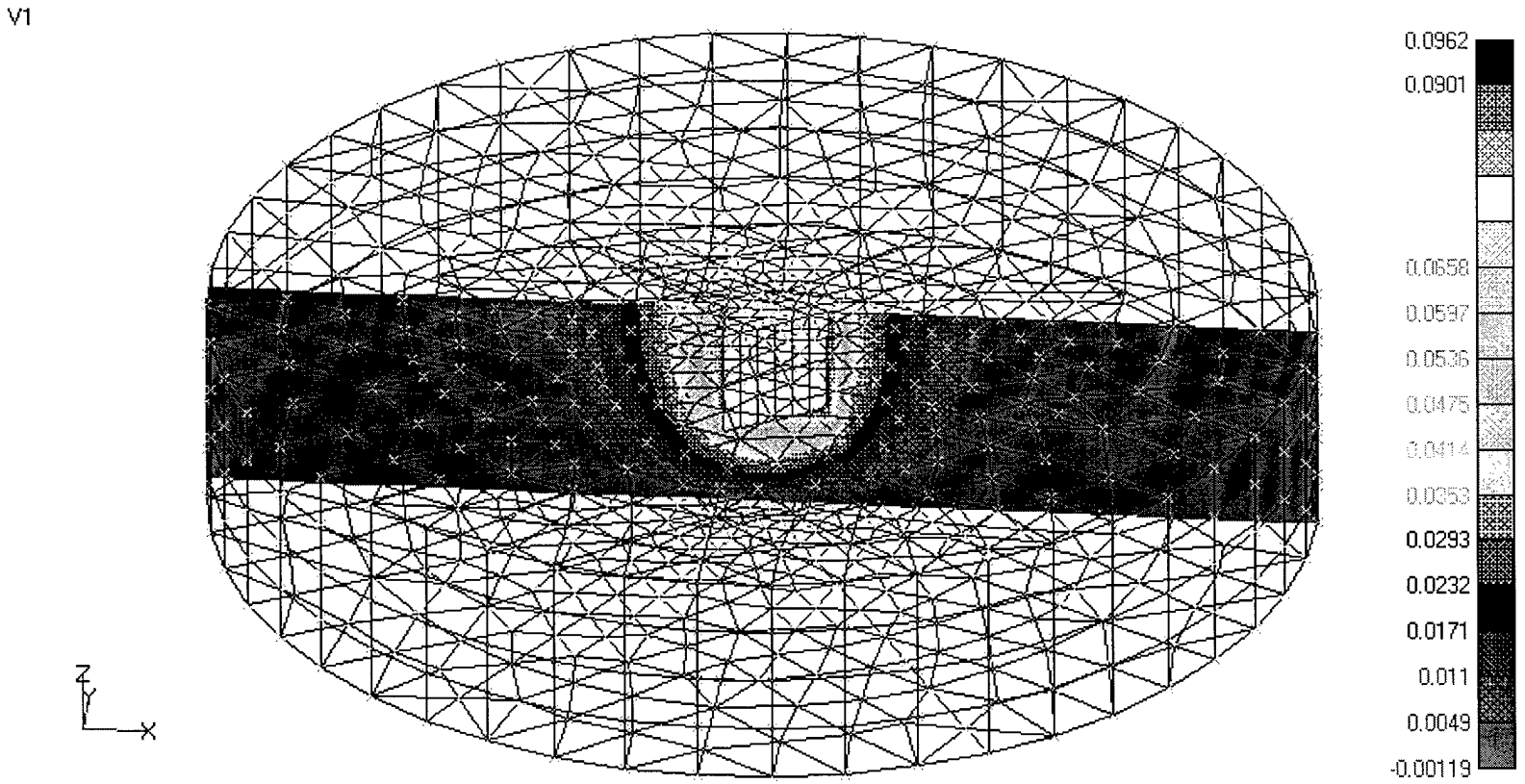

Vertical Load = 6,000,000 lbs
Linear Elastic-Perfectly Plastic Sandy Soil (Linear Extended Drucker-Prager)
E = 864,000 psf, $\upsilon = 0.3$, Slope Angle = 42.6°, Dilation Angle = 21.5°
Pile, AISI 4340 Steel

Figure-B23. Pile Vertical Displacements (Triangular Section)

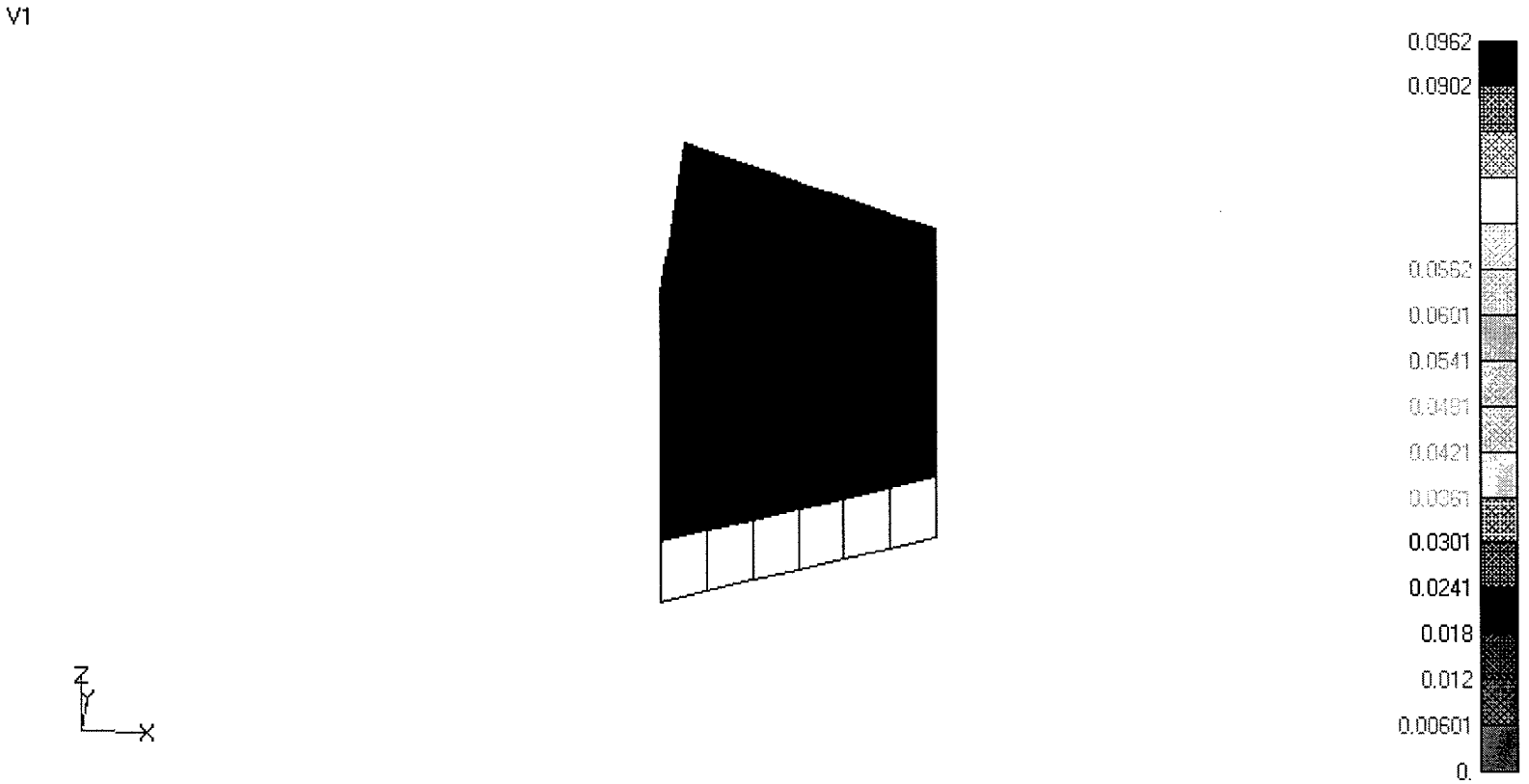

Vertical Load = 6,000,000 lbs
Linear Elastic-Perfectly Plastic Sandy Soil (Linear Extended Drucker-Prager)
E = 864,000 psf, $\upsilon = 0.3$, Slope Angle = 42.6°, Dilation Angle = 21.5°
Pile, AISI 4340 Steel

Figure-B24. Soil Minor Principal Stresses (Triangular Section)

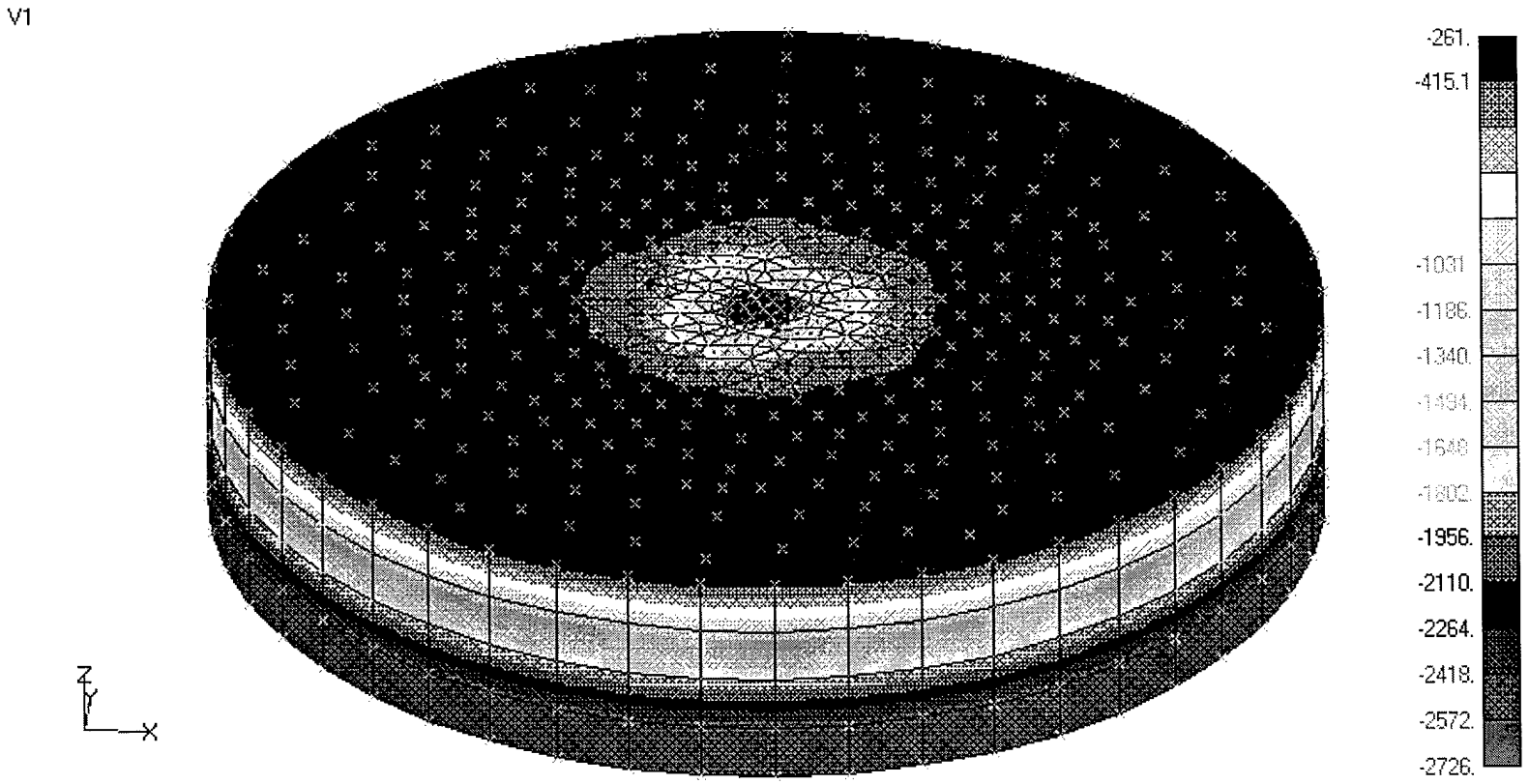

Vertical Load = 6,000,000 lbs
Linear Elastic-Perfectly Plastic Sandy Soil (Linear Extended Drucker-Prager)
E = 864,000 psf, $\upsilon = 0.3$, Slope Angle = 42.6°, Dilation Angle = 21.5°
Pile, AISI 4340 Steel

Figure-B25. Soil Minor Principal Stresses on a Vertical Plane (Triangular Section)

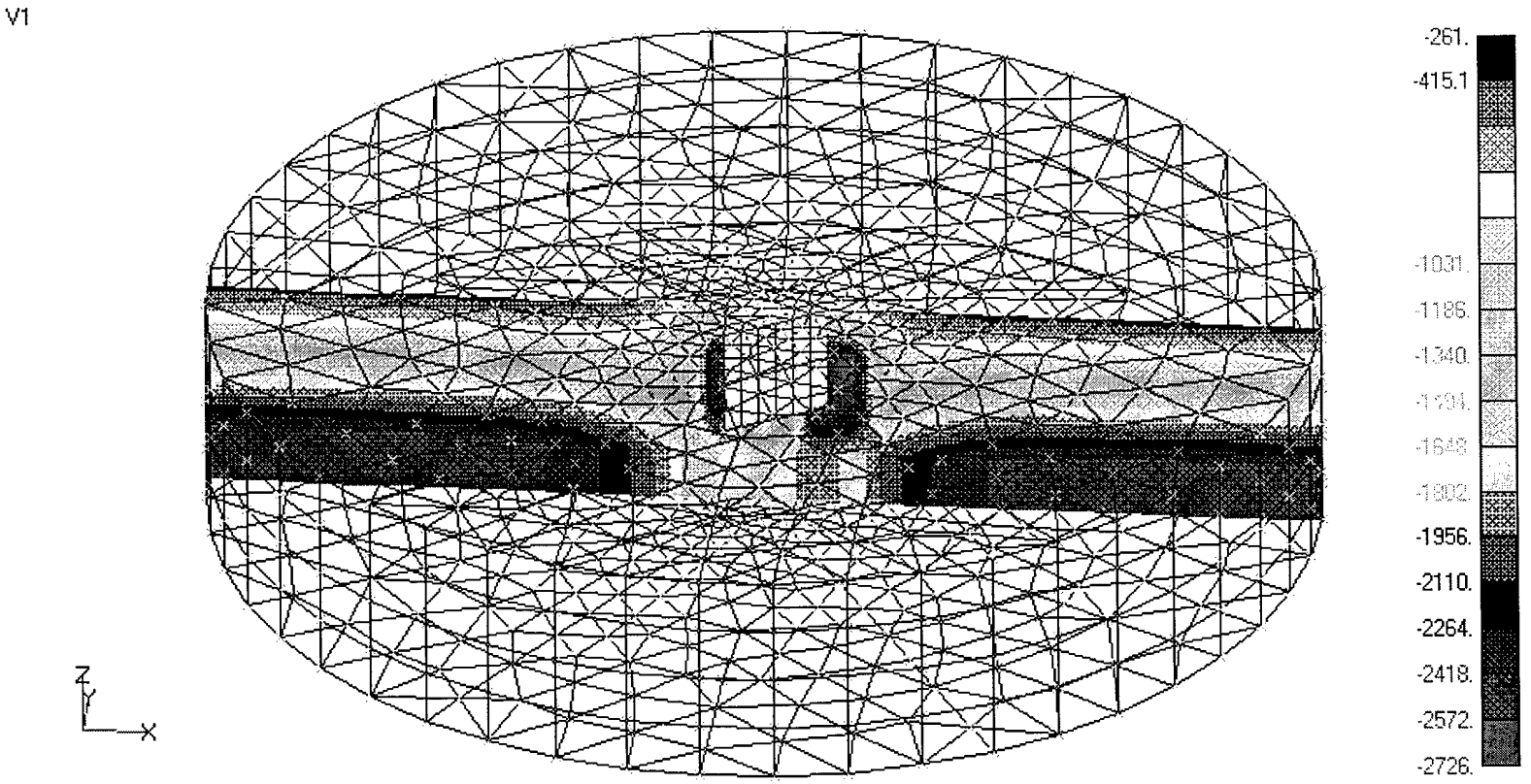

Vertical Load = 6,000,000 lbs
Linear Elastic-Perfectly Plastic Sandy Soil (Linear Extended Drucker-Prager)
E = 864,000 psf, $\upsilon = 0.3$, Slope Angle = 42.6°, Dilation Angle = 21.5°
Pile, AISI 4340 Steel

Figure-B26. Pile von Mises Stresses on the Pile Surface (Triangular Section)

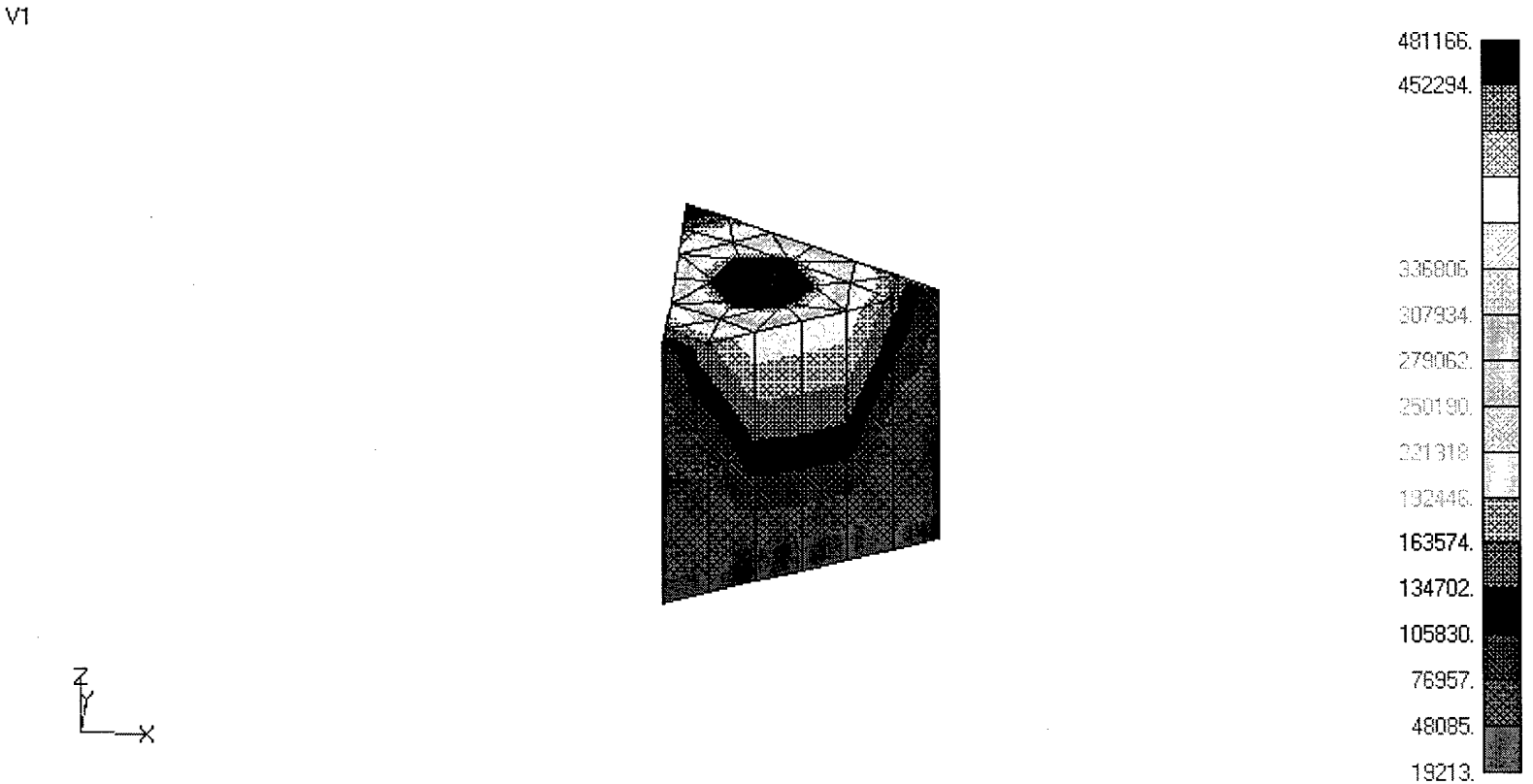

Vertical Load = 6,000,000 lbs
Linear Elastic-Perfectly Plastic Sandy Soil (Linear Extended Drucker-Prager)
E = 864,000 psf, $\upsilon = 0.3$, Slope Angle = 42.6°, Dilation Angle = 21.5°
Pile, AISI 4340 Steel

Figure-B27. Horizontal Displacements (Y-shaped Section)

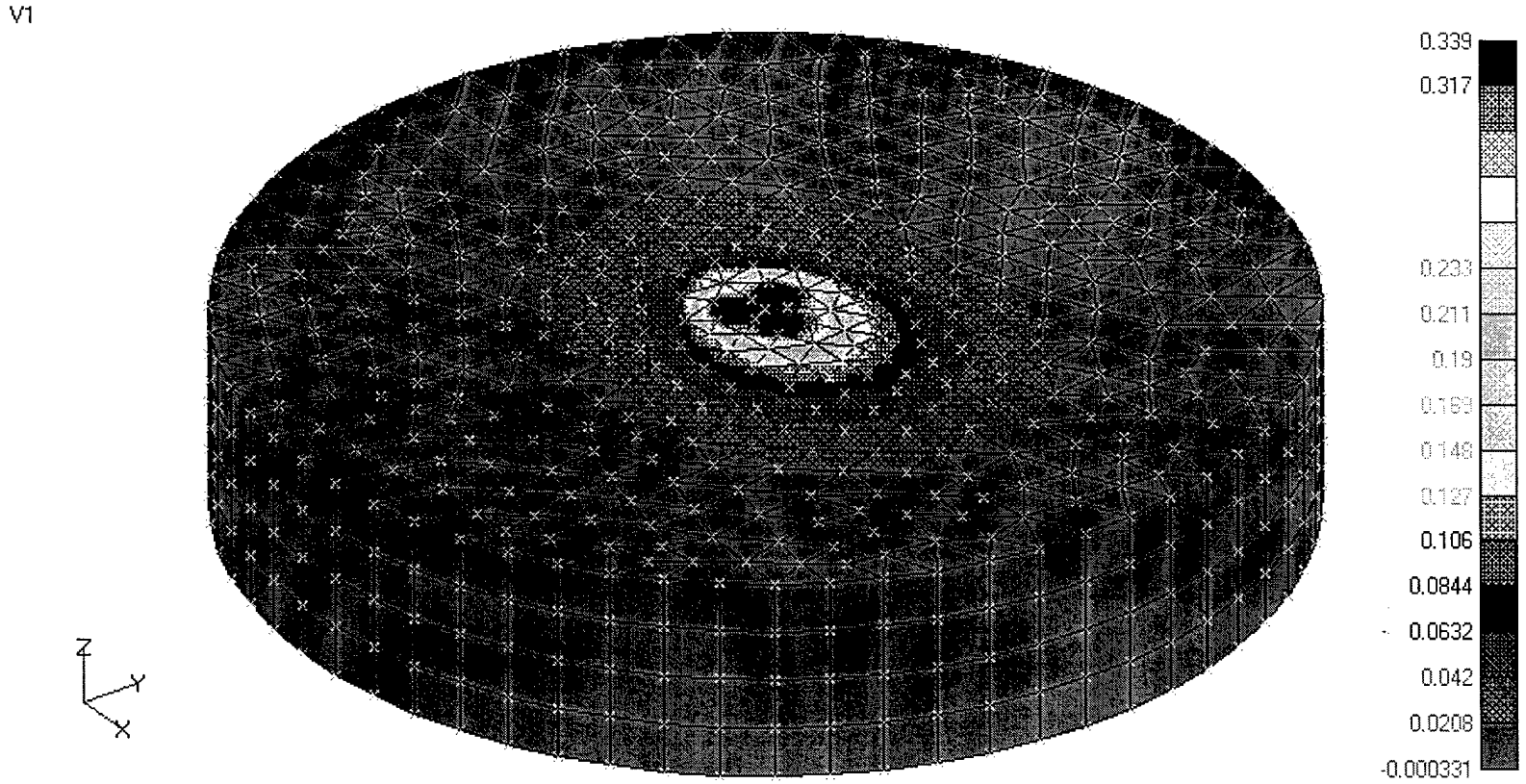

Horizontal Load = 6,500,000 lbs
Linear Elastic-Perfectly Plastic Sandy Soil (Linear Extended Drucker-Prager)
E = 864,000 psf, υ = 0.3, Slope Angle = 42.6°, Dilation Angle = 21.5°
Pile, AISI 4340 Steel

Figure-B28. Horizontal Displacements on a Vertical Plane along the Horizontal Load Direction (Y-shaped Section)

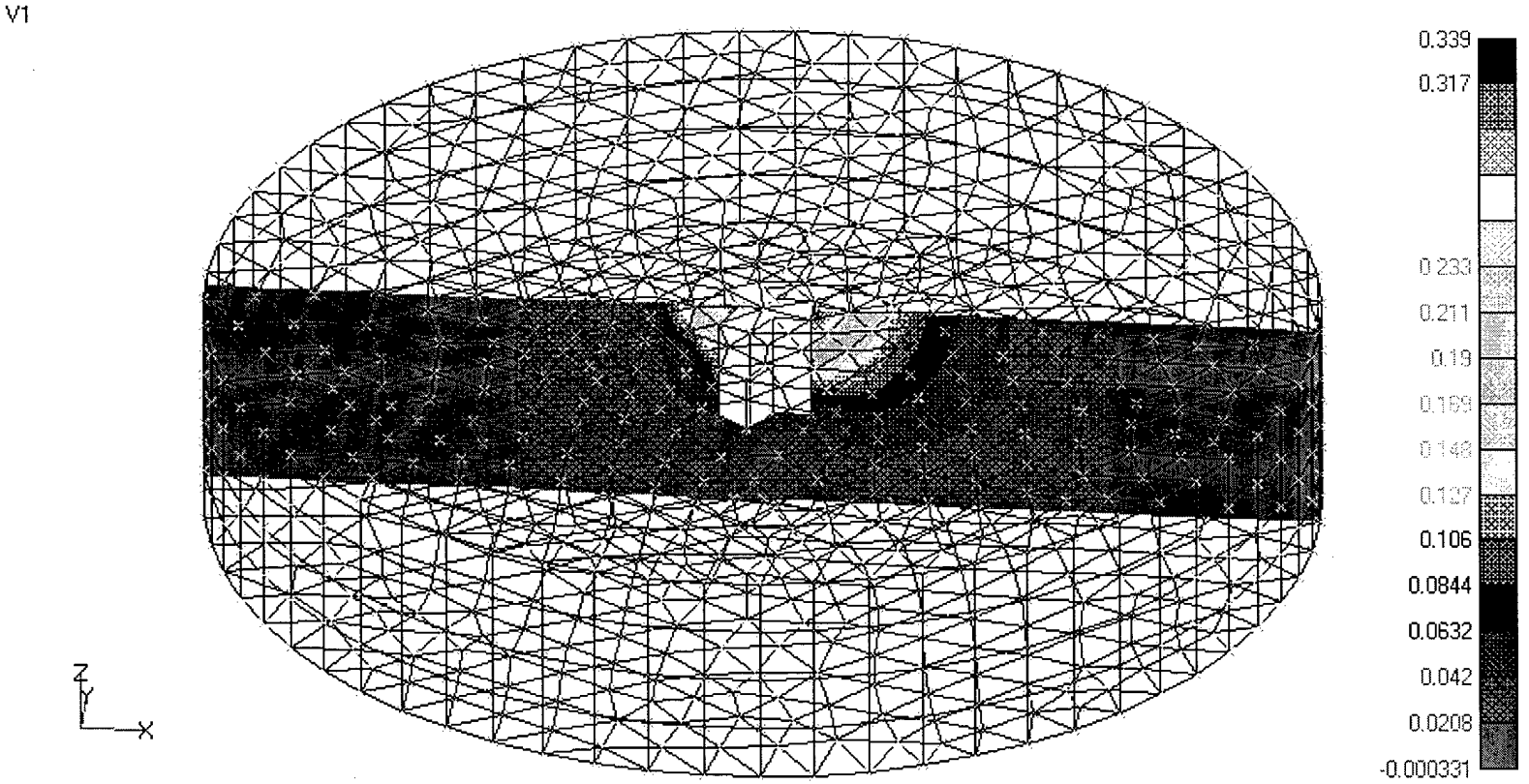

Horizontal Load = 6,500,000 lbs
Linear Elastic-Perfectly Plastic Sandy Soil (Linear Extended Drucker-Prager)
E = 864,000 psf, υ = 0.3, Slope Angle = 42.6°, Dilation Angle = 21.5°
Pile, AISI 4340 Steel

Figure-B29. Pile Total Displacements (Y-shaped Section)

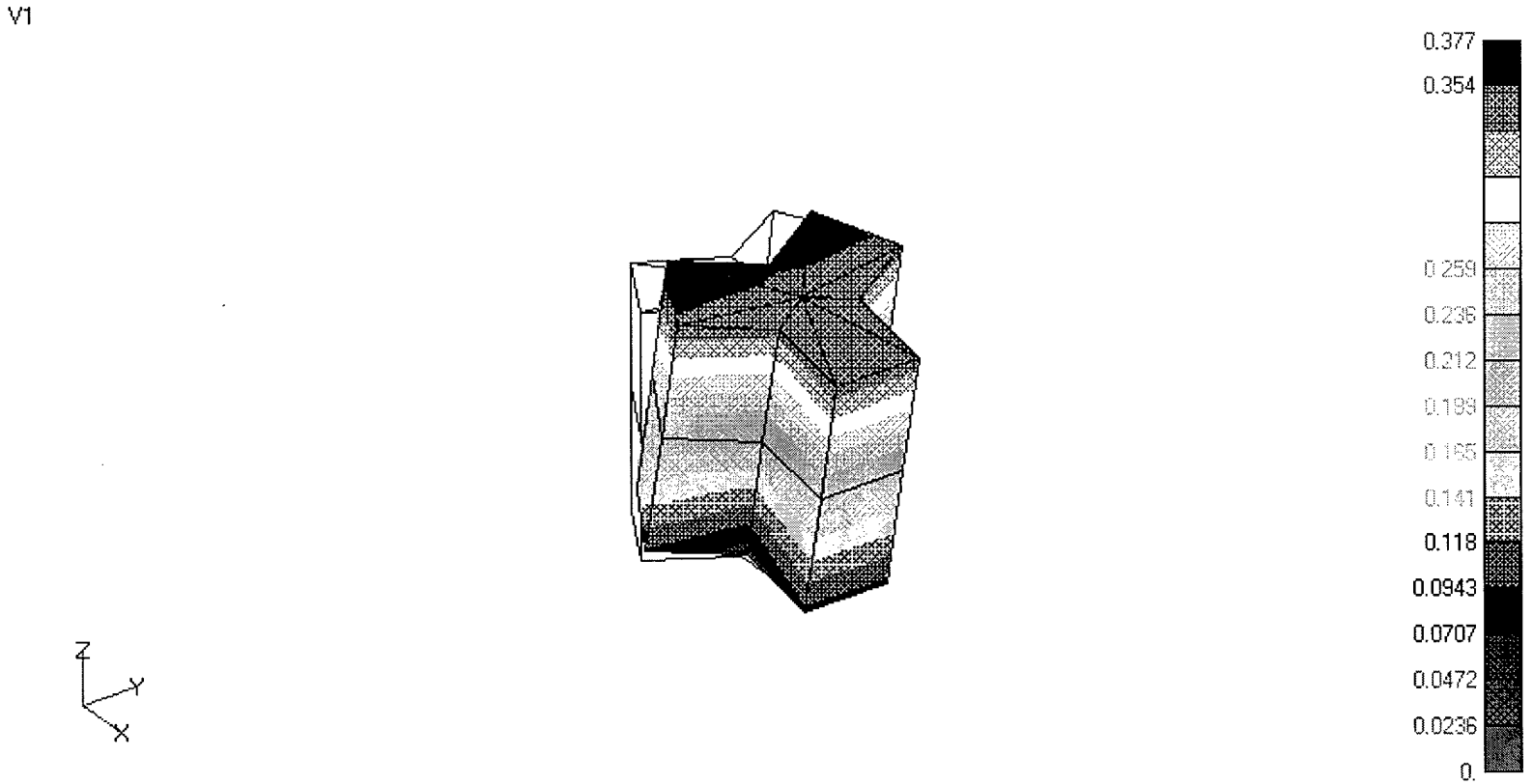

Horizontal Load = 6,500,000 lbs
Linear Elastic-Perfectly Plastic Sandy Soil (Linear Extended Drucker-Prager)
E = 864,000 psf, $\upsilon = 0.3$, Slope Angle = 42.6°, Dilation Angle = 21.5°
Pile, AISI 4340 Steel

Figure-B30. Soil Minor Principal Stresses (Y-shaped Section)

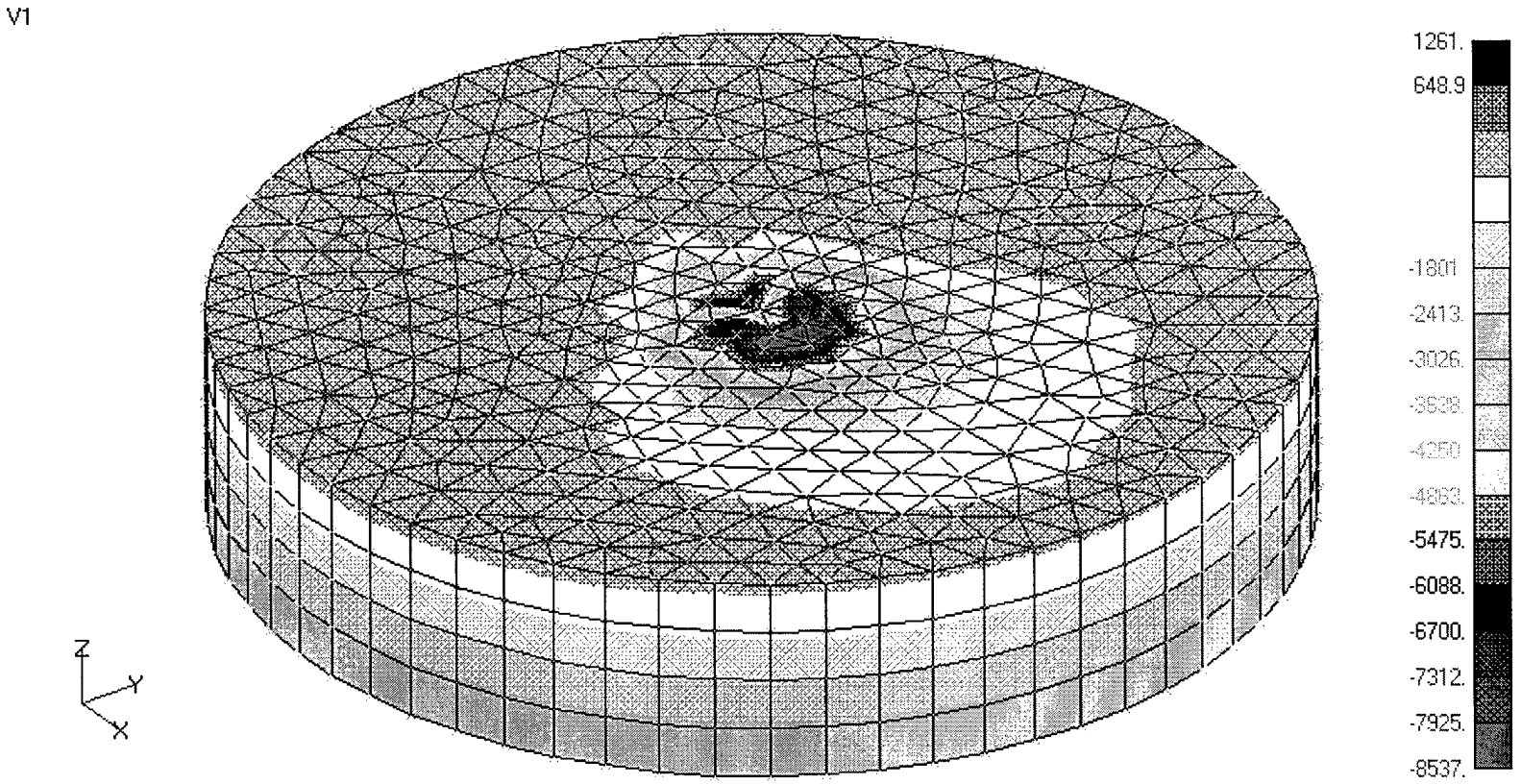

Horizontal Load = 6,500,000 lbs
Linear Elastic-Perfectly Plastic Sandy Soil (Linear Extended Drucker-Prager)
E = 864,000 psf, $\upsilon = 0.3$, Slope Angle = 42.6°, Dilation Angle = 21.5°
Pile, AISI 4340 Steel

Figure-B31. Soil Minor Principal Stresses on a Vertical Plane along the Horizontal Load Direction (Y-shaped Section)

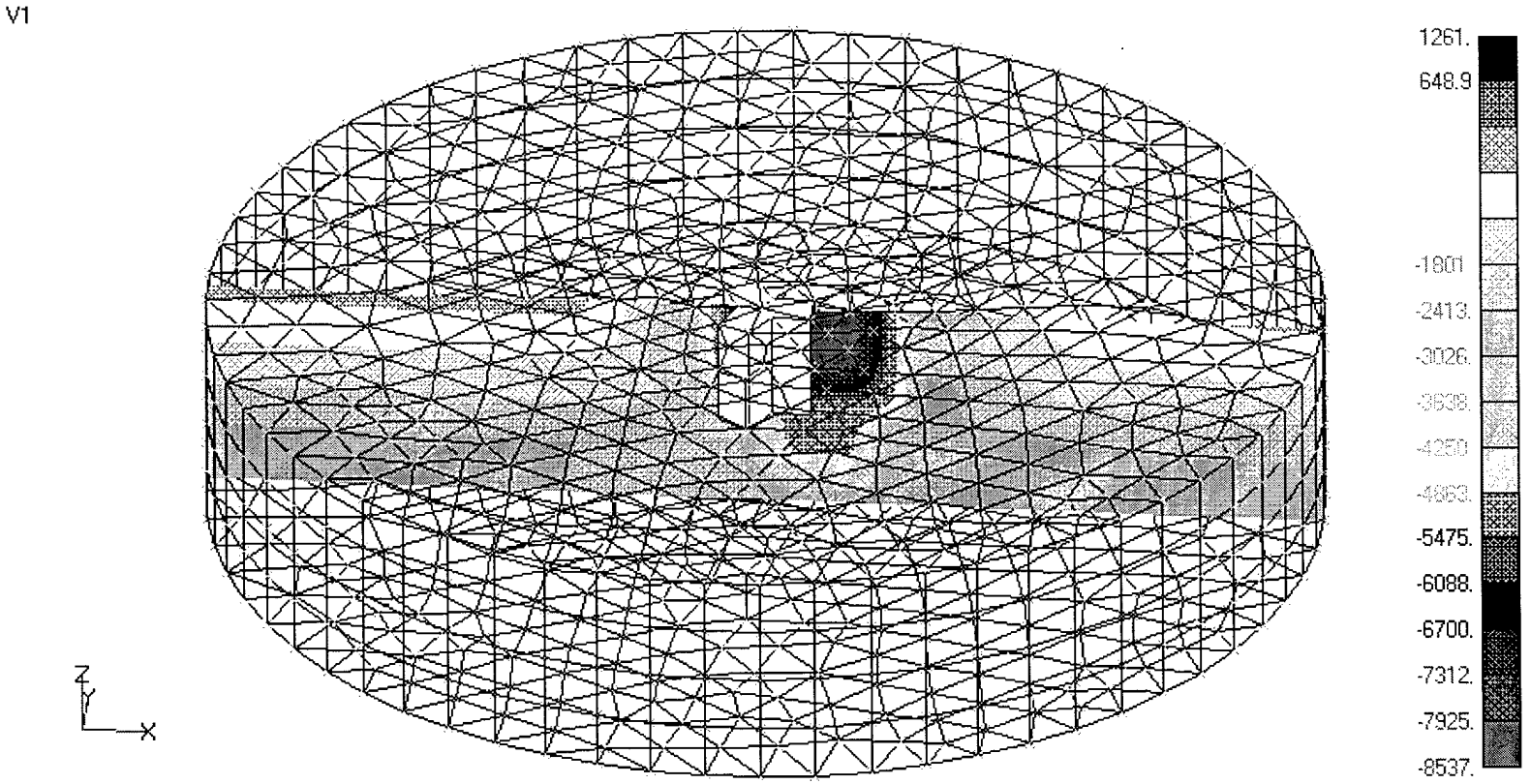

Horizontal Load = 6,500,000 lbs
Linear Elastic-Perfectly Plastic Sandy Soil (Linear Extended Drucker-Prager)
E = 864,000 psf, υ = 0.3, Slope Angle = 42.6°, Dilation Angle = 21.5°
Pile, AISI 4340 Steel

Figure-B32. Horizontal Normal Pile Stresses on the Pile Surface (Y-shaped Section)

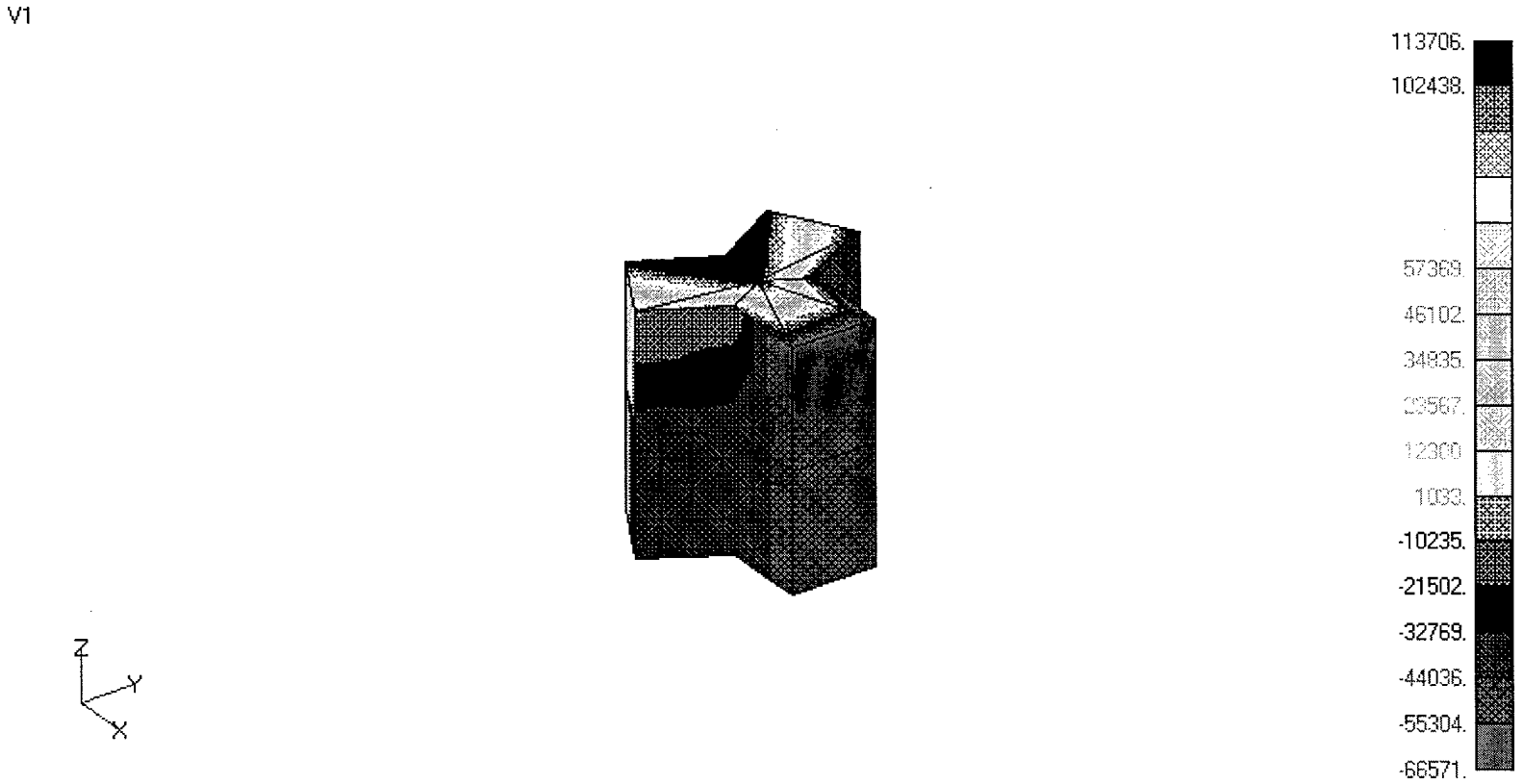

Horizontal Load = 6,500,000 lbs
Linear Elastic-Perfectly Plastic Sandy Soil (Linear Extended Drucker-Prager)
E = 864,000 psf, υ = 0.3, Slope Angle = 42.6°, Dilation Angle = 21.5°
Pile, AISI 4340 Steel

Figure-B33. Pile von Mises Stresses on the Pile Surface (Y-shaped Section)

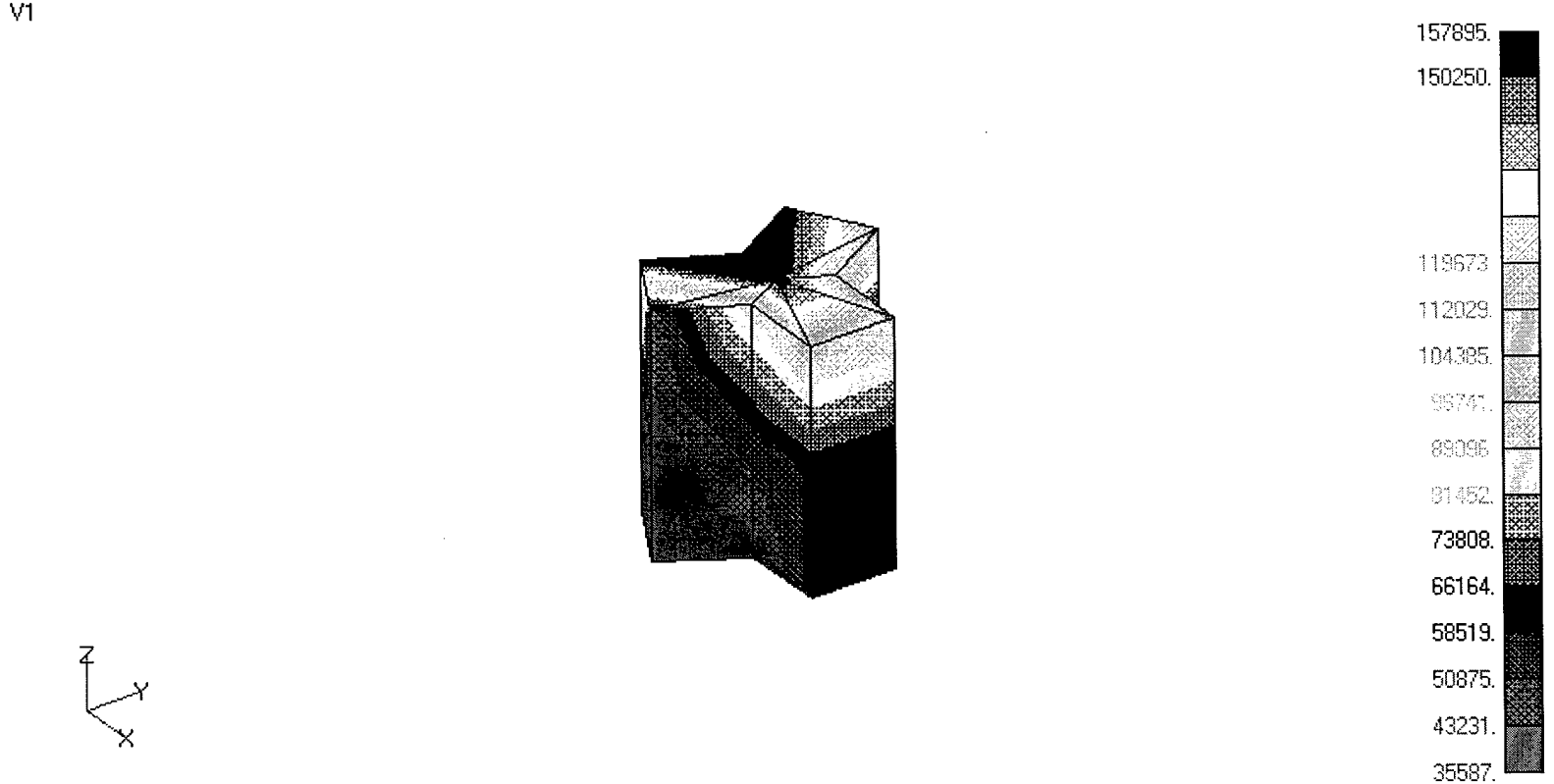

Horizontal Load = 6,500,000 lbs
Linear Elastic-Perfectly Plastic Sandy Soil (Linear Extended Drucker-Prager)
E = 864,000 psf, υ = 0.3, Slope Angle = 42.6°, Dilation Angle = 21.5°
Pile, AISI 4340 Steel

Figure-B34. Vertical Displacements (Y-shaped Section)

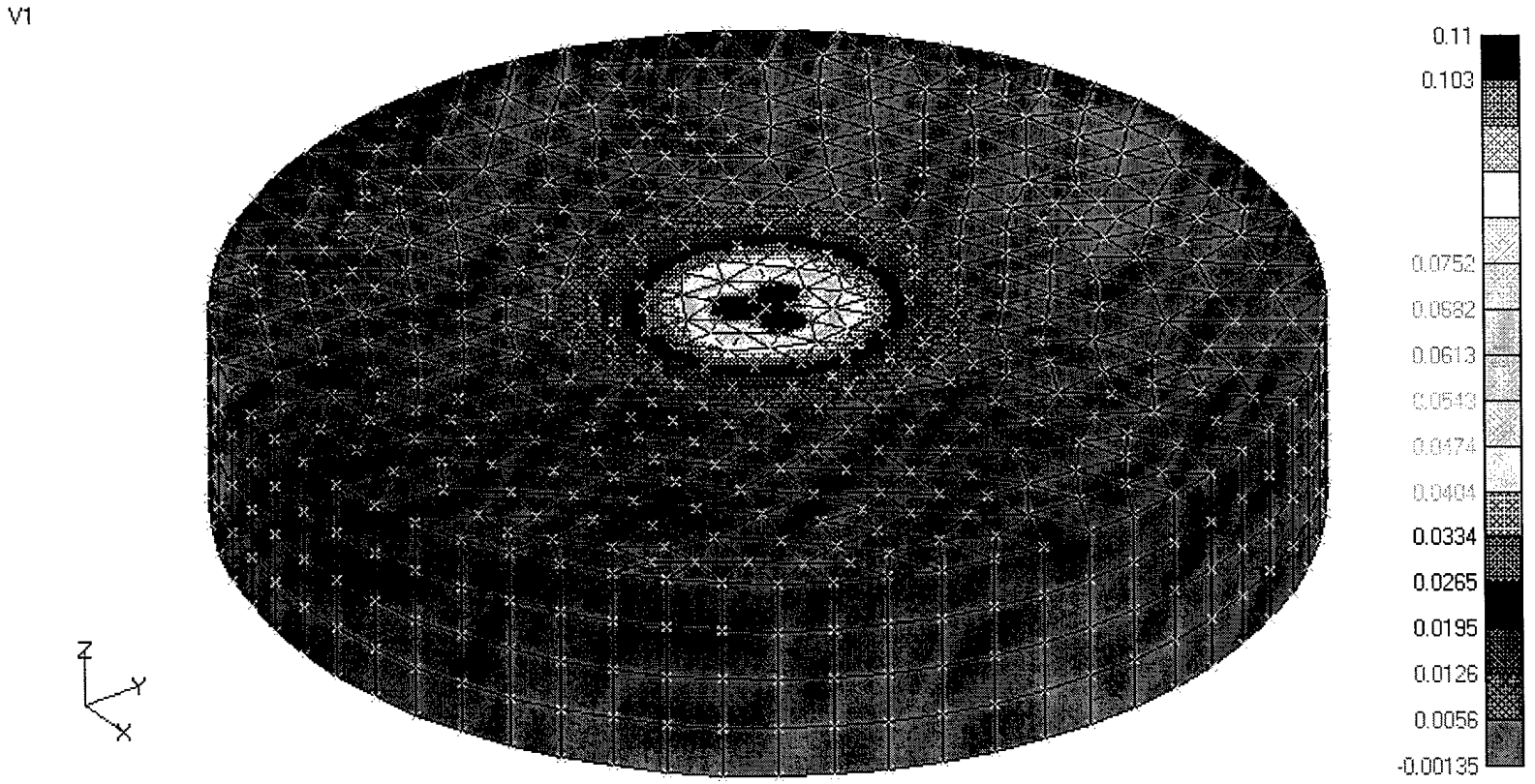

Vertical Load = 6,500,000 lbs
Linear Elastic-Perfectly Plastic Sandy Soil (Linear Extended Drucker-Prager)
E = 864,000 psf, $\upsilon = 0.3$, Slope Angle = 42.6°, Dilation Angle = 21.5°
Pile, AISI 4340 Steel

Figure-B35. Vertical Displacements on a Vertical Plane (Y-shaped Section)

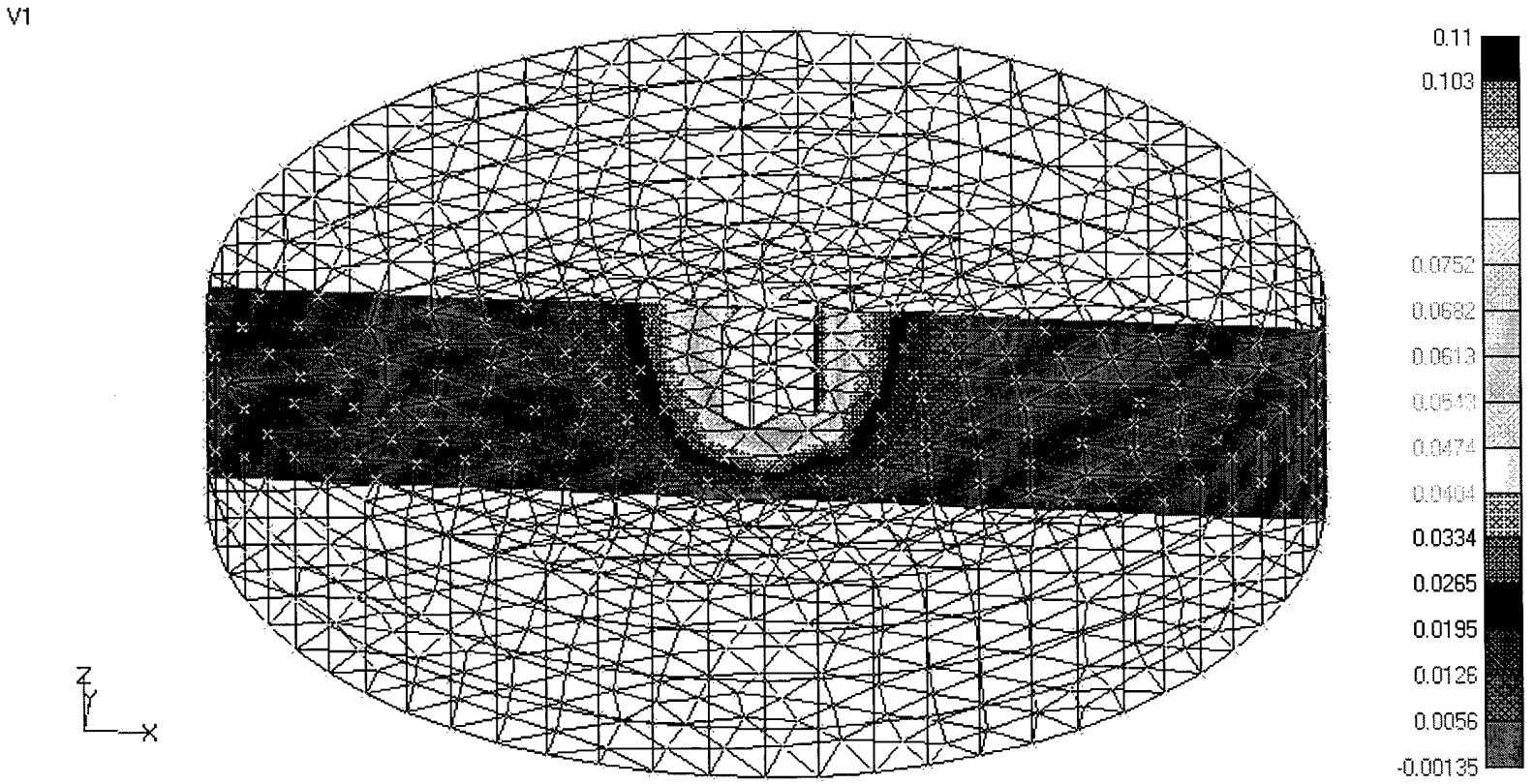

Vertical Load = 6,500,000 lbs
Linear Elastic-Perfectly Plastic Sandy Soil (Linear Extended Drucker-Prager)
E = 864,000 psf, υ = 0.3, Slope Angle = 42.6°, Dilation Angle = 21.5°
Pile, AISI 4340 Steel

Figure-B36. Pile Vertical Displacements (Y-shaped Section)

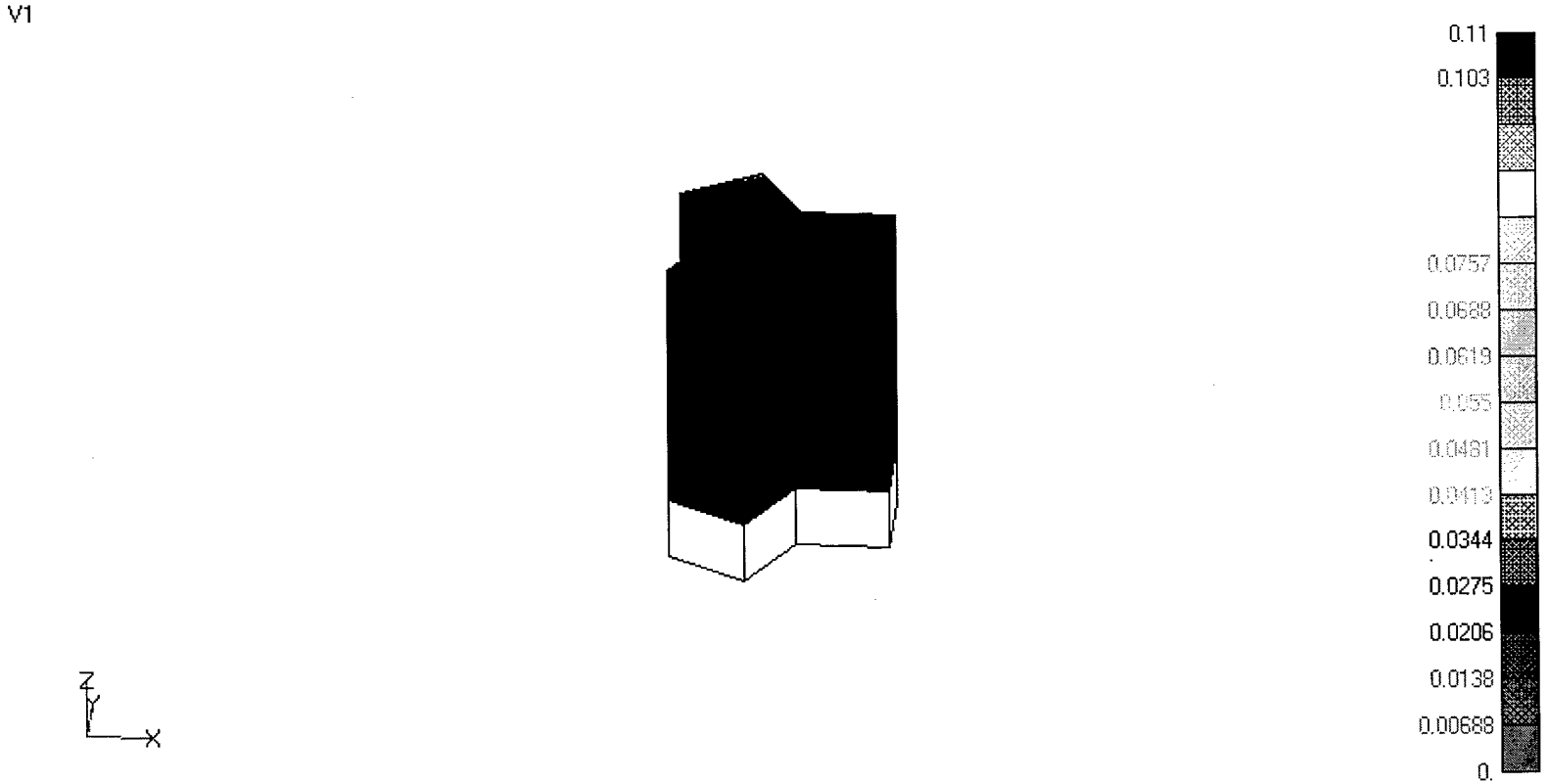

Vertical Load = 6,500,000 lbs
Linear Elastic-Perfectly Plastic Sandy Soil (Linear Extended Drucker-Prager)
E = 864,000 psf, $\upsilon = 0.3$, Slope Angle = 42.6°, Dilation Angle = 21.5°
Pile, AISI 4340 Steel

Figure-B37. Soil Minor Principal Stresses (Y-shaped Section)

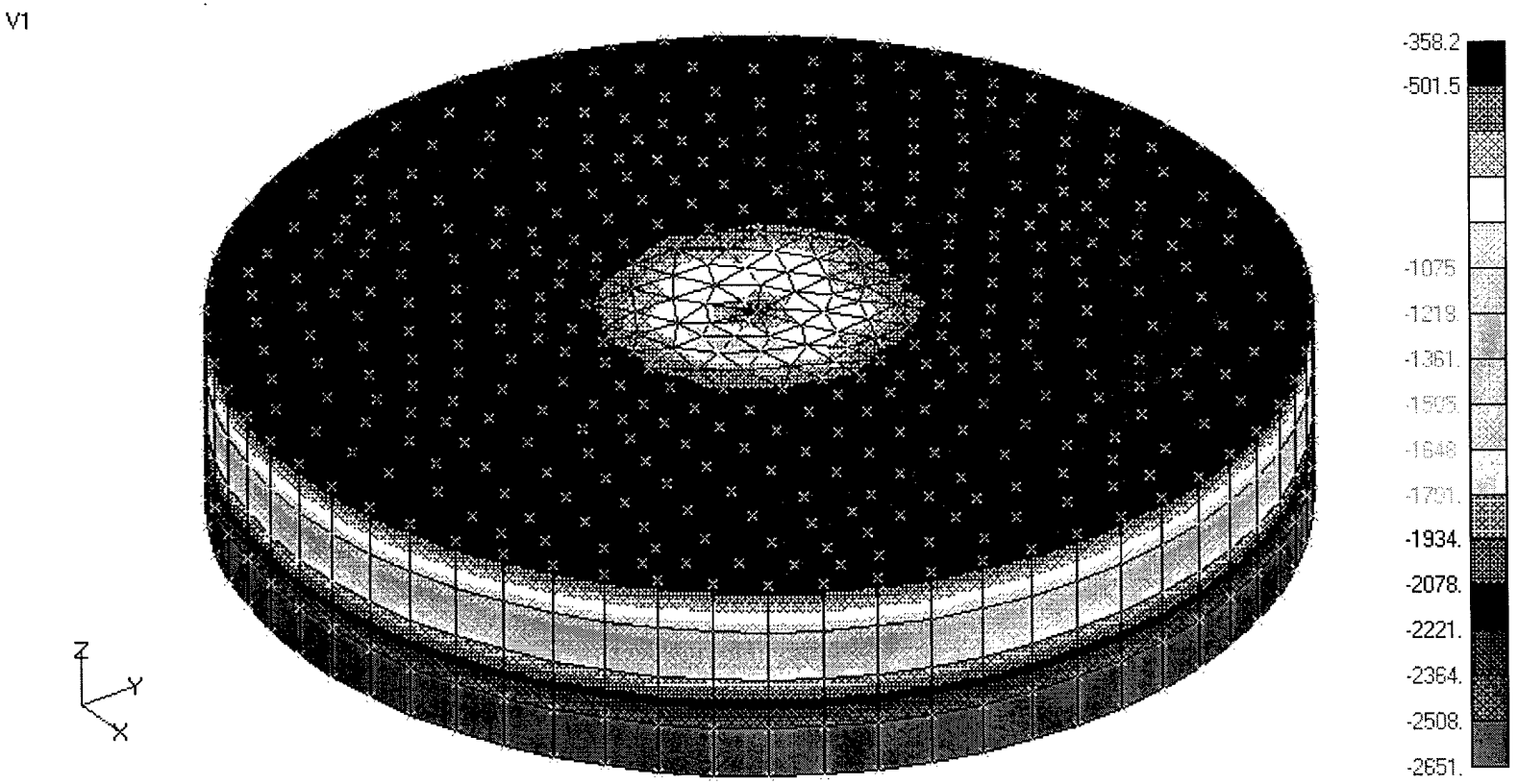

Vertical Load = 6,500,000 lbs
Linear Elastic-Perfectly Plastic Sandy Soil (Linear Extended Drucker-Prager)
E = 864,000 psf, υ = 0.3, Slope Angle = 42.6°, Dilation Angle = 21.5°
Pile, AISI 4340 Steel

Figure-B38. Soil Minor Principal Stresses on a Vertical Plane (Y-shaped Section)

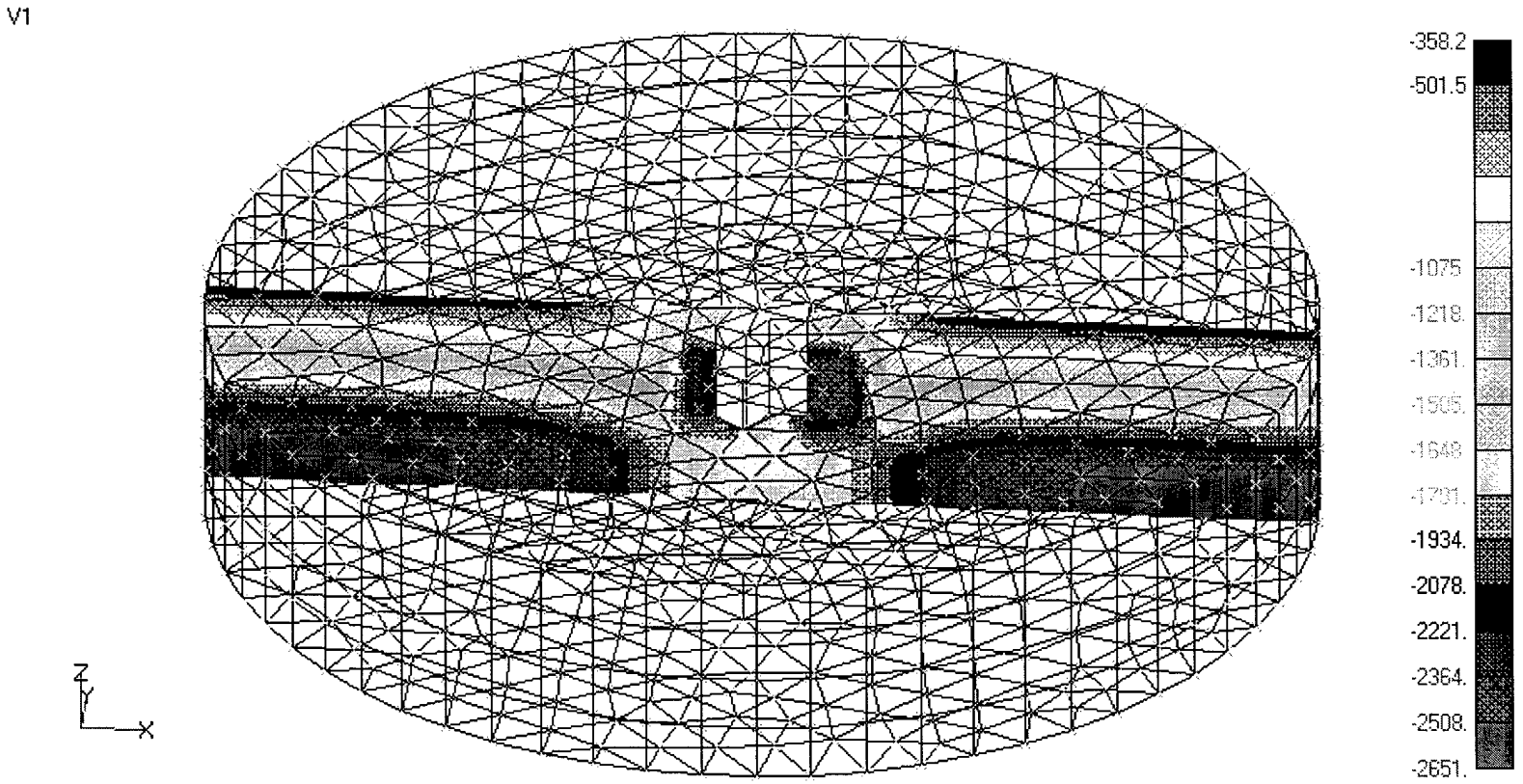

Vertical Load = 6,500,000 lbs
Linear Elastic-Perfectly Plastic Sandy Soil (Linear Extended Drucker-Prager)
E = 864,000 psf, υ = 0.3, Slope Angle = 42.6°, Dilation Angle = 21.5°
Pile, AISI 4340 Steel

Figure-B39. Pile von Mises Stresses on the Pile Surface (Y-shaped Section)

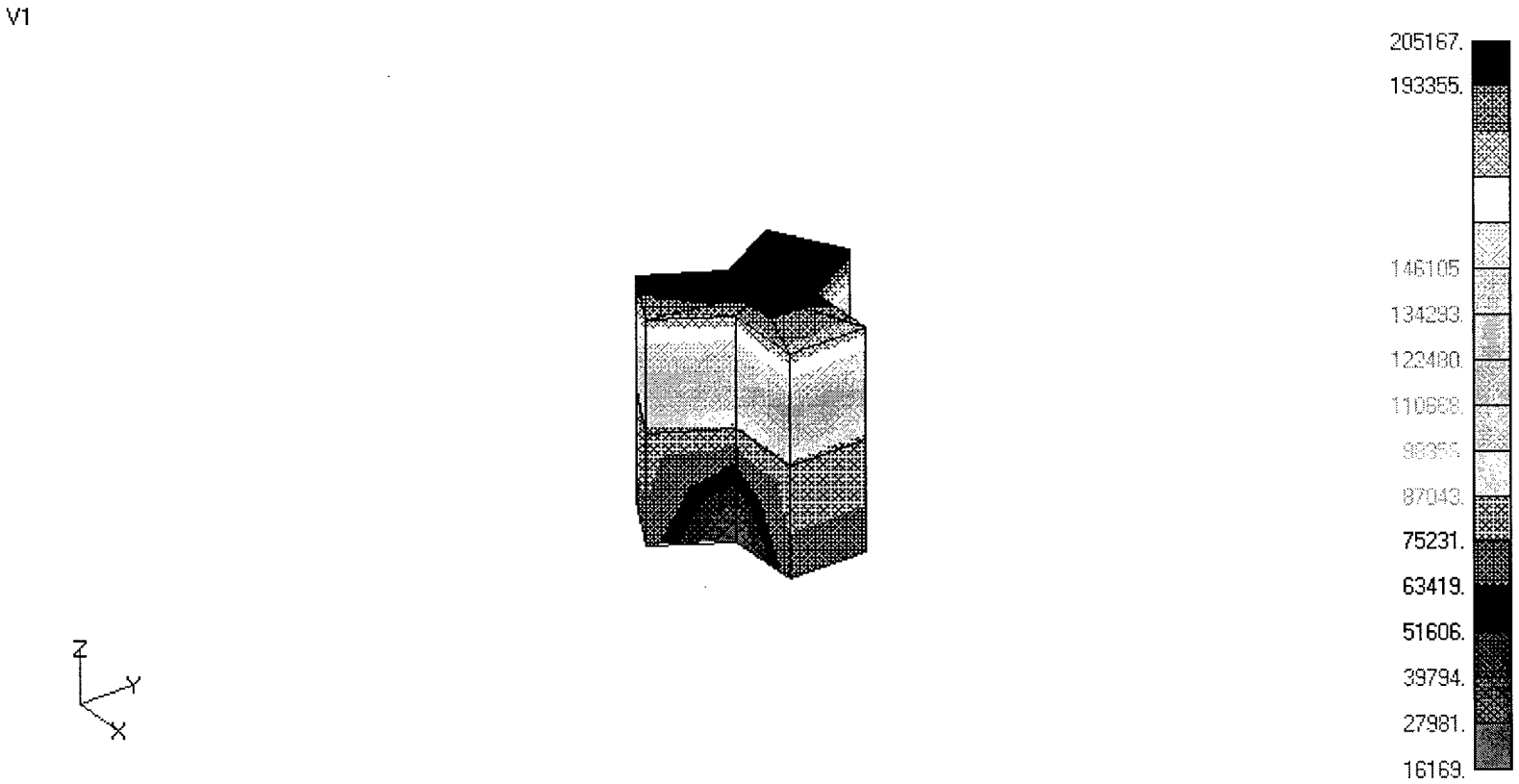

Vertical Load = 6,500,000 lbs
Linear Elastic-Perfectly Plastic Sandy Soil (Linear Extended Drucker-Prager)
E = 864,000 psf, υ = 0.3, Slope Angle = 42.6°, Dilation Angle = 21.5°
Pile, AISI 4340 Steel
Figure-C1. Horizontal Displacements (Circular Section)

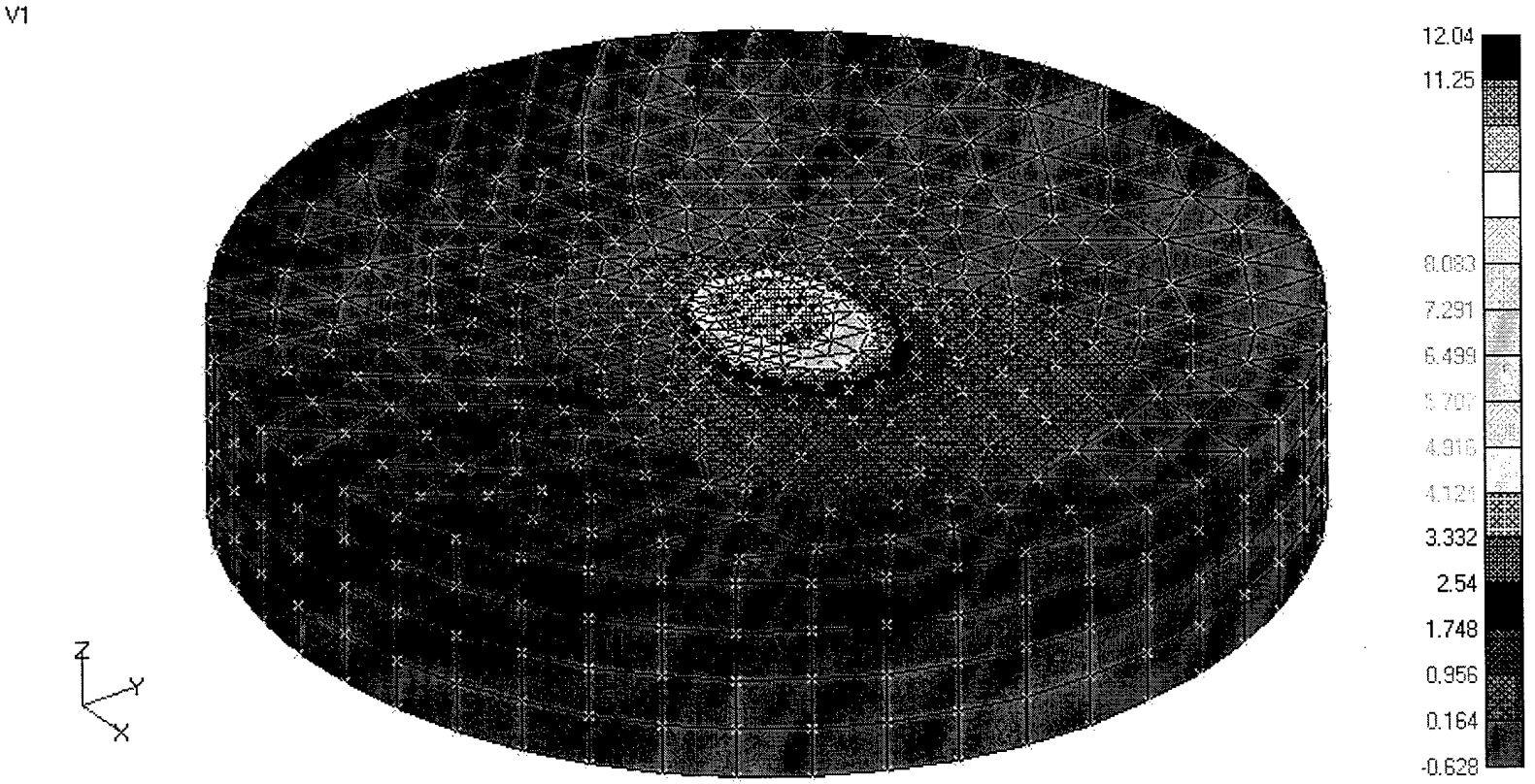

Horizontal Load = 1,900,000 lbs
Linear Elastic-Perfectly Plastic Clayey Soil (Hyperbolic Extended Drucker-Prager)
E = 30,000 psf, υ = 0.499, Slope Angle = 10.2°, Dilation Angle = 10.2°
Pile, AISI 4340 Steel

Figure-C2. Horizontal Displacements on a Vertical Plane along the Horizontal Load Direction (Circular Section)

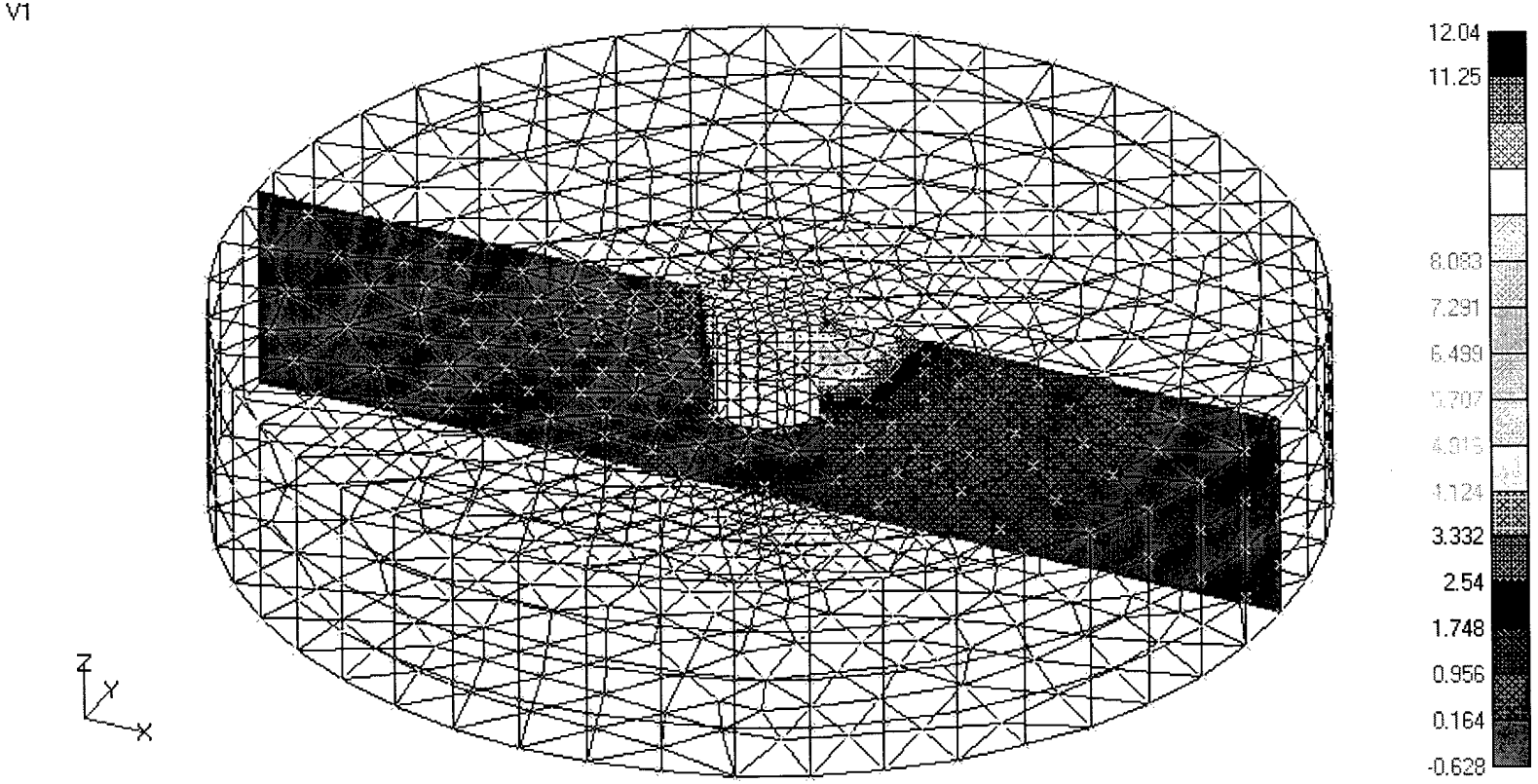

Horizontal Load = 1,900,000 lbs
Linear Elastic-Perfectly Plastic Clayey Soil (Hyperbolic Extended Drucker-Prager)
E = 30,000 psf, $\upsilon = 0.499$, Slope Angle = 10.2^{o}, Dilation Angle = 10.2^{o}
Pile, AISI 4340 Steel

Figure-C3. Pile Total Displacements (Circular Section)

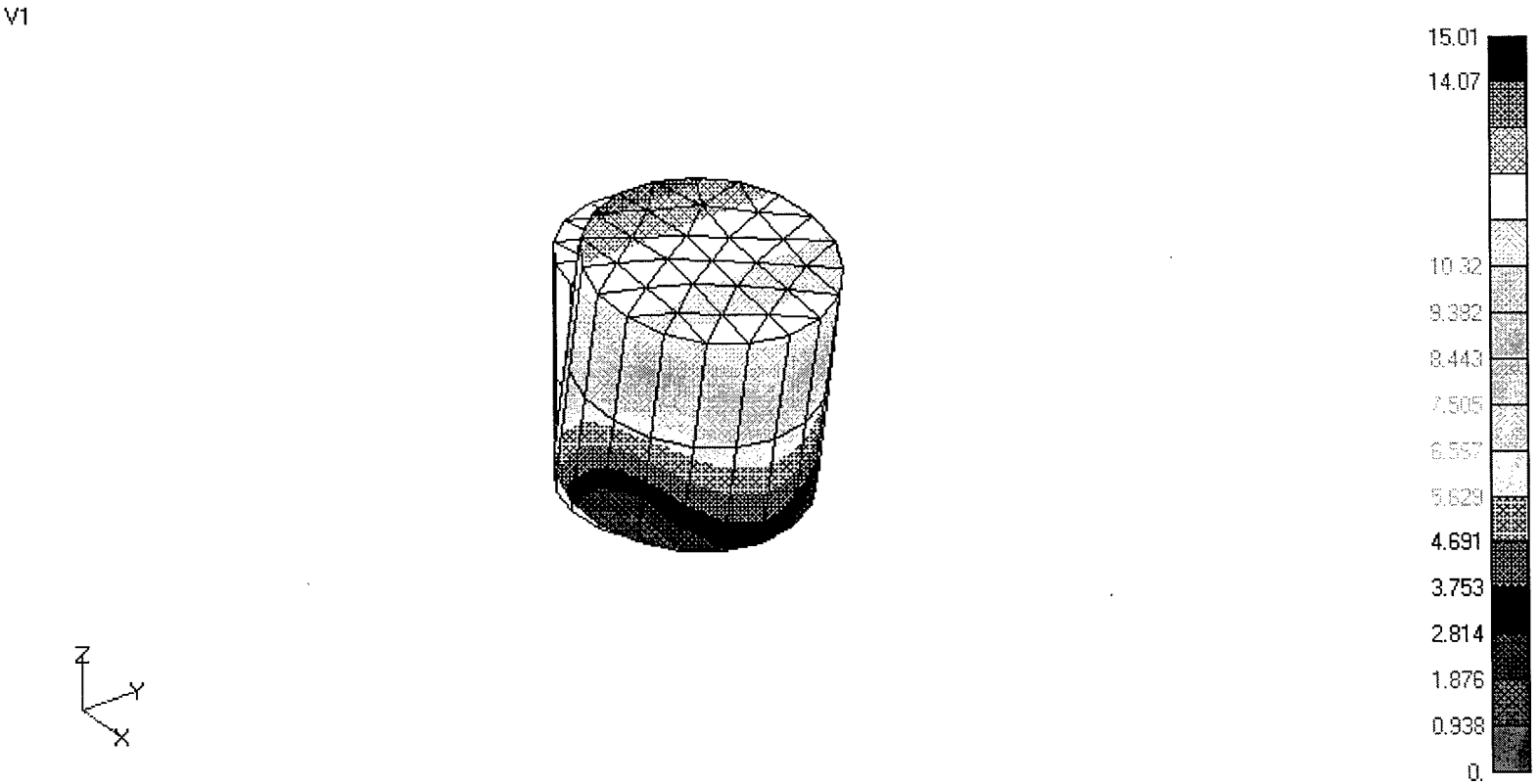

Horizontal Load = 1,900,000 lbs
Linear Elastic-Perfectly Plastic Clayey Soil (Hyperbolic Extended Drucker-Prager)
E = 30,000 psf, υ = 0.499, Slope Angle = 10.2°, Dilation Angle = 10.2°
Pile, AISI 4340 Steel

Figure-C4. Soil Minor Principal Stresses (Circular Section)

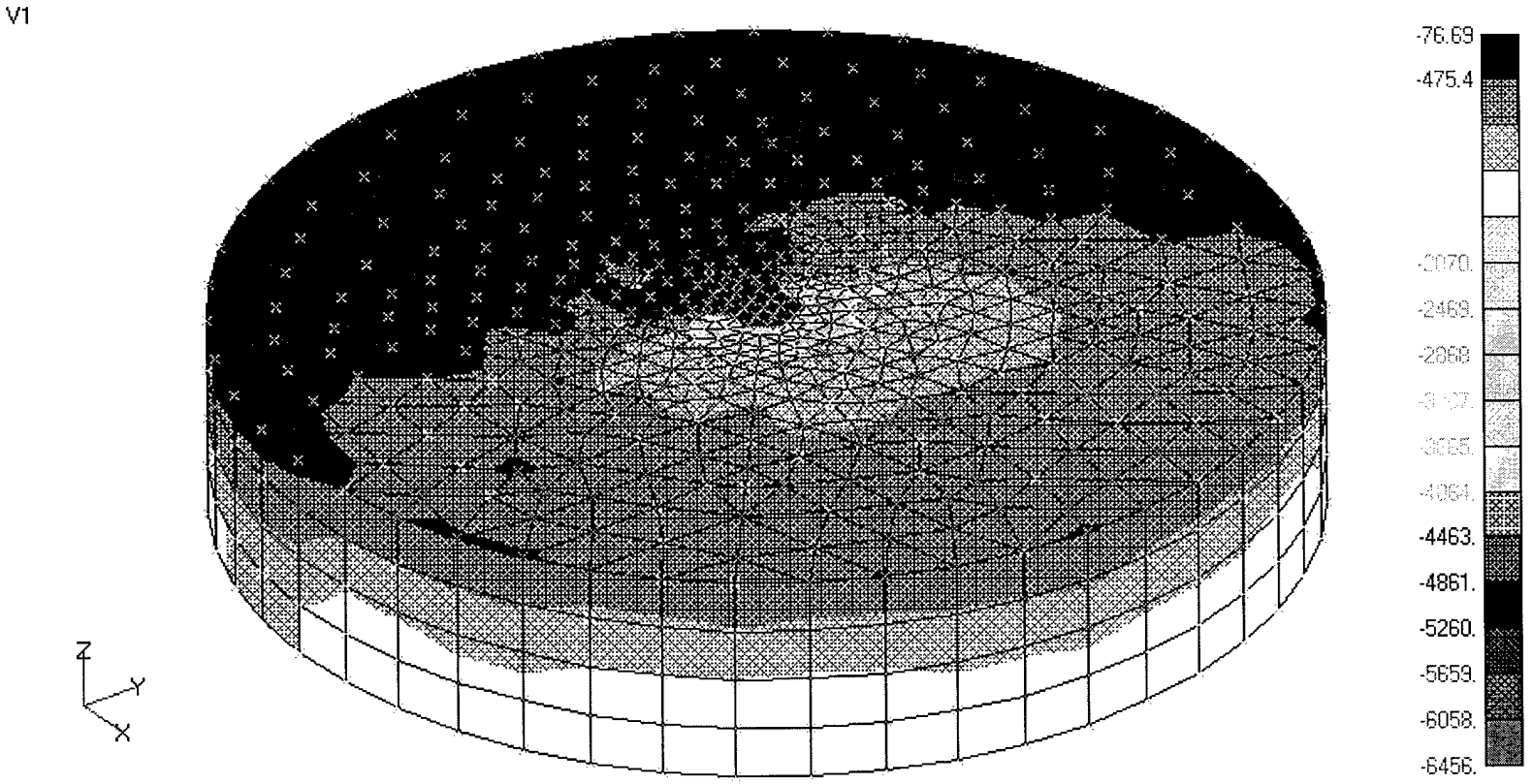

Horizontal Load = 1,900,000 lbs
Linear Elastic-Perfectly Plastic Clayey Soil (Hyperbolic Extended Drucker-Prager)
E = 30,000 psf, υ = 0.499, Slope Angle = 10.2°, Dilation Angle = 10.2°
Pile, AISI 4340 Steel

Figure-C5. Soil Minor Principal Stresses on a Vertical Plane along the Horizontal Load Direction (Circular Section)

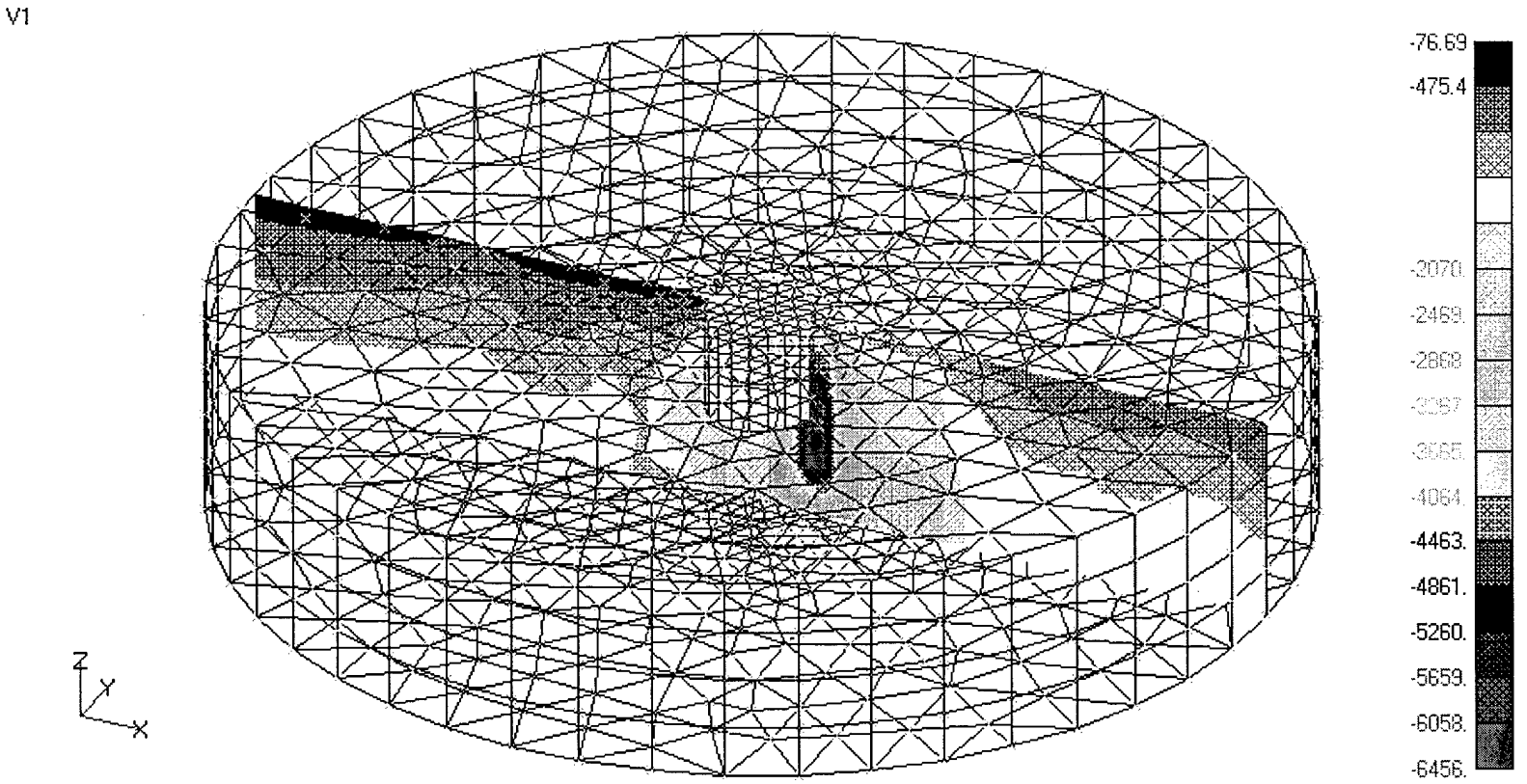

Horizontal Load = 1,900,000 lbs
Linear Elastic-Perfectly Plastic Clayey Soil (Hyperbolic Extended Drucker-Prager)
E = 30,000 psf, $\upsilon = 0.499$, Slope Angle = 10.2^{o}, Dilation Angle = 10.2^{o}
Pile, AISI 4340 Steel

Figure-C6. Horizontal Normal Pile Stresses on the Pile Surface (Circular Section)

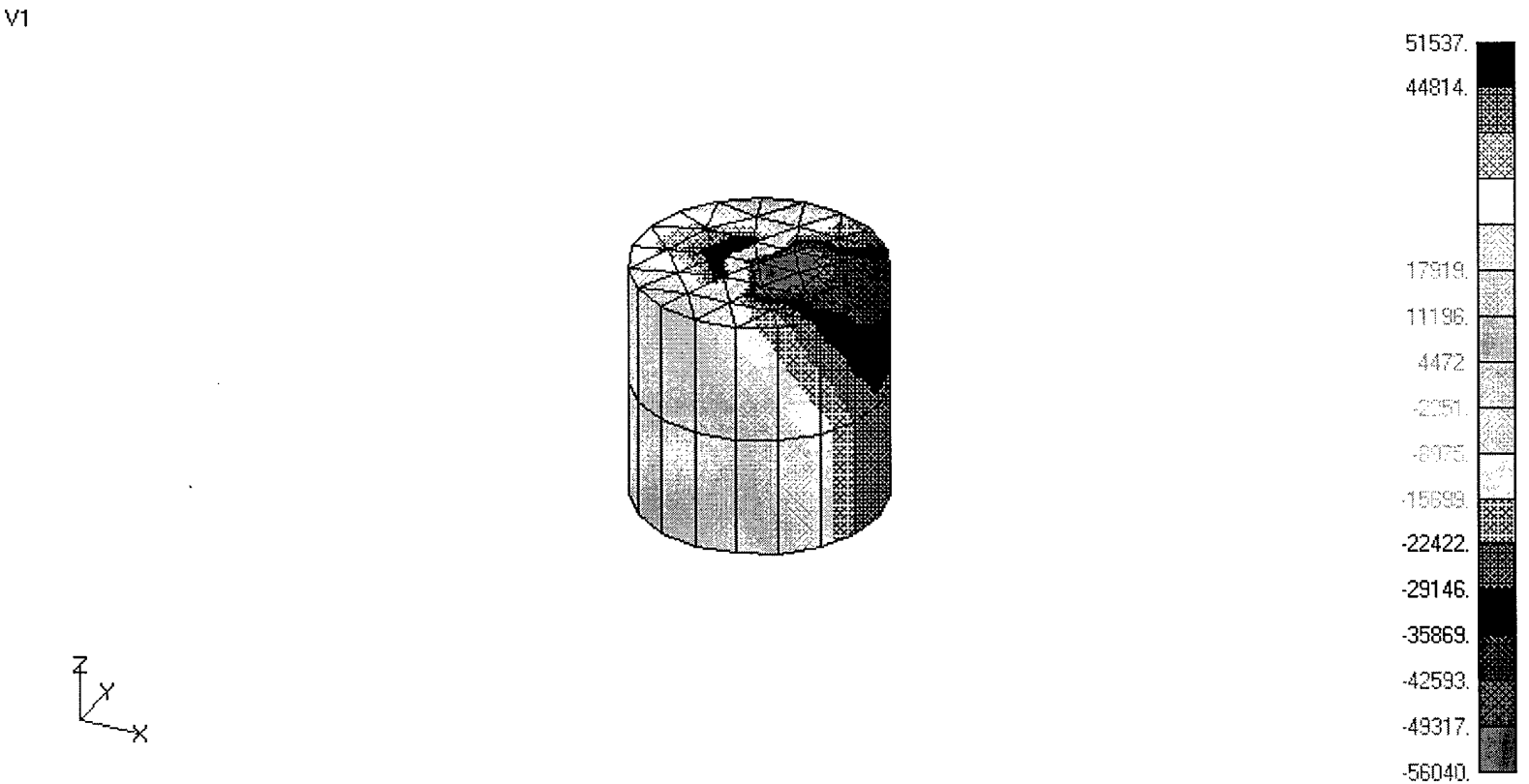

Horizontal Load = 1,900,000 lbs
Linear Elastic-Perfectly Plastic Clayey Soil (Hyperbolic Extended Drucker-Prager)
E = 30,000 psf, υ = 0.499, Slope Angle = 10.2°, Dilation Angle = 10.2°
Pile, AISI 4340 Steel

Figure-C7. Pile von Mises Stresses on the Pile Surface (Circular Section)

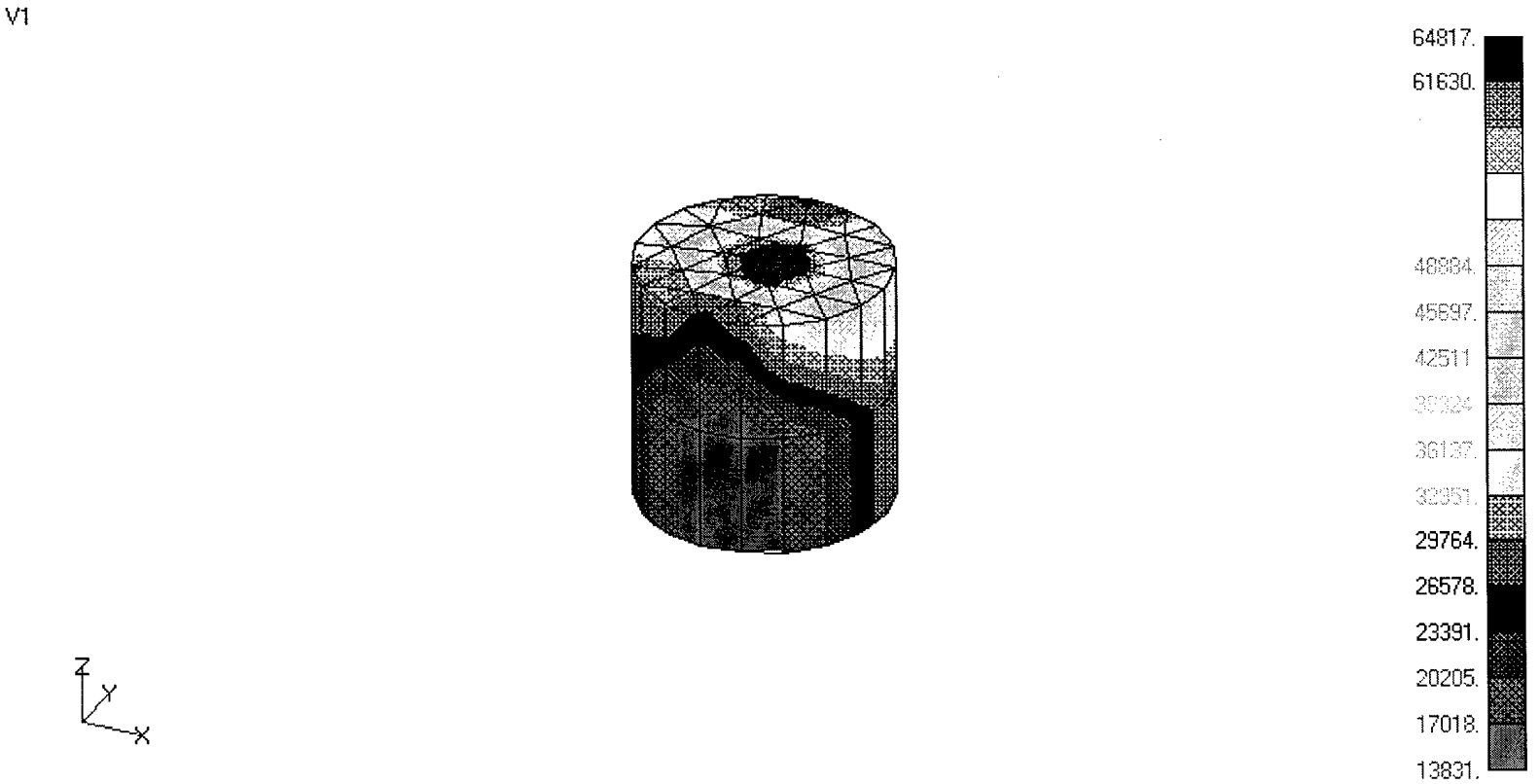

Horizontal Load = 1,900,000 lbs
Linear Elastic-Perfectly Plastic Clayey Soil (Hyperbolic Extended Drucker-Prager)
E = 30,000 psf, υ = 0.499, Slope Angle = 10.2°, Dilation Angle = 10.2°
Pile, AISI 4340 Steel

Figure-C8. Vertical Displacements (Circular Section)

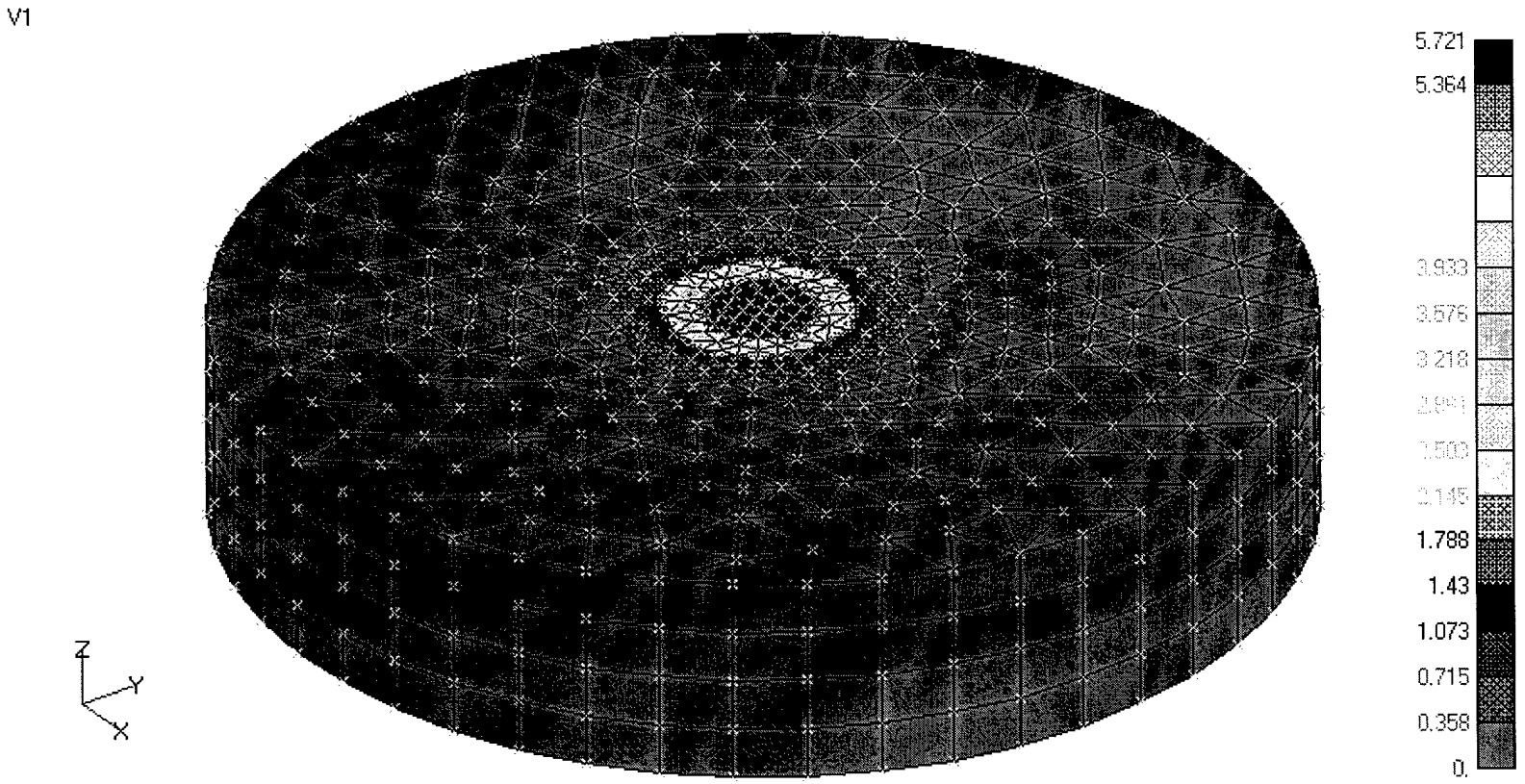

Vertical Load = 2,300,000 lbs
Linear Elastic-Perfectly Plastic Clayey Soil (Hyperbolic Extended Drucker-Prager)
E = 30,000 psf, υ = 0.499, Slope Angle = 10.2°, Dilation Angle = 10.2°
Pile, AISI 4340 Steel

Figure-C9. Vertical Displacements on a Vertical Plane (Circular Section)

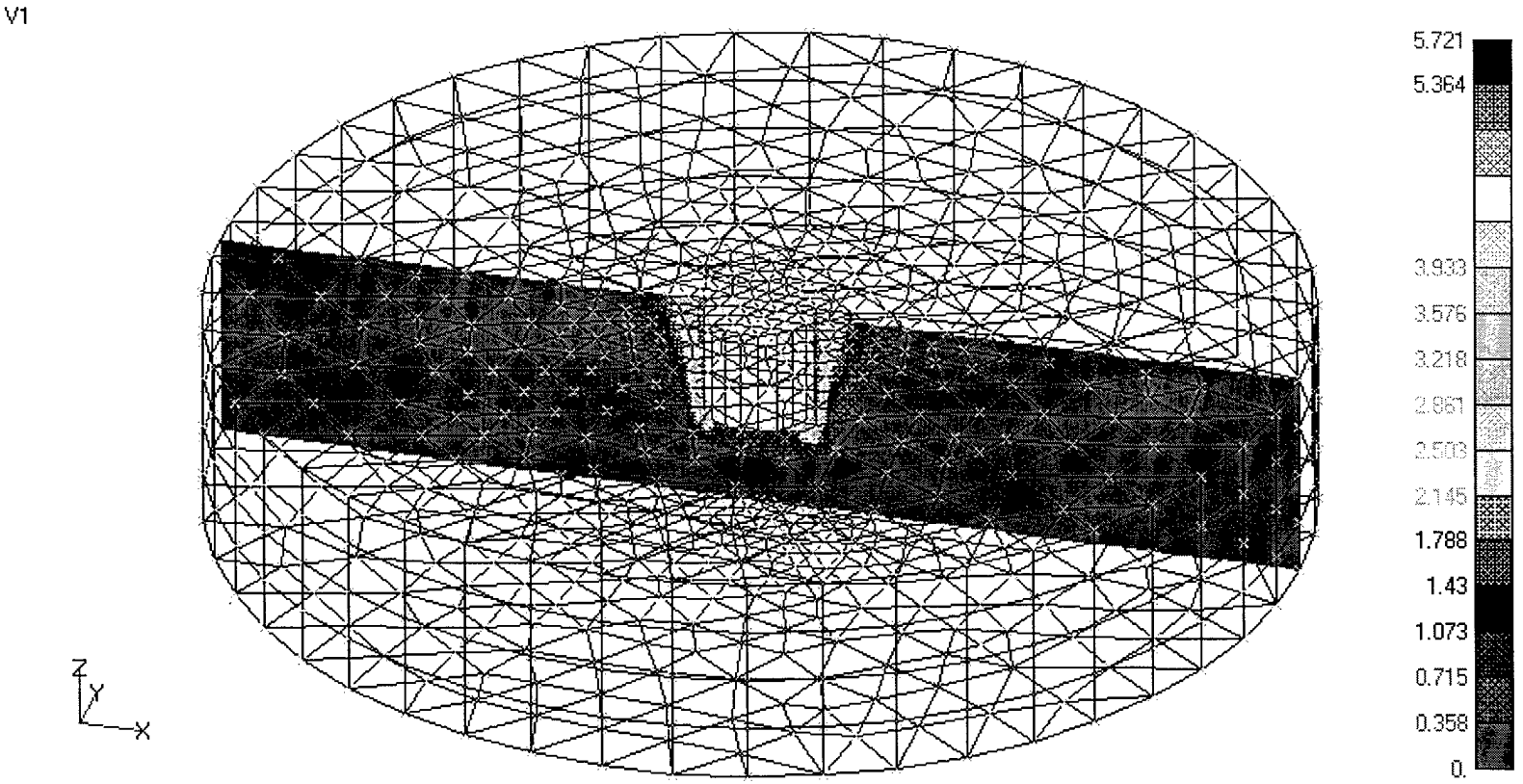

Vertical Load = 2,300,000 lbs
Linear Elastic-Perfectly Plastic Clayey Soil (Hyperbolic Extended Drucker-Prager)
E = 30,000 psf, υ = 0.499, Slope Angle = 10.2°, Dilation Angle = 10.2°
Pile, AISI 4340 Steel

Figure-C10. Pile Vertical Displacements (Circular Section)

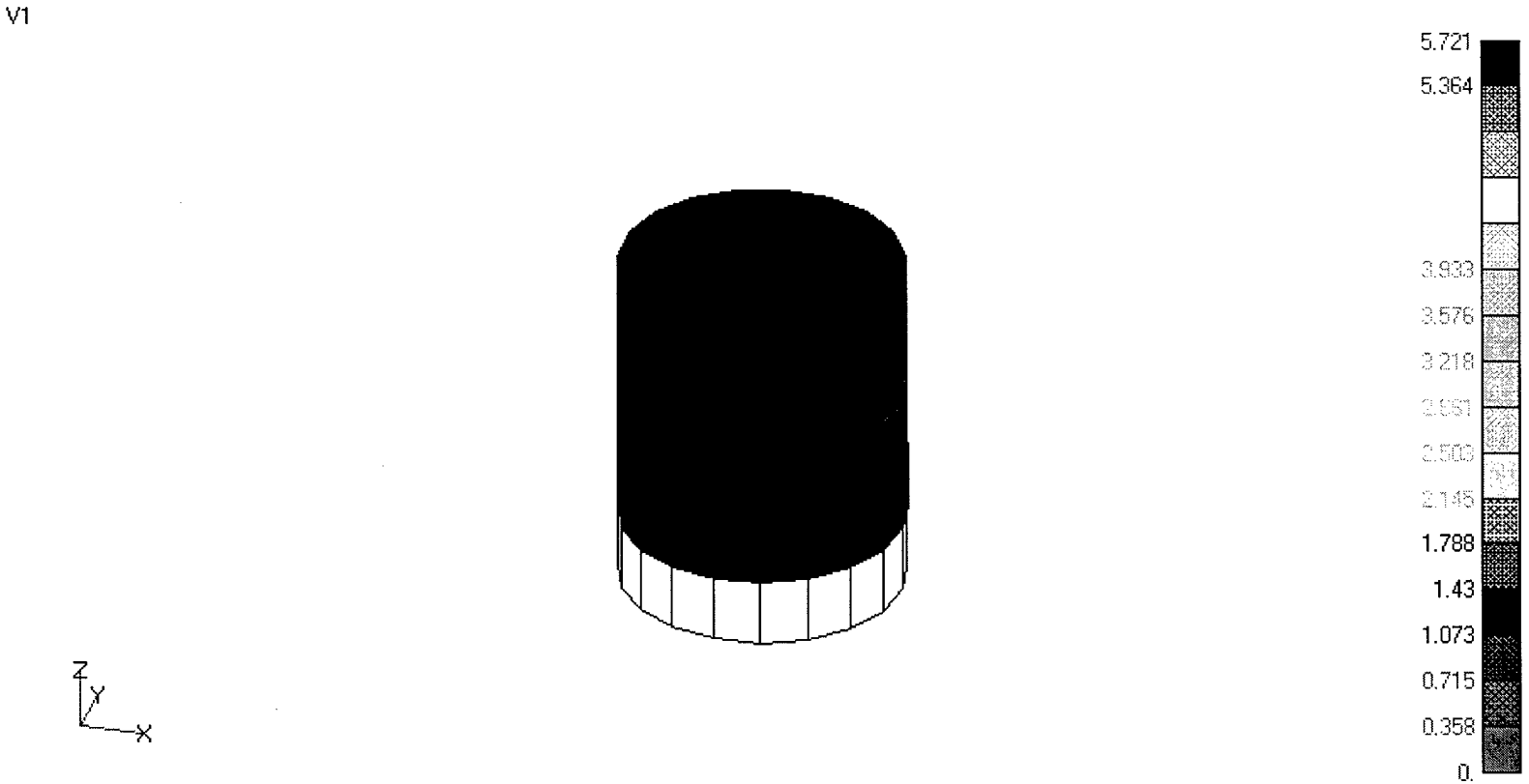

Vertical Load = 2,300,000 lbs
Linear Elastic-Perfectly Plastic Clayey Soil (Hyperbolic Extended Drucker-Prager)
E = 30,000 psf, υ = 0.499, Slope Angle = 10.2°, Dilation Angle = 10.2°
Pile, AISI 4340 Steel

Figure-C11. Soil Minor Principal Stresses on a Vertical Plane (Circular Section)

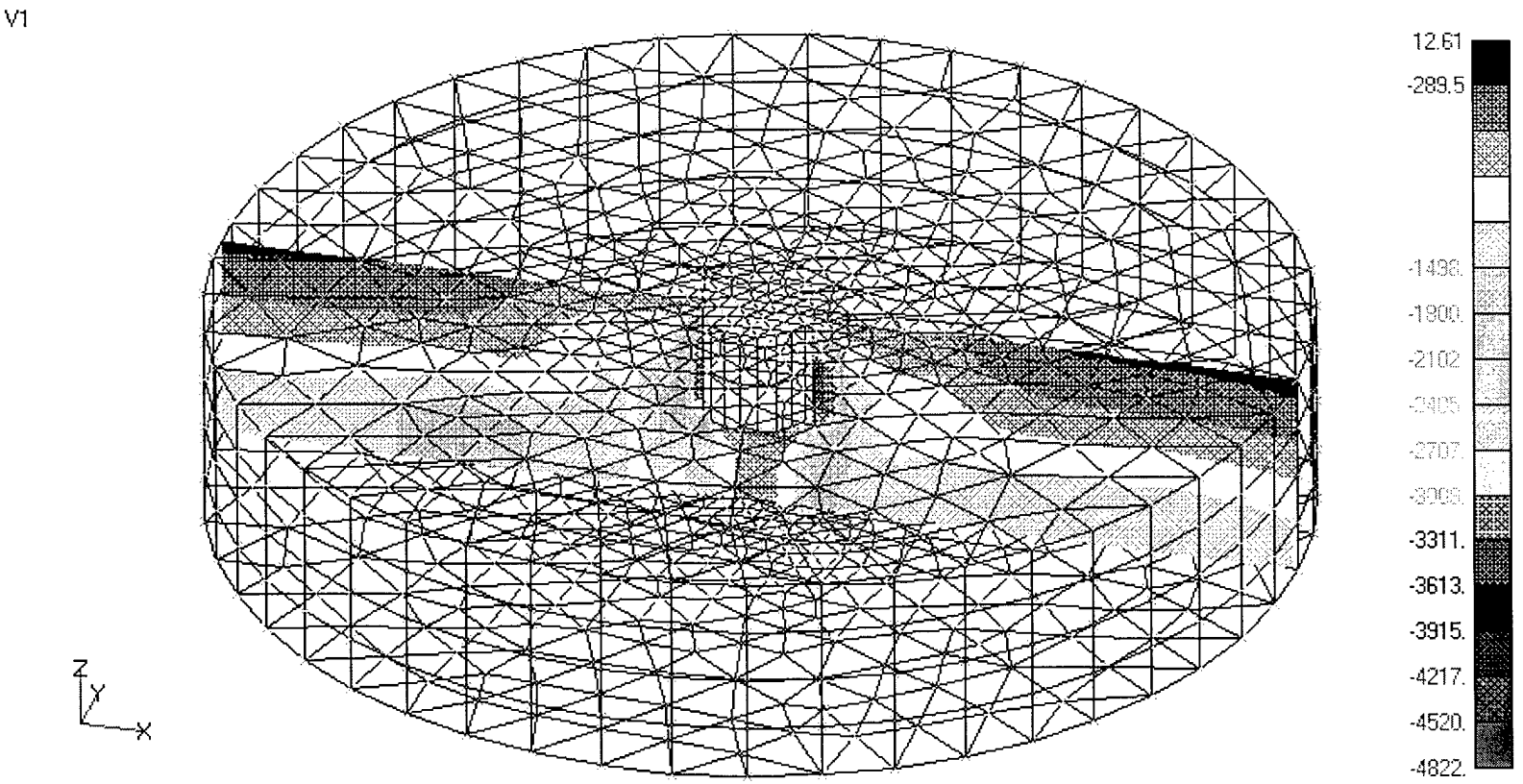

Vertical Load = 2,300,000 lbs
Linear Elastic-Perfectly Plastic Clayey Soil (Hyperbolic Extended Drucker-Prager)
E = 30,000 psf, υ = 0.499, Slope Angle = 10.2°, Dilation Angle = 10.2°
Pile, AISI 4340 Steel

Figure-C12. Soil Minor Principal Stresses on the Pile Surface (Circular Section)

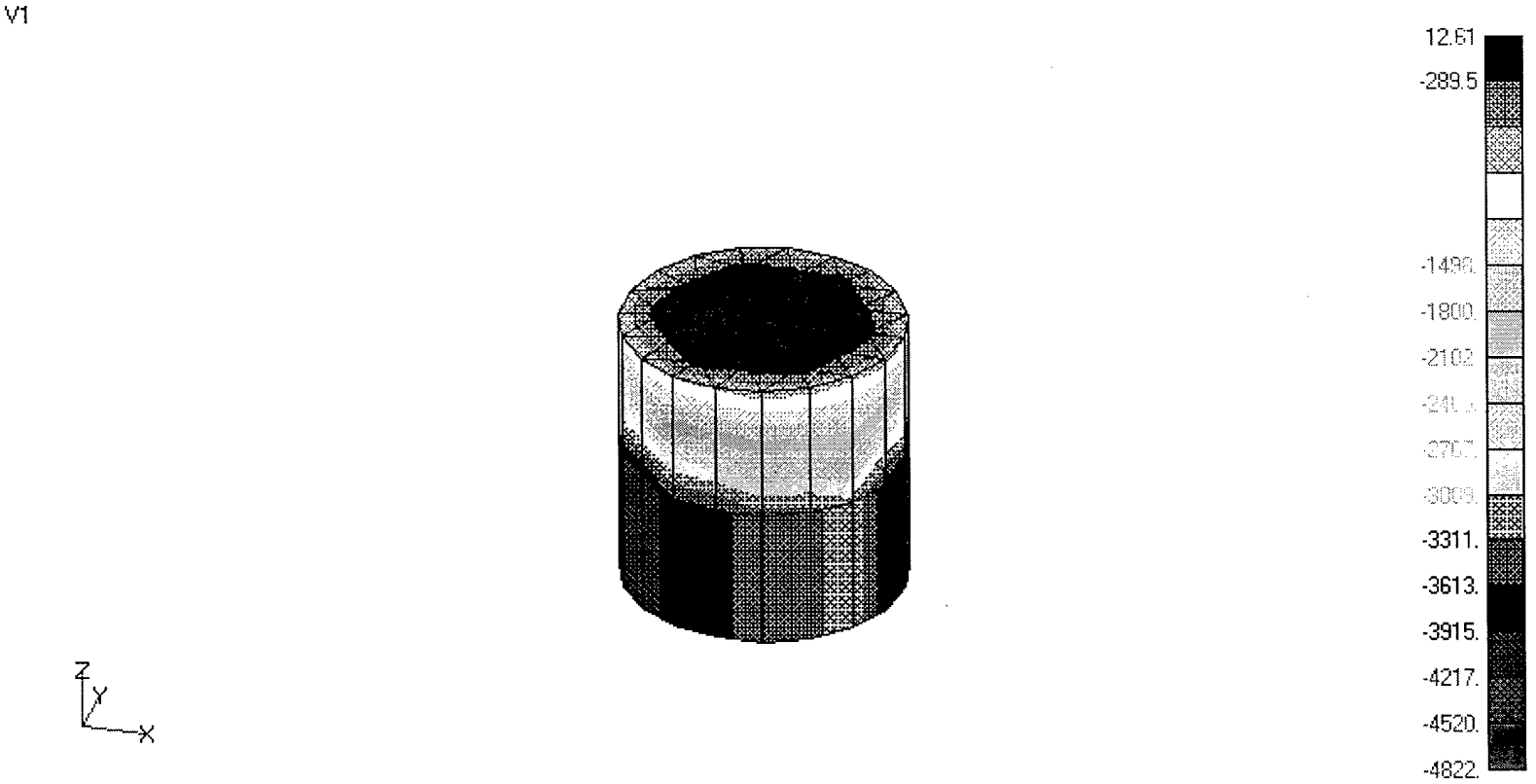

Vertical Load = 2,300,000 lbs
Linear Elastic-Perfectly Plastic Clayey Soil (Hyperbolic Extended Drucker-Prager)
E = 30,000 psf, $\upsilon = 0.499$, Slope Angle = 10.2°, Dilation Angle = 10.2°
Pile, AISI 4340 Steel

Figure-C13. Pile von Mises Stresses on the Pile Surface (Circular Section)

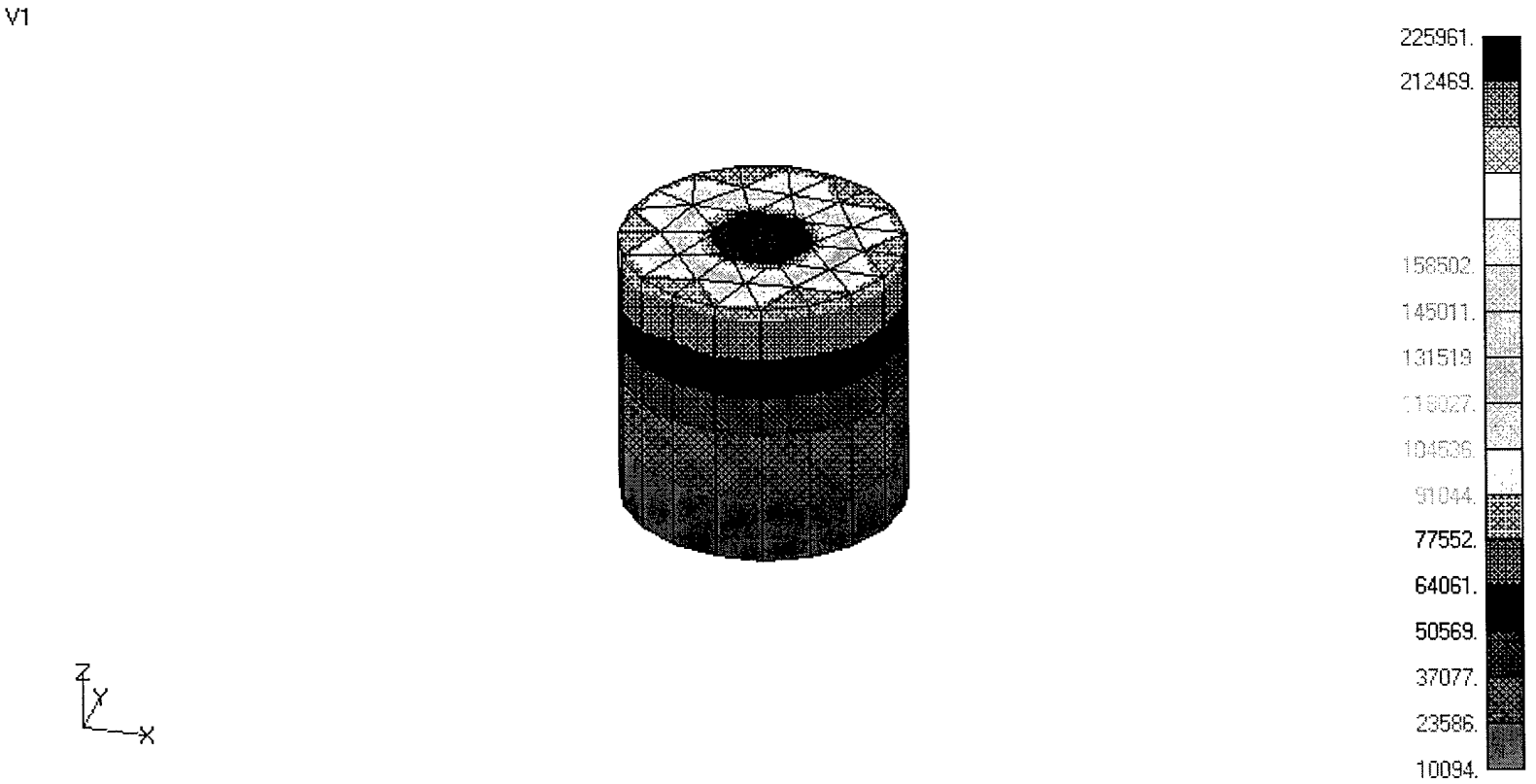

Vertical Load = 2,300,000 lbs
Linear Elastic-Perfectly Plastic Clayey Soil (Hyperbolic Extended Drucker-Prager)
E = 30,000 psf, υ = 0.499, Slope Angle = 10.2°, Dilation Angle = 10.2°
Pile, AISI 4340 Steel

Figure-C14. Horizontal Displacements (Triangular Section)

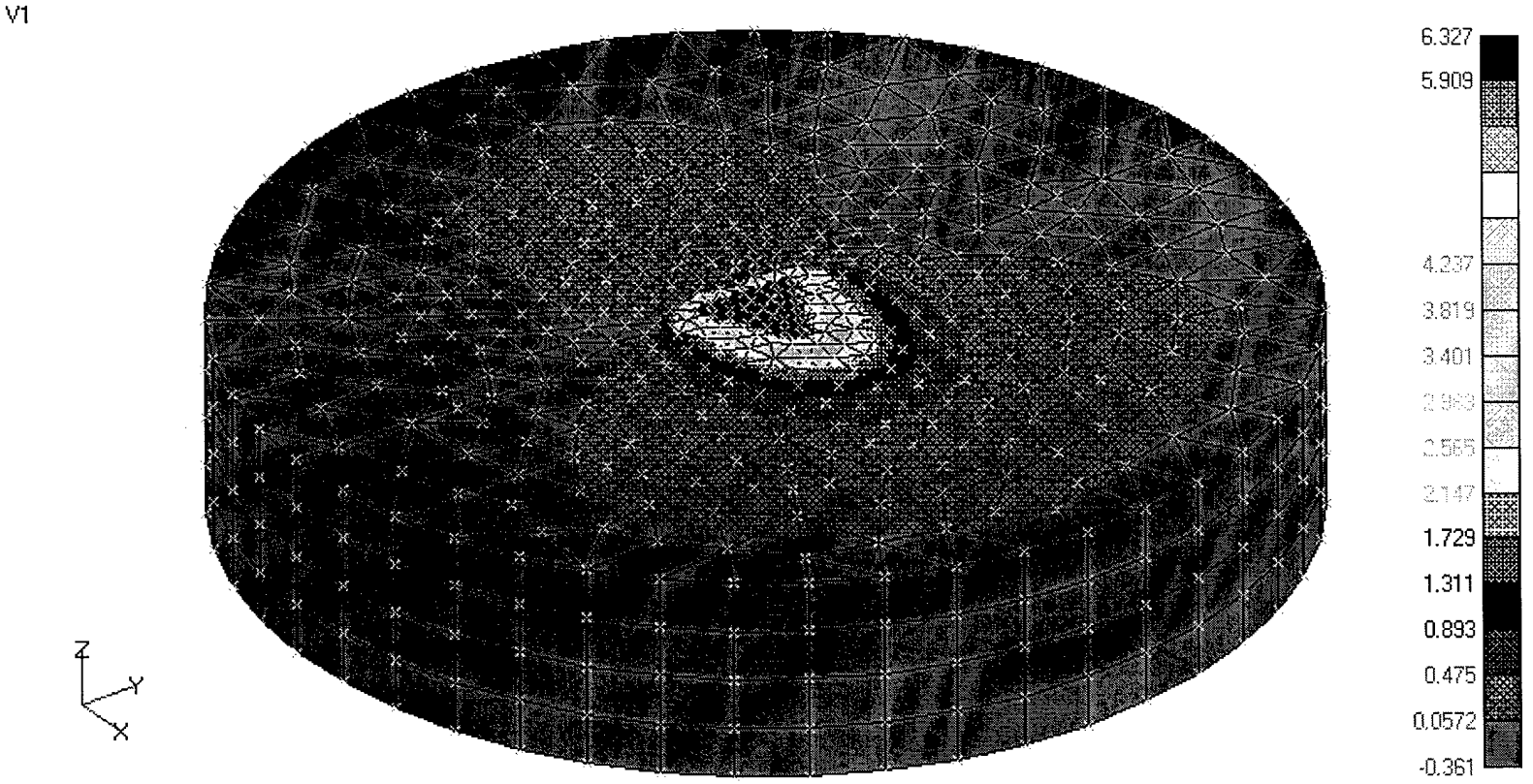

Horizontal Load = 1,800,000 lbs
Linear Elastic-Perfectly Plastic Clayey Soil (Hyperbolic Extended Drucker-Prager)
E = 30,000 psf, υ = 0.499, Slope Angle = 10.2°, Dilation Angle = 10.2°
Pile, AISI 4340 Steel

Figure-C15. Horizontal Displacements on a Vertical Plane along the Horizontal Load Direction (Triangular Section)

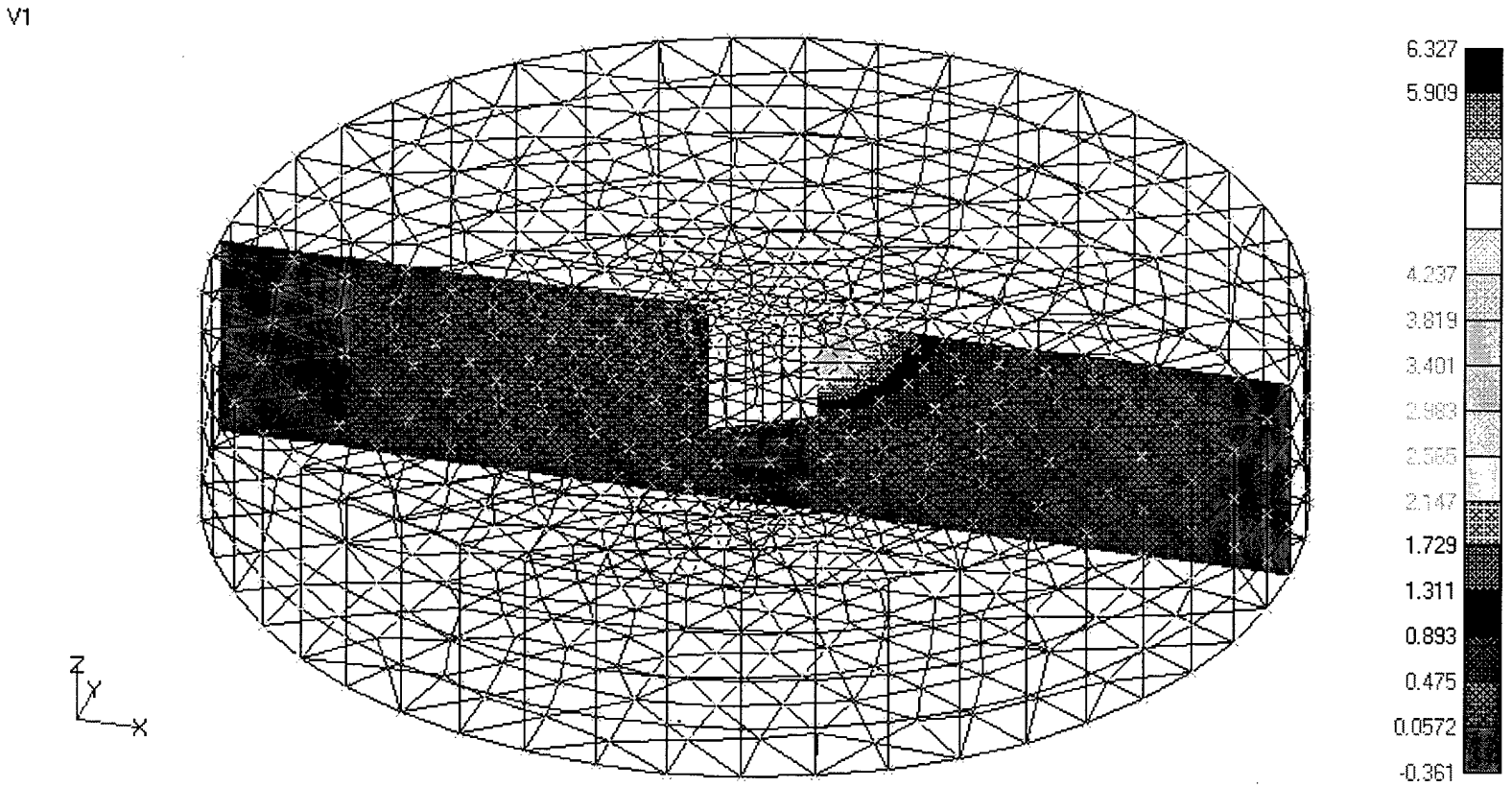

Horizontal Load = 1,800,000 lbs
Linear Elastic-Perfectly Plastic Clayey Soil (Hyperbolic Extended Drucker-Prager)
E = 30,000 psf, υ = 0.499, Slope Angle = 10.2°, Dilation Angle = 10.2°
Pile, AISI 4340 Steel

Figure-C16. Pile Total Displacements (Triangular Section)

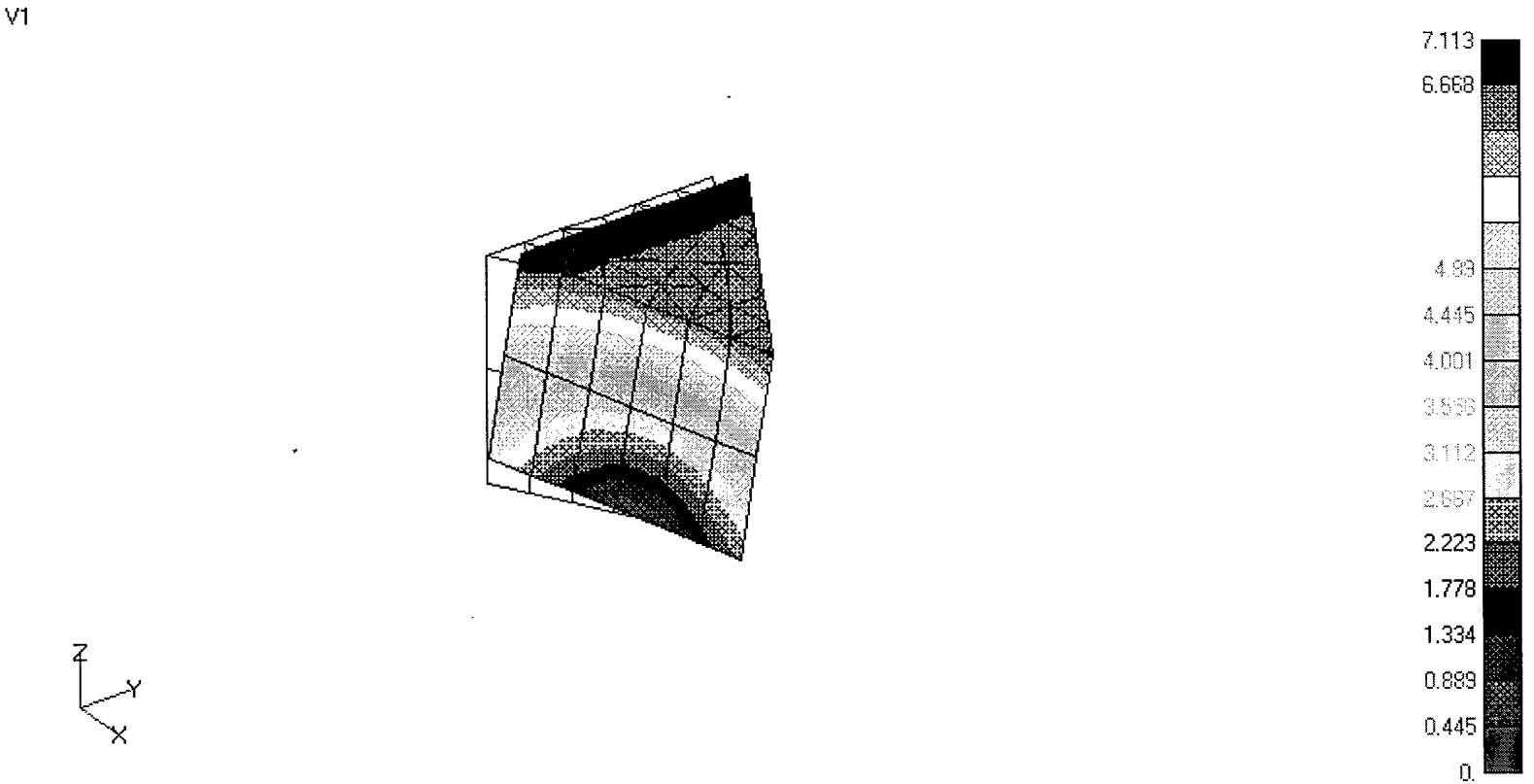

Horizontal Load = 1,800,000 lbs
Linear Elastic-Perfectly Plastic Clayey Soil (Hyperbolic Extended Drucker-Prager)
E = 30,000 psf, $\upsilon = 0.499$, Slope Angle = 10.2^{o}, Dilation Angle = 10.2^{o}
Pile, AISI 4340 Steel

Figure-C17. Soil Minor Principal Stresses (Triangular Section)

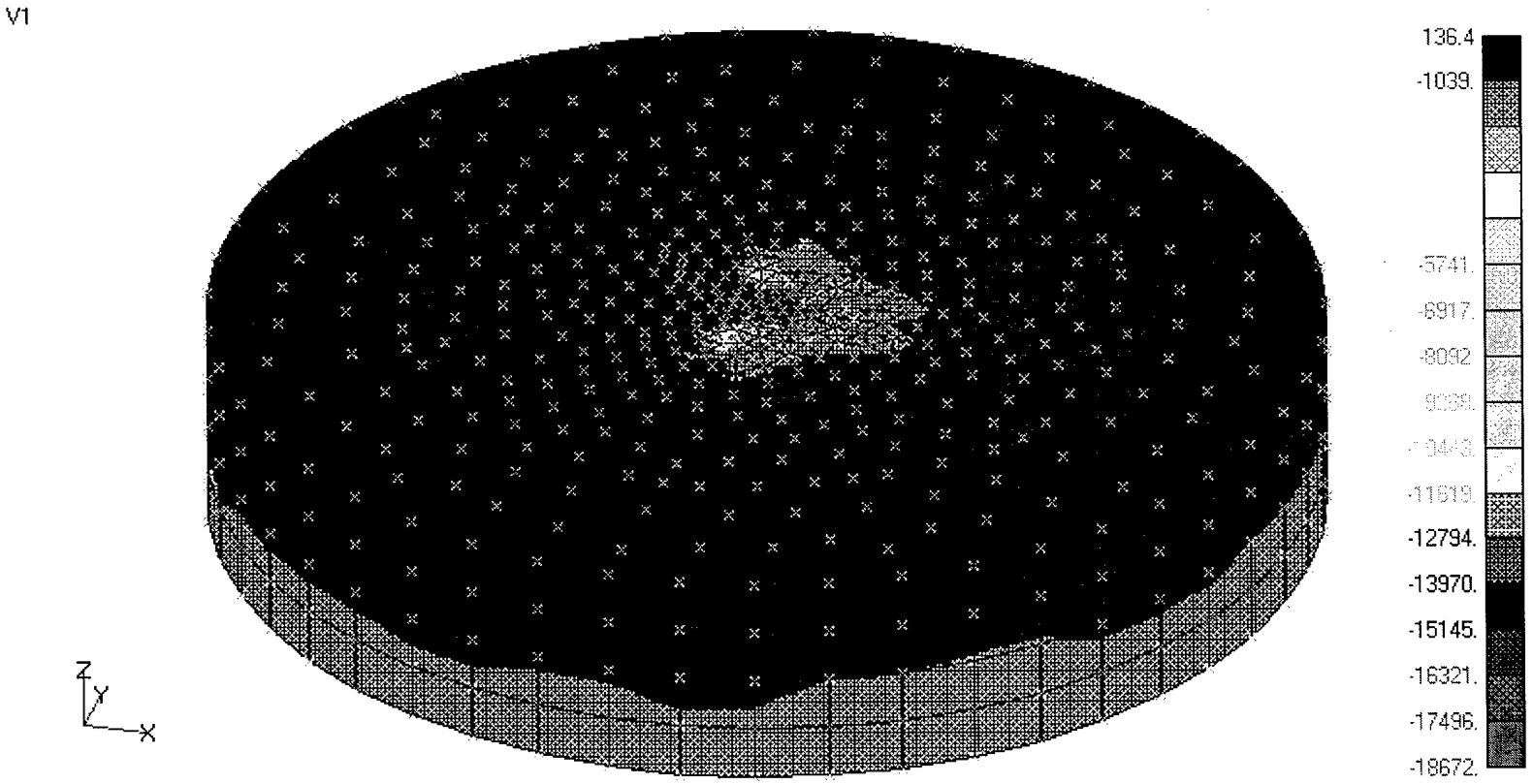

Horizontal Load = 1,800,000 lbs
Linear Elastic-Perfectly Plastic Clayey Soil (Hyperbolic Extended Drucker-Prager)
E = 30,000 psf, $\upsilon = 0.499$, Slope Angle = 10.2^{o}, Dilation Angle = 10.2^{o}
Pile, AISI 4340 Steel

Figure-C18. Soil Minor Principal Stresses on a Vertical Plane along the Horizontal Load Direction (Triangular Section)

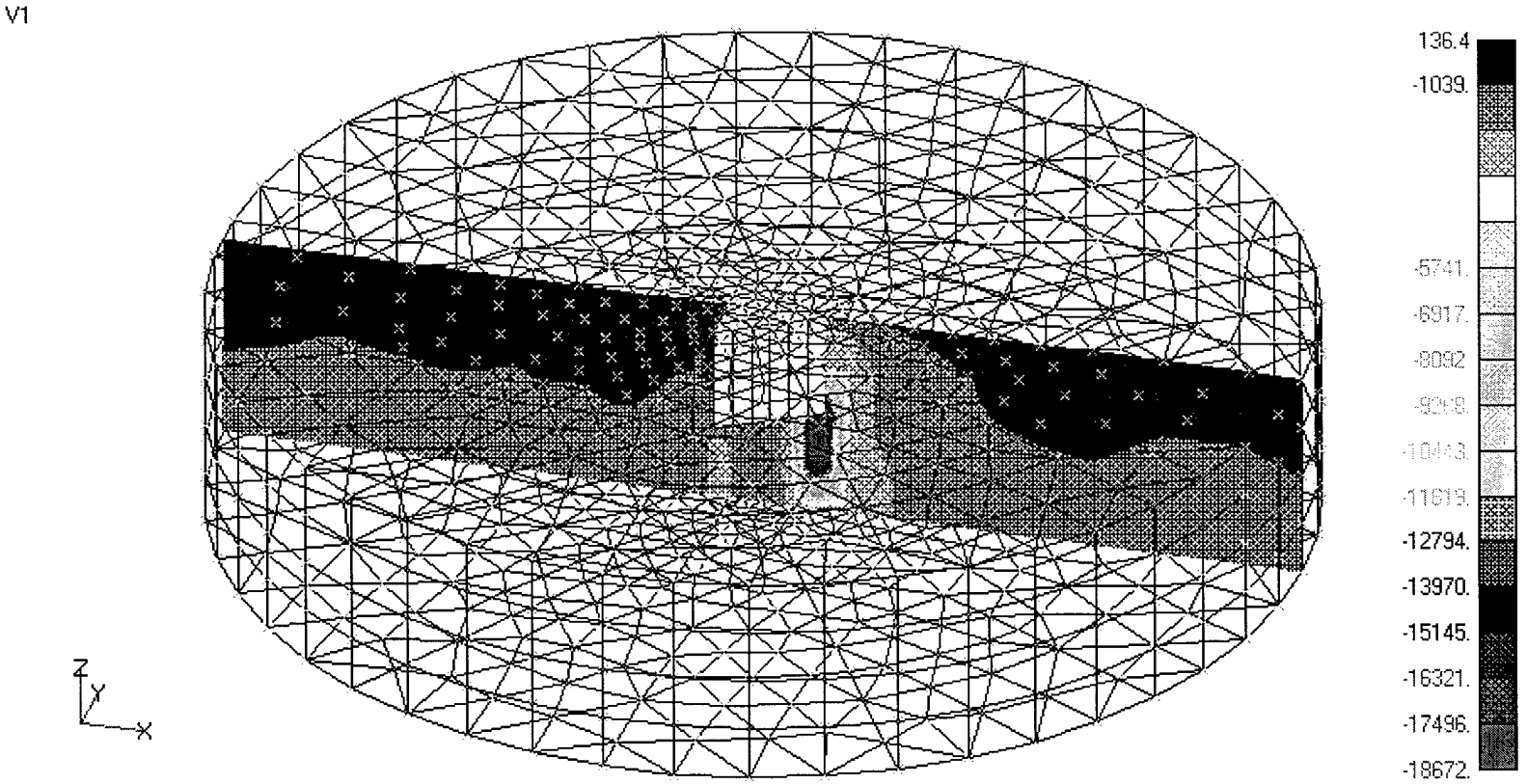

Horizontal Load = 1,800,000 lbs
Linear Elastic-Perfectly Plastic Clayey Soil (Hyperbolic Extended Drucker-Prager)
E = 30,000 psf, υ = 0.499, Slope Angle = 10.2°, Dilation Angle = 10.2°
Pile, AISI 4340 Steel

Figure-C19. Horizontal Normal Pile Stresses on the Pile Surface (Triangular Section)

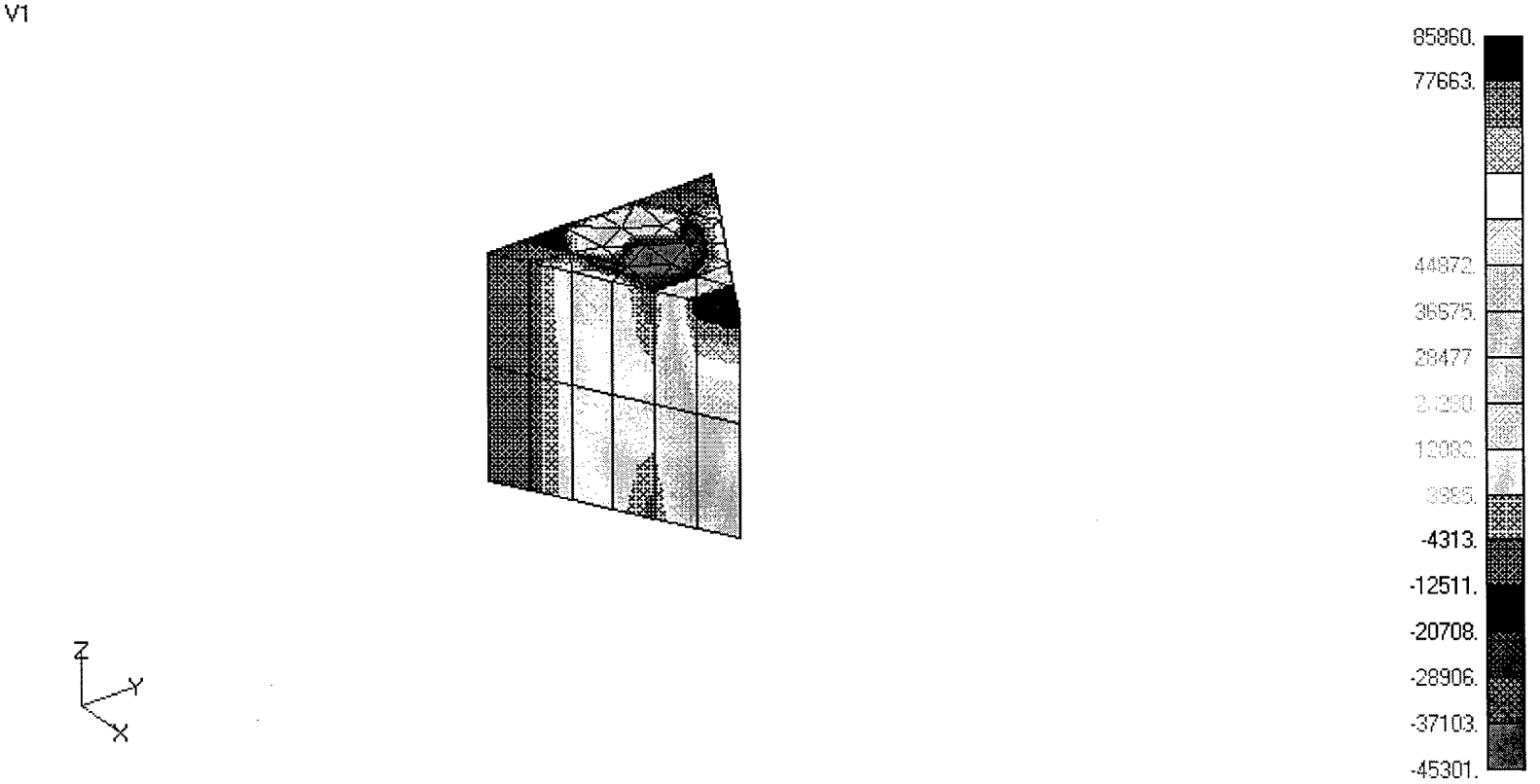

Horizontal Load = 1,800,000 lbs
Linear Elastic-Perfectly Plastic Clayey Soil (Hyperbolic Extended Drucker-Prager)
E = 30,000 psf, υ = 0.499, Slope Angle = 10.2°, Dilation Angle = 10.2°
Pile, AISI 4340 Steel

Figure-C20. Pile von Mises Stresses on the Pile Surface (Triangular Section)

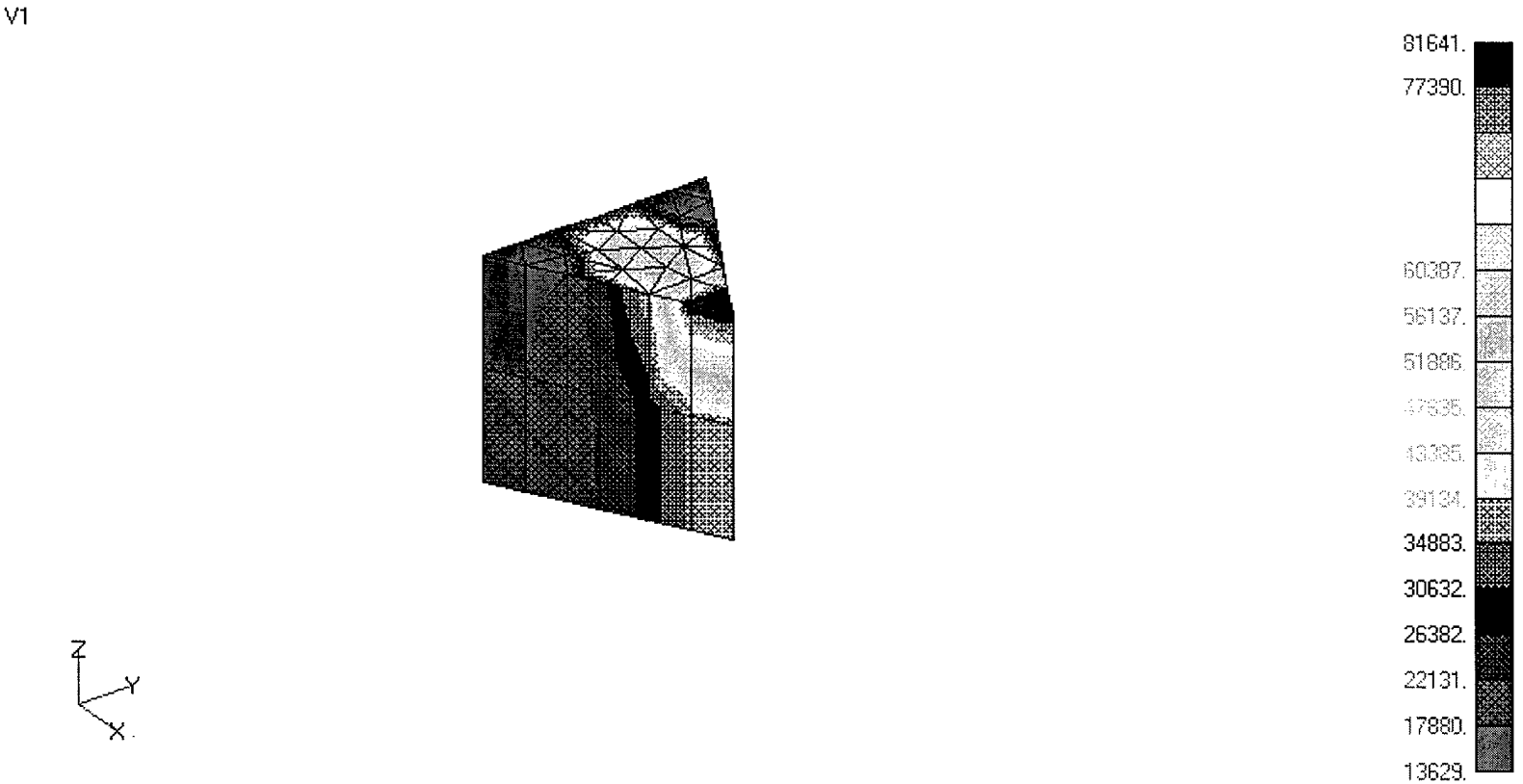

Horizontal Load = 1,800,000 lbs
Linear Elastic-Perfectly Plastic Clayey Soil (Hyperbolic Extended Drucker-Prager)
E = 30,000 psf, υ = 0.499, Slope Angle = 10.2°, Dilation Angle = 10.2°
Pile, AISI 4340 Steel

Figure-C21. Vertical Displacements (Triangular Section)

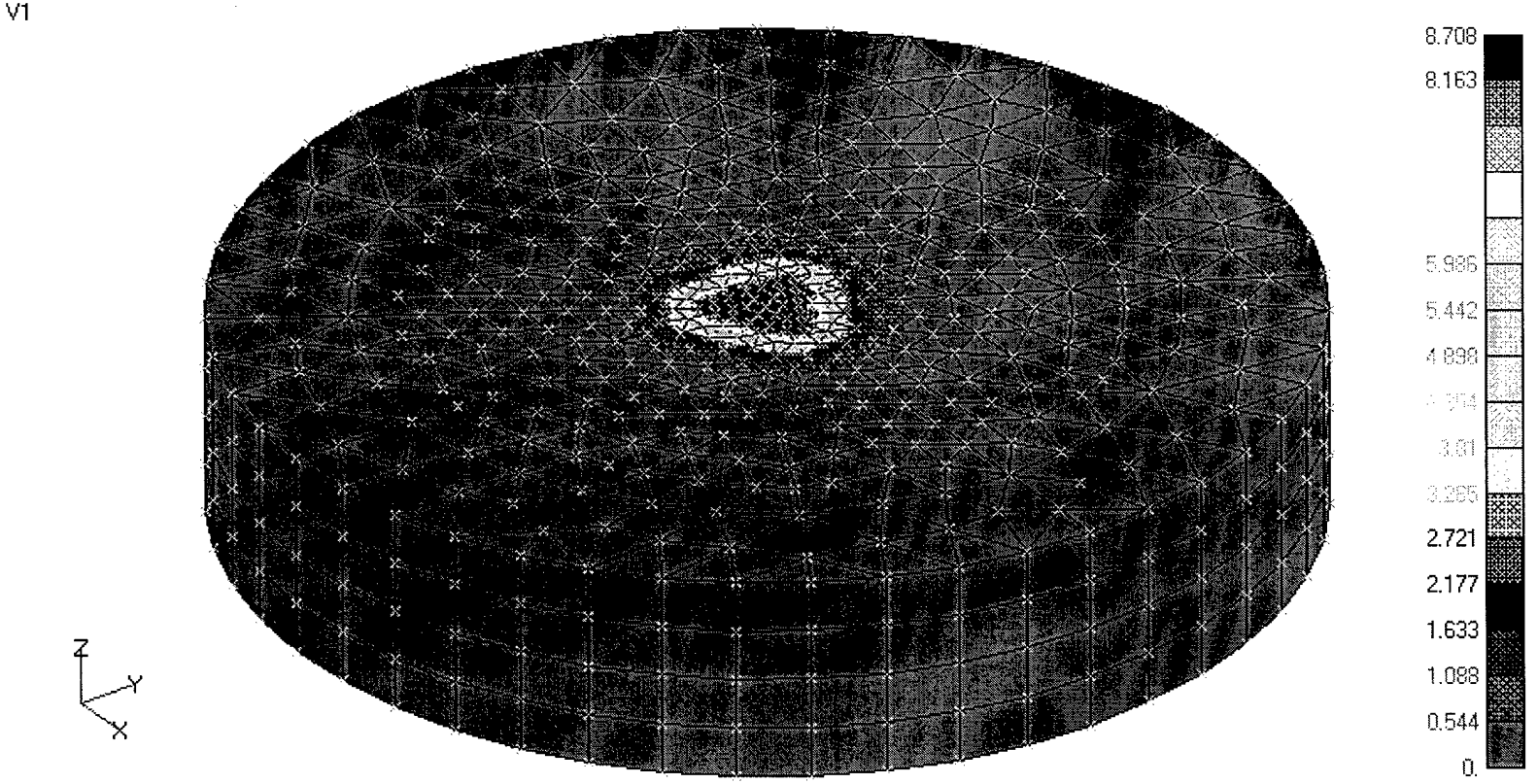

Vertical Load = 2,100,000 lbs
Linear Elastic-Perfectly Plastic Clayey Soil (Hyperbolic Extended Drucker-Prager)
E = 30,000 psf, $\upsilon = 0.499$, Slope Angle = 10.2°, Dilation Angle = 10.2°
Pile, AISI 4340 Steel

Figure-C22. Vertical Displacements on a Vertical Plane (Triangular Section)

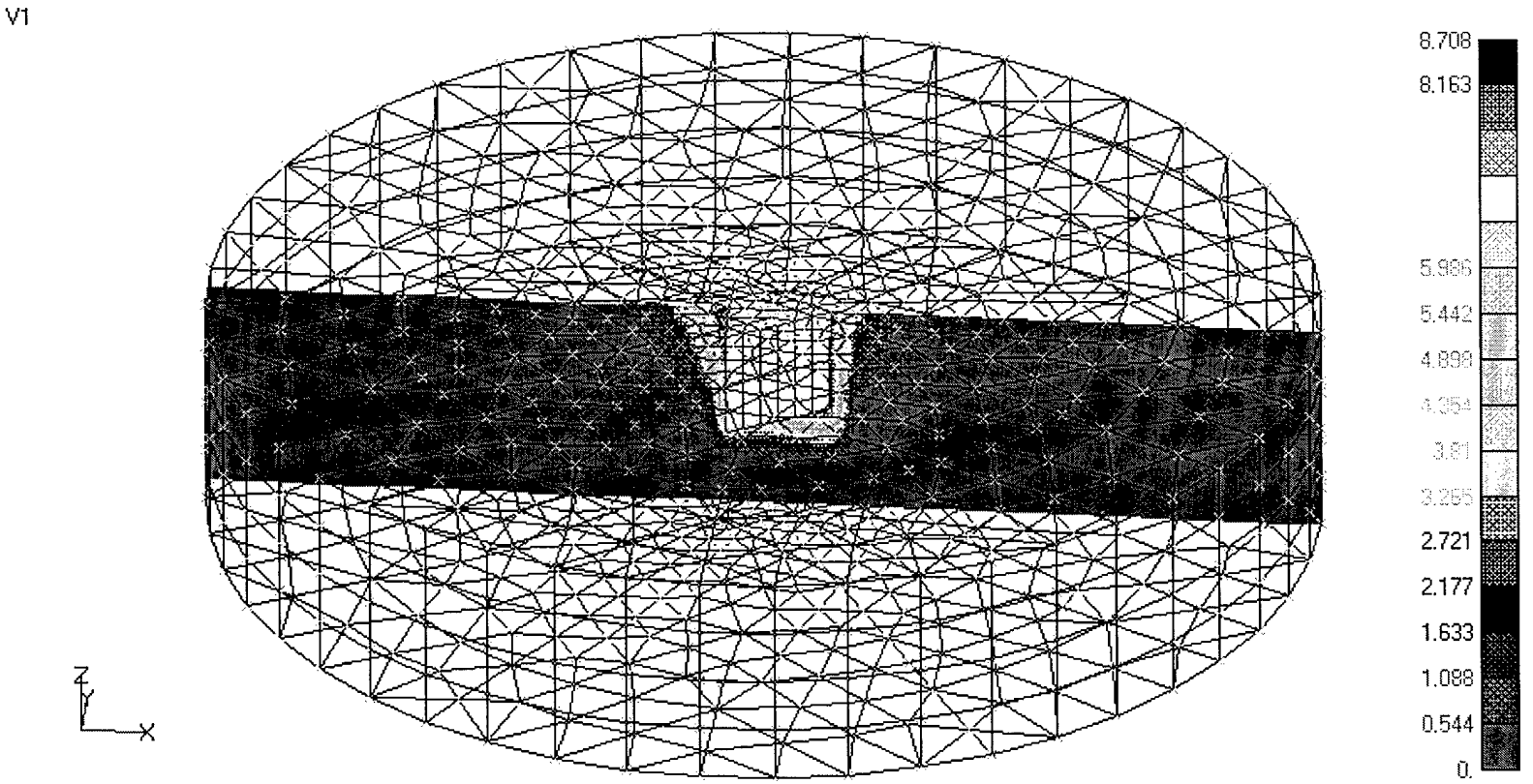

Vertical Load = 2,100,000 lbs
Linear Elastic-Perfectly Plastic Clayey Soil (Hyperbolic Extended Drucker-Prager)
E = 30,000 psf, υ = 0.499, Slope Angle = 10.2°, Dilation Angle = 10.2°
Pile, AISI 4340 Steel

Figure-C23. Pile Vertical Displacements (Triangular Section)

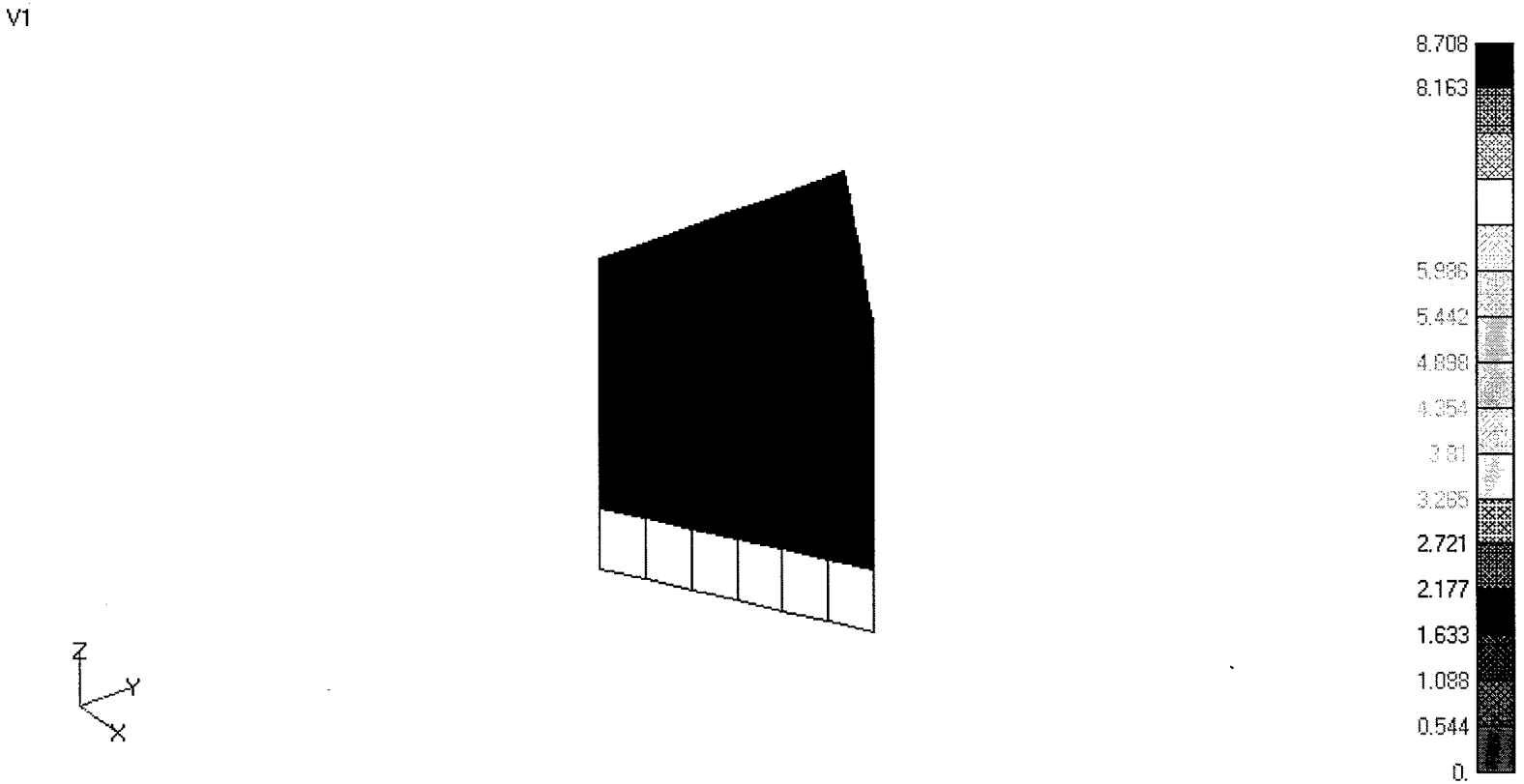

Vertical Load = 2,100,000 lbs
Linear Elastic-Perfectly Plastic Clayey Soil (Hyperbolic Extended Drucker-Prager)
E = 30,000 psf, υ = 0.499, Slope Angle = 10.2°, Dilation Angle = 10.2°
Pile, AISI 4340 Steel

Figure-C24. Soil Minor Principal Stresses on a Vertical Plane (Triangular Section)

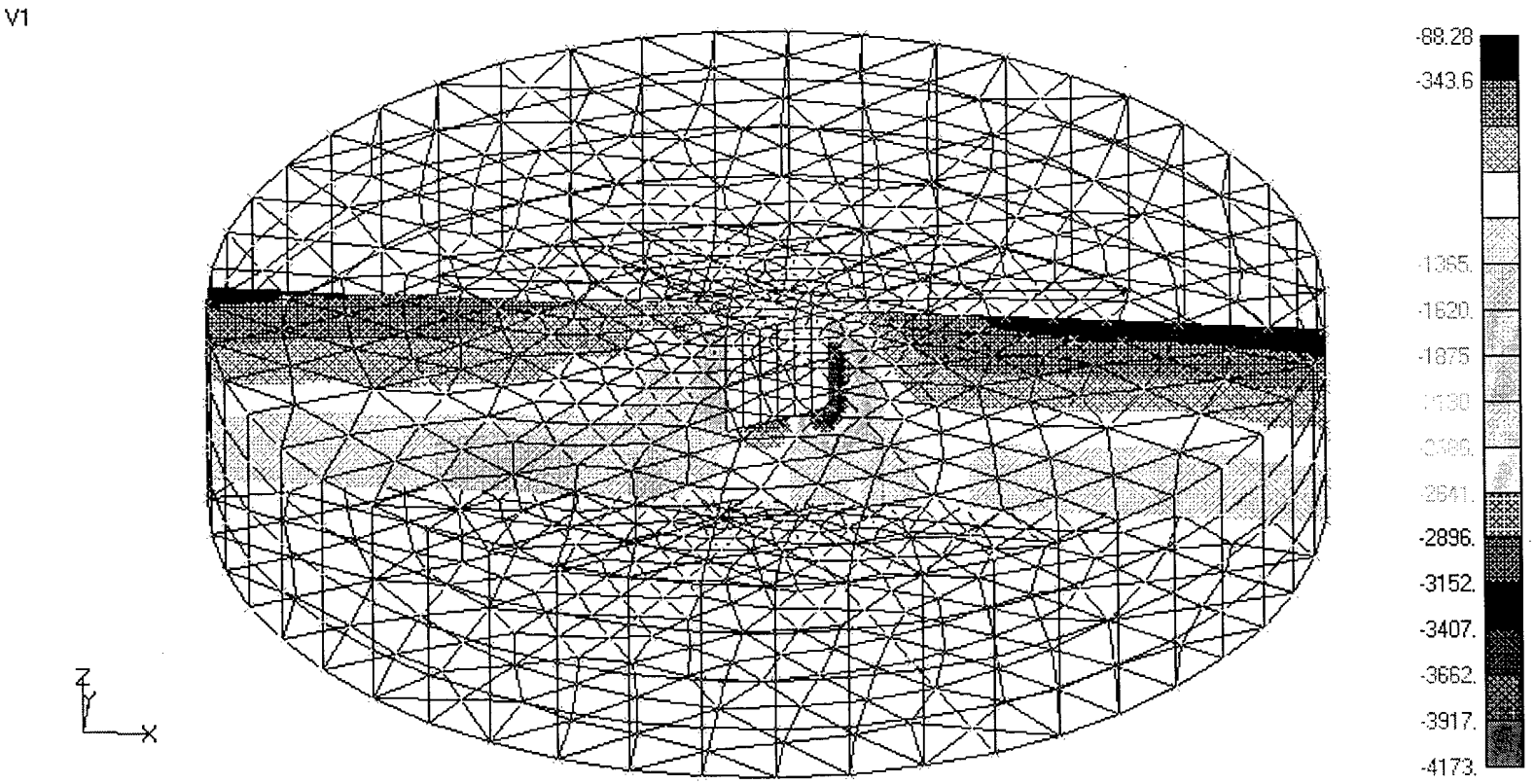

Vertical Load = 2,100,000 lbs
Linear Elastic-Perfectly Plastic Clayey Soil (Hyperbolic Extended Drucker-Prager)
E = 30,000 psf, υ = 0.499, Slope Angle = 10.2°, Dilation Angle = 10.2°
Pile, AISI 4340 Steel

Figure-C25. Soil Minor Principal Stresses on the Pile Surface (Triangular Section)

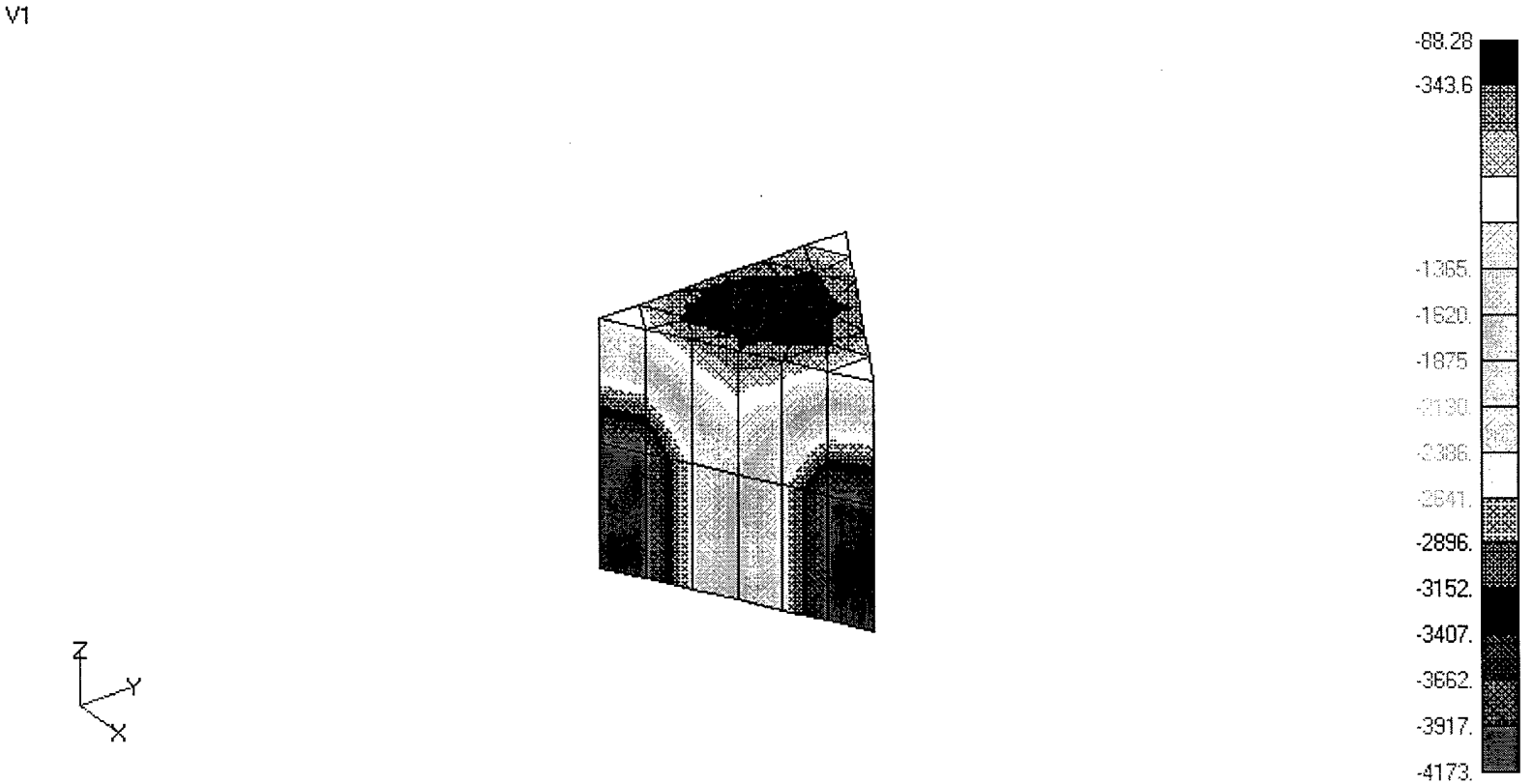

Vertical Load = 2,100,000 lbs
Linear Elastic-Perfectly Plastic Clayey Soil (Hyperbolic Extended Drucker-Prager)
E = 30,000 psf, υ = 0.499, Slope Angle = 10.2°, Dilation Angle = 10.2°
Pile, AISI 4340 Steel

Figure-C26. Pile von Mises Stresses on the Pile Surface (Triangular Section)

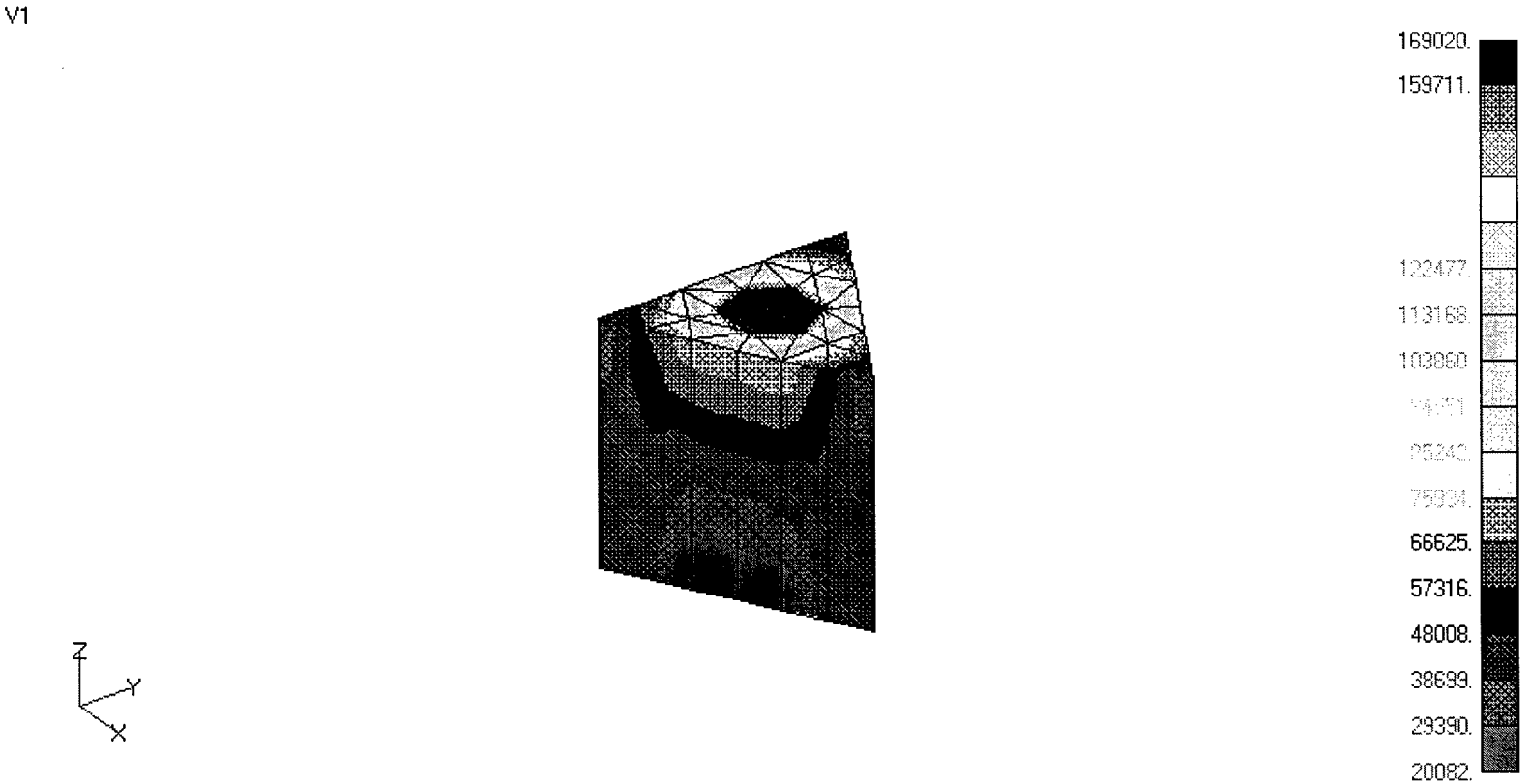

Vertical Load = 2,100,000 lbs
Linear Elastic-Perfectly Plastic Clayey Soil (Hyperbolic Extended Drucker-Prager)
E = 30,000 psf, υ = 0.499, Slope Angle = 10.2°, Dilation Angle = 10.2°
Pile, AISI 4340 Steel

Figure-C27. Horizontal Displacements (Y-shaped Section)

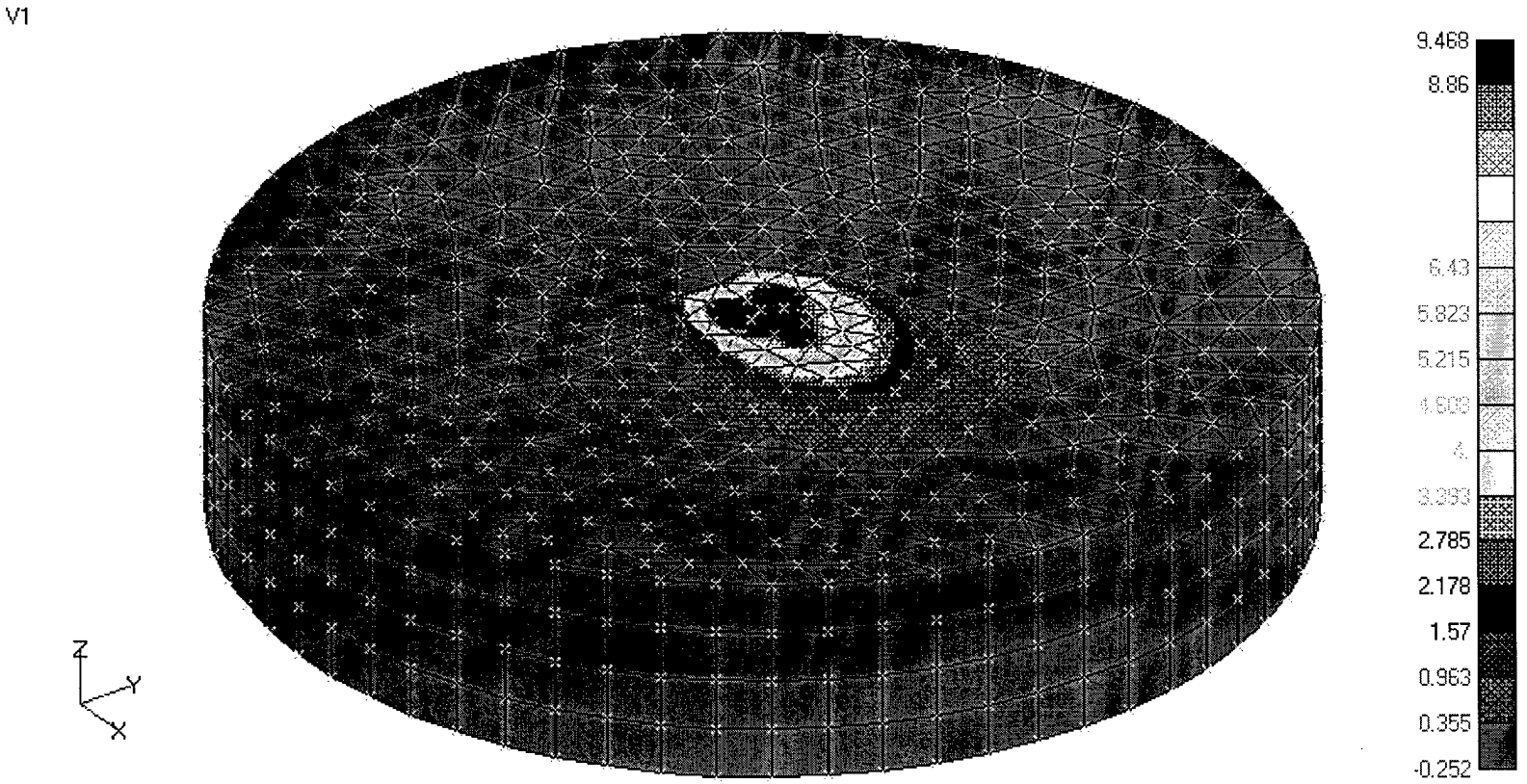

Horizontal Load = 1,900,000 lbs
Linear Elastic-Perfectly Plastic Clayey Soil (Hyperbolic Extended Drucker-Prager)
E = 30,000 psf, υ = 0.499, Slope Angle = 10.2°, Dilation Angle = 10.2°
Pile, AISI 4340 Steel

Figure-C28. Horizontal Displacements on a Vertical Plane along the Horizontal Load Direction (Y-shaped Section)

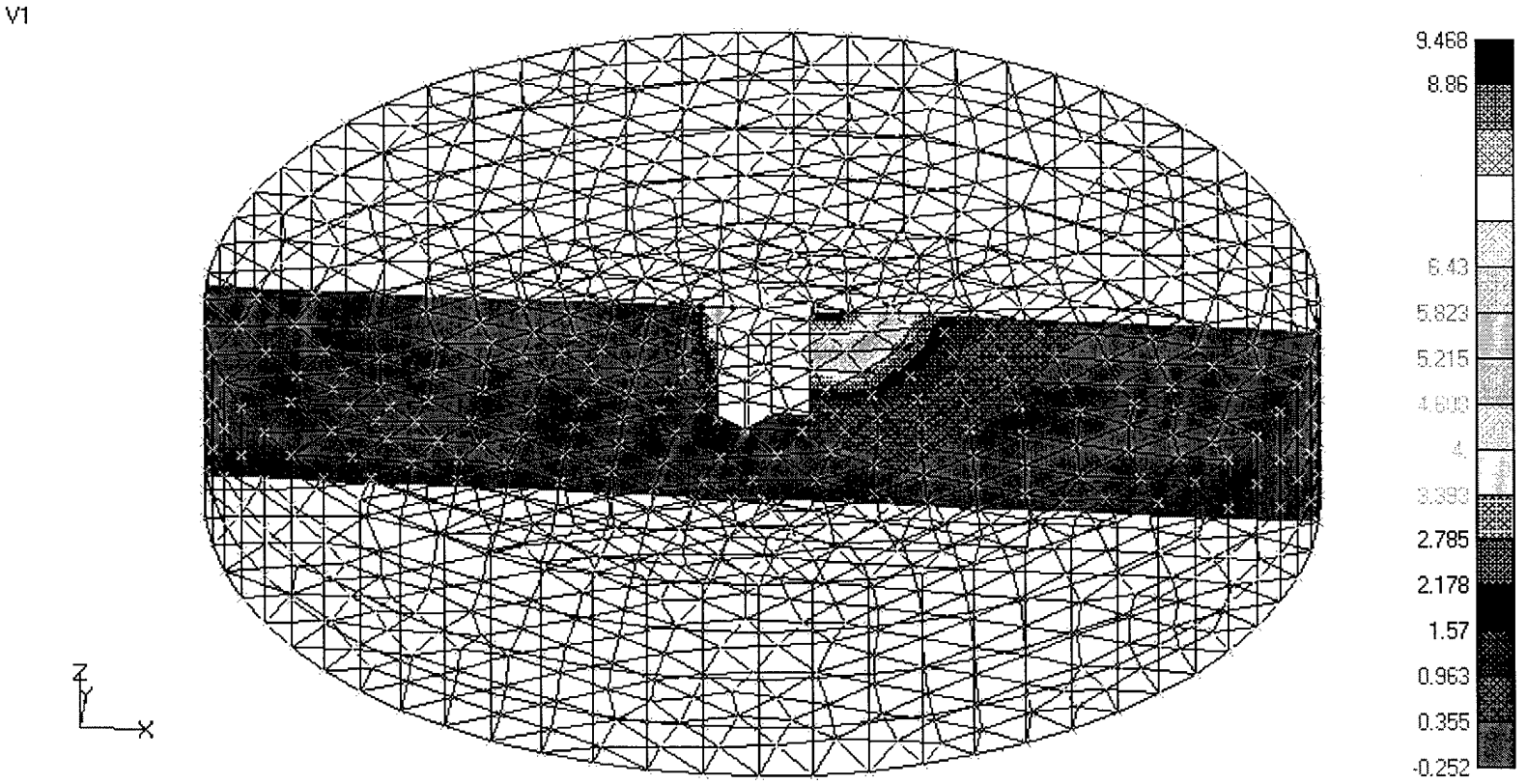

Horizontal Load = 1,900,000 lbs
Linear Elastic-Perfectly Plastic Clayey Soil (Hyperbolic Extended Drucker-Prager)
E = 30,000 psf, υ = 0.499, Slope Angle = 10.2°, Dilation Angle = 10.2°
Pile, AISI 4340 Steel

Figure-C29. Pile Total Displacements (Y-shaped Section)

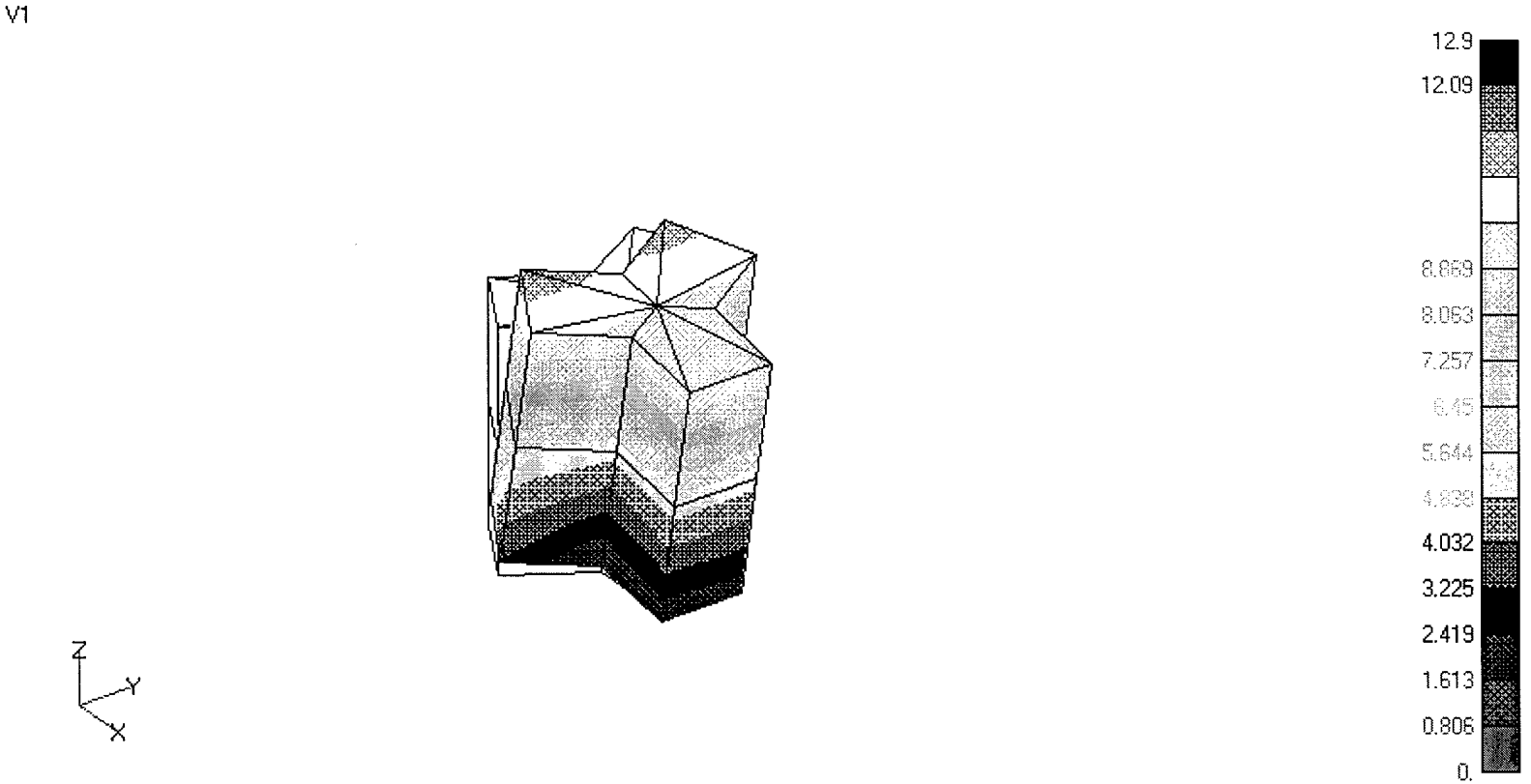

Horizontal Load = 1,900,000 lbs
Linear Elastic-Perfectly Plastic Clayey Soil (Hyperbolic Extended Drucker-Prager)
E = 30,000 psf, υ = 0.499, Slope Angle = 10.2°, Dilation Angle = 10.2°
Pile, AISI 4340 Steel

Figure-C30. Soil Minor Principal Stresses (Y-shaped Section)

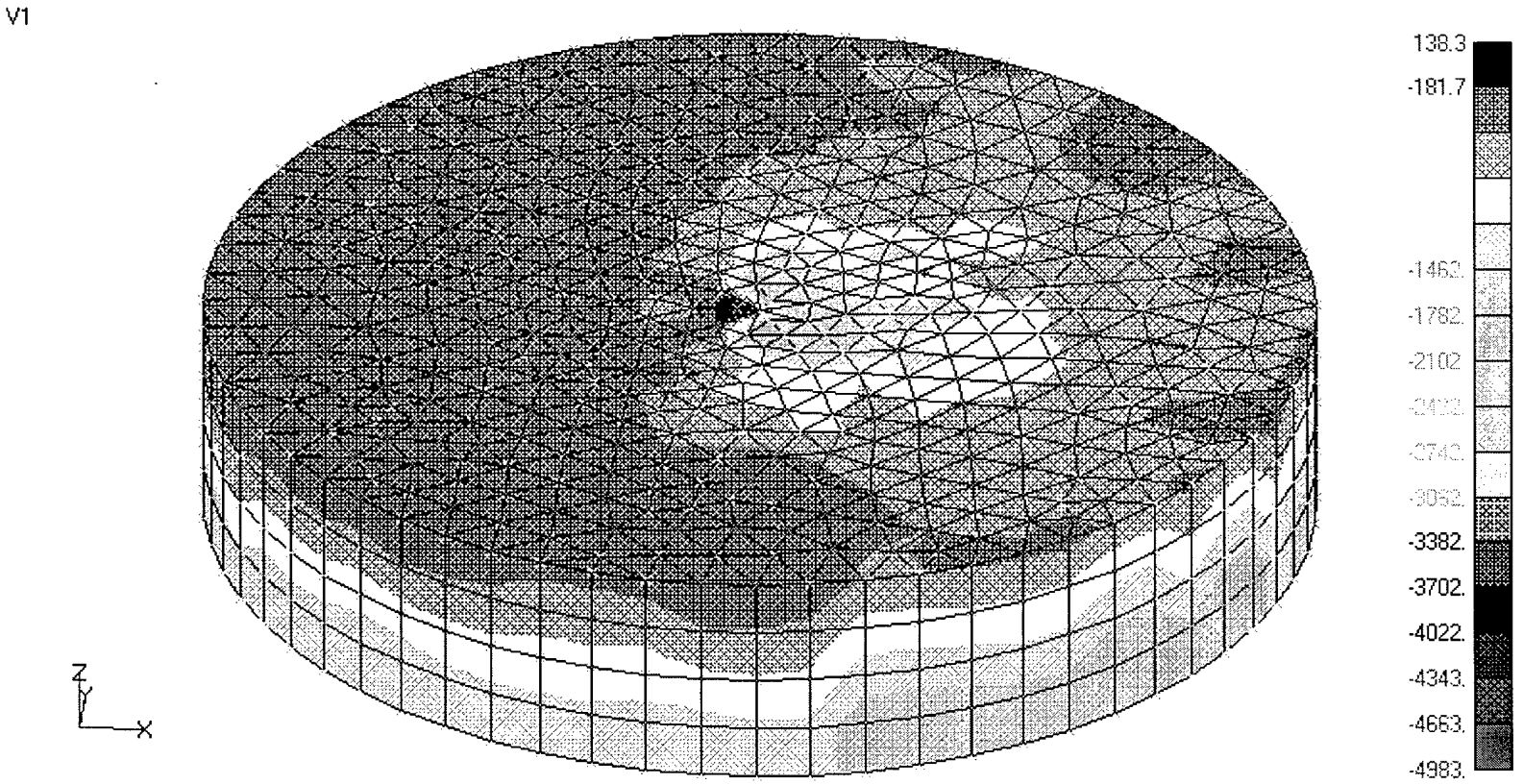

Horizontal Load = 1,900,000 lbs
Linear Elastic-Perfectly Plastic Clayey Soil (Hyperbolic Extended Drucker-Prager)
E = 30,000 psf, $\upsilon = 0.499$, Slope Angle = 10.2^{o}, Dilation Angle = 10.2^{o}
Pile, AISI 4340 Steel

Figure-C31. Soil Minor Principal Stresses on a Vertical Plane along the Horizontal Load Direction (Y-shaped Section)

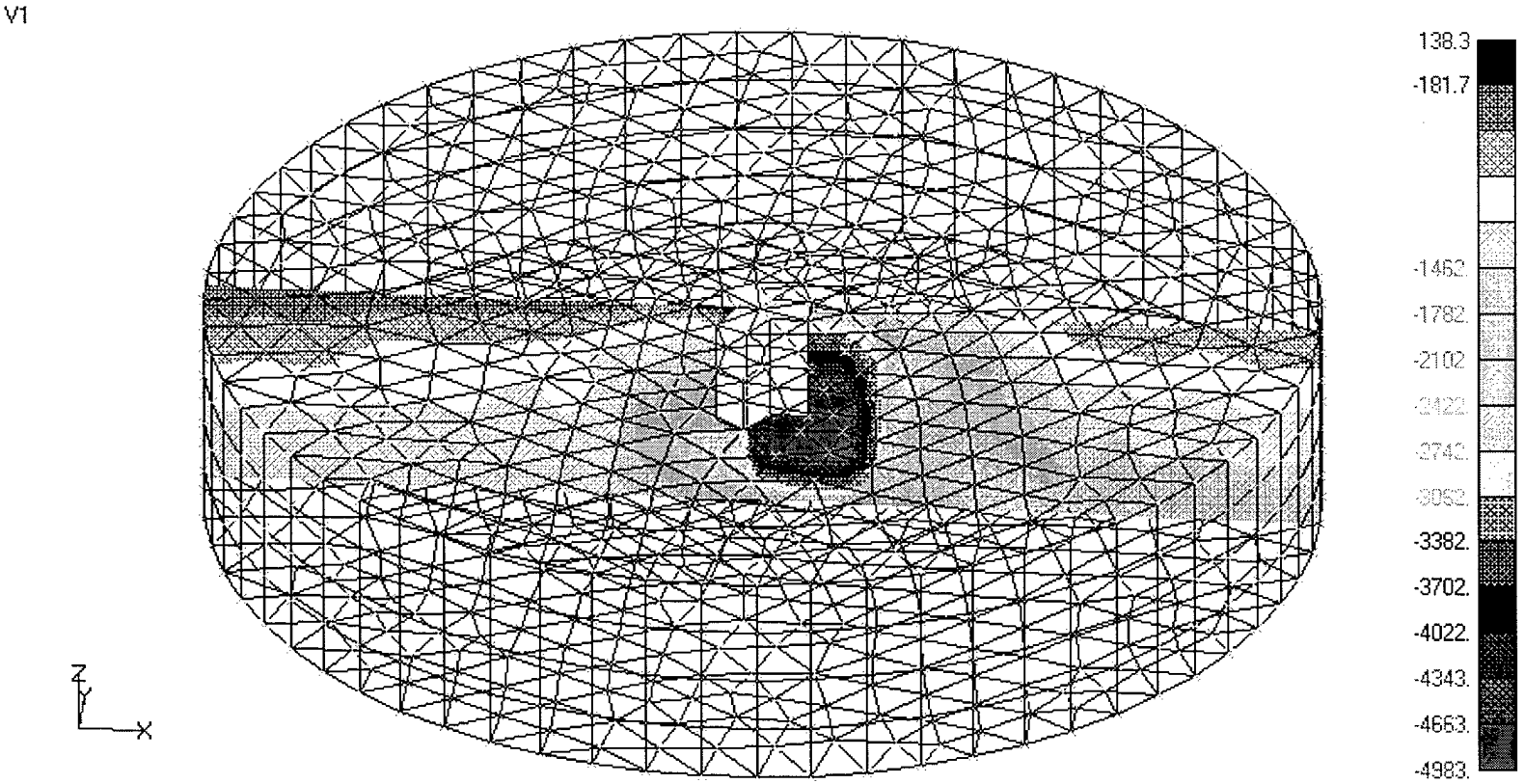

Horizontal Load = 1,900,000 lbs
Linear Elastic-Perfectly Plastic Clayey Soil (Hyperbolic Extended Drucker-Prager)
E = 30,000 psf, υ = 0.499, Slope Angle = 10.2°, Dilation Angle = 10.2°
Pile, AISI 4340 Steel

Figure-C32. Horizontal Normal Pile Stresses on the Pile Surface (Y-shaped Section)

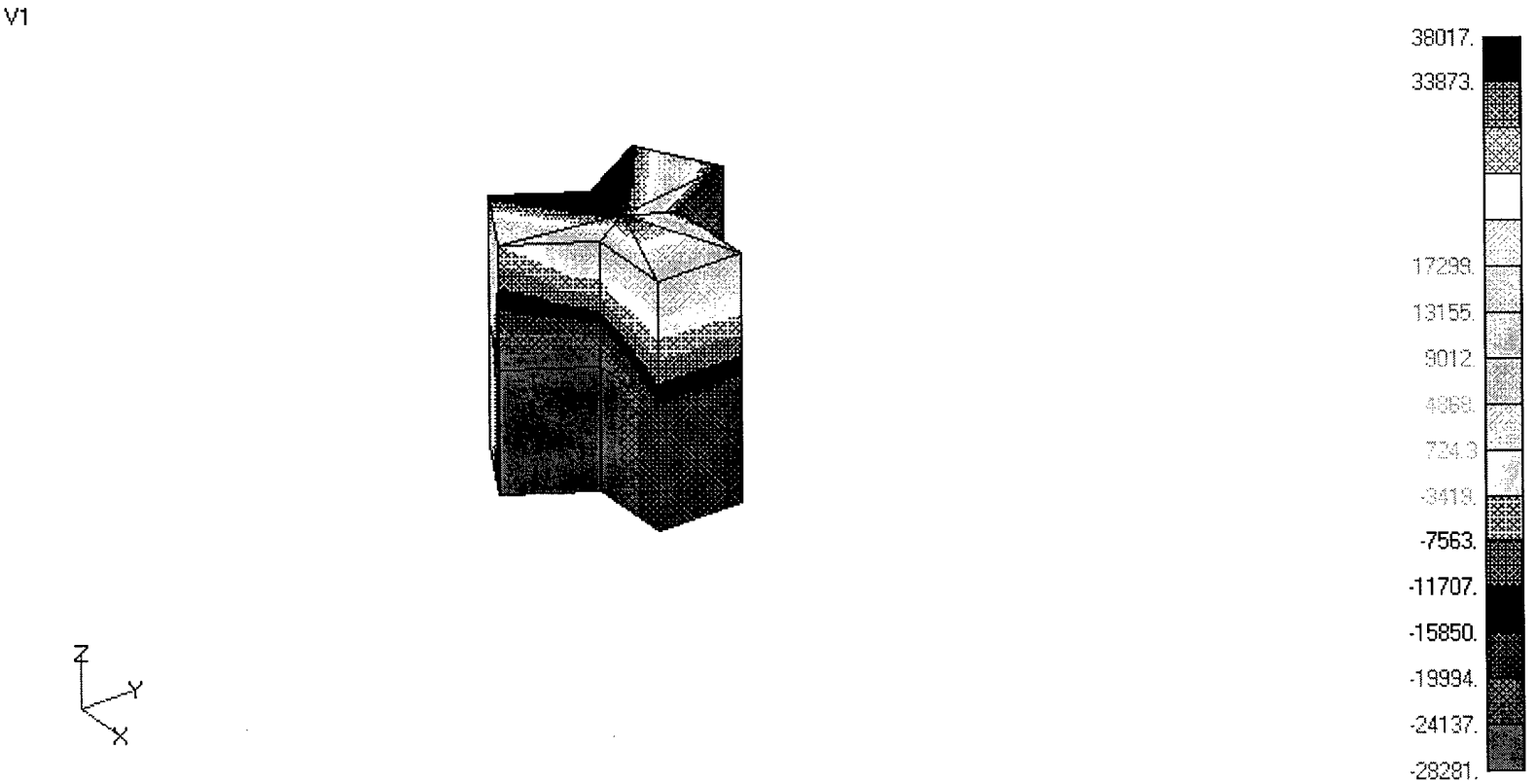

Horizontal Load = 1,900,000 lbs
Linear Elastic-Perfectly Plastic Clayey Soil (Hyperbolic Extended Drucker-Prager)
E = 30,000 psf, υ = 0.499, Slope Angle = 10.2°, Dilation Angle = 10.2°
Pile, AISI 4340 Steel

Figure-C33. Pile von Mises Stresses on the Pile Surface (Y-shaped Section)

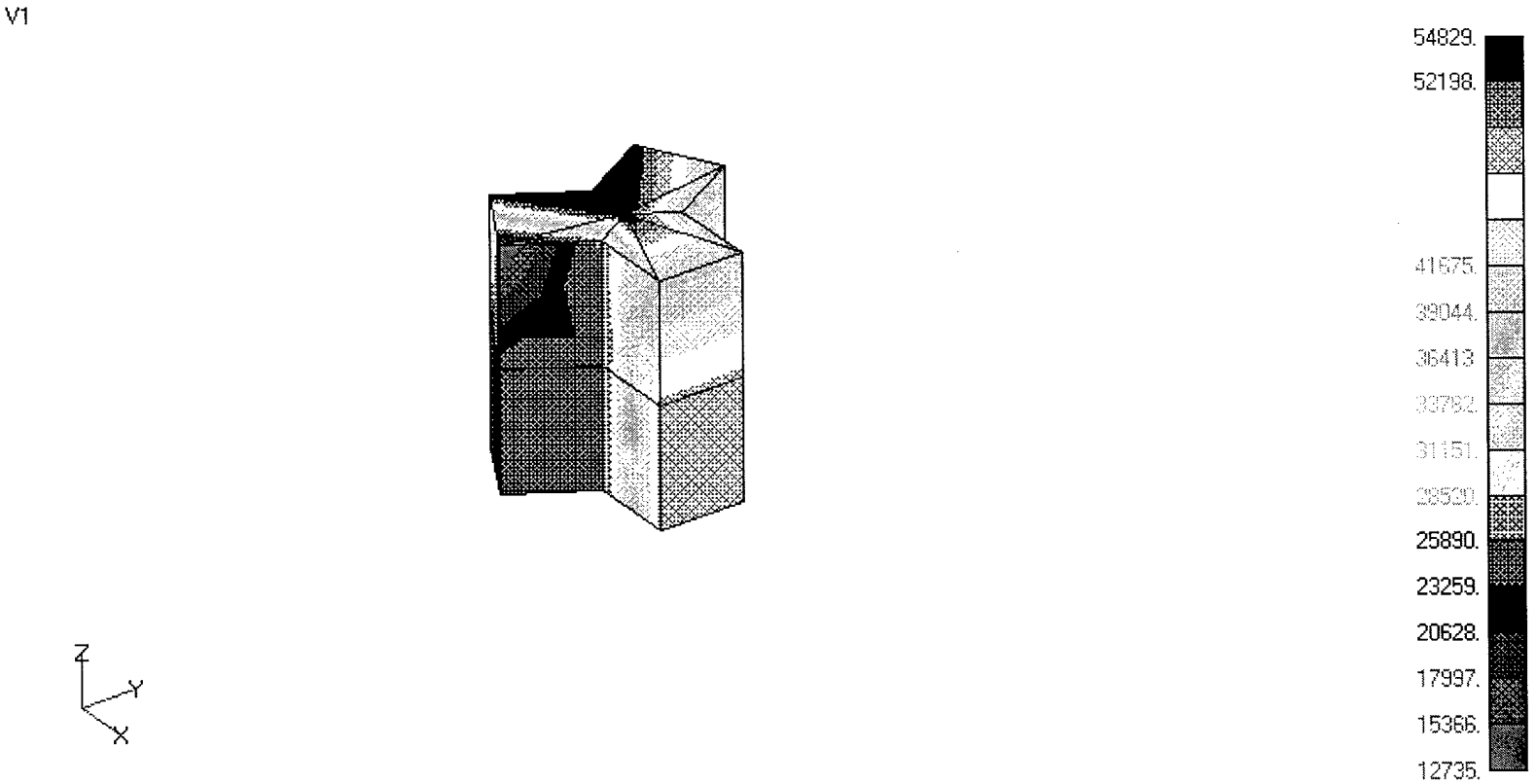

Horizontal Load = 1,900,000 lbs
Linear Elastic-Perfectly Plastic Clayey Soil (Hyperbolic Extended Drucker-Prager)
E = 30,000 psf, υ = 0.499, Slope Angle = 10.2°, Dilation Angle = 10.2°
Pile, AISI 4340 Steel

Figure-C34. Vertical Displacements (Y-shaped Section)

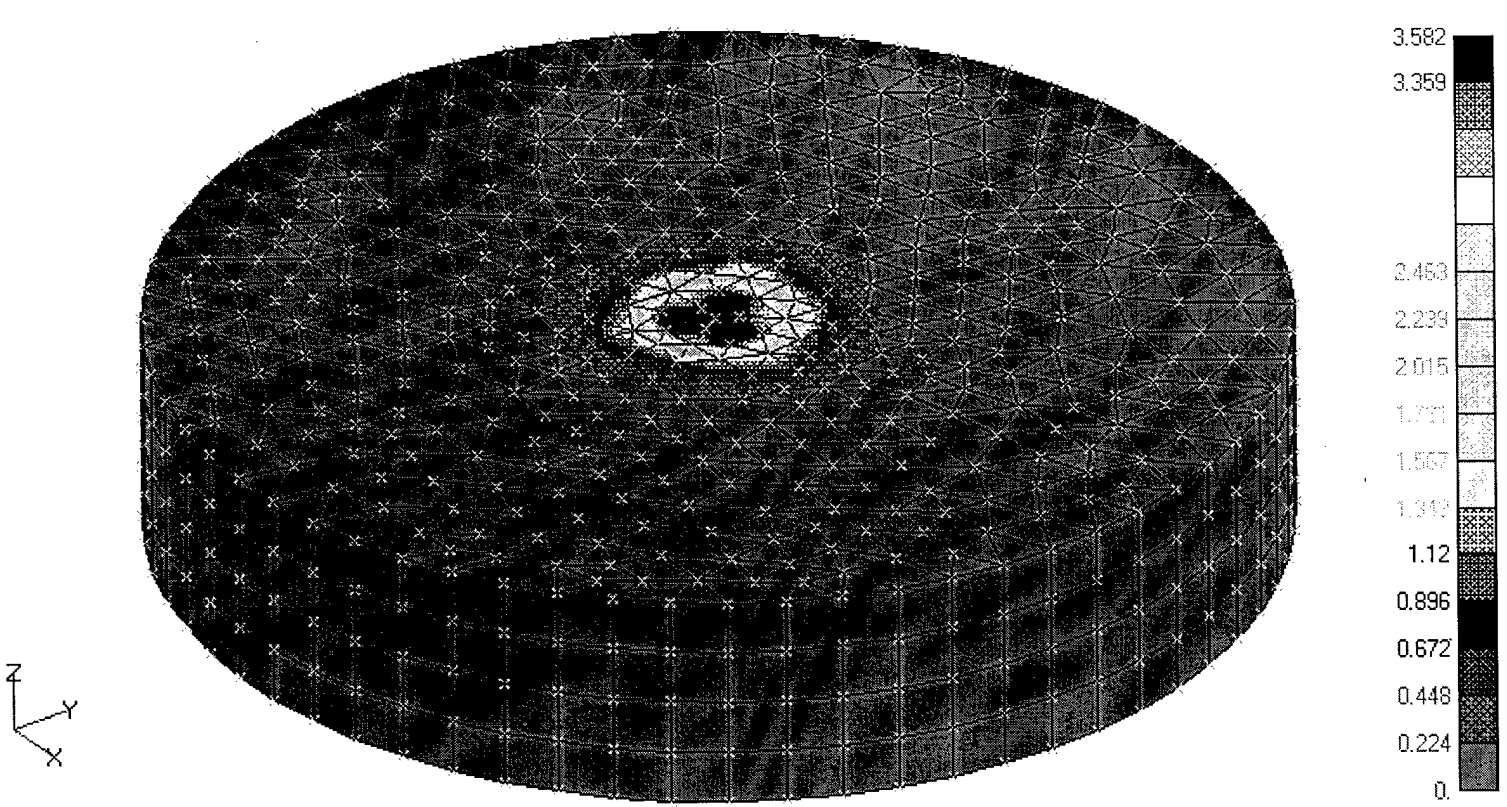

Vertical Load = 2,200,000 lbs
Linear Elastic-Perfectly Plastic Clayey Soil (Hyperbolic Extended Drucker-Prager)
E = 30,000 psf, υ = 0.499, Slope Angle = 10.2°, Dilation Angle = 10.2°
Pile, AISI 4340 Steel

Figure-C35. Vertical Displacements on a Vertical Plane (Y-shaped Section)

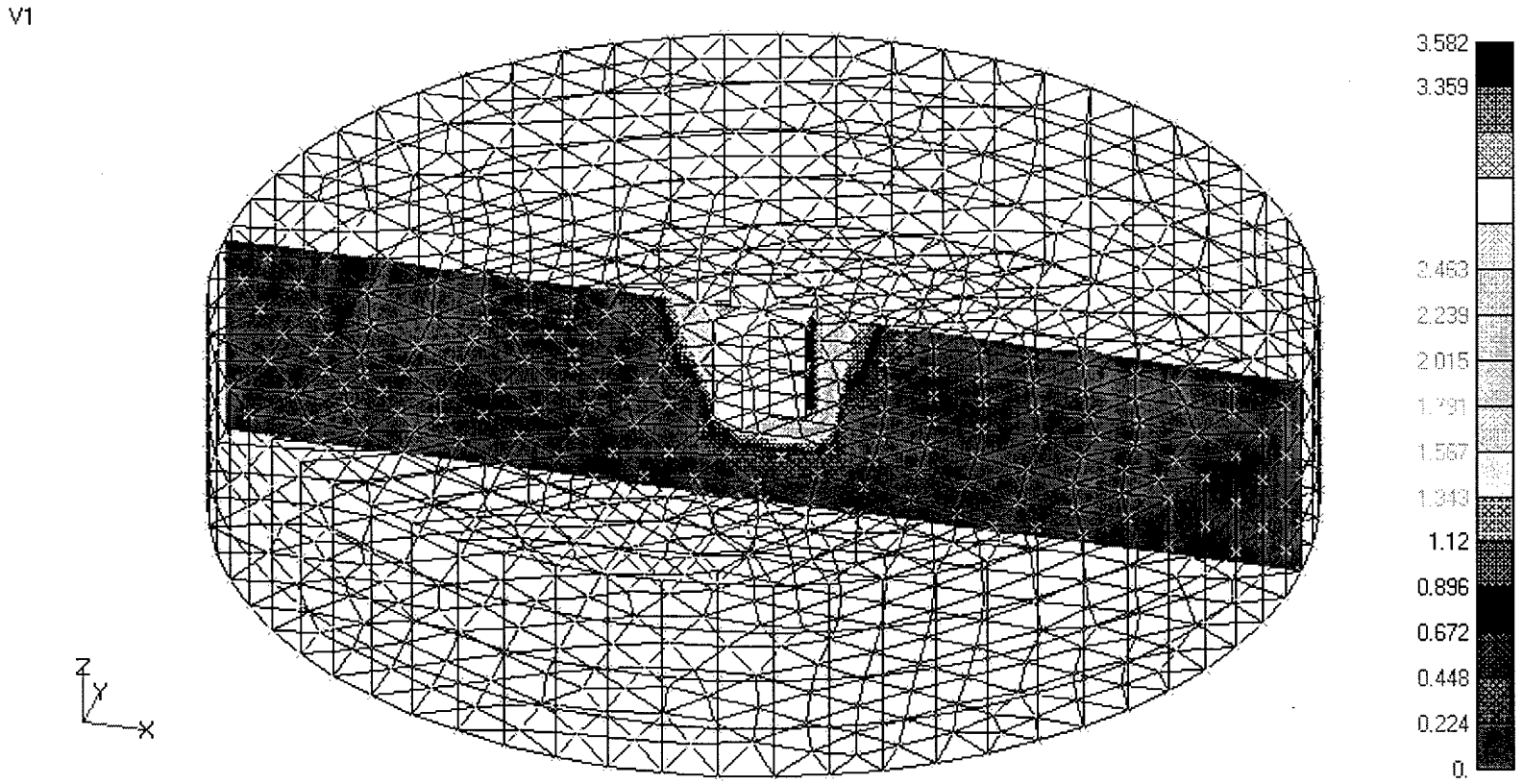

Vertical Load = 2,200,000 lbs
Linear Elastic-Perfectly Plastic Clayey Soil (Hyperbolic Extended Drucker-Prager)
E = 30,000 psf, υ = 0.499, Slope Angle = 10.2°, Dilation Angle = 10.2°
Pile, AISI 4340 Steel

Figure-C36. Pile Vertical Displacements (Y-shaped Section)

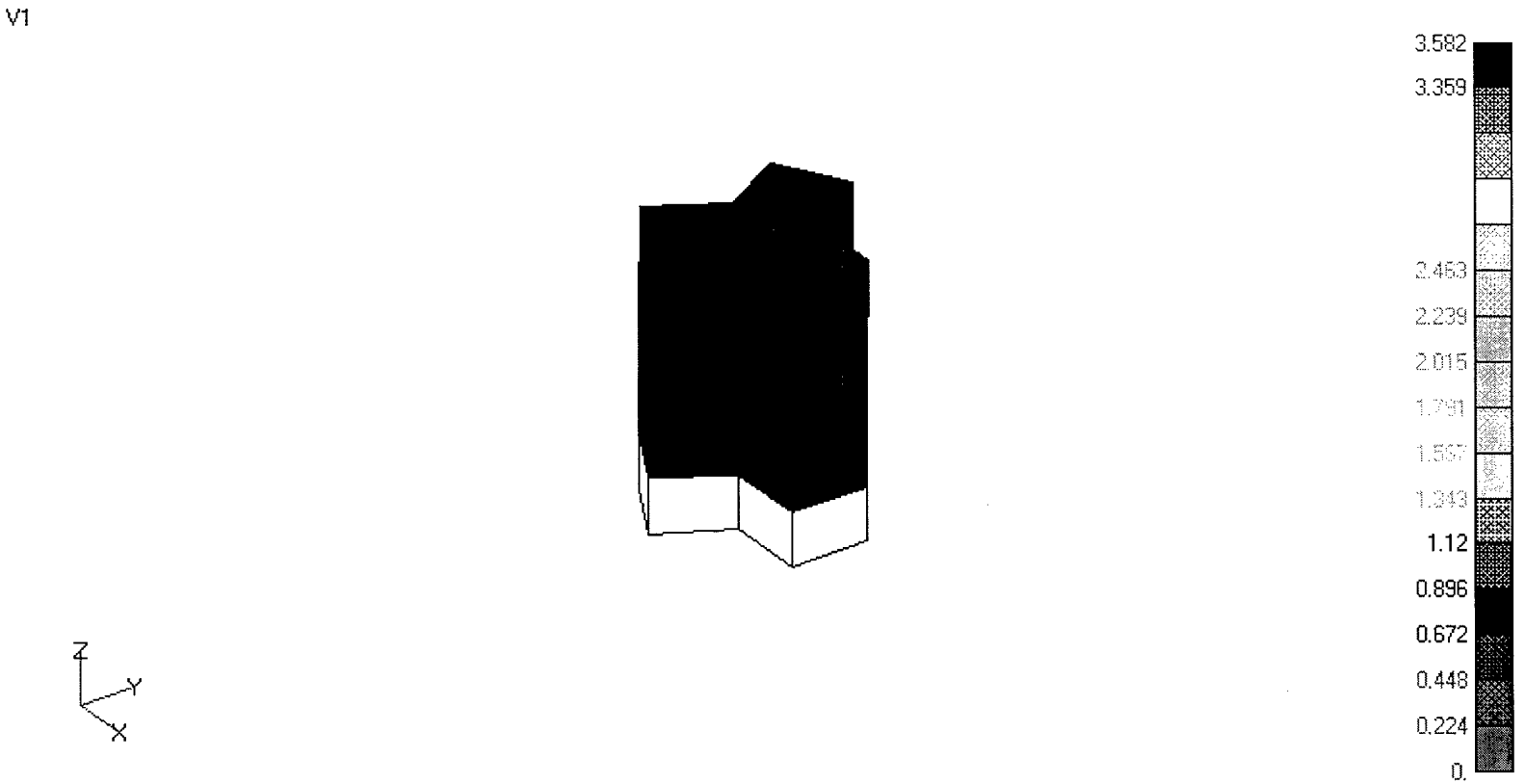

Vertical Load = 2,200,000 lbs
Linear Elastic-Perfectly Plastic Clayey Soil (Hyperbolic Extended Drucker-Prager)
E = 30,000 psf, υ = 0.499, Slope Angle = 10.2°, Dilation Angle = 10.2°
Pile, AISI 4340 Steel

Figure-C37. Soil Minor Principal Stresses on a Vertical Plane (Y-shaped Section)

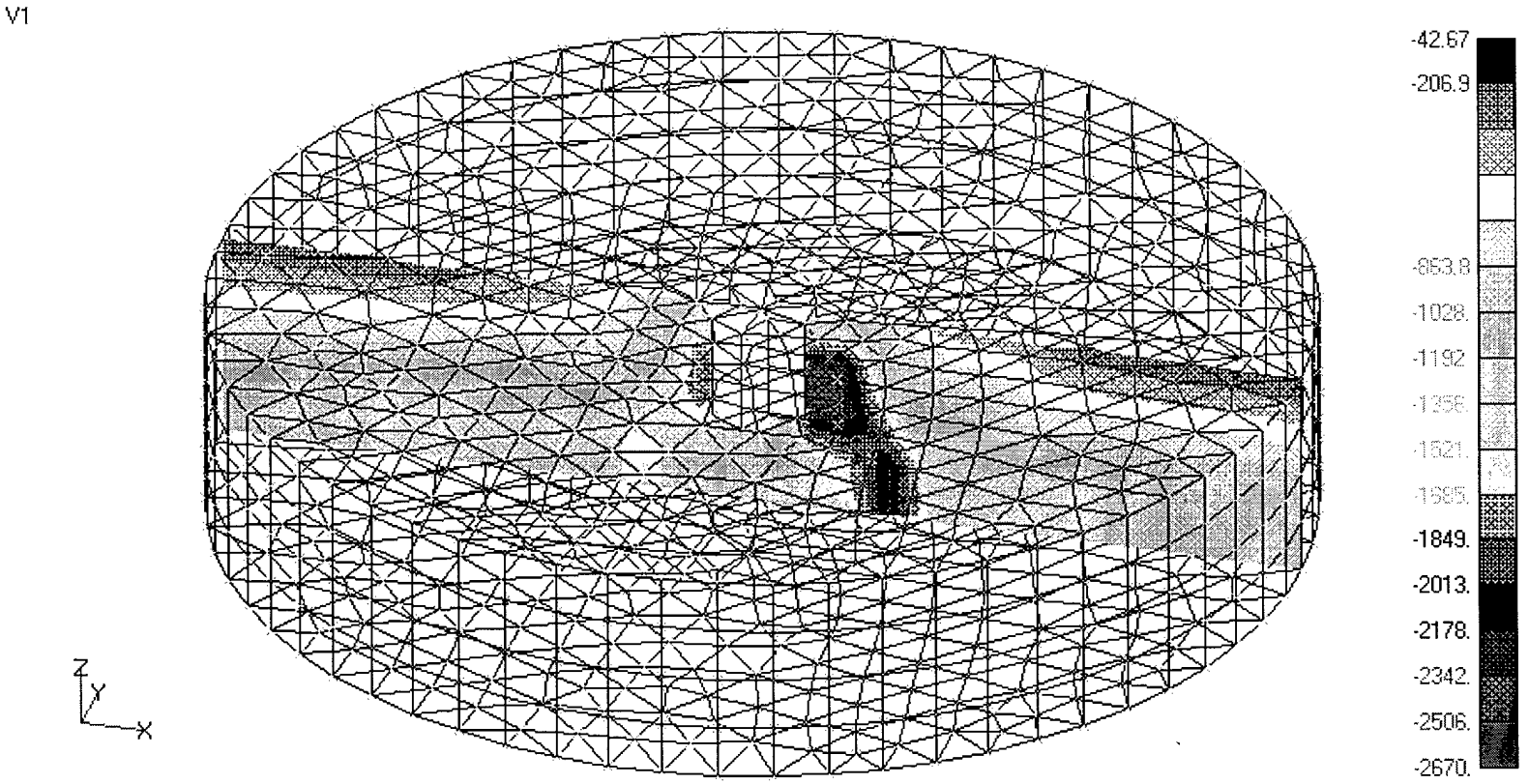

Vertical Load = 2,200,000 lbs
Linear Elastic-Perfectly Plastic Clayey Soil (Hyperbolic Extended Drucker-Prager)
E = 30,000 psf, $\upsilon = 0.499$, Slope Angle = 10.2^{o}, Dilation Angle = 10.2^{o}
Pile, AISI 4340 Steel

Figure-C38. Soil Minor Principal Stresses on the Pile Surface (Y-shaped Section)

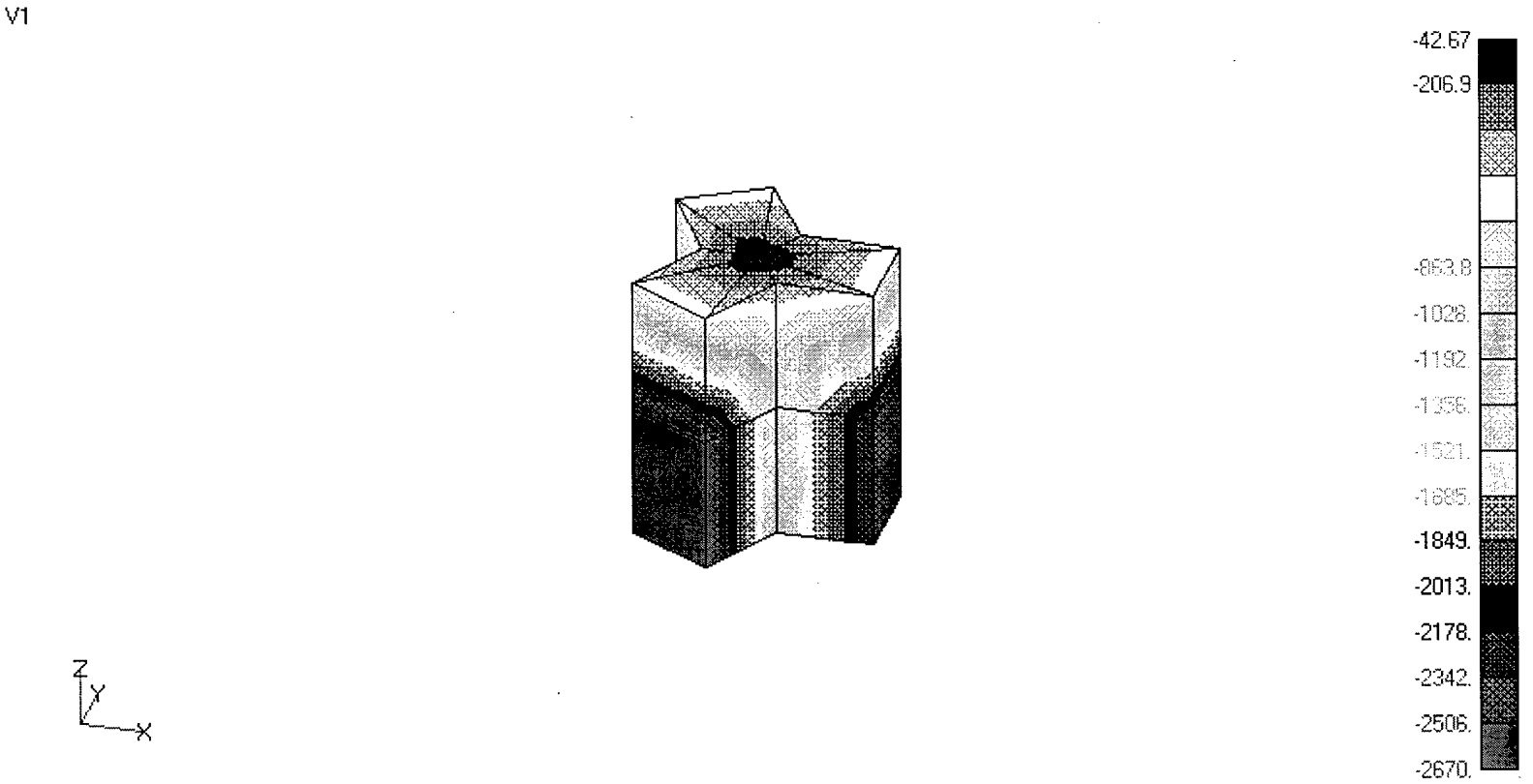

Vertical Load = 2,200,000 lbs
Linear Elastic-Perfectly Plastic Clayey Soil (Hyperbolic Extended Drucker-Prager)
E = 30,000 psf, υ = 0.499, Slope Angle = 10.2°, Dilation Angle = 10.2°
Pile, AISI 4340 Steel

Figure-C39. Pile von Mises Stresses on the Pile Surface (Y-shaped Section)

V1

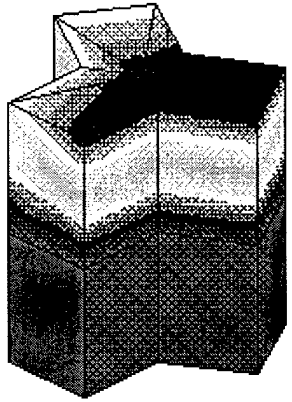

Vertical Load = 2,200,000 lbs
Linear Elastic-Perfectly Plastic Clayey Soil (Hyperbolic Extended Drucker-Prager)
E = 30,000 psf, $\upsilon = 0.499$, Slope Angle = 10.2°, Dilation Angle = 10.2°
Pile, AISI 4340 Steel

Figure-D1. Horizontal Displacements (Circular Pile with 15-ft Flange in Sand)

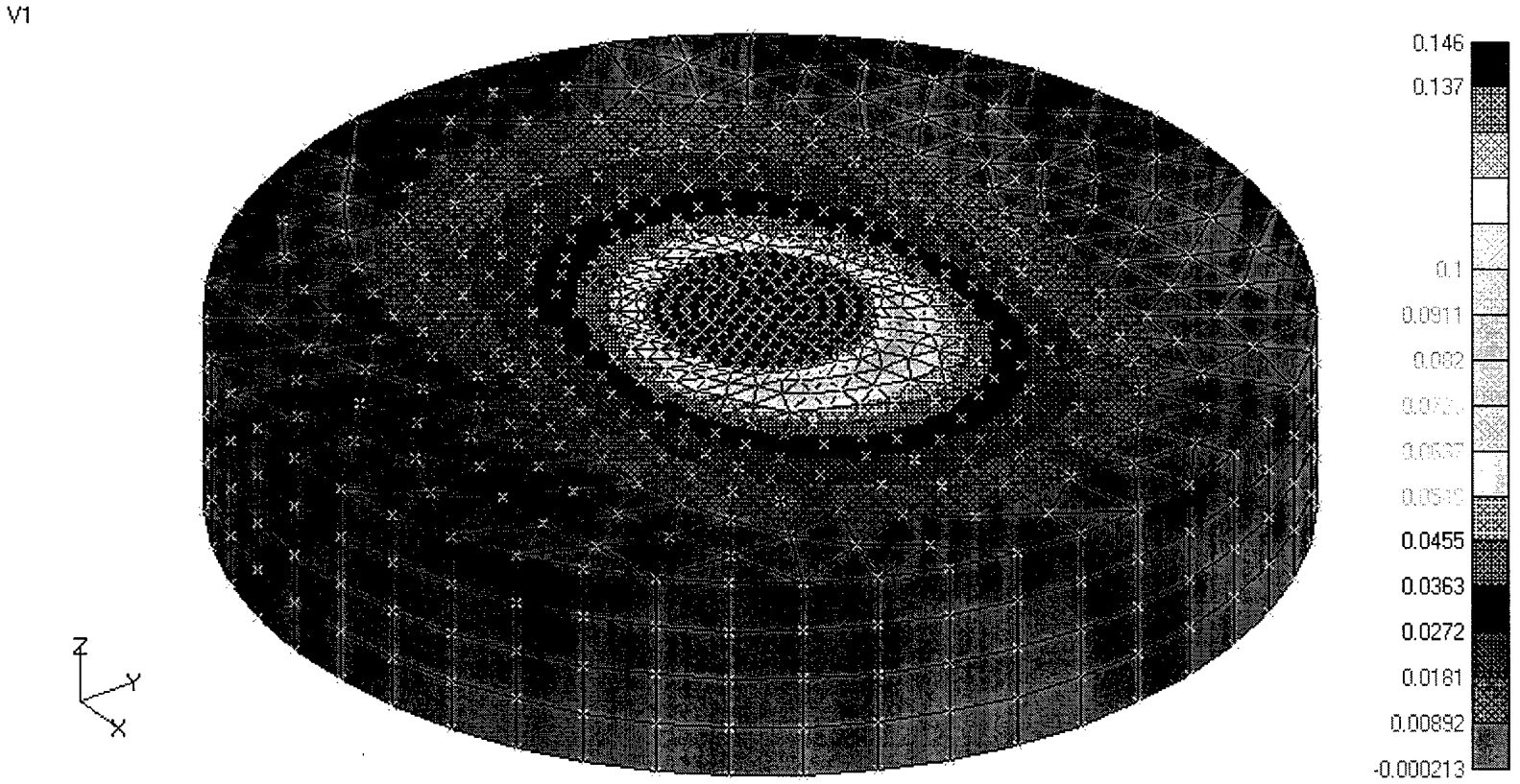

Horizontal Load = 8,000,000 lbs
Linear Elastic-Perfectly Plastic Clayey Soil (Linear Extended Drucker-Prager)
E = 864,000 psf, $\upsilon = 0.3$, Slope Angle = 46.2°, Dilation Angle = 21.5°
Pile, AISI 4340 Steel

Figure-D2. Horizontal Displacements on a Vertical Plane along the Horizontal Load Direction (Circular Pile with 15-ft Flange in Sand)

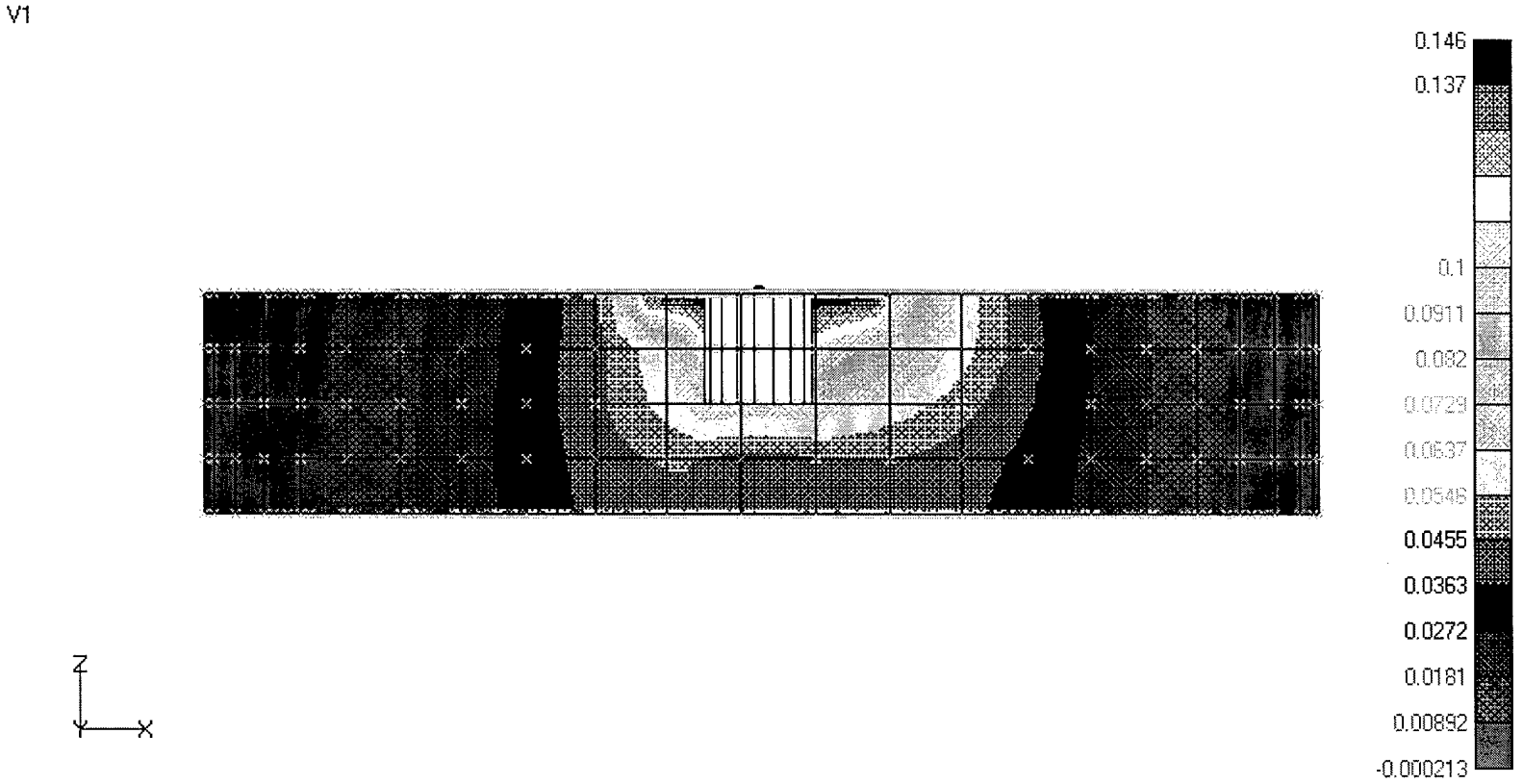

Horizontal Load = 8,000,000 lbs
Linear Elastic-Perfectly Plastic Clayey Soil (Linear Extended Drucker-Prager)
E = 864,000 psf, υ = 0.3, Slope Angle = 46.2°, Dilation Angle = 21.5°
Pile, AISI 4340 Steel

Figure-D3. Pile Total Displacements (Circular Pile with 15-ft Flange in Sand)

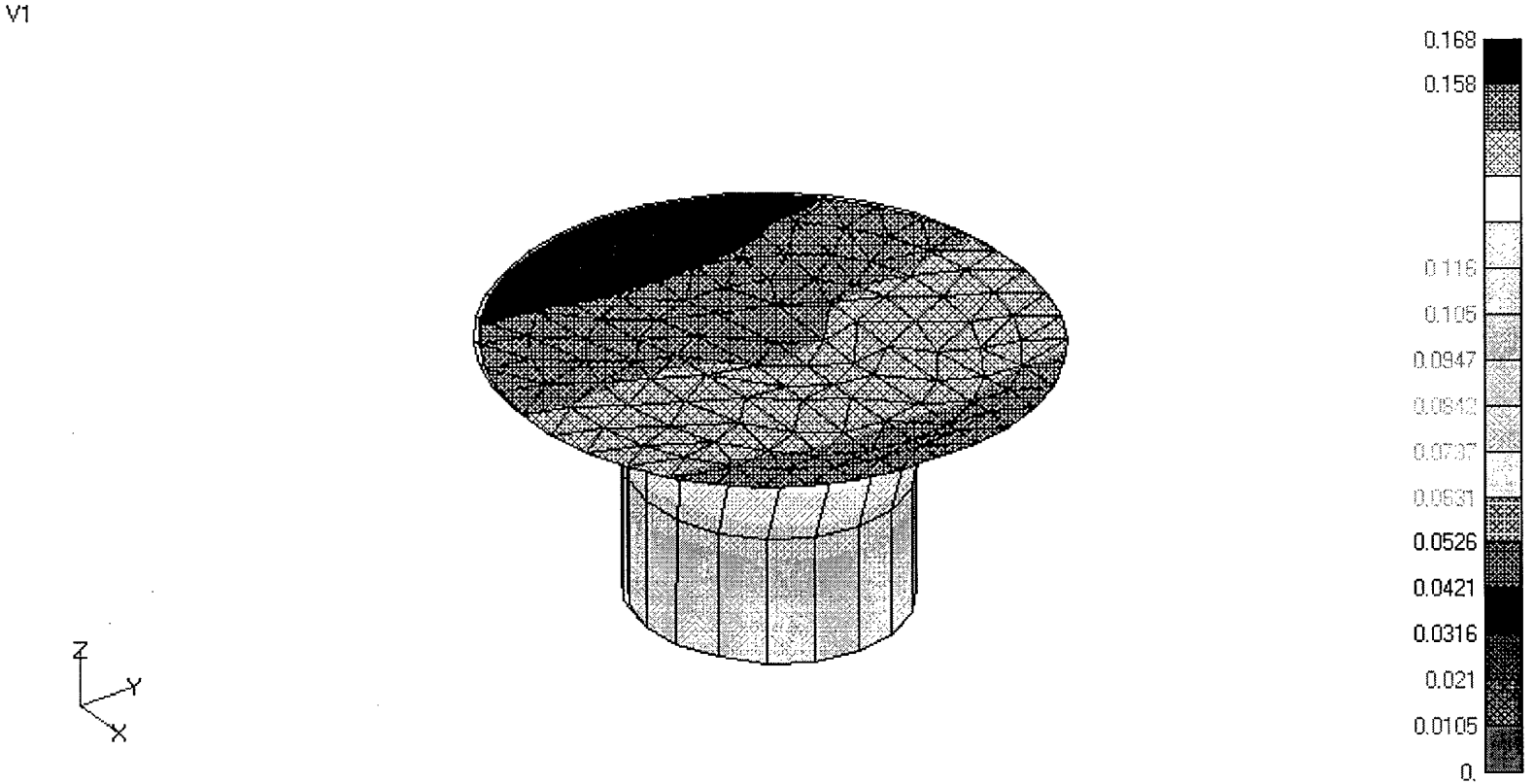

Horizontal Load = 8,000,000 lbs
Linear Elastic-Perfectly Plastic Clayey Soil (Linear Extended Drucker-Prager)
E = 864,000 psf, $\upsilon = 0.3$, Slope Angle = 46.2°, Dilation Angle = 21.5°
Pile, AISI 4340 Steel

Figure-D4. Soil Minor Principal Stresses on a Vertical Plane along the Horizontal Load Directrion (Circular Pile with 15-ft Flange in Sand)

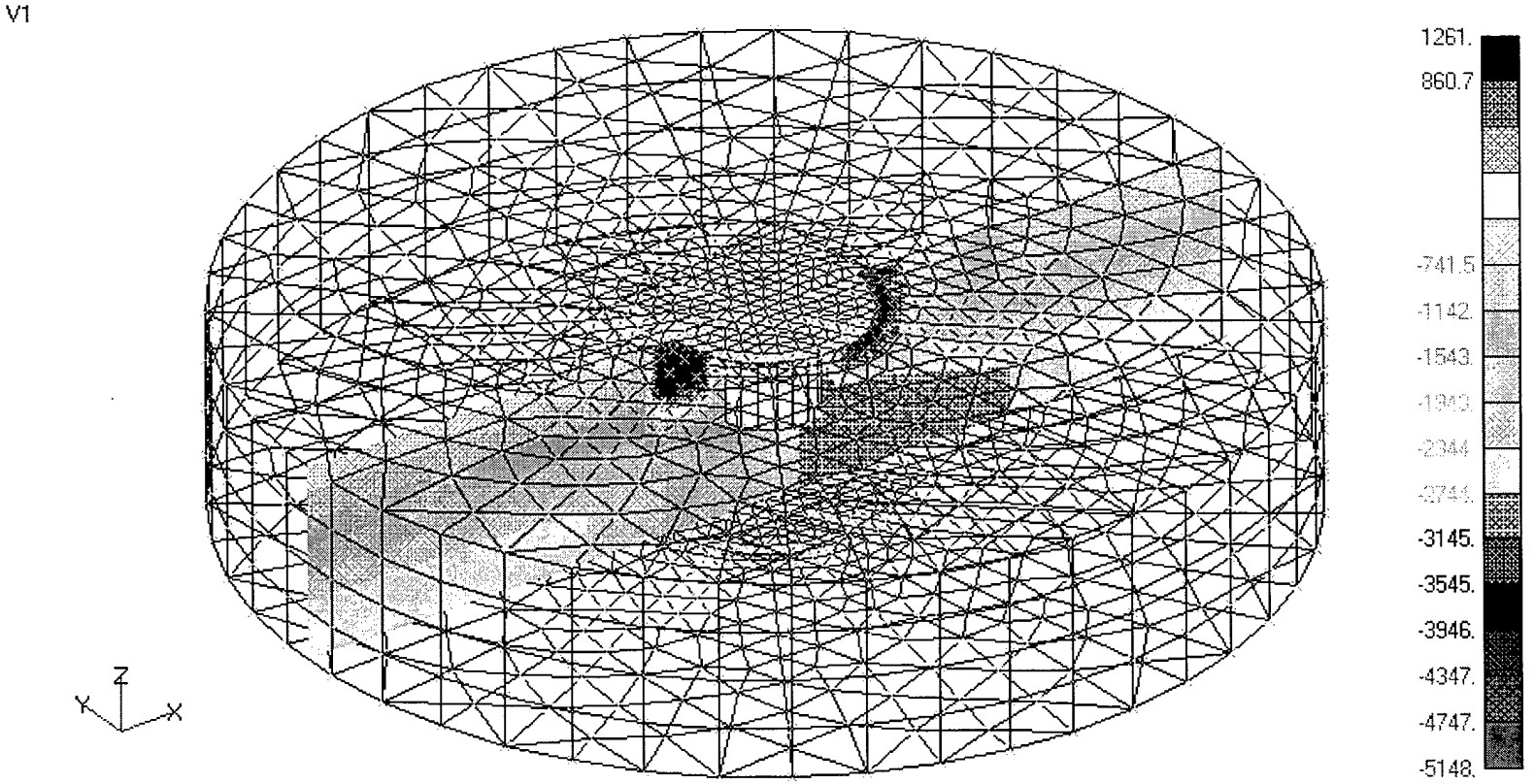

Horizontal Load = 8,000,000 lbs
Linear Elastic-Perfectly Plastic Clayey Soil (Linear Extended Drucker-Prager)
E = 864,000 psf, υ = 0.3, Slope Angle = 46.2°, Dilation Angle = 21.5°
Pile, AISI 4340 Steel

Figure-D5. Soil Minor Principal Stresses on the Pile Surface (Circular Pile with 15-ft Flange in Sand)

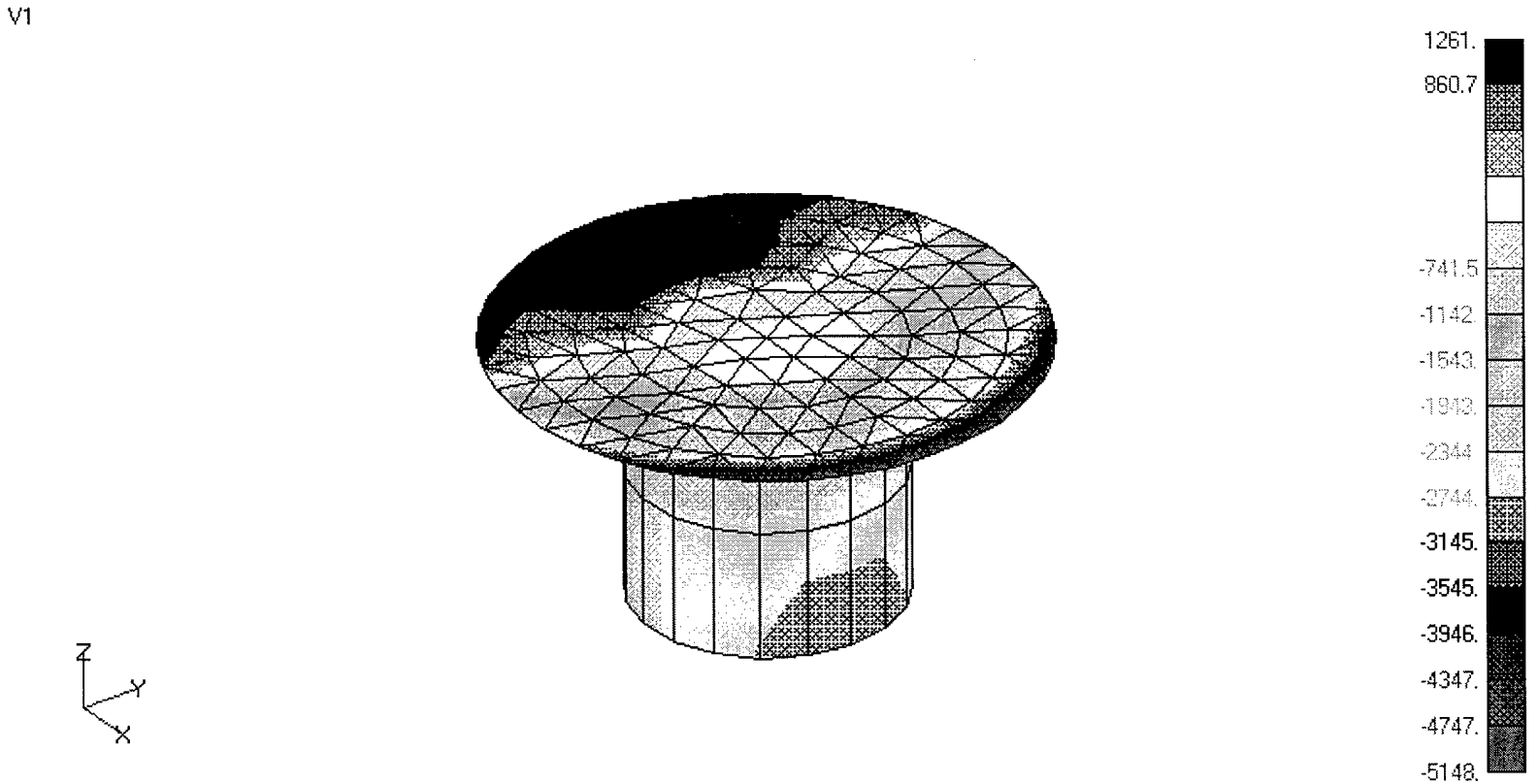

Horizontal Load = 8,000,000 lbs
Linear Elastic-Perfectly Plastic Clayey Soil (Linear Extended Drucker-Prager)
E = 864,000 psf, υ = 0.3, Slope Angle = 46.2°, Dilation Angle = 21.5°
Pile, AISI 4340 Steel

Figure-D6. Pile von Mises Stresses on the Pile Surface (Circular Pile with 15-ft Flange in Sand)

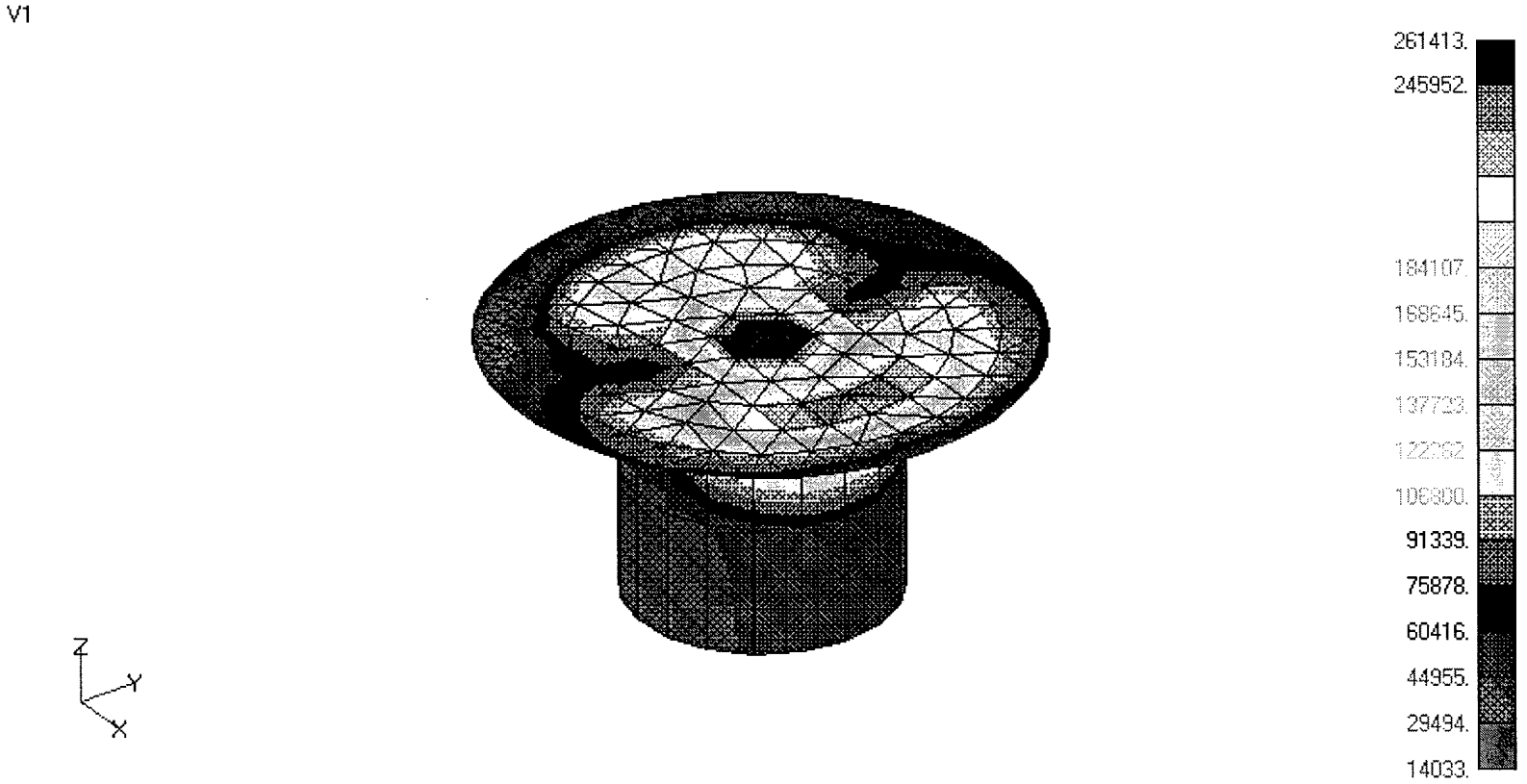

Horizontal Load = 8,000,000 lbs
Linear Elastic-Perfectly Plastic Clayey Soil (Linear Extended Drucker-Prager)
E = 864,000 psf, υ = 0.3, Slope Angle = 46.2°, Dilation Angle = 21.5°
Pile, AISI 4340 Steel

Figure-D7. Horizontal Displacements (Circular Pile with 15-ft Flange in Clay)

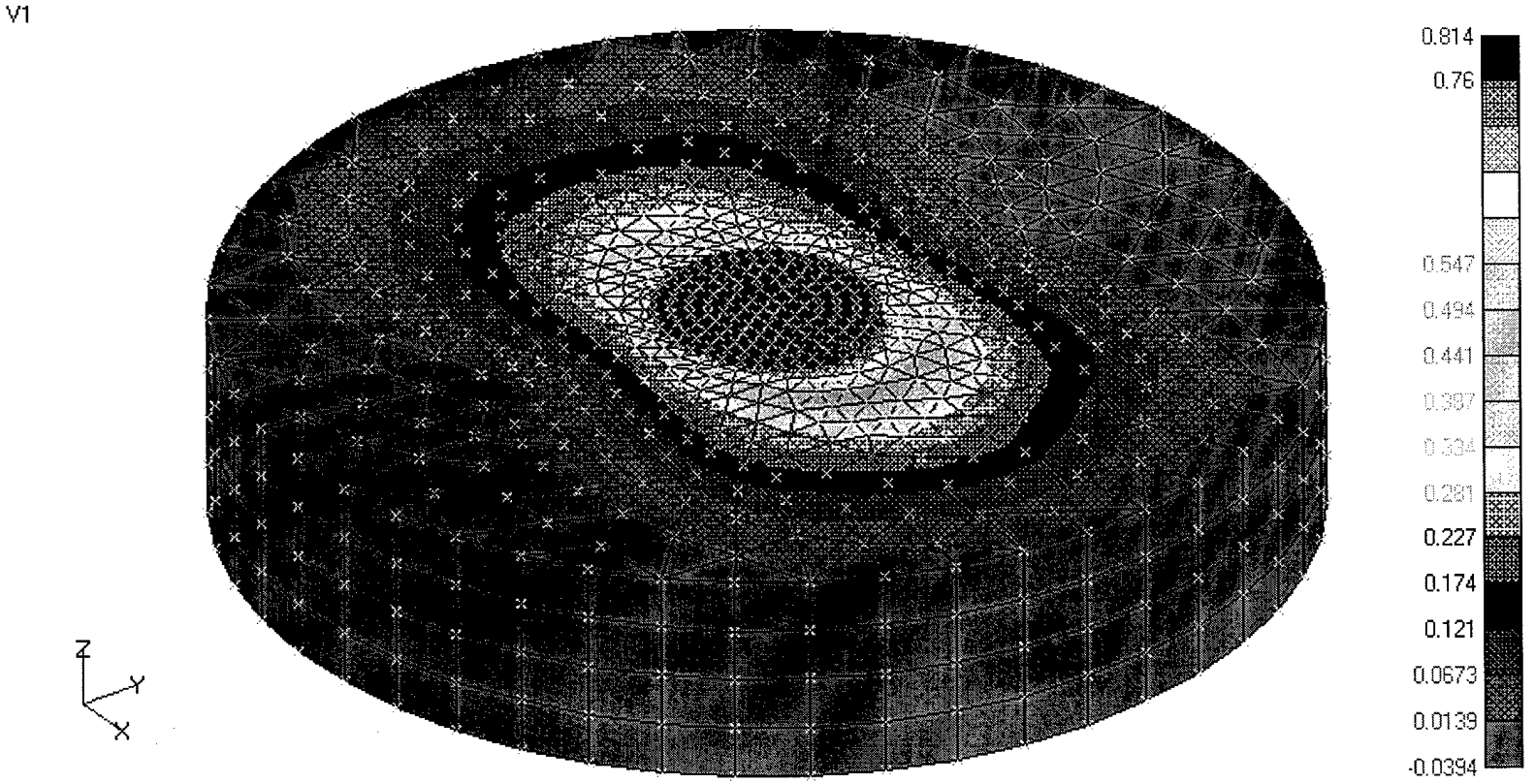

Horizontal Load = 2,100,000 lbs
Linear Elastic-Perfectly Plastic Clayey Soil (Hyperbolic Extended Drucker-Prager)
E = 30,000 psf, υ = 0.499, Slope Angle = 10.2°, Dilation Angle = 10.2°
Pile, AISI 4340 Steel

Figure-D8. Horizontal Displacements on a Vertical Plane along the Horizontal Load Direction (Circular Pile with 15-ft Flange in Clay)

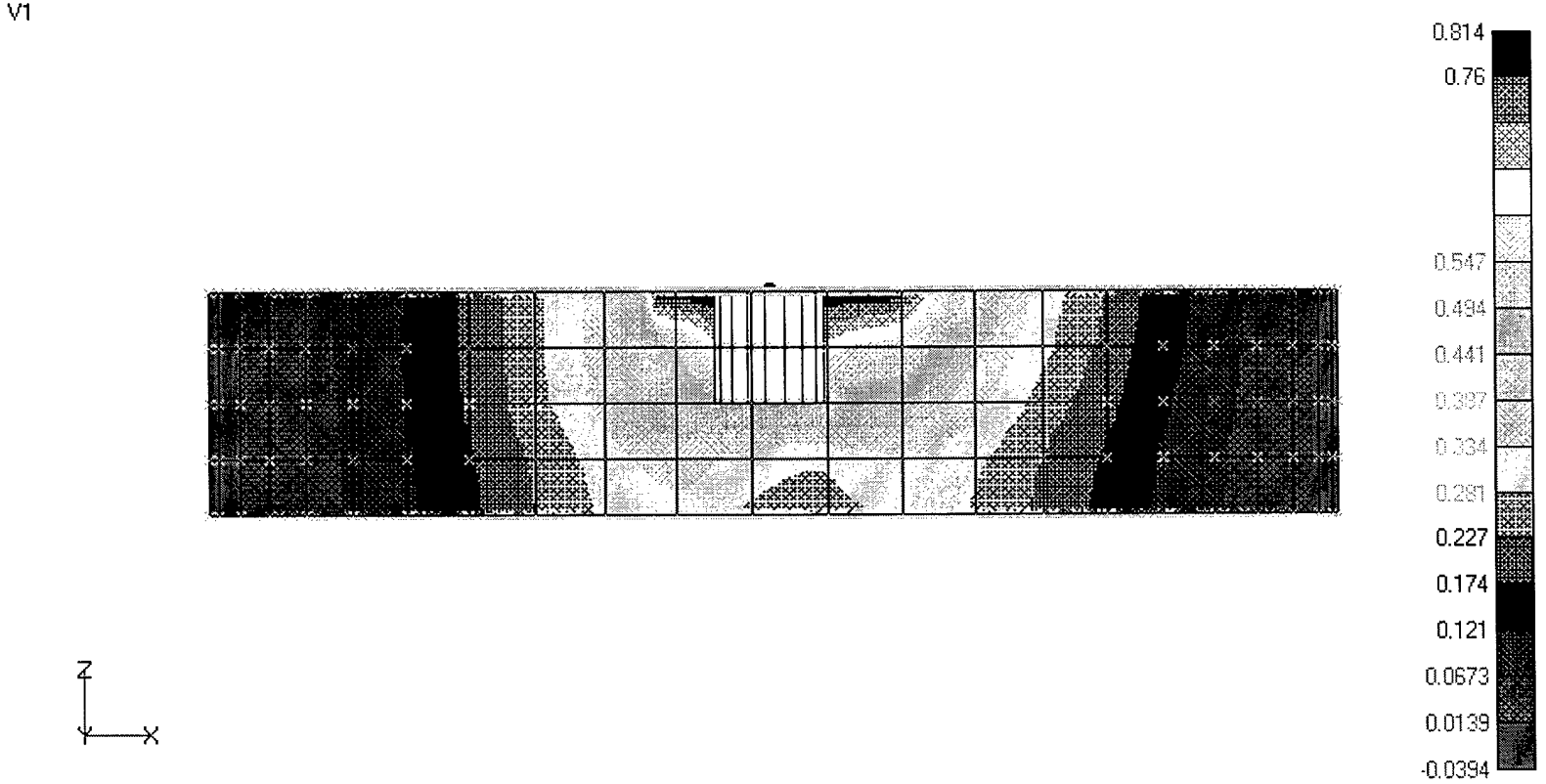

Horizontal Load = 2,100,000 lbs
Linear Elastic-Perfectly Plastic Clayey Soil (Hyperbolic Extended Drucker-Prager)
E = 30,000 psf, υ = 0.499, Slope Angle = 10.2°, Dilation Angle = 10.2°
Pile, AISI 4340 Steel

Figure-D9. Pile Total Displacements (Circular Pile with 15-ft Flange in Clay)

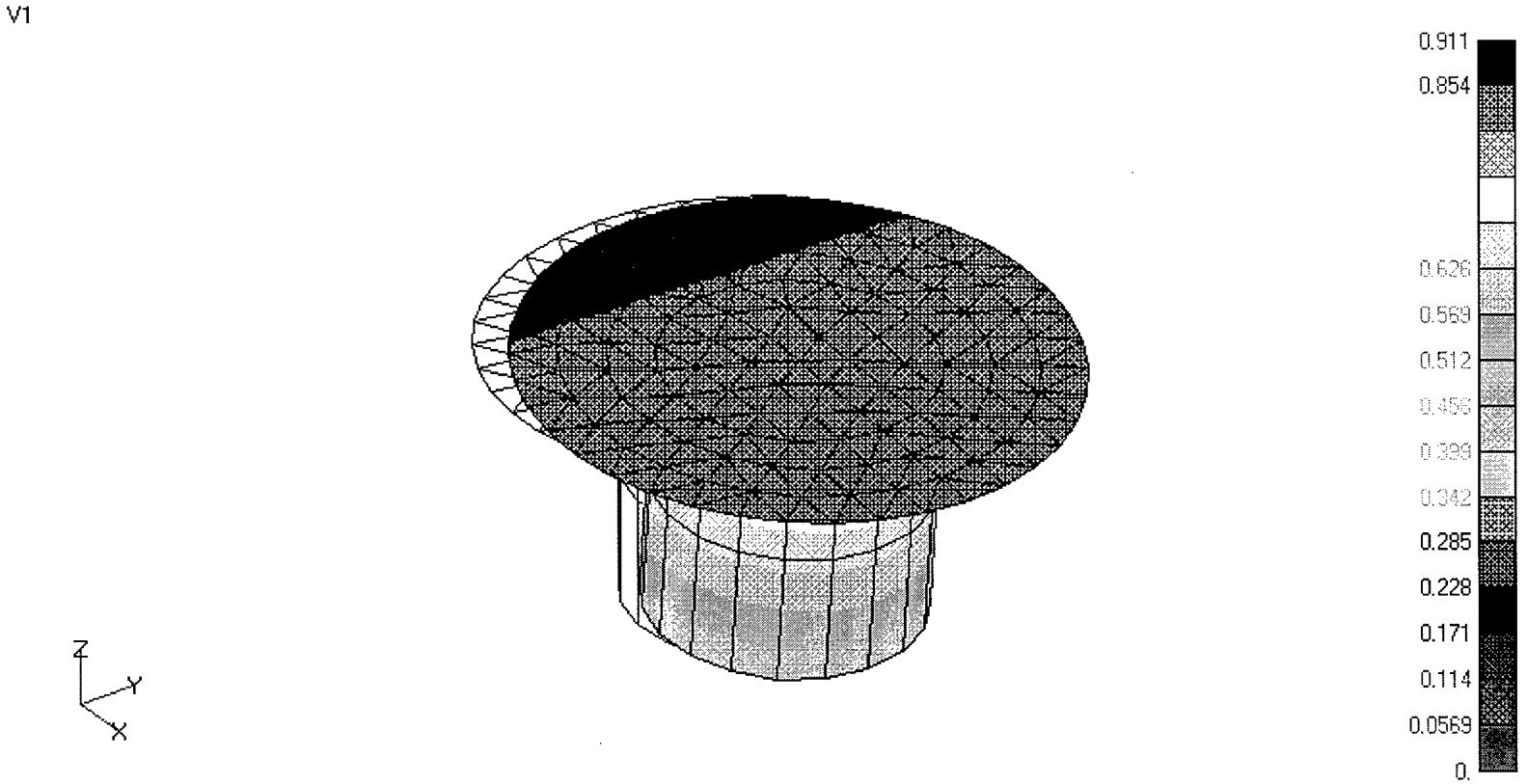

Horizontal Load = 2,100,000 lbs
Linear Elastic-Perfectly Plastic Clayey Soil (Hyperbolic Extended Drucker-Prager)
E = 30,000 psf, υ = 0.499, Slope Angle = 10.2°, Dilation Angle = 10.2°
Pile, AISI 4340 Steel

Figure-D10. Soil Minor Principal Stresses on a Vertical Plane along the Horizontal Load Direction (Circular Pile with 15-ft Flange in Clay)

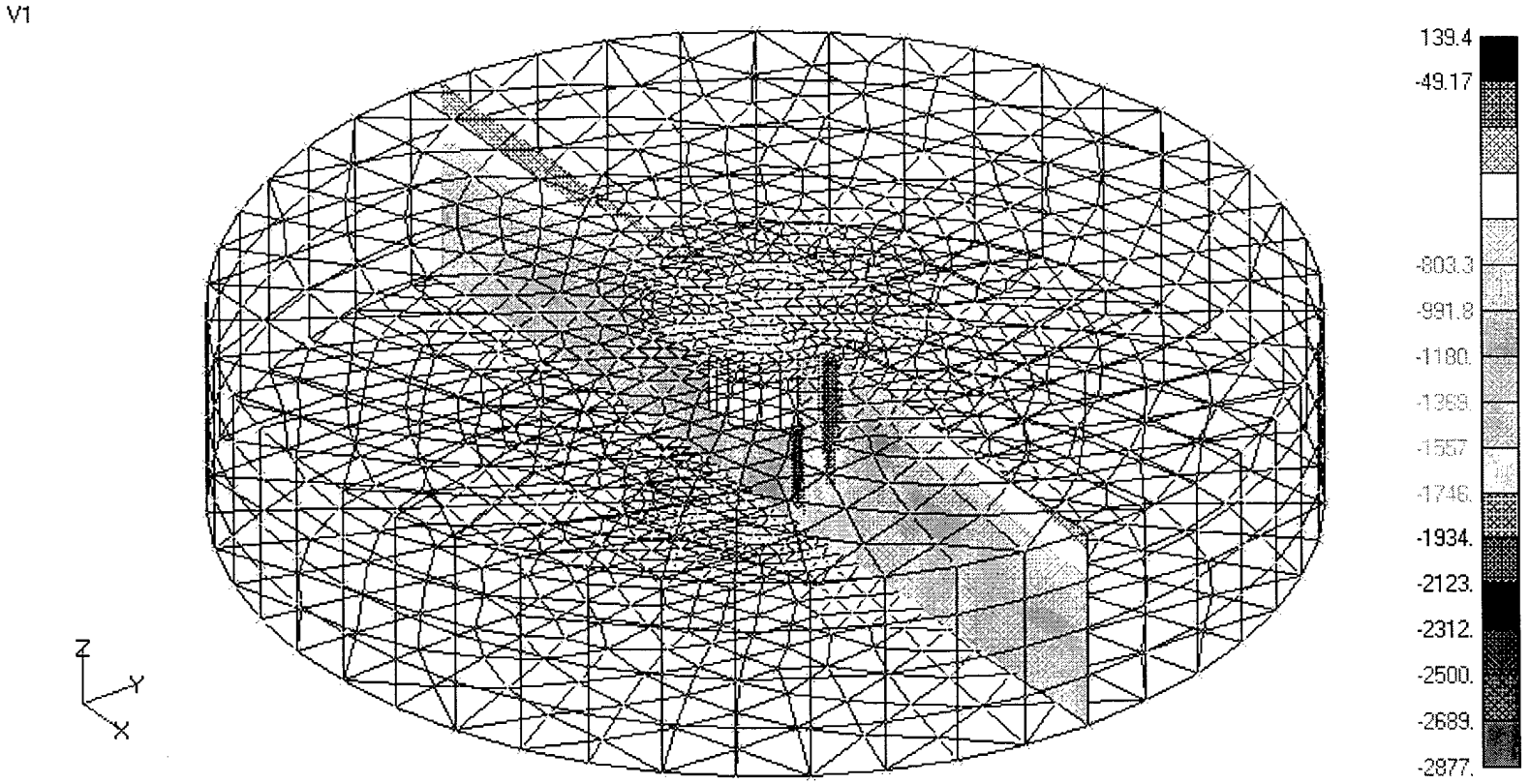

Horizontal Load = 2,100,000 lbs
Linear Elastic-Perfectly Plastic Clayey Soil (Hyperbolic Extended Drucker-Prager)
E = 30,000 psf, υ = 0.499, Slope Angle = 10.2°, Dilation Angle = 10.2°
Pile, AISI 4340 Steel

Figure-D11. Soil Minor Principal Stresses on the Pile Surface (Circular Pile with 15-ft Flange in Clay)

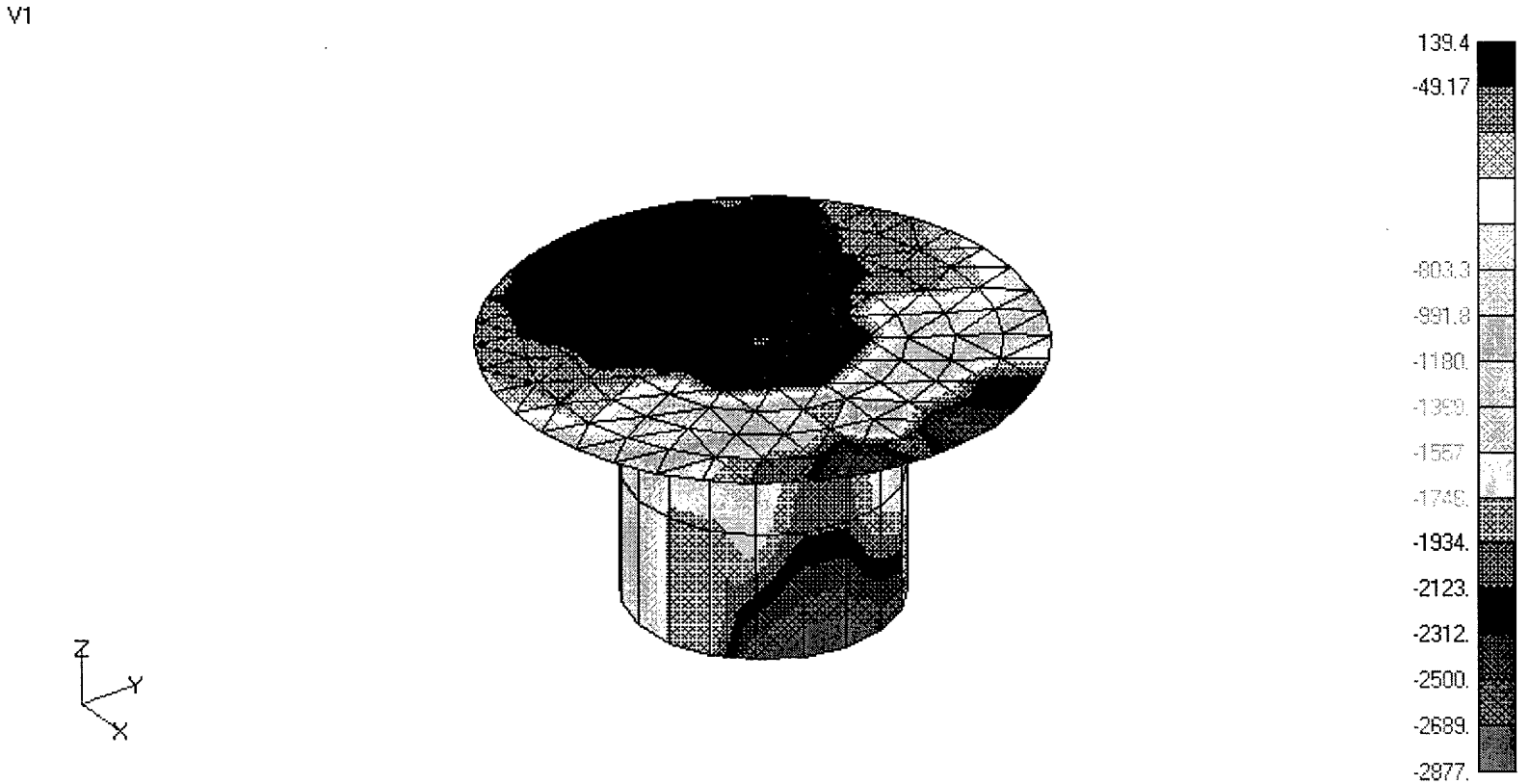

Horizontal Load = 2,100,000 lbs
Linear Elastic-Perfectly Plastic Clayey Soil (Hyperbolic Extended Drucker-Prager)
E = 30,000 psf, υ = 0.499, Slope Angle = 10.2°, Dilation Angle = 10.2°
Pile, AISI 4340 Steel

Figure-D12. Pile von Mises Stresses on the Pile Surface (Circular Pile with 15-ft Flange in Clay)

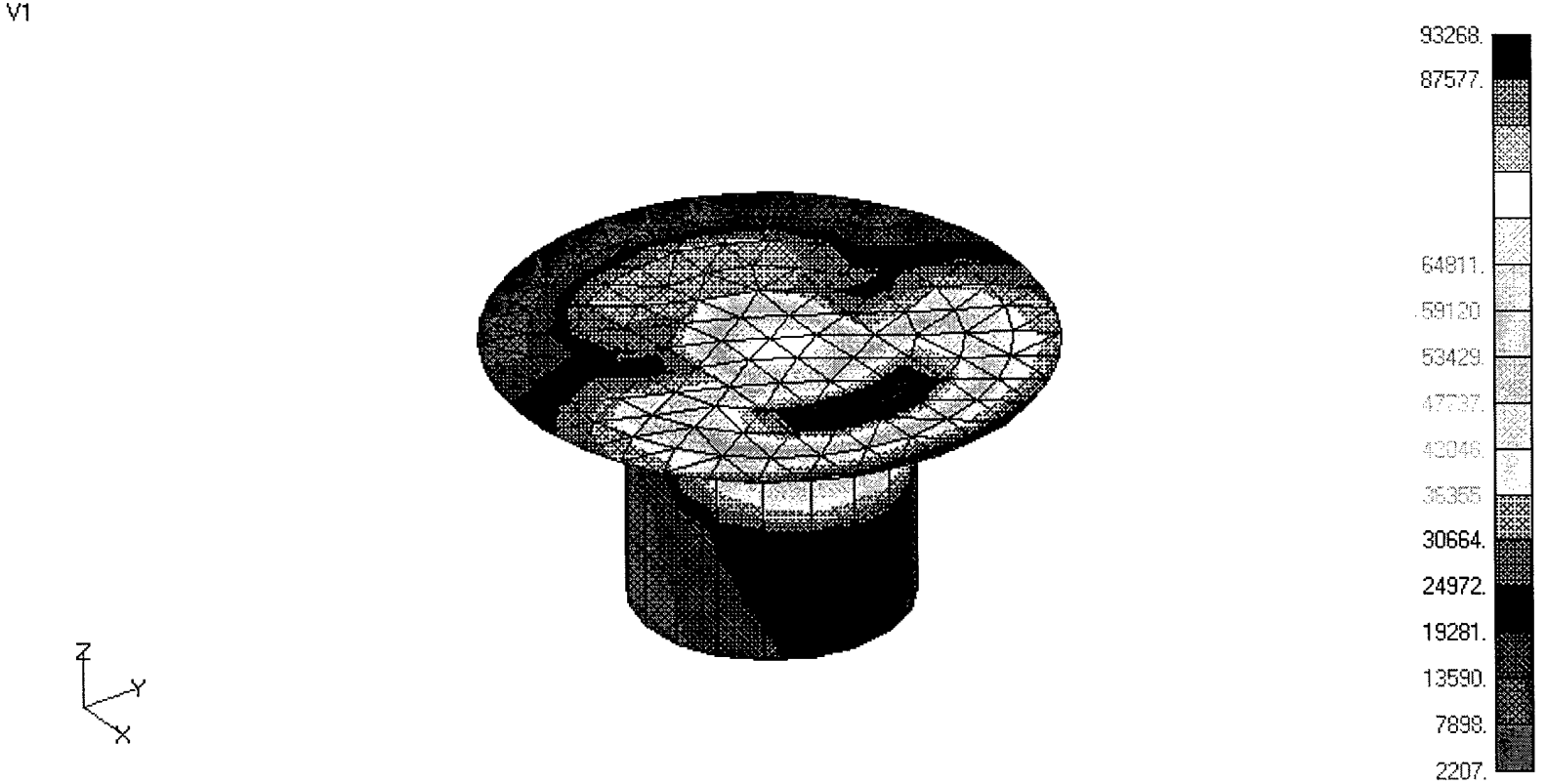

Horizontal Load = 2,100,000 lbs
Linear Elastic-Perfectly Plastic Clayey Soil (Hyperbolic Extended Drucker-Prager)
E = 30,000 psf, υ = 0.499, Slope Angle = 10.2°, Dilation Angle = 10.2°
Pile, AISI 4340 Steel

Figure-E1. Horizontal Displacements on a Vertical Plane along the Horizontal Load Direction (Load at the Middle of the Pile in Clay)

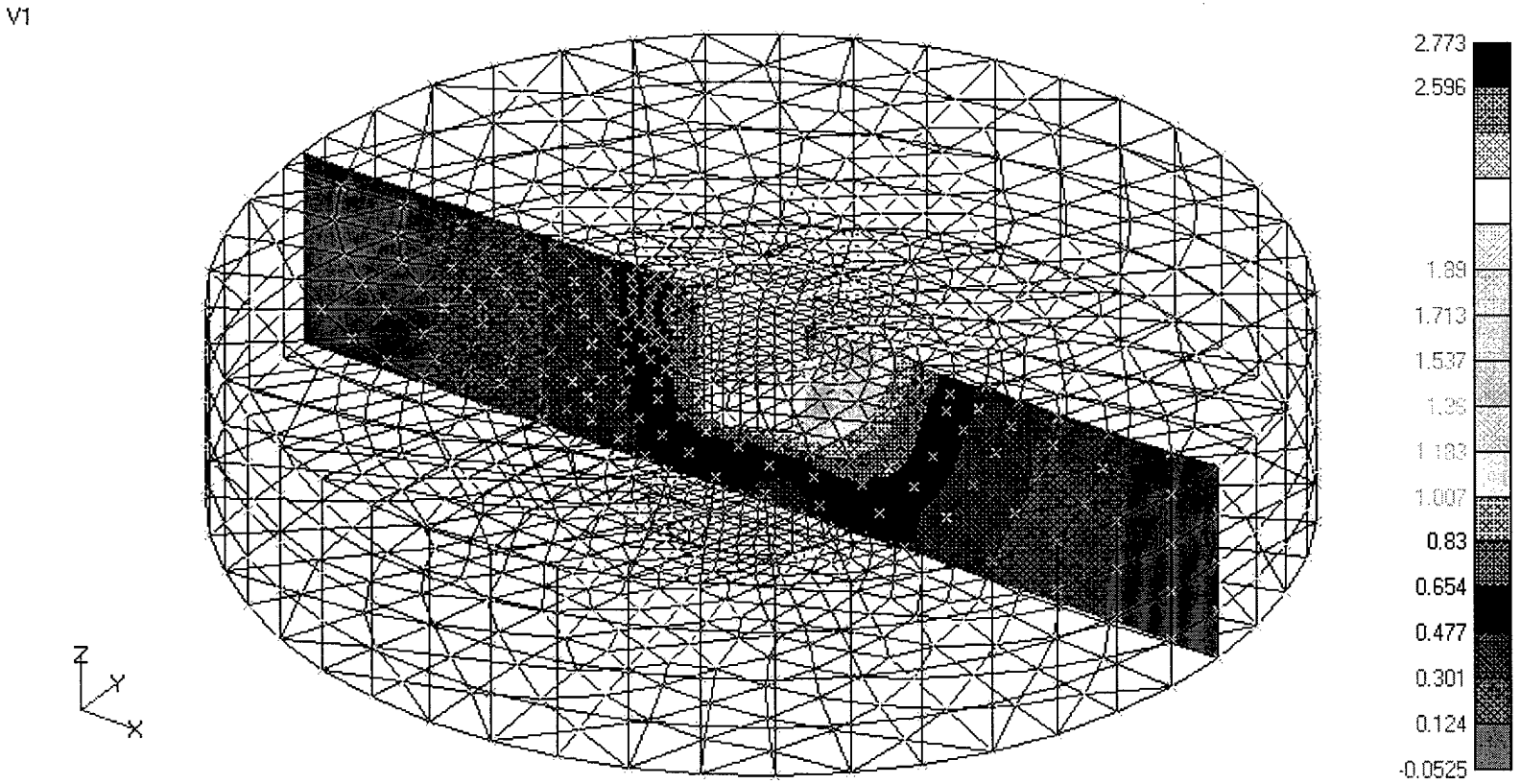

Horizontal Load = 3,000,000 lbs
Linear Elastic-Perfectly Plastic Clayey Soil (Hyperbolic Extended Drucker-Prager)
E = 30,000 psf, υ = 0.499, Slope Angle = 10.2°, Dilation Angle = 10.2°
Pile, AISI 4340 Steel

Figure-E2. Pile Total Displacements (Load at the Middle of the Pile in Clay)

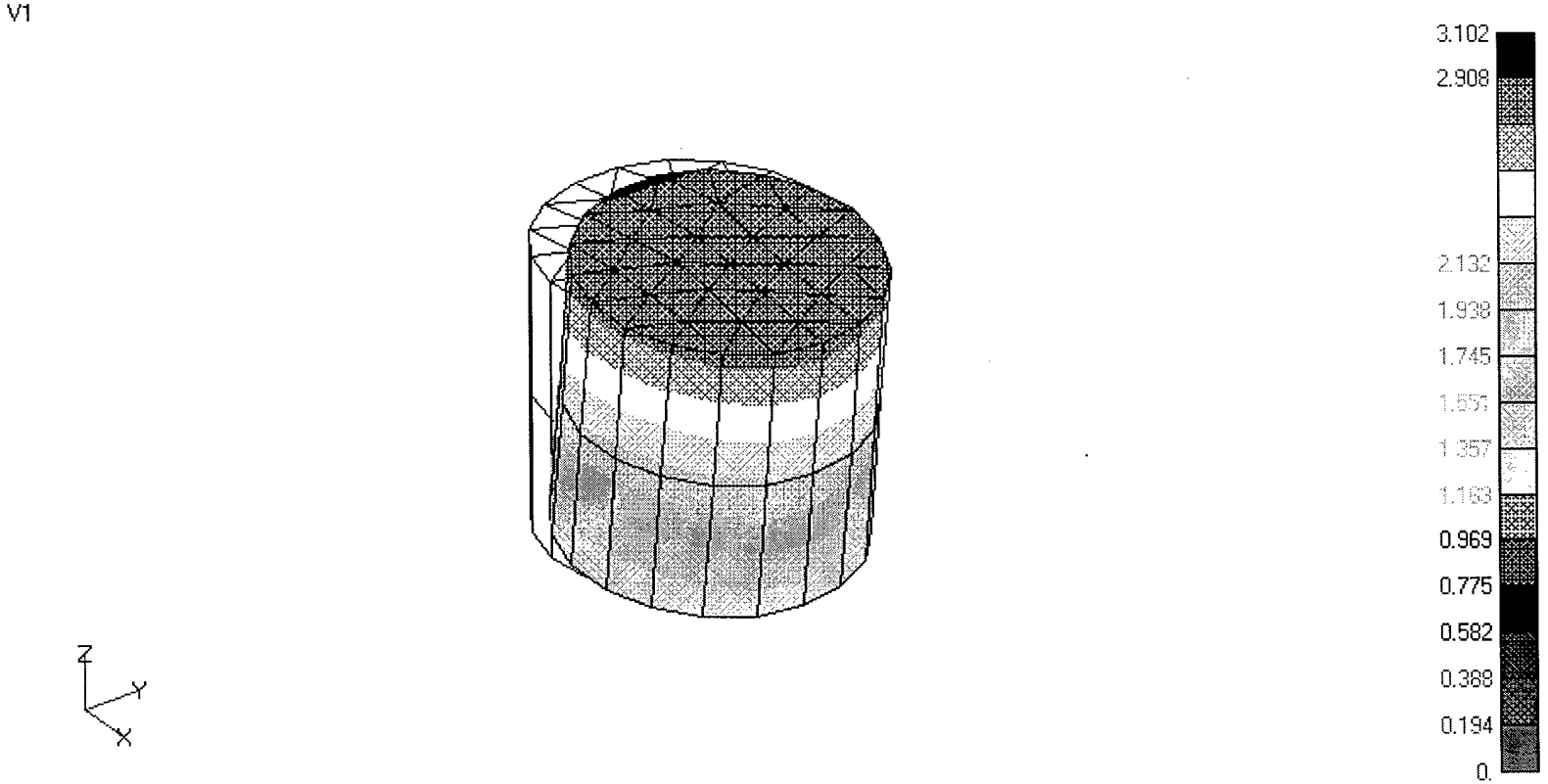

Horizontal Load = 3,000,000 lbs
Linear Elastic-Perfectly Plastic Clayey Soil (Hyperbolic Extended Drucker-Prager)
E = 30,000 psf, υ = 0.499, Slope Angle = 10.2°, Dilation Angle = 10.2°
Pile, AISI 4340 Steel

Figure-E3. Soil Minor Principal Stresses on a Vertical Plane along the Horizontal Load Direction (Load at the Middle of the Pile in Clay)

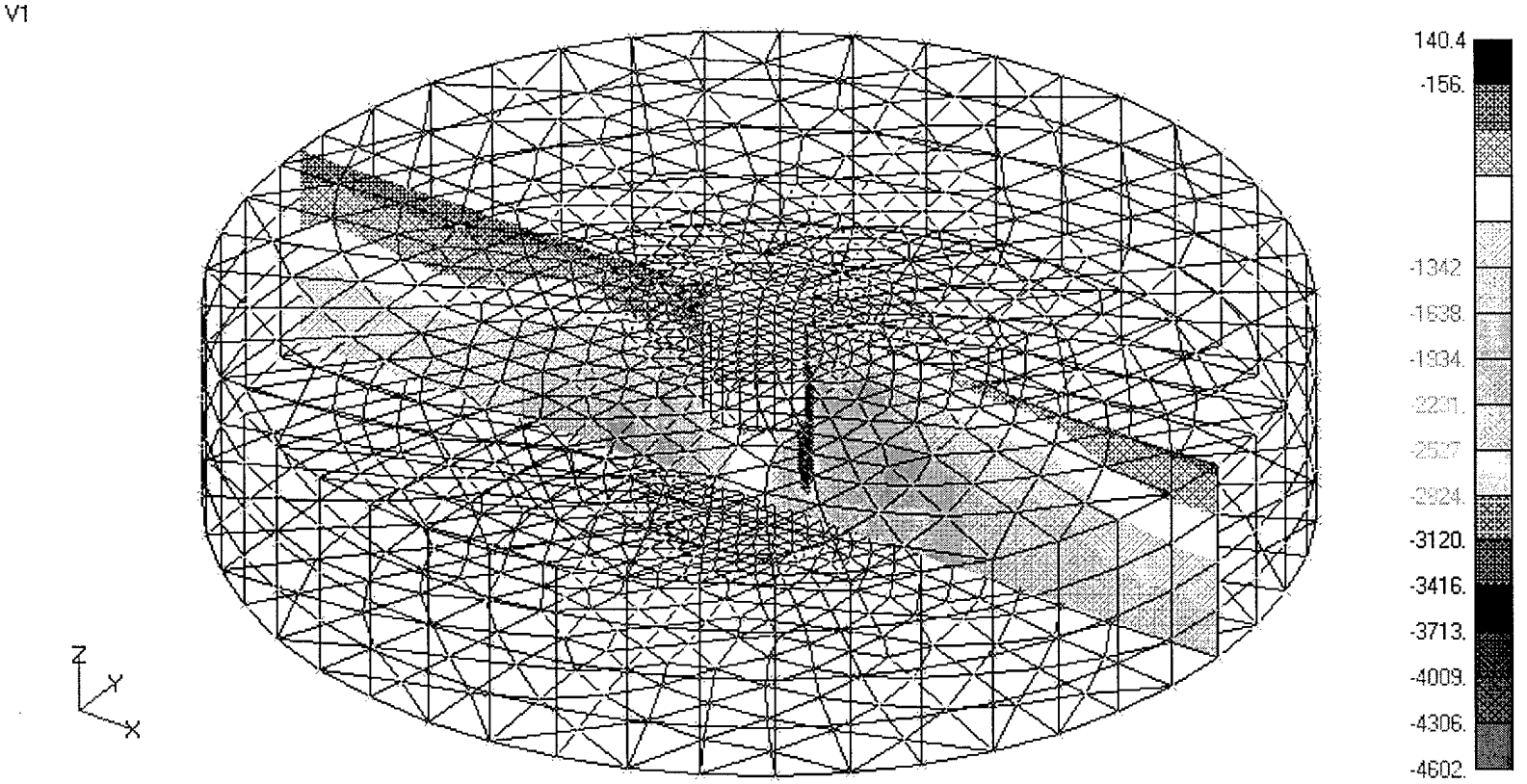

Horizontal Load = 3,000,000 lbs
Linear Elastic-Perfectly Plastic Clayey Soil (Hyperbolic Extended Drucker-Prager)
E = 30,000 psf, υ = 0.499, Slope Angle = 10.2°, Dilation Angle = 10.2°
Pile, AISI 4340 Steel

Figure-E4. Soil Minor Principal Stresses on the Pile Surface (Load at the Middle of the Pile in Clay)

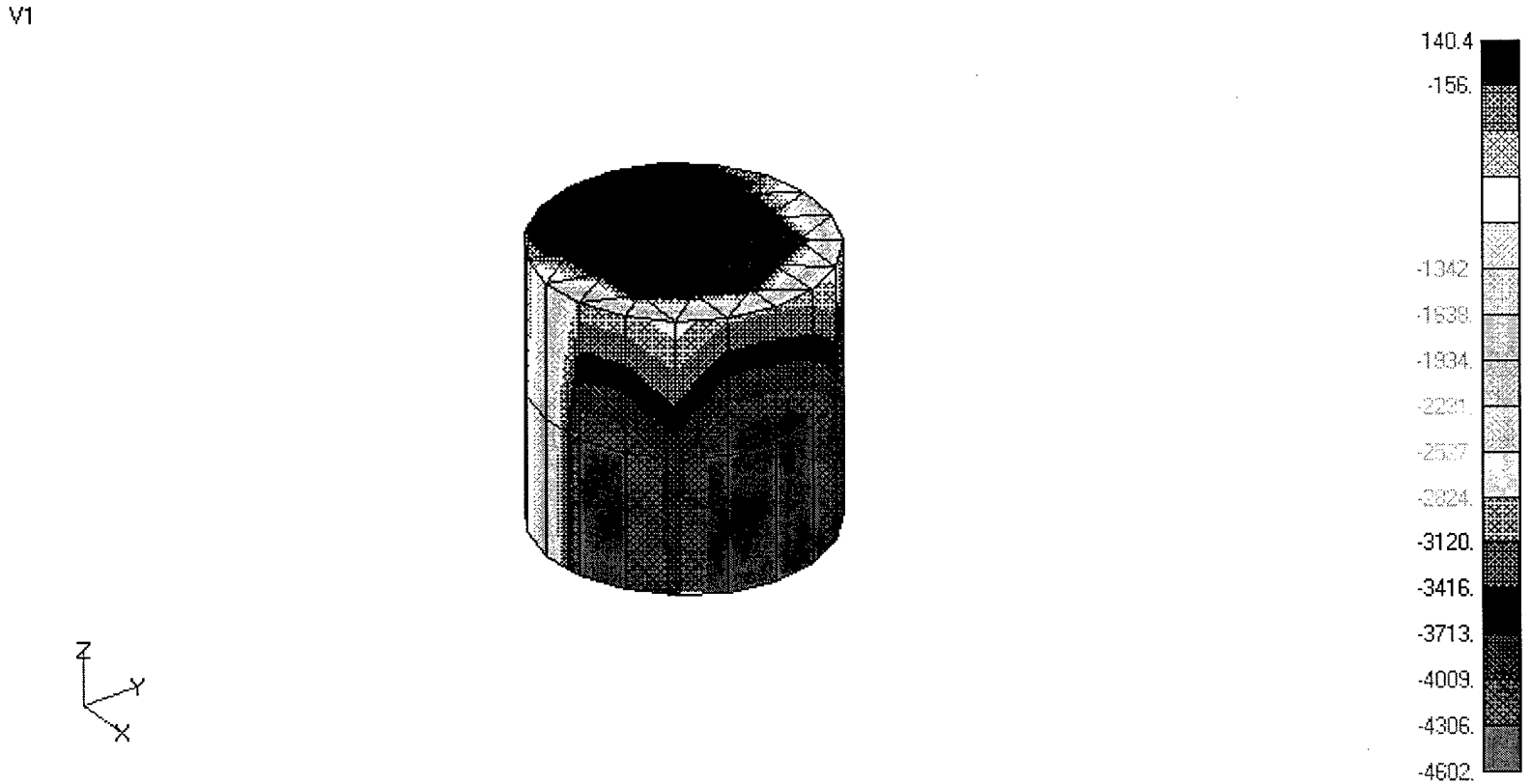

Horizontal Load = 3,000,000 lbs
Linear Elastic-Perfectly Plastic Clayey Soil (Hyperbolic Extended Drucker-Prager)
E = 30,000 psf, υ = 0.499, Slope Angle = 10.2°, Dilation Angle = 10.2°
Pile, AISI 4340 Steel

Figure-E5. Pile von Mises Stresses on the Pile Surface (Load at the Middle of the Pile in Clay)

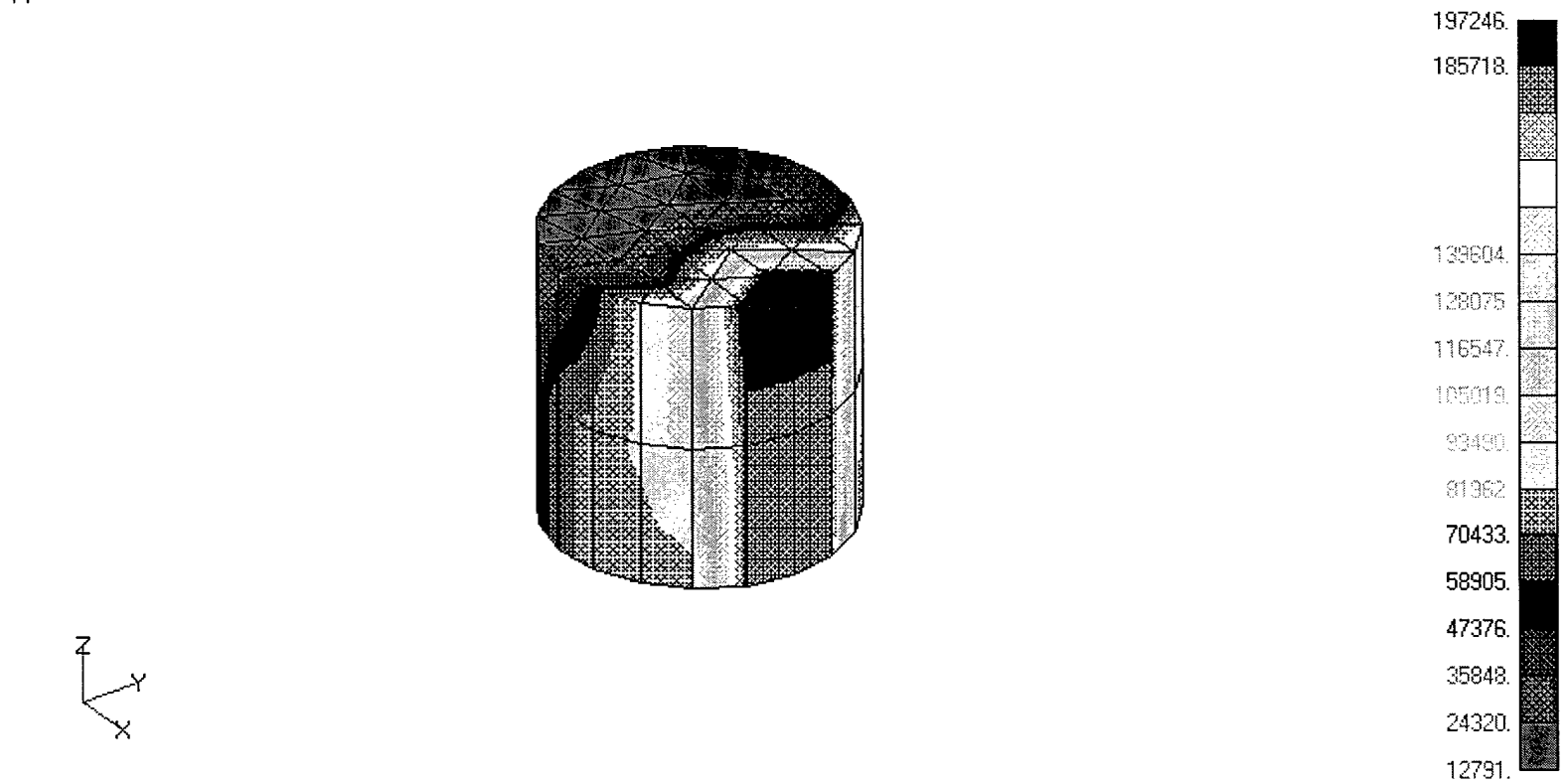

Horizontal Load = 3,000,000 lbs
Linear Elastic-Perfectly Plastic Clayey Soil (Hyperbolic Extended Drucker-Prager)
E = 30,000 psf, υ = 0.499, Slope Angle = 10.2°, Dilation Angle = 10.2°
Pile, AISI 4340 Steel

Figure-E6. Horizontal Displacements on a Vertical Plane along the Horizontal Load Direction (Load at the Bottom of the Pile in Clay)

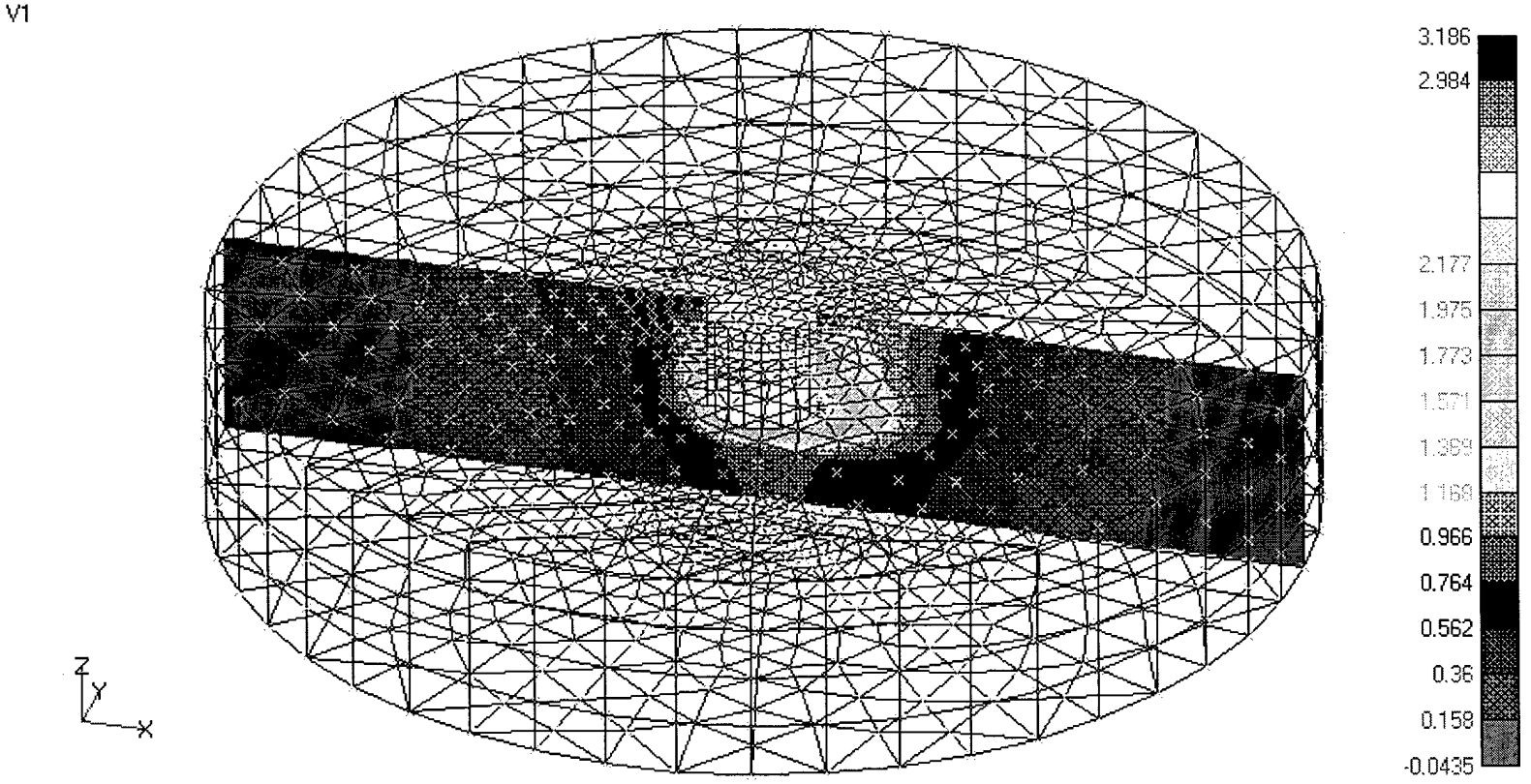

Horizontal Load = 3,000,000 lbs
Linear Elastic-Perfectly Plastic Clayey Soil (Hyperbolic Extended Drucker-Prager)
E = 30,000 psf, υ = 0.499, Slope Angle = 10.2°, Dilation Angle = 10.2°
Pile, AISI 4340 Steel

Figure-E7. Pile Total Displacements (Load at the Bottom of the Pile in Clay)

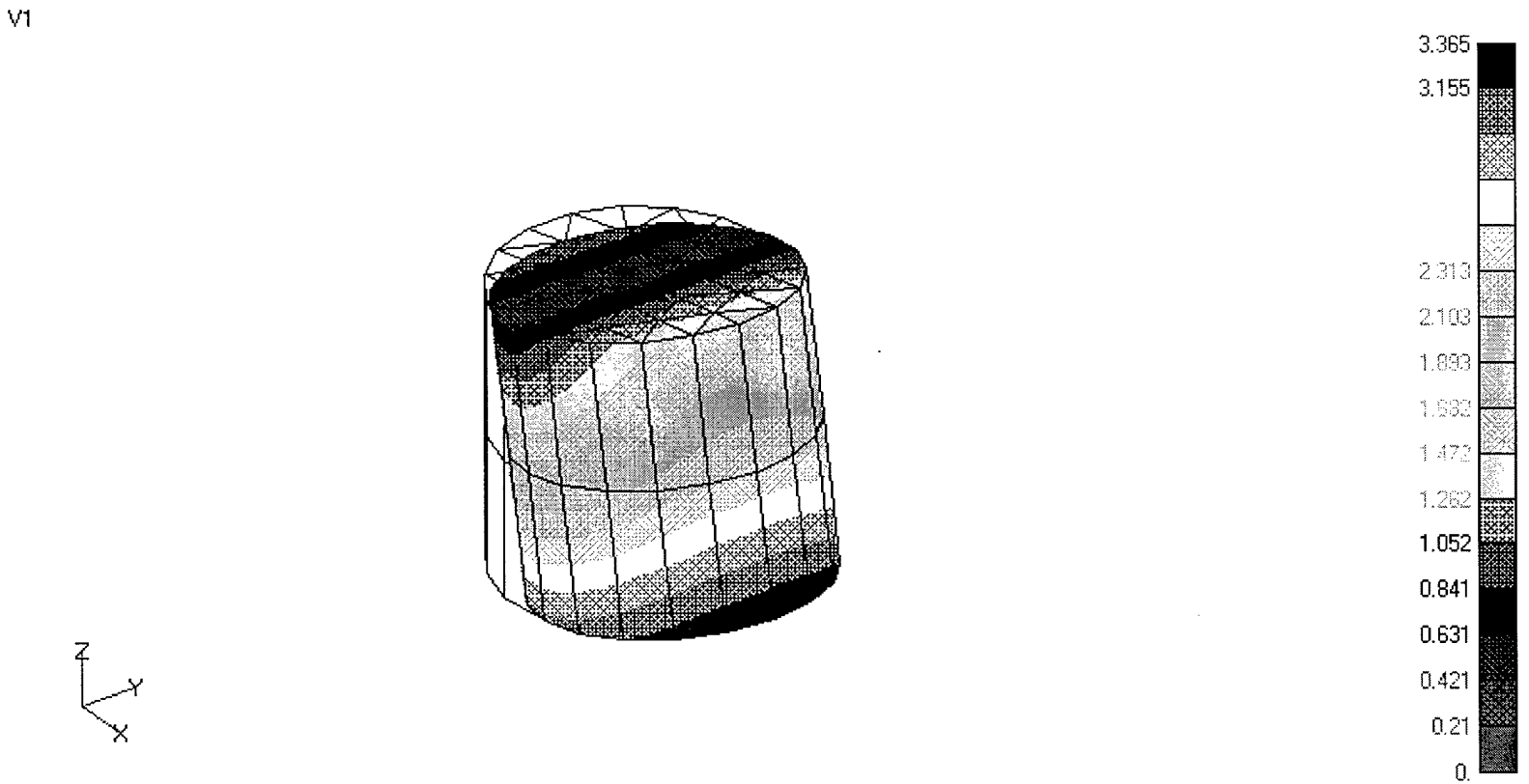

Horizontal Load = 3,000,000 lbs
Linear Elastic-Perfectly Plastic Clayey Soil (Hyperbolic Extended Drucker-Prager)
E = 30,000 psf, $\upsilon = 0.499$, Slope Angle = 10.2°, Dilation Angle = 10.2°
Pile, AISI 4340 Steel

Figure-E8. Soil Minor Principal Stresses on a Vertical Plane along the Horizontal Load Direction (Load at the Bottom of the Pile in Clay)

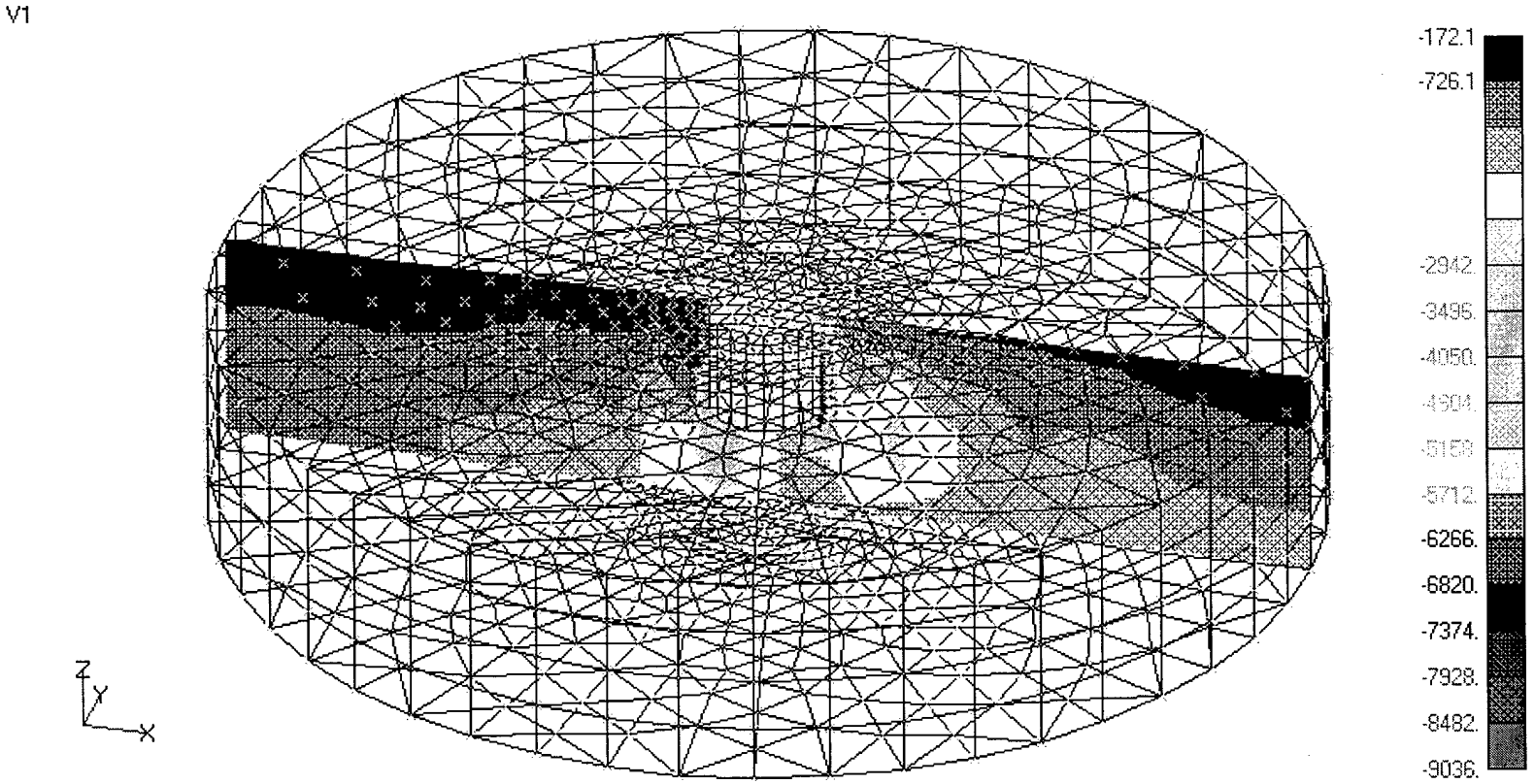

Horizontal Load = 3,000,000 lbs
Linear Elastic-Perfectly Plastic Clayey Soil (Hyperbolic Extended Drucker-Prager)
E = 30,000 psf, υ = 0.499, Slope Angle = 10.2°, Dilation Angle = 10.2°
Pile, AISI 4340 Steel

Figure-E9. Soil Minor Principal Stresses on the Pile Surface (Load at the Bottom of the Pile in Clay)

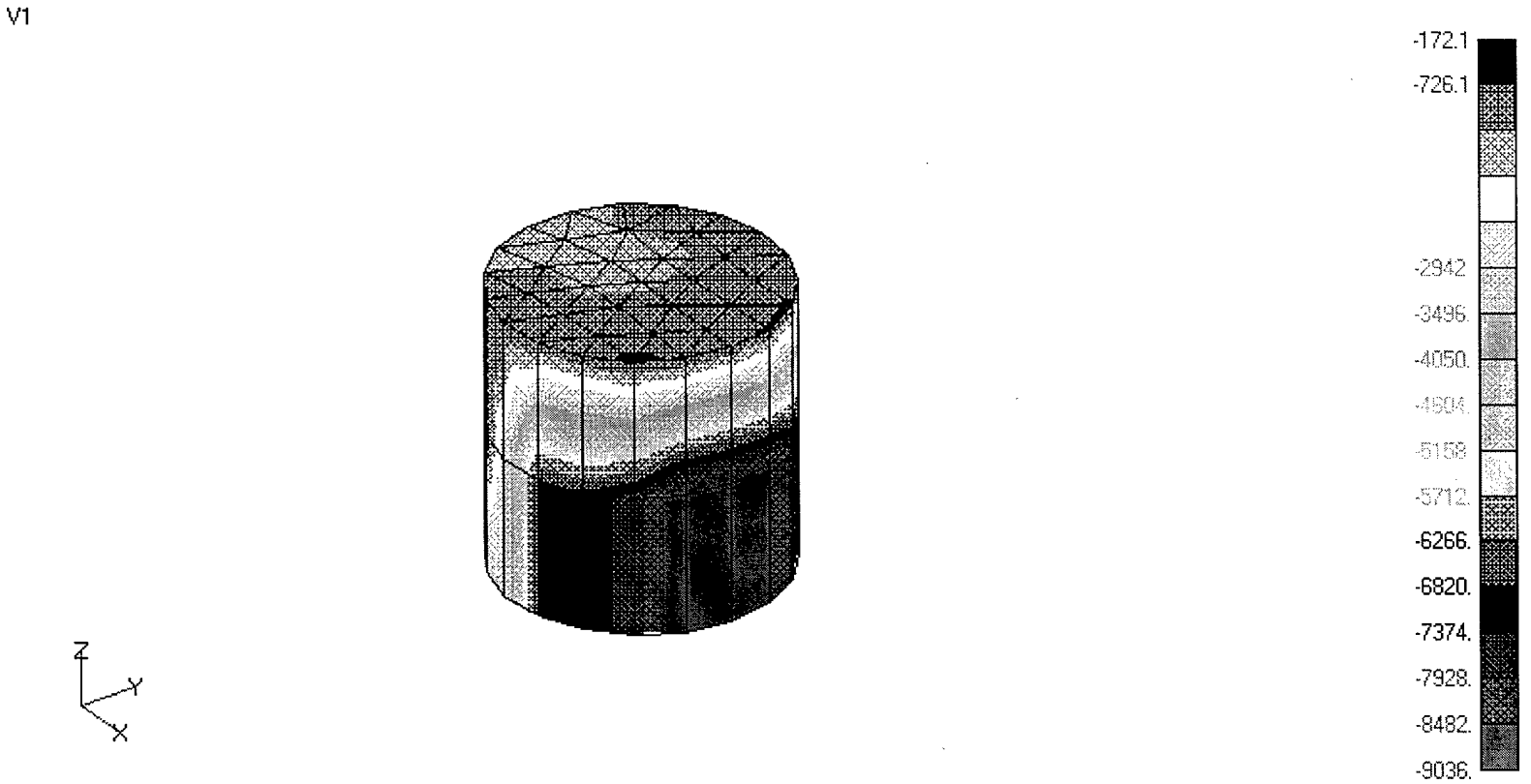

Horizontal Load = 3,000,000 lbs
Linear Elastic-Perfectly Plastic Clayey Soil (Hyperbolic Extended Drucker-Prager)
E = 30,000 psf, $\upsilon = 0.499$, Slope Angle = 10.2°, Dilation Angle = 10.2°
Pile, AISI 4340 Steel

Figure-E10. Pile von Mises Stresses on the Pile Surface (Load at the Bottom of the Pile in Clay)

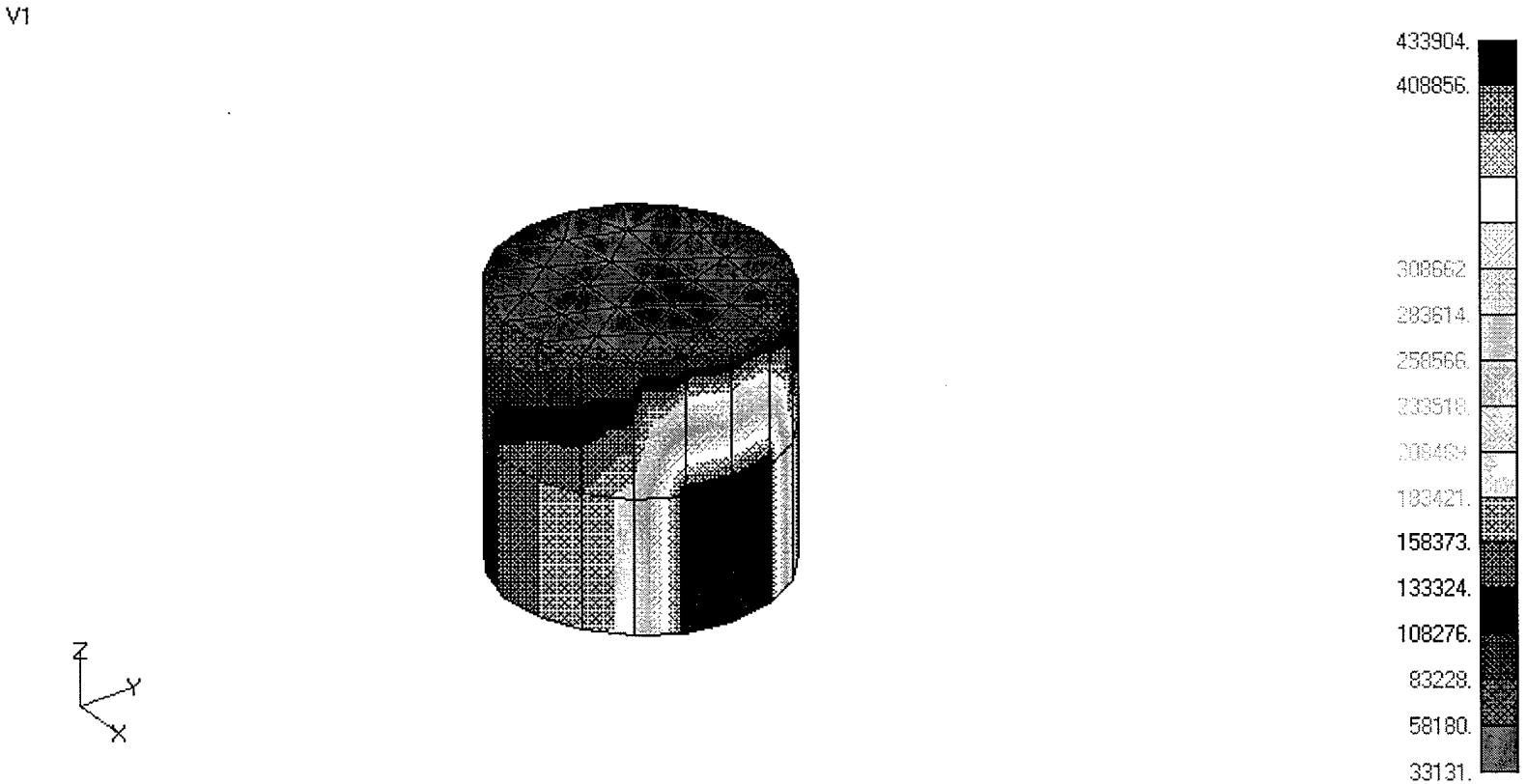

Horizontal Load = 3,000,000 lbs
Linear Elastic-Perfectly Plastic Clayey Soil (Hyperbolic Extended Drucker-Prager)
E = 30,000 psf, υ = 0.499, Slope Angle = 10.2°, Dilation Angle = 10.2°
Pile, AISI 4340 Steel

Figure-E11. Horizontal Displacements on a Vertical Plane along the Horizontal Load Direction (Load at the Middle of the Pile in Sand)

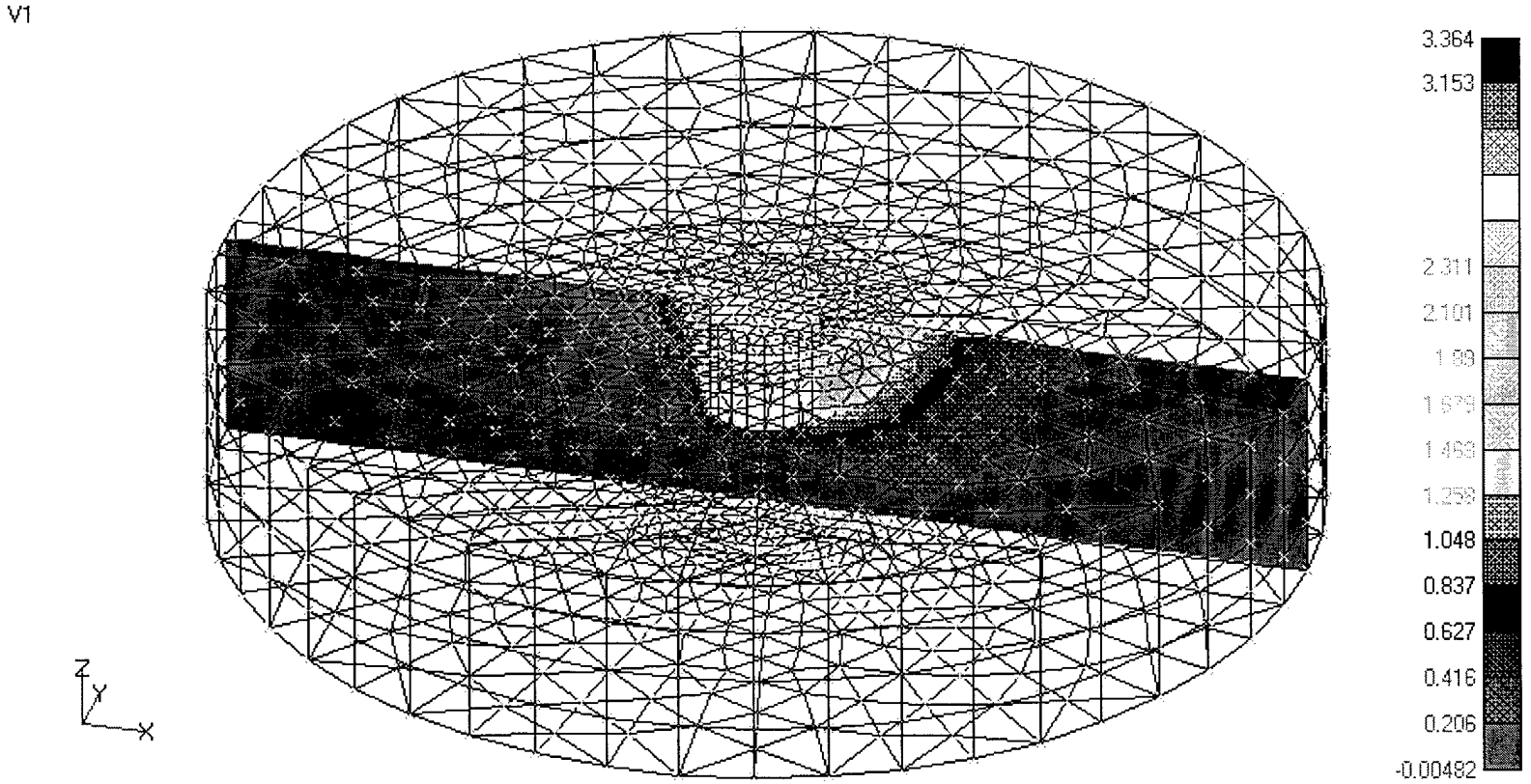

Horizontal Load = 24,000,000 lbs
Linear Elastic-Perfectly Plastic Sandy Soil (Linear Extended Drucker-Prager)
E = 864,000 psf, υ = 0.3, Slope Angle = 46.2°, Dilation Angle = 21.5°
Pile, AISI 4340 Steel

Figure-E12. Pile Total Displacements (Load at the Middle of the Pile in Sand)

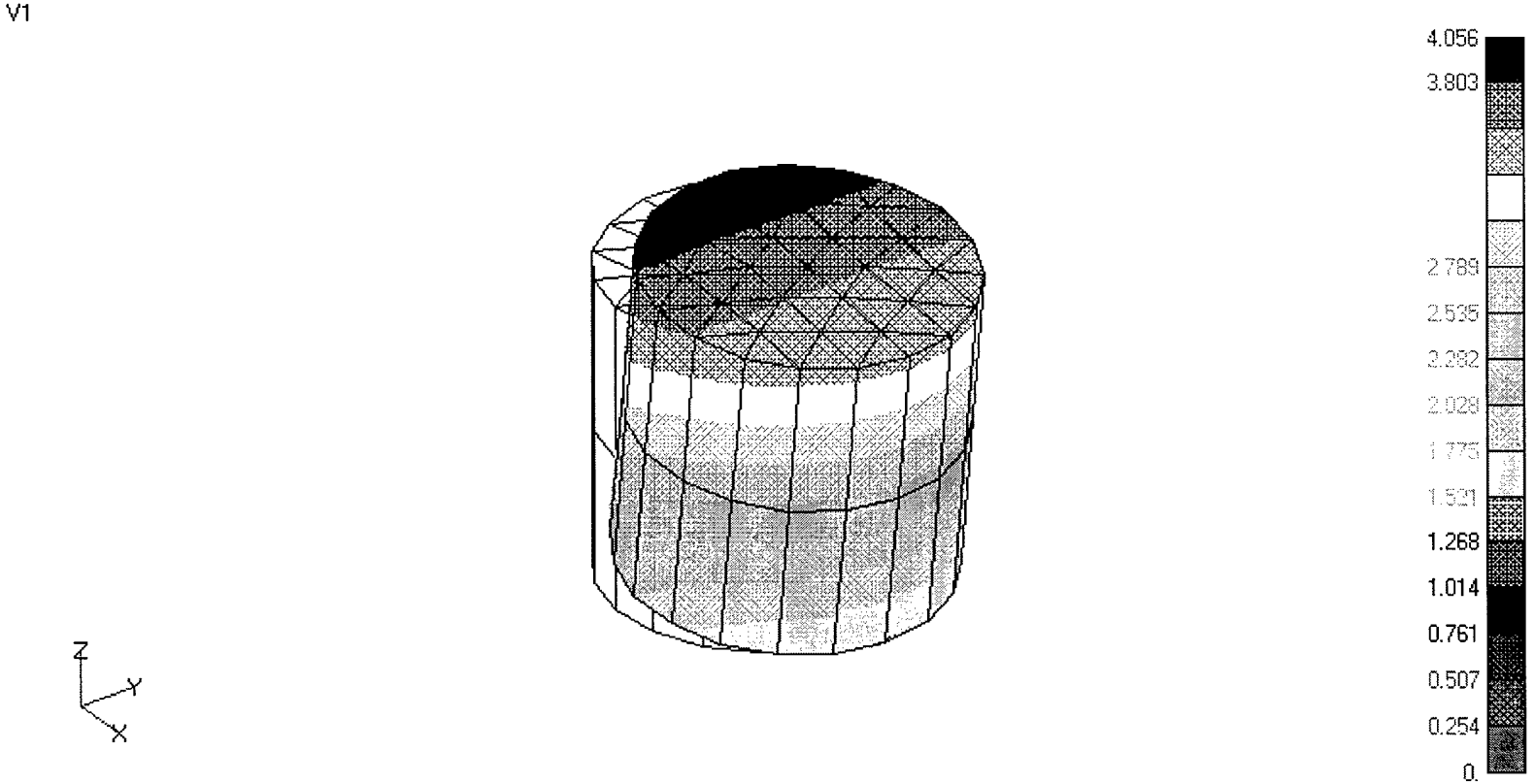

Horizontal Load = 24,000,000 lbs
Linear Elastic-Perfectly Plastic Sandy Soil (Linear Extended Drucker-Prager)
E = 864,000 psf, $\upsilon = 0.3$, Slope Angle = 46.2°, Dilation Angle = 21.5°
Pile, AISI 4340 Steel

Figure-E13. Soil Minor Principal Stresses on a Vertical Plane along the Horizontal Load Direction (Load at the Middle of the Pile in Sand)

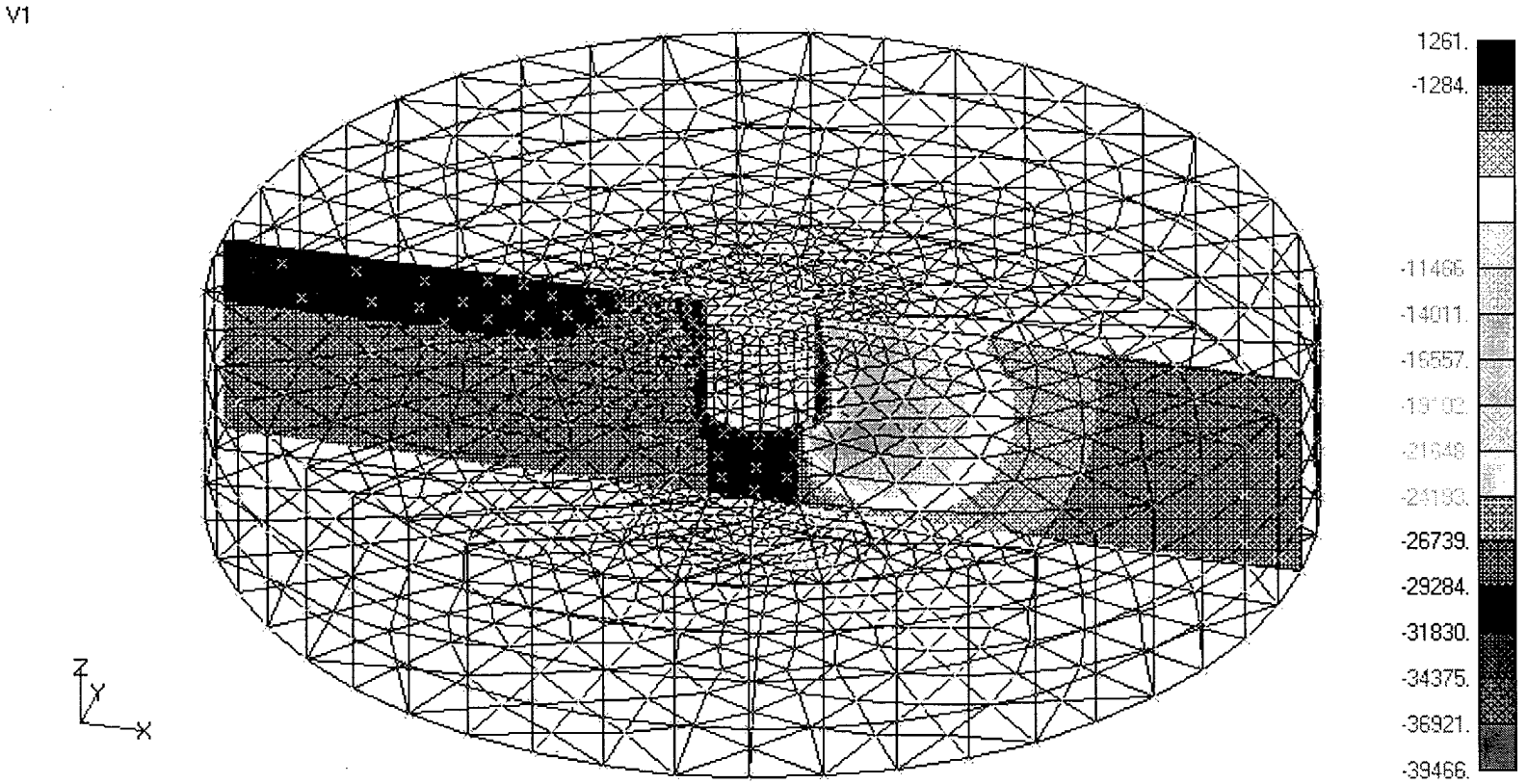

Horizontal Load = 24,000,000 lbs
Linear Elastic-Perfectly Plastic Sandy Soil (Linear Extended Drucker-Prager)
E = 864,000 psf, υ = 0.3, Slope Angle = 46.2°, Dilation Angle = 21.5°
Pile, AISI 4340 Steel

Figure-E14. Soil Minor Principal Stresses on the Pile Surface (Load at the Middle of the Pile in Sand)

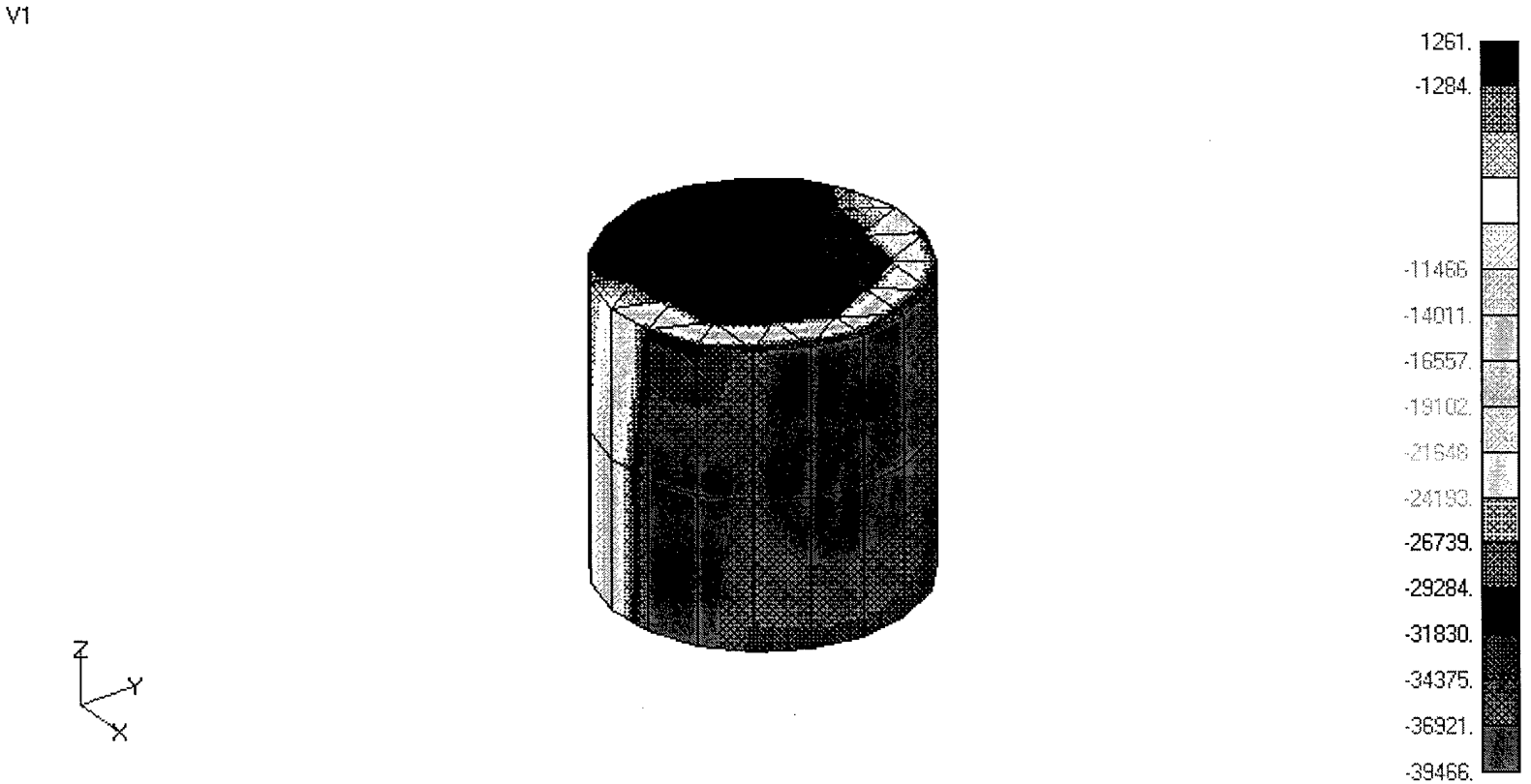

Horizontal Load = 24,000,000 lbs
Linear Elastic-Perfectly Plastic Sandy Soil (Linear Extended Drucker-Prager)
E = 864,000 psf, $\upsilon = 0.3$, Slope Angle = 46.2°, Dilation Angle = 21.5°
Pile, AISI 4340 Steel

Figure-E15. Pile von Mises Stresses on the Pile Surface (Load at the Middle of the Pile in Sand)

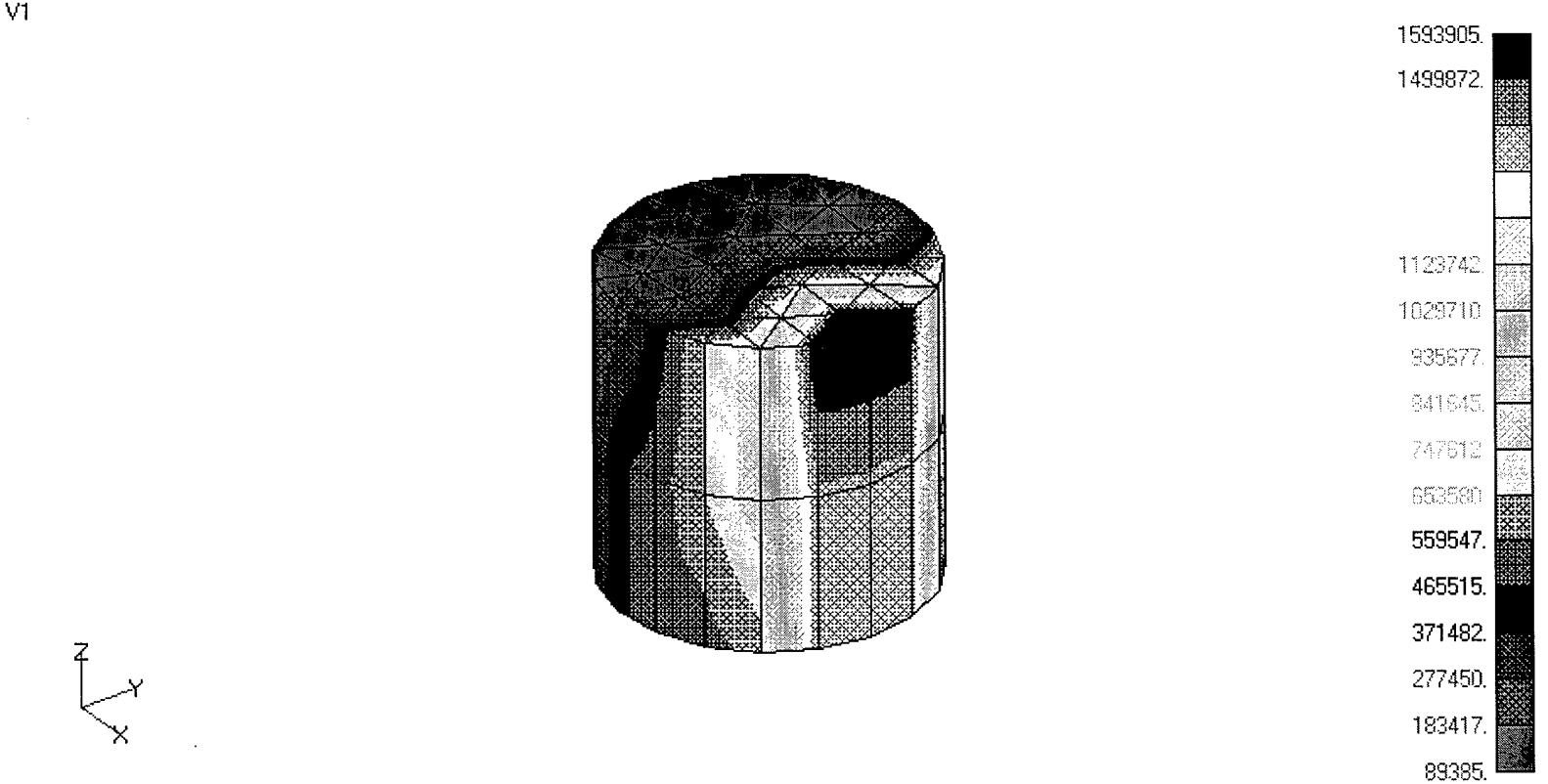

Horizontal Load = 24,000,000 lbs
Linear Elastic-Perfectly Plastic Sandy Soil (Linear Extended Drucker-Prager)
E = 864,000 psf, υ = 0.3, Slope Angle = 46.2°, Dilation Angle = 21.5°
Pile, AISI 4340 Steel

Figure-E16. Horizontal Displacements on a Vertical Plane along the Horizontal Load Direction (Load at the Bottom of the Pile in Sand)

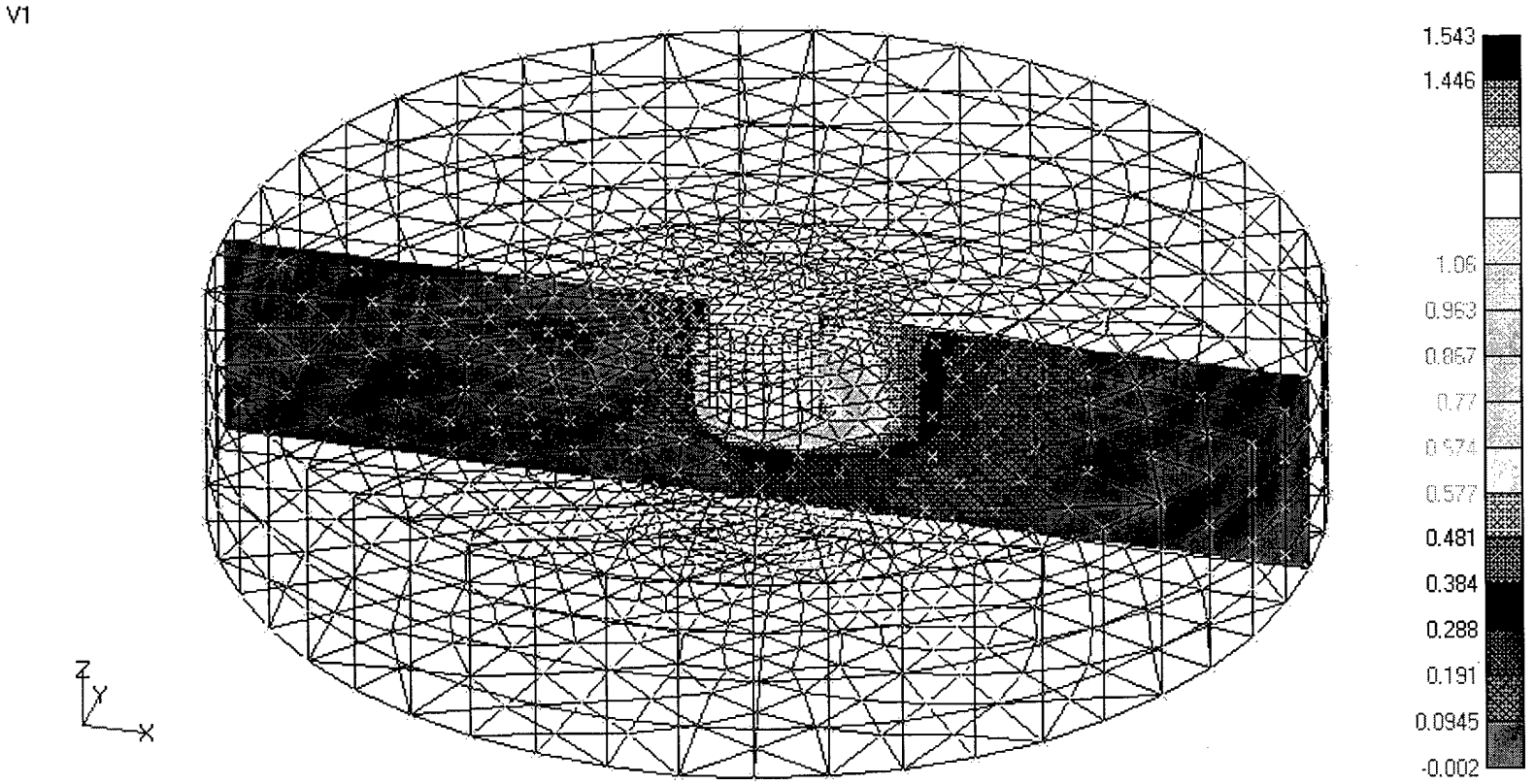

Horizontal Load = 20,000,000 lbs
Linear Elastic-Perfectly Plastic Sandy Soil (Linear Extended Drucker-Prager)
E = 864,000 psf, υ = 0.3, Slope Angle = 46.2°, Dilation Angle = 21.5°
Pile, AISI 4340 Steel

Figure-E17. Pile Total Displacements (Load at the Bottom of the Pile in Sand)

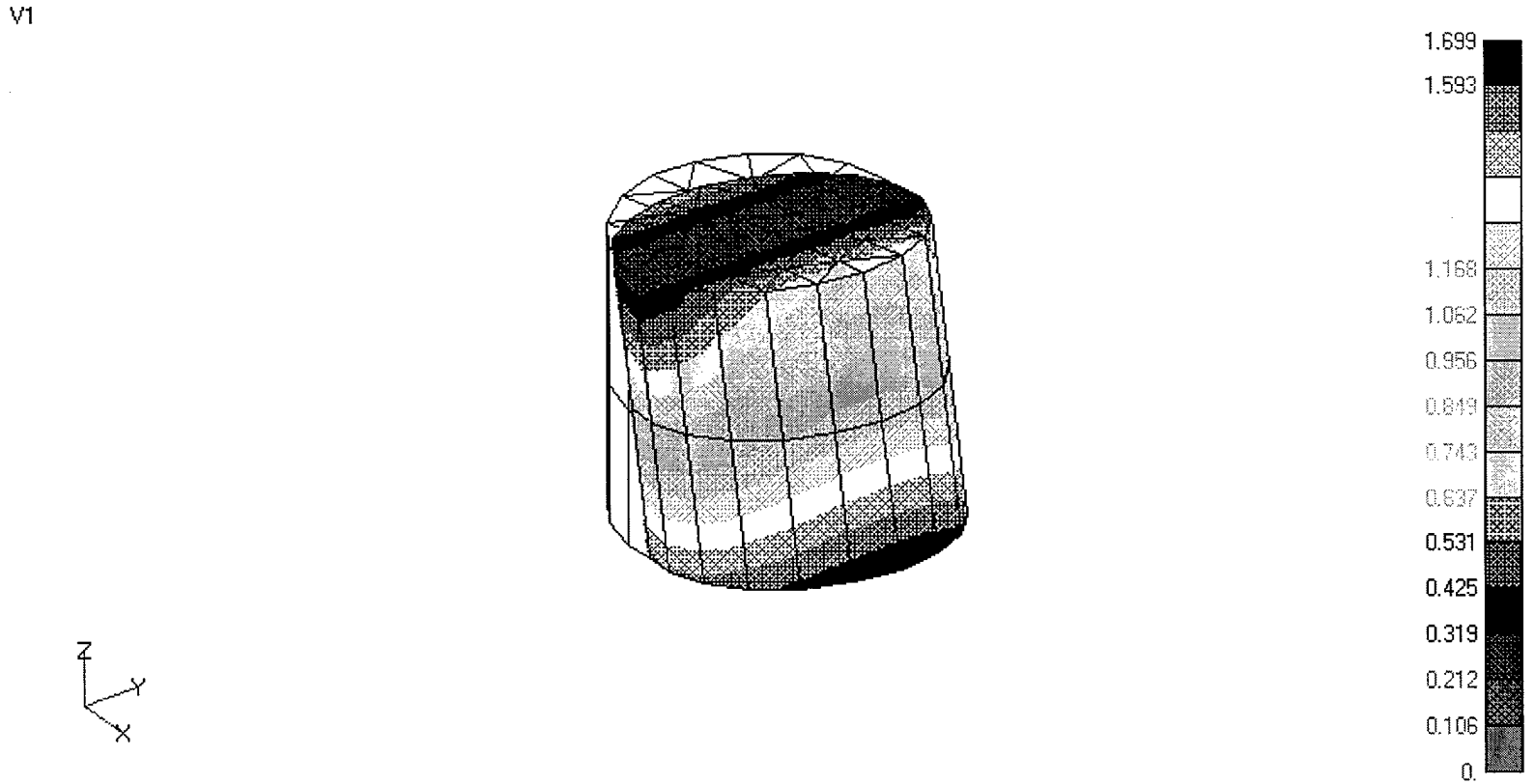

Horizontal Load = 20,000,000 lbs
Linear Elastic-Perfectly Plastic Sandy Soil (Linear Extended Drucker-Prager)
E = 864,000 psf, υ = 0.3, Slope Angle = 46.2°, Dilation Angle = 21.5°
Pile, AISI 4340 Steel

Figure-E18. Soil Minor Principal Stresses on a Vertical Plane along the Horizontal Load Direction (Load at the Bottom of the Pile in Sand)

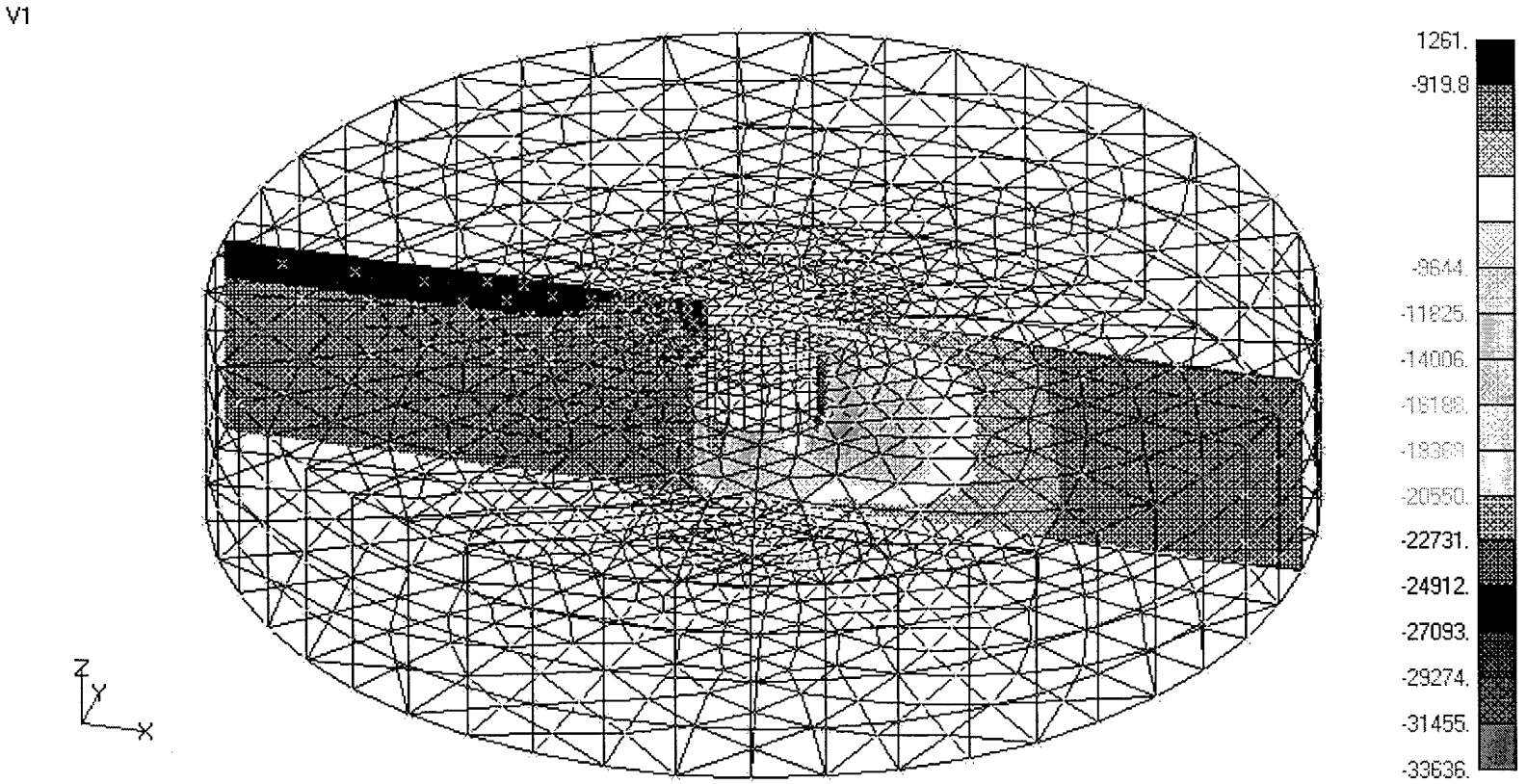

Horizontal Load = 20,000,000 lbs
Linear Elastic-Perfectly Plastic Sandy Soil (Linear Extended Drucker-Prager)
E = 864,000 psf, $\upsilon = 0.3$, Slope Angle = 46.2°, Dilation Angle = 21.5°
Pile, AISI 4340 Steel

Figure-E19. Soil Minor Principal Stresses on the Pile Surface (Load at the Bottom of the Pile in Sand)

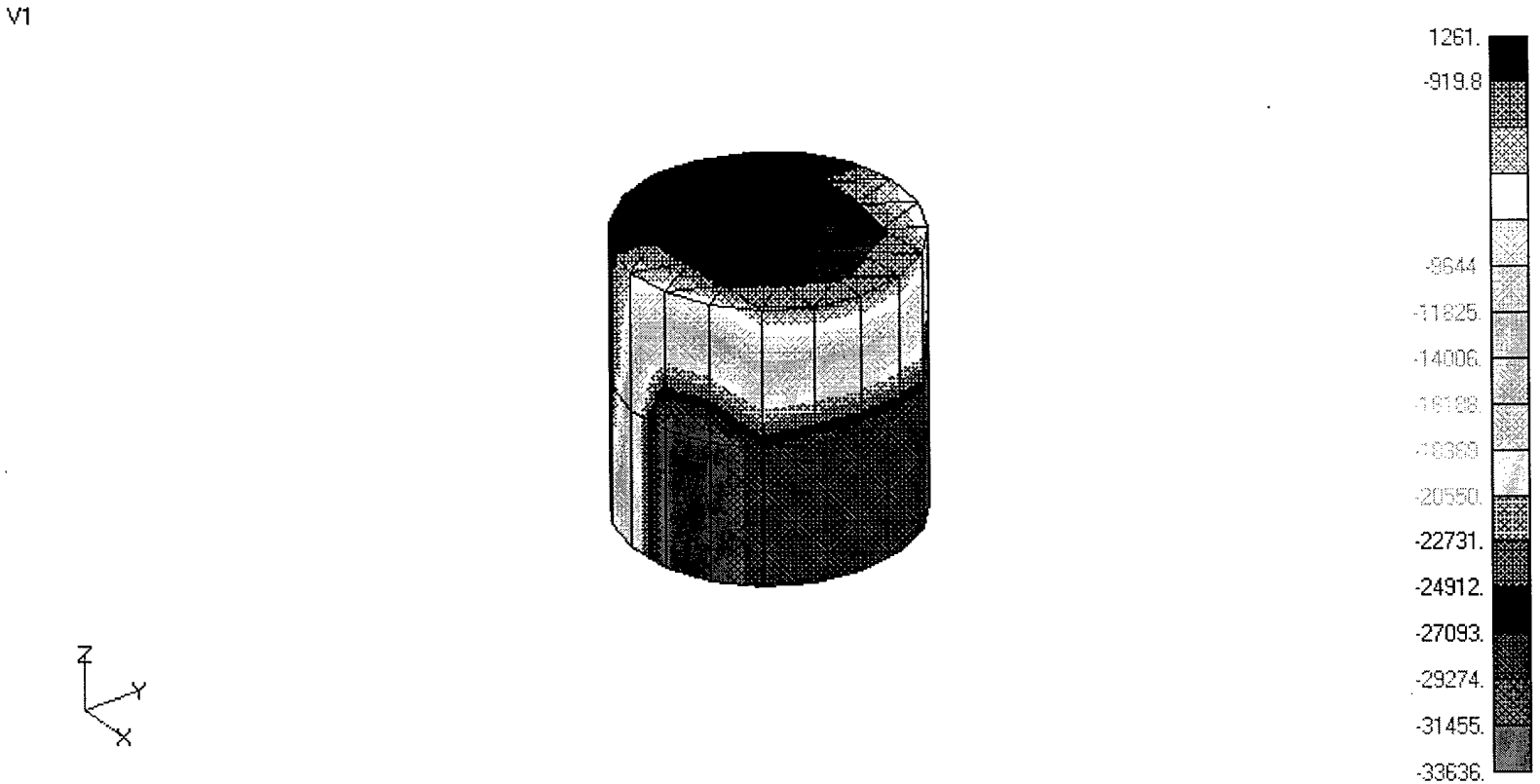

Horizontal Load = 20,000,000 lbs
Linear Elastic-Perfectly Plastic Sandy Soil (Linear Extended Drucker-Prager)
E = 864,000 psf, $\upsilon = 0.3$, Slope Angle = 46.2°, Dilation Angle = 21.5°
Pile, AISI 4340 Steel

Figure-E20. Pile von Mises Stresses on the Pile Surface (Load at the Bottom of the Pile in Sand)

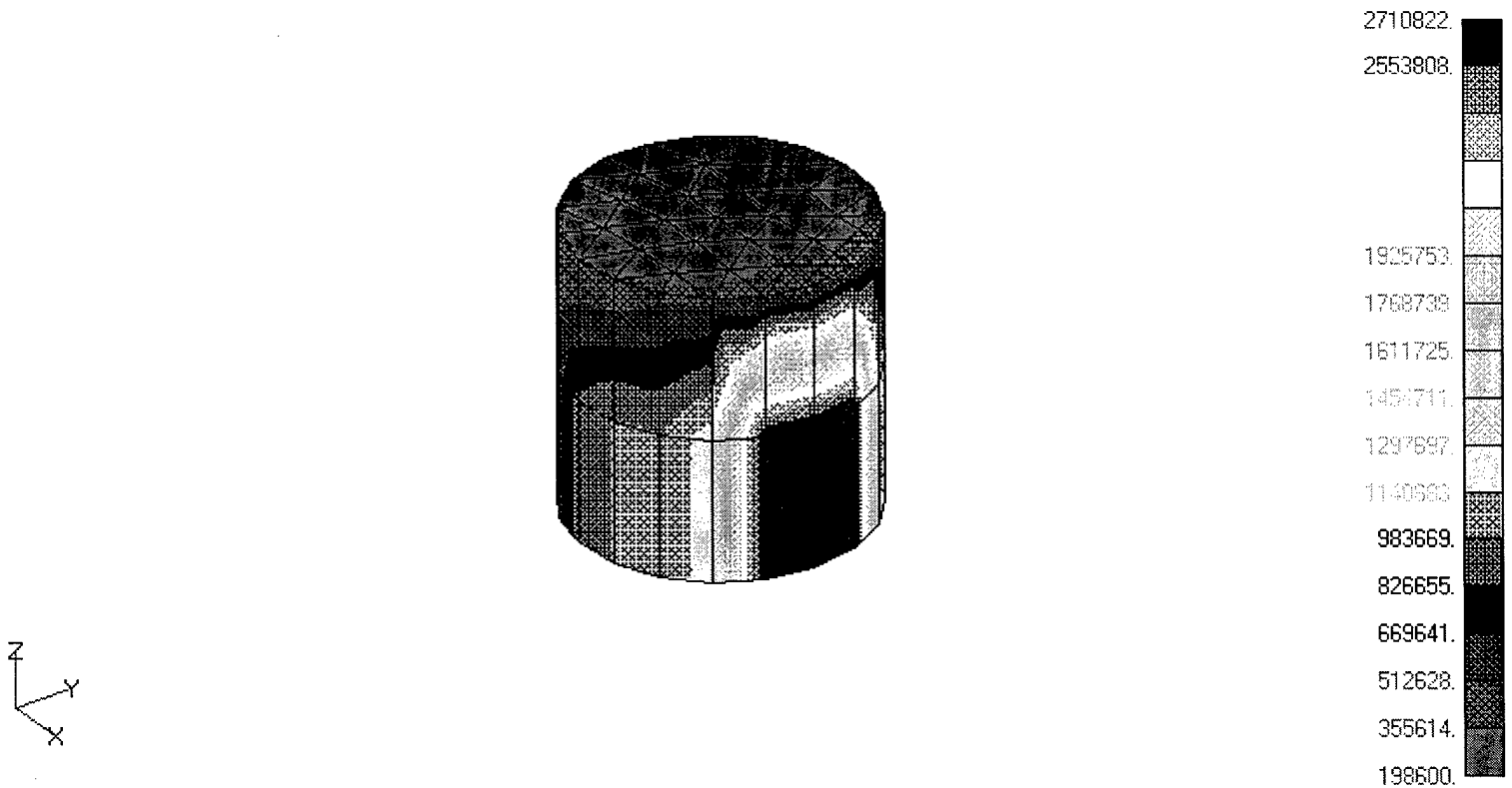

Horizontal Load = 20,000,000 lbs
Linear Elastic-Perfectly Plastic Sandy Soil (Linear Extended Drucker-Prager)
E = 864,000 psf, $\upsilon = 0.3$, Slope Angle = 46.2°, Dilation Angle = 21.5°
Pile, AISI 4340 Steel

Figure-F1. Horizontal Displacements (Telescopic Pile in Sand)

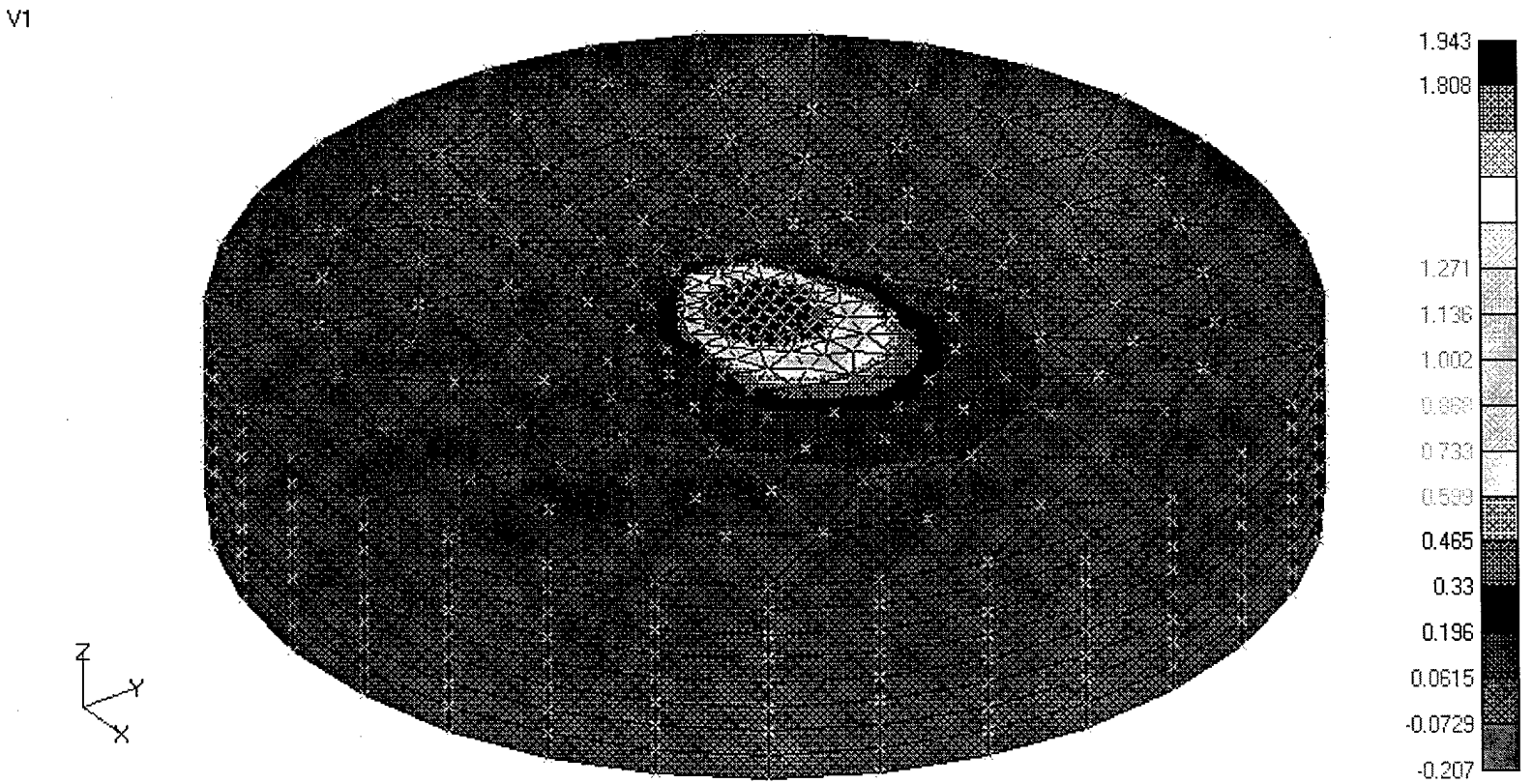

Horizontal Load = 12,000,000 lbs
Linear Elastic-Perfectly Plastic Sandy Soil (Linear Extended Drucker-Prager)
E = 864,000 psf, υ = 0.3, Slope Angle = 46.2°, Dilation Angle = 21.5°
Pile, AISI 4340 Steel

Figure-F2. Horizontal Displacements on a Vertical Plane along the Horizontal Load Direction (Telescopic Pile in Sand)

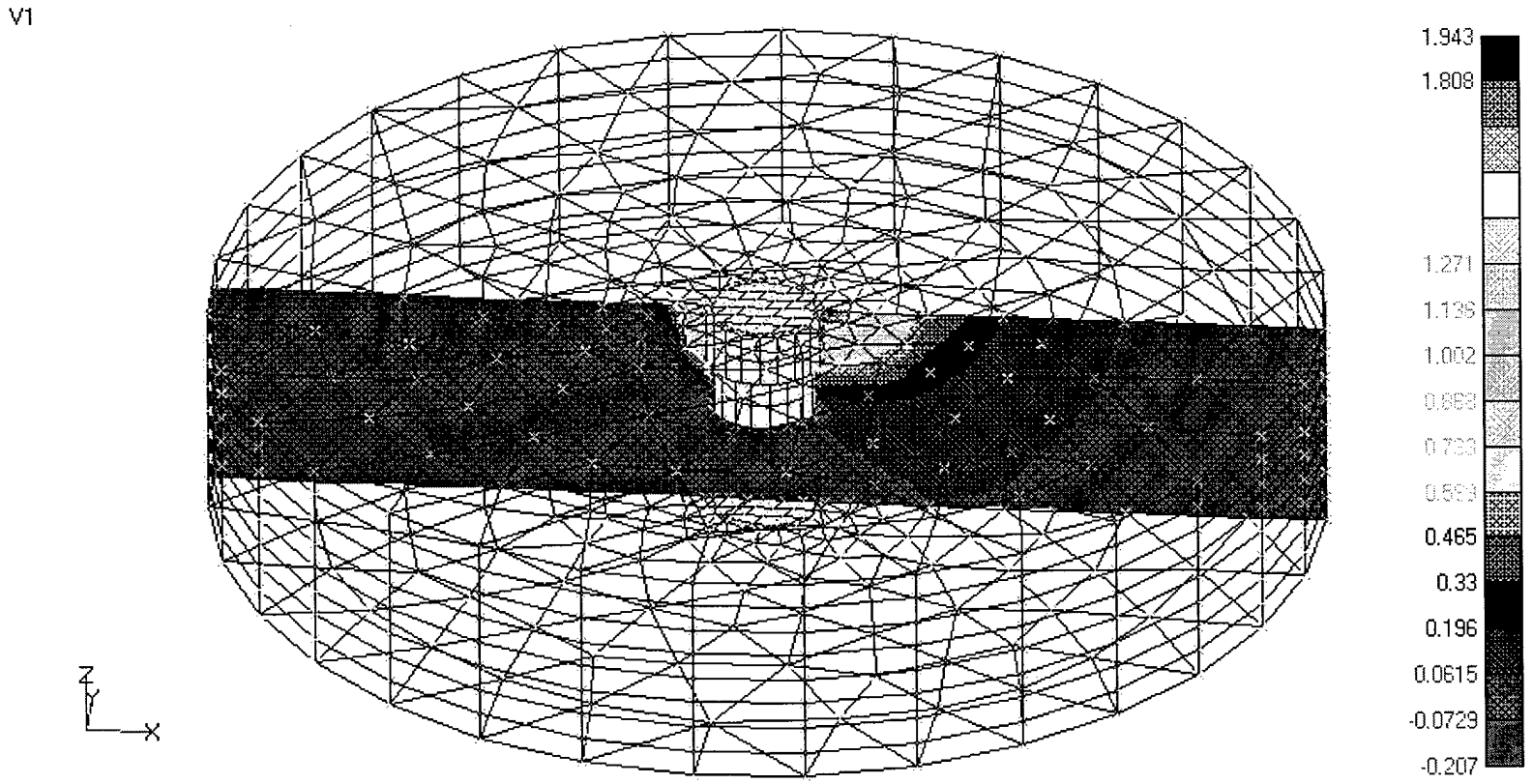

Horizontal Load = 12,000,000 lbs
Linear Elastic-Perfectly Plastic Sandy Soil (Linear Extended Drucker-Prager)
E = 864,000 psf, $\upsilon = 0.3$, Slope Angle = 46.2°, Dilation Angle = 21.5°
Pile, AISI 4340 Steel

Figure-F3. Pile Total Displacements (Telescopic Pile in Sand)

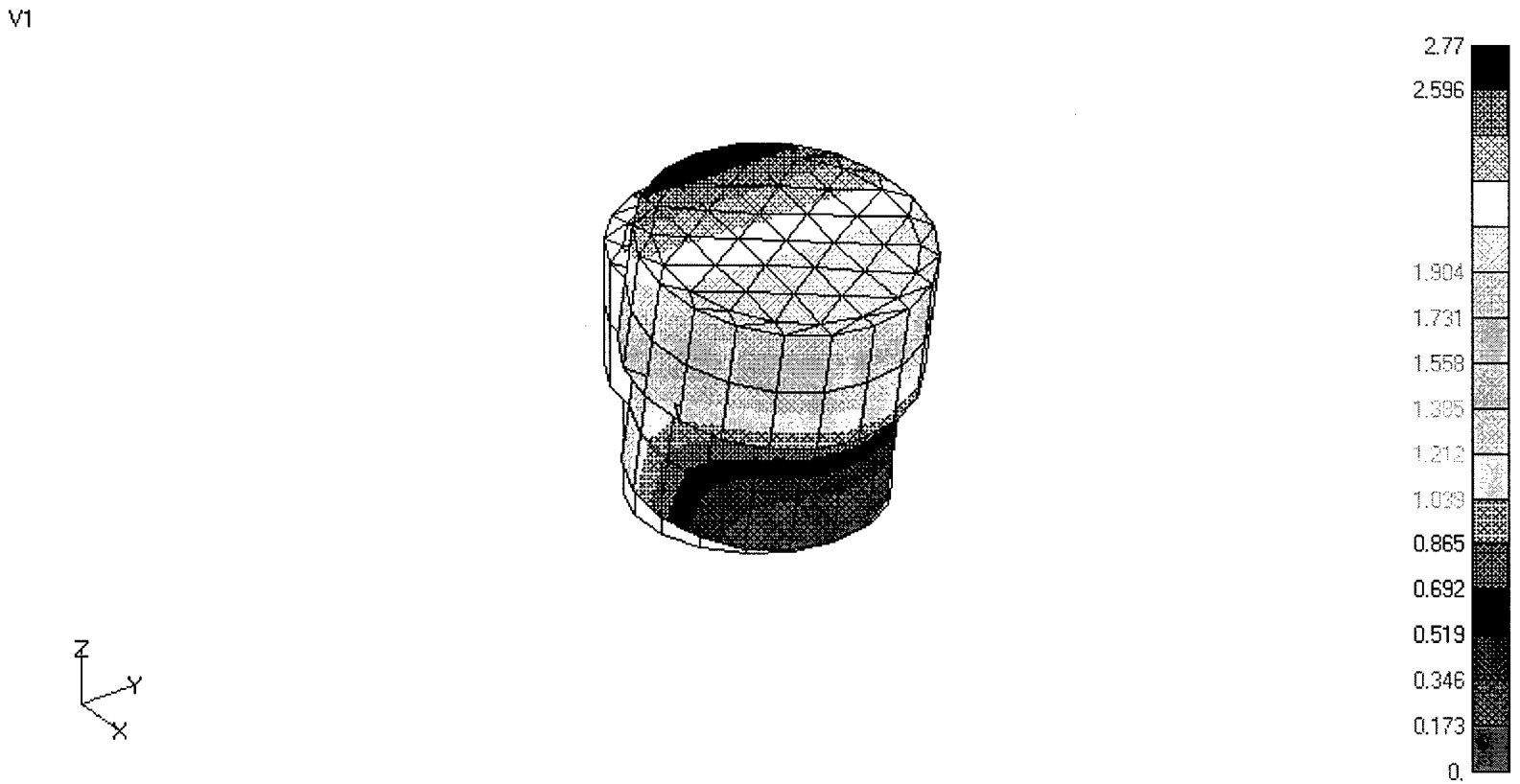

Horizontal Load = 12,000,000 lbs
Linear Elastic-Perfectly Plastic Sandy Soil (Linear Extended Drucker-Prager)
E = 864,000 psf, υ = 0.3, Slope Angle = 46.2°, Dilation Angle = 21.5°
Pile, AISI 4340 Steel

Figure-F4. Soil Minor Principal Stresses (Telescopic Pile in Sand)

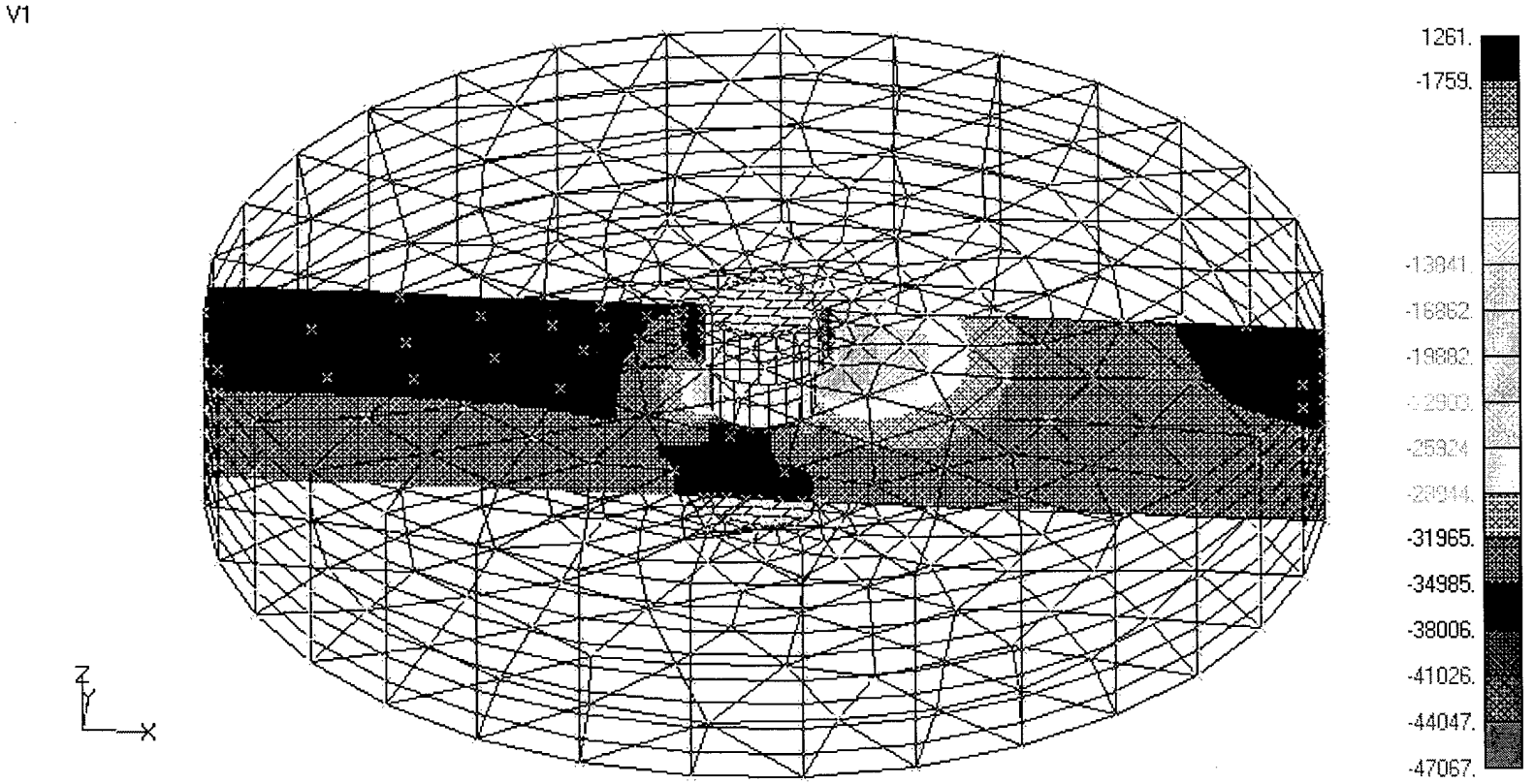

Horizontal Load = 12,000,000 lbs
Linear Elastic-Perfectly Plastic Sandy Soil (Linear Extended Drucker-Prager)
E = 864,000 psf, $\upsilon = 0.3$, Slope Angle = 46.2°, Dilation Angle = 21.5°
Pile, AISI 4340 Steel

Figure-F5. Soil Minor Principal Stresses on a Vertical Plane along the Horizontal Load Direction (Telescopic Pile in Sand)

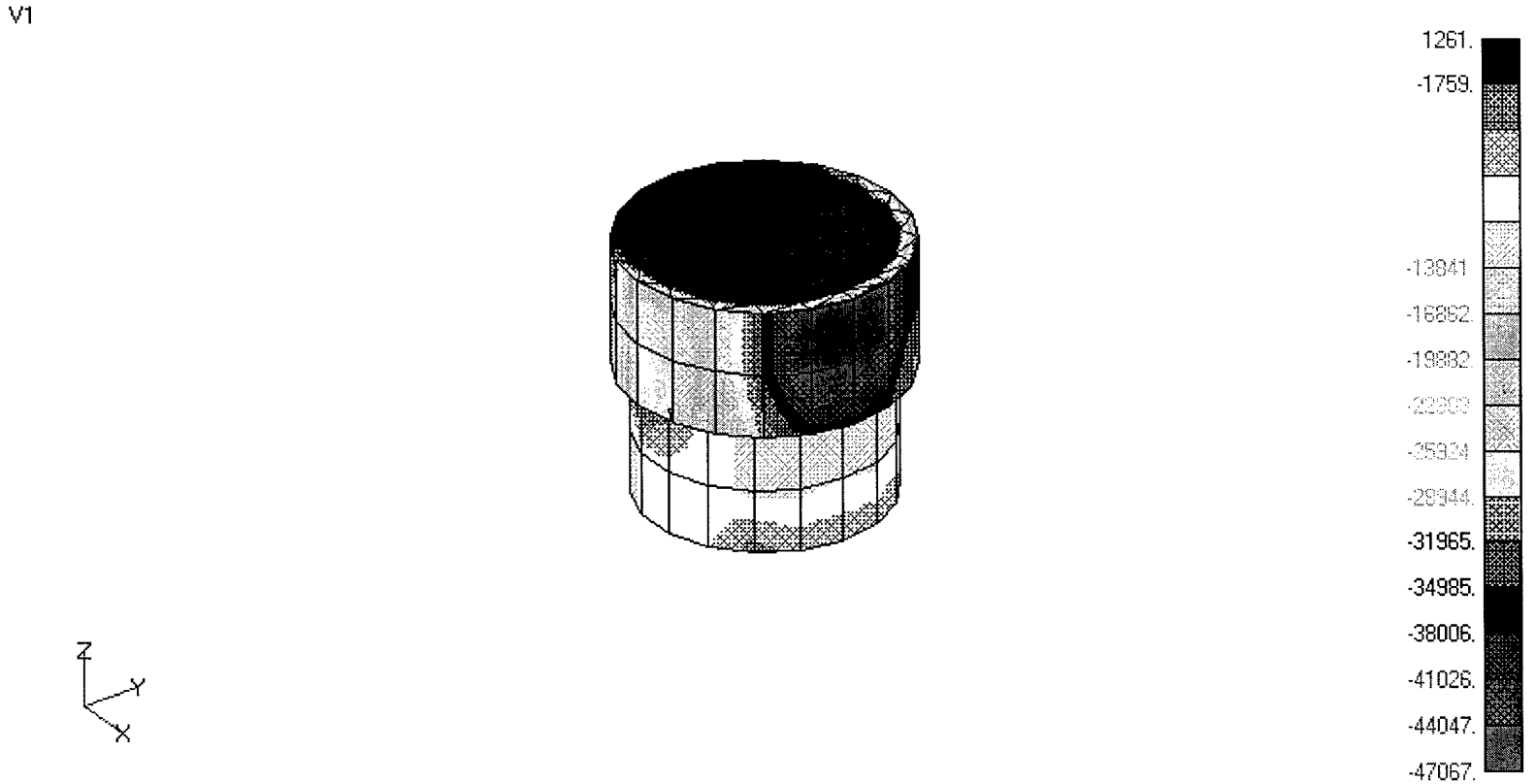

Horizontal Load = 12,000,000 lbs
Linear Elastic-Perfectly Plastic Sandy Soil (Linear Extended Drucker-Prager)
E = 864,000 psf, υ = 0.3, Slope Angle = 46.2°, Dilation Angle = 21.5°
Pile, AISI 4340 Steel

Figure-F6. Pile von Mises Stresses on the Pile Surface (Telescopic Pile in Sand)

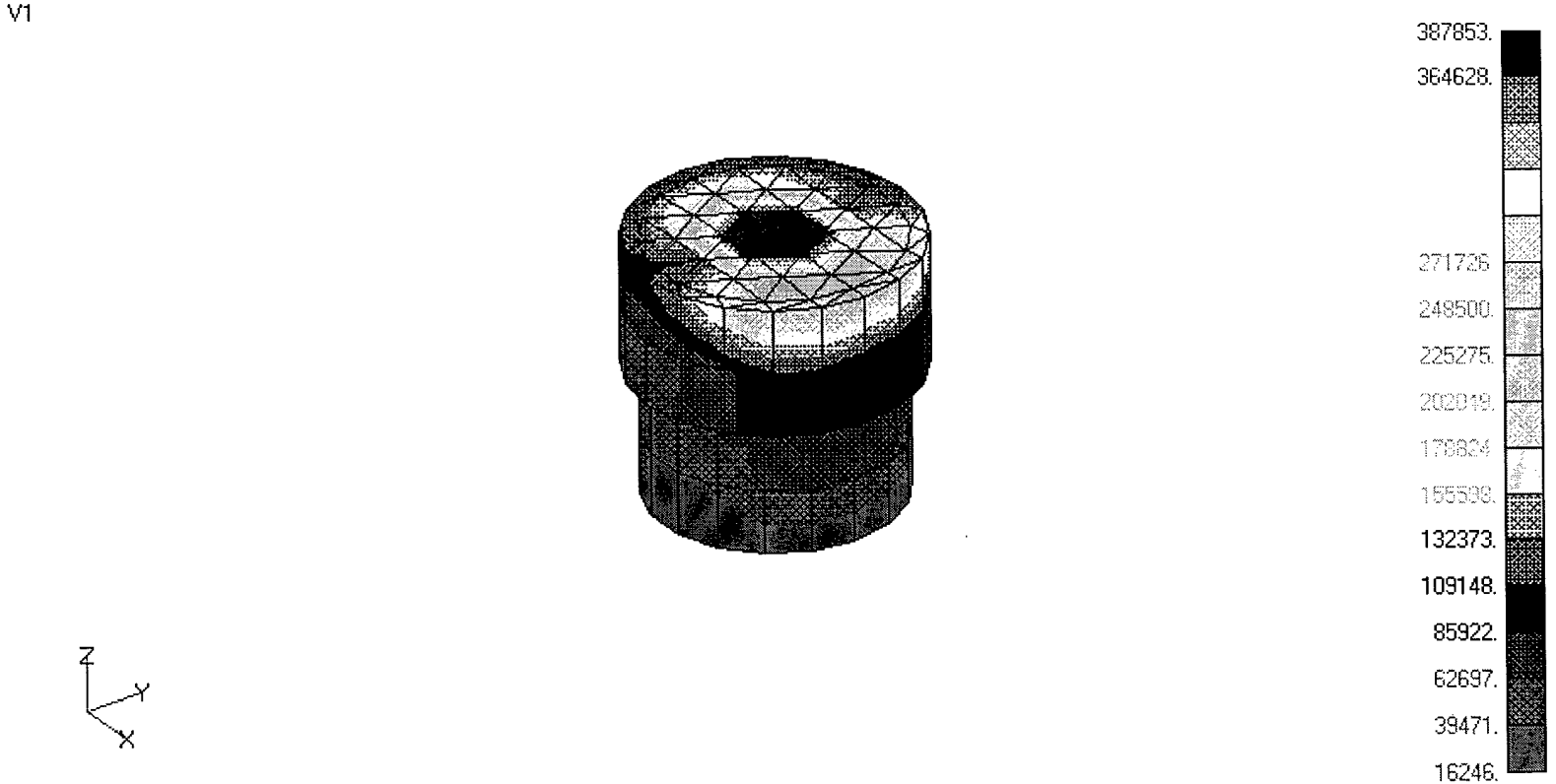

Horizontal Load = 12,000,000 lbs
Linear Elastic-Perfectly Plastic Sandy Soil (Linear Extended Drucker-Prager)
E = 864,000 psf, υ = 0.3, Slope Angle = 46.2°, Dilation Angle = 21.5°
Pile, AISI 4340 Steel

Figure-F7. Horizontal Displacements (Telescopic Pile in Clay)

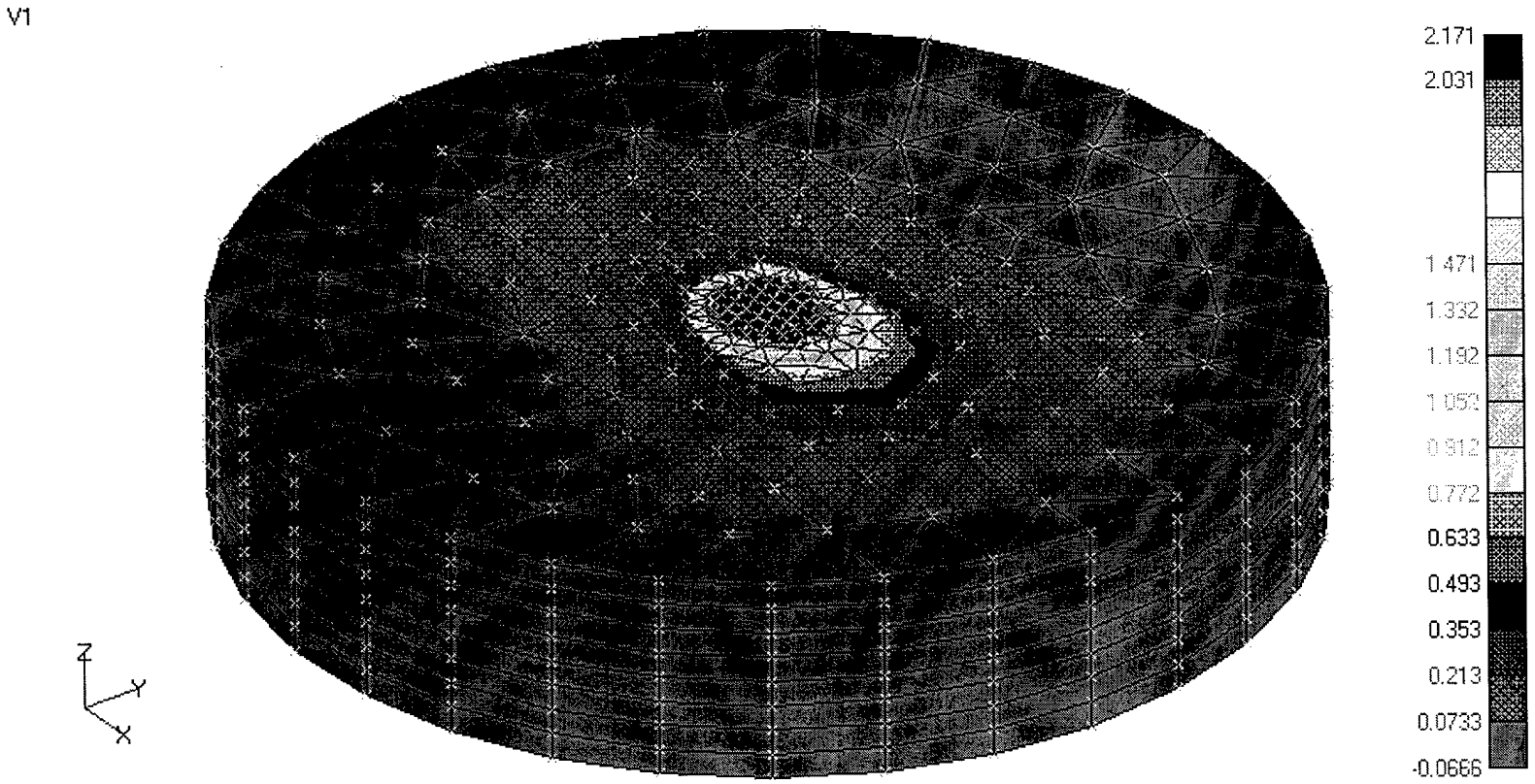

Horizontal Load = 1,600,000 lbs
Linear Elastic-Perfectly Plastic Clayey Soil (Hyperbolic Extended Drucker-Prager)
E = 30,000 psf, $\upsilon = 0.499$, Slope Angle = 10.2°, Dilation Angle = 10.2°
Pile, AISI 4340 Steel

Figure-F8. Horizontal Displacements on a Vertical Plane along the Horizontal Load Direction (Telescopic Pile in Clay)

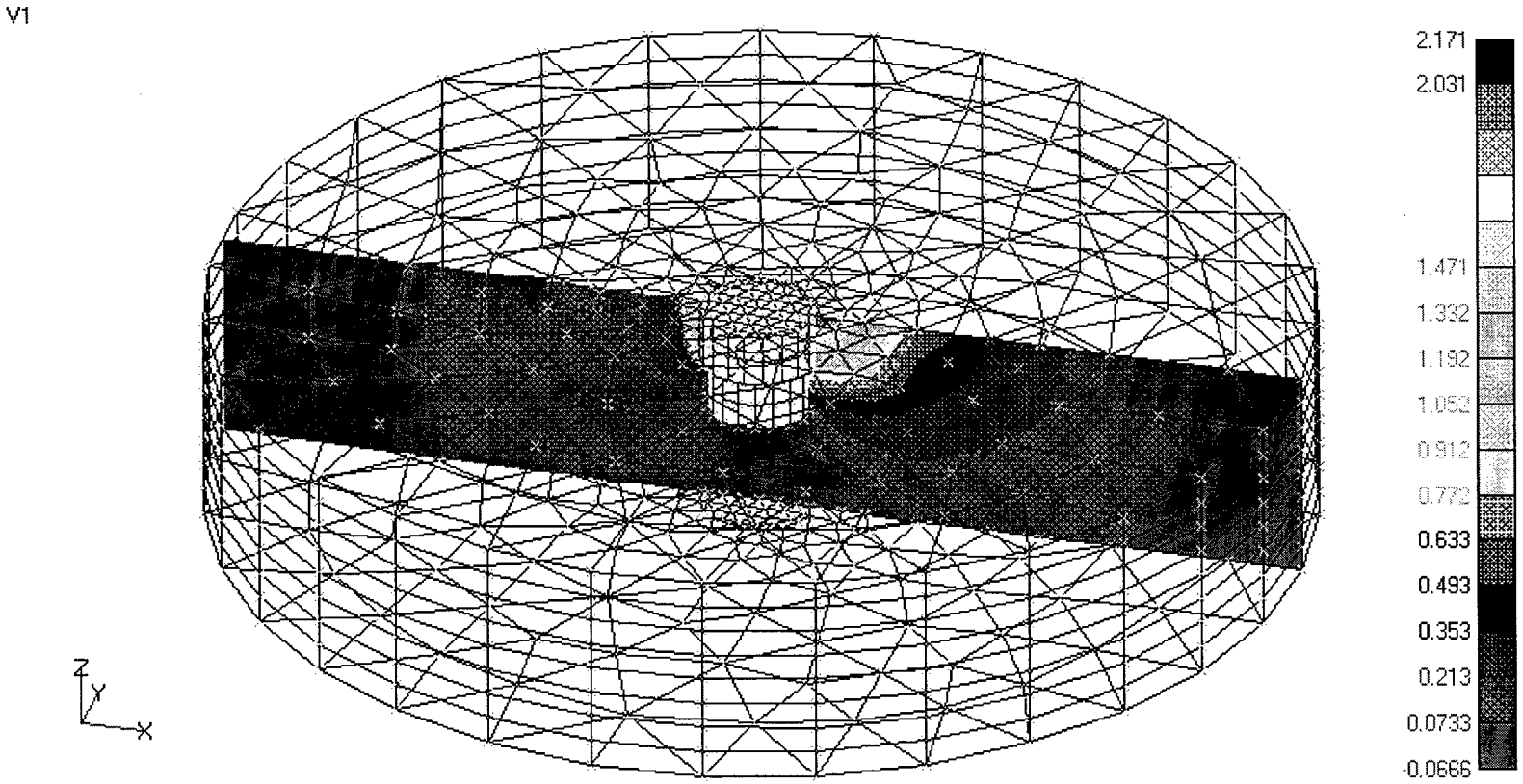

Horizontal Load = 1,600,000 lbs
Linear Elastic-Perfectly Plastic Clayey Soil (Hyperbolic Extended Drucker-Prager)
E = 30,000 psf, υ = 0.499, Slope Angle = 10.2°, Dilation Angle = 10.2°
Pile, AISI 4340 Steel

Figure-F9. Pile Total Displacements (Telescopic Pile in Clay)

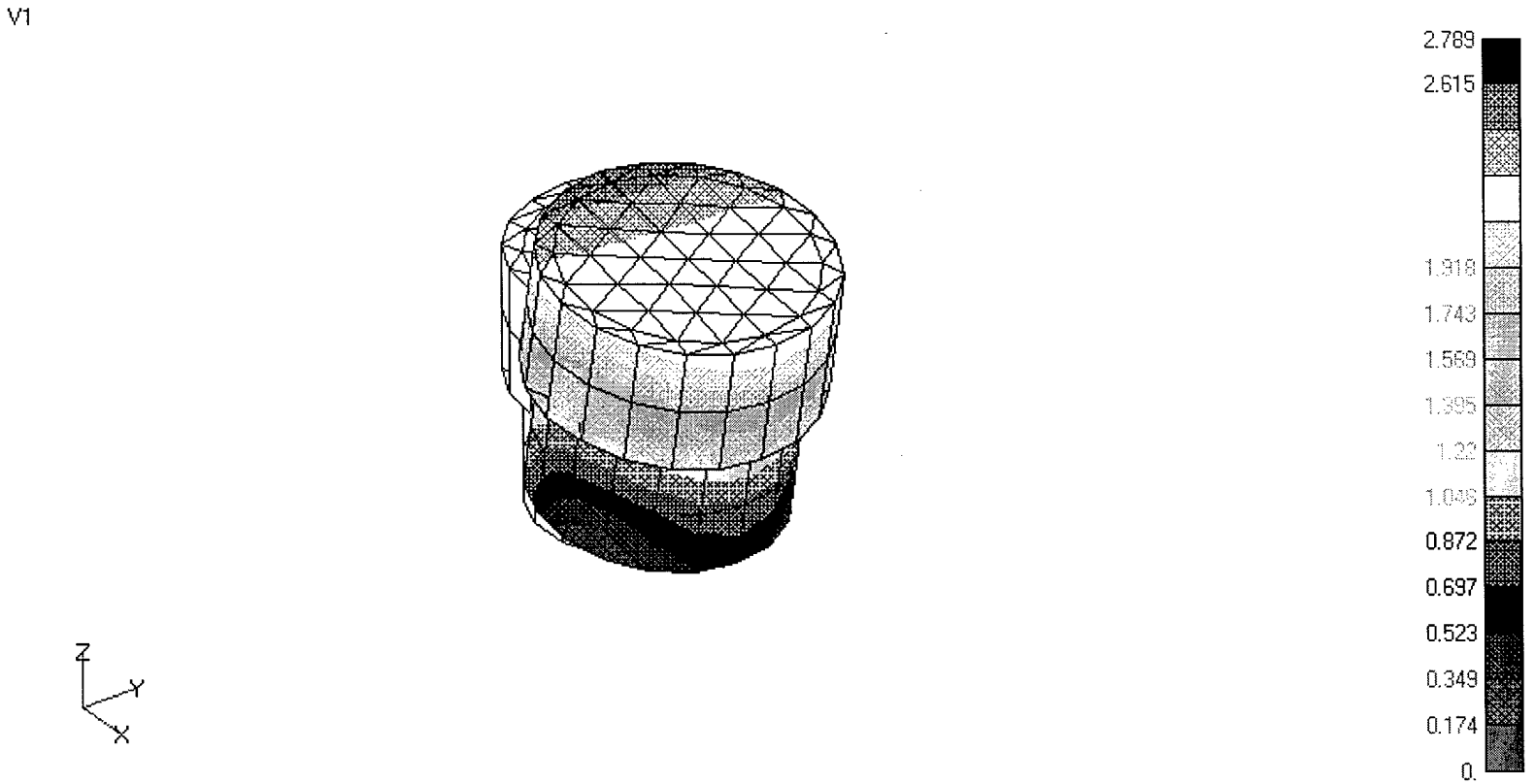

Horizontal Load = 1,600,000 lbs
Linear Elastic-Perfectly Plastic Clayey Soil (Hyperbolic Extended Drucker-Prager)
E = 30,000 psf, υ = 0.499, Slope Angle = 10.2°, Dilation Angle = 10.2°
Pile, AISI 4340 Steel

Figure-F10. Soil Minor Principal Stresses (Telescopic Pile in Clay)

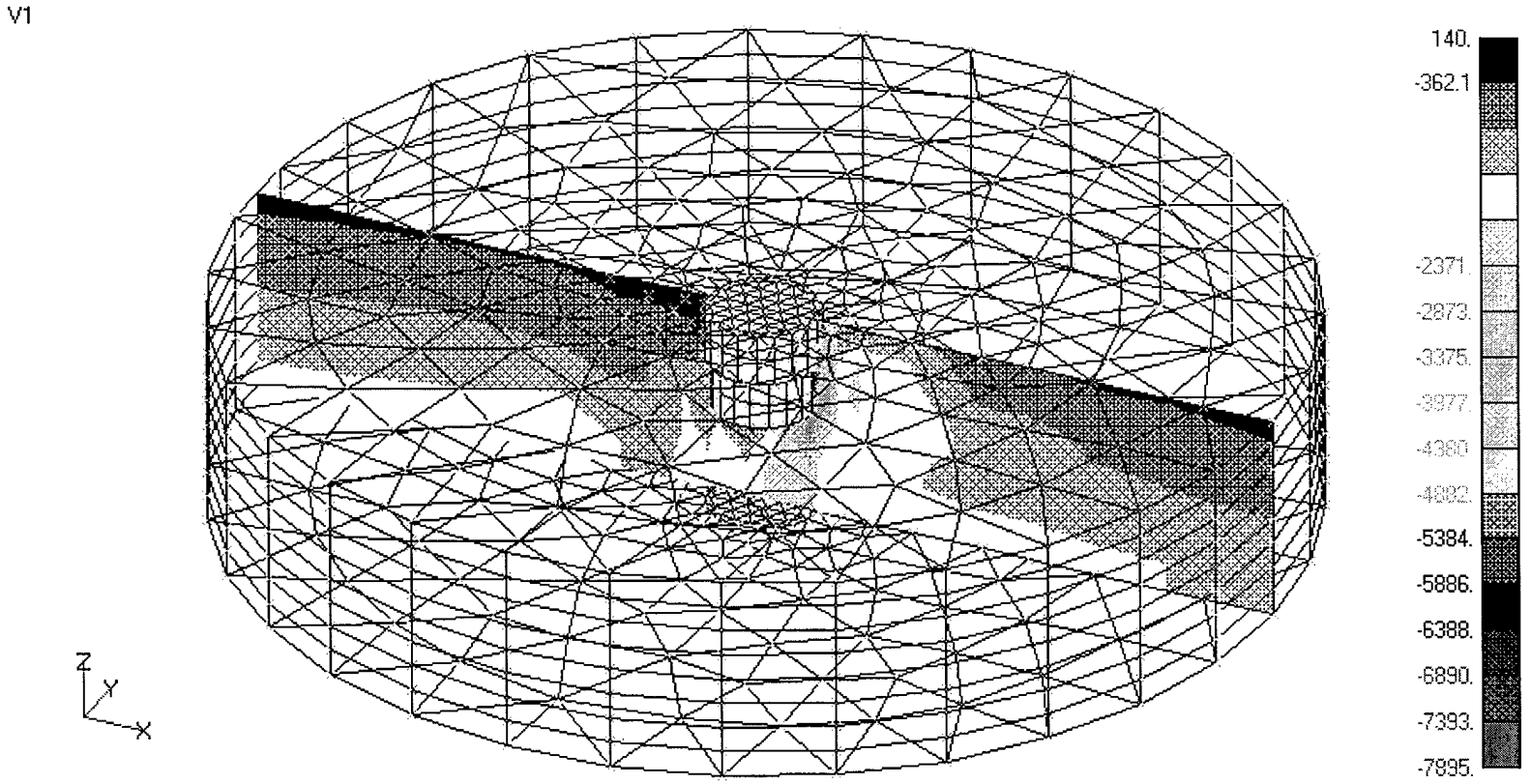

Horizontal Load = 1,600,000 lbs
Linear Elastic-Perfectly Plastic Clayey Soil (Hyperbolic Extended Drucker-Prager)
E = 30,000 psf, $\upsilon = 0.499$, Slope Angle = 10.2^{o}, Dilation Angle = 10.2^{o}
Pile, AISI 4340 Steel

Figure-F11. Soil Minor Principal Stresses on a Vertical Plane along the Horizontal Load Direction (Telescopic Pile in Clay)

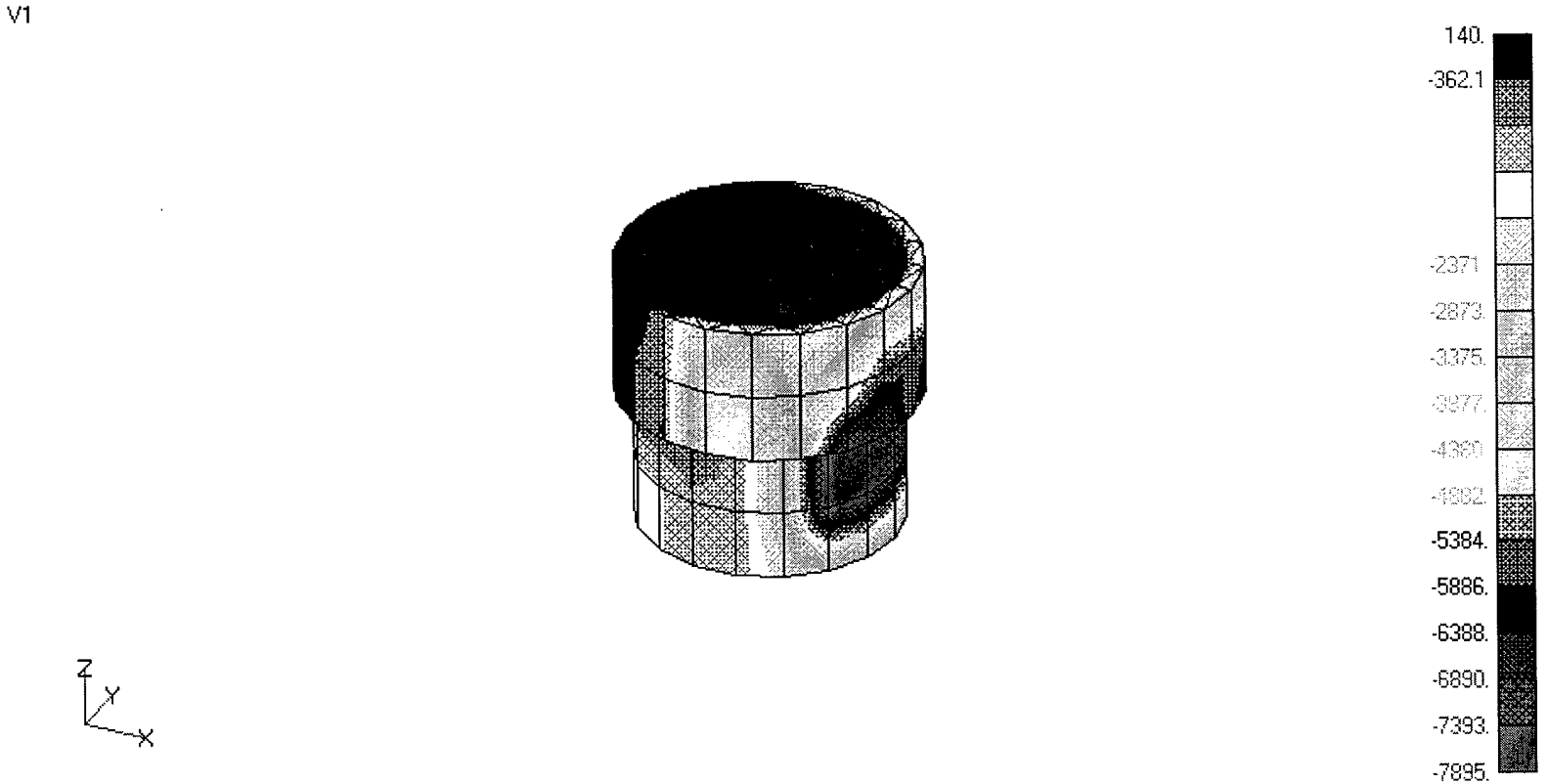

Horizontal Load = 1,600,000 lbs
Linear Elastic-Perfectly Plastic Clayey Soil (Hyperbolic Extended Drucker-Prager)
E = 30,000 psf, $\upsilon = 0.499$, Slope Angle = 10.2°, Dilation Angle = 10.2°
Pile, AISI 4340 Steel

Figure-F12. Pile von Mises Stresses on the Pile Surface (Telescopic Pile in Clay)

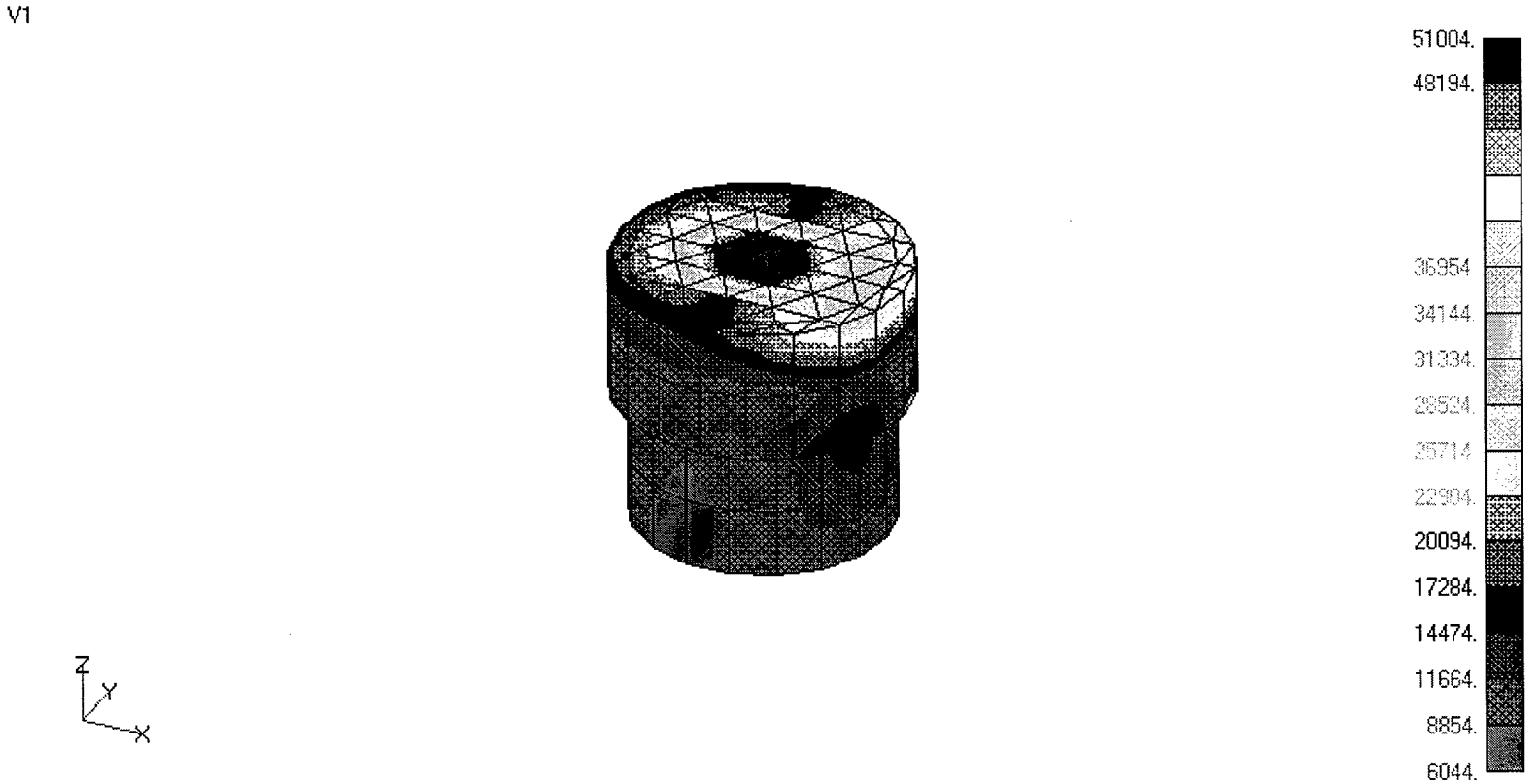

Horizontal Load = 1,600,000 lbs
Linear Elastic-Perfectly Plastic Clayey Soil (Hyperbolic Extended Drucker-Prager)
E = 30,000 psf, $\upsilon = 0.499$, Slope Angle = 10.2°, Dilation Angle = 10.2°
Pile, AISI 4340 Steel

Figure-G1. Horizontal Displacements (Circular Pile in Layered Soil-2)

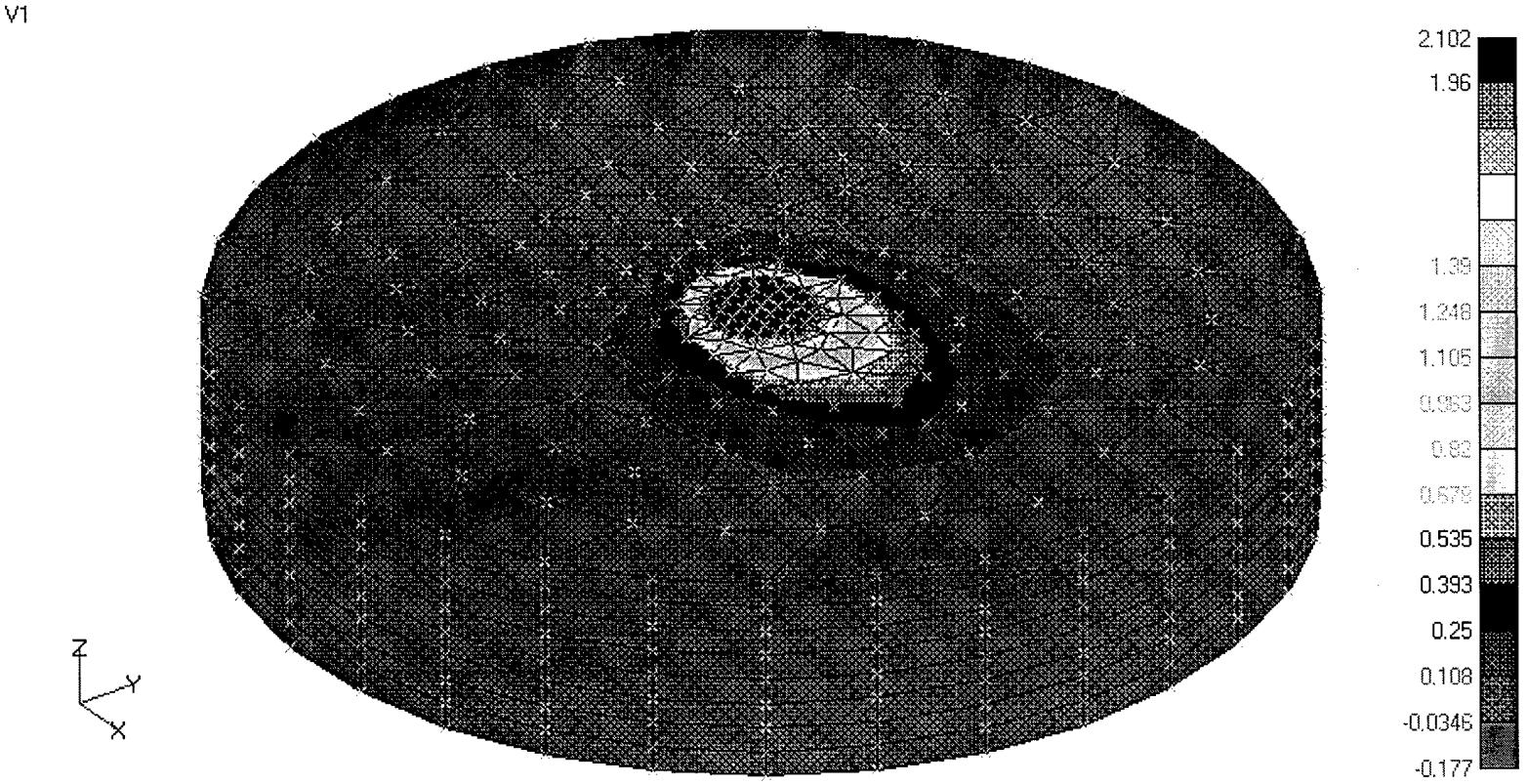

Horizontal Load = 5,000,000 lbs
Linear Elastic-Perfectly Plastic Clayey Soil (Hyperbolic Extended Drucker-Prager)
E = 30,000 psf, υ = 0.499, Slope Angle = 10.2°, Dilation Angle = 10.2°
Linear Elastic-Perfectly Plastic Sandy Soil (Linear Extended Drucker-Prager)
E = 864,000 psf, υ = 0.3, Slope Angle = 46.2°, Dilation Angle = 21.5°
Pile, AISI 4340 Steel

Figure-G2. Horizontal Displacements on a Vertical Plane along the Horizontal Load Direction (Circular Pile in Layered Soil-2)

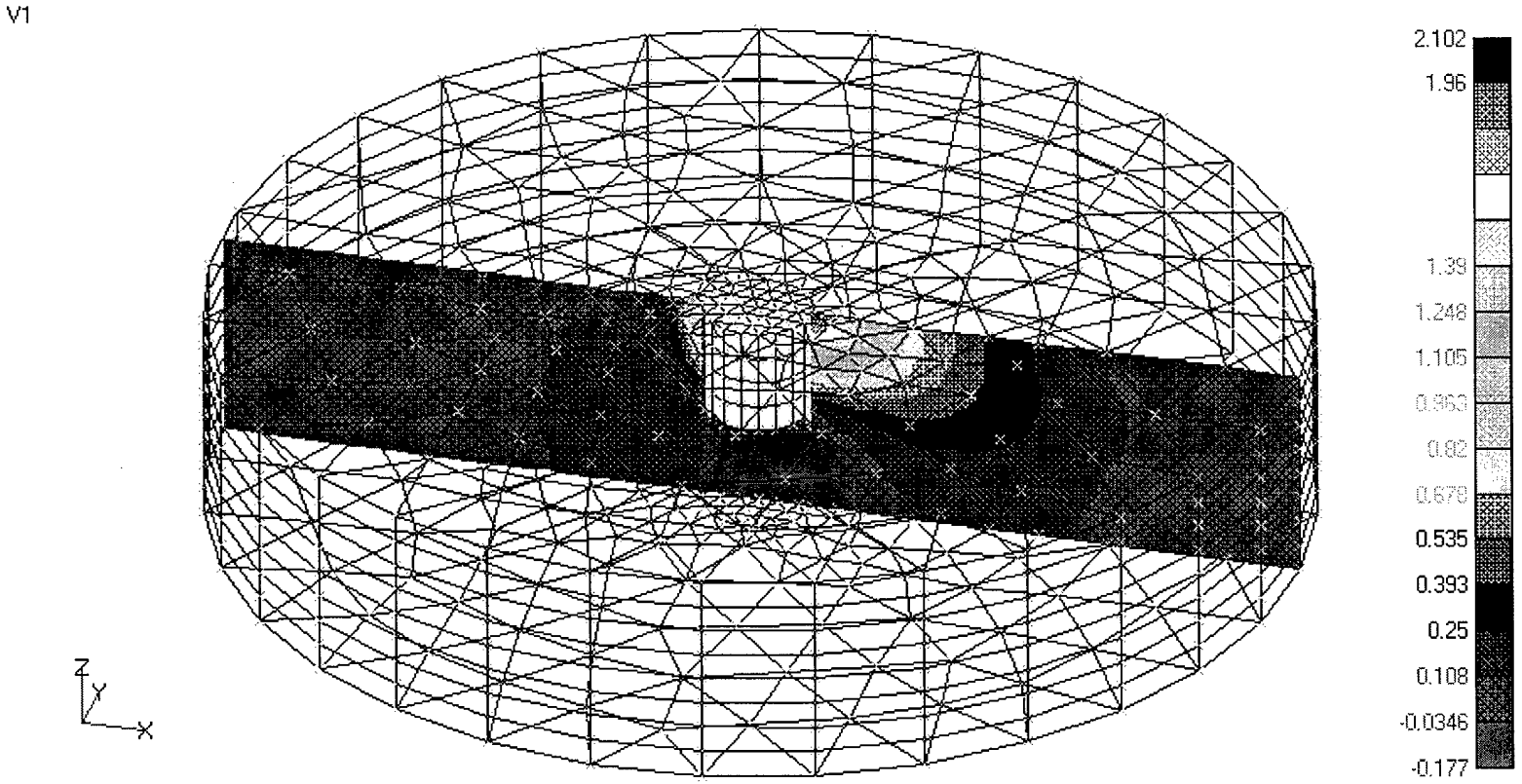

Horizontal Load = 5,000,000 lbs
Linear Elastic-Perfectly Plastic Clayey Soil (Hyperbolic Extended Drucker-Prager)
E = 30,000 psf, υ = 0.499, Slope Angle = 10.2°, Dilation Angle = 10.2°
Linear Elastic-Perfectly Plastic Sandy Soil (Linear Extended Drucker-Prager)
E = 864,000 psf, υ = 0.3, Slope Angle = 46.2°, Dilation Angle = 21.5°
Pile, AISI 4340 Steel

Figure-G3. Pile Total Displacements (Circular Pile in Layered Soil-2)

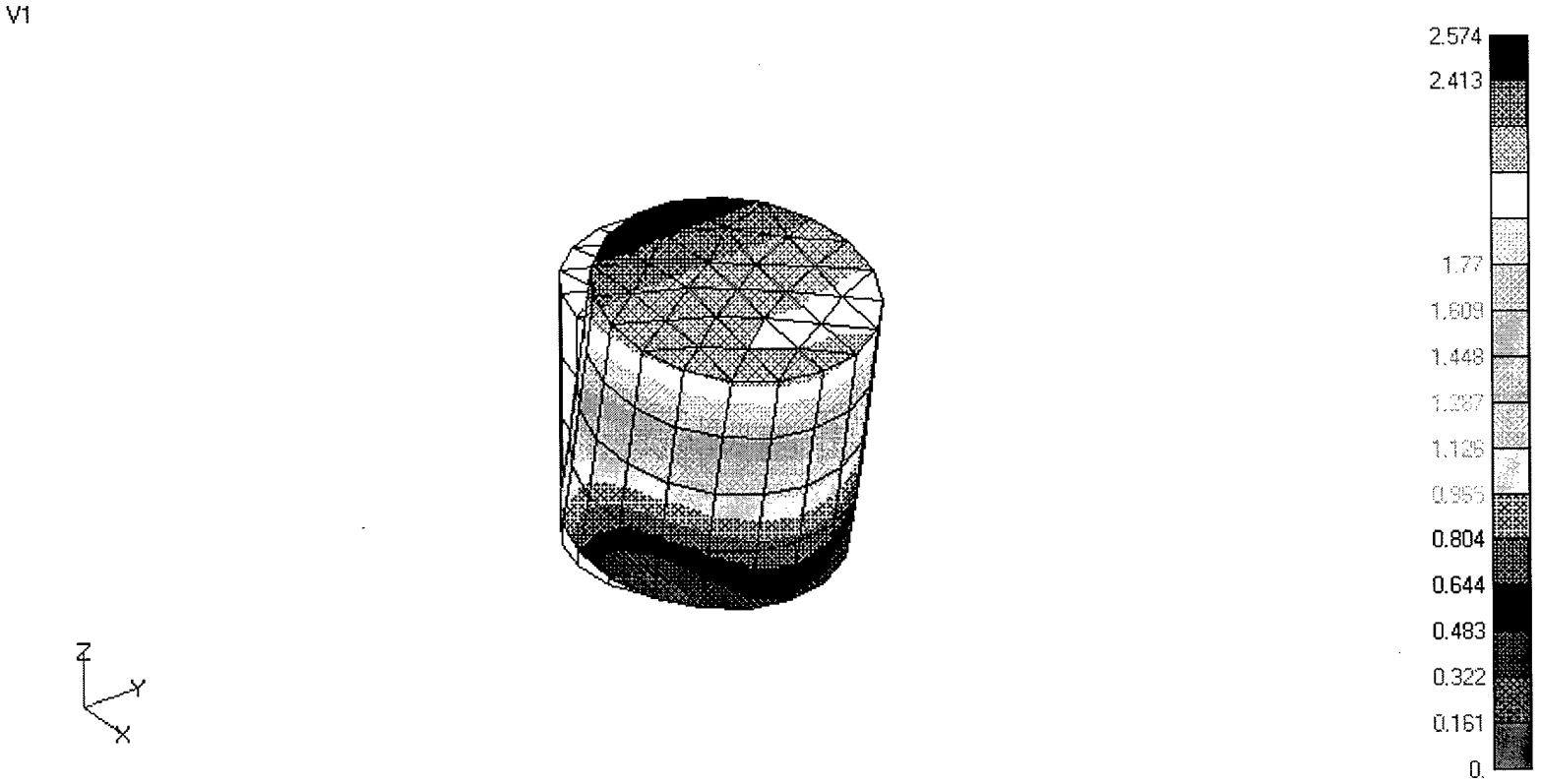

Horizontal Load = 5,000,000 lbs
Linear Elastic-Perfectly Plastic Clayey Soil (Hyperbolic Extended Drucker-Prager)
E = 30,000 psf, υ = 0.499, Slope Angle = 10.2°, Dilation Angle = 10.2°
Linear Elastic-Perfectly Plastic Sandy Soil (Linear Extended Drucker-Prager)
E = 864,000 psf, υ = 0.3, Slope Angle = 46.2°, Dilation Angle = 21.5°
Pile, AISI 4340 Steel

Figure-G4..Soil Minor Principal Stresses (Circular Pile in Layered Soil-2)

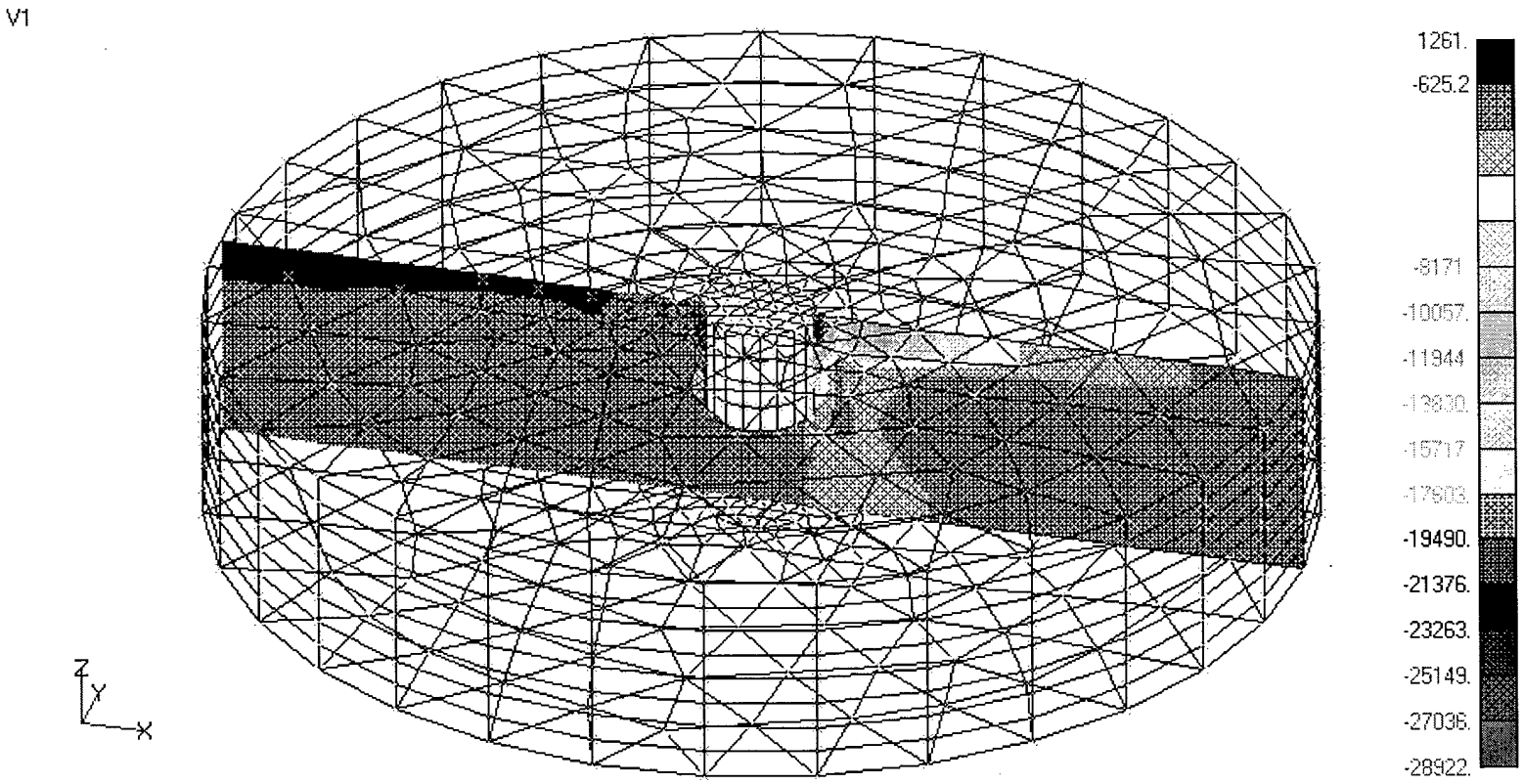

Horizontal Load = 5,000,000 lbs
Linear Elastic-Perfectly Plastic Clayey Soil (Hyperbolic Extended Drucker-Prager)
E = 30,000 psf, υ = 0.499, Slope Angle = 10.2°, Dilation Angle = 10.2°
Linear Elastic-Perfectly Plastic Sandy Soil (Linear Extended Drucker-Prager)
E = 864,000 psf, υ = 0.3, Slope Angle = 46.2°, Dilation Angle = 21.5°
Pile, AISI 4340 Steel

Figure-G5. Soil Minor Principal Stresses on a Vertical Plane along the Horizontal Load Direction (Circular Pile in Layered Soil-2)

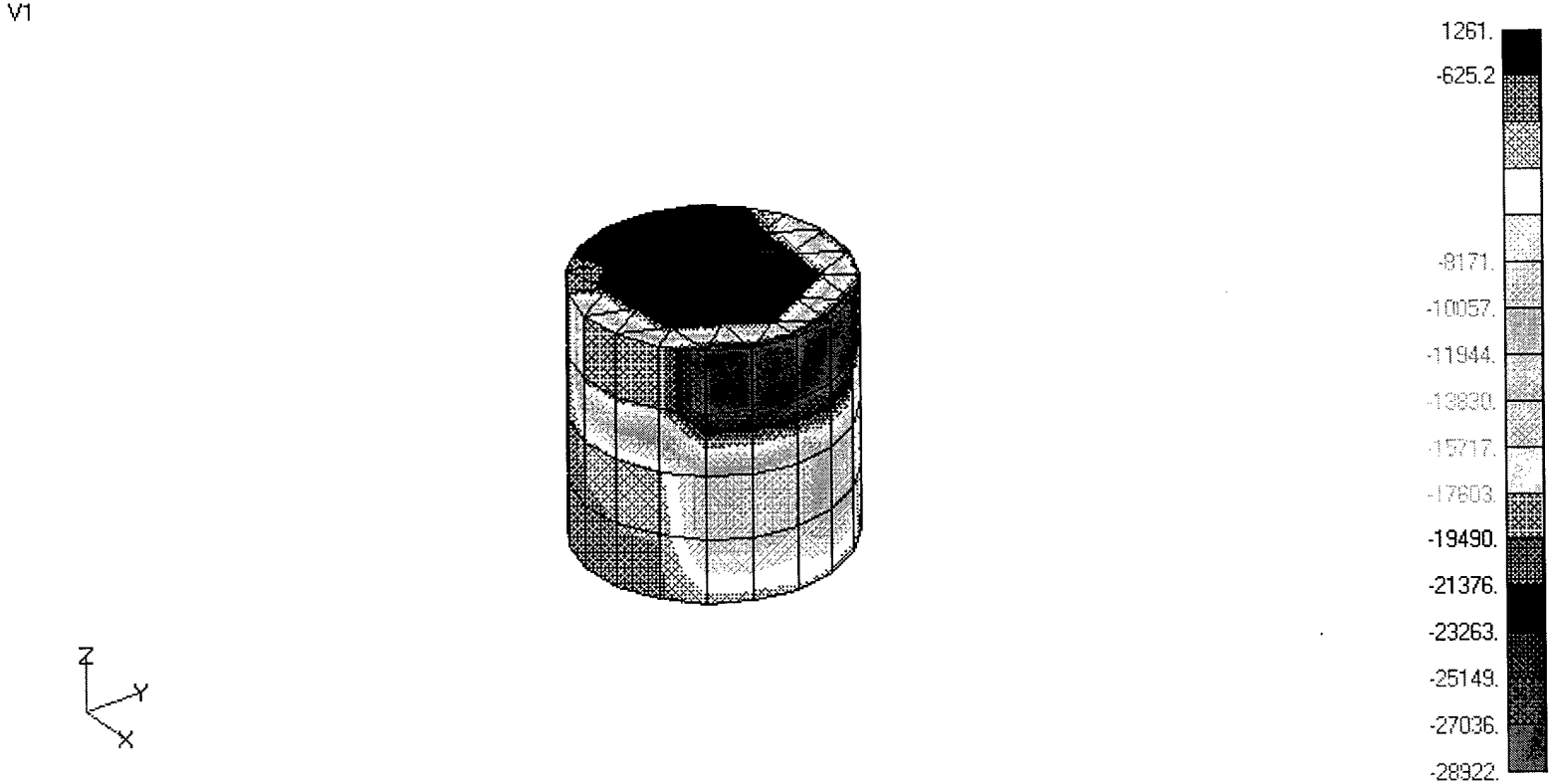

Horizontal Load = 5,000,000 lbs
Linear Elastic-Perfectly Plastic Clayey Soil (Hyperbolic Extended Drucker-Prager)
E = 30,000 psf, υ = 0.499, Slope Angle = 10.2°, Dilation Angle = 10.2°
Linear Elastic-Perfectly Plastic Sandy Soil (Linear Extended Drucker-Prager)
E = 864,000 psf, υ = 0.3, Slope Angle = 46.2°, Dilation Angle = 21.5°
Pile, AISI 4340 Steel

Figure-G6. Pile von Mises Stresses on the Pile Surface (Circular Pile in Layered Soil-2)

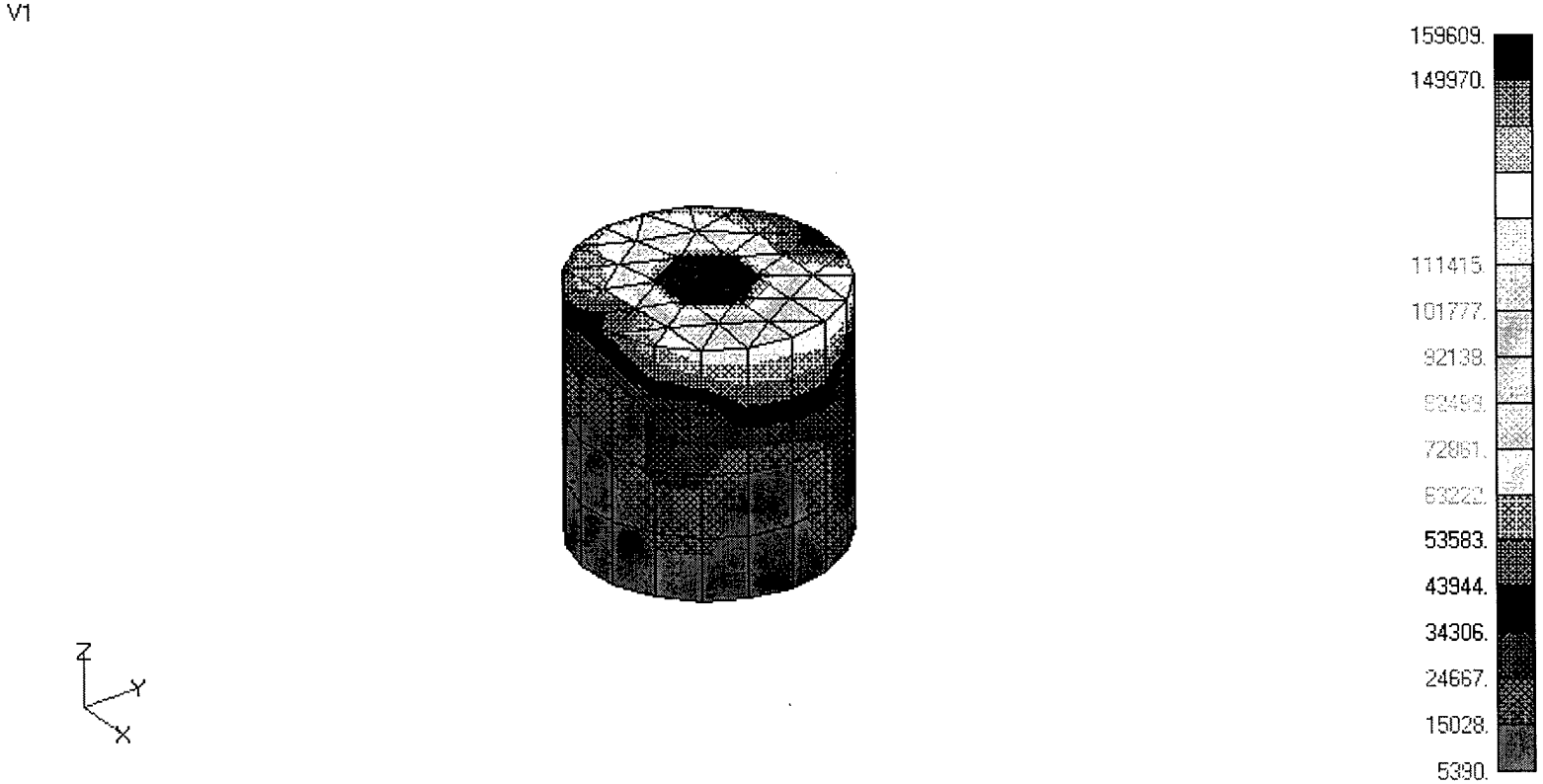

Horizontal Load = 5,000,000 lbs
Linear Elastic-Perfectly Plastic Clayey Soil (Hyperbolic Extended Drucker-Prager)
E = 30,000 psf, υ = 0.499, Slope Angle = 10.2°, Dilation Angle = 10.2°
Linear Elastic-Perfectly Plastic Sandy Soil (Linear Extended Drucker-Prager)
E = 864,000 psf, υ = 0.3, Slope Angle = 46.2°, Dilation Angle = 21.5°
Pile, AISI 4340 Steel

Figure-G7. Horizontal Displacements (Circular Pile in Layered Soil-6)

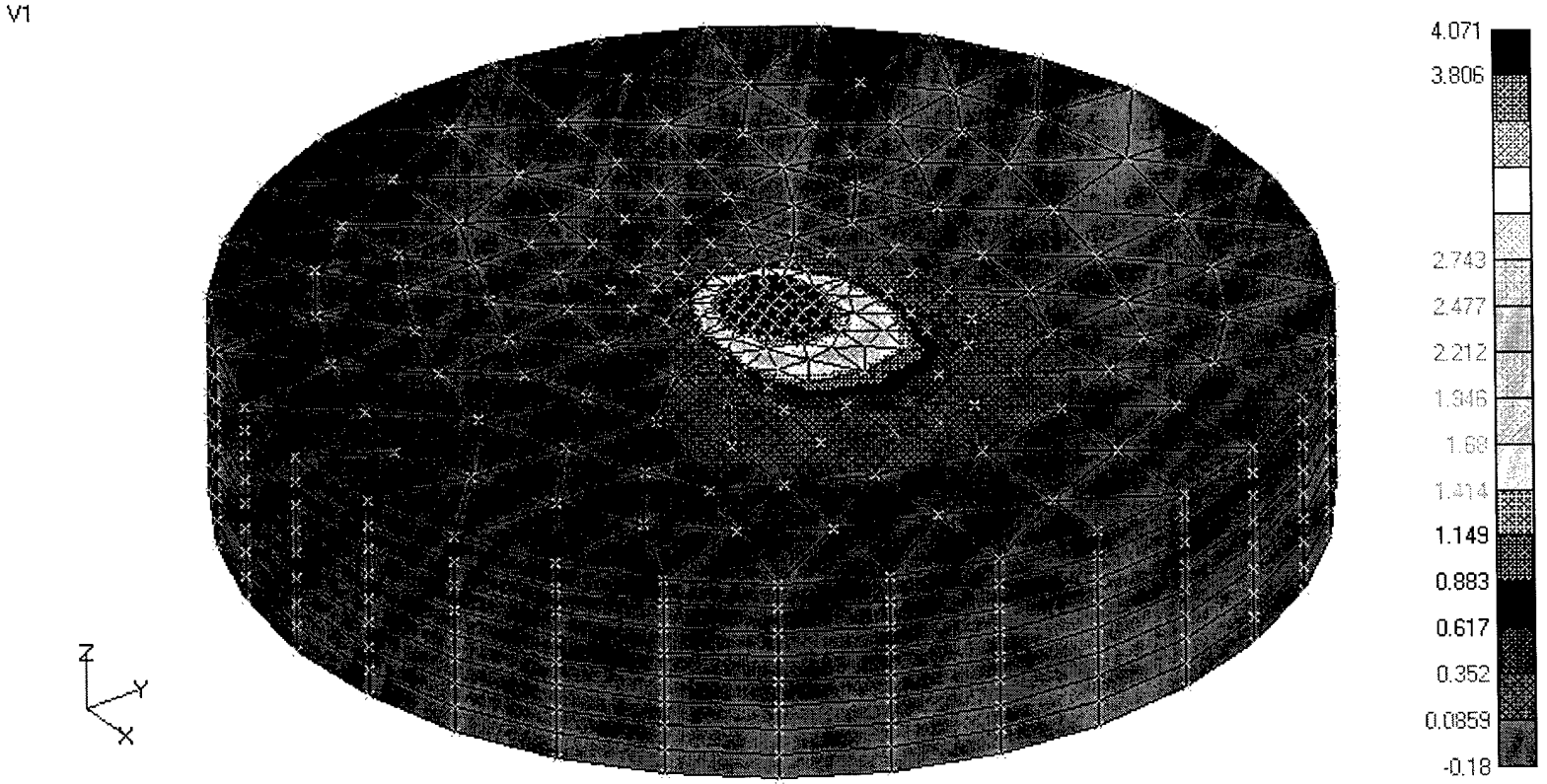

Horizontal Load = 4,500,000 lbs
Linear Elastic-Perfectly Plastic Clayey Soil (Hyperbolic Extended Drucker-Prager)
E = 30,000 psf, υ = 0.499, Slope Angle = 10.2°, Dilation Angle = 10.2°
Linear Elastic-Perfectly Plastic Sandy Soil (Linear Extended Drucker-Prager)
E = 864,000 psf, υ = 0.3, Slope Angle = 46.2°, Dilation Angle = 21.5°
Pile, AISI 4340 Steel

Figure-G8. Horizontal Displacements on a Vertical Plane along the Horizontal Load Direction (Circular Pile in Layered Soil-6)

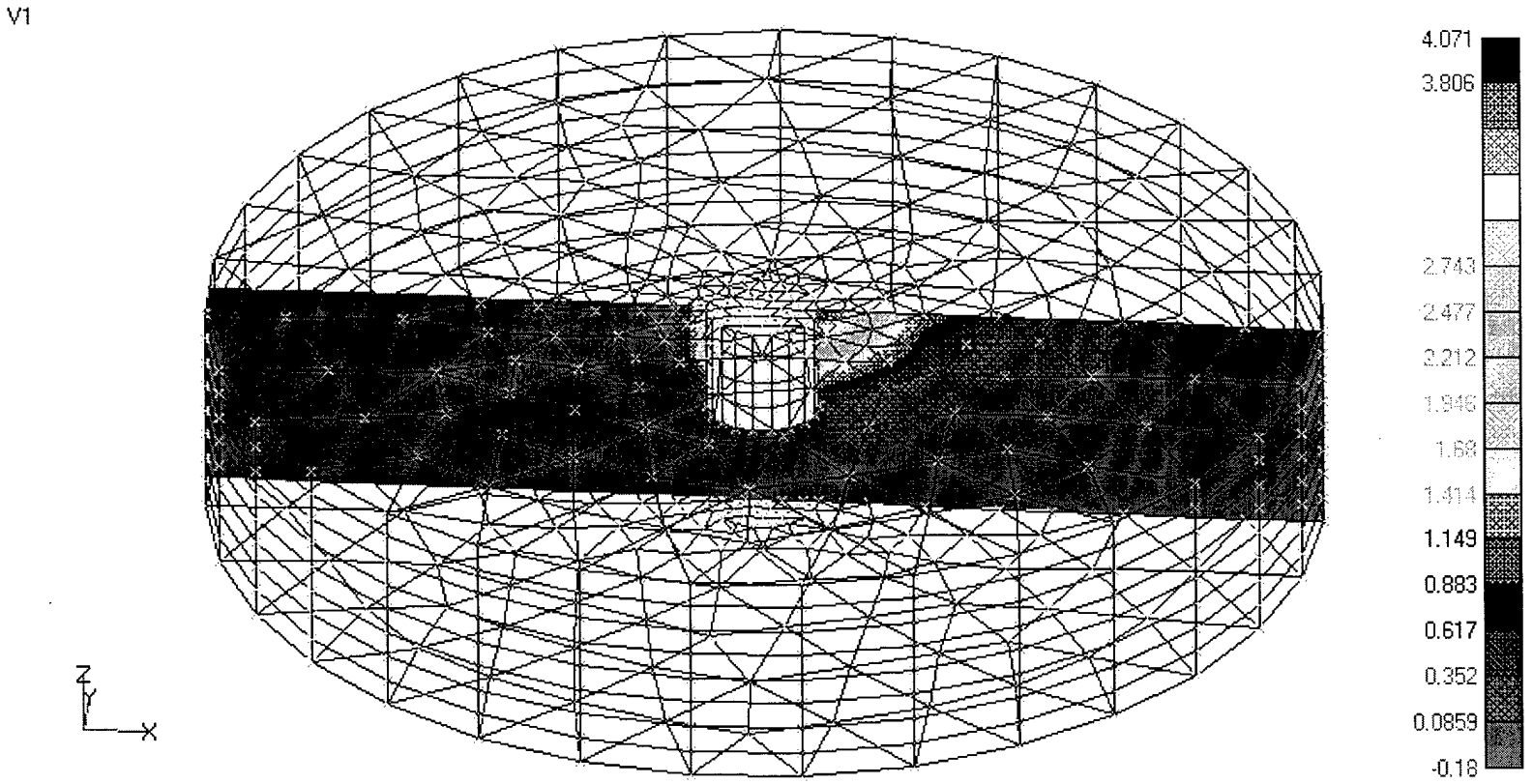

Horizontal Load = 4,500,000 lbs
Linear Elastic-Perfectly Plastic Clayey Soil (Hyperbolic Extended Drucker-Prager)
E = 30,000 psf, υ = 0.499, Slope Angle = 10.2°, Dilation Angle = 10.2°
Linear Elastic-Perfectly Plastic Sandy Soil (Linear Extended Drucker-Prager)
E = 864,000 psf, υ = 0.3, Slope Angle = 46.2°, Dilation Angle = 21.5°
Pile, AISI 4340 Steel

Figure-G9. Pile Total Displacements (Circular Pile in Layered Soil-6)

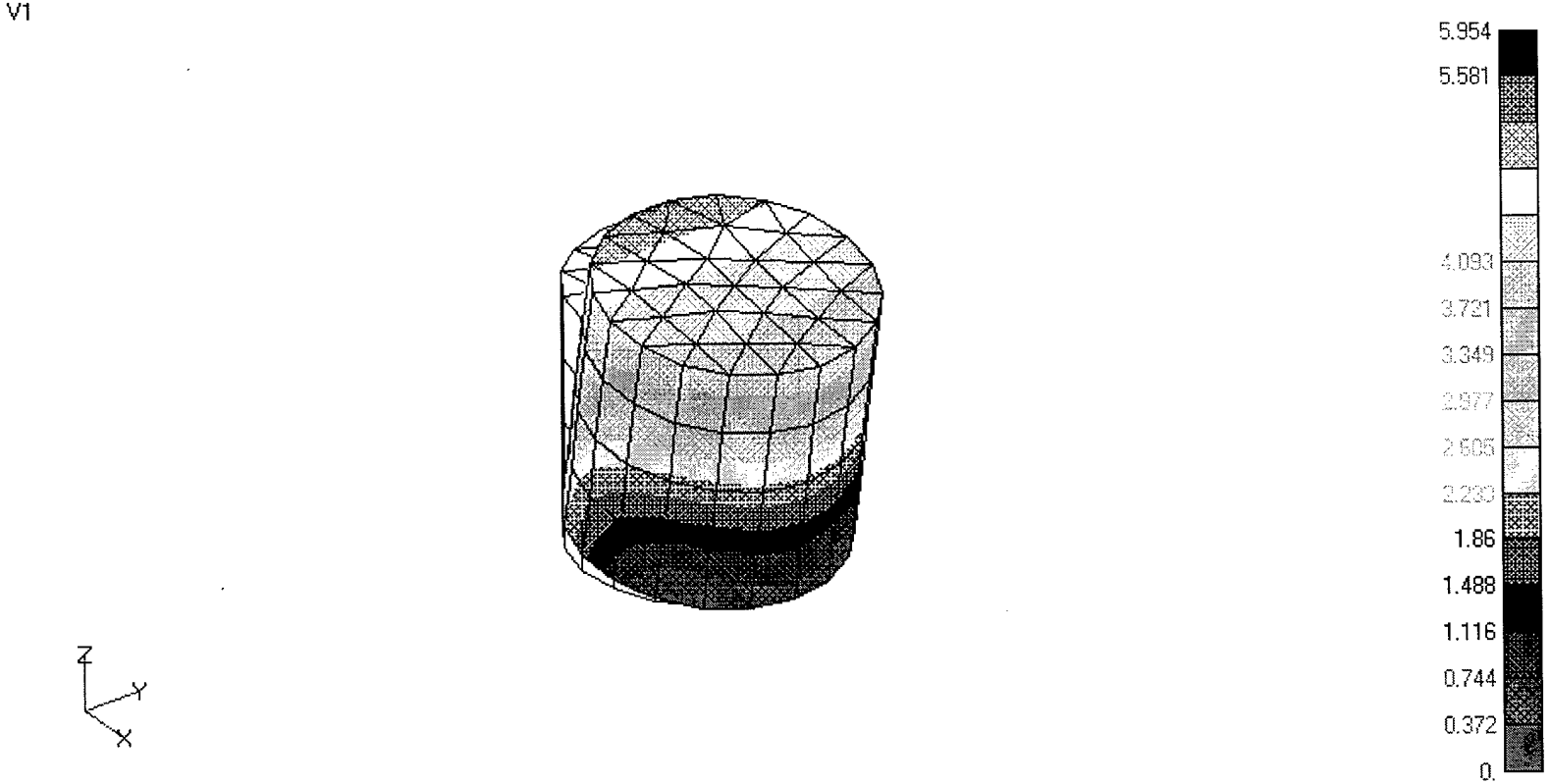

Horizontal Load = 4,500,000 lbs
Linear Elastic-Perfectly Plastic Clayey Soil (Hyperbolic Extended Drucker-Prager)
E = 30,000 psf, υ = 0.499, Slope Angle = 10.2°, Dilation Angle = 10.2°
Linear Elastic-Perfectly Plastic Sandy Soil (Linear Extended Drucker-Prager)
E = 864,000 psf, υ = 0.3, Slope Angle = 46.2°, Dilation Angle = 21.5°
Pile, AISI 4340 Steel

Figure-G10. Soil Minor Principal Stresses (Circular Pile in Layered Soil-6)

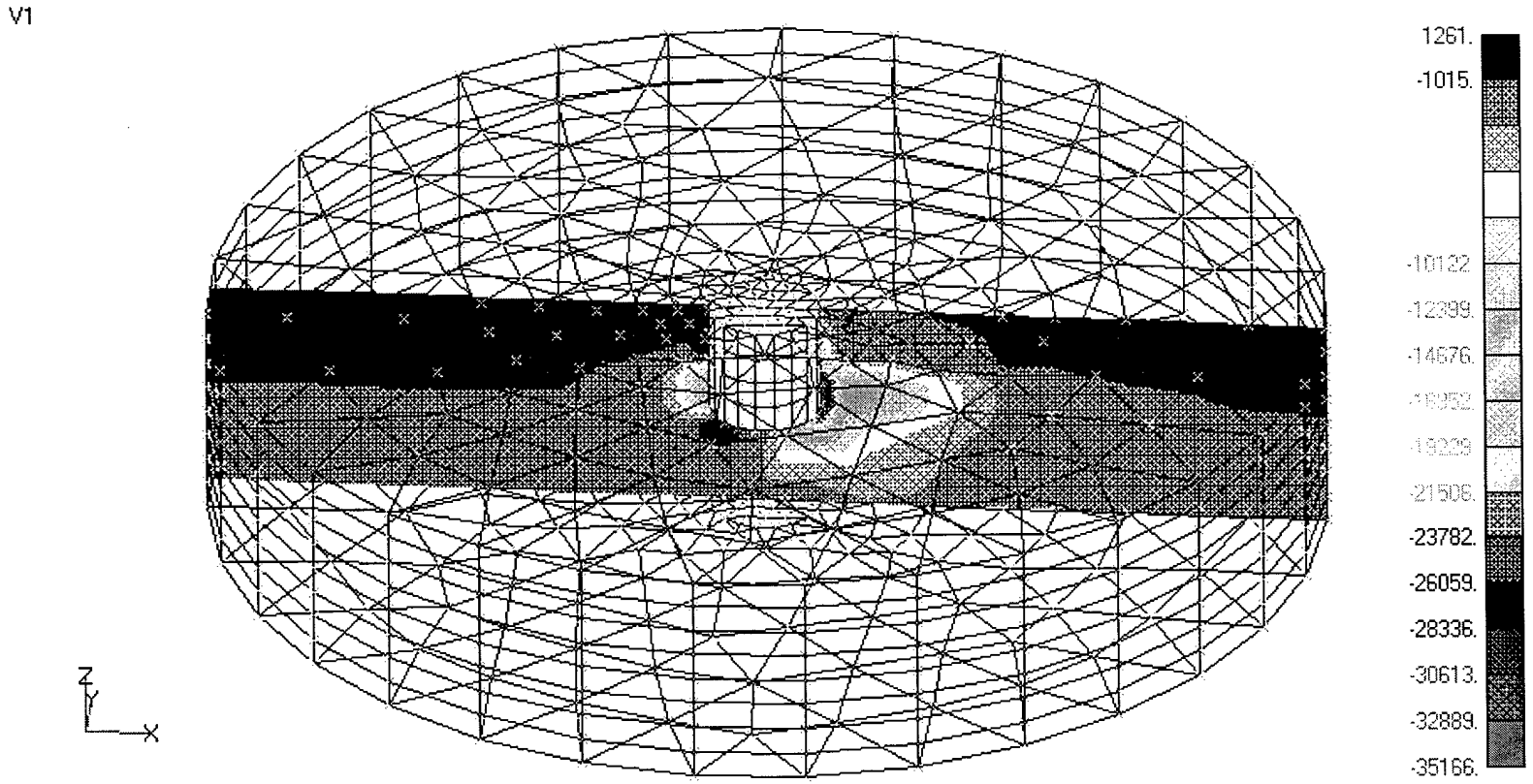

Horizontal Load = 4,500,000 lbs
Linear Elastic-Perfectly Plastic Clayey Soil (Hyperbolic Extended Drucker-Prager)
E = 30,000 psf, υ = 0.499, Slope Angle = 10.2°, Dilation Angle = 10.2°
Linear Elastic-Perfectly Plastic Sandy Soil (Linear Extended Drucker-Prager)
E = 864,000 psf, υ = 0.3, Slope Angle = 46.2°, Dilation Angle = 21.5°
Pile, AISI 4340 Steel

Figure-G11. Soil Minor Principal Stresses on a Vertical Plane along the Horizontal Load Direction (Circular Pile in Layered Soil-6)

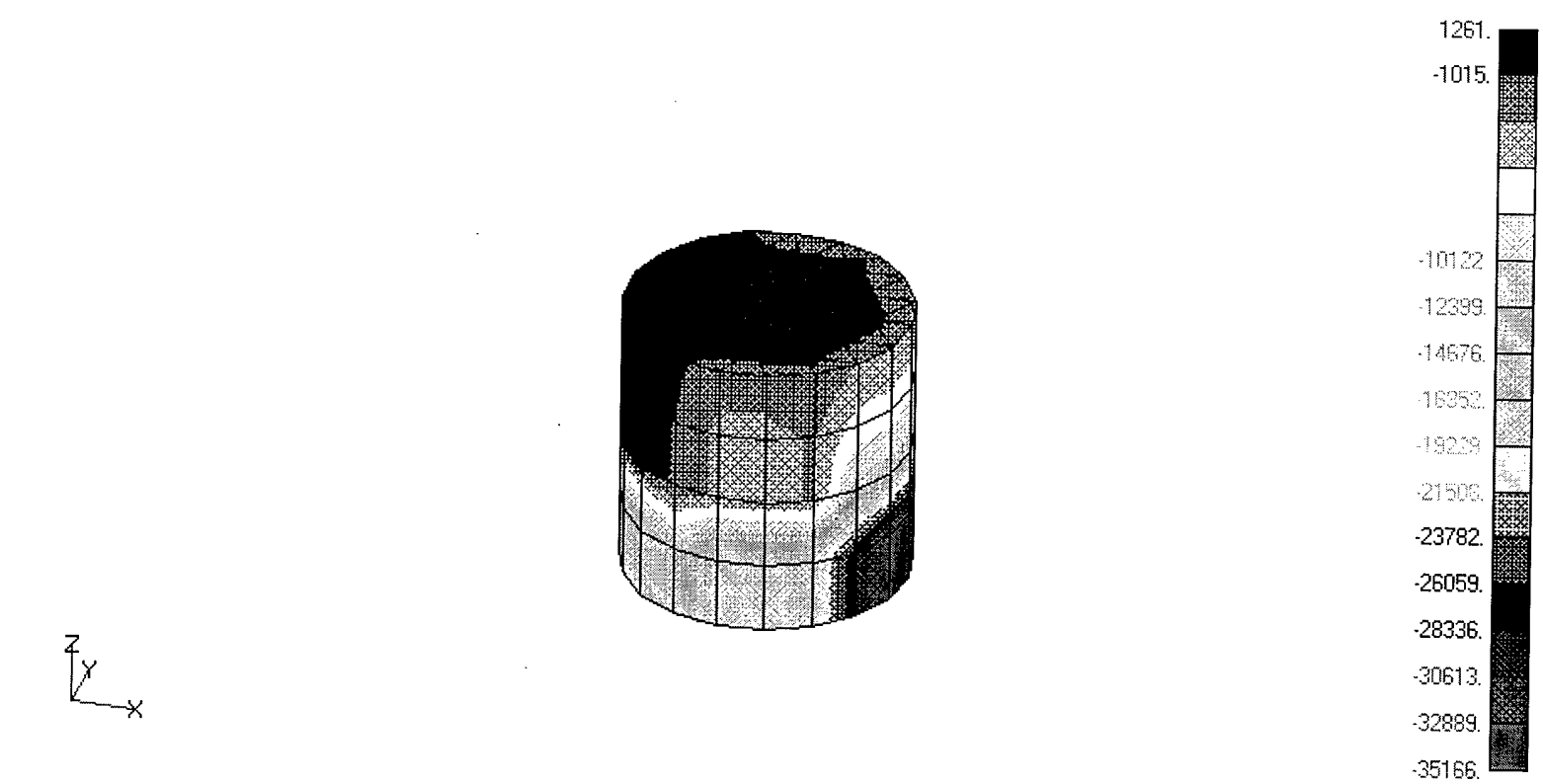

Horizontal Load = 4,500,000 lbs
Linear Elastic-Perfectly Plastic Clayey Soil (Hyperbolic Extended Drucker-Prager)
E = 30,000 psf, υ = 0.499, Slope Angle = 10.2°, Dilation Angle = 10.2°
Linear Elastic-Perfectly Plastic Sandy Soil (Linear Extended Drucker-Prager)
E = 864,000 psf, υ = 0.3, Slope Angle = 46.2°, Dilation Angle = 21.5°
Pile, AISI 4340 Steel

Figure-G12. Pile von Mises Stresses on the Pile Surface (Circular Pile in Layered Soil-6)

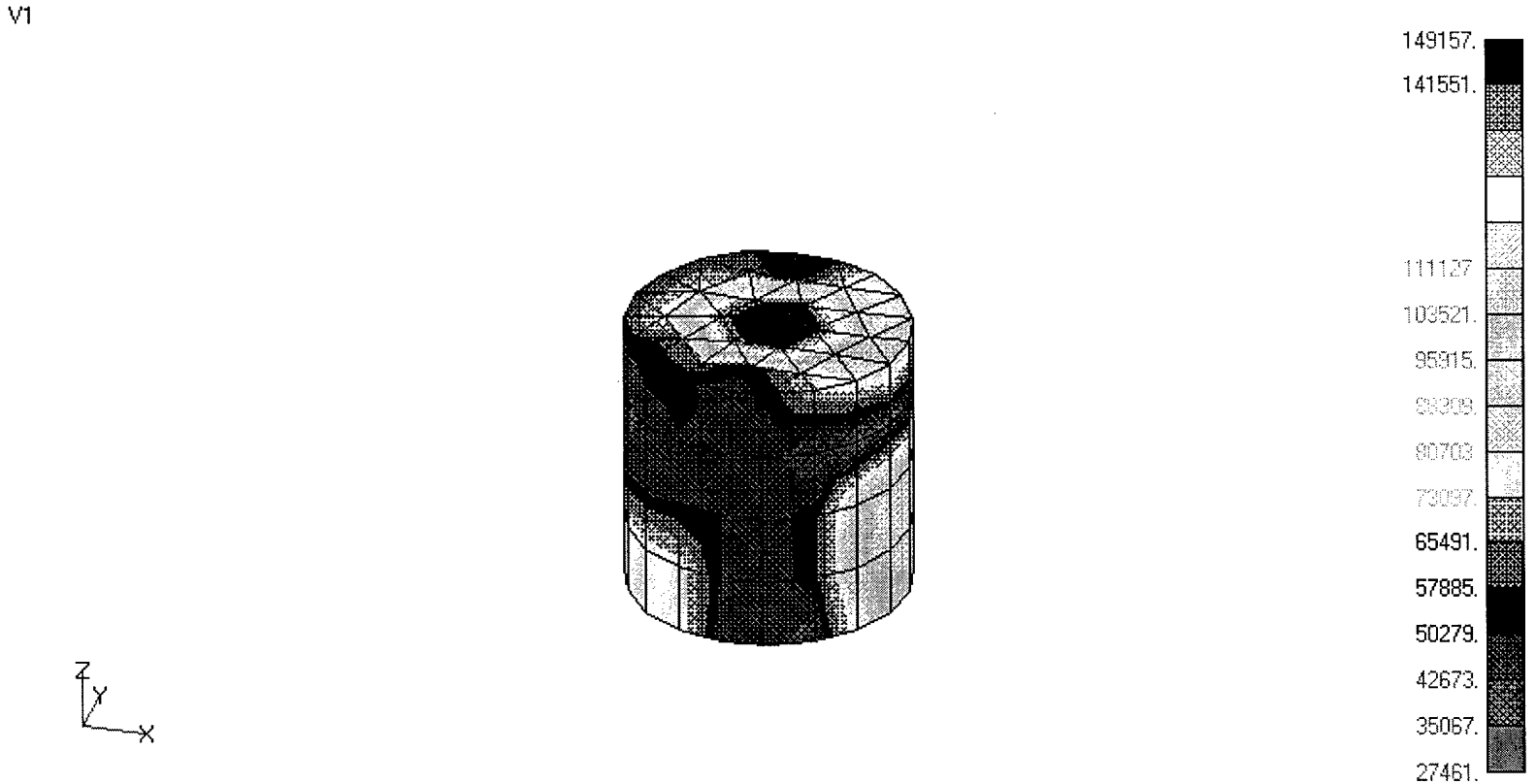

Horizontal Load = 4,500,000 lbs
Linear Elastic-Perfectly Plastic Clayey Soil (Hyperbolic Extended Drucker-Prager)
E = 30,000 psf, υ = 0.499, Slope Angle = 10.2°, Dilation Angle = 10.2°
Linear Elastic-Perfectly Plastic Sandy Soil (Linear Extended Drucker-Prager)
E = 864,000 psf, υ = 0.3, Slope Angle = 46.2°, Dilation Angle = 21.5°
Pile, AISI 4340 Steel